REPORT

Appendix 7.1 - Marine Physical Environment Numerical Modelling

Wave, Hydrodynamic and Plume Dispersion Modelling Report

Client:	ScottishPower Renewables UK Ltd
Reference:	PC3749-RHD-XX-XX-RP-X-0001
Status:	S0/P01.01
Date:	28 November 2025

Haskoning
Enhancing Society Together

HASKONING UK LTD.

Telecom House
125-135 Preston Road
Brighton
BN1 6AF
United Kingdom
Water & Maritime
VAT registration number: 792428892

Phone: +44 (0)1444 458551
Email: info@uk.haskoning.com
Website: haskoning.com

Document title:	Appendix 7.1 - Marine Physical Environment Numerical Modelling
Subtitle:	Wave, Hydrodynamic and Plume Dispersion Modelling Report
Reference:	PC3749-RHD-XX-XX-RP-X-0001
Your reference	MCW-DWF-ENV-REP-RHS-000045
Status:	S0/P01.01
Date:	28 November 2025
Project name:	Machair Windfarm EIA
Project number:	PC3749
Author(s):	JC
Drafted by:	JC, DXL and TC
Checked by:	KH
Date:	
Approved by:	
Date:	
Classification:	Project related

Table of Contents

Table of Tables

Table of Figures

Acronyms

ADCP	Acoustic Doppler Current Profiler
BNG	British National Grid
BODC	British Oceanographic Data Centre
CFL	Courant–Friedrichs–Lewy
CSD	Cutter Suction Dredger
DHI	Danish Hydraulic Institute
EA	Environment Agency
EIA	Environmental Impact Assessment
EMODnet	European Marine Observation and Data Network
ERA5	EC MWF Reanalysis v5 (ERA5). ERA5 is the fifth generation EC MWF reanalysis for the global climate and weather for the past 8 decades, and for the global wave for the past 4 decades.
GEV	Generalized Extreme Value
GPD	Generalized Pareto Distribution
HD	Hydrodynamic
Hs	Significant wave height
IAC	Inter-Array Cable
IHO	International Hydrographic Organization
km	Kilometre
LAT	Lowest Astronomic Tide
ME	Mean Error

MSL	Mean Sea Level
MW	Megawatt
MWD	Mean Wave Direction
NE	Northeast
NRW	Natural Resource Wales
NW	Northwest
OSP	Offshore Substation Platform
POT	Peak Over Threshold
R	Correlation Coefficient
RMSE	Root Mean Square Error
SE	Southeast
SI	International Units System
SSC	Suspended Sediment Concentration
Std	Standard Deviation
SW	Spectral Wave
SWLB	Seawatch LiDAR Buoy
SWM	Seawatch Midi Buoy
Tp	Peak wave period
TSHD	Trailing Suction Hopper Dredger
UK	United Kingdom
UKHO	United Kingdom Hydrographic Office

WAFO	Wave Analysis for Fatigue and Oceanography
WDA	Windfarm Development Area
WS	Wave Scan Buoy
WSW	West southwest
WTG	Wind Turbine Generator

1 Introduction

1.1 Project Background

1.1.1 Machairwind Limited have enlisted the expertise of Haskoning to undertake a numerical modelling study of waves, hydrodynamics and sediment transport for the proposed MachairWind Windfarm Development Area (WDA). The modelling study forms part of the larger Environmental Impact Assessment (EIA) which is required in the consenting process for the proposed WDA.

1.1.2 The WDA is located off the northwest of Islay and west of Colonsay, with the proposed WDA covering a spatial extent of 448 km^2, as shown in the Project overview in **Figure 1-1**.

1.1.3 This technical report will focus on the numerical modelling study only.

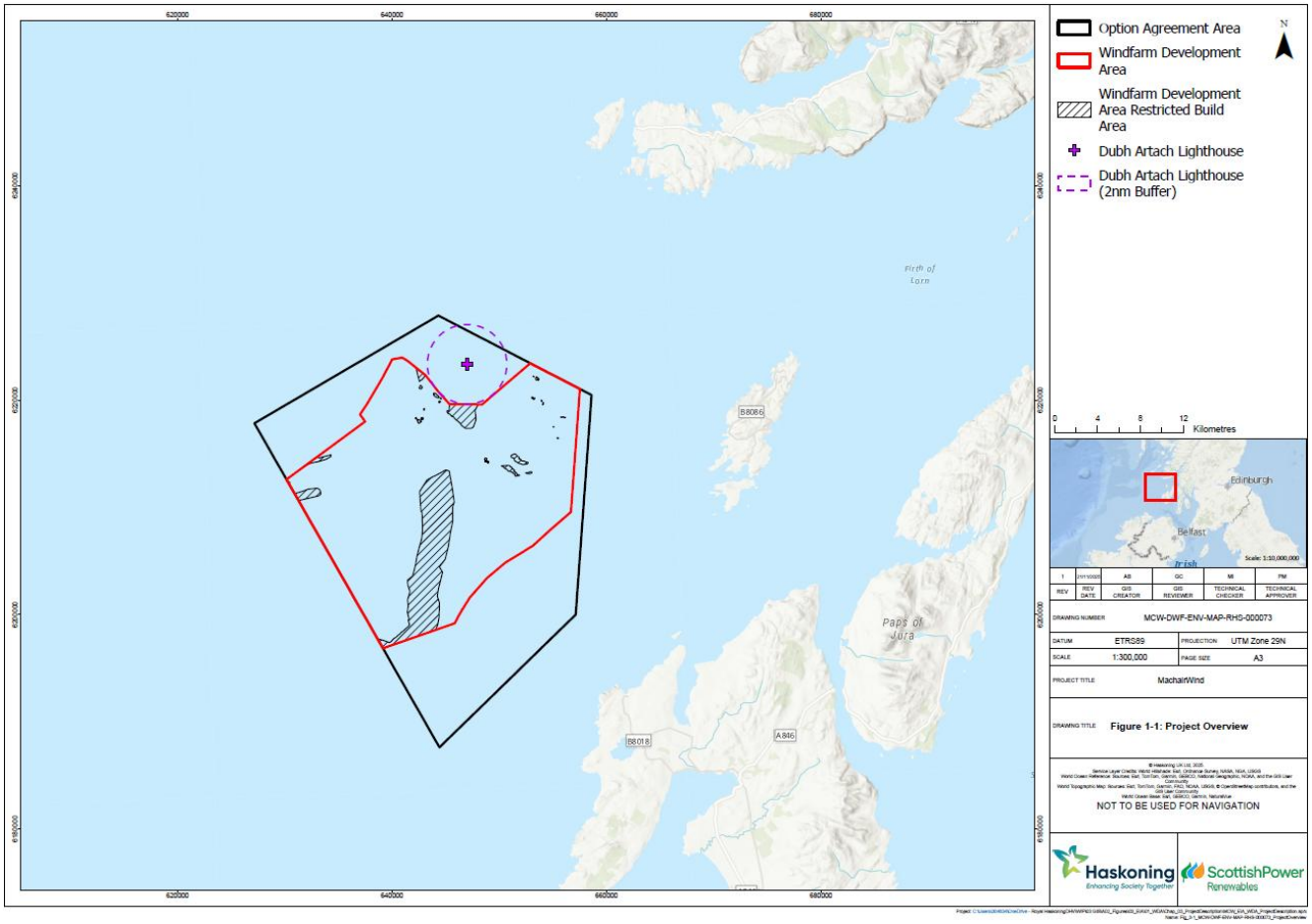

Figure 1-1: Project overview

1.2 Scope

1.2.1 The aim of the numerical modelling study was to quantify the potential change in wave climate, hydrodynamics and suspended sediment concentrations (SSC) in response to the proposed WDA infrastructure, where results of the study will supplement the EIA to investigate the impact

of any change in waves in the surrounding coastal environment, designated areas and sensitive receptors.

1.2.2 The scope of works to achieve this aim was a derivation of offshore extreme wave and wind climate, development and calibration of spectral wave (SW) model, hydrodynamic model and sediment transport model, simulation of wave climate and tidal conditions for baseline (no WDA) and with WDA options in place to quantify the change, and SSC and deposition during construction.

1.2.3 Out of the three foundation options proposed for wind turbine generators (WTG) (monopiles, pin-pile jackets and suction bucket jackets), monopiles were considered as a worst-case (with respect to the blocking effect in wave propagation) due to the larger diameter of the single structure, compared with the jackets which are held by multiple smaller piles. The monopiles were modelled for two indicative layouts, 15 MW (144 turbines) and 24 MW (91 turbines). The exact structure dimensions and locations are discussed in more detail in **Section 4.3**.

1.2.4 In sediment dispersion modelling, monopiles were considered as a worst-case with respect to quantity of sediment release from drilling. However, for sediment release from bed preparation, suction bucket jackets are considered as a worst-case.

1.2.5 The model results will be used to define a ‘Zone of Influence’ where the wave climate is affected by the WDA.

1.3 Datum, Units and Convention

1.3.1 For the wave modelling study, the vertical datum used was relative to Lowest Astronomic Tide Level (m LAT) at the survey location.

1.3.2 All distances and measurements in this study refer to standard base SI (International Units System) units.

1.3.3 The horizontal reference for all distances and coordinates in this study is to British National Grid, m (BNG).

1.3.4 The convention of both wave and wind direction through the modelling study is in degrees relative to true north. When describing directions as a narrative, the direction the waves are coming from is used, for example, a southwesterly wave reflects a wave approaching from the southwest.

2 Approach

2.1 Wave Modelling

2.1.1 The proposed wave modelling approach was to apply the MIKE21 SW wave transformation model developed by Danish Hydraulic Institute (DHI), to simulate extreme wave conditions at the WDA for baseline and with WDA infrastructure options to understand the potential impact of a change in wave climate on surrounding coastal areas.

2.1.2 The MIKE21-SW model is industry standard software for simulating the growth and transformation of wind and swell waves in coastal areas.

2.1.3 Boundary conditions for the MIKE21-SW model were obtained from widely used sources, MetOffice United Kingdom (UK) hindcast wave model, EC MWF Reanalysis v5 (ERA5) global atmospheric model and NORA3 high resolution atmospheric model of Arctic and North Seas.

2.1.4 The MIKE21-SW model development included the most recent bathymetric data to the model domain and a calibration of predicted wave climate to measured wave data from the Project's one-year metocean campaign at two survey locations (S1 and S2) and Centre for Ecology, Fisheries and Aquaculture Science (CEFAS) 'Blackstone's' wave buoy.

2.2 Hydrodynamic Modelling

2.2.1 For the hydrodynamics, MIKE21-HD (Hydrodynamic) software developed by DHI was chosen. In this study, two hydrodynamic models with different scales and grid resolutions were used. For the large-scale tidal hydrodynamics, Haskoning's UK and Ireland Regional model was adopted. For the detailed tidal hydrodynamics around the Project area, a local model was developed using fine mesh. This local model was nested in the large-scale regional model. Further details of these two models are presented in **Section 5.1**.

2.2.2 At the open boundaries of the regional model, water levels were used, which vary in time and along the boundaries. The input data for these boundaries were extracted from the Global Tidal Model of DHI. The boundary conditions of the local model are provided by the regional model.

2.2.3 The local hydrodynamic model development included the most recent bathymetric data to the model domain as the wave model.

2.3 Sediment Dispersion Modelling

2.3.1 For the purpose of the sediment dispersion model, the local hydrodynamic model was developed into a 3D hydrodynamic model using MIKE3-HD by introducing vertical mesh. The sediment dispersion model was then built in MIKE3-MT, and coupled with the 3D hydrodynamic model built in MIKE3-HD. The computational mesh of MIKE3-MT is identical to the local hydrodynamic model.

3 Input Data

3.1 Bathymetry

3.1.1 The bathymetry data for this numerical modelling study comprises the following datasets, where these are combined to provide the most suitable coverage in terms of resolution and survey period:

1) High resolution multibeam bathymetric survey of the WDA collected in 2023 (yellow polygon in **Figure 3-1**). **Figure 3-2** shows a close-up with the bathymetry around the WDA (red outline);

2) Open-source bathymetry data from the United Kingdom Hydrographic Office (UKHO) Admiralty Seabed Portal (**Ref 9**). This is a collection of measured datasets covering a range of time periods (green polygon in **Figure 3-1**); and

3) The remaining areas of the domain are covered by European Marine Observation and Data Network (EMODnet 2024) gridded bathymetric data on a 100 m horizontal grid (**Ref 4**).

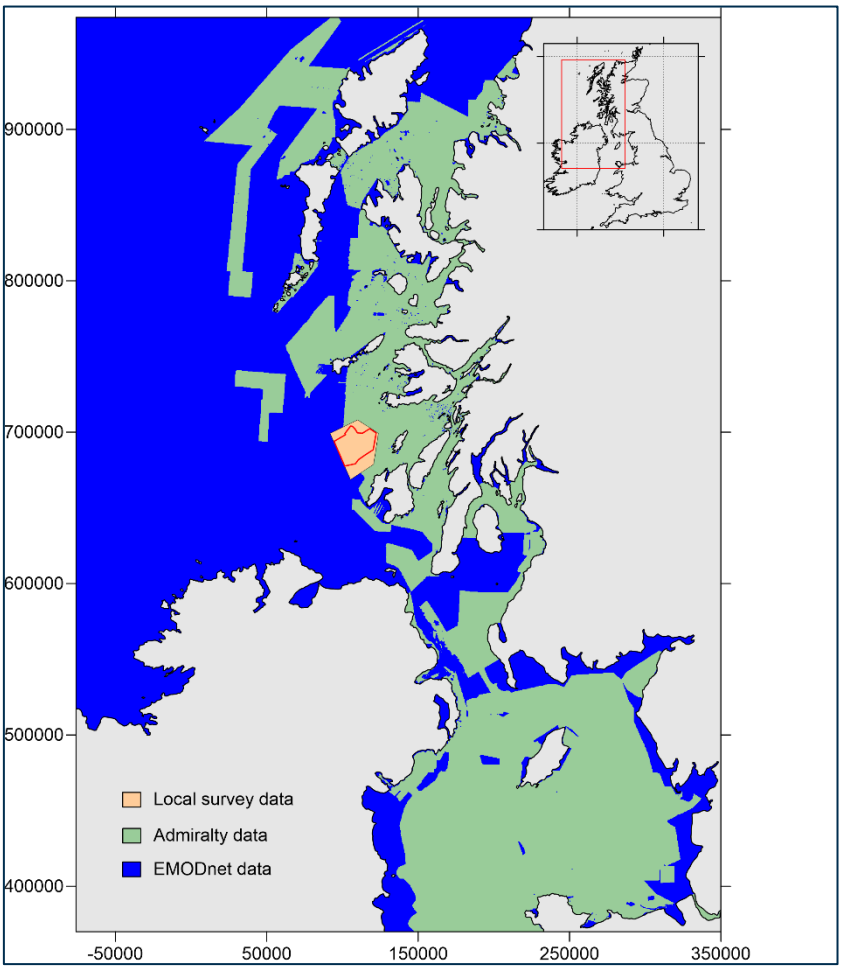

Figure 3-1: Wave model bathymetric datasets (red line indicates the proposed WDA)

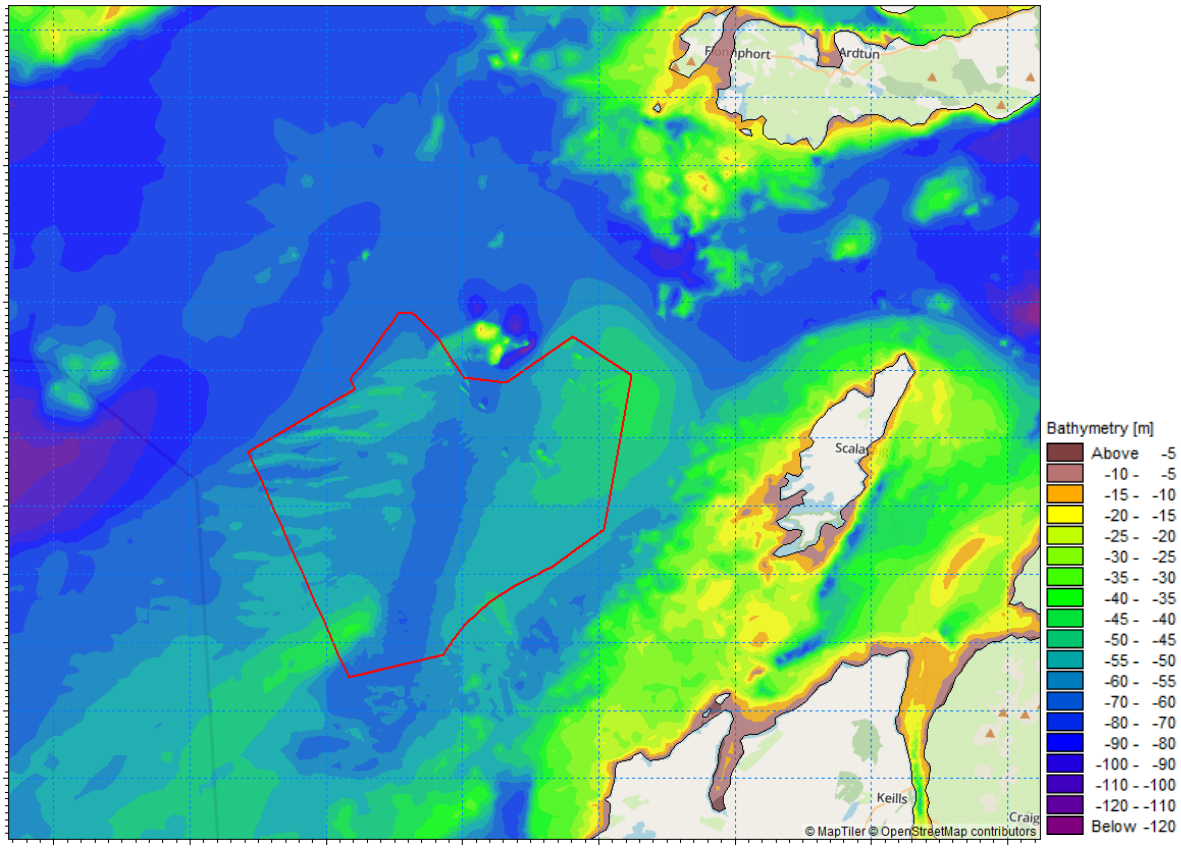

Figure 3-2: Bathymetry around the Machair WDA (red outline)

3.2 Measured Metocean Data

3.2.1 A comprehensive metocean survey was undertaken within the WDA and on the indicative cable corridor by Fugro from April 2023 to May 2024 (**Ref 5** and **Ref 6**). The survey included the deployment of surface buoys to measure wind and wave climate and seabed mounted frames to measure water level, wave climate and other parameters. The location of the survey sites is presented in **Figure 3-3** below.

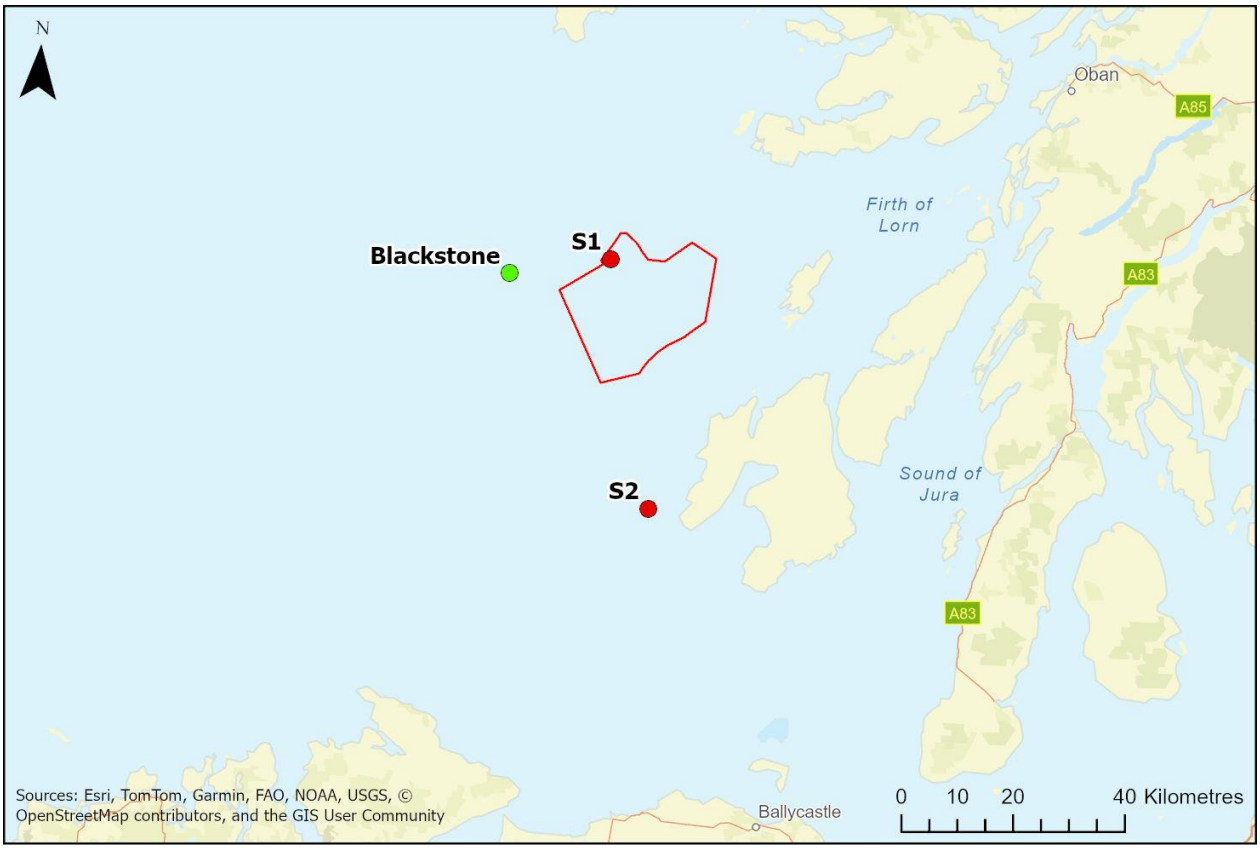

Figure 3-3: Metocean survey locations S1 (56° 05.919'N, 006° 45.893'W) and S2 (55° 41.779'N, 006° 36.854'W) [see Section 3.4 for details on Cefas WaveNet buoy Blackstone]

Waves

3.2.2 At S1 wave data was collected via two surface buoys Seawatch Midi Buoy (SWM) and Seawatch LiDAR Buoy (SWLB) and one seabed mounted frame 'SIG'. At S2, wave data was collected via one surface buoy Wave Scan Buoy (WS) and one seabed mounted frame (SIG). An example of the wave data collected at S2 via the seabed mounted frame is presented in **Figure 3-4** and **Table 3-1**.

3.2.3 Initial analysis of the data indicates the predominant wave climate is arriving from west southwest (WSW) to northwest (NW), with strong seasonality observed in the winter months (December – March) which typically have more frequent and larger energetic storm events, and the summer months typically are calmer, with smaller and less frequent storm events. The largest storm event of the survey period came on the 21/12/2023, with a measured significant wave height (Hs) of 8.97 m at S2 (SIG').

3.2.4 Through review of the data, it was concluded the most complete wave datasets which covered the full survey period were 'SWM' at S1 and 'SIG' at S2, these would be used for wave model calibration.

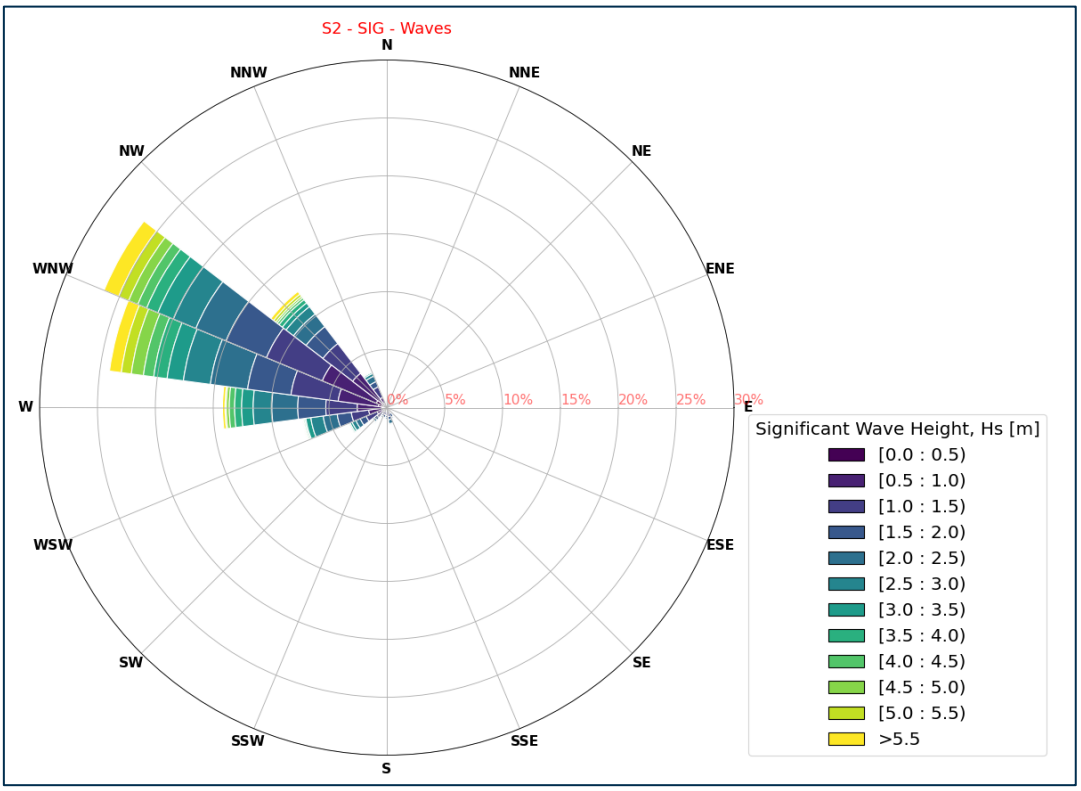

Figure 3-4: Measured Hs at S2 – SIG

Table 3-1: Frequency of occurrence of Hs at S2 - SIG

Month	% Occurrence of Hs (m) – S2 - SIG							
	0-1	1-2	2-3	3-4	4-5	5-6	6-7	>7
Jan	0.1%	2.9%	1.8%	1.1%	0.7%	0.6%	0.4%	0.1%
Feb	0.2%	2.0%	1.2%	1.0%	1.7%	1.0%	0.1%	0.0%
Mar	0.4%	4.3%	1.8%	0.6%	0.2%	0.3%	0.2%	0.0%
Apr	2.6%	2.7%	1.5%	0.9%	0.3%	0.1%	0.0%	0.0%
May	4.4%	7.3%	3.2%	0.5%	0.0%	0.0%	0.0%	0.0%
Jun	5.4%	1.0%	1.1%	0.0%	0.0%	0.0%	0.0%	0.0%
Jul	3.7%	2.5%	1.1%	0.5%	0.0%	0.0%	0.0%	0.0%
Aug	2.0%	4.5%	1.2%	0.1%	0.0%	0.0%	0.0%	0.0%
Sep	0.9%	3.0%	2.2%	1.1%	0.3%	0.0%	0.0%	0.0%
Oct	0.5%	4.2%	2.0%	0.9%	0.2%	0.0%	0.0%	0.0%
Nov	0.6%	2.9%	2.6%	0.6%	0.6%	0.3%	0.0%	0.0%
Dec	1.0%	1.0%	2.0%	1.3%	1.0%	1.0%	0.3%	0.2%
Total	**21.7%**	**38.4%**	**21.6%**	**8.5%**	**5.1%**	**3.3%**	**1.0%**	**0.3%**

Wind

3.2.5 Meteorological data was collected at S1 which covered the full survey period from April 2023 to May 2024, this data is presented in **Figure 3-5** and **Table 3-2**. The predominant wind direction is approaching the site from SW to NW.

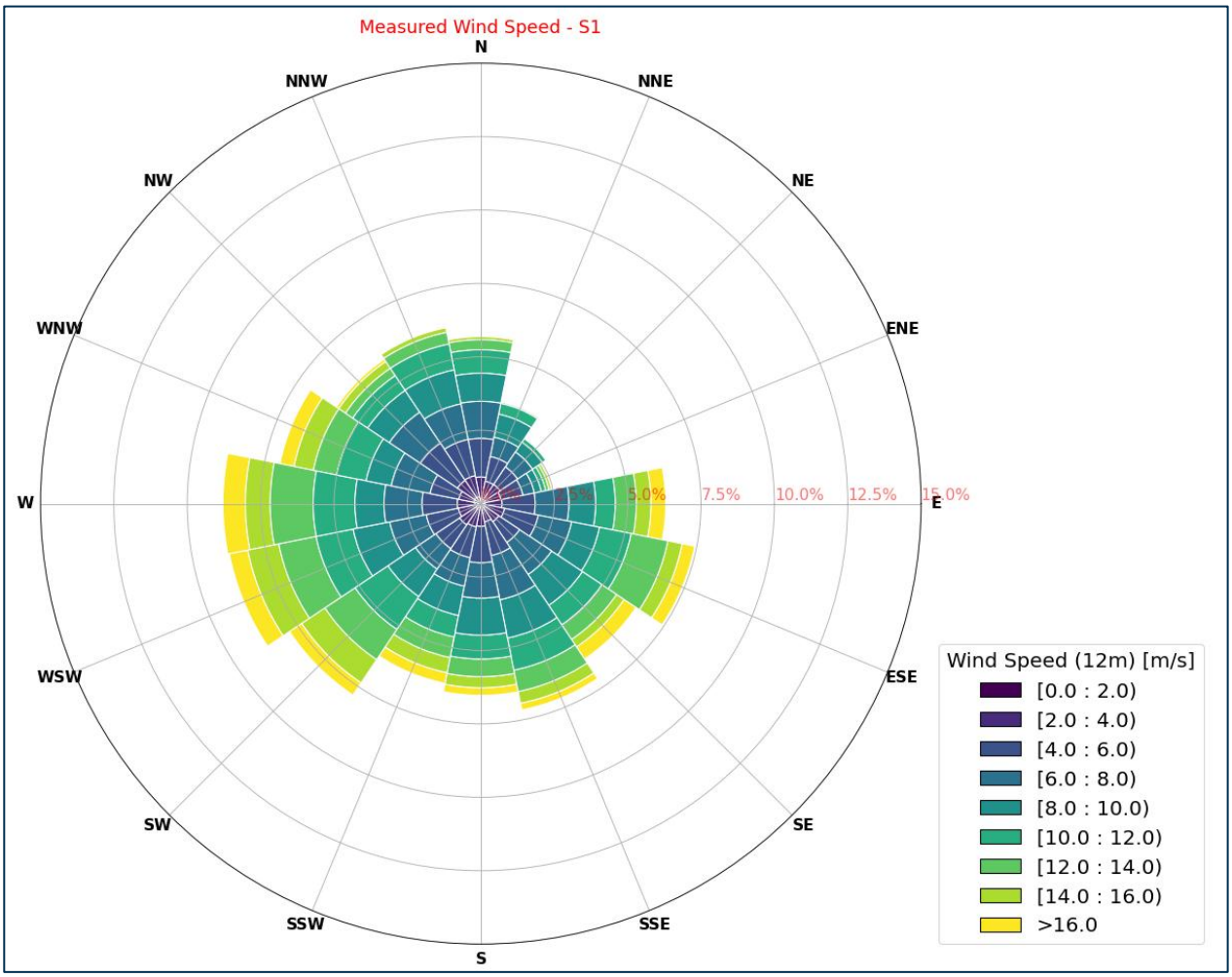

Figure 3-5: Measured wind speed at 12 m elevation – S1

Table 3-2: Frequency of occurrence of wind speed at S1

Month	% Occurrence of Wind Speed (m/s) – S1							
	0-2	2-5	5-8	8-11	11-14	14-17	17-20	>20
Jan	0.3%	1.1%	1.4%	2.1%	1.6%	1.2%	0.6%	0.2%
Feb	0.1%	0.8%	1.6%	2.1%	1.9%	1.2%	0.2%	0.0%
Mar	0.2%	0.8%	1.7%	2.6%	2.0%	1.0%	0.1%	0.0%
Apr	0.5%	1.5%	2.2%	2.0%	1.1%	0.7%	0.2%	0.0%
May	0.3%	2.6%	4.1%	1.1%	0.3%	0.0%	0.0%	0.0%
Jun	0.6%	3.5%	3.0%	0.8%	0.2%	0.0%	0.0%	0.0%
Jul	0.3%	1.7%	3.3%	1.8%	1.2%	0.2%	0.0%	0.0%
Aug	0.4%	1.5%	2.8%	2.5%	1.0%	0.2%	0.0%	0.0%
Sep	0.3%	1.5%	2.3%	1.8%	1.3%	0.9%	0.1%	0.0%
Oct	0.2%	0.6%	1.2%	2.2%	3.2%	0.8%	0.3%	0.0%
Nov	0.1%	1.4%	2.4%	1.8%	1.2%	1.0%	0.2%	0.0%
Dec	0.6%	0.8%	1.1%	1.5%	2.0%	1.6%	0.7%	0.1%
Total	**3.9%**	**17.9%**	**27.0%**	**22.4%**	**17.1%**	**8.8%**	**2.5%**	**0.3%**

Water Level

3.2.6 Measured water levels from 01 May 2023 to 01 March 2024 were downloaded from British Oceanographic Data Centre (BODCp) recorded at an A-Class Portrush tide gauge (**Ref 2**). The location of this tide gauge is shown in **Figure 3-6** and the coordinates of this location are provided in **Table 3-3**. These measured water levels were used to calibrate the regional model.

3.2.7 Water level measurement data from 28 April 2023 to 31 May 2024 at 2 locations were collected by Fugro (**Ref 5** and **Ref 6**). The locations of these two surface buoys are shown in **Figure 3-6** and the coordinates of these locations are provided in **Table 3-3**. These measured water levels were used to calibrate both the regional and local model.

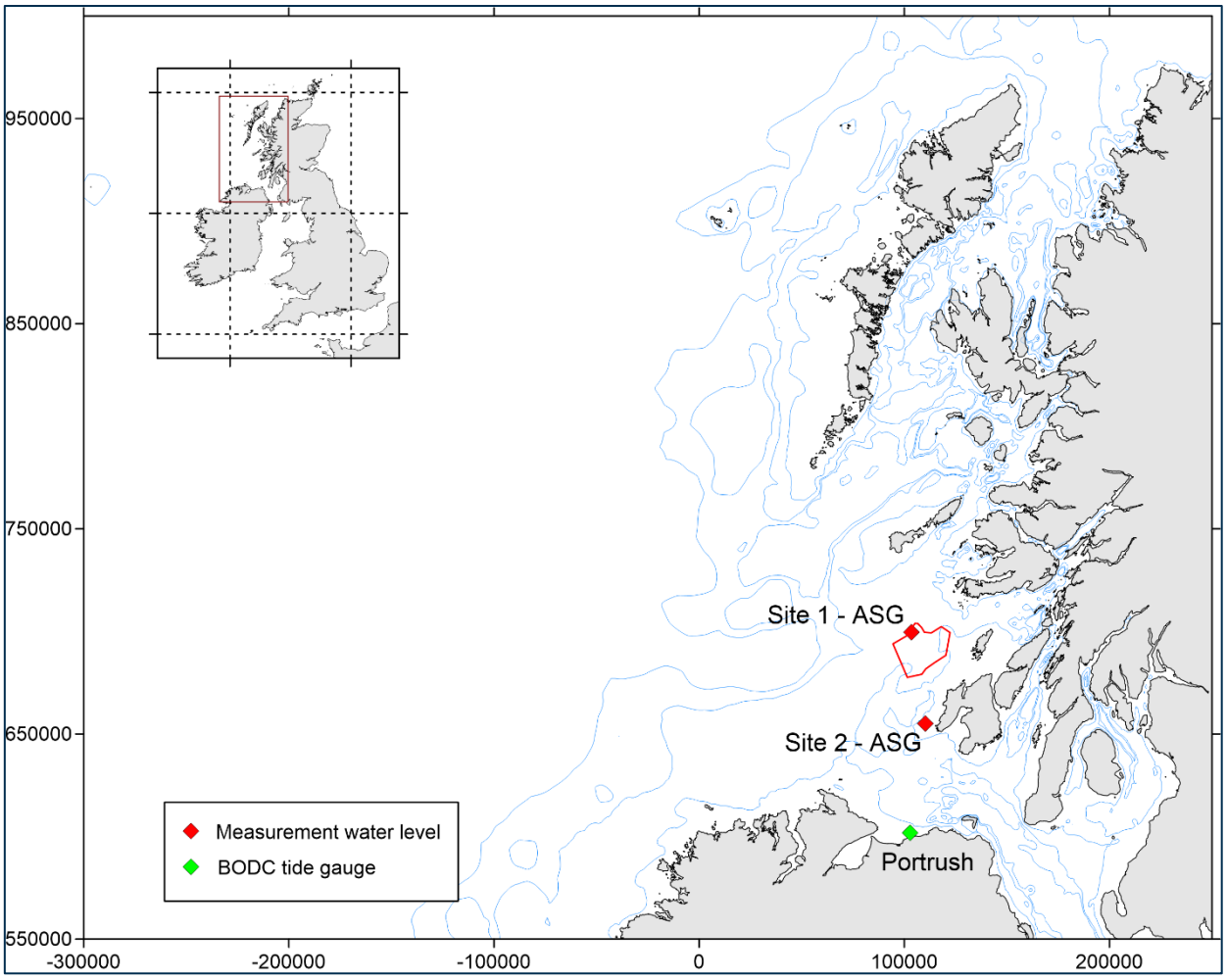

Figure 3-6:Location of tidal gauges (red line indicates the WDA)

Table 3-3: Locations of the measured water levels

ID	Station name	Longitude	Latitude	Time interval (minute)	Duration	Description
1	Site 1-ASG	-6.77º	56.09º	10	28/4/2023 - 31/5/2024	Water level
2	Site 2-ASG	-6.61º	55.70º	10	29/4/2023 - 31/3/2024	Water level
3	Portrush	-6.66º	55.20º	15	1/5/2023 - 31/3/2024	Water level

Currents

3.2.8 The measured current data was collected by Fugro (**Figure 3-7**), using two surface buoys and two seabed mounted Acoustic Doppler Current Profiler (ADCP) frames. A description of the measured data including locations is provided in **Table 3-4** and a detailed summary of data collection methods and Haskoning data review is provided in report – "PC3479-RHD-XX-XX-ME-X-0001-Machair Windfarm Metocean Data Review R1.docx".

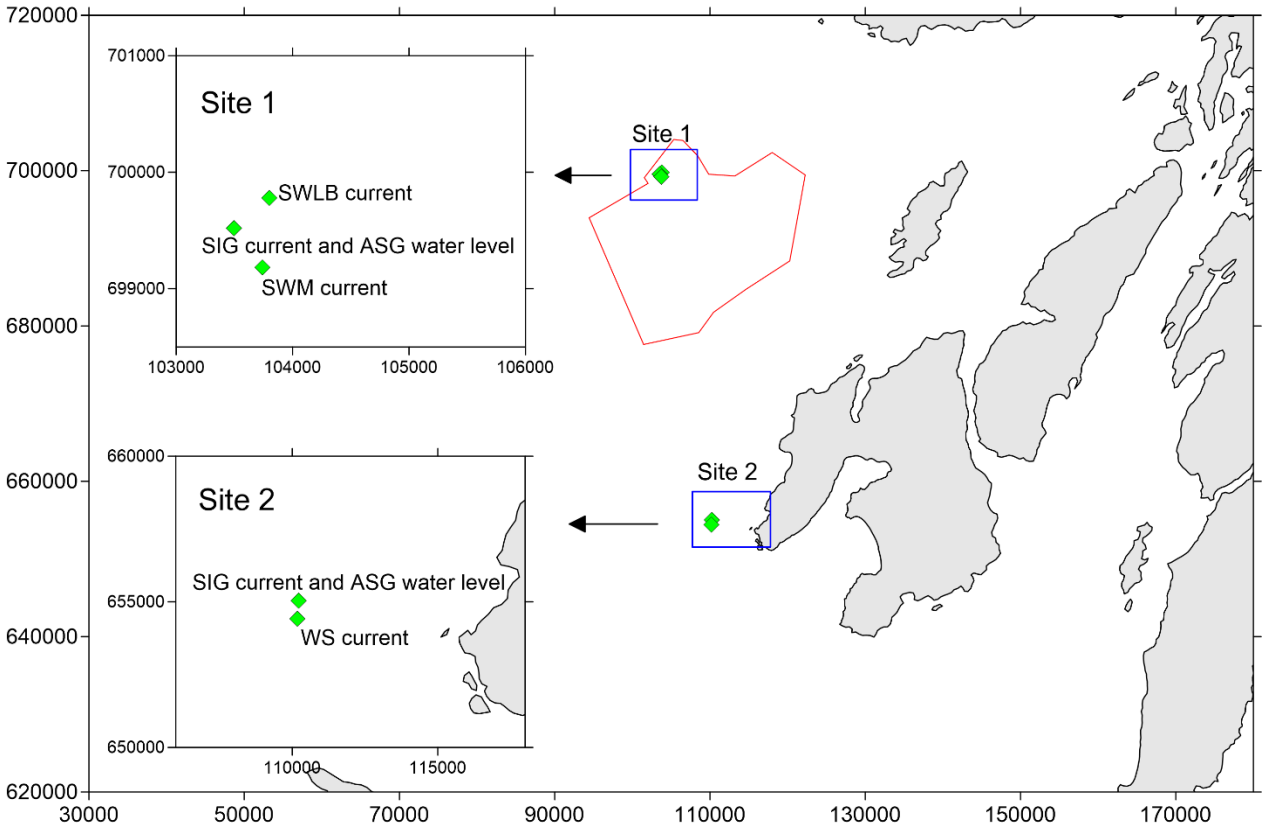

Figure 3-7: Location of current and water level measurements (red line indicates the proposed WDA)

Table 3-4: Locations of the measured current speed

ID	Station name	Longitude	Latitude	Time interval (minute)	Duration
1	Site 1 - SWLB current	-6.764º	56.098º	10	28/4/2023 - 24/4/2024
2	Site 1 - SIG current	-6.769º	56.096º	10	28/4/2023 - 31/5/2024
3	Site 1 - SWM current	-6.765º	56.093º	10	28/4/2023 - 31/5/2024
4	Site 2 - SIG current	-6.614º	55.701º	10	29/4/2023 - 31/5/2024
5	Site 2 - WS current	-6.614º	55.696º	10	29/4/2023 - 14/3/2024

3.3 Hindcast Data

3.3.1 Hindcast wave data for the modelling study was obtained from the MetOffice UK high resolution WAVEWATCH III model. The hindcast dataset of SW parameters (sH, peak wave period (Tp) and mean wave direction) covers 1980 – 2024 at 3 hourly intervals, simulated on a high-resolution horizontal grid of 3 km to 1.5 km in coastal areas. To drive the MIKE21-SW model for the study, a total of 256 data points were extracted from the MetOffice hindcast wave model, along with the proposed boundary of the MIKE21-SW model (see **Section 4.1**). Wave spreading was not readily available from the MetOffice model, so this parameter was obtained from the reanalysis dataset from the ERA5 global wave model, on a 0.5° horizontal grid.

3.3.2 Hindcast wind data for the study was obtained from the reanalysis dataset from the ERA5 global atmospheric model. The dataset of U and V wind speed vectors covers 1980 – 2024 at 1 hourly interval, simulated on a global horizontal grid of 0.5°, approximately 25 km to 30 km at the location of the WDA. A series of 380 data points were extracted from the ERA5 global model to provide a 2D data array for model simulations.

3.3.3 Additional hindcast wind data was also obtained from the high-resolution Norwegian reanalysis 3 km atmospheric model of the Arctic and North Sea (NORA3). This dataset was for comparison purposes in the model calibration process, where the primary hindcast wind dataset was from ERA5 as the MetOffice UK wave model (used for wave boundary conditions) is forced by this.

3.4 Wave Buoy Data

3.4.1 In addition to survey data collected at S1 and S2, measured wave buoy data at Blackstone's wave buoy was also obtained from the CEFAS online WaveNet data portal, covering the full period of the survey period (**Ref 3**). The data point is located at 56°3.717'N, 007°3.400'W as shown in **Figure 3-3**.

3.5 Predicted Water Levels

3.5.1 A long time series of predicted astronomic tide levels at the closest standard port of Iona, was obtained for the wave modelling study. The time series was generated from the International Hydrographic Organization (IHO) tidal database. Due to deep water at calibration sites, it is not expected that accuracy of water levels would affect model calibration.

3.6 Coastline

3.6.1 The coastline for the model domain was digitized using Google Earth Pro, 2025.

3.7 Extreme Value Analysis

Approach

3.7.1 An extreme value analysis of the offshore wave climate was undertaken to determine the offshore forcing conditions for the WDA wave impact assessment. Following the analysis of the survey data (**Section 3.2**), the predominant approaching wave directions which would be the focus for the assessment are SW through to NW, in 30 degree sectors as follows, 240°N (225°N to 255°N), 270°N (255°N to 285°N), 300°N (285°N to 315°N) and 330°N (315°N to 345°N). In addition to this, these directions of wave approach are of interest for the impact of the WDA on surrounding coastal areas.

3.7.2 The long time series of hindcast MetOffice wave data (1980- 2024) was used for the extreme wave analysis at two offshore locations, as presented in **Figure 3-8**. The southern location for waves from 240°N and 270°N, then the northern location for waves from 300°N and 330°N. The offshore location of each point is selected so the hindcast data is at the proposed model boundary (see **Section 4.1**). To understand whether any model error or uncertainty in the hindcast data lead to the extreme values being under or over predicted compared with measured data, a validation of the MetOffice hindcast wave data is also presented in the following section.

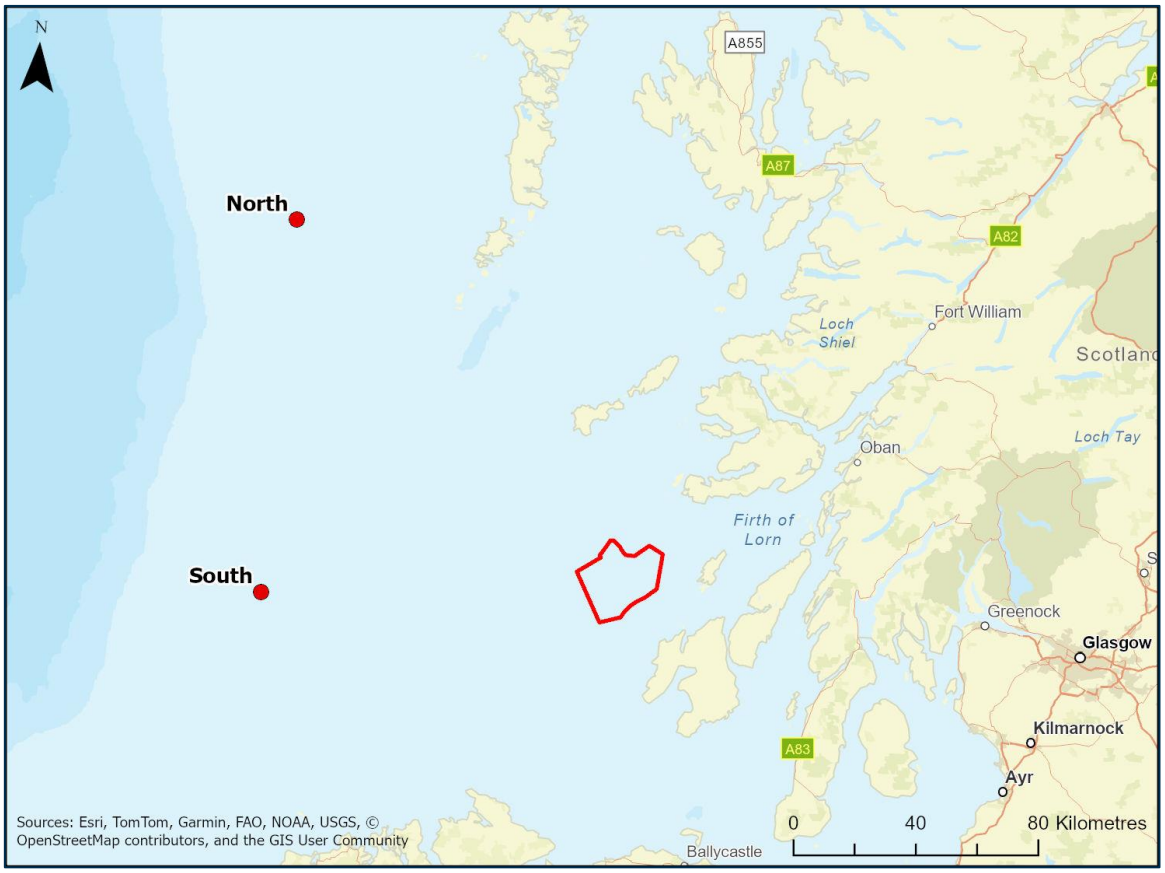

Figure 3-8: MetOffice data points for offshore EVA (red line indicates the proposed WDA)

3.7.3 The extreme analysis of the wave climate was carried out using an in-house MATLAB tool developed by Haskoning, utilizing the Peak Over Threshold (POT) method. The tool is based on the Wave Analysis for Fatigue and Oceanography (WAFO), a third generation of MATLAB routines for handling statistical modelling, calculation of random waves and wave characteristics and their statistical distributions developed by Lund University (**Ref 8**).

3.7.4 Of the four distribution types available within the tool (Generalized Extreme Value (GEV), Generalized Pareto Distribution (GPD), Weibull and Gumbel), the Weibull distribution provided the best fit to the data for all directional sectors in the analysis. Where the 'best fit' was determined through a combination of visual comparison of graphical outputs, assessment of parameter stability plots, magnitude of computed error and width of 95% confidence intervals, where a large range in 95% confidence intervals typically indicates a greater degree of uncertainty in the predicted value.

3.7.5 For each directional sector (240°N, 270°N, 300°N and 330°N) and return period (1 in 1 year, 1 in 50 year and 1 in 100 year) the extreme wave analysis was undertaken to derive extreme offshore wave conditions to force the MIKE21-SW model.

Hs / Tp / Wind Speed Relationship

3.7.6 For each extreme wave height, a corresponding Tp was determined through a wave steepness relationship on the highest 3 waves for each dataset (directional sector and return period).

3.7.7 Similarly, a corresponding wind speed was determined through fitting a linear relationship between ERA5 wind speed data and Hs. The 95th percentile wave height was used as a threshold for deriving the linear relationship, to ensure low waves did not skew the linear trendline.

3.7.8 This was repeated at both the south and north offshore points used for the extreme wave climate data. This 'corresponding' wind speed is used to transform extreme waves under average wind conditions and provide no additional growth or introduce decay of extreme waves as they propagate from the model boundary to the WDA. The wind speed relationships at the south and north point are presented in **Figure 3-9** and **Figure 3-10**, respectively.

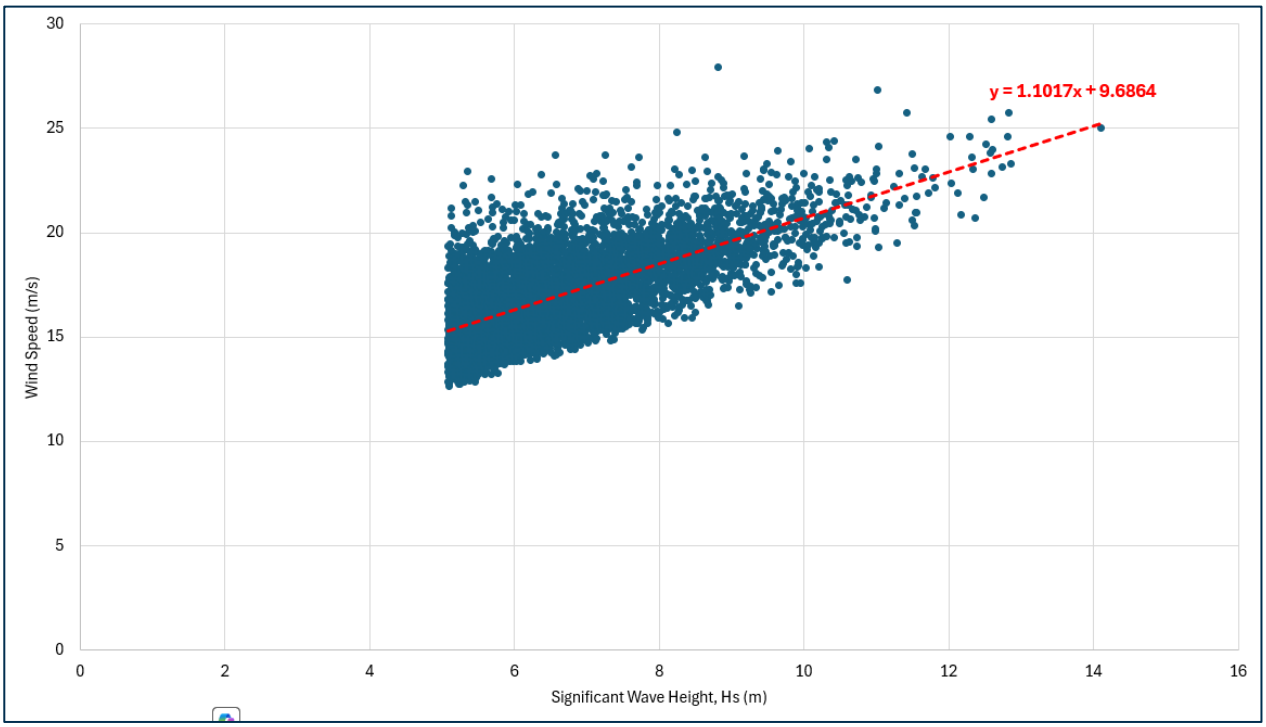

Figure 3-9: Hs / wind speed relationship derived for south point

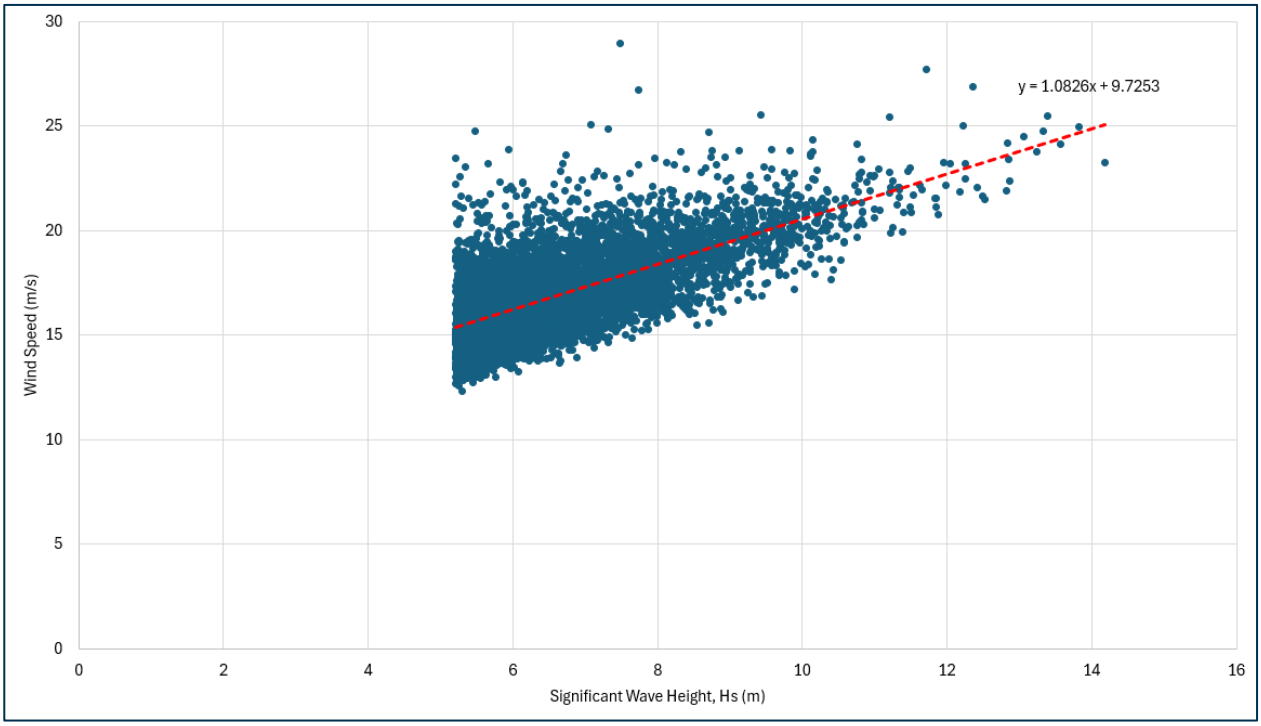

Figure 3-10: Hs / wind speed relationship derived for north point

Validation of MetOffice Hindcast Data

3.7.9 To ensure that the MetOffice hindcast wave data, which forms the basis of the extreme value analysis, is not under or over estimating the wave model boundary conditions for the production

simulations of extreme wave climate, a validation of the data (map shown in **Figure 3-11**) is presented in **Figure 3-12**.

3.7.10 The validation compares MetOffice hindcast wave model data against measured wave data at the location of the M4 wave buoy. The location of this wave buoy is greater than 110m which is of similar depth to the 'North' (112m) and 'South' (125m) locations used for the extreme values analysis of MetOffice data.

3.7.11 The scatter plot which compares the MetOffice modelled and measured data at 3 hourly intervals between 2006 – 2024 (no data between 2011 and 2018), along with associated error statistics.

3.7.12 The scatter plot suggests that for all magnitude of wave heights, the MetOffice hindcast model predicts the wave height reasonably well compared to measured data at M4. It can be concluded from this comparison that at the extremes, which are the focus of this study, there is no clear bias between modelled and measured data, indicating that the model is not consistently over or under predicting the extremes.

3.7.13 It is also worth noting that the extreme wave heights derived in this study are to be used as a representative extreme climate to understand changes to waves due to the WDA and should not be used for design conditions for the structures.

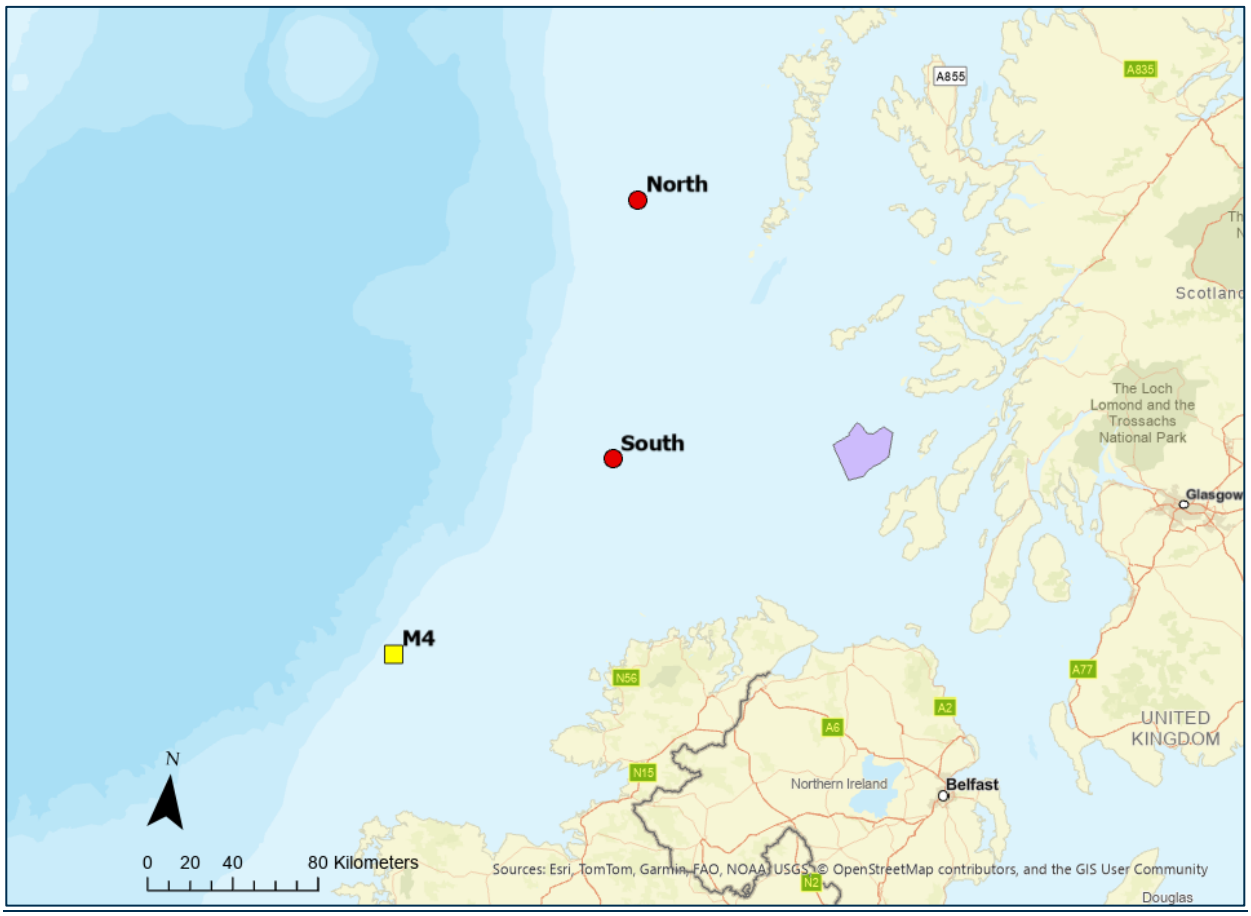

Figure 3-11: Location of MetOffice boundary conditions, M4 wave buoy and project boundary

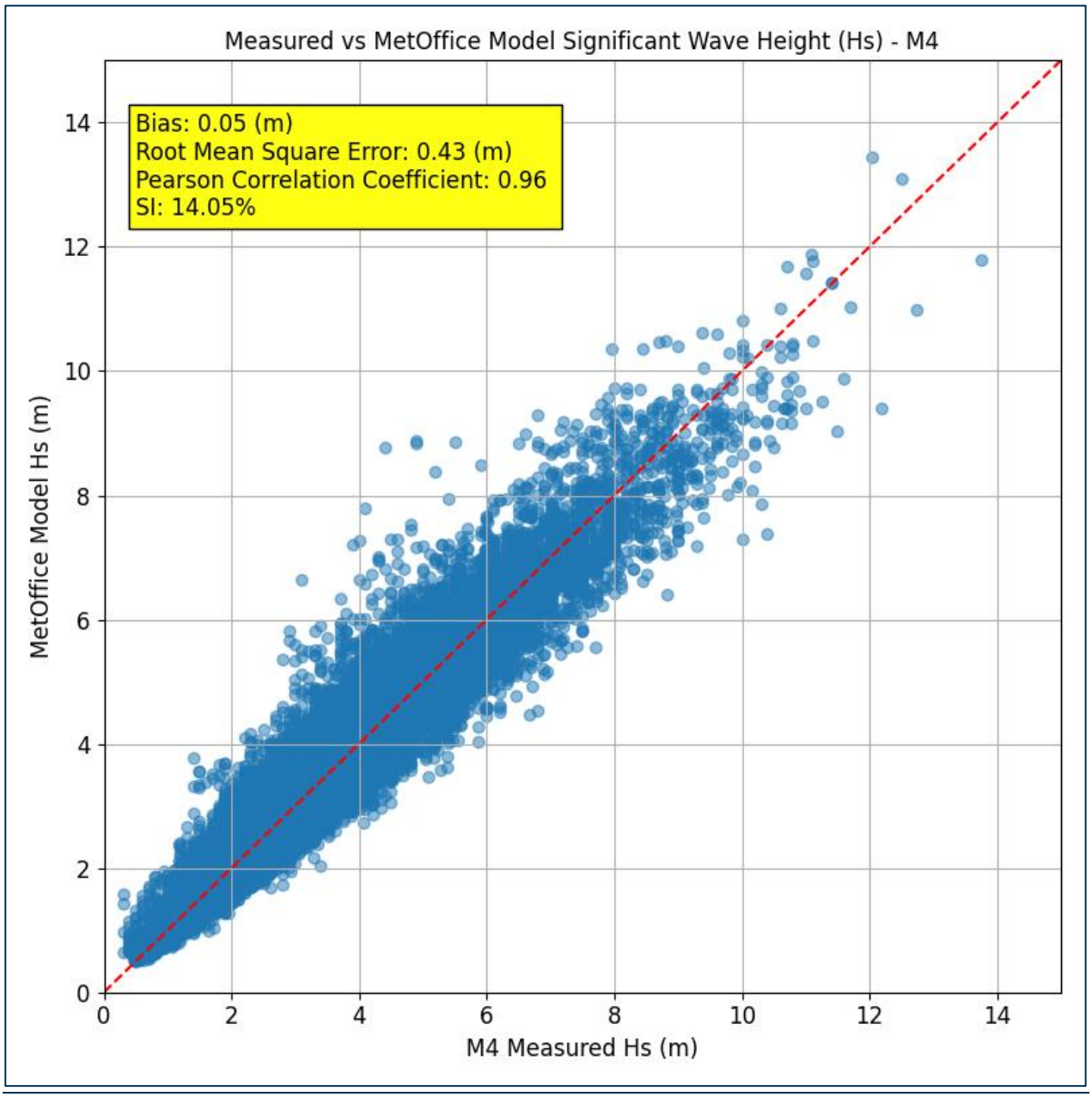

Figure 3-12: Scatter plot and error statistics comparing MetOffice hindcast wave height with M4 measured wave height (2006 – 2024)

Results

3.7.14 The results of the extreme wave analysis of the offshore hindcast wave climate are presented in **Table 3-5**. The table presents the derived extreme wave height for 3 return periods (1 in 1 year, 1 in 50 year and 1 in 100 year) and 4 directional sectors (240°N (225°N to 255°N), 270°N (255°N to 285°N), 300°N (285°N to 315°N) and 330°N (315°N to 345°N)). Along with this, the corresponding Tp and wind speed are also presented.

3.7.15 These results provide boundary conditions for the model simulations to derive an extreme wave climate at the WDA.

3.7.16 The extreme Weibull distributions for each directional sector are presented in **Figure 3-13 - Figure 3-16**.

Table 3-5: Extreme wave analysis results

Directional Sector (°N)	Parameter	Return Period (Year)		
		1	50	100
240	Hs (m)	8.83	13.17	13.93
	Tp (s)	13.29	16.23	16.69
	Wind Speed (m/s)	19.41	24.20	25.03
270	Hs (m)	9.91	14.01	14.69
	Tp (s)	14.99	17.82	18.25
	Wind Speed (m/s)	20.60	25.12	25.87
300	Hs (m)	8.42	12.45	13.09
	Tp (s)	13.67	16.63	17.05
	Wind Speed (m/s)	18.84	23.20	23.90
330	Hs (m)	6.58	10.85	11.58
	Tp (s)	11.45	14.70	15.19
	Wind Speed (m/s)	16.85	21.47	22.26

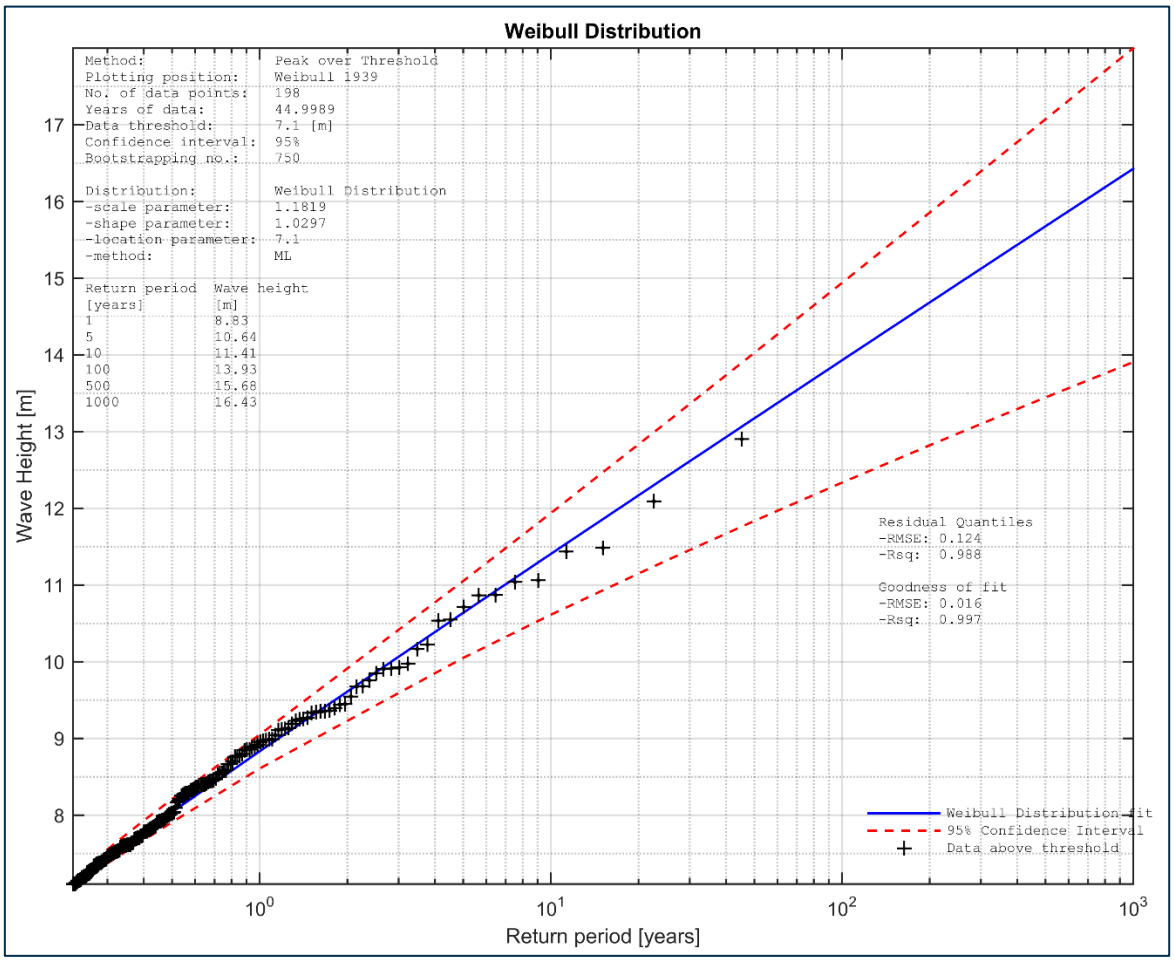

Figure 3-13: Extreme Weibull distribution for 240°N directional sector (south point)

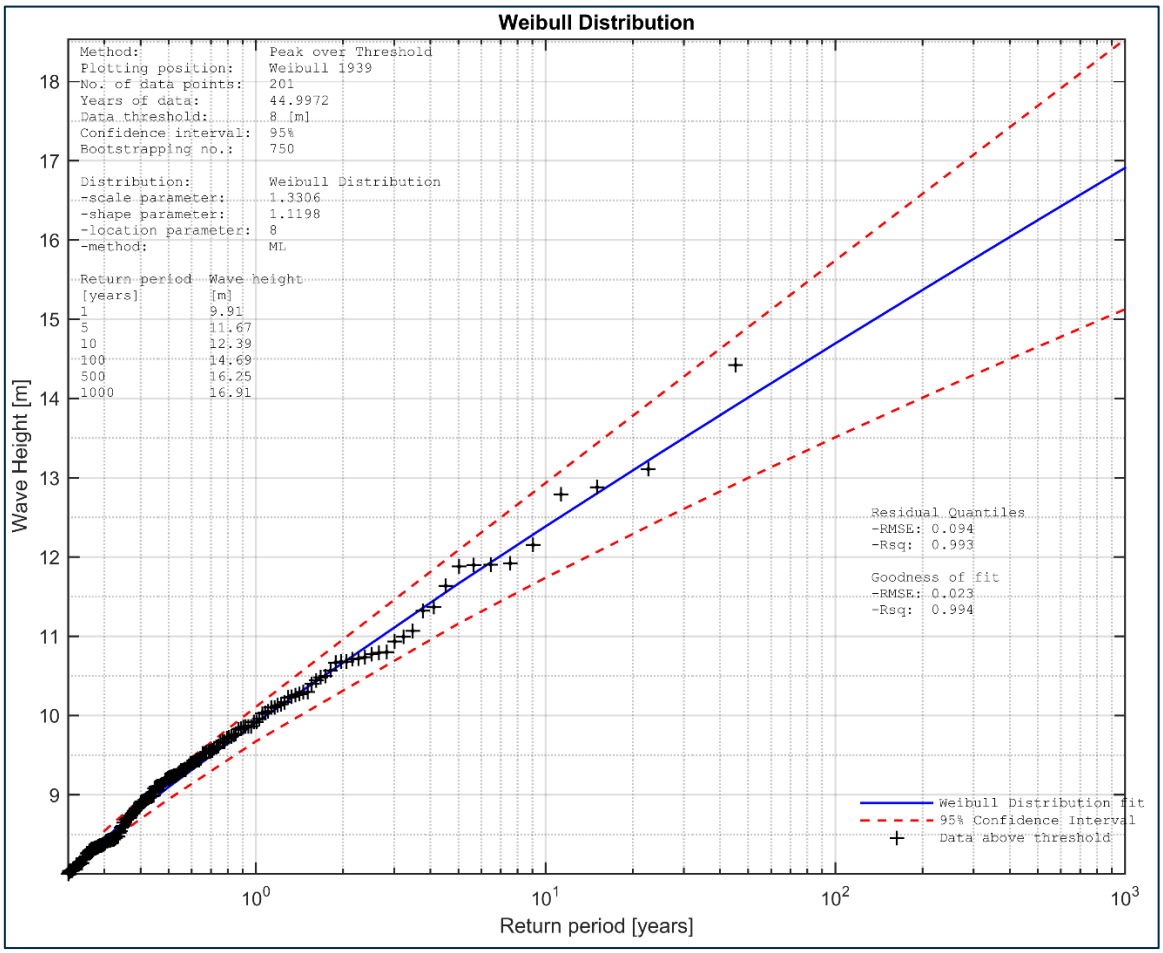

Figure 3-14: Extreme Weibull distribution for 270°N directional sector (south point)

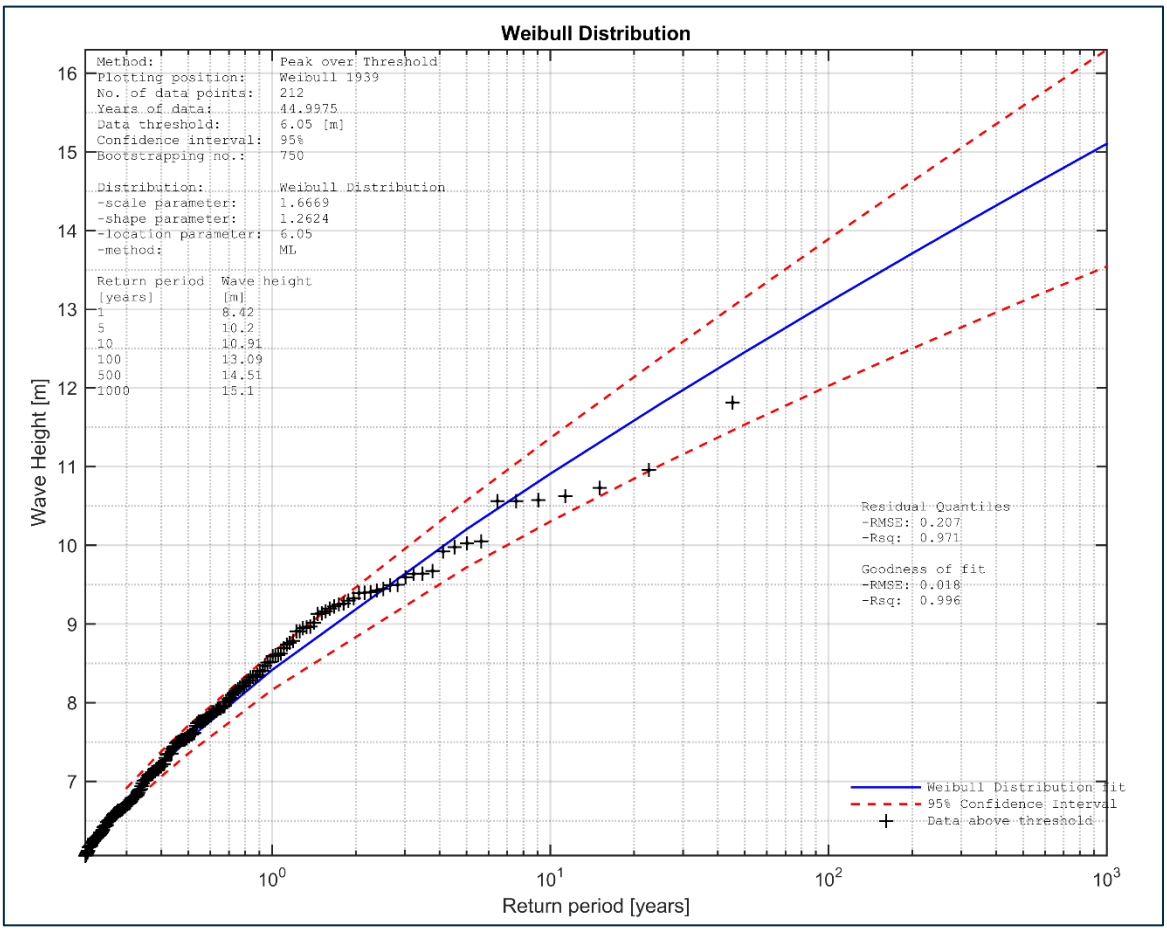

Figure 3-15: Extreme Weibull distribution for 300°N directional sector (north point)

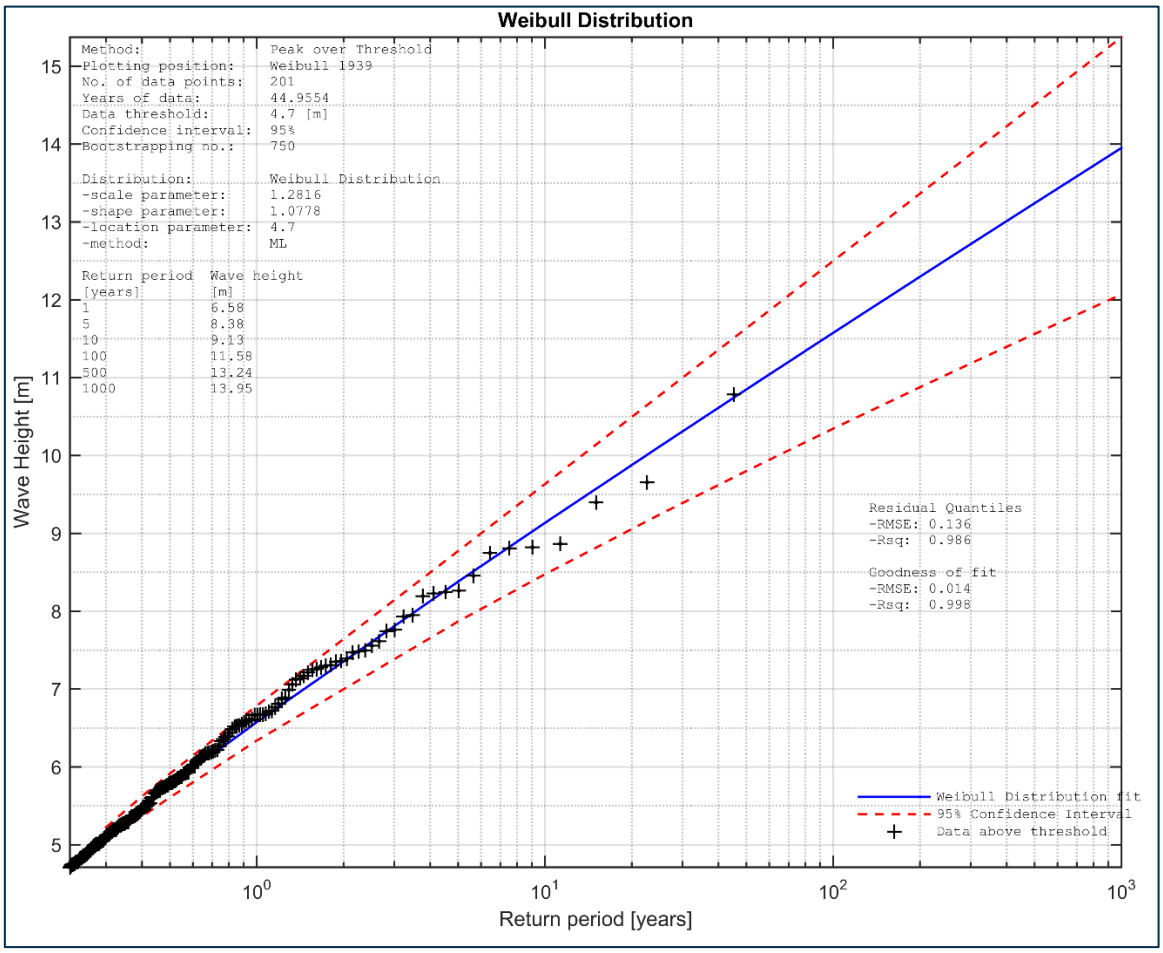

Figure 3-16: Extreme Weibull distribution for 330°N directional sector (north point)

MetOffice Data Verification

3.7.17 As a verification of the hindcast MetOffice data used as input to the extreme value analysis, a comparison of measured Hs at S1 was made with MetOffice hindcast Hs extracted at the same location. This comparison is presented for August 2023 to December 2023 (**Figure 3-17**) and December 2023 to February 2024 (**Figure 3-18**).

3.7.18 The comparison shows that the MetOffice model performs well at re-creating the measured wave heights during storm events, therefore, is deemed suitable to be used for the extreme values analysis and any adjustment on the derived extreme values is not required.

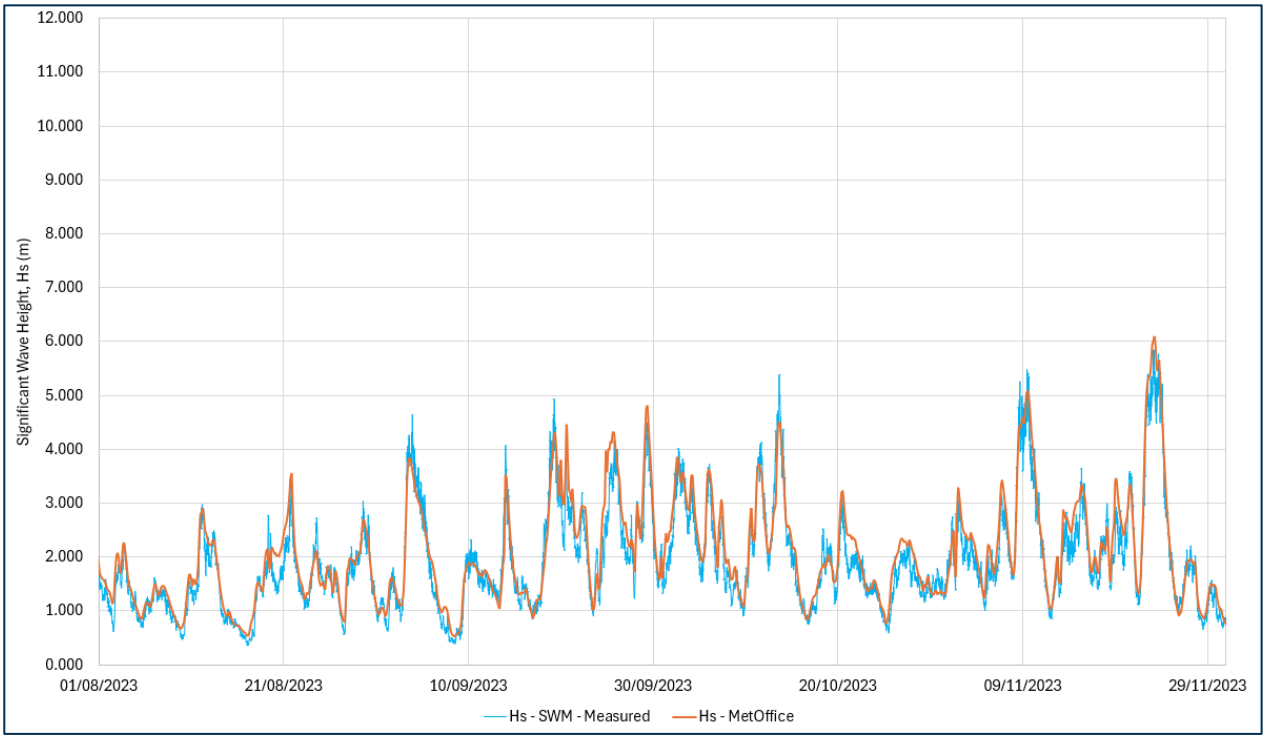

Figure 3-17: Comparison between measured and modelled (MetOffice hindcast) Hs at S1 – August 2023 to December 2023

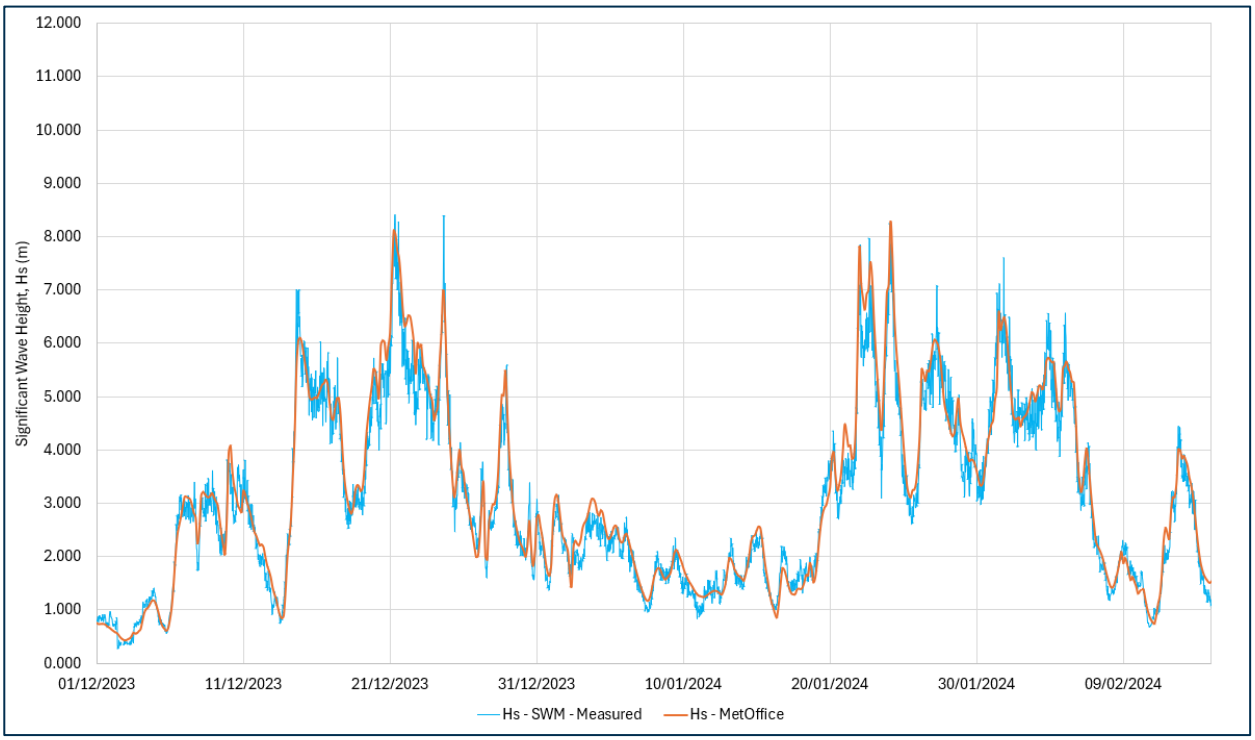

Figure 3-18: Comparison between measured and modelled (MetOffice hindcast) Hs at S1 – December 2023 to February 2024

4 Wave Modelling

4.1 Model Development

Domain and Mesh

4.1.1 The model domain and computational mesh are presented in **Figure 4-1** and **Figure 4-2**, for the calibration and assessment simulations, respectively. Due to the computational demand required to simulate the MIKE21-SW model for the full 1-year survey period, a coarser computational mesh was used for the model calibration process, then refined around the WDA for the production simulations around the WDA and coastal regions.

4.1.2 The computational mesh size for the calibration model varied between 3 kilometres (km) at the offshore boundaries and 1 km close to the survey locations. In contrast to this, for the assessment simulations the size varied between 2 km at the offshore boundaries, 500 m to 300 m in coastal regions and 50 m at the WDA.

4.1.3 In the model calibration, it was found that the resolution of the mesh was demonstrated to have little effect on simulated wave heights at the survey locations (**Section 4.2**). However, the higher resolution of mesh was applied for accurately resolving the effect of the WDA structures on the wave climate. The resolution of the computational mesh through the WDA is presented in **Figure 4-2**, along with the WDA boundary, WTG's and OSP's indicative locations.

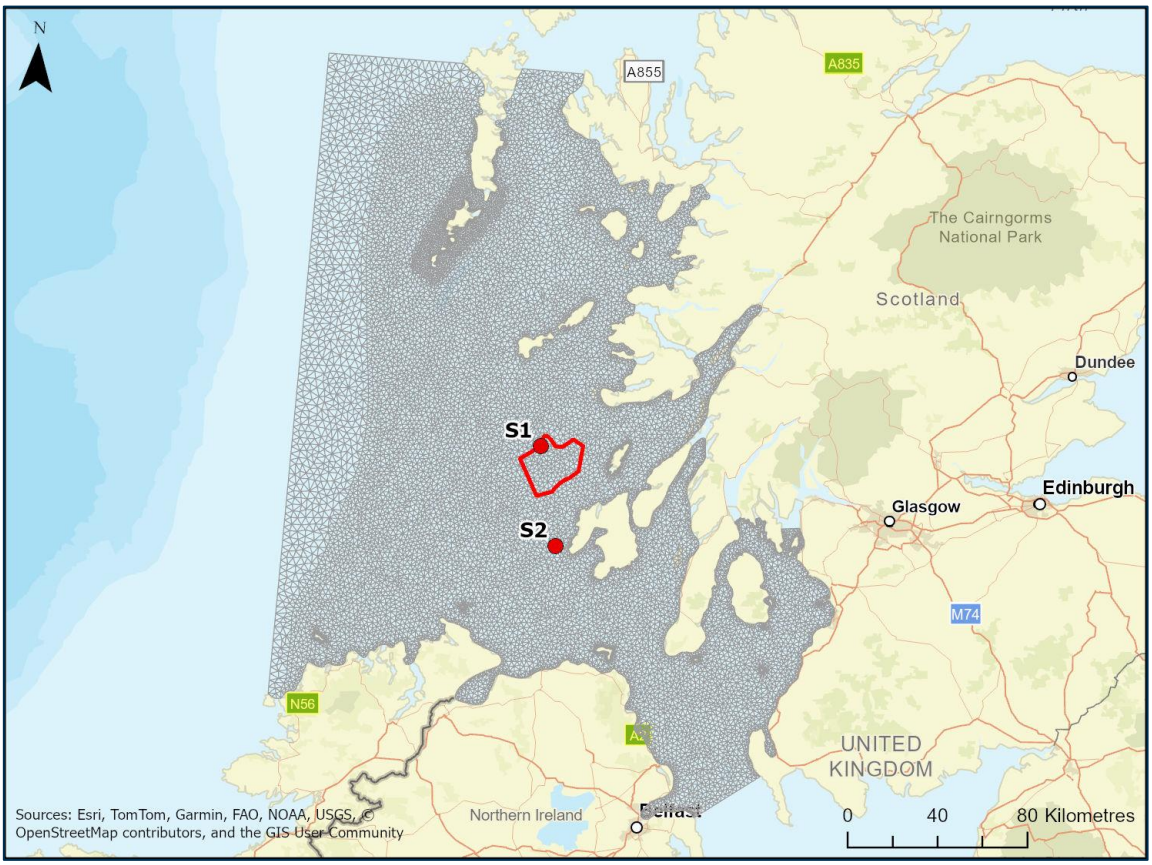

Figure 4-1: MIK21-SW computational mesh for model calibration (red line indicates the proposed WDA)

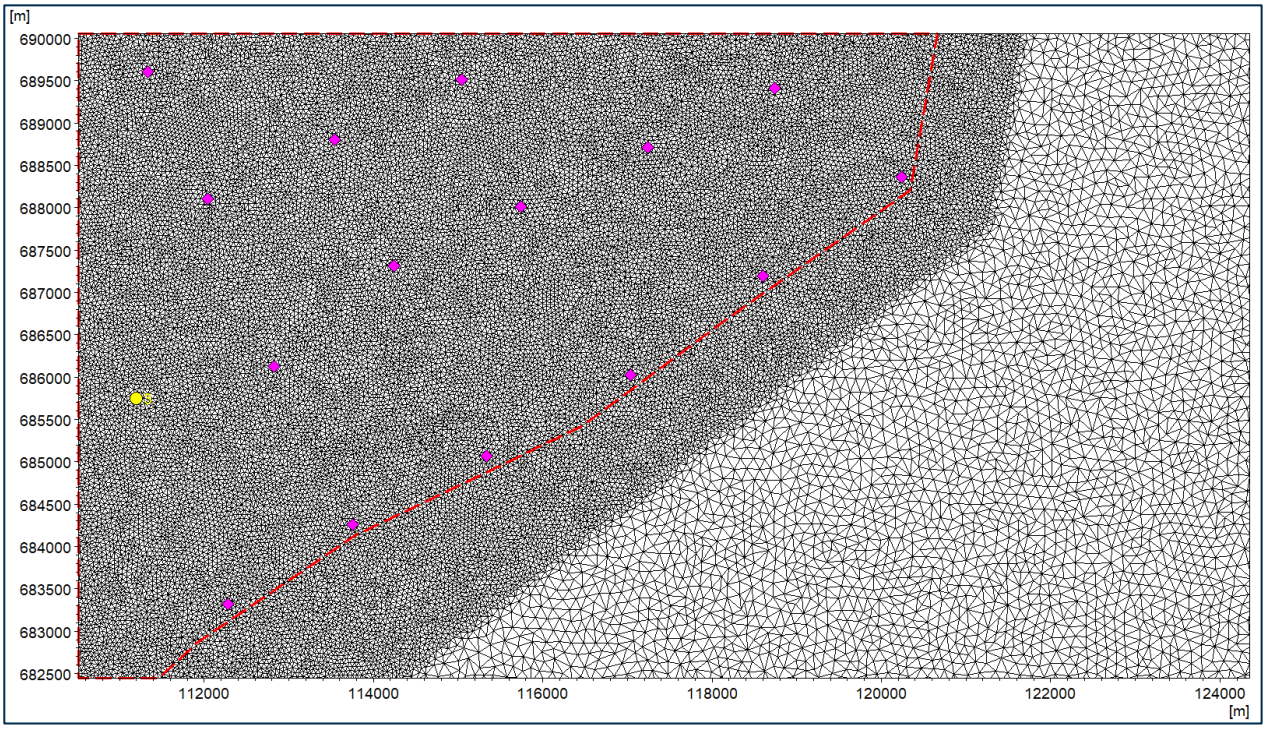

Figure 4-2: Detailed computational mesh around WDA (red dash line indicates the outline) for the assessment simulations

4.2 Model Calibration and Validation

4.2.1 The calibration of the MIKE21-SW model consisted of a 1 year simulation covering the full survey period from May 2023 to May 2024, where measured wave data was available at S1 and S2 project survey sites and compared with the predicted model outputs of sH, (m), Tp (s) and mean wave direction (MWD) (°N).

4.2.2 The first stage of model calibration was optimizing the accuracy of the boundary conditions. This included testing the wave model boundary conditions from the MetOffice hindcast model as spatially constant along each boundary or varying spatially. Besides this, the type of wind forcing data to be used, whether ERA5 or NORA3 would provide the optimal match between measured and modelled data. In addition to this, simulations with and without varying water level were undertaken, although due to water depth at both survey sites, varying water levels did not make a difference.

4.2.3 The optimal model boundary conditions as a result of the model calibration process were found to be wave conditions from MetOffice UK hindcast model as varying along the boundary at 5 km resolution, wind forcing from the ERA5 global atmospheric hindcast model and wave spectral width varying along the boundary at approximately 25 km resolution from the ERA5 global wave hindcast model.

4.2.4 The second stage of model calibration focused on a range of model settings which primarily affected wave growth due to wind interaction with the sea surface, transformation of the wave spectra between the boundary and WDA and energy dissipation of waves. Water depths of 40 m at S1 and S2 meant it was not necessary to investigate the effects of bottom friction or wave breaking parameters in the model settings, as these would have no influence on model results.

Model Settings

4.2.5 The model settings explored for each of the above processes are summarised below:

- Transformation of wave spectra:
  - Spectral formulation (directional decoupled or fully spectral);
  - Time formulation (quasi stationary or instationary); and
  - Directional discretisation.
- Wave growth due to wind:
  - Air-sea interaction (growth parameter, type, charnock parameter).
- Wave energy dissipation:
  - White capping parameters (Cdis and Ddis).

4.2.6 The model settings for the final calibration run are presented below in **Table 4-1**, along with the varying of each model parameter which was investigated during the calibration process.

Table 4-1: MIKE21-SW model settings used for assessment simulations

Model Setting	Selected Value
Spectral formulation	Fully spectral (directionally decoupled)
Time formulation	Instationary (quasi stationary)
Directional discretisation	36 (16 – 60)
Air-sea interaction	Growth parameter: 1.2 (1.0 – 1.3) Type: coupled (uncoupled) Charnock parameter: 0.006 (0.03)

Model Setting	Selected Value
White capping	Cdis: 1.33 (1.15 – 1.6) Ddis: 0.5 (0.3 – 0.7
Diffraction	No diffraction
Bottom friction	Nikuradse: 0.005m
Wave Breaking	Gamma: 0.8

Quantifying Model Error / Uncertainty

4.2.7 Error and uncertainty in the performance of the MIKE21-SW model is assessed using a variety of statistical parameters, comparing the modelled and measured Hs (m). These are based on recent guidance from the Environment Agency (EA) in 2022 (**Ref 7**).

4.2.8 The parameters used are model bias (m), root mean square error 'RMSE' (m), Pearson correlation coefficient and scatter index 'SI' (%). The guidance sets out requirements of RMSE and SI, which define a suitable performance for wave model calibration and validation, as follows:

A – Design: RMSE <= 0.3 m OR SI <20%
B – Appraisal: RMSE <= 0.4 m OR SI 20% to 25%
U – Unsatisfactory: RMSE > 0.5 m OR SI > 30%

4.2.9 The wave model calibration in this study sought after the best achievable model performance given the available data and project timeline, although as a guide, the application of the wave model to the Project is most closely aligned to 'Appraisal' therefore, the model calibration focused on meeting these requirements of model performance.

Calibration Results

4.2.10 The results of the wave model calibration between May 2023 and May 2024 at S1 and S2 project survey sites are presented in the following figures and tables, as time series, scatter plots and statistical error tables.

4.2.11 Timeseries plots comparing measured and modelled wave parameters (Hs, Tp and MWD) at S1 are presented in **Figure 4-3** to **Figure 4-8**, where the time period of 2 months is focused for each plot. Timeseries plots comparing measured and modelled wave parameters (Hs, Tp and MWD) at S2 are presented in **Figure 4-10** to **Figure 4-15**, where the time period of 2 months is focused for each plot.

4.2.12 Scatter plots comparing measured and modelled Hs at S1 and S2 are presented in **Figure 4-9** and **Figure 4-16**, respectively.

4.2.13 Error statistics (Bias, RMSE, correlation coefficient and SI) which quantify model performance in predicting Hs at S1 and S2 for the entire calibration period (May 2023 – May 2024) are presented in **Table 4-2**.

4.2.14 In general, at both sites the model is shown to perform very well in predicting Hs, Tp and mean wave direction throughout the calibration period. For some selected storm events (>6 m), the model is shown to slightly under and over predict Hs, yet, given this is not a consistent bias across all storms, this can be attributed to the quality of boundary conditions rather than the choice of model settings.

4.2.15 Comparing the computed model error statistics of Hs with those EA guidelines described above, it is clear that the performance of the MIKE21-SW model meets the 'Design' criteria of <20% for SI, with 14.27% and 14.92% at S1 and S2, respectively. And it is close to the 'Design' criteria of <=0.3 m for RMSE, with 0.31 m at S1 and S2. Given that the EA guidance requires one of the above statistical parameters to be met for adequate calibration (RMSE or SI), it can be concluded that the 'Design' standard for model calibration is achieved, and the model is suitable to be taken forward to simulate the wave climate at the WDA.

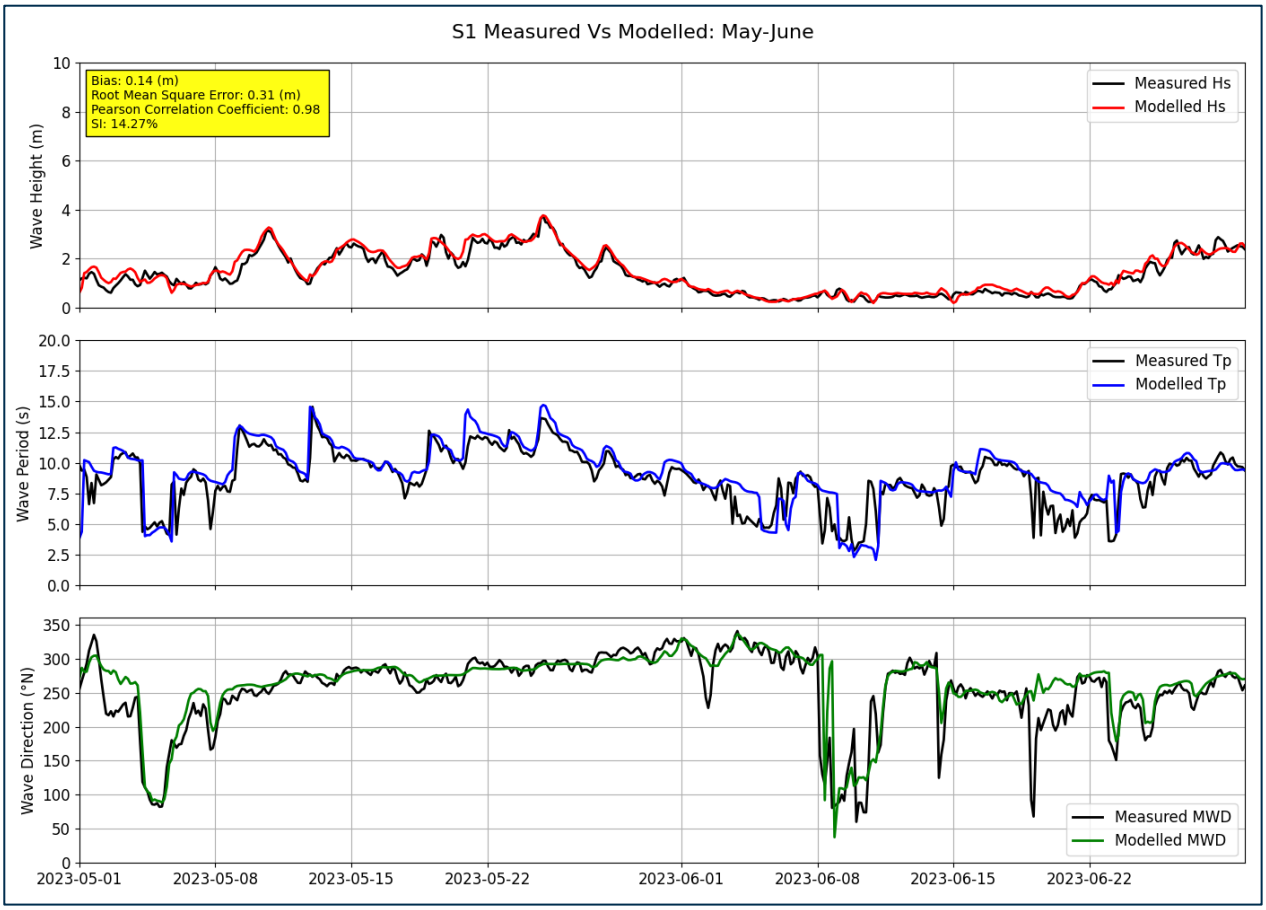

Figure 4-3: MIKE21-SW wave model calibration results at S1, May 2023 – June 2023

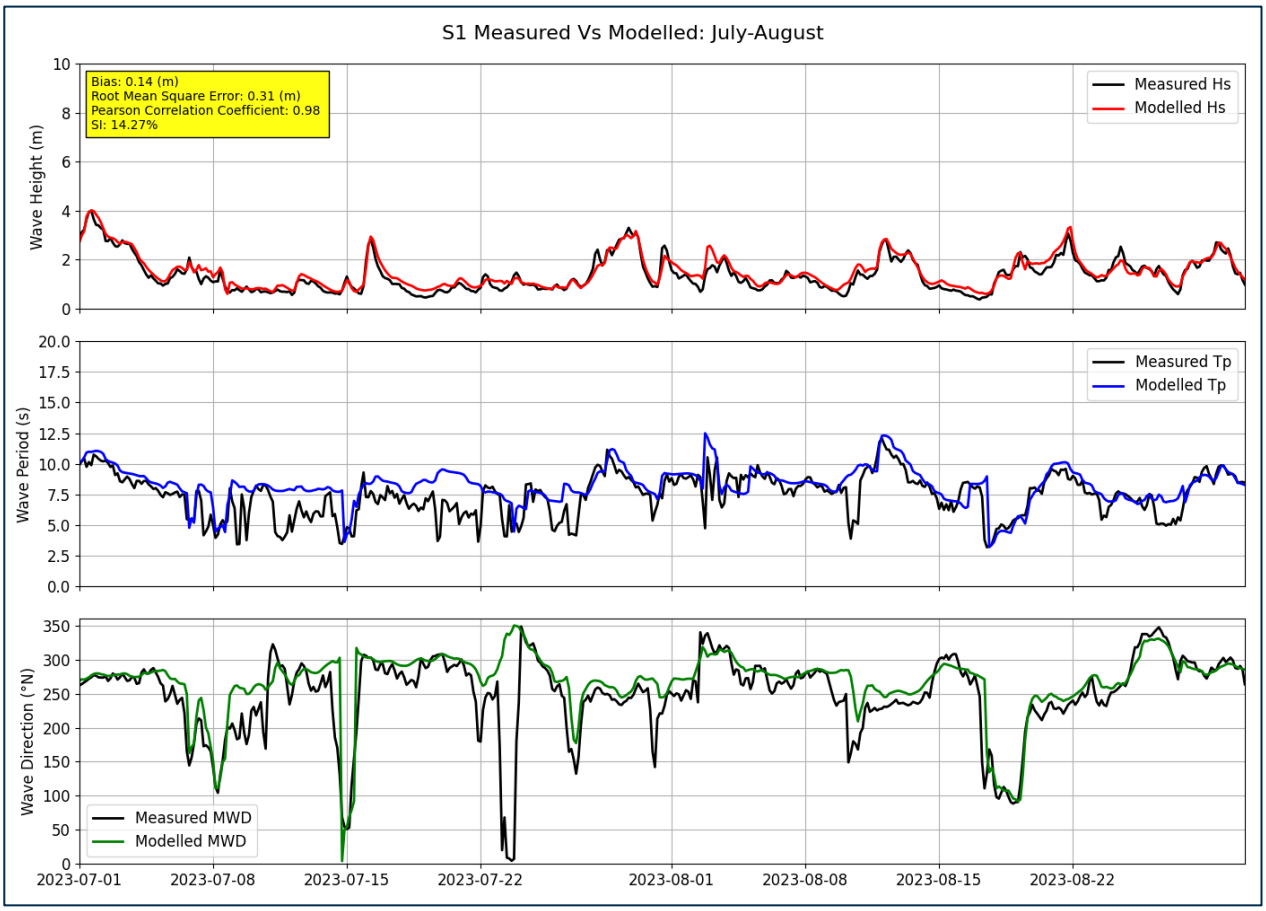

Figure 4-4: MIKE21-SW wave model calibration results at S1, July 2023 – August 2023

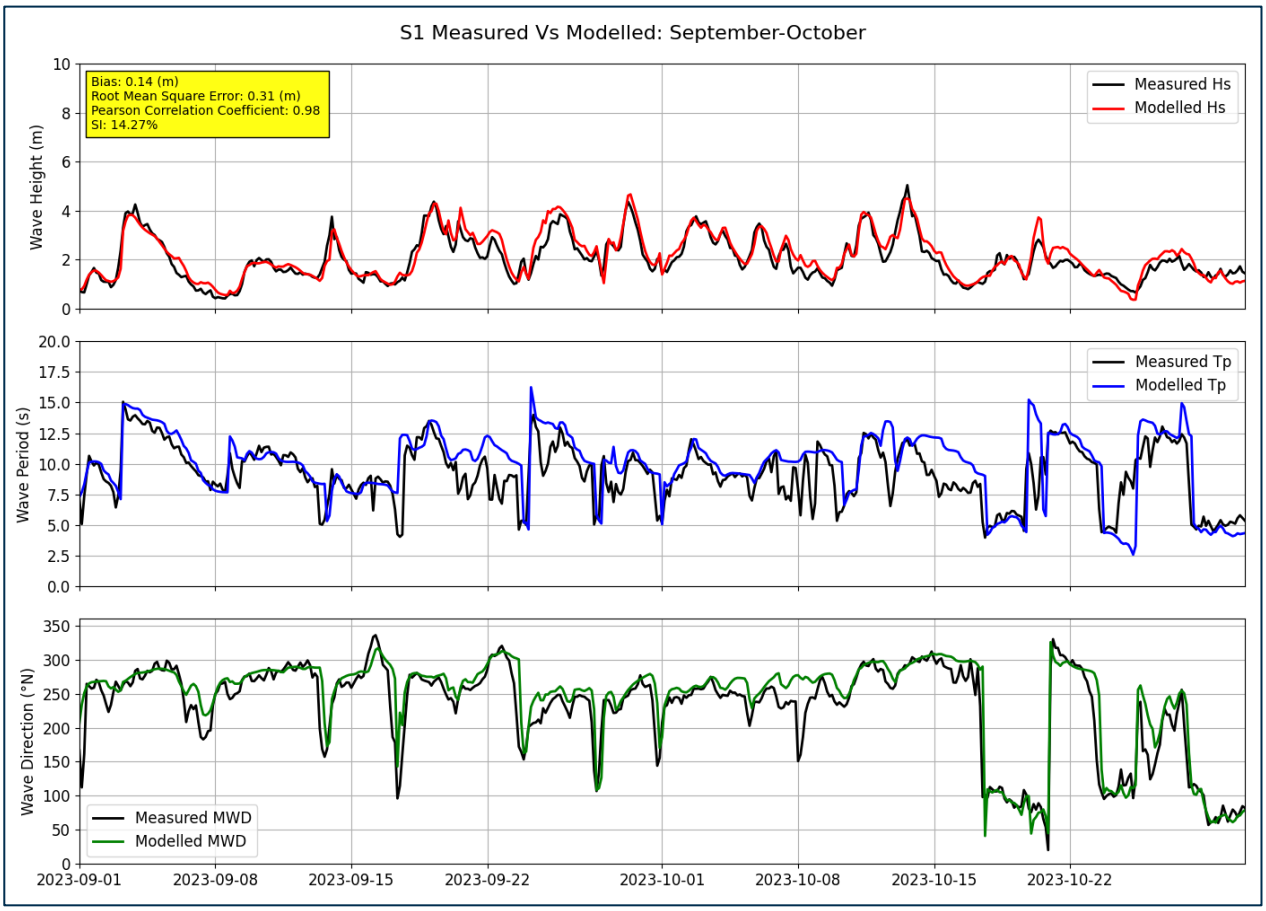

Figure 4-5: MIKE21-SW wave model calibration results at S1, September 2023 – October 2023

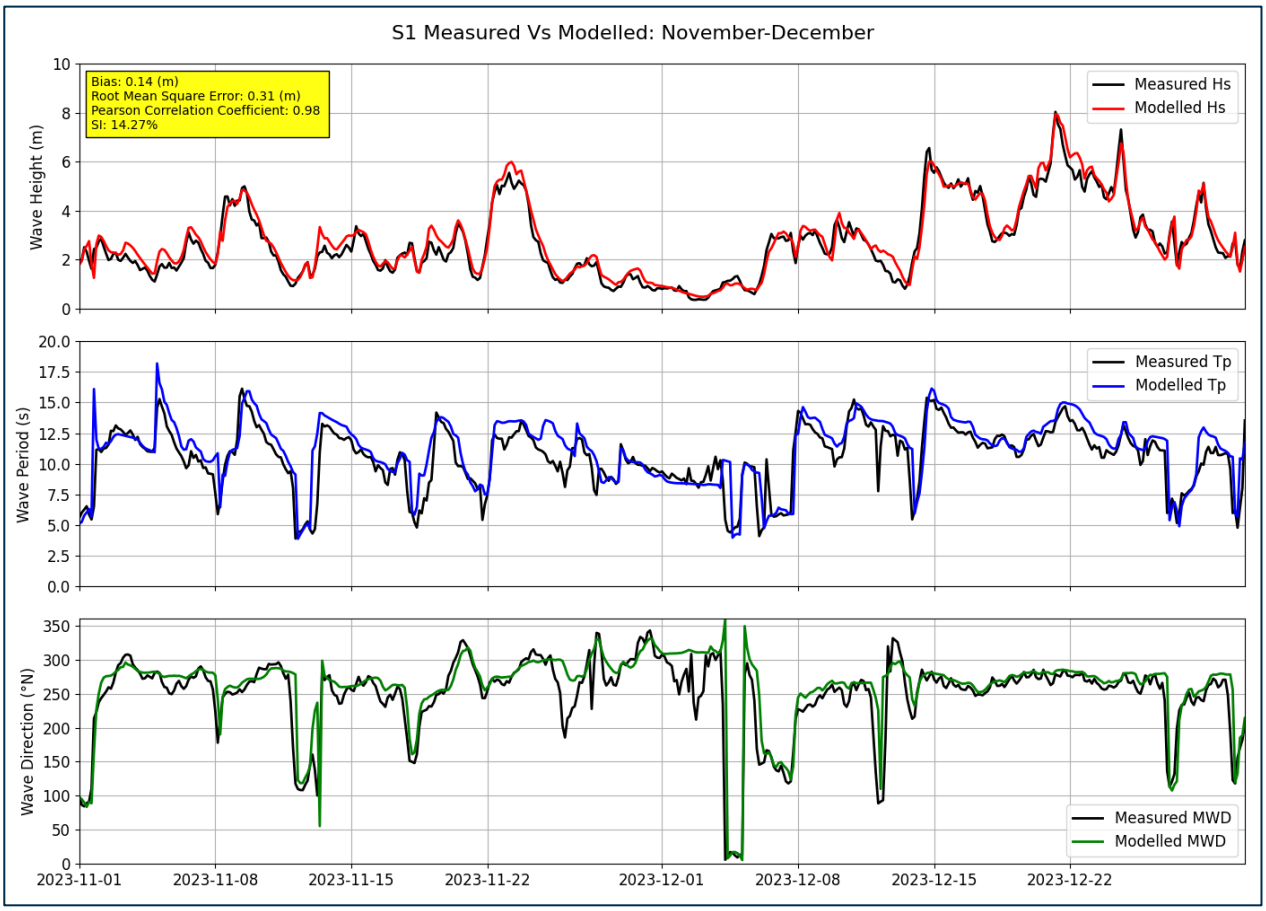

Figure 4-6: MIKE21-SW wave model calibration results at S1, November 2023 – December 2023

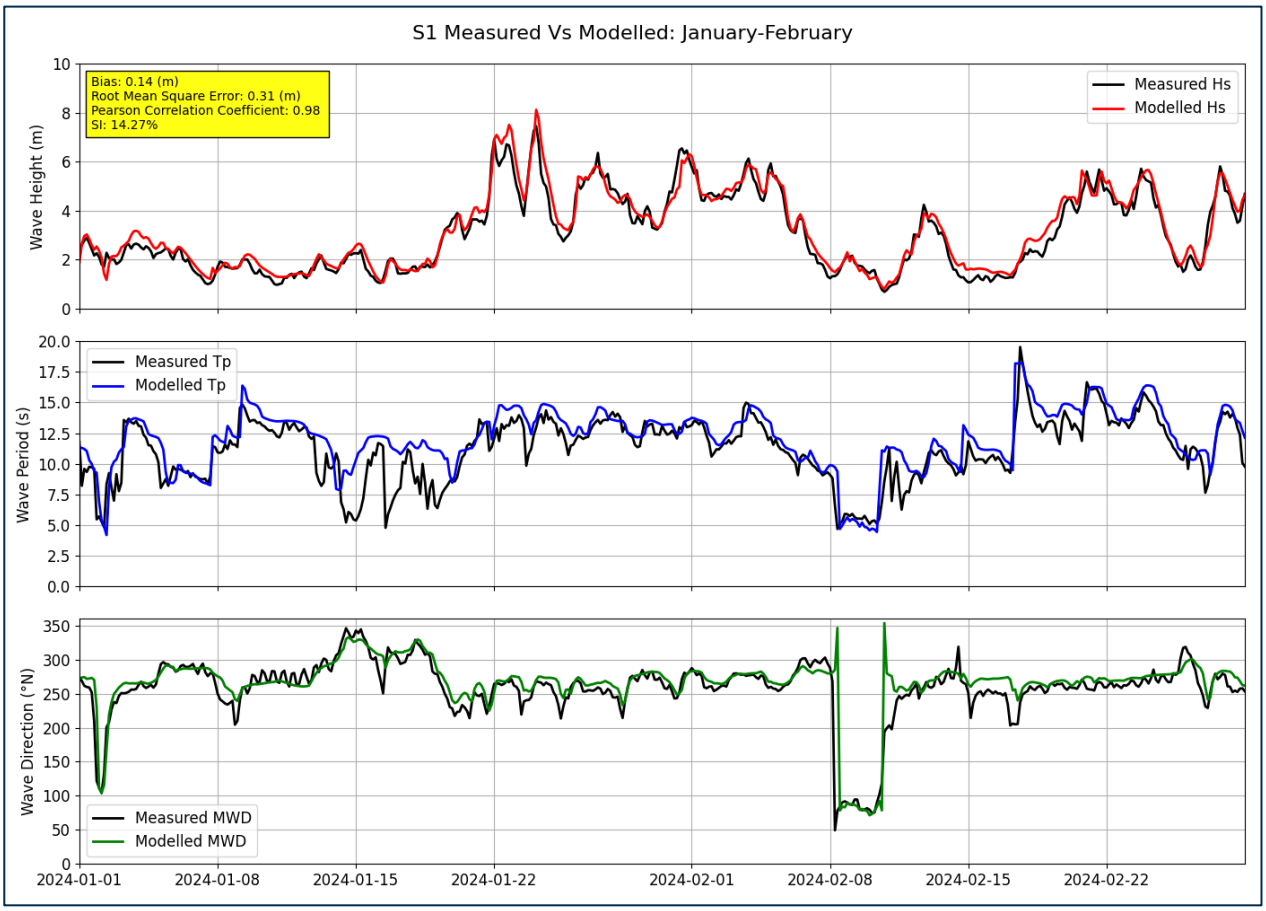

Figure 4-7: MIKE21-SW wave model calibration results at S1, January 2024 – February 2024

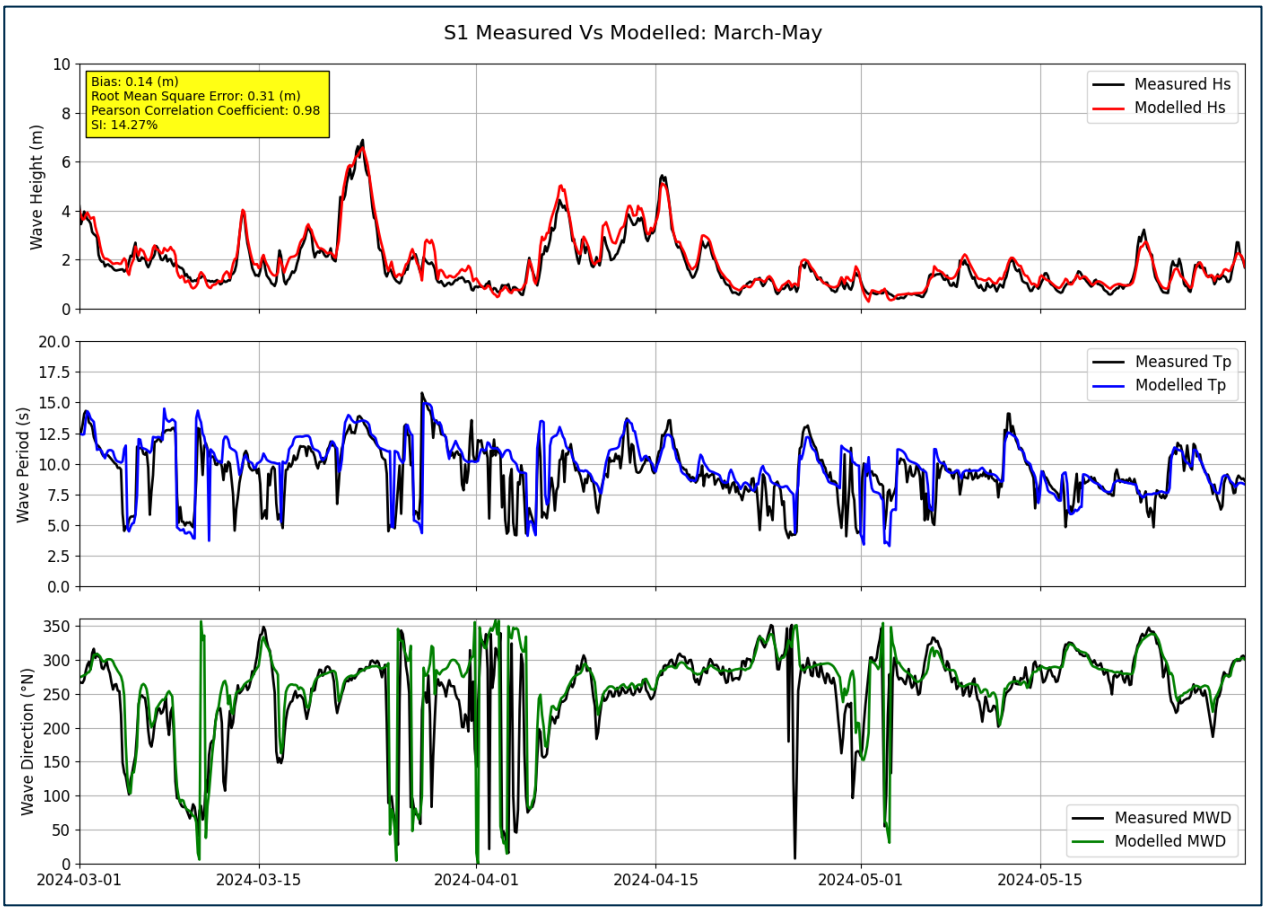

Figure 4-8: MIKE21-SW wave model calibration results at S1, March 2024 – May 2024

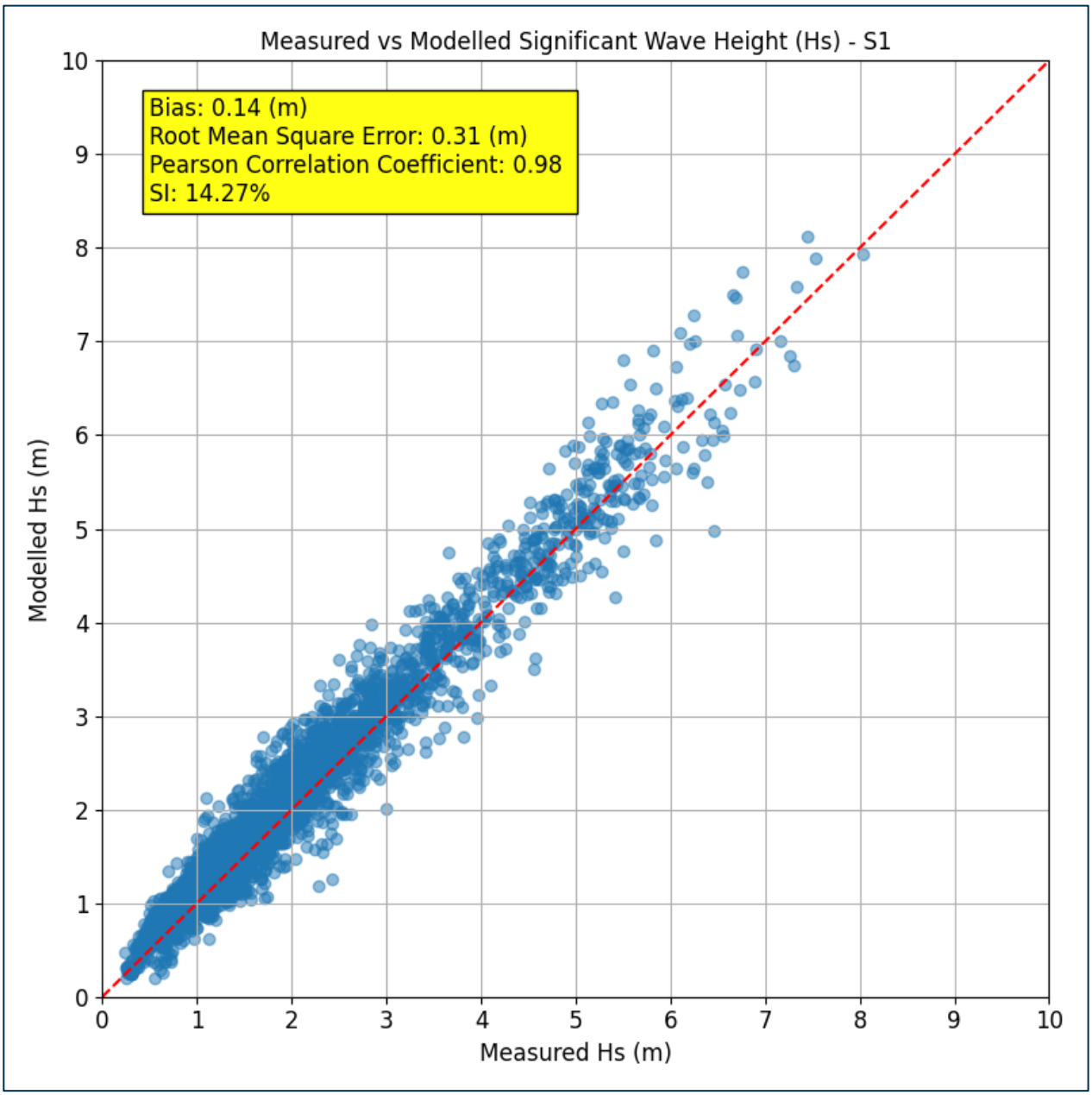

Figure 4-9: Measured Vs modelled Hs at S1, May 2023 – May 2024

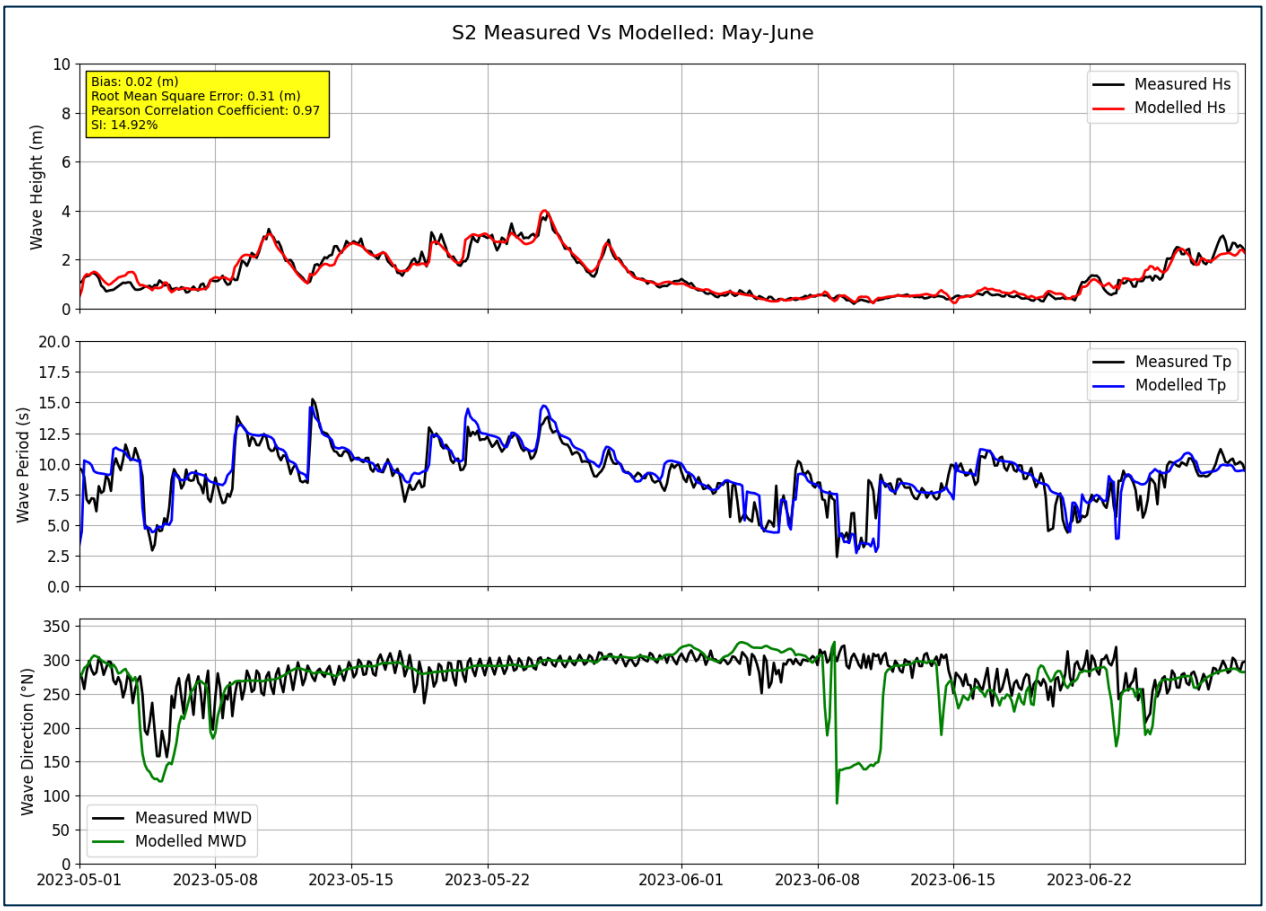

Figure 4-10: MIKE21-SW wave model calibration results at S2, May 2023 – June 2023

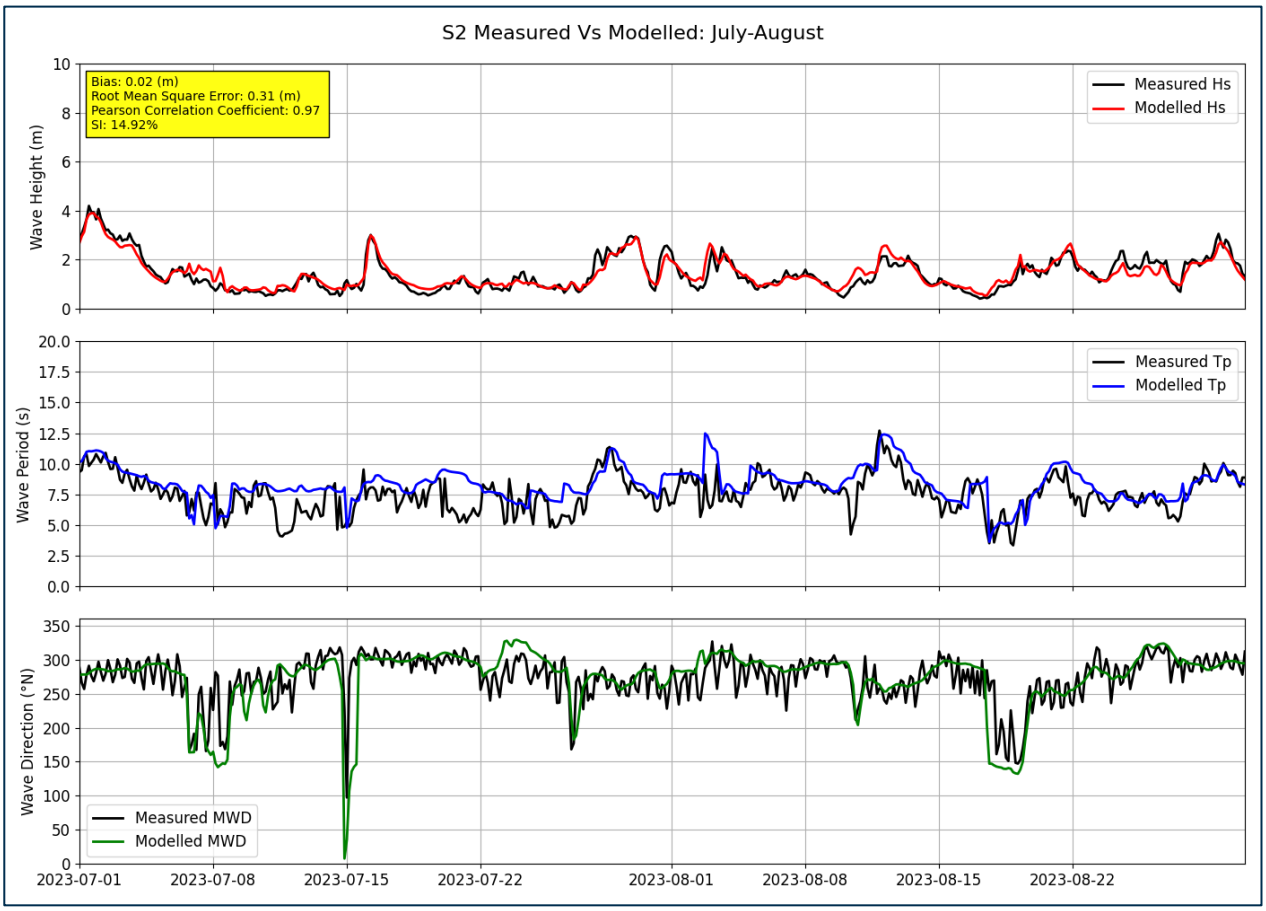

Figure 4-11: MIKE21-SW wave model calibration results at S2, July 2023 – August 2023

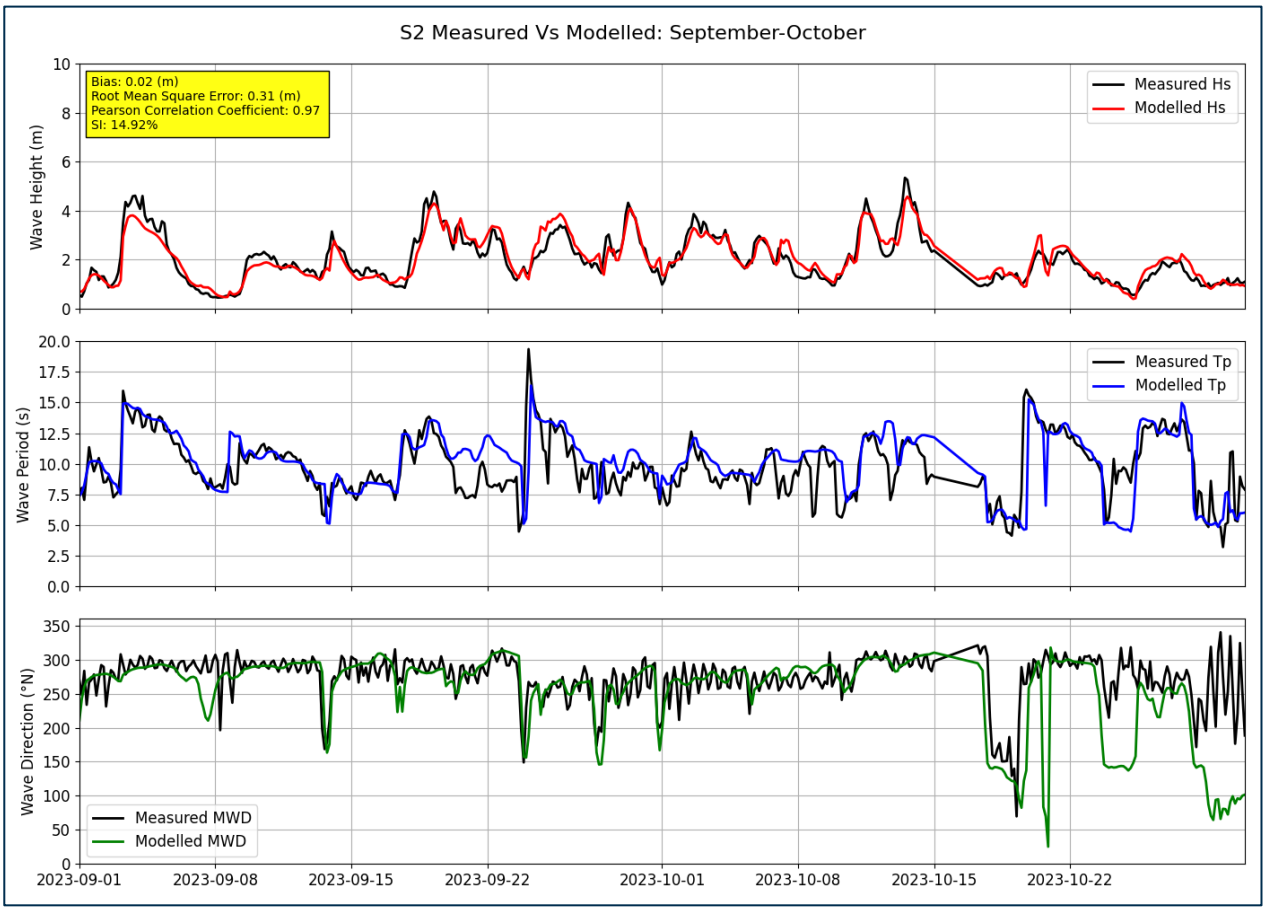

Figure 4-12: MIKE21-SW wave model calibration results at S2, September 2023 – October 2023

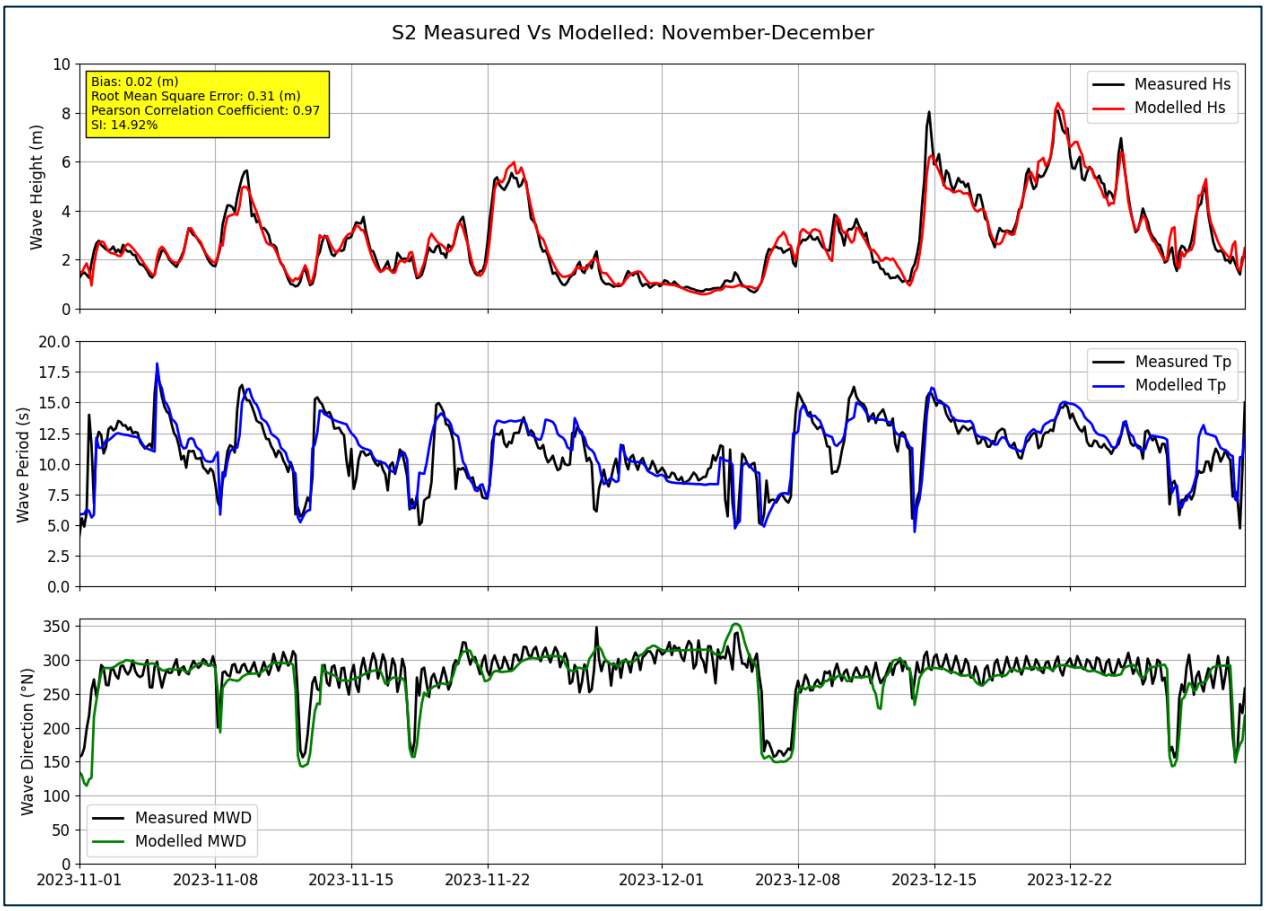

Figure 4-13: MIKE21-SW wave model calibration results at S2, November 2023 – December 2023

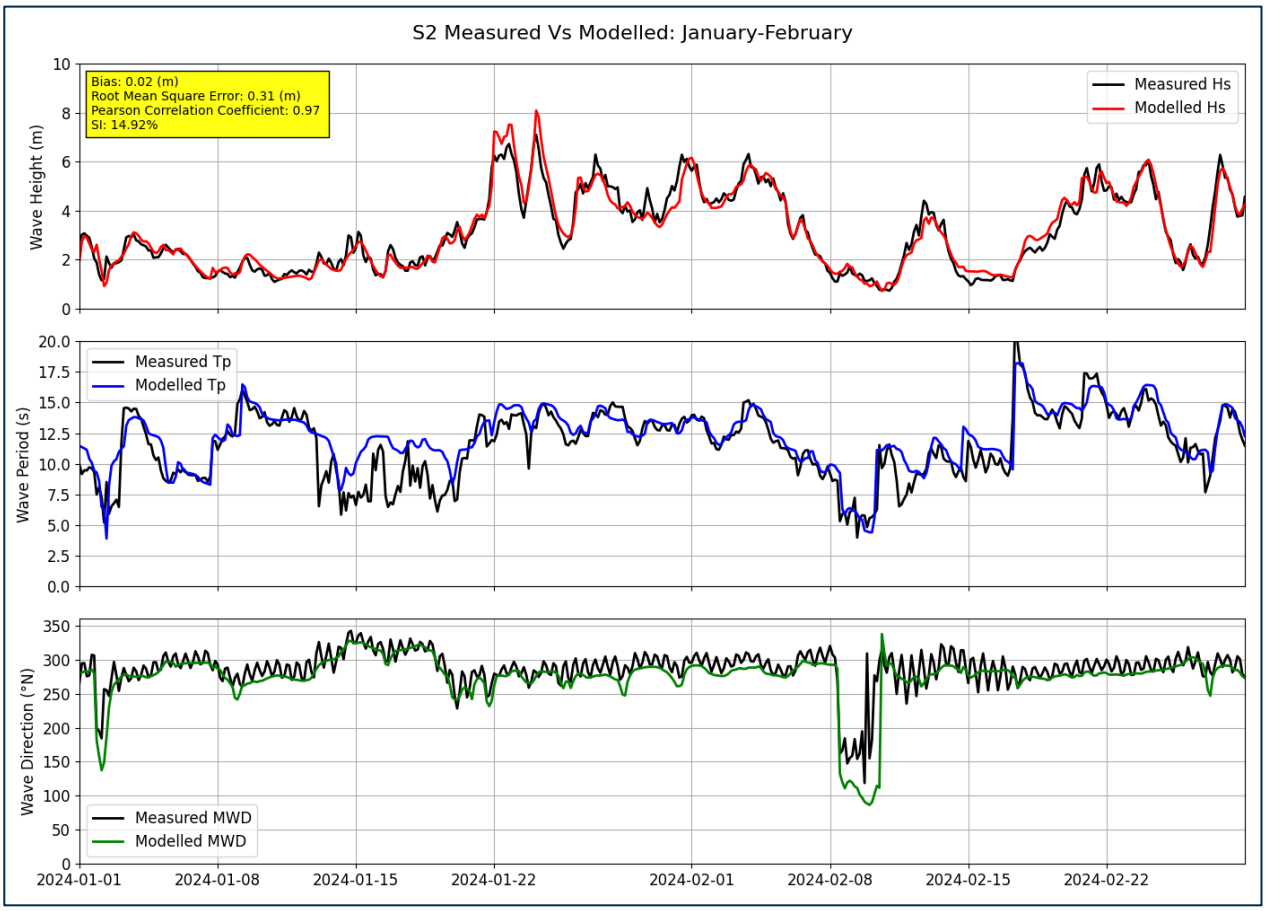

Figure 4-14: MIKE21-SW wave model calibration results at S2, January 2024 – February 2024

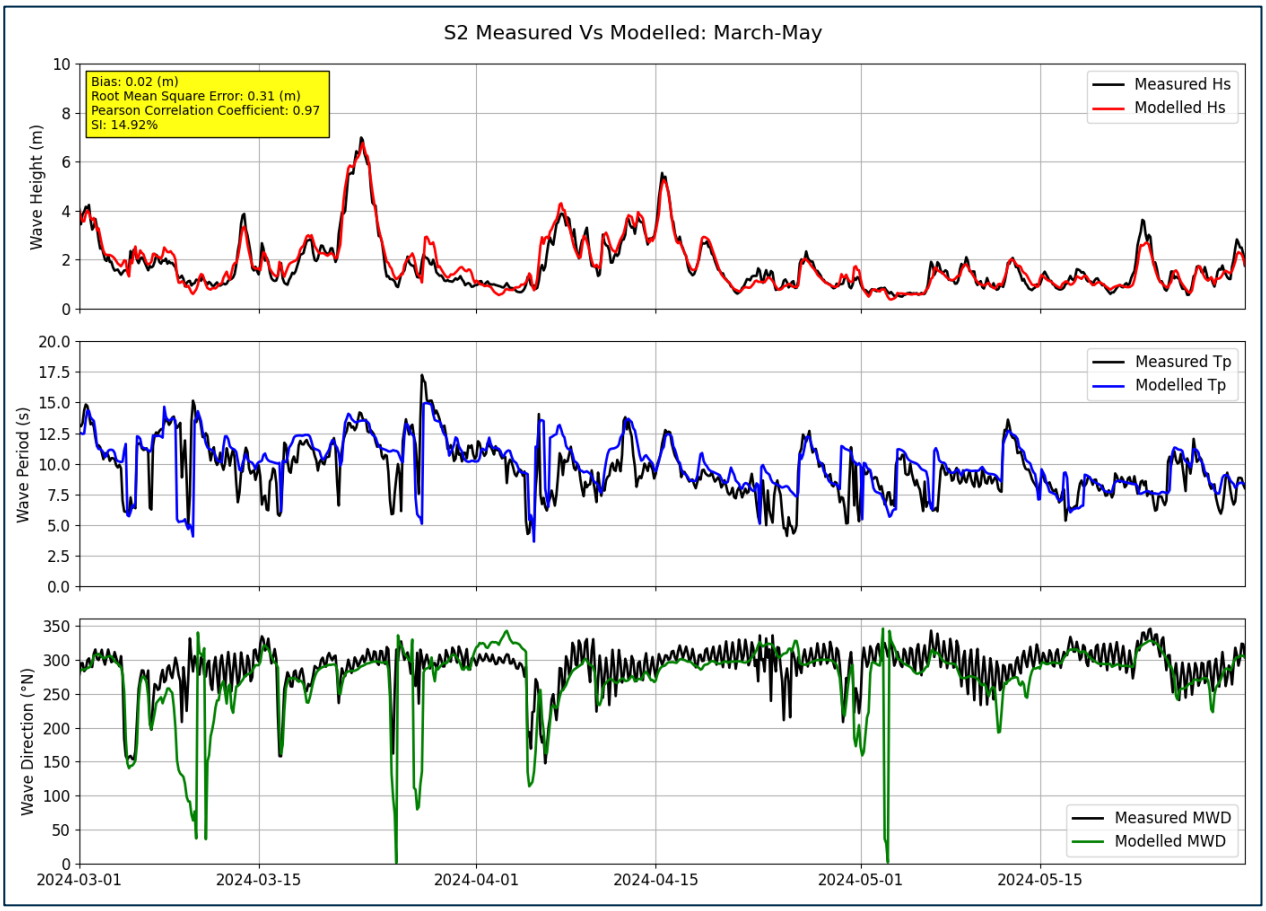

Figure 4-15: MIKE21-SW wave model calibration results at S2, March 2024 – May 2024

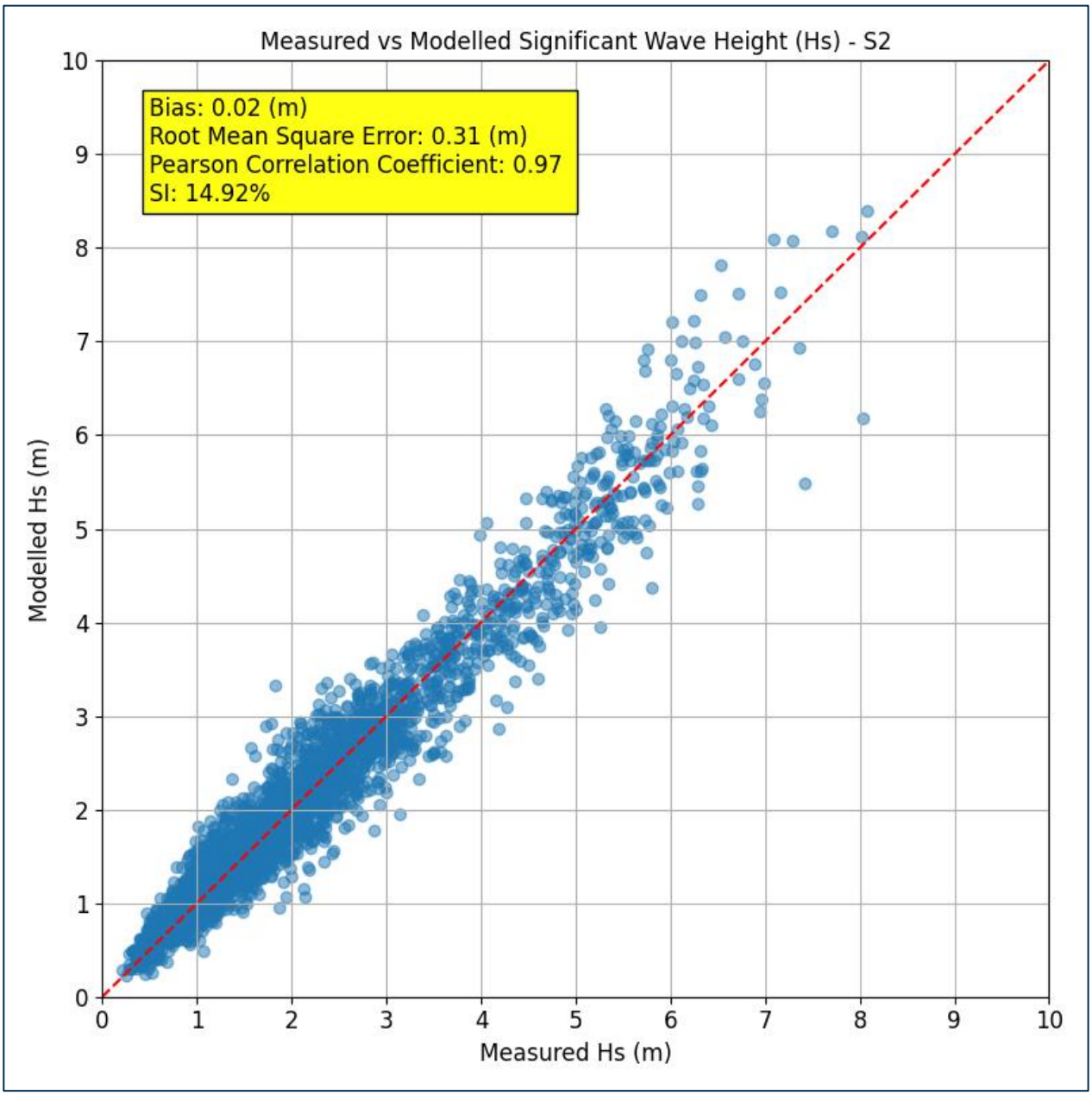

Figure 4-16: Measured Vs modelled Hs at S2, May 2023 – May 2024

Table 4-2: Hs error statistics for MIKE21-SW wave model calibration at S1 and S2

Indicator	S1	S2
Model Bias (m)	0.14	0.02
Root Mean Square Error, RMSE (m)	0.31	0.31
Pearson Correlation Coefficient, σ	0.98	0.97
Scatter Index, SI (%)	14.27	14.92

Model Validation

4.2.16 Following the model calibration summarized above, an independent model validation (without any change of model settings) was undertaken for the same period (May 2023 – May 2024) but at a separate location, the Blackstone's wave buoy, which is located approximately 20 km offshore of the S1 survey site.

4.2.17 Similarly to model calibration results, the model validation results are presented as time-series plots comparing measured and modelled wave parameters (Hs, Tp and MWD) at the Blackstone's wave buoy in **Figure 4-17** to **Figure 4-22**.

4.2.18 A scatter plot comparing measured and modelled Hs at Blackstone's wave buoy is presented in **Figure 4-23**.

4.2.19 Error statistics (Bias, RMSE, correlation coefficient and SI) which quantify model performance to predict Hs at Blackstone's wave buoy for the entire validation period (May 2023 – May 2024) are presented in **Table 4-3**.

4.2.20 The results of the model validation exercise again show a very good comparison between modelled and measured wave climate. The computed error statistics on Hs indicate that model performance is suitable to meet the 'Design' criteria in the EA guidance for both RMSE (0.30 m) and SI (12.86%).

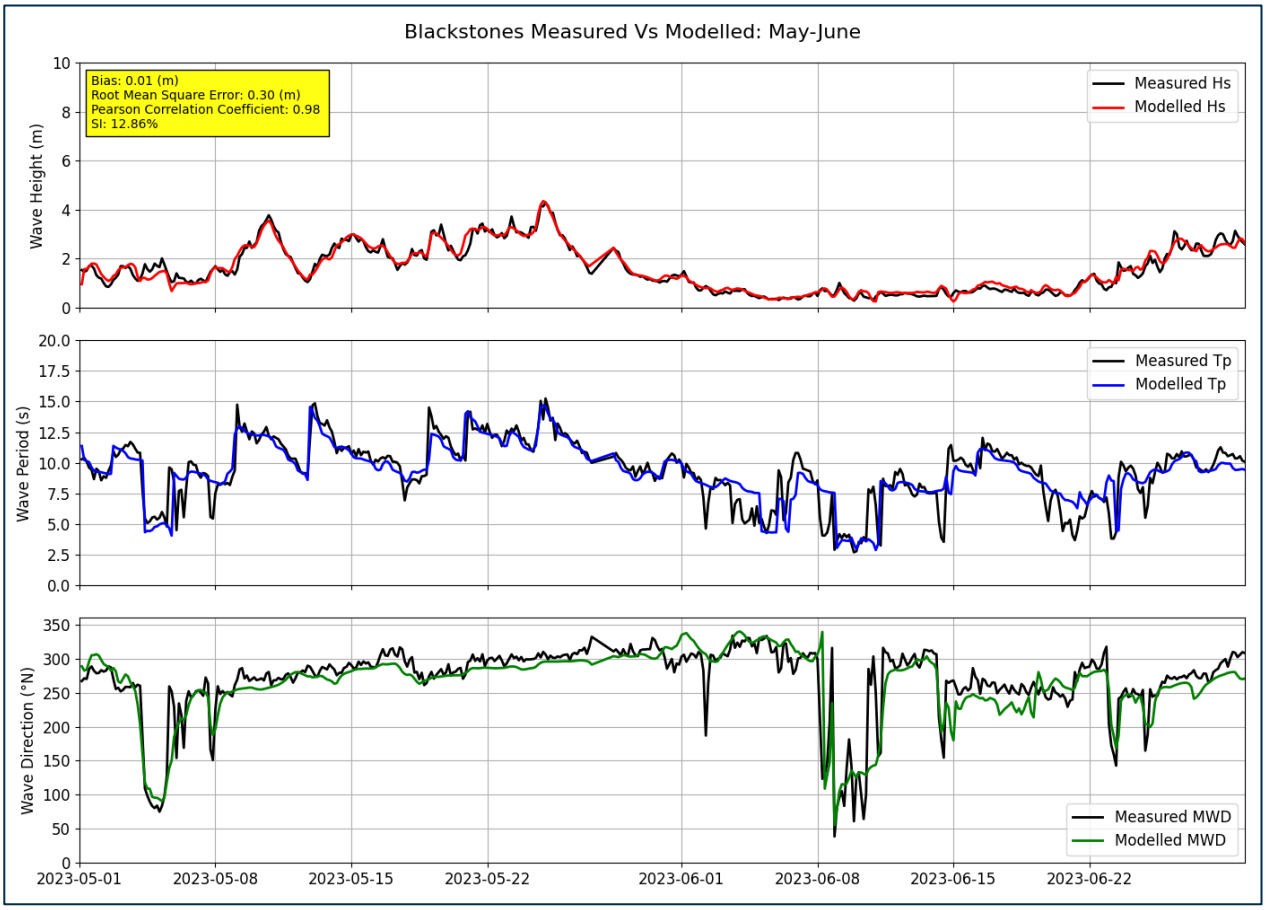

Figure 4-17: MIKE21-SW wave model validation results at Blackstone's wave buoy, May 2023 – June 2023

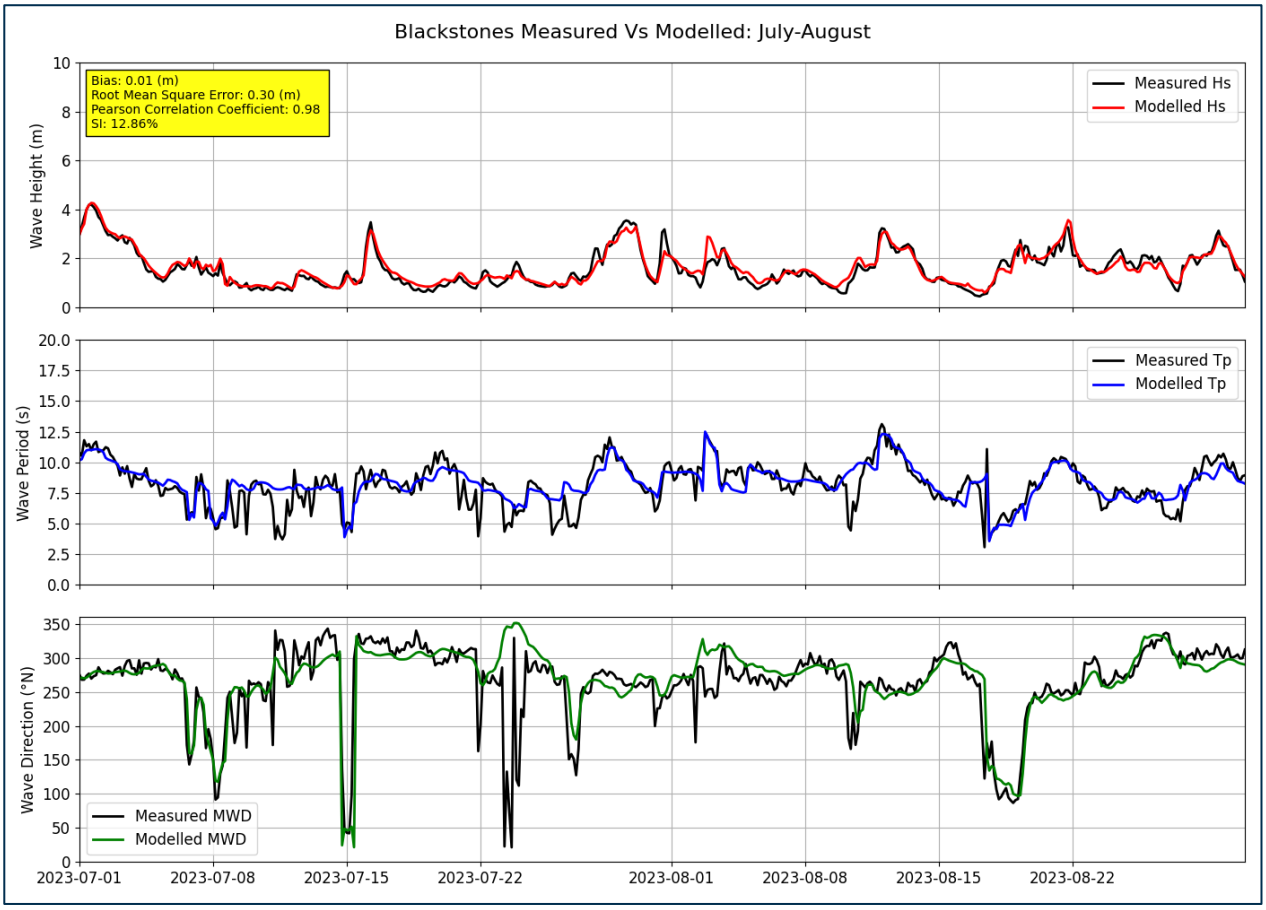

Figure 4-18: MIKE21-SW wave model validation results at Blackstone's wave buoy, July 2023 – August 2023

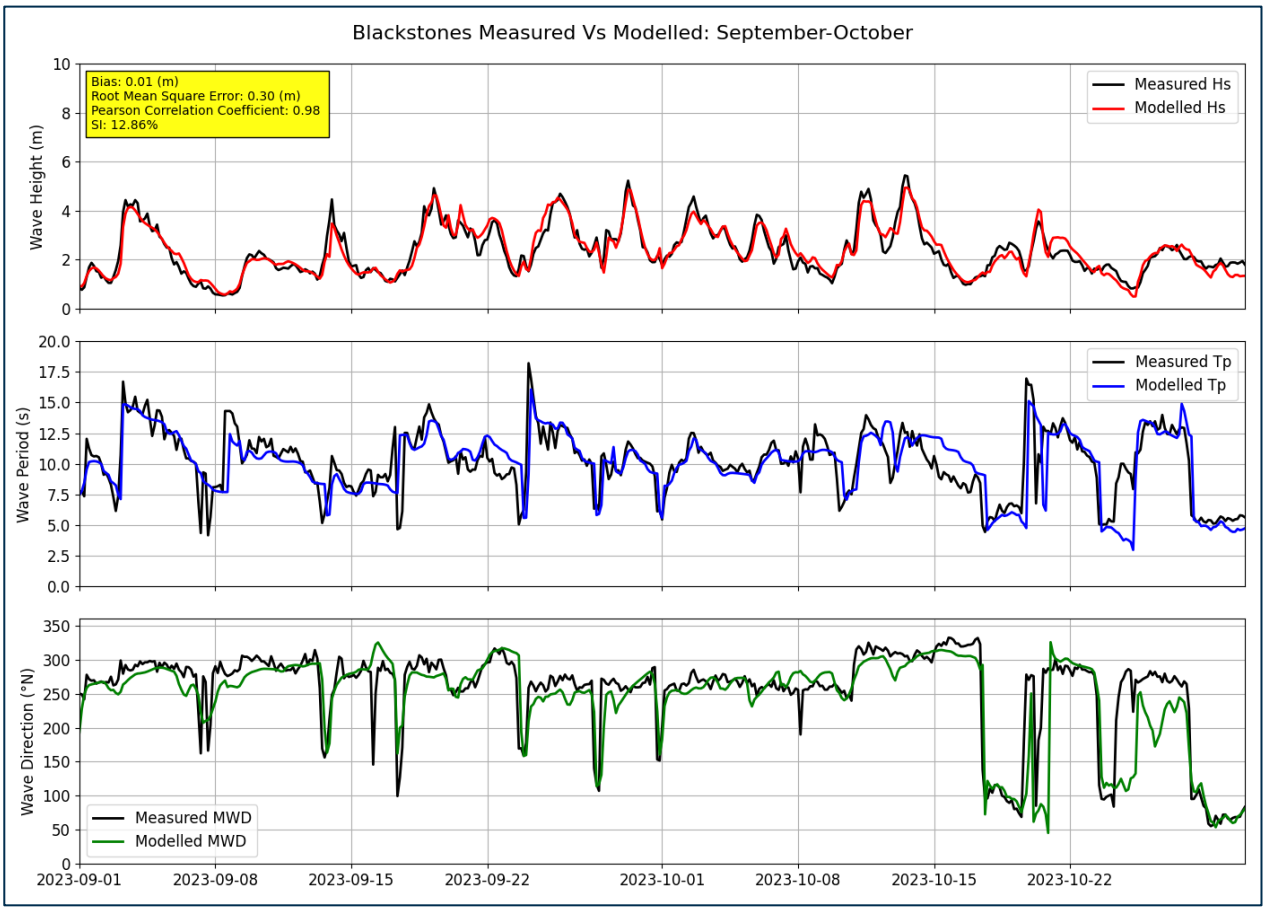

Figure 4-19: MIKE21-SW wave model validation results at Blackstone's wave buoy, September 2023 – October 2023

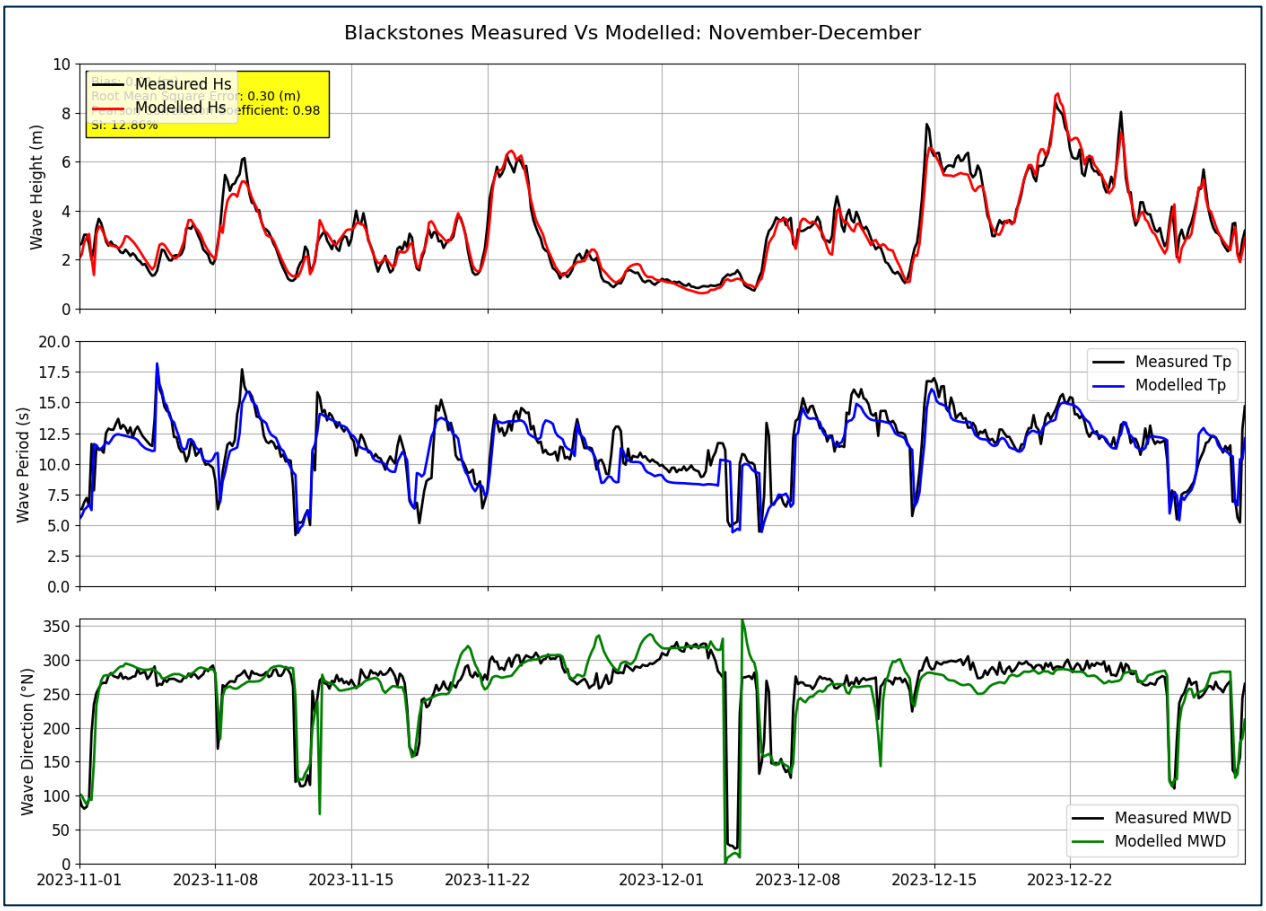

Figure 4-20: MIKE21-SW wave model validation results at Blackstone's wave buoy, November 2023 – December 2023

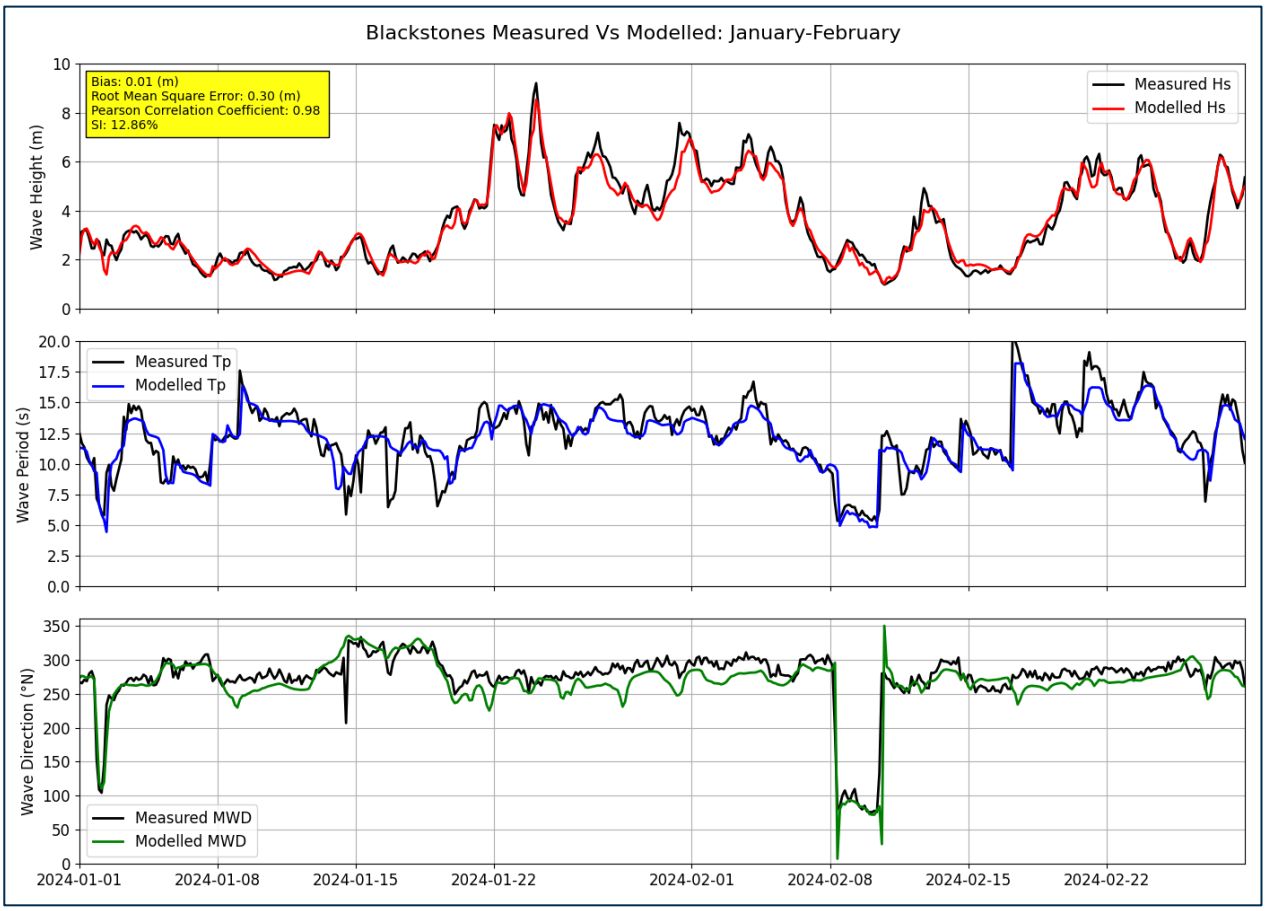

Figure 4-21: MIKE21-SW wave model validation results at Blackstone's wave buoy, January 2024 – February 2024

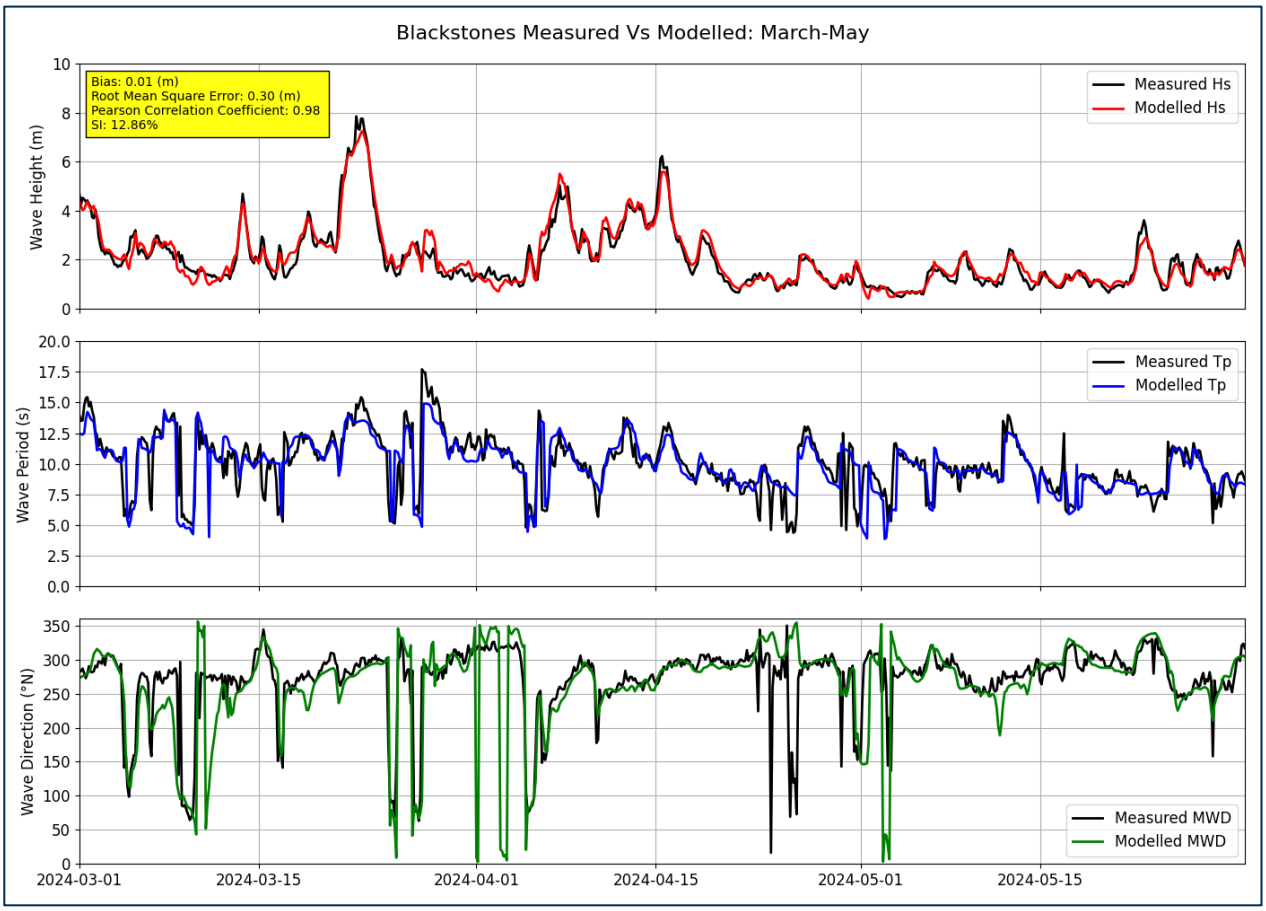

Figure 4-22: MIKE21-SW wave model validation results at Blackstone's wave buoy, March 2024 – May 2024

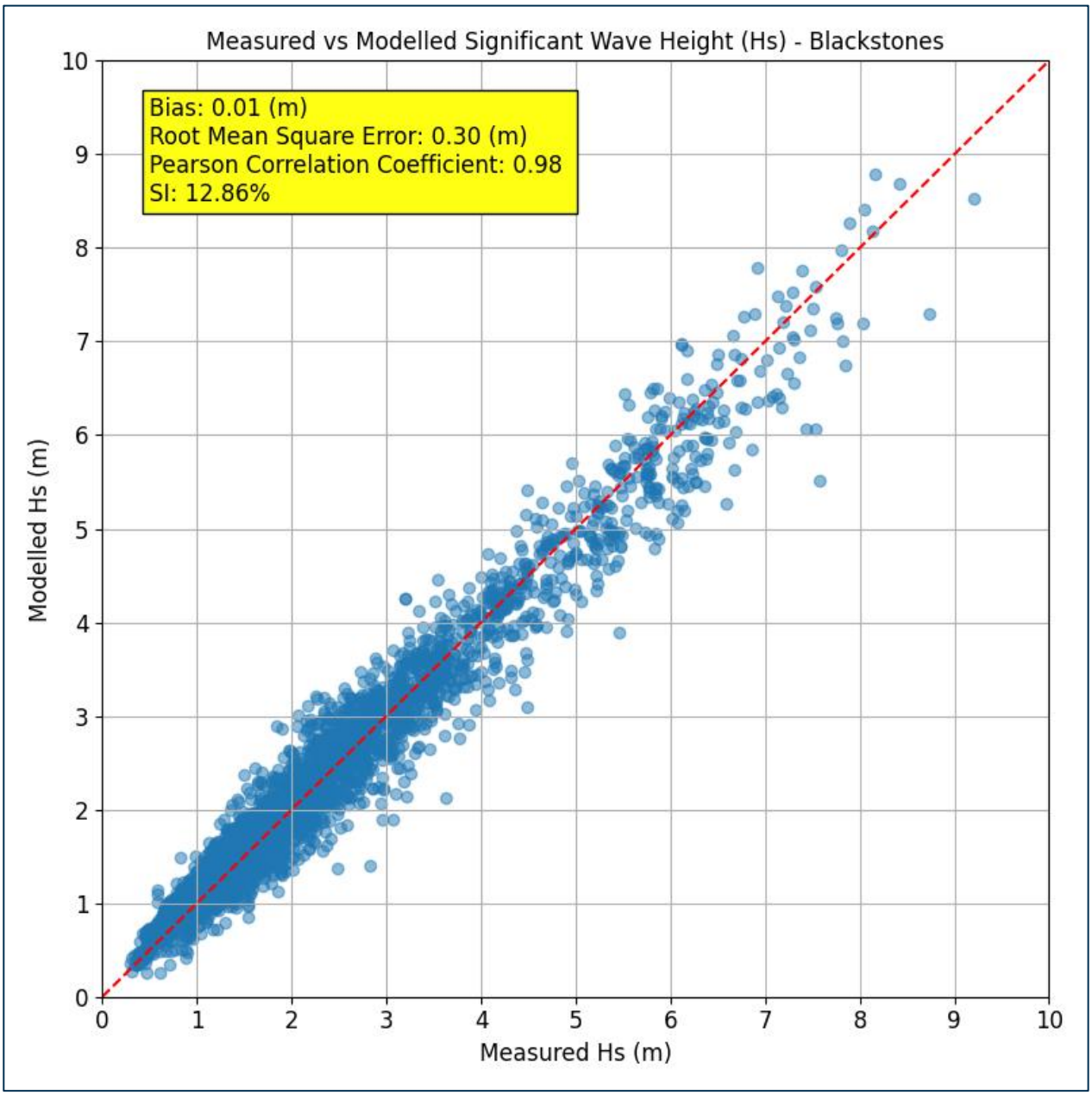

Figure 4-23: Measured Vs modelled Hs at Blackstone's wave buoy, May 2023 – May 2024

Table 4-3: Hs error statistics for MIKE21-SW wave model validation

Indicator	Blackstone's Wave Buoy
Model Bias (m)	0.01
Root Mean Square Error, RMSE (m)	0.30
Pearson Correlation Coefficient, σ	0.98
Scatter Index, SI (%)	12.86

Sensitivity to Mesh Resolution

4.2.21 Due to the computational demand of the 1-year calibration period, a coarse mesh throughout coastal areas and around the WDA of 1 km was adopted. Then to ensure that the mesh refinement for the assessment simulations did not affect the model performance and associated settings, a sensitivity test on a refined mesh was undertaken, simulating a 22-day period around the storm event on the 22/12/2023, where peak Hs reached up to 8 m at S1.

4.2.22 The results of the sensitivity test, presented in **Figure 4-24** below indicate that the mesh resolution leads to an indistinguishable change on the predicted wave climate and the refined mesh does not hinder the model performance reported in the model calibration and validation study.

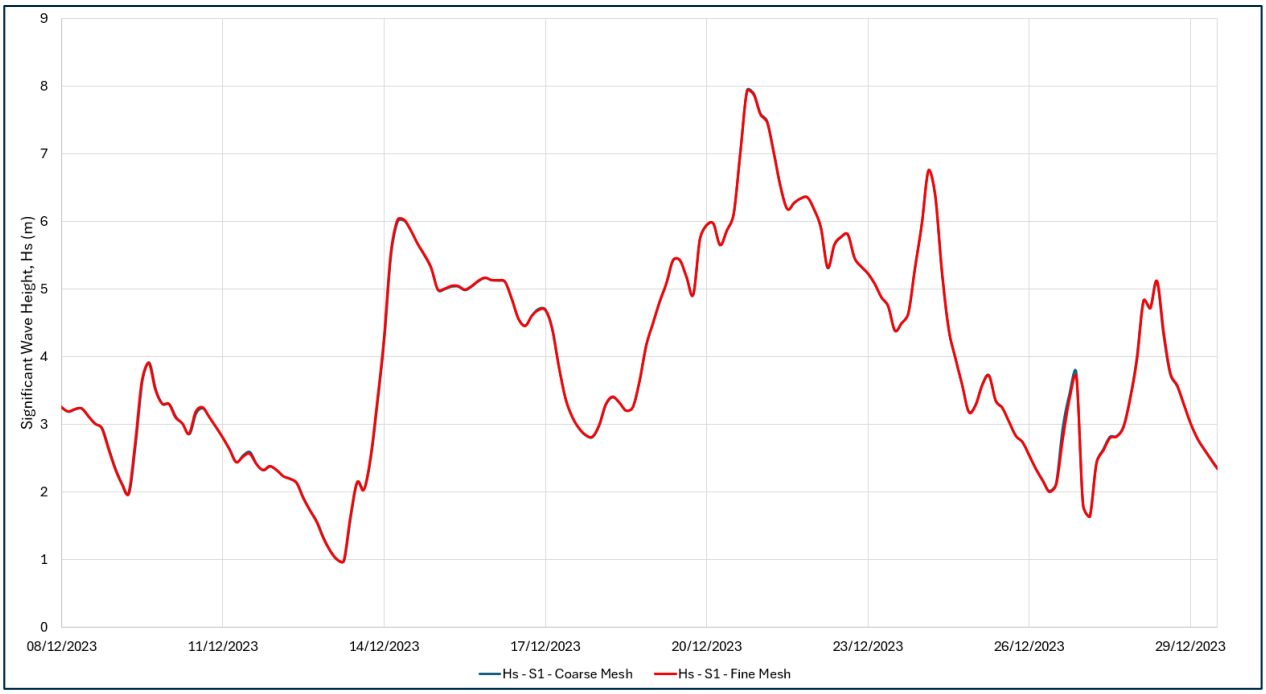

Figure 4-24 Modelled wave height in mesh sensitivity test

4.3 Model Results

Scenarios

4.3.1 The WDA turbine indicative layouts which were modelled in the assessment are presented in **Table 4-4** and **Figure 4-25**. These four layouts are based on two WTG size options of 15 MW and 24 MW, on monopiles. Each of the 15 MW and 24 MW turbine layouts show two options: a 'dense perimeter' and 'even spread' of WTGs. All layouts also include 2 OSP's in the same proposed location for all. OSPs are modelled using a series of monopile structures.

4.3.2 In the MIKE21-SW model setup, the monopiles were input as a sub-grid feature using coordinates, structure type (circular pile) and diameter.

4.3.3 The extreme wave climate from 4 directions of approach was modelled (240°N, 270°N, 300°N and 330°N) and for 3 return periods, 1 in 1 year, 1 in 50 year and 1 in 100 year, using the following approach:

- Establish the worst-case direction(s) for the 1 in 1 year return period;
- Establish the worst-case layout using the worst-case direction(s) for 1 in 1 year return period; and
- Run 3 assessment simulations for 1 in 1 year, 1 in 50 year and 1 in 100 year return periods of the worst-case directions and the worst-case layout.

4.3.4 The focus of the assessment was the difference in wave climate between the proposed WDA layout and baseline scenario (no WDA).

Table 4-4: WDA layout information

Type	Indicative Layout	Number	Structure	Diameter (m)
WTG	15 MW – Even Spread	144	Monopile	13.0
WTG	15 MW – Dense Perimeter	144	Monopile	13.0
WTG	24 MW – Even Spread	91	Monopile	15.0
WTG	24 MW – Dense Perimeter	91	Monopile	15.0
OSP	All	2	6 * Monopile (each OSP)	15.0

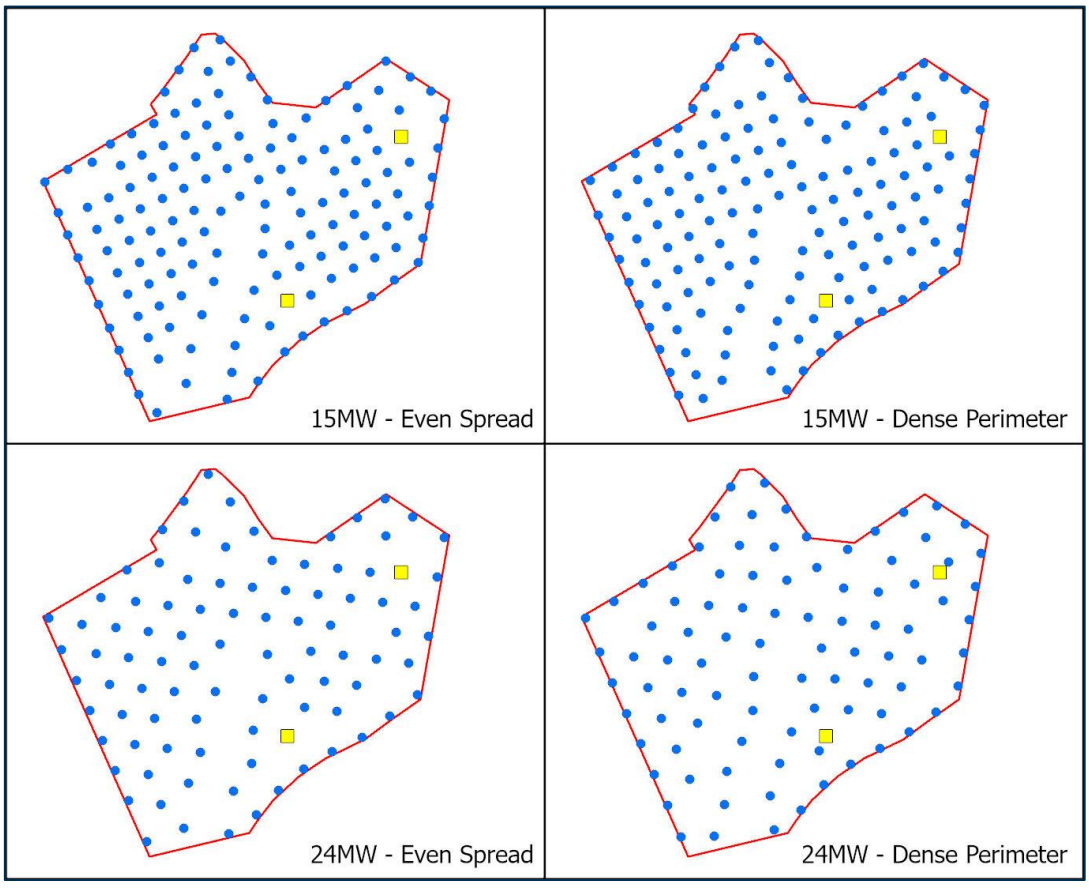

Figure 4-25: Indicative WTG (in blue) and OSP (in yellow) locations

Worst-case Direction(s)

4.3.5 To establish the worst-case wave direction(s), waves from 240°N, 270°N, 300°N and 330°N for 1 in 1 year return period were simulated for the baseline case (no WDA) and the 15 MW even spread monopile indicative layout, where the percentage difference in wave height was assessed as follows:

- % Difference (240°N 15 MW even spread monopile – 240°N baseline);
- % Difference (270°N 15 MW even spread monopile – 270°N baseline);
- % Difference (300°N 15 MW even spread monopile – 300°N baseline); and
- % Difference (330°N 15 MW even spread monopile – 330°N baseline).

4.3.6 The predicted percentage difference in wave height to establish the worst-case wave direction(s) is presented in **Figure 5-2 - Figure 5-5** below. The model results demonstrate that the WDA will result in the greatest change to waves from 330°N, with a change of 0.5% - 1% extending up to 5 km southeast (SE) of the WDA. In contrast to this, waves from 270°N are predicted to be the least affected by the WDA. This can be attributed to the offshore Tp of waves from each direction (**Table 3-5**), where the smallest wave period will result in the greatest effect from the WDA. Change to waves approaching from 240°N is shown to be less pronounced than from 330°N. Despite this, there is potential for this change to be material, due to the direction of the change and its proximity to the Isle of Colonsay, although the changes do not reach the coastline.

4.3.7 Therefore, in conclusion to this, the worst-case wave directions taken forward to the assessment simulations are waves from 240°N and 330°N.

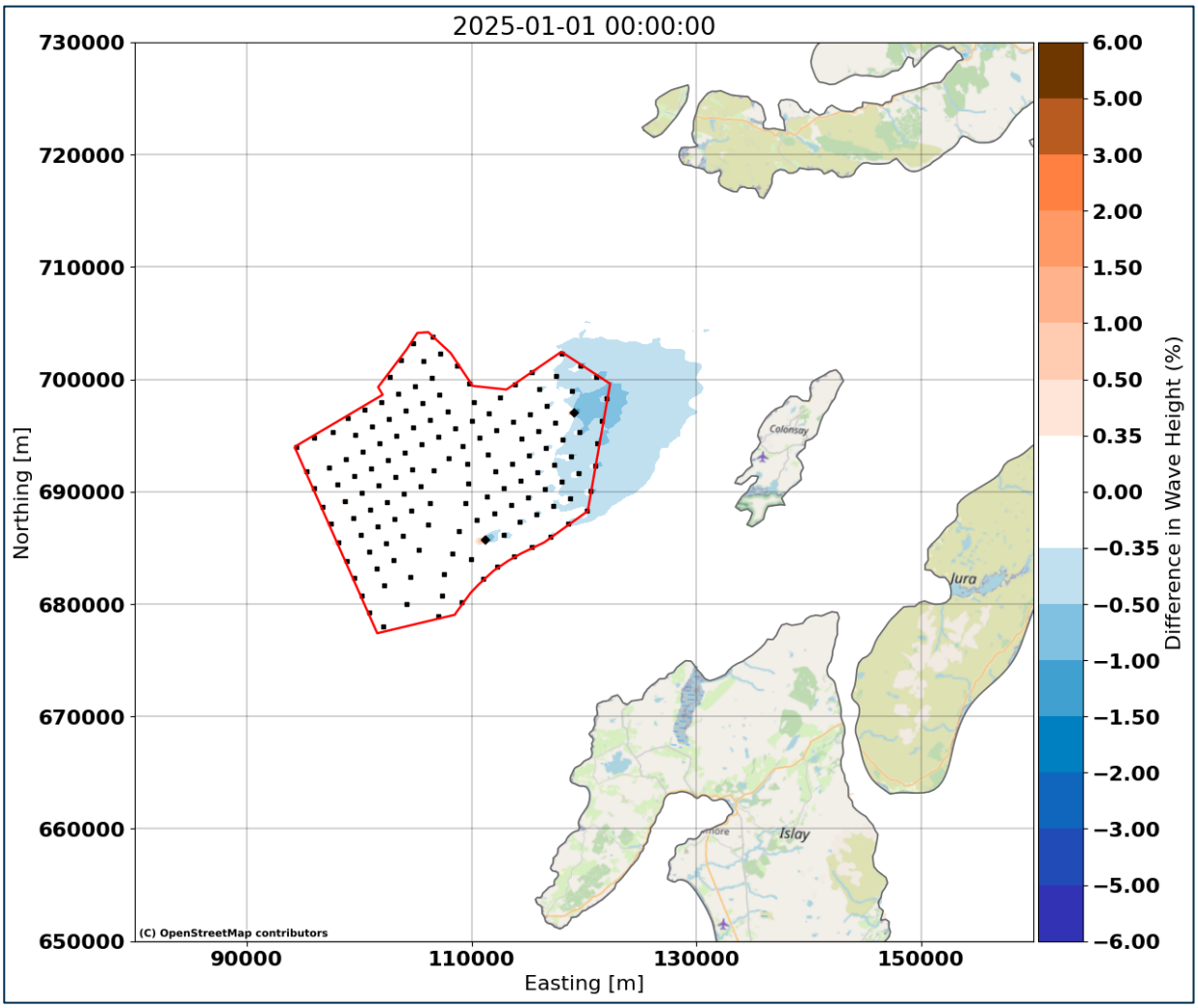

Figure 4-26: Difference in wave height (%) for 1 in 1 year from 240°N – 15 MW even spread monopile

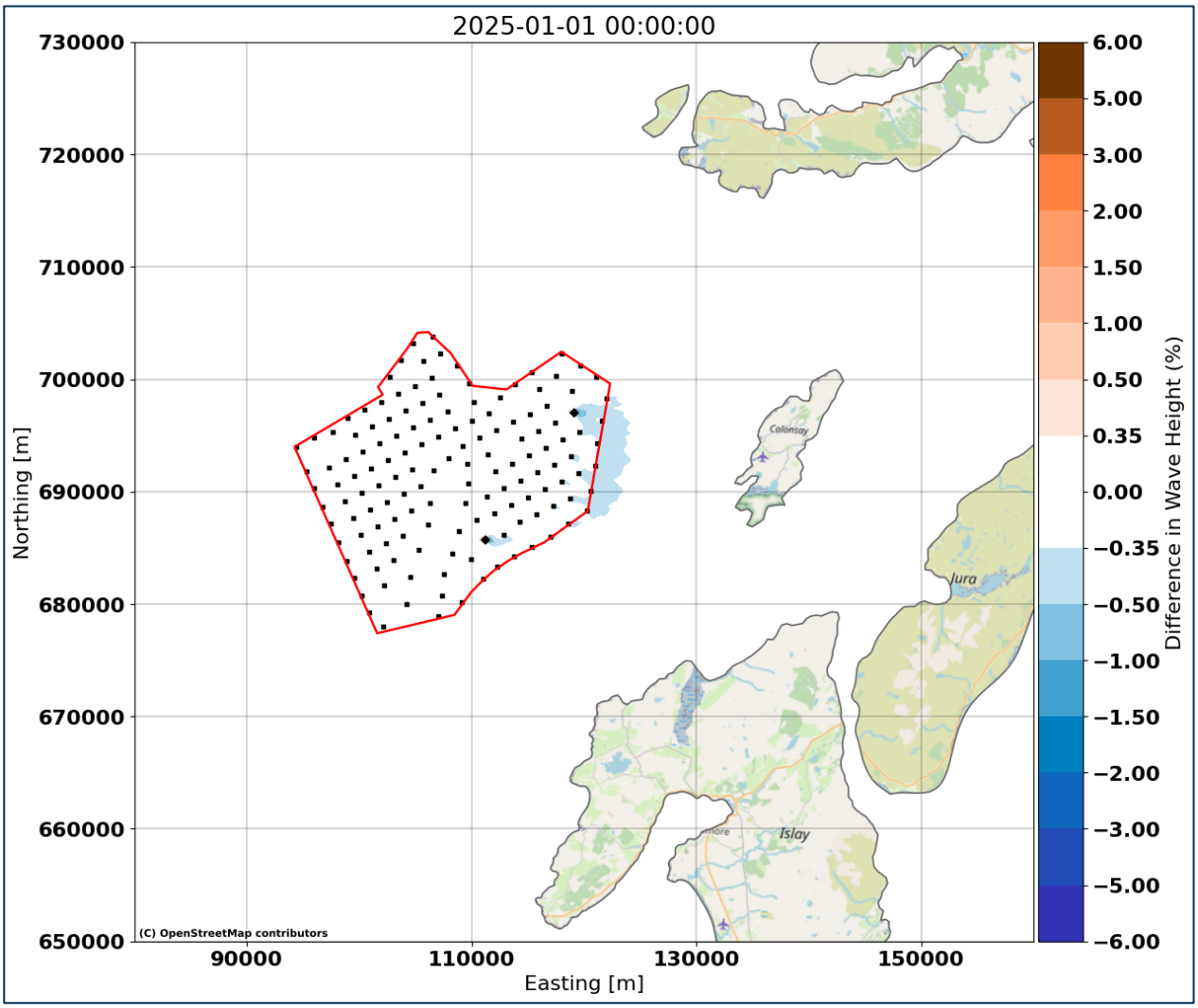

Figure 4-27: Difference in wave height (%) for 1 in 1 year from 270°N – 15 MW even spread monopile

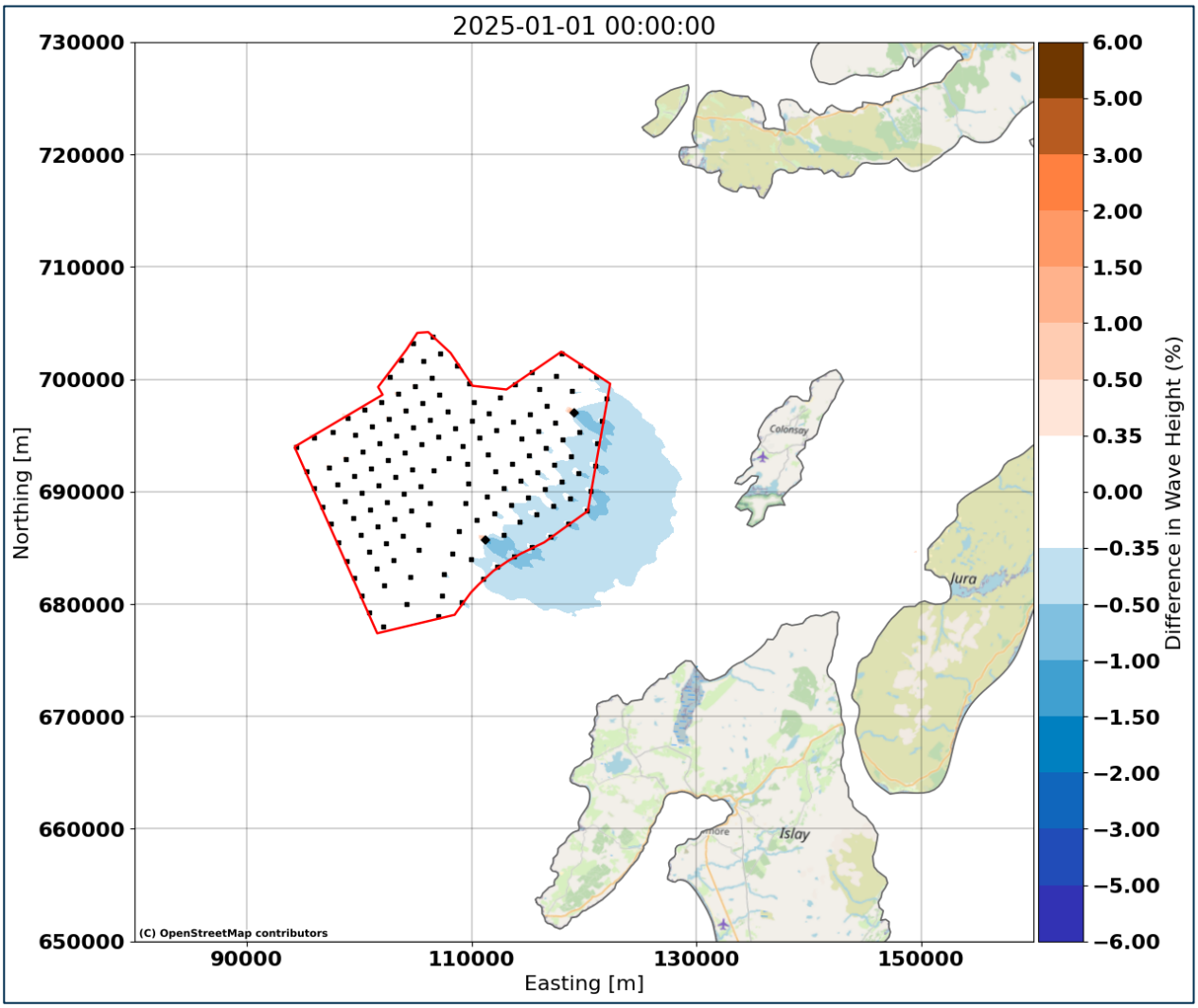

Figure 4-28: Difference in wave height (%) for 1 in 1 year from 300°N – 15 MW even spread monopile

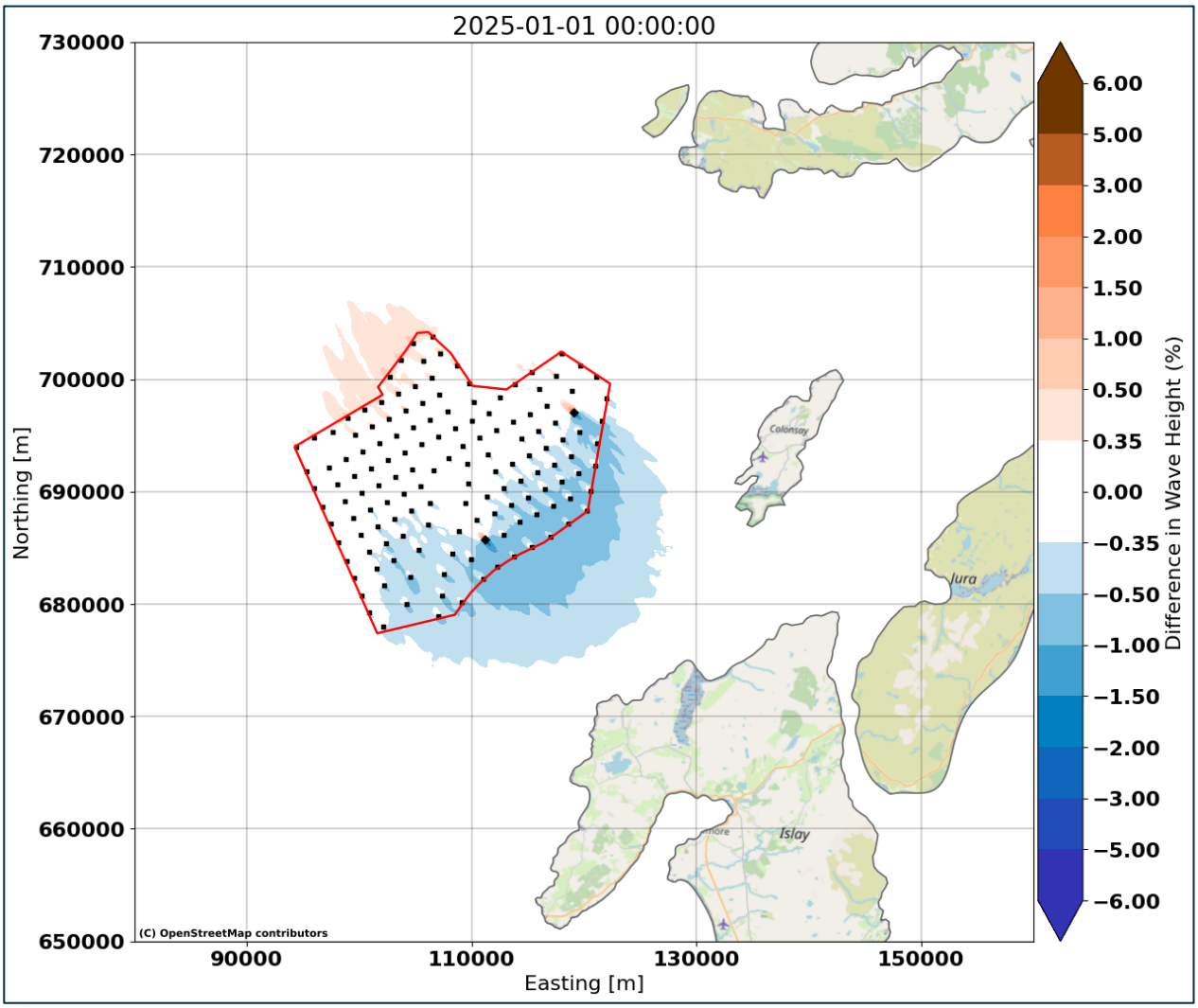

Figure 4-29: Difference in wave height (%) for 1 in 1 year from 330°N – 15 MW even spread monopile

Worst-case Layout

4.3.8 To establish the worst-case layout, waves from 240°N and 330°N (based on section above) for 1 in 1 year return period were simulated for the baseline case (no WDA) and each proposed WDA layout, where the percentage difference in wave height was assessed as follows:

- % Difference (15 MW even spread monopile – baseline);
- % Difference (15 MW dense spread monopile – baseline);
- % Difference (24 MW even spread monopile – baseline); and
- % Difference (24 MW dense spread monopile – baseline).

4.3.9 The predicted percentage difference in wave height to establish the worst-case layout is presented in **Figure 4-30** to **Figure 4-33** for waves from 240°N and **Figure 4-34** to **Figure 4-37** for waves from 330°N. The model results demonstrate that although the predicted percentage difference as a result of each of the layouts is small, the 15 MW even spread is demonstrated to have the largest effect in the wake of the WDA, with the largest area of 0.35% to 1% change.

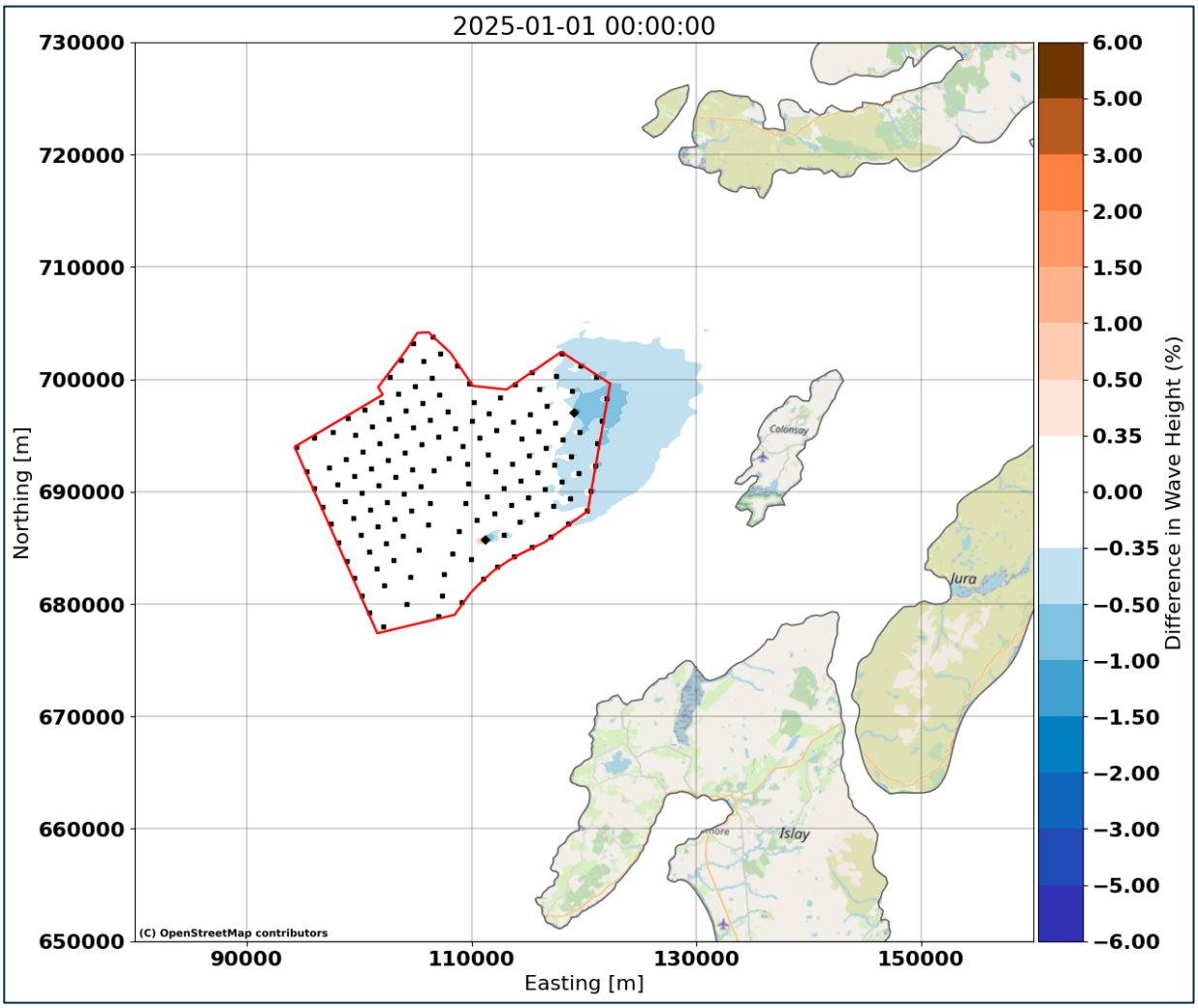

Figure 4-30: Difference in wave height (%) for 1 in 1 year from 240°N – 15 MW even spread monopile

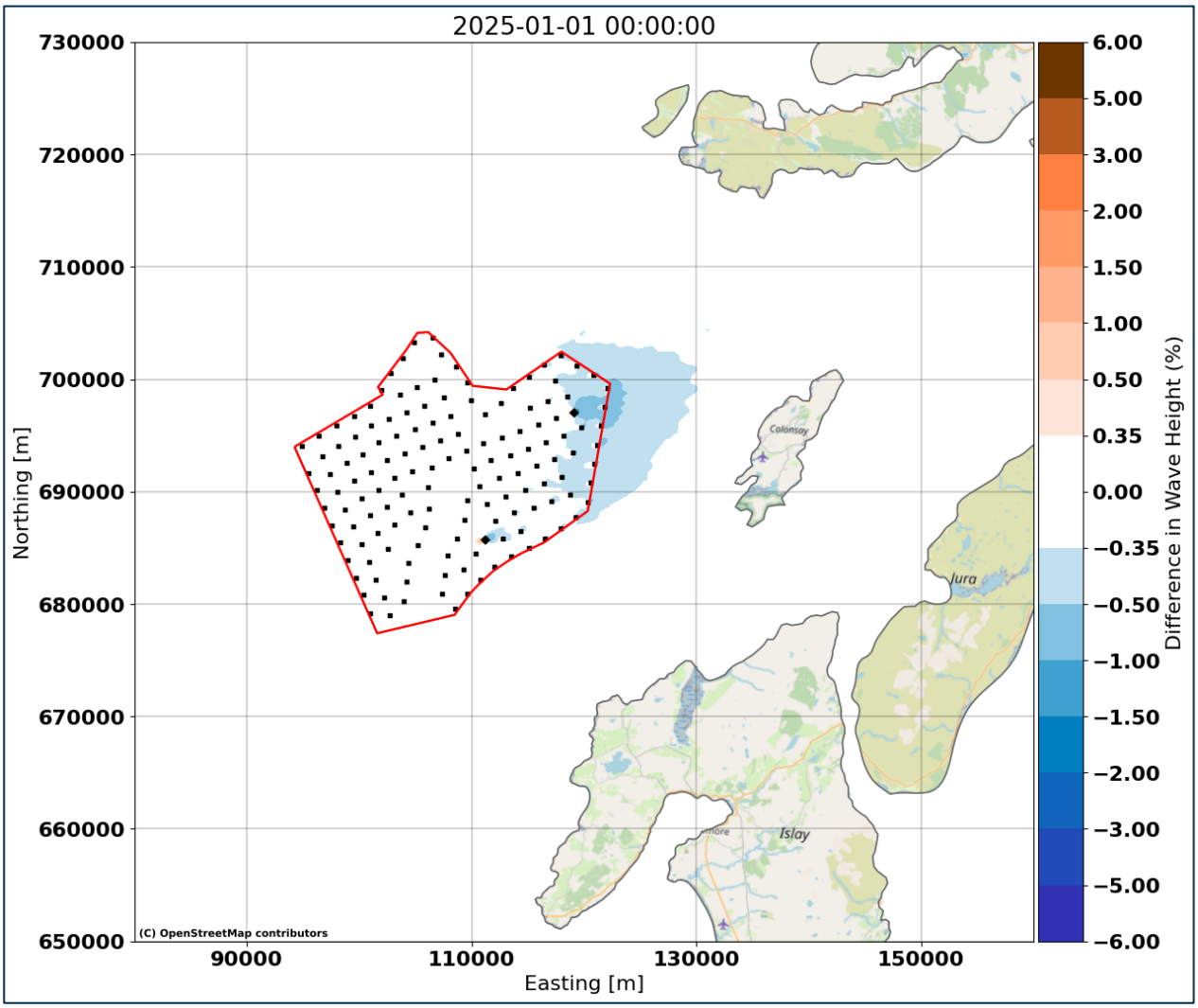

Figure 4-31: Difference in wave height (%) for 1 in 1 year from 240°N – 15 MW dense perimeter monopile

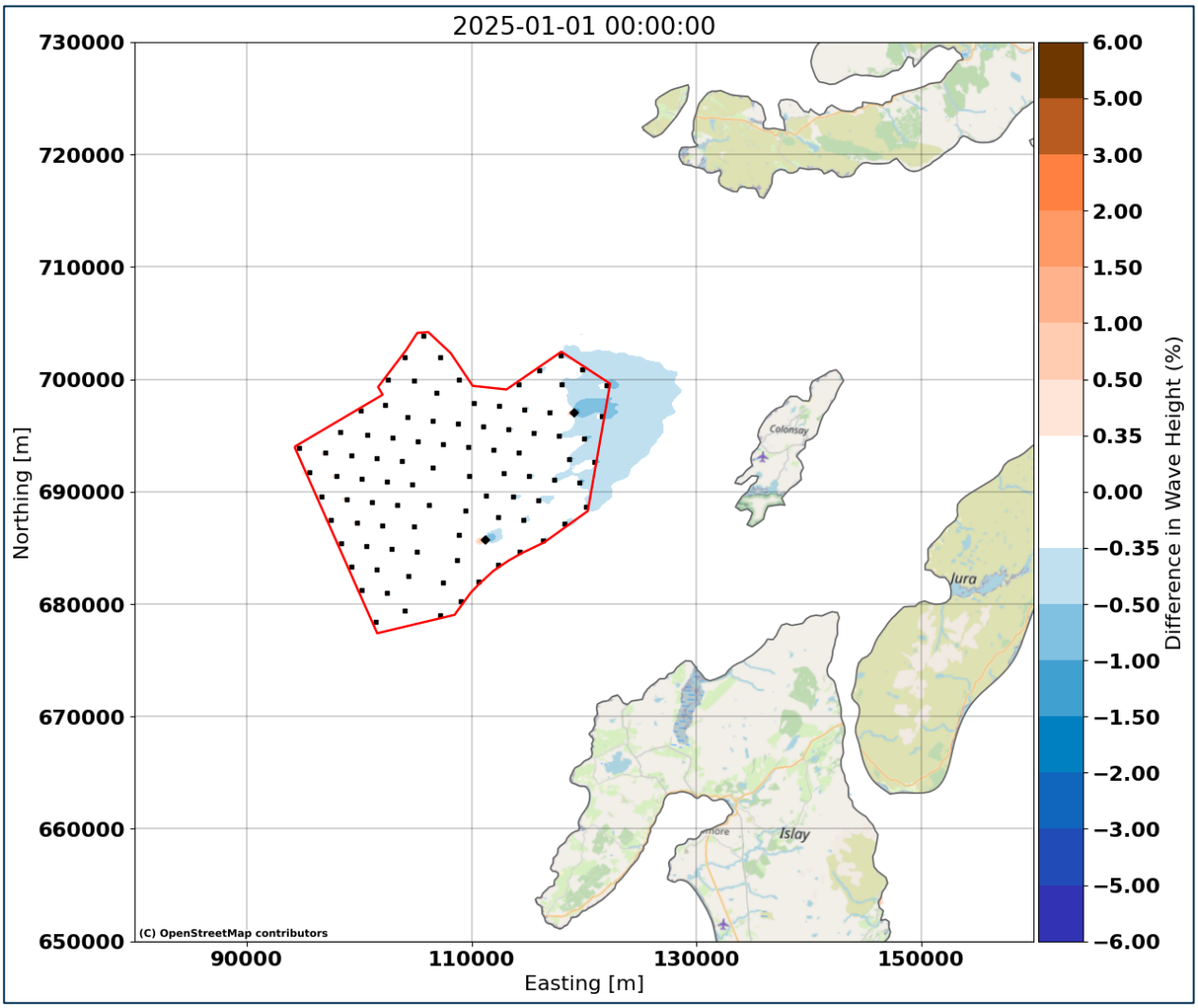

Figure 4-32: Difference in wave height (%) for 1 in 1 year from 240°N – 24 MW even spread monopile

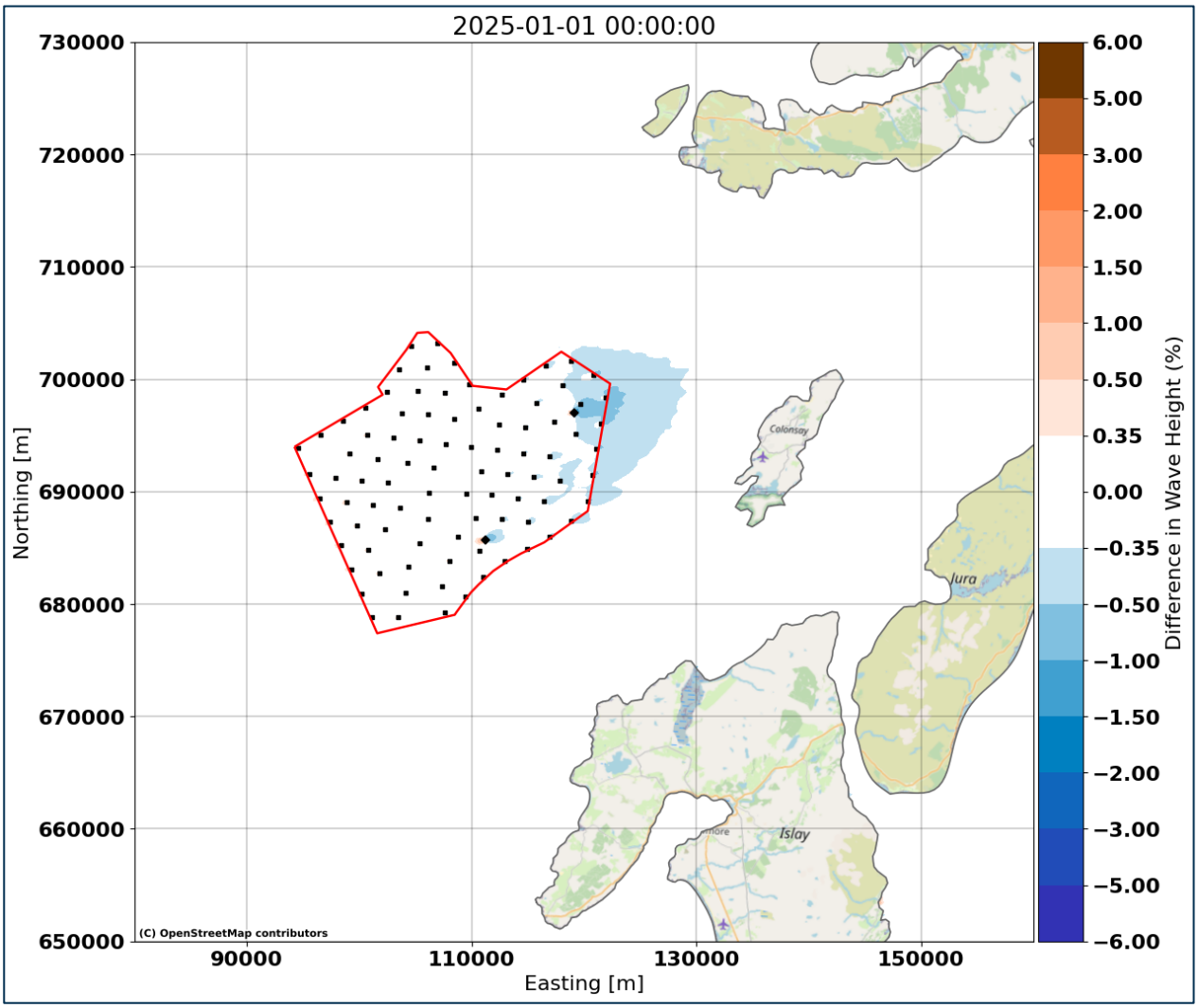

Figure 4-33: Difference in wave height (%) for 1 in 1 year from 240°N – 24 MW dense perimeter monopile

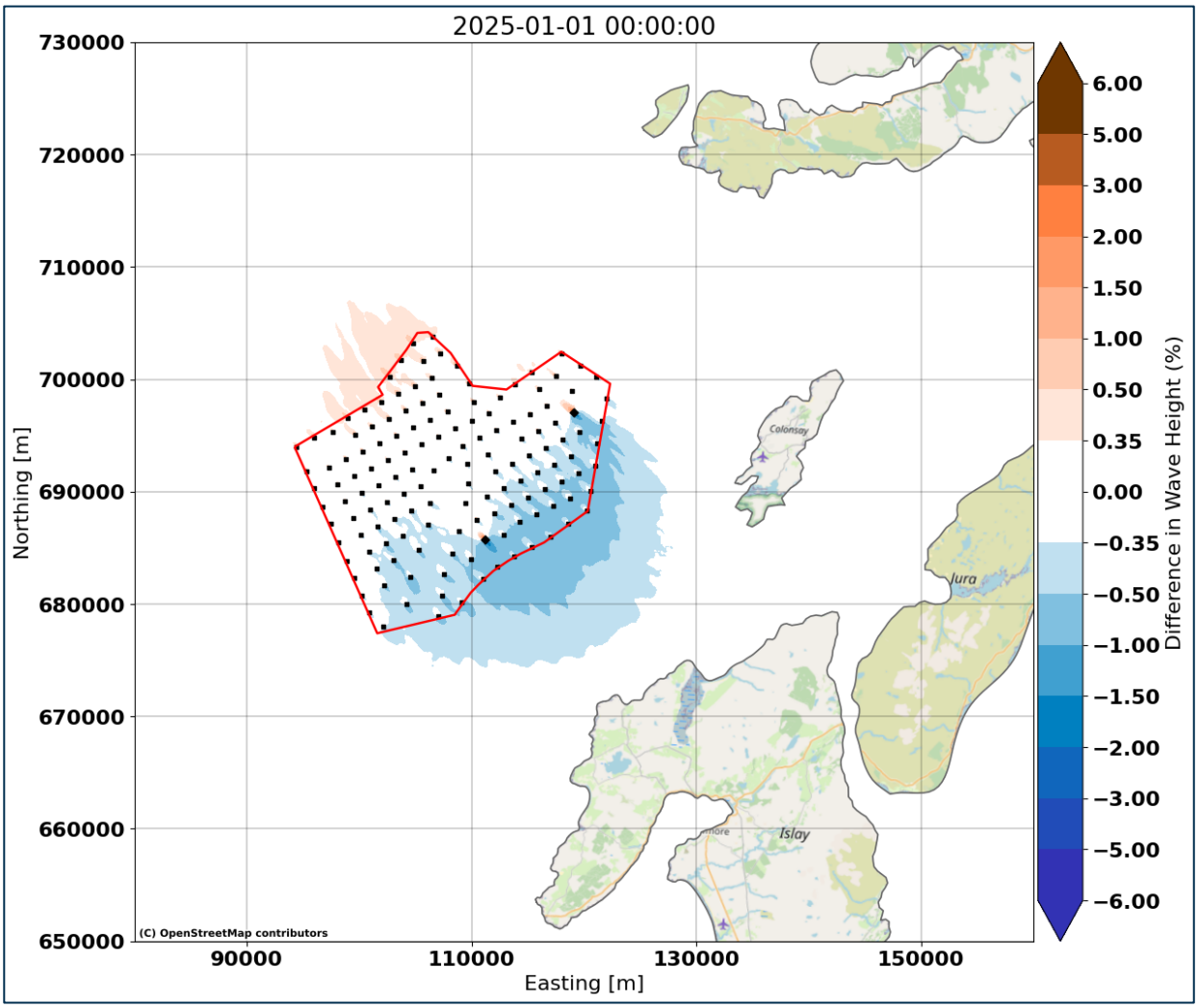

Figure 4-34: Difference in wave height (%) for 1 in 1 year from 330°N – 15 MW even spread monopile

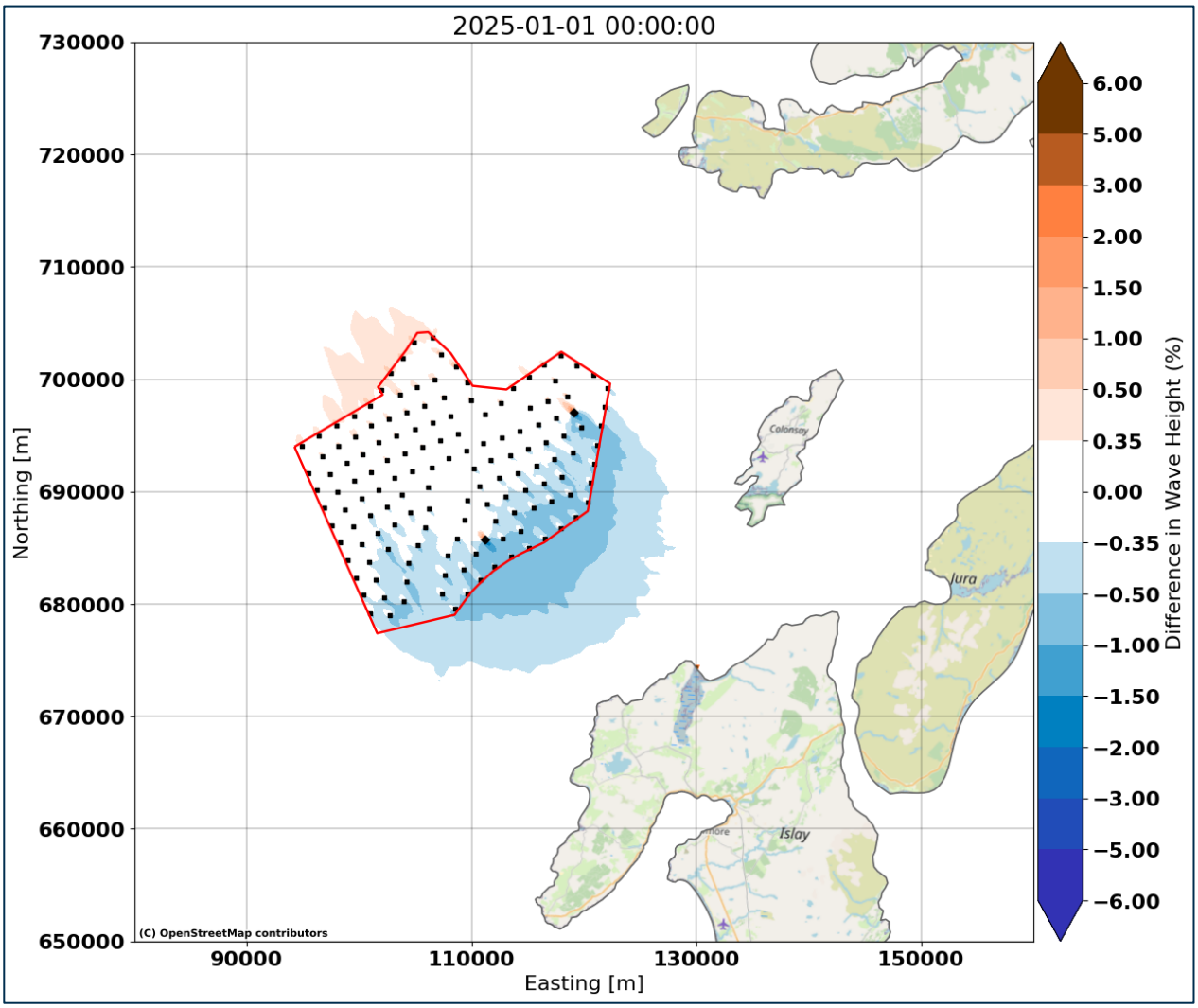

Figure 4-35: Difference in wave height (%) for 1 in 1 year from 330°N – 15 MW dense perimeter monopile

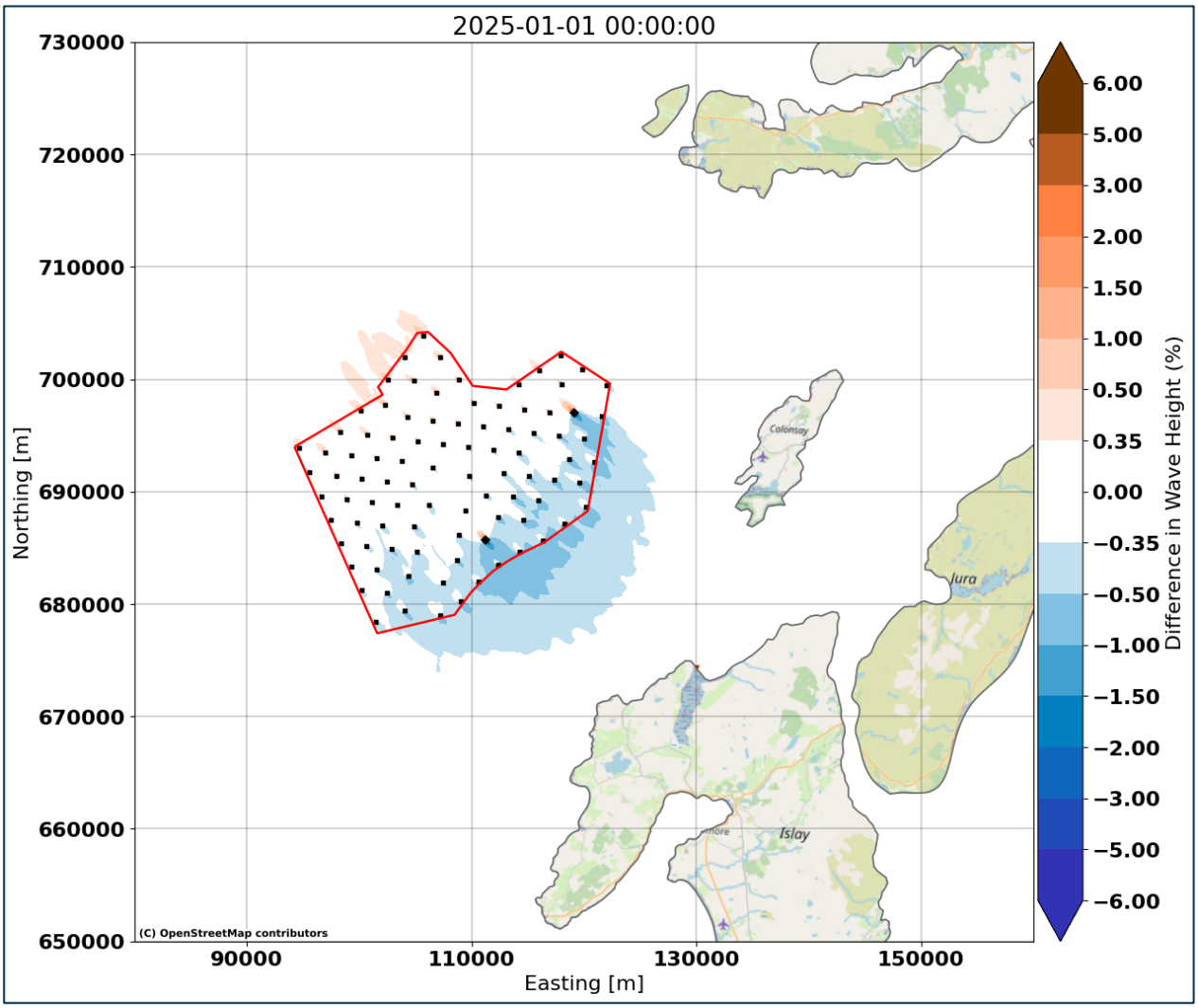

Figure 4-36: Difference in wave height (%) for 1 in 1 year from 330°N – 24 MW even spread monopile

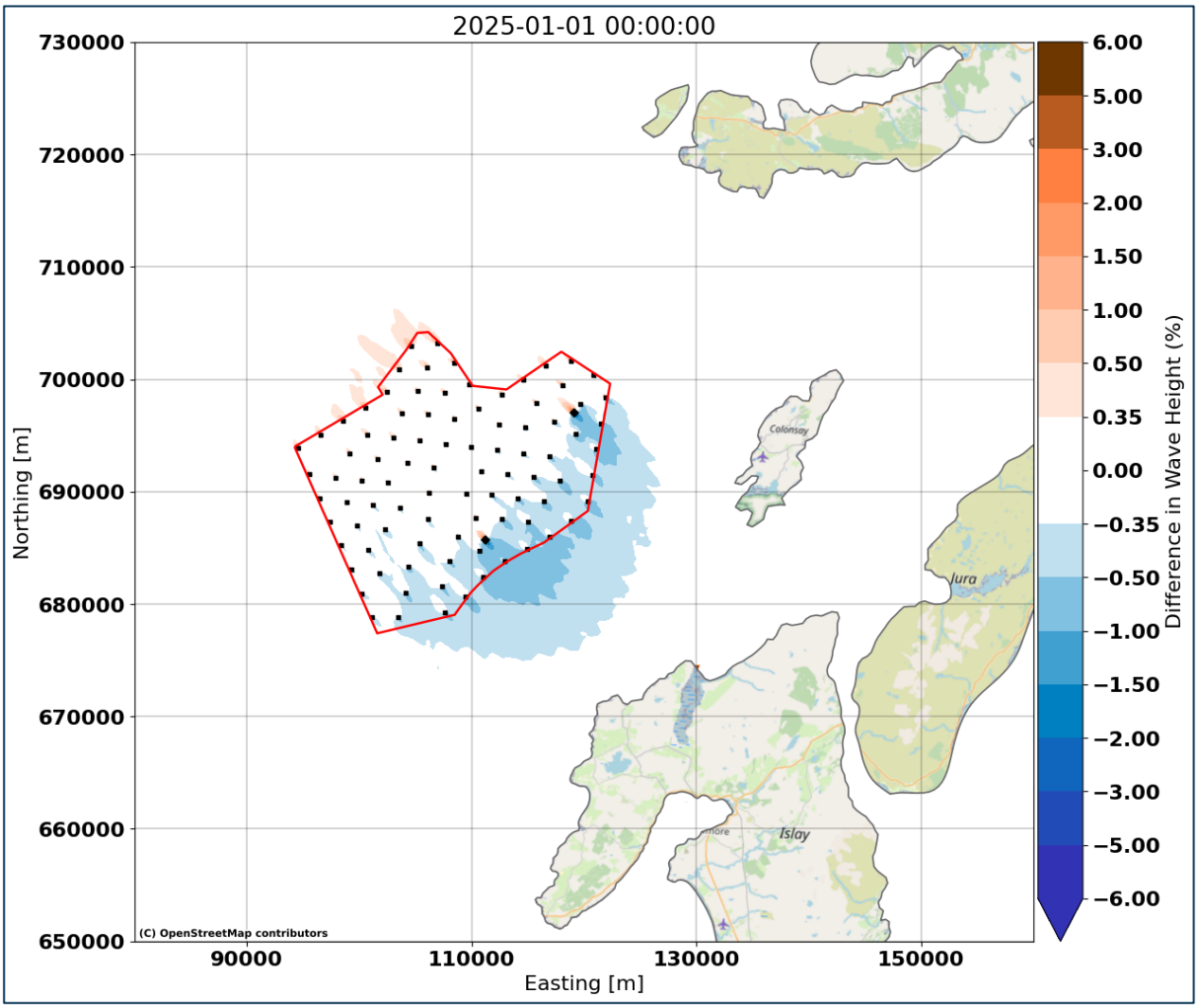

Figure 4-37: Difference in wave height (%) for 1 in 1 year from 330°N – 24 MW dense perimeter monopile

Assessment Simulations

4.3.10 Using the worst-case wave directions (240°N and 330°N) and worst-case layout (15 MW even spread monopile) established in the above sections, the predicted absolute difference in wave height (m) and percentage difference in wave height is presented in the following figures, for the 1 in 1 year, 1 in 50 year and 1 in 100 year return periods. All return periods for waves approaching from 240°N are presented in **Figure 4-38** to **Figure 4-43** and all return periods for waves approaching from 330°N are presented in **Figure 4-44** to **Figure 4-49**.

4.3.11 For 240°N, the largest difference in wave climate is predicted for the 1 in 1 year return period, where a percentage difference in wave height of 0.5% - 1% is predicted to extend up to 1.5 km northeast (NE) of WDA and 0.35% - 0.5% is predicted to extend up to 10 km NE of the WDA. Although the results demonstrate that a percentage difference of >0.35% does not reach the coastline. For the 1 in 50 year and 1 in 100 year simulations, the predicted percentage difference in wave climate is considerably reduced, with 0.35% - 1% difference almost entirely contained within the WDA.

4.3.12 For 330°N, the largest difference in wave climate is predicted for the 1 in 1 year return period, where a percentage difference in wave height of 0.5% - 1% is predicted to extend up to 5 km SE of the WDA and 0.35% - 0.5% is predicted to extend up to 12 km SE of the WDA. Although the results demonstrate that a percentage difference of >0.35% does not reach the coastline. For the 1 in 50 year and 1 in 100 year simulations, the predicted percentage difference in wave climate is considerably reduced, with 0.5% - 1% difference contained within the WDA and 0.35% - 0.5% extending up to 3 km SE of the WDA.

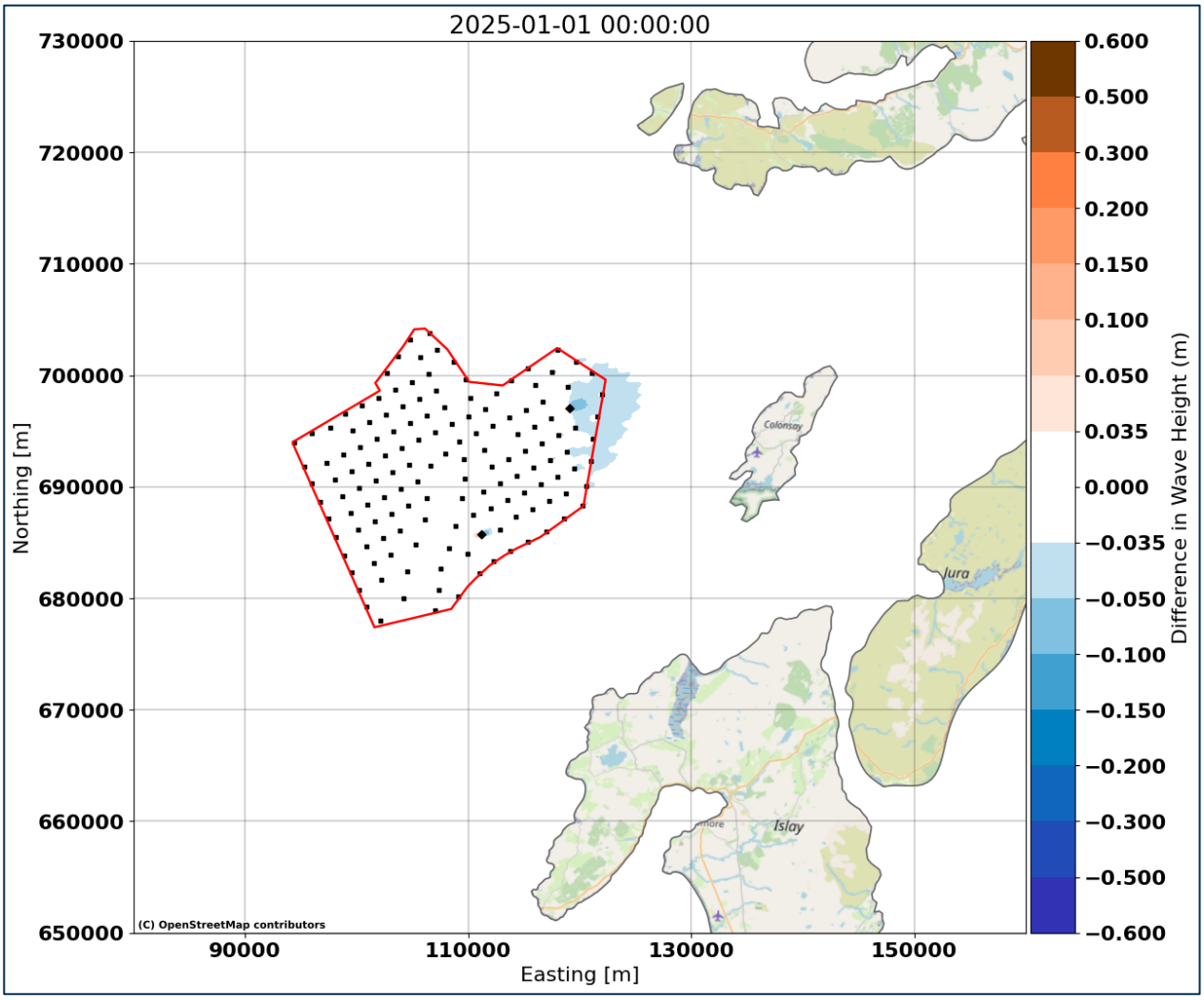

Figure 4-38: Difference in wave height (m) for 1 in 1 year from 240°N – 15 MW even spread monopile

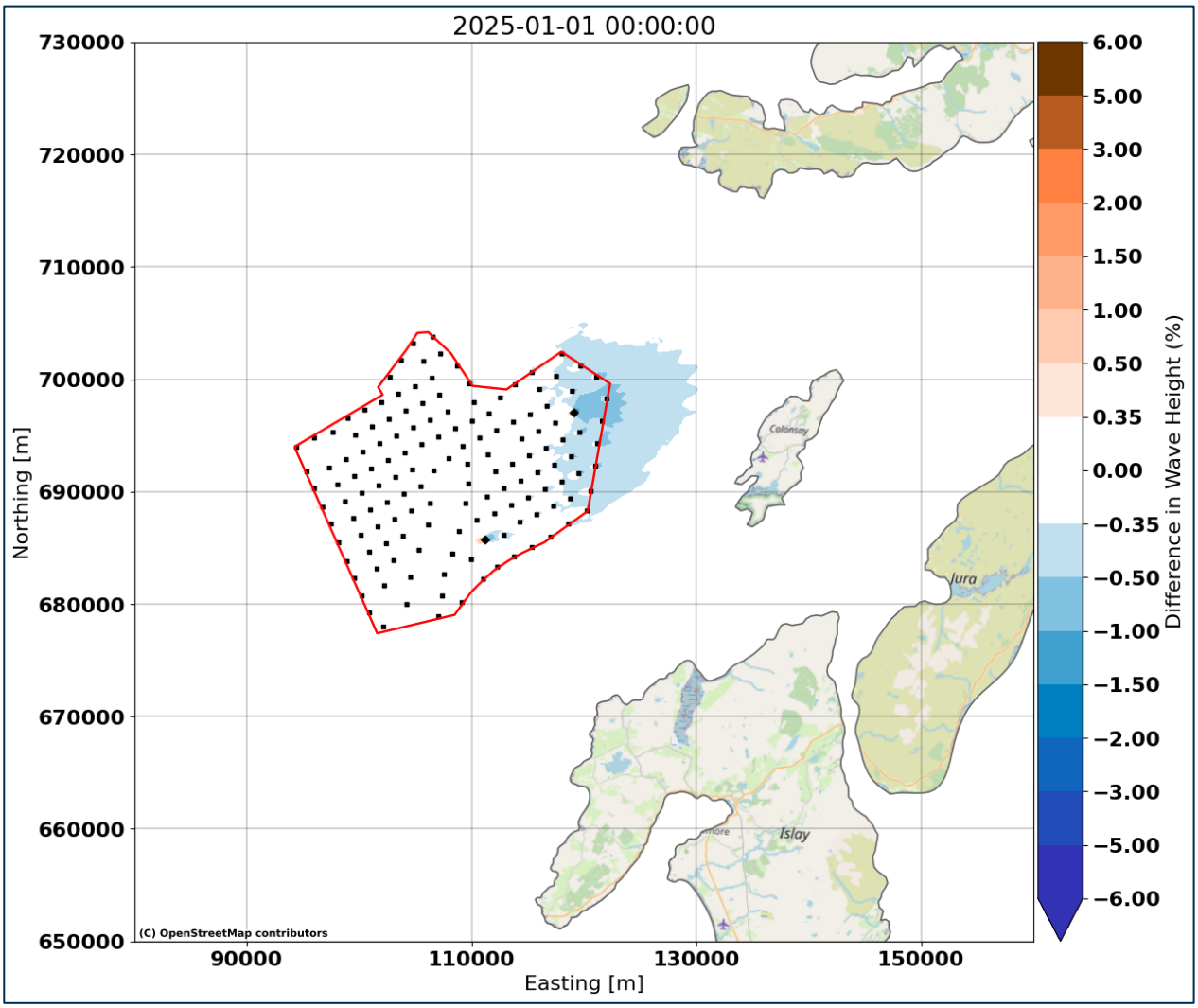

Figure 4-39: Difference in wave height (%) for 1 in 1 year from 240°N – 15 MW even spread monopile

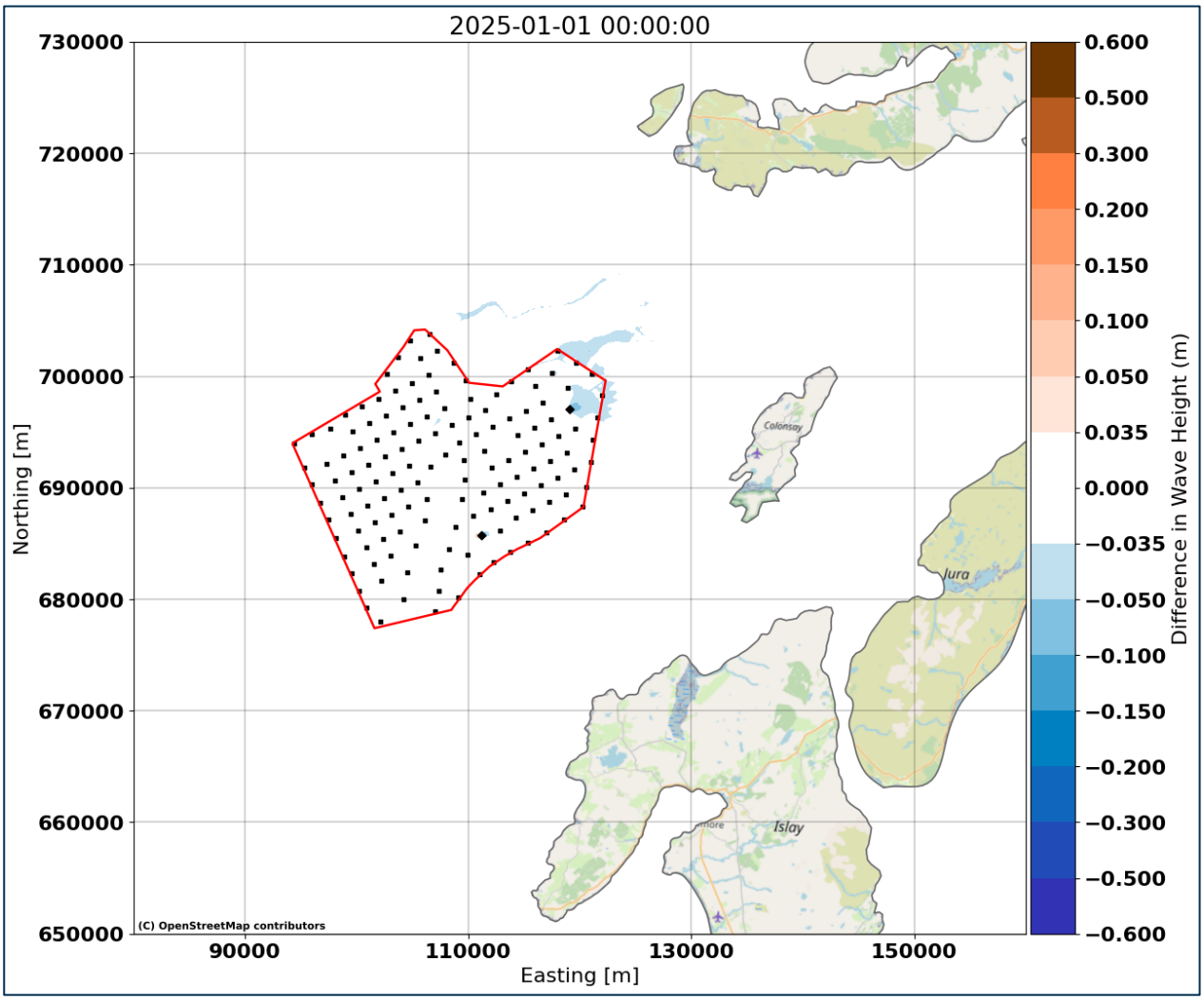

Figure 4-40: Difference in wave height (m) for 1 in 50 year from 240°N – 15 MW even spread monopile

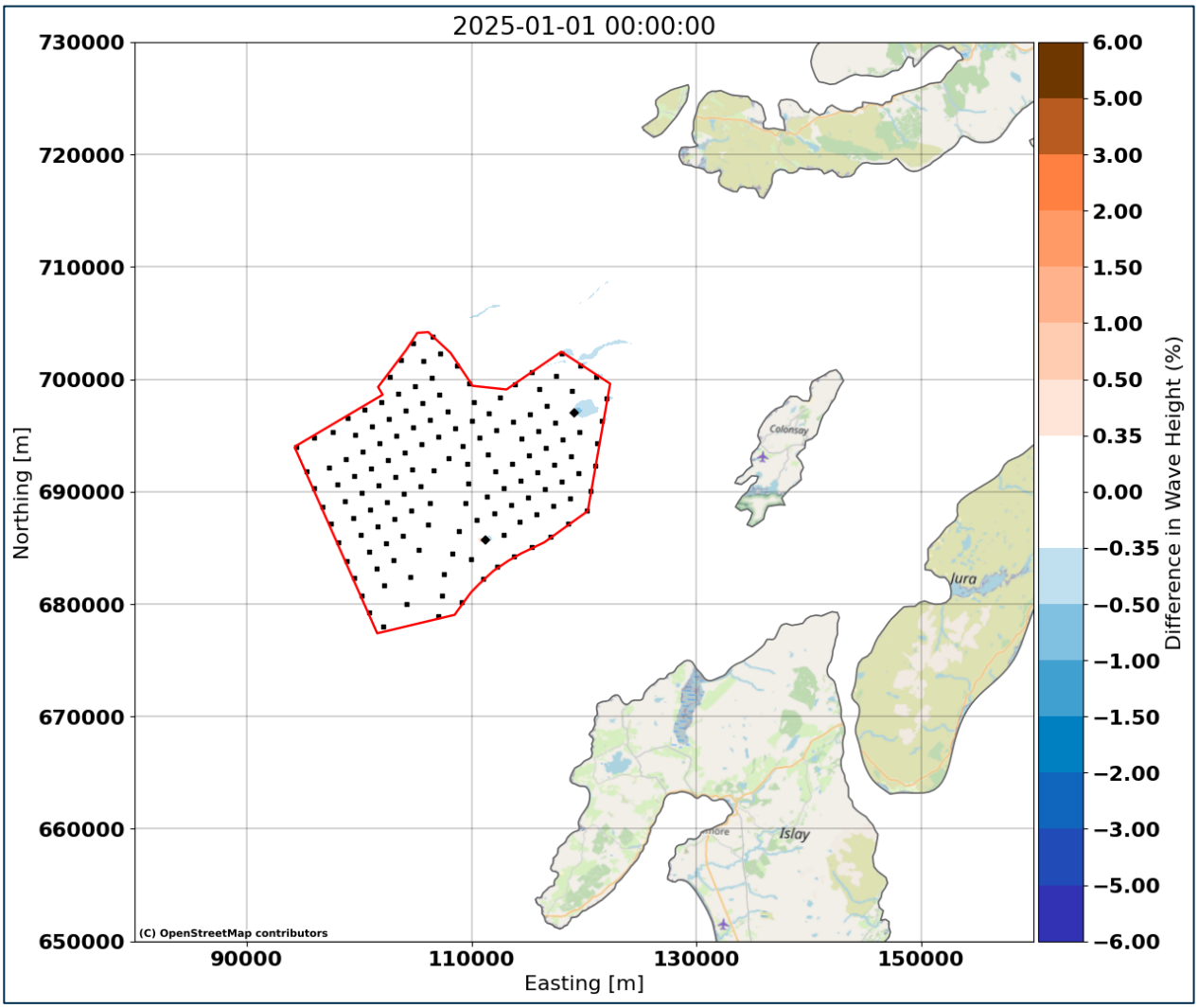

Figure 4-41: Difference in wave height (%) for 1 in 50 year from 240°N – 15 MW even spread monopile

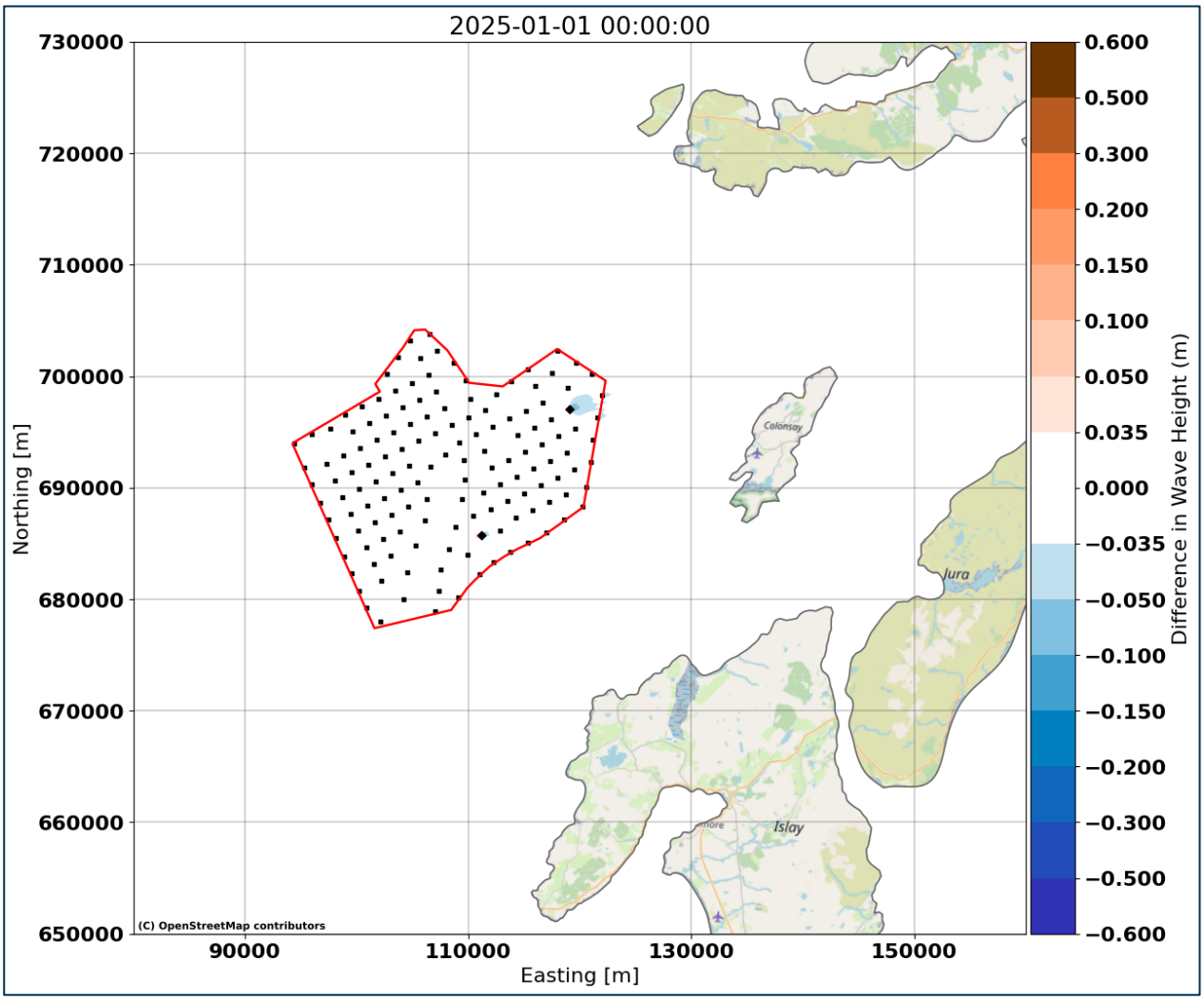

Figure 4-42: Difference in wave height (m) for 1 in 100 year from 240°N – 15 MW even spread monopile

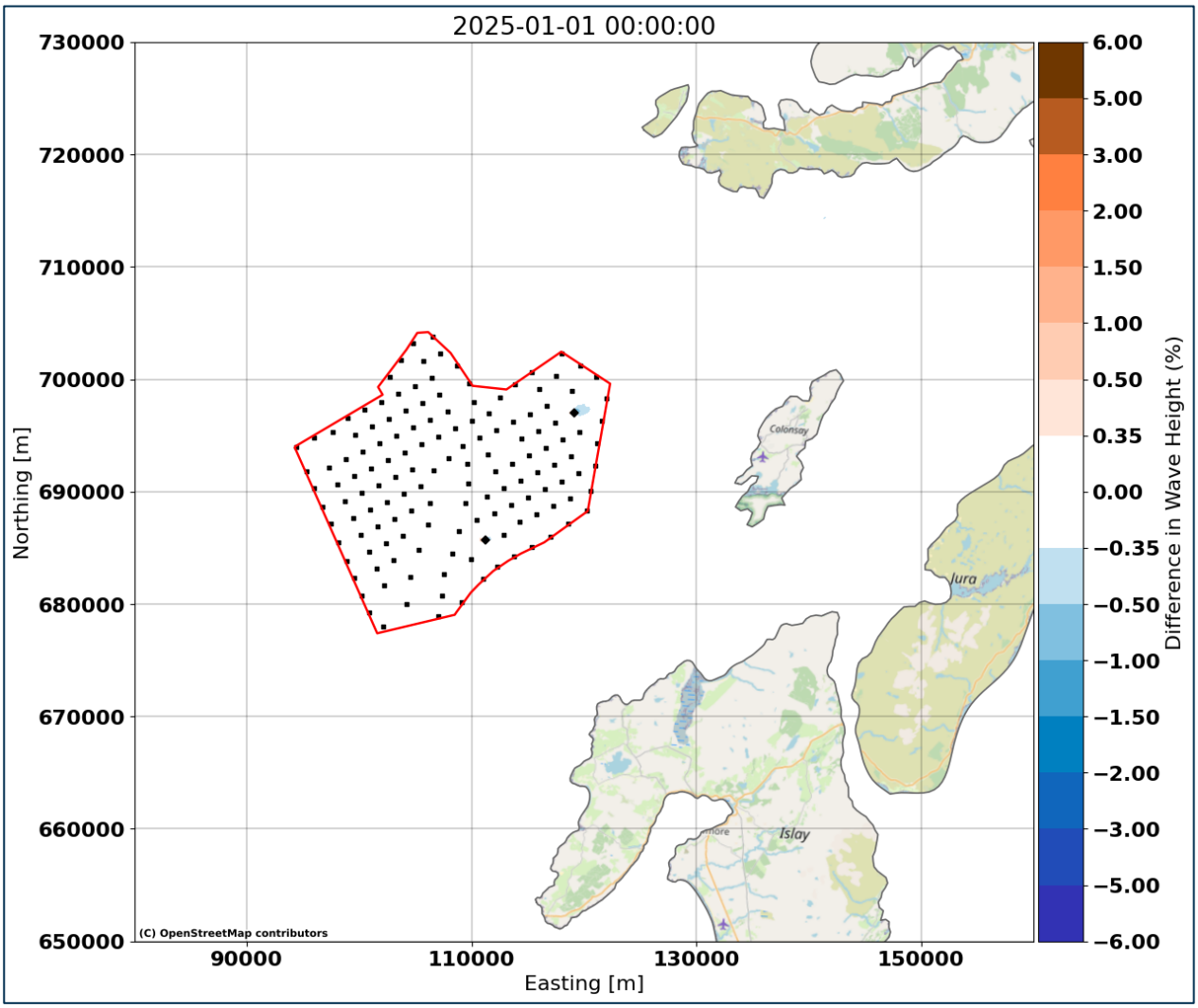

Figure 4-43: Difference in wave height (%) for 1 in 100 year from 240°N – 15 MW even spread monopile

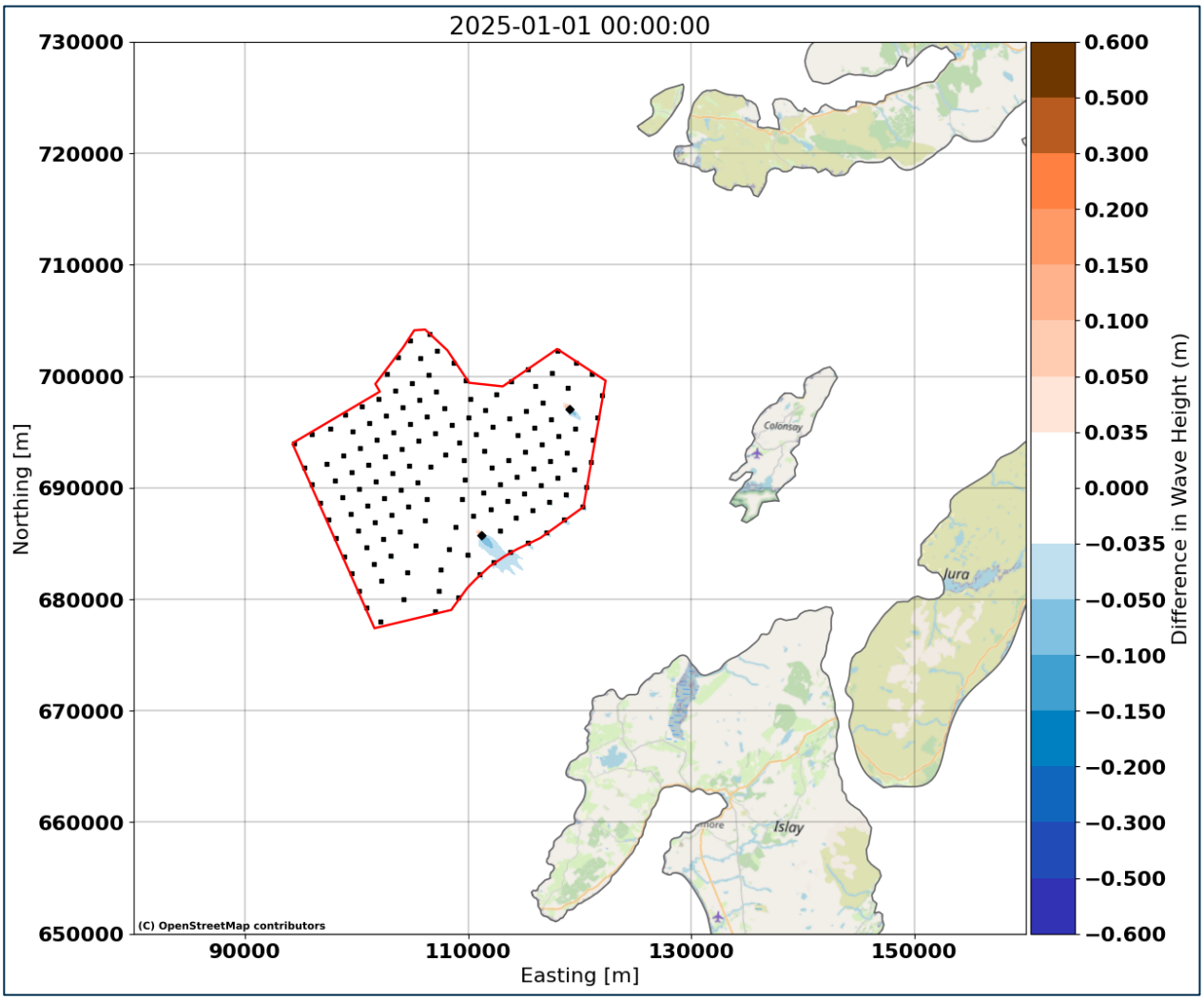

Figure 4-44: Difference in wave height (m) for 1 in 1 year from 330°N – 15 MW even spread monopile

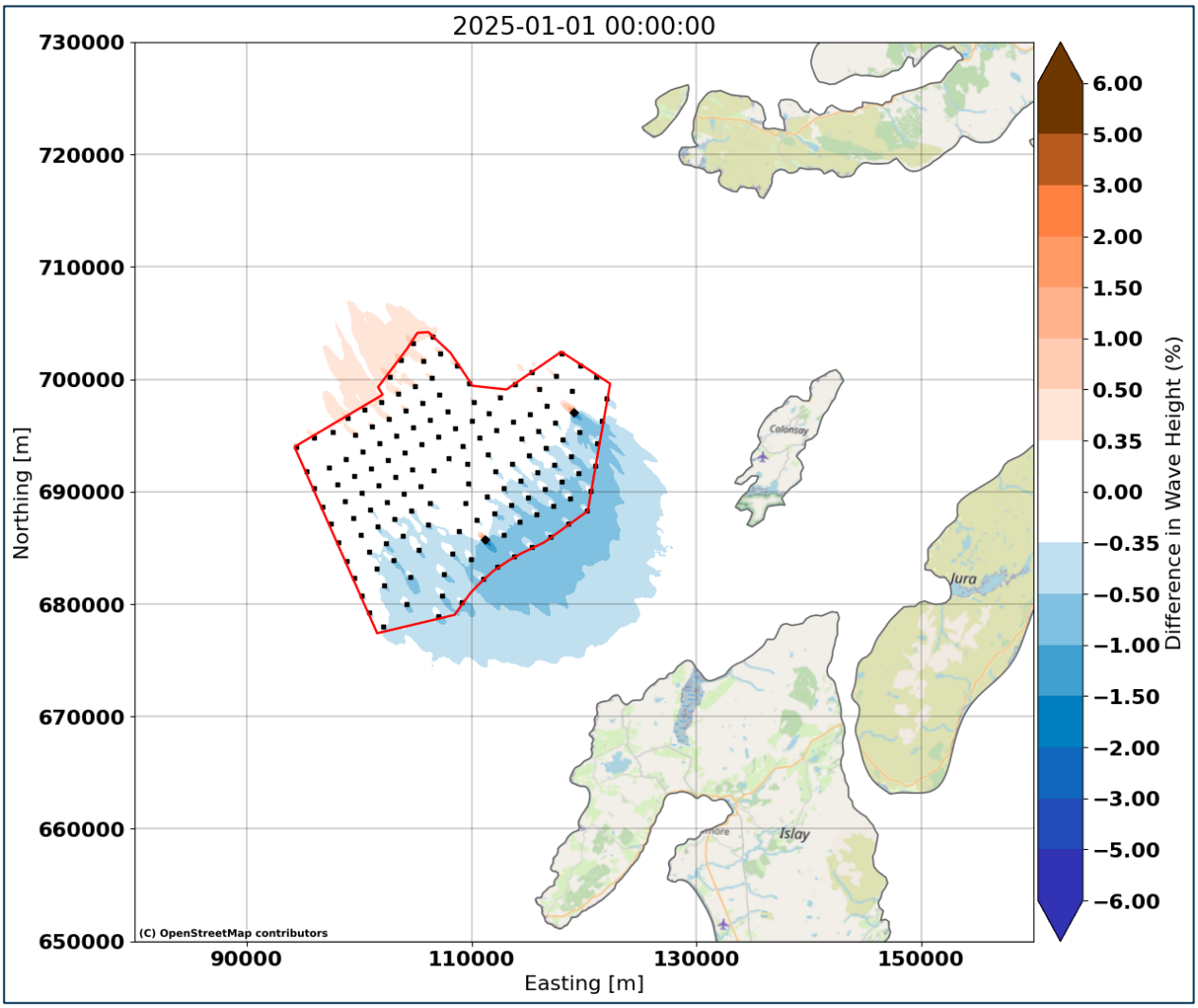

Figure 4-45: % difference in wave height (m) for 1 in 1 year from 330°N – 15 MW even spread monopile

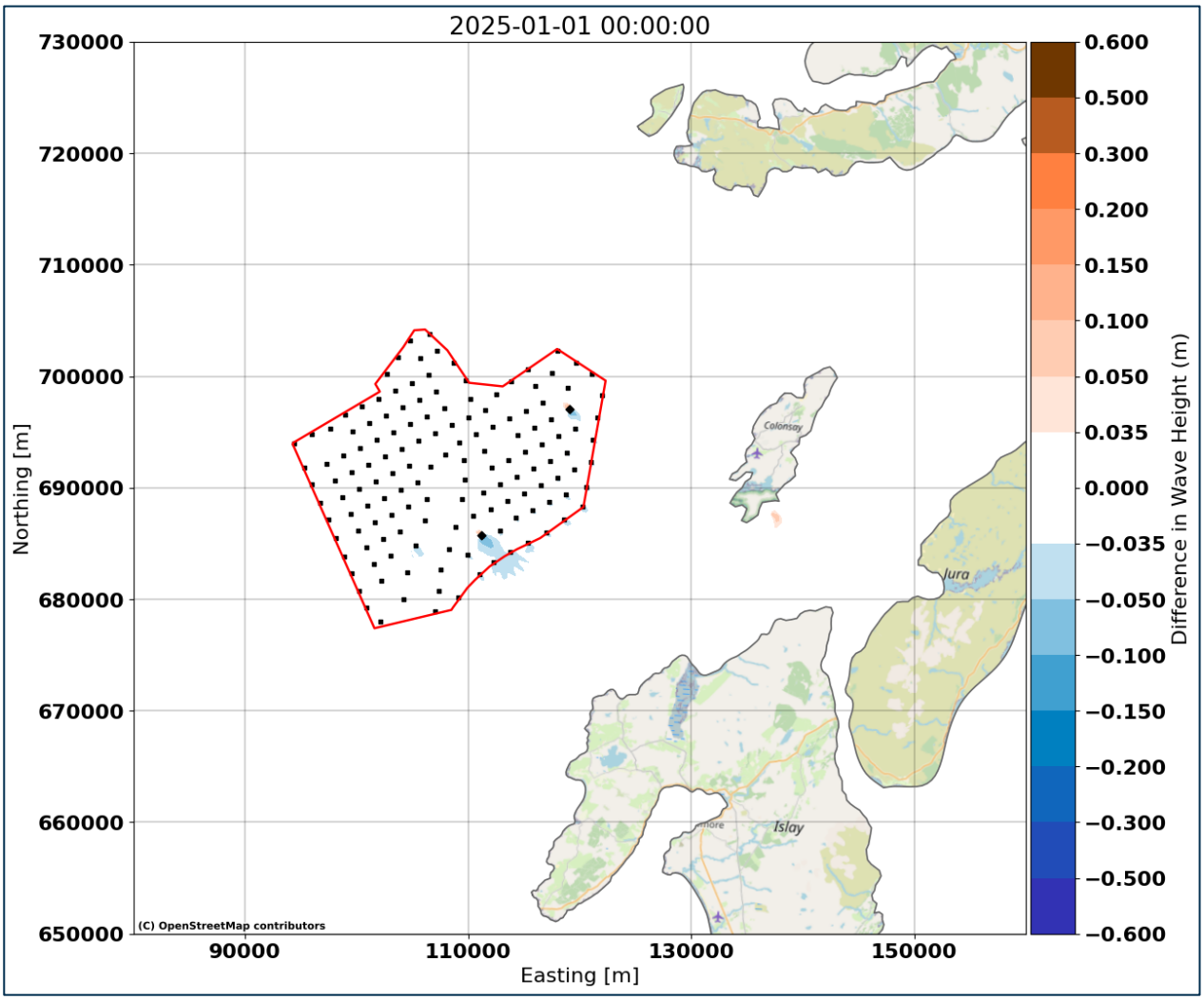

Figure 4-46: Difference in wave height (m) for 1 in 50 year from 330°N – 15 MW even spread monopile

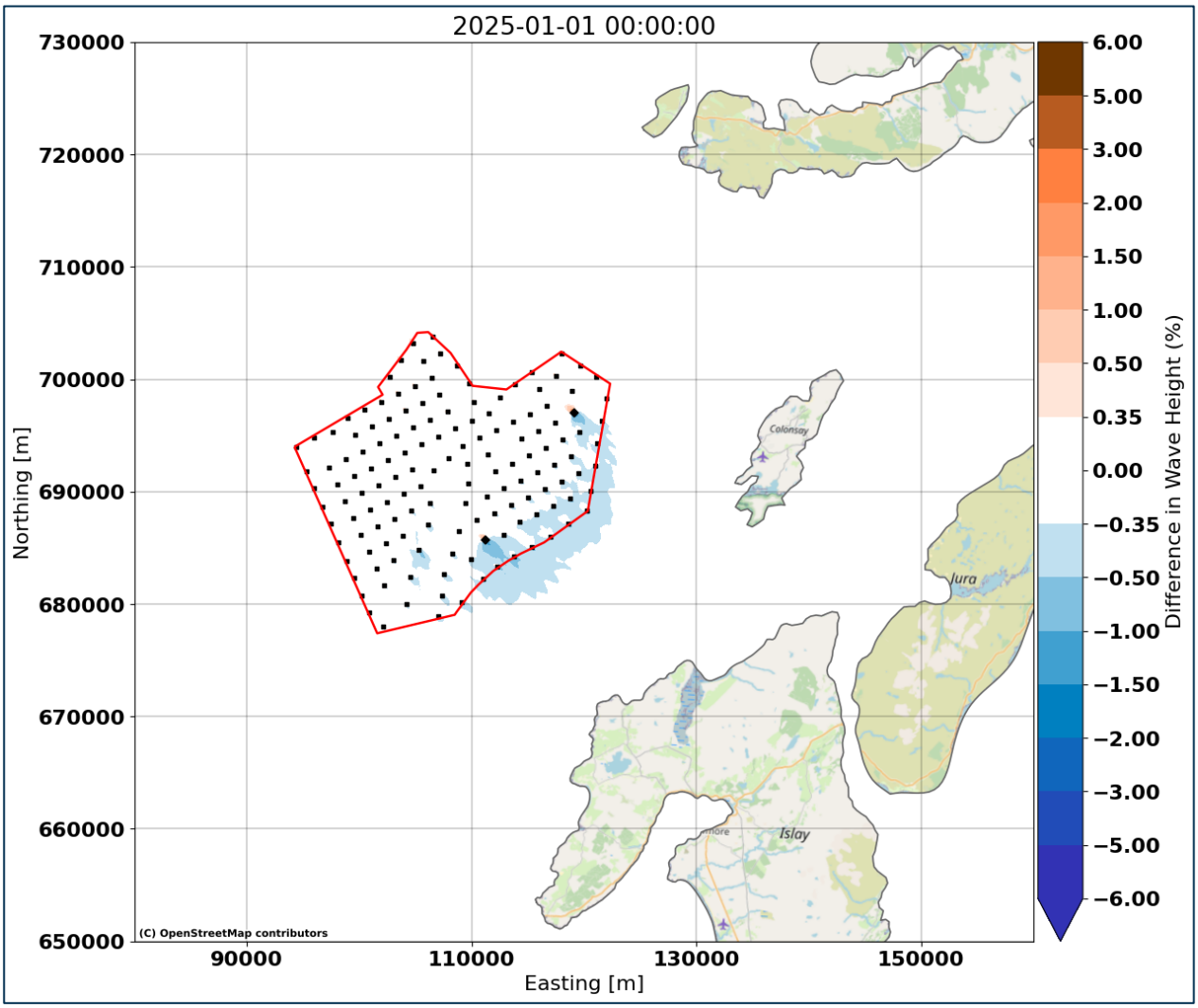

Figure 4-47: % difference in wave height (m) for 1 in 50 year from 330°N – 15 MW even spread monopile

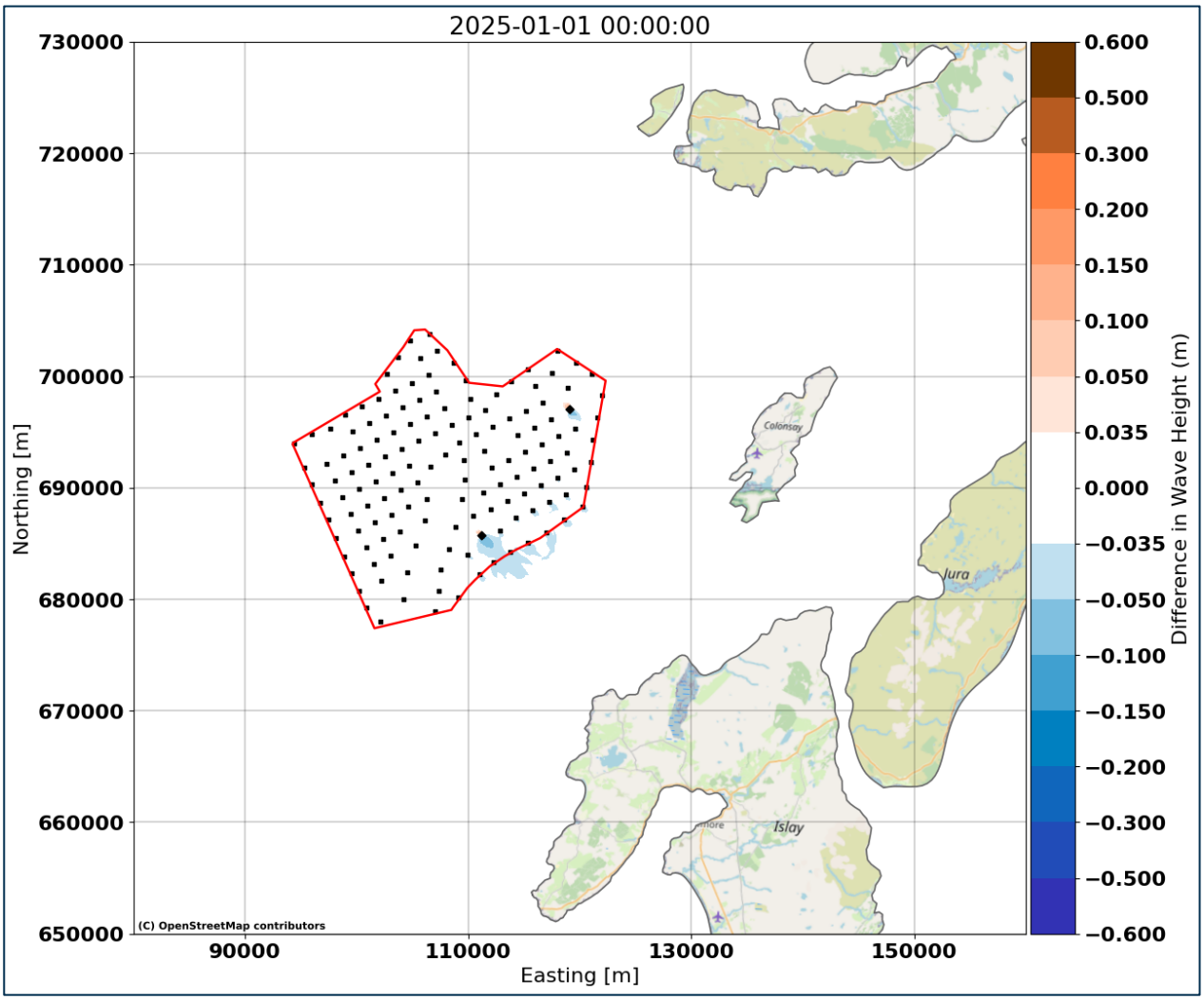

Figure 4-48: Difference in wave height (m) for 1 in 100 year from 330°N – 15 MW even spread monopile

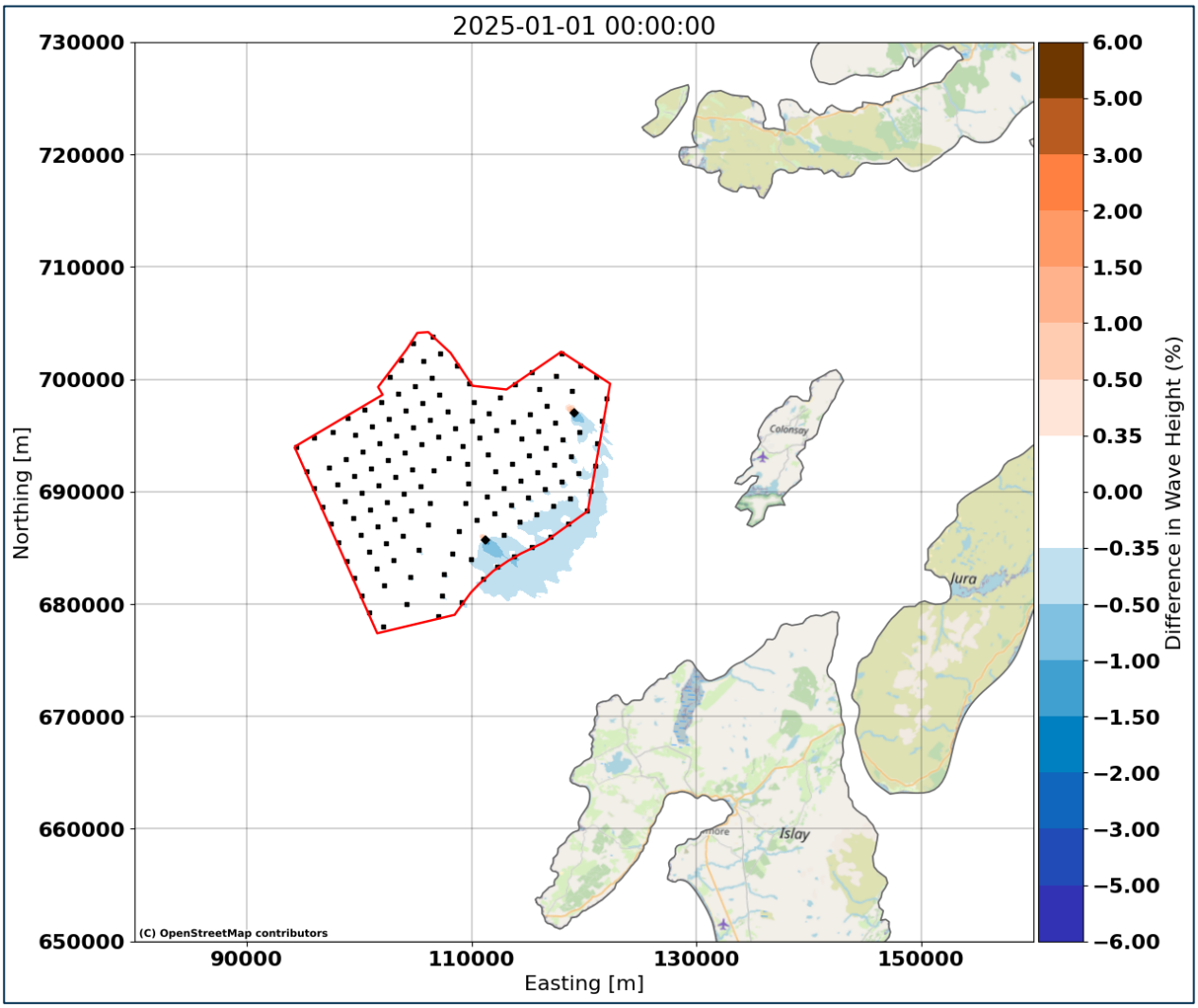

Figure 4-49: % difference in wave height (m) for 1 in 100 year from 330°N – 15 MW even spread monopile

4.4 Summary and Conclusions on Wave Modelling

4.4.1 A wave transformation modelling study has been undertaken using MIKE21 SW, to investigate the potential effect of the WDA on the surrounding wave climate, in which, results will supplement the relevant EIA chapters.

4.4.2 The study included the successful development, calibration and validation of a MIKE21-SW model, where the predicted wave climate showed good agreement with measured data at the two project survey sites, S1 (Hs, RMSE = 0.31 m, SI = 14.27%) and S2 (Hs, RMSE = 0.31 m, SI = 14.92%), as well as the Blackstone's wave buoy (Hs, RMSE = 0.30 m, SI = 12.86%). The model calibration was deemed suitable to be taken forward to the assessment simulations for the WDA, in line with the 'Design' criteria (RMSE <= 0.3 m OR SI <20%) set out in Jacobs and EA (2022) guidance to numerical modelling in the coastal zone.

4.4.3 This calibrated and validated model was applied to the assessment simulations for the WDA, where the worst-case wave directions (240°N and 330°N) and worst-case layout (15 MW even

spread monopile) were established, before simulating these for the 1 in 1 year, 1 in 50 year and 1 in 100 year return periods.

4.4.4 Model results showing absolute and percentage difference in wave climate (layout – baseline) due to the WDA, indicate that the most pronounced impact on wave climate occurs during the 1 in 1 year return period for waves from 330°N. In this case, the percentage difference in wave height reaches 0.5% - 1%, extending up to 5 km SE of the WDA. In addition to this, the percentage difference of 0.35% - 0.5% extends up to 12 km SE of the WDA. However, it is important to note that the threshold of >0.35% does not extend as far as the coastline in this direction.

4.4.5 Similarly for waves from 240°N, the most pronounced change is predicted for the 1 in 1 year return period, where a percentage difference in wave height of 0.5% - 1% is predicted to extend up to 1.5 km NE of WDA and 0.35% - 0.5% is predicted to extend up to 10 km NE of the WDA. Although the results demonstrate that a percentage difference of >0.35% does not reach the coastline.

4.4.6 For the 1 in 50 year and 1 in 100 year return periods, the predicted percentage differences in wave climate are notably reduced. Here, the 0.5% - 1% change remains contained entirely within the WDA boundary, and the 0.35% - 0.5% difference extends only as far as 3 km SE of the WDA for waves from 330°N and is almost entirely contained within the WDA for waves from 240°N.

4.4.7 Overall, the wave transformation modelling study demonstrates that the influence of the worst-case monopile layout on local wave heights is <1% outside of the boundary of the WDA, and along coastal regions in the wake of the WDA is <0.35%.

4.4.8 On the uncertainty surrounding modelled extreme wave climate at the site, model calibration showed good agreement between measured and modelled data for the largest storms in the calibration window (2023 – 2024), where wave heights up to 8.5 m were measured. In addition to this, the validation of the MetOffice boundary conditions suggested that there was no clear bias between measured (M4 wave buoy) and modelled data at the offshore location, indicating no clear over or underestimation of extreme wave heights.

4.4.9 Despite the good agreement at the extremes between measured and modelled data, it is important to note that the extreme wave climate derived in this report should not be used for design conditions of the Project infrastructure, and rather is used in this case to model the change in wave climate due to the WDA layout.

4.4.10 In addition to this, the wave modelling study has demonstrated that the largest change in wave climate due to the WDA was for the extreme event with the lower Tp and therefore wave height (1 in 1 year, 330°N), where both the model calibration and validation showed good agreement between measured and modelled data for these wave events.

5 Hydrodynamic Modelling

5.1 Model Development

Model Mesh and Bathymetry – Regional Model

5.1.1 The computational mesh consists of 292,000 elements and 143,000 nodes. As the regional model was developed for simulation of the large-scale circulation patterns, the mesh resolution is relatively coarse, ranging from 1 km to 5 km. In general, the grid resolution increases towards the coastline to capture the effect of nearshore shallow water (see **Figure 5-1**).

5.1.2 The model bathymetry and grid were constructed based on EMODnet bathymetry data and Admiralty Maritime Data Solutions' data with coastline positions digitized from Google Earth. The model bathymetry, shown in **Figure 5-2** was created by combining the bathymetric data.

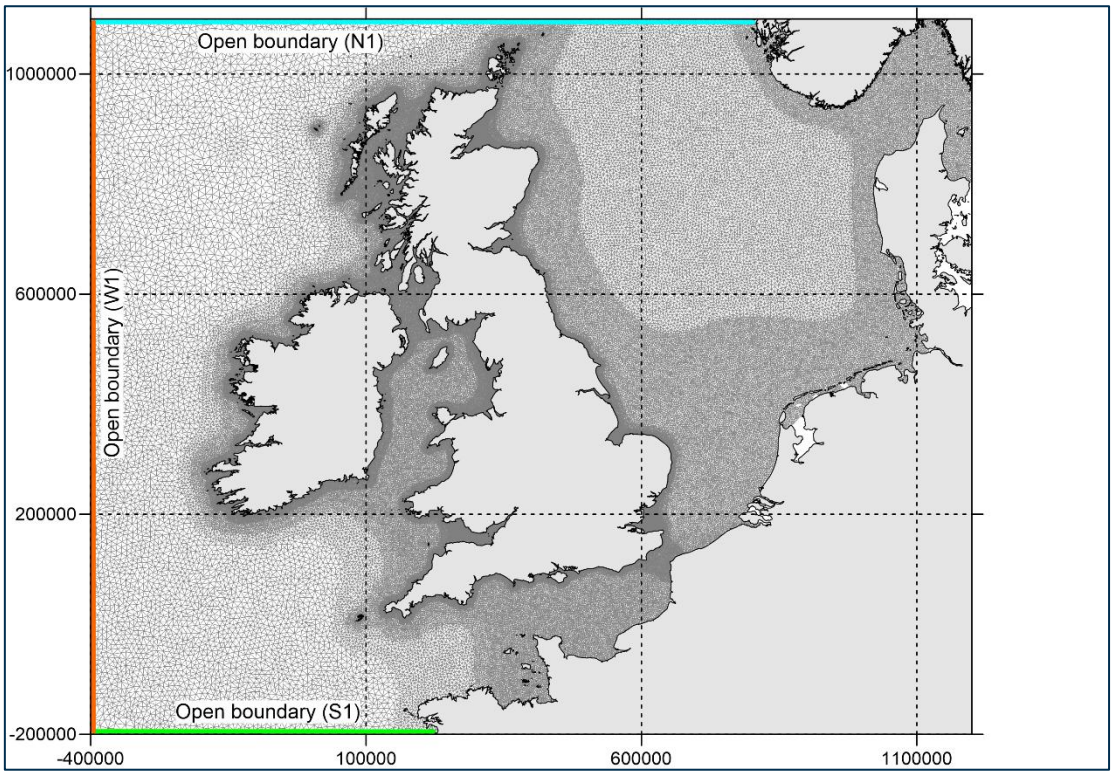

Figure 5-1: Computational mesh of the regional HD model

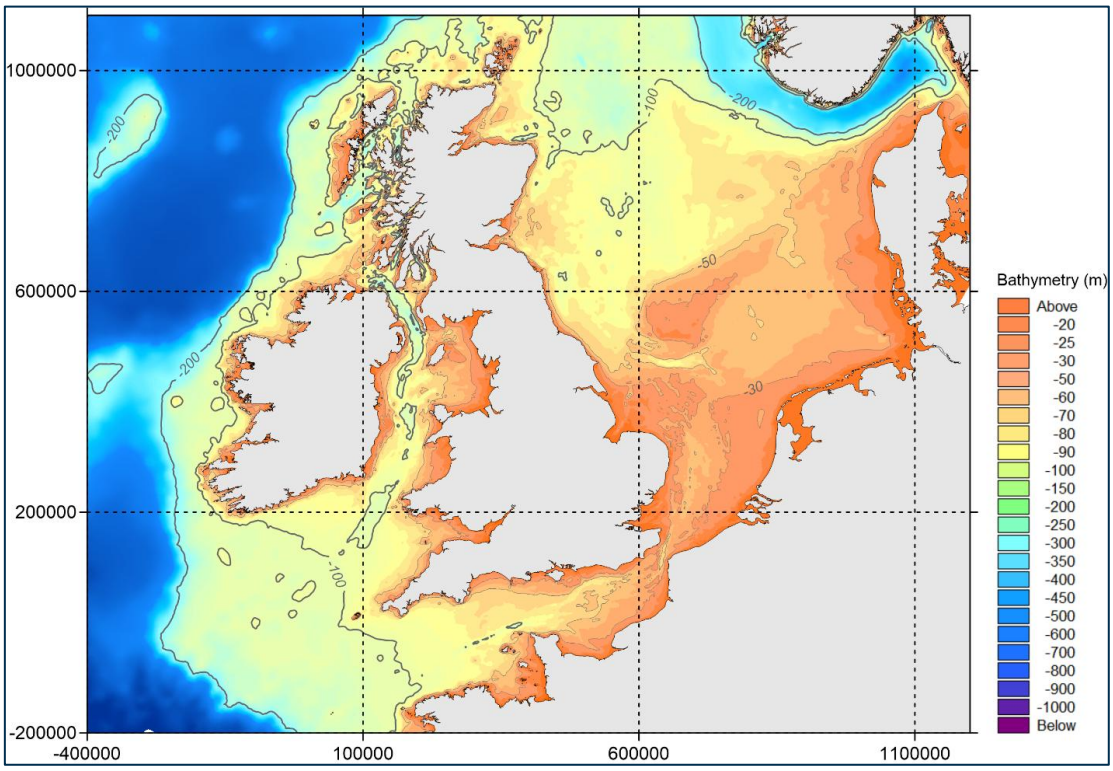

Figure 5-2: Regional HD model bathymetry m Mean Sea Level (MSL)

Local Model

5.1.3 Like the regional model, the flexible mesh was adopted in the local model. A coarser grid (500 - 1000 m) was used in remote areas and a finer grid (100-150 m) in the areas of interest.

5.1.4 The computational mesh for the model calibration consists of 141,835 elements and 76,402 nodes (see **Figure 5-3**) and bathymetry shown in **Figure 5-4**.

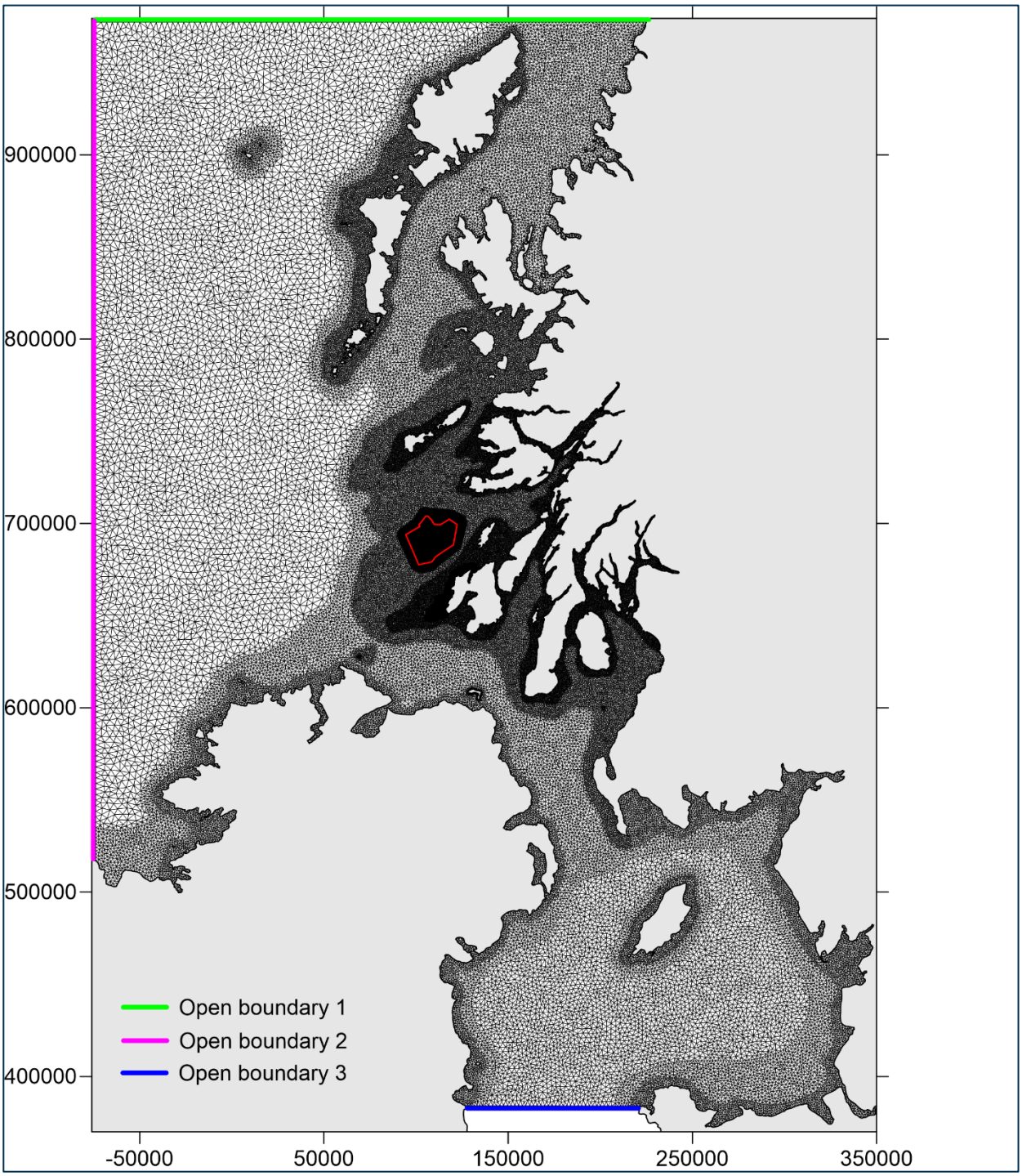

Figure 5-3: Local model computational mesh (red line indicates the proposed WDA)

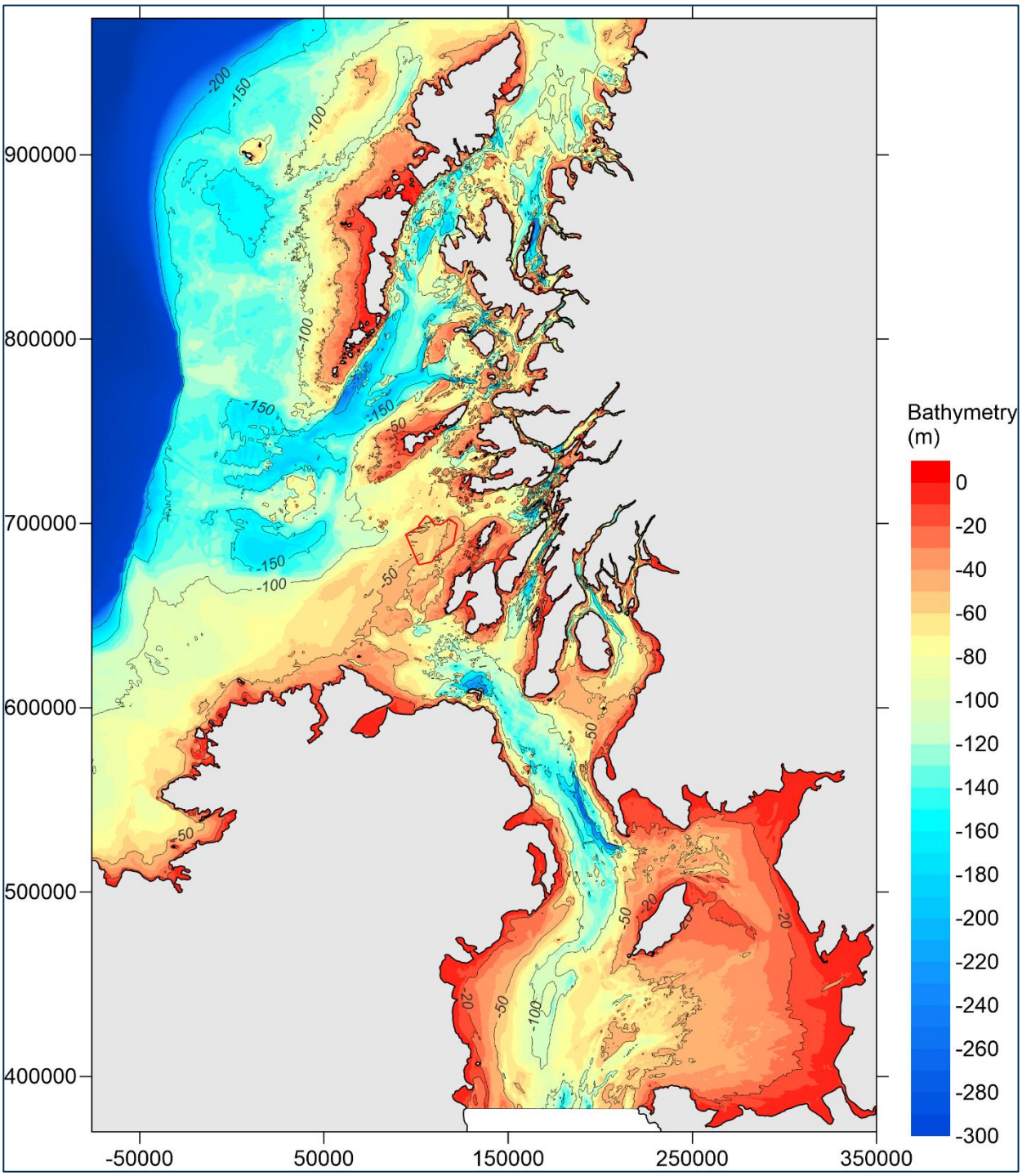

Figure 5-4: Bathymetry of the local model domain (referenced to ODN) (red line indicates the proposed WDA)

Boundary Conditions

5.1.5 At the open boundaries of the regional model, water levels were used, which vary in time and along the boundaries. The input data for these boundaries were extracted (at locations N1, S1 and W1 as in **Figure 5-1**) from the Global Tidal Model of DHI with a spatial resolution of 0.25° × 0.25°. The data represents the major diurnal (K1, O1, P1 and Q1) and semidiurnal tidal constituents (M2, S2, N2 and K2) based on OPEX/POSEIDON altimetry data.

5.1.6 **Figure 5-3** shows the boundaries of the local model. The open boundary is set as velocity and water level boundaries varying in time. The velocity and water level along these boundaries were extracted from the regional model.

5.2 Model Calibration and Validation

Approach

5.2.1 After reviewing the survey of bathymetry data and velocity measurements within the WDA, a 2D hydrodynamic model was adopted for calibration, instead of a 3D model and for assessing the impact of the windfarm on hydrodynamics for the following reasons:

- Analysis of the measured current speed and direction data reveals small vertical variation, particularly between surface and middle layers. Both sites demonstrate almost uniform flow characteristics throughout the water column (see **Figure 5-5** to **Figure 5-8**). The WDA has an approximate average water depth of 50 - 55 meters.

- The current regime at both Site 1 and Site 2 is predominantly influenced by tidal forces. At Site 1, tidal currents account for approximately 90% of the total flow velocity, and over 98% at Site 2 (see Sections 7.4 and 7.10 of the survey report – **Ref 6**). A 2D hydrodynamic model is sufficient to simulate the tidal current regime in the WDA. This approach offers reliable results while optimizing computational efficiency.

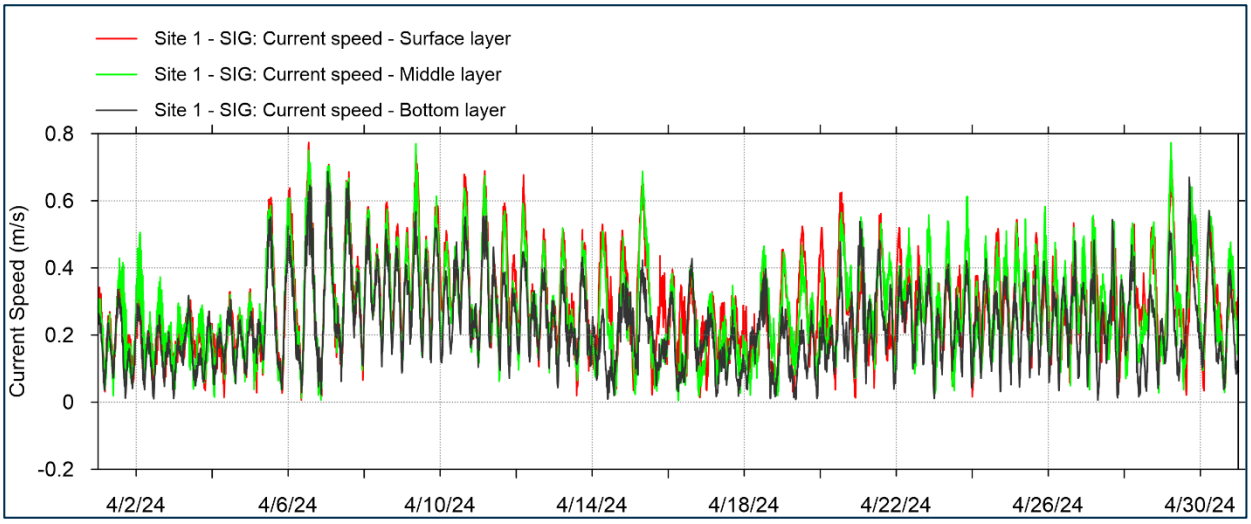

Figure 5-5: Current speed measurements at three depths (bottom, middle, surface) at Site 1 - SIG station, April 2024.

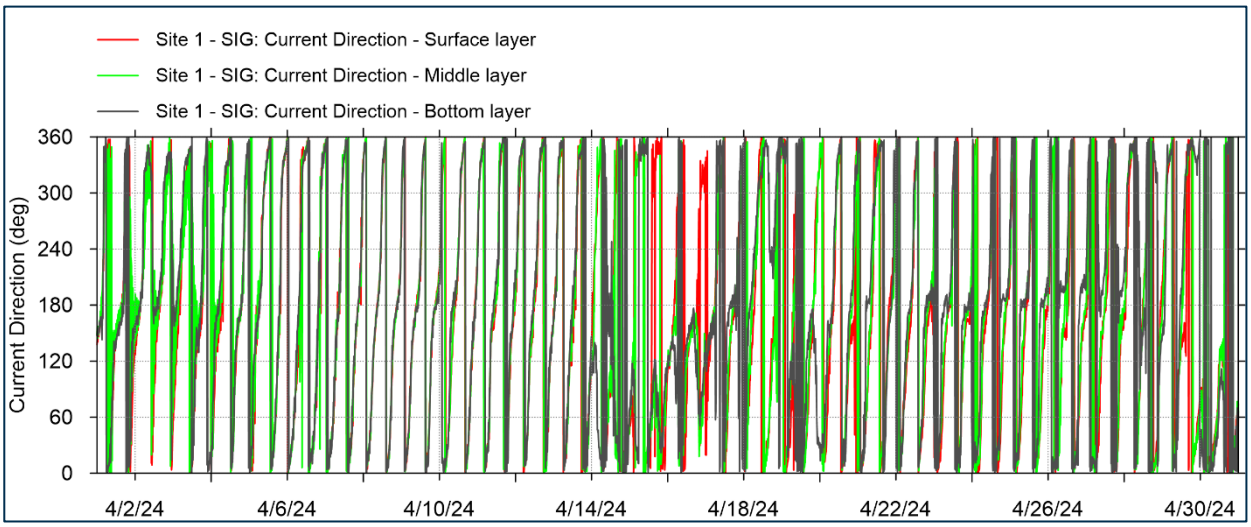

Figure 5-6: Current direction measurements at three depths (bottom, middle, surface) at Site 1 - SIG station, April 2024.

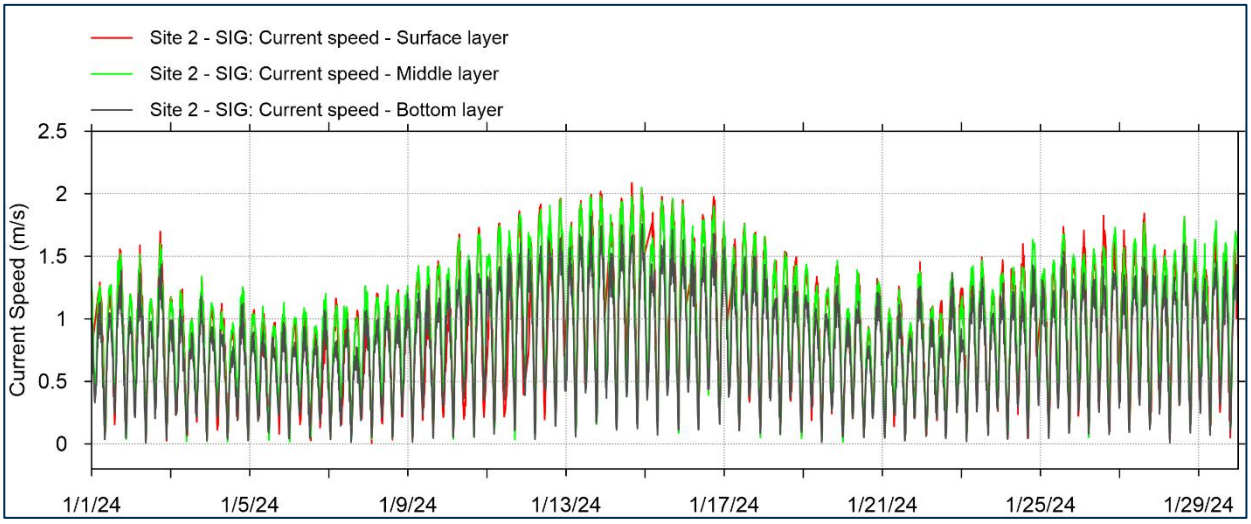

Figure 5-7: Current speed measurements at three depths (bottom, middle, surface) at Site 2 - SIG station, January 2024.

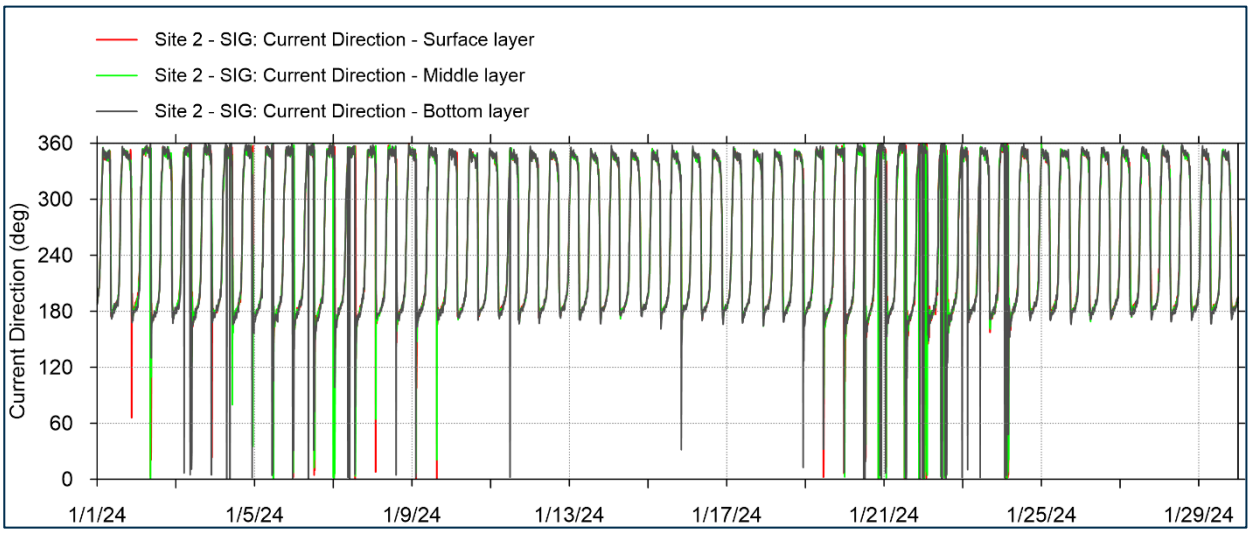

Figure 5-8: Current direction measurements at three depths (bottom, middle, surface) at Site 2 - SIG station, January 2024.

Quantifying Model Error / Uncertainty

5.2.2 Error and uncertainty of the MIKE21-HD model is assessed using a variety of statistical parameters, comparing the modelled and measured water levels and current speeds. These are based on guidance from the EA in 2022 (**Ref 7**) and ABPmer (2013) (**Ref 1**), where both documents have been widely used in metocean studies around the UK and the latter is adopted by National Resources Wales (NRW) for the application of numerical models in the coastal zone.

5.2.3 The parameters used are mean error 'ME' (m), root mean square error 'RMSE' (m), standard deviation 'Std' (m) and correlation coefficient 'R'. These parameters are assessed on a simulation of a full spring-neap tidal cycle.

5.2.4 For comparison of water levels, the required statistical error for model calibration is variable between each guidance document. The EA (2022) set out a requirement of RMSE <= 0.1 m for 'Design', 'Appraisal' and 'Strategic' applications of the hydrodynamic model. However, it requests error statistics are calculated for a length of >19years, 5-19 years and >1 year for 'Design', 'Appraisal' and 'Strategic' applications respectively. In this study, only the tide data recorded at Portrush covers a period greater than a year. Whereas the ABPmer (2013) states that water level differences between measured and modelled should be within +/- 0.2 m and percentage water level differences should be within 15% of spring tidal ranges and 20% of neap tidal ranges. Yet, additional guidance is given that optimal model calibration would be achieved if water level differences between measured and modelled values were within 10 cm, 10% or RMSE <0.1 m, although these values depend on the actual tidal range at the site.

5.2.5 For comparison of current speeds, EA (2022) do not state any specific requirements for error levels in model calibration. The ABPmer (2013) study suggested that adequate model calibration is achieved if modelled flow speeds are within 0.2 m/s or +/- 10% – 20% measured speeds. Although it is stated that these values are dependent on the actual magnitude of current speeds. When applying the hydrodynamic model to assessment scenarios, the uncertainty envelope due to errors in modelled current speeds should be clearly defined.

Regional Model Calibration (Water Level)

5.2.6 For this study, the regional model has been re-calibrated using measured water levels recorded at Site 1 - ASG and Site 2-ASG in July 2023 and January 2024. Water level calibration results for the Portrush station are available for May 2023 and January 2024.

5.2.7 Re-calibration performance is assessed by both visual comparison and quantifying errors using statistical parameters including Correlation Coefficient and RMSE . **Figure 5-9** to **Figure 5-14** show the modelled and measured water levels and **Table 5-1** and **Table 5-2** show calculated statistics.

5.2.8 Comparing the model error statistics to the guidance set out above, the calibration at Portrush (where over one year data is available) is shown the meet the required error set out in both the EA (2022) and ABPmer (2013) guidance, with a RMSE of 0.09 m.

5.2.9 At S1 for both spring and neap tide the RMSE is <= 0.1 m, which satisfies the ABPmer (2013) guidance. At S2 the RMSE is 0.13 m and 0.12 m for spring and neap tide phases, respectively. Although this is slightly above the 0.1 m RMSE guidance set out by ABPmer (2013), these values remain within the 10% of the spring (4 m) and neap (2 m) tidal ranges. Therefore, it can be concluded that the regional model performs well in recreating measured water levels at the WDA and surrounding areas.

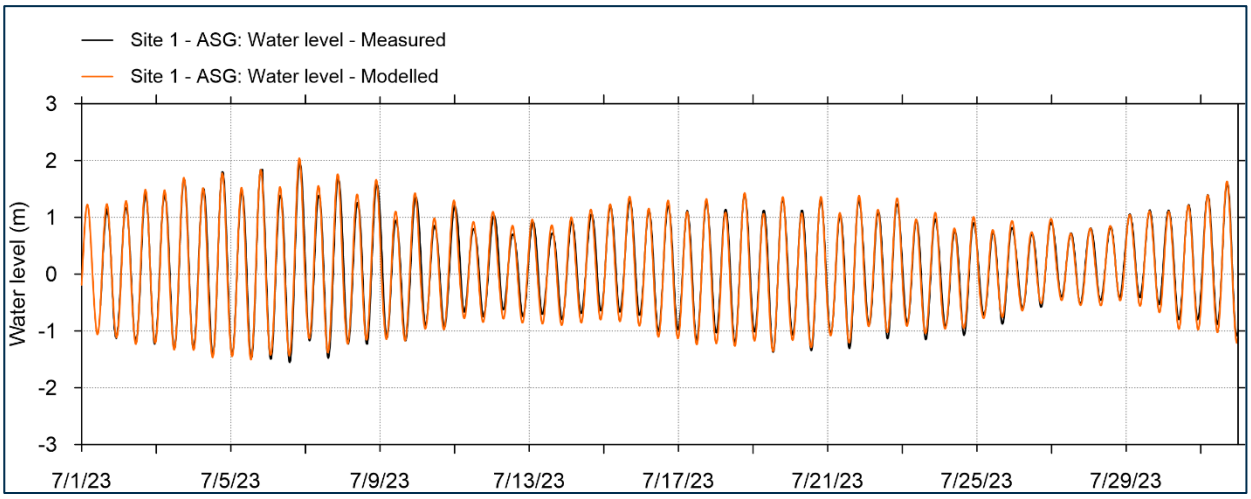

Figure 5-9: Time series comparison between simulated vs observed water levels at Site 1 - ASG in July 2023 (Regional model)

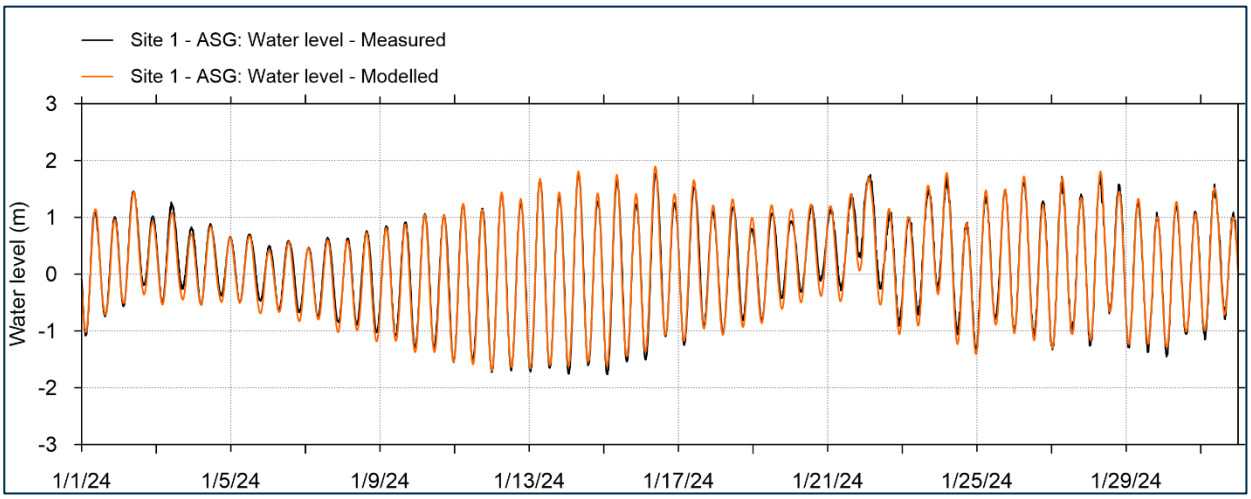

Figure 5-10: Time series comparison between simulated vs observed water levels at Site 1 - ASG in January 2024 (Regional model)

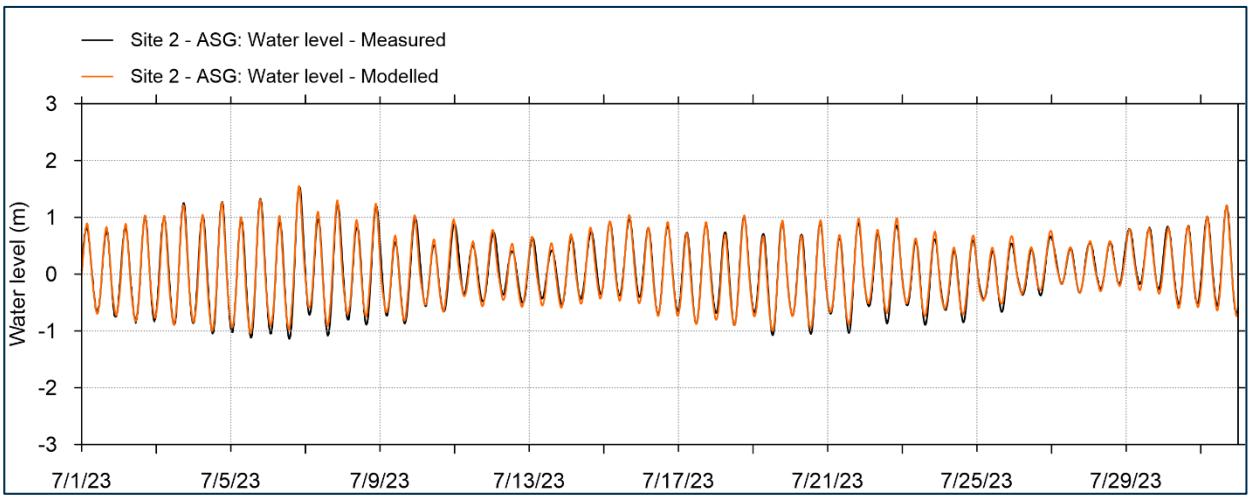

Figure 5-11: Time series comparison between simulated vs observed water levels at Site 2 - ASG in July 2023 (Regional model)

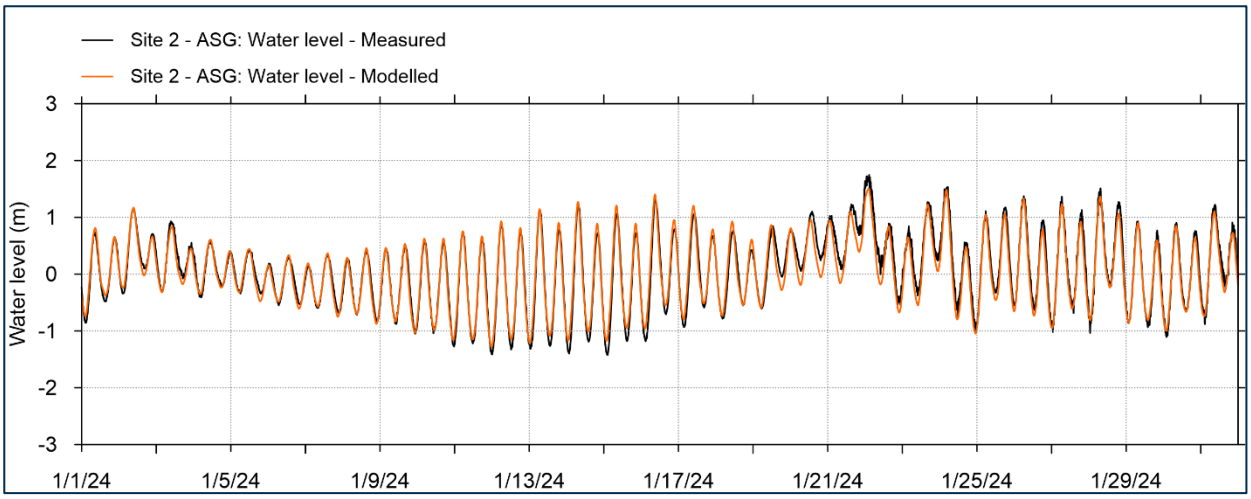

Figure 5-12: Time series comparison between simulated vs observed water levels at Site 2- ASG in January 2024 (Regional model)

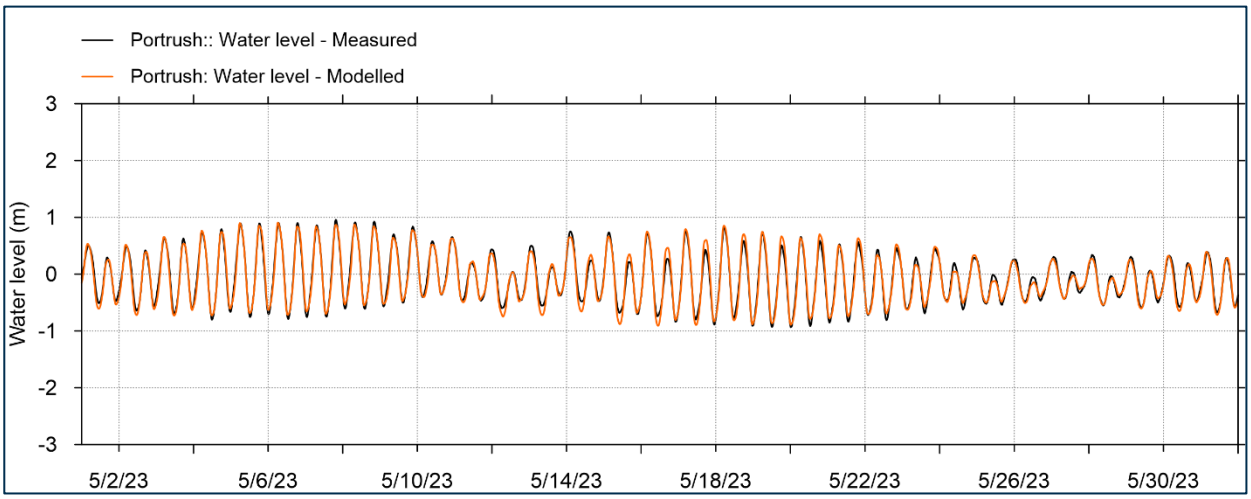

Figure 5-13: Time series comparison between simulated vs observed water levels at Portrush in May 2023 (Regional model)

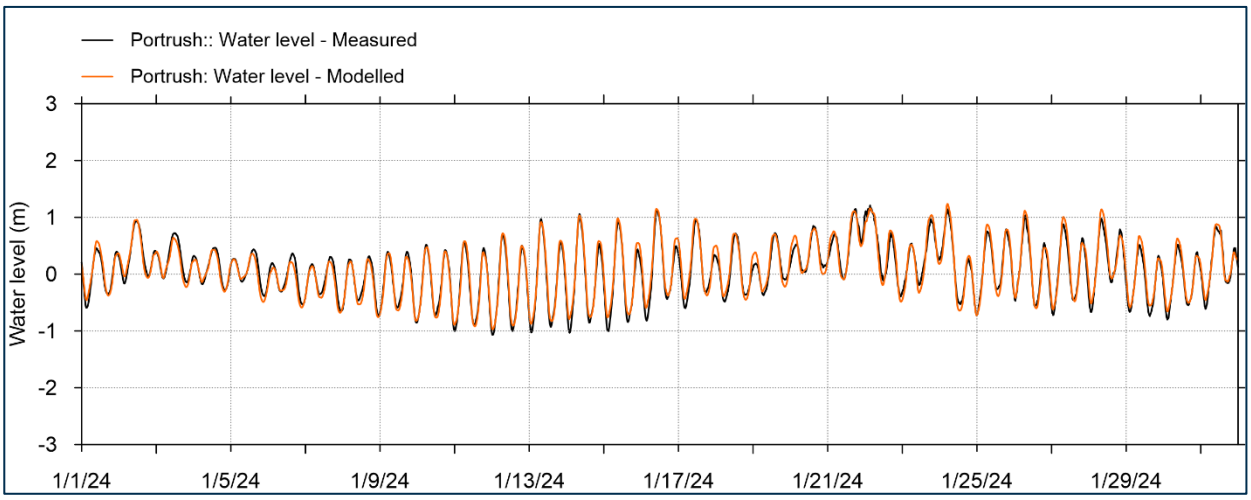

Figure 5-14: Time series comparison between simulated vs observed water levels at Portrush in January 2024 (Regional model)

Table 5-1: Model errors in water level during spring tide (Regional model)

Name of station	ME (m)	RMSE (m)	Std (m)	R
Site 1 - ASG	-0.04	0.10	0.10	0.99
Site 2 - ASG	-0.07	0.13	0.10	0.97
Portrush	-0.01	0.10	0.08	0.98

Note: *ME: Mean Error; RMSE: Root Mean Square Error; Std: Std. dev of Residuals; R: Coefficient of Determination*

Table 5-2: Model errors in water level during neap tide (Regional model)

Name of station	ME (m)	RMSE (m)	Std (m)	R
Site 1 - ASG	-0.06	0.09	0.07	0.98
Site 2 - ASG	0.01	0.12	0.12	0.95
Portrush	0.01	0.09	0.09	0.96

Note: *ME: Mean Error; RMSE: Root Mean Square Error; Std: Std. dev of Residuals; R: Coefficient of Determination*

Local Model Calibration (Water Level)

5.2.10 For this study, the local model has been calibrated using measured water levels recorded at Site 1 - ASG and Site 2-ASG in July 2023 and January 2024. Calibration performance is

assessed by both visual comparison and quantifying errors using statistical parameters including Correlation Coefficient and RMSE. Timeseries comparison of measured and modelled water levels are presented in **Figure 5-15** and **Figure 5-16** for Site 1 and **Figure 5-17** and **Figure 5-18** for Site 2. **Table 5-3** and **Table 5-4** present these model error statistics for Site 1 and Site 2, respectively.

5.2.11 At S1 for July 2023, January 2024 and both spring and neap tide the RMSE is <= 0.15 m and at S2 the RMSE is 0.15 m for July 2023 and 0.23 m for January 2024, then 0.19 m and 0.17 m for spring and neap tide phases, respectively. Although this is slightly above the 0.1 m RMSE guidance set out by ABPmer (2013), these values remain within the 10% of the spring (4m) and neap (2 m) tidal ranges. Therefore, it can be concluded that the local model performs well in recreating measured water levels at the WDA and surrounding areas.

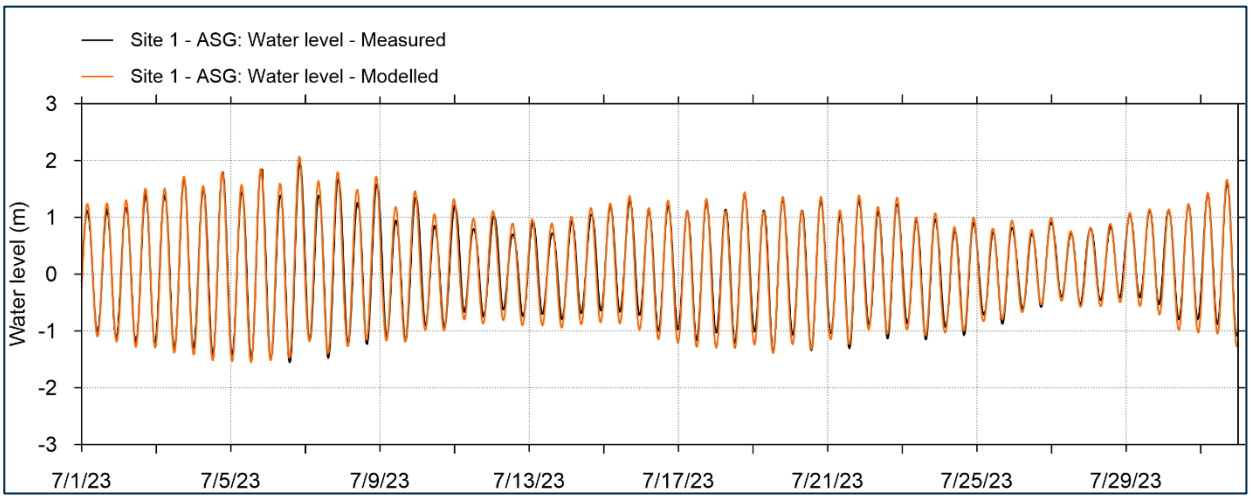

Figure 5-15: Time series comparison between simulated vs observed water levels at Site 1 - ASG in July 2023 (Local model)

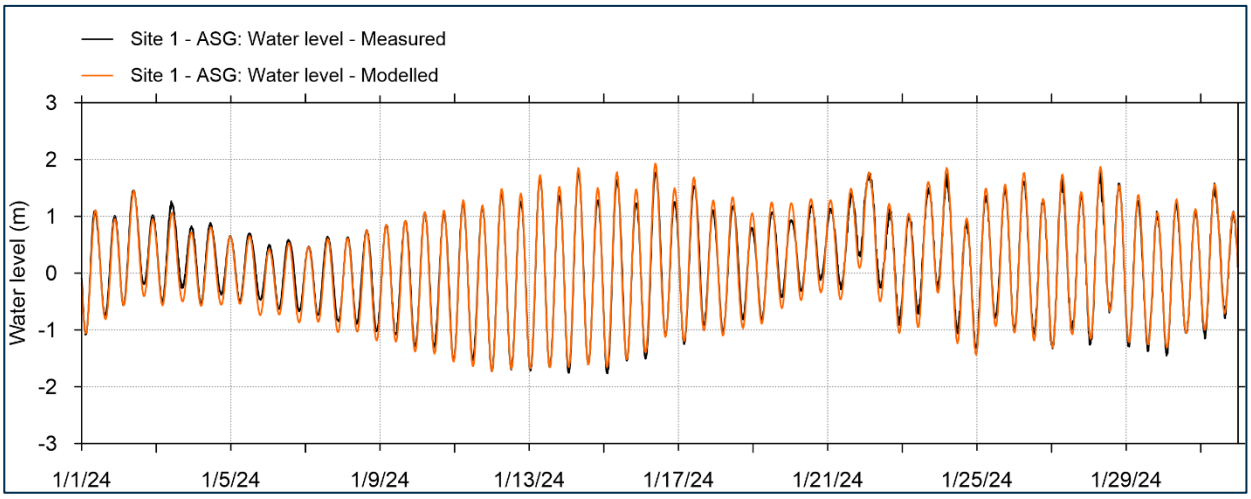

Figure 5-16: Time series comparison between simulated vs observed water levels at Site 1 - ASG in January 2024 (Local model)

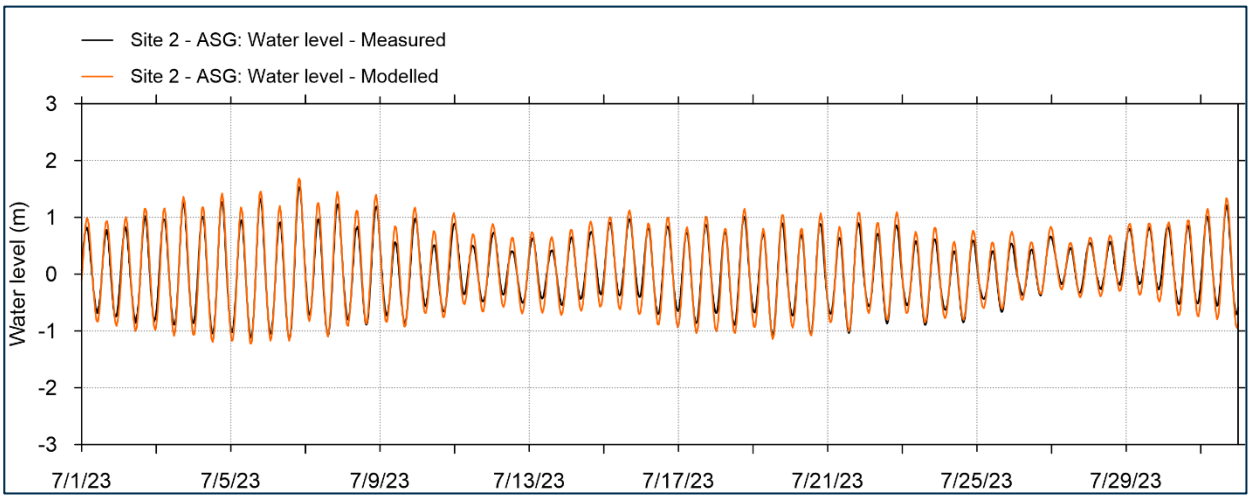

Figure 5-17: Time series comparison between simulated vs observed water levels at Site 2 - ASG in July 2023 (Local model)

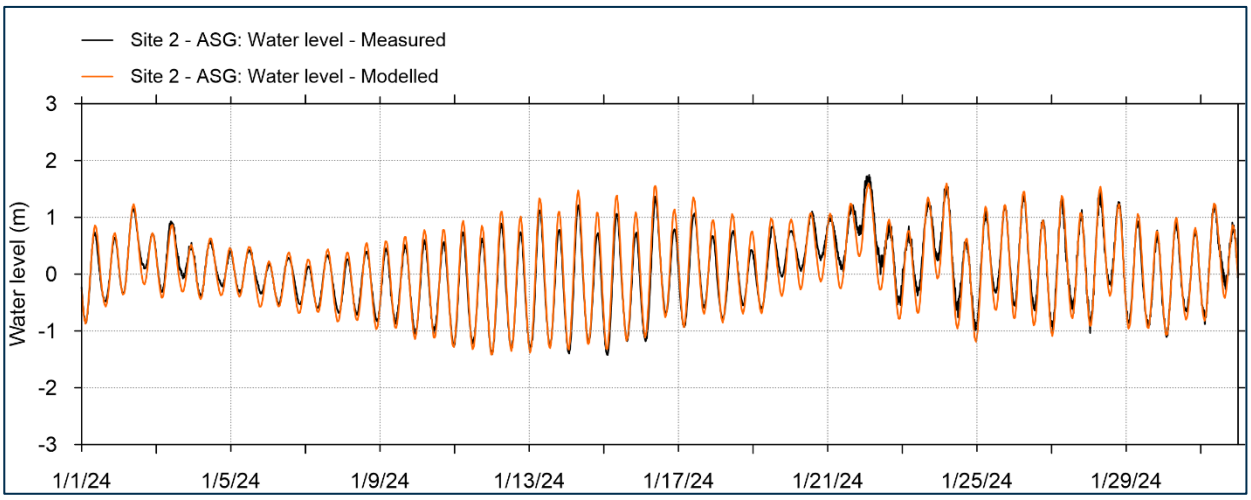

Figure 5-18: Time series comparison between simulated vs observed water levels at Site 2 - ASG in January 2024 (Local model)

Table 5-3: Model errors in water level at Site 1 – ASG (for local model)

Name of station	ME (m)	RMSE (m)	Std (m)	R
July 2023	-0.06	0.14	0.12	0.98
January 2024	-0.02	0.13	0.12	0.98
Spring tide (January 2024)	-0.06	0.11	0.09	0.99
Neap tide (January 2024)	-0.01	0.14	0.14	0.98

Note: *ME: Mean Error; RMSE: Root Mean Square Error; Std: Std. dev of Residuals; R: Coefficient of Determination*

Table 5-4: Model errors in water level at Site 2 – ASG (for local model)

Name of station	ME (m)	RMSE (m)	Std (m)	R
July 2023	-0.08	0.15	0.13	0.98
January 2024	-0.17	0.23	0.16	0.95
Spring tide (January 2024)	-0.15	0.19	0.12	0.98
Neap tide (January 2024)	-0.03	0.17	0.17	0.93

Note: *ME: Mean Error; RMSE: Root Mean Square Error; Std: Std. dev of Residuals; R: Coefficient of Determination*

Local Model Calibration (Currents)

5.2.12 The local model has been also calibrated using measured current data recorded at 5 locations (Site 1 - SIG current speed; Site 1 - SWLB current speed; Site 1 - SWM current speed; Site 2 – SIG; Site 2 - SWLB current speed).

5.2.13 The velocity data recorded at Site 1, specifically for stations SIG, SWLB, and SWM - were of low quality, which negatively impacted calibration outcomes at certain times. These data quality issues were documented in Section 7.4 of the survey report: "*On examination of the current profiles from the Nortek Signature, suspect data throughout the deployment were observed to affect bins 15 to 30, appearing as higher frequency variations than usually expected*" and "*Additionally, the SWLB current profile displayed interference in the upper 10 m of the water column throughout the deployment*".

5.2.14 Accordingly, we selected an appropriate time period for statistical analysis, excluding the period with abnormally high velocities for the velocity measurement stations at Site 1. The time periods used for statistical analysis of the measured against modelled data at Site 1 are presented in **Table 5-5** to **Table 5-7** and Site 2 are presented in **Table 5-8** and **Table 5-9**.

5.2.15 Model calibration performance is assessed by both visual comparison and quantifying errors using statistical parameters including Correlation Coefficient and RMSE. **Figure 5-19** to **Figure** 5-30 show the modelled and measured current speed and direction while **Table 5-5** to **Table 5-7** present quantified errors for stations at Site 1.

5.2.16 **Figure 5-31** to **Figure 5-38** show the modelled and measured current speed and direction **Table 5-8** and **Table 5-9** presents the quantified errors for stations at Site 2.

5.2.17 In all cases the RMSE in predicted current speeds is <0.2 m/s, which concludes a good model calibration based on the ABPmer (2013) guidance detailed above, this provides confidence in using the model to assess potential impact on tidal currents and associated bed shear stress.

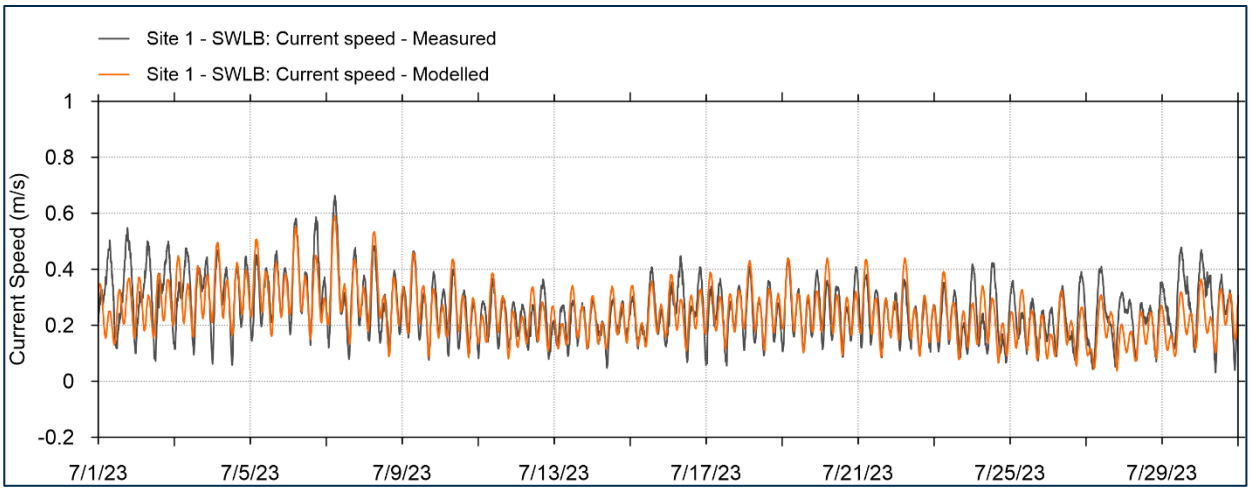

Figure 5-19: Time series comparison between simulated vs observed current speeds at Site 1 – SWLB in July 2024 (Local model)

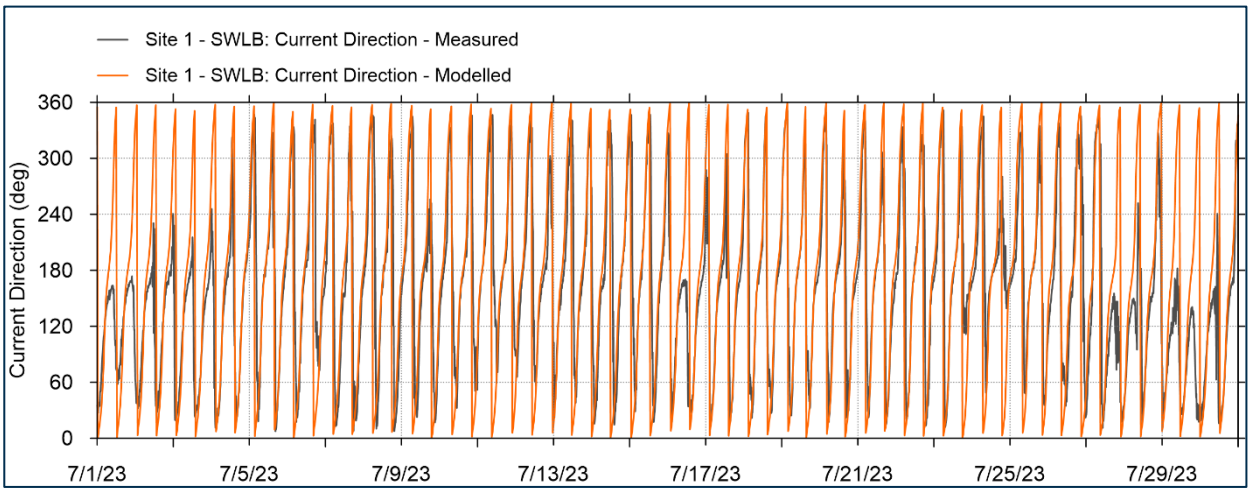

Figure 5-20: Time series comparison between simulated vs observed current directions at Site 1 – SWLB in July 2024 (Local model)

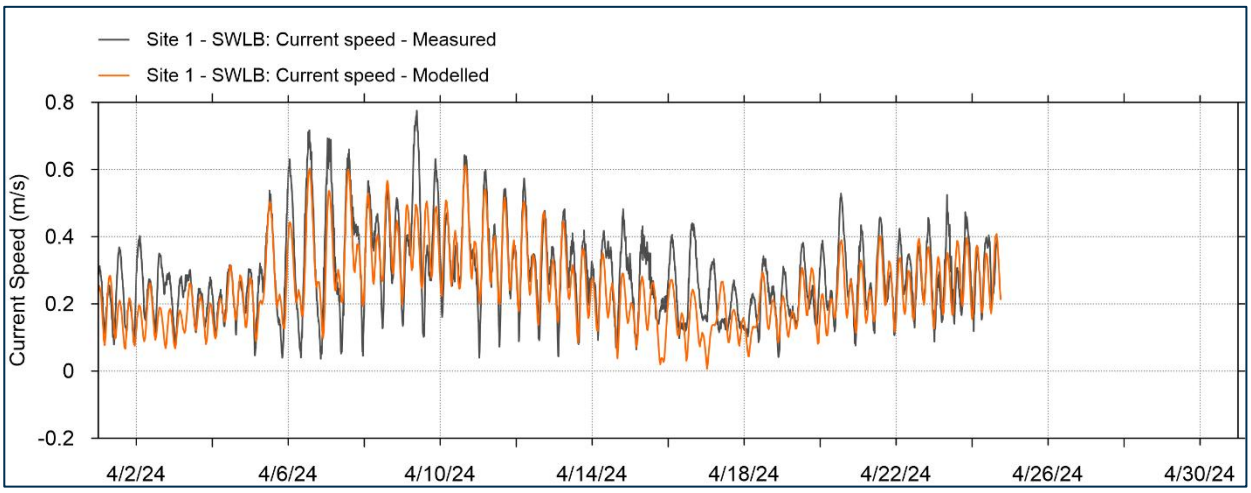

Figure 5-21: Time series comparison between simulated vs observed current speeds at Site 1 – SWLB in April 2024 (Local model)

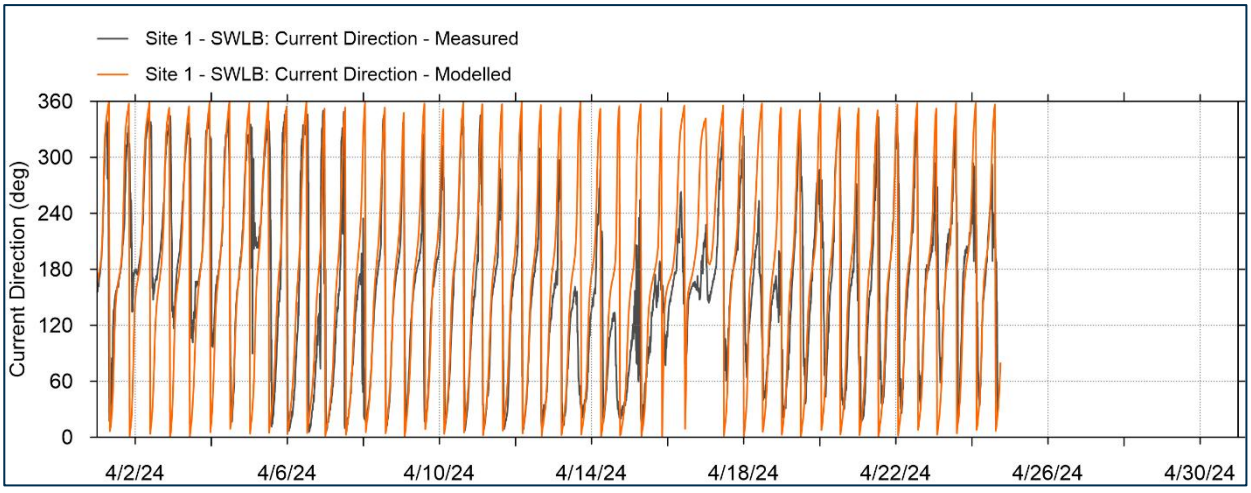

Figure 5-22: Time series comparison between simulated vs observed current directions at Site 1 – SWLB in April 2024 (Local model)

Table 5-5: Model errors in current speed at Site 1 – SWLB (local model)

Time	ME (m/s)	RMSE (m/s)	Std (m/s)	R
July 2023	0.01	0.06	0.06	0.61
April 2024	0.04	0.08	0.07	0.67
Spring tide (2 July – 10 July 2023)	-0.01	0.05	0.05	0.8
Neap tide (25 July – 30 July 2023)	0.05	0.08	0.06	0.63

Note: *ME: Mean Error; RMSE: Root Mean Square Error; Std: Std. dev of Residuals; R: Coefficient of Determination*

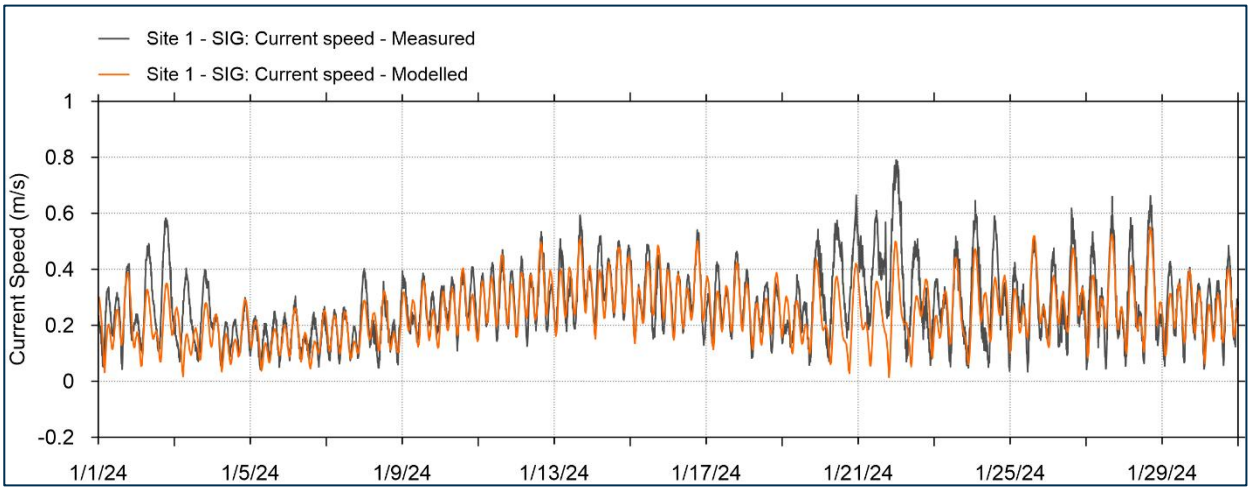

Figure 5-23: Time series comparison between simulated vs observed current speeds at Site 1 – SIG in January 2024 (Local model)

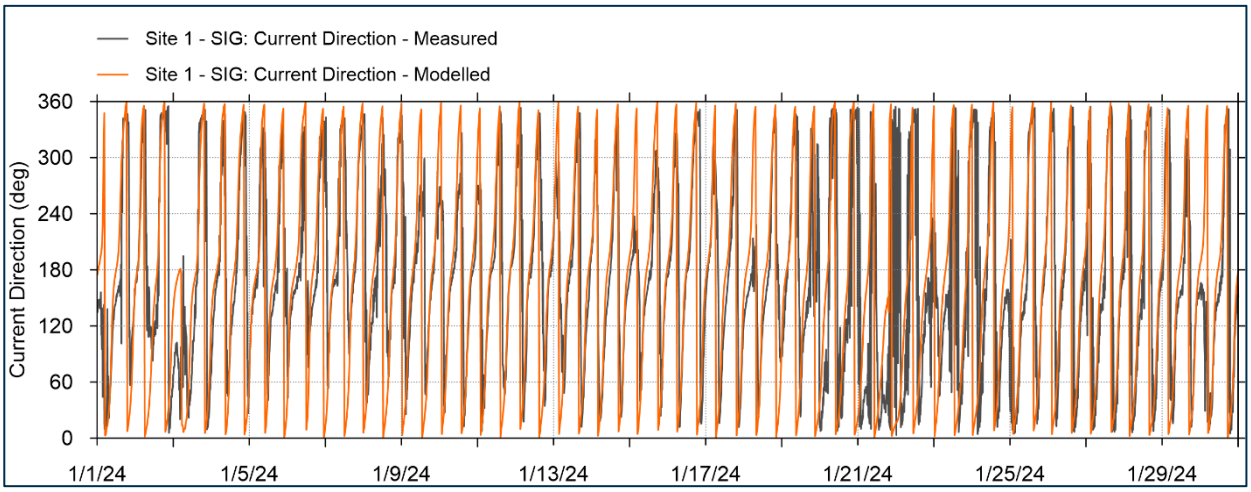

Figure 5-24: Time series comparison between simulated vs observed current directions at Site 1 – SIG in January 2024 (Local model)

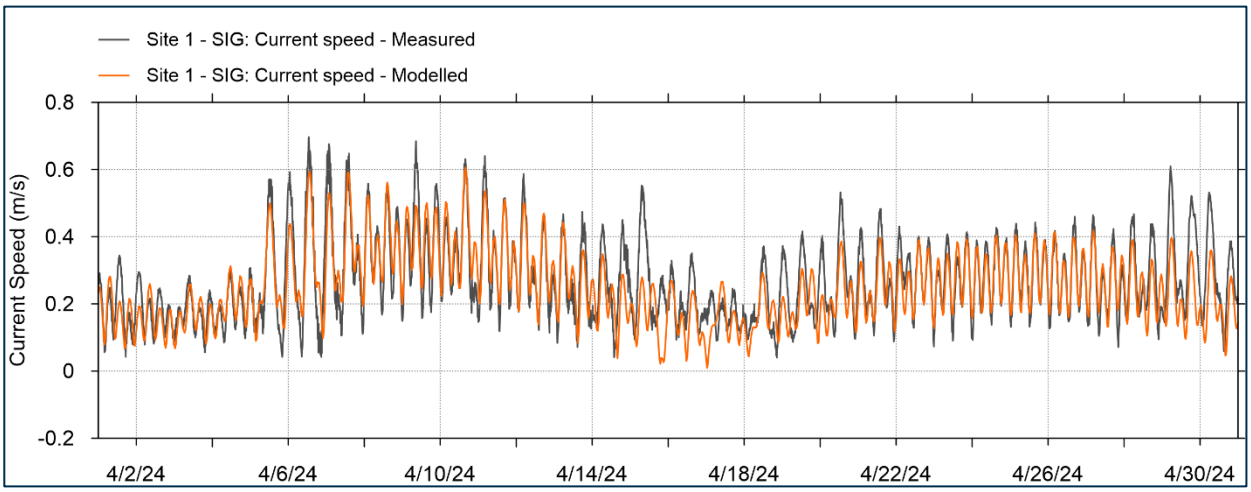

Figure 5-25: Time series comparison between simulated vs observed current speeds at Site 1 – SIG in April 2024 (Local model)

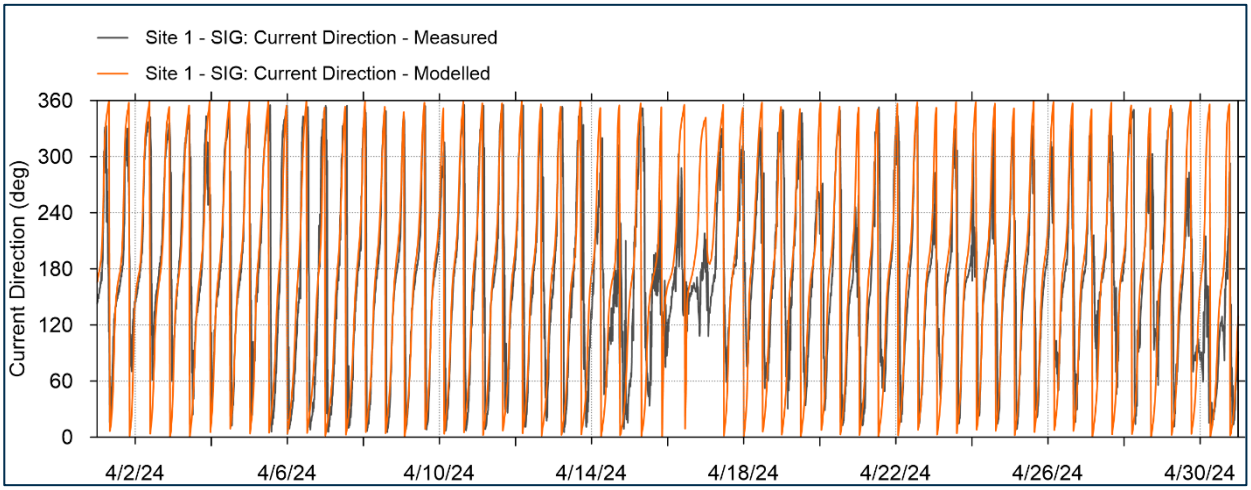

Figure 5-26: Time series comparison between simulated vs observed current directions at Site 1 – SIG in April 2024 (Local model)

Table 5-6: Model errors in current speed at Site 1 - SIG (local model)

Time	ME (m/s)	RMSE (m/s)	Std (m/s)	R
January 2024	0.03	0.08	0.08	0.60
April 2024	0.01	0.07	0.06	0.70
Spring tide (10 Jan to 19 Jan 2024)	0.01	0.05	0.05	0.75
Neap tide (3 Jan to 8 Jan 2024)	0.01	0.05	0.05	0.60

Note: *ME: Mean Error; RMSE: Root Mean Square Error; Std: Std. dev of Residuals; R: Coefficient of Determination*

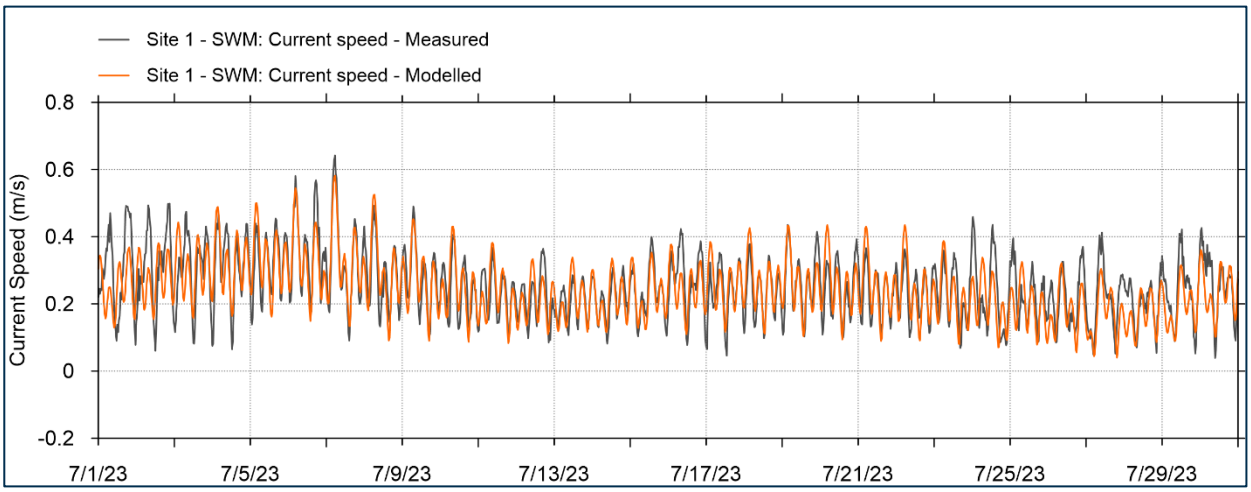

Figure 5-27: Time series comparison between simulated vs observed current speeds at Site 1 – SWM in July 2023 (Local model)

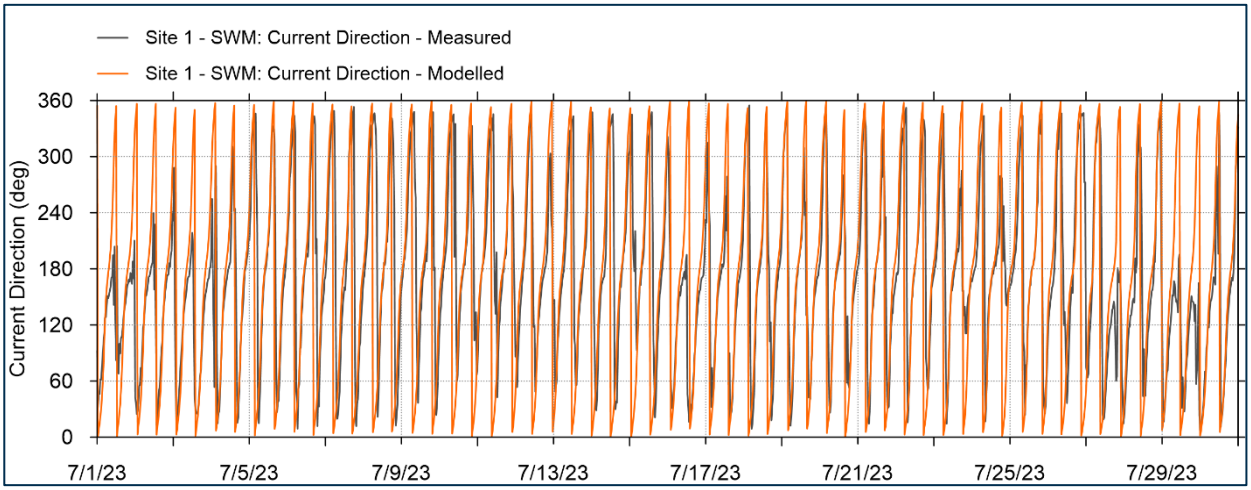

Figure 5-28: Time series comparison between simulated vs observed current directions at Site 1 – SWLB in July 2023 (Local model)

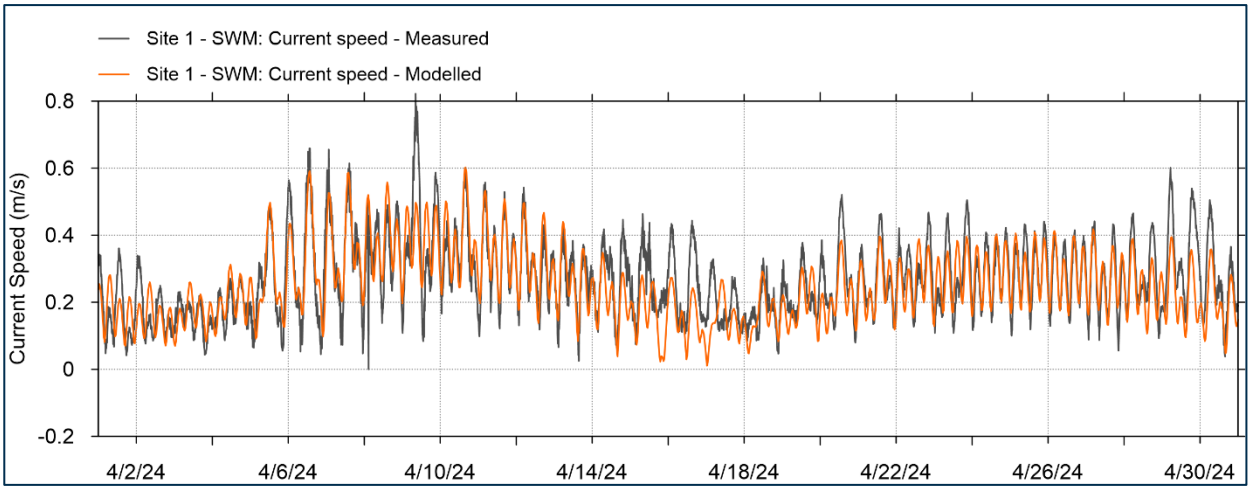

Figure 5-29: Time series comparison between simulated vs observed current speeds at Site 1 – SWLB in April 2024 (Local model)

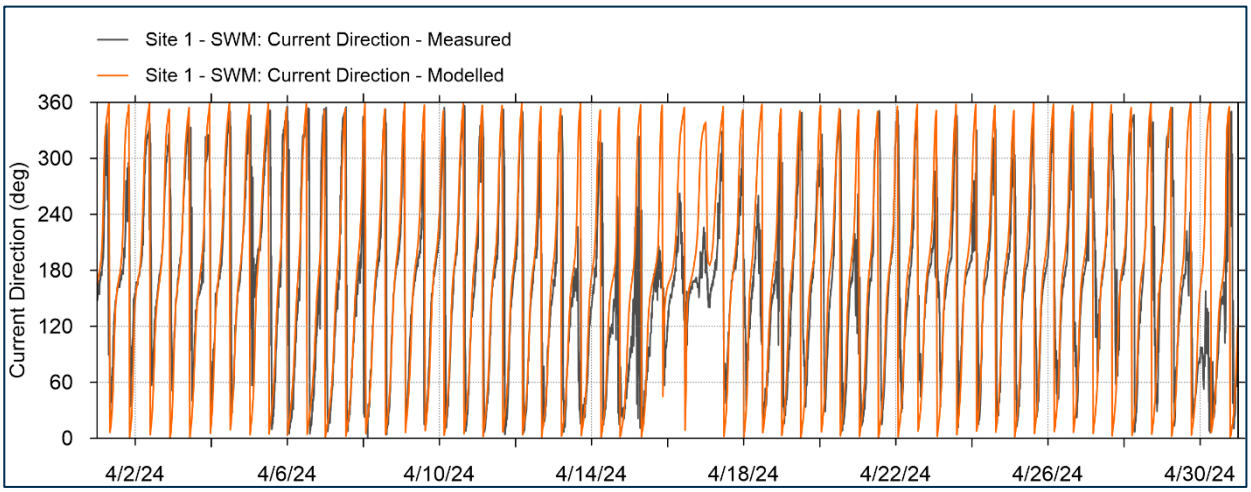

Figure 5-30: Time series comparison between simulated vs observed current directions at Site 1 – SWLB in April 2024 (Local model)

Table 5-7: Model errors in current speed at Site 1 - SWM (local model)

Time	ME (m/s)	RMSE (m/s)	Std (m/s)	R
July 2023	0.01	0.06	0.06	0.58
April 2024	0.01	0.07	0.07	0.61
Spring tide (2 July – 10 July 2023)	0.00	0.06	0.06	0.65
Neap tide (25 July – 30 July 2023)	0.04	0.07	0.05	0.63

Note: *ME: Mean Error; RMSE: Root Mean Square Error; Std: Std. dev of Residuals; R: Coefficient of Determination*

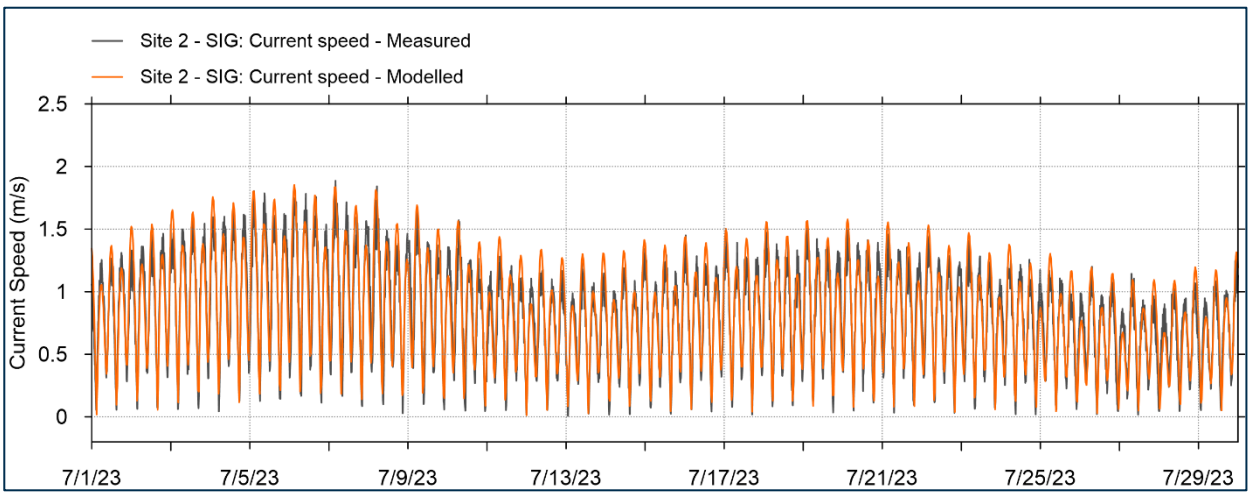

Figure 5-31: Time series comparison between simulated vs observed current speeds at Site 2 – SIG in July 2023 (Local model)

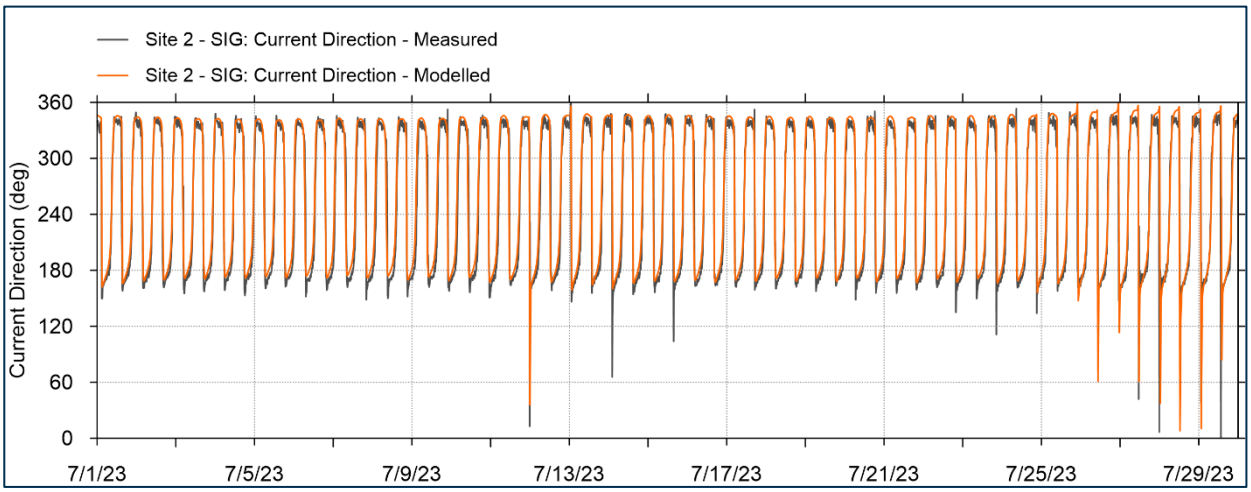

Figure 5-32: Time series comparison between simulated vs observed current directions at Site 2 – SIG in July 2023 (Local model)

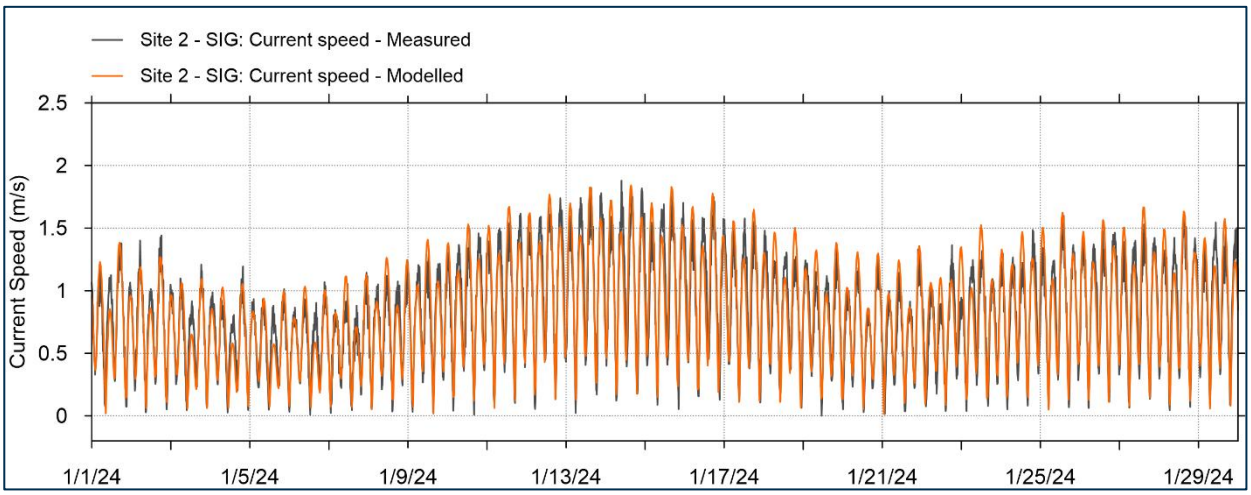

Figure 5-33: Time series comparison between simulated vs observed current speeds at Site 2 – SIG in January 2024 (Local model)

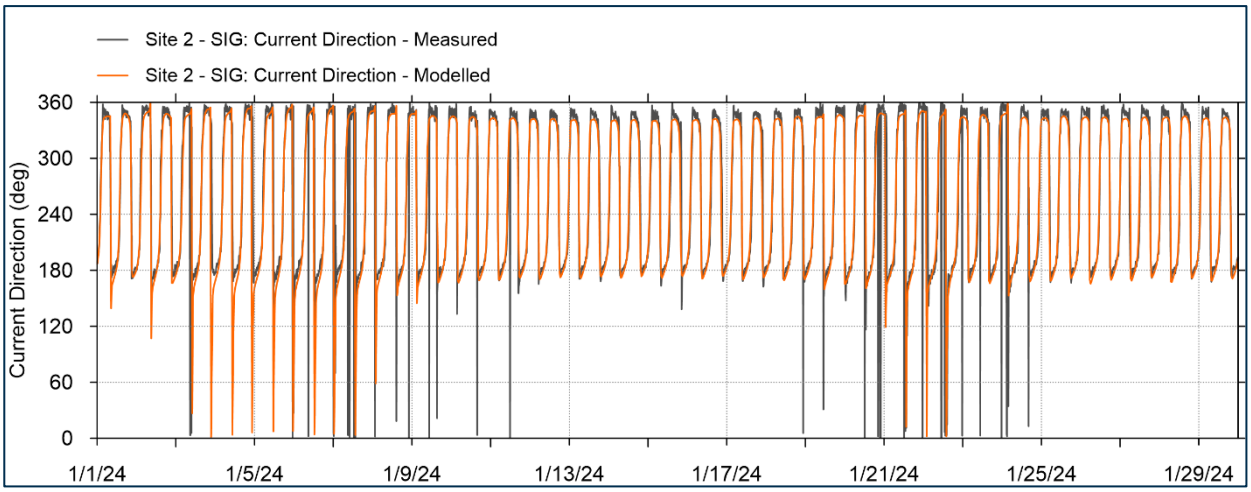

Figure 5-34: Time series comparison between simulated vs observed current directions at Site 2 – SIG in January 2024 (Local model)

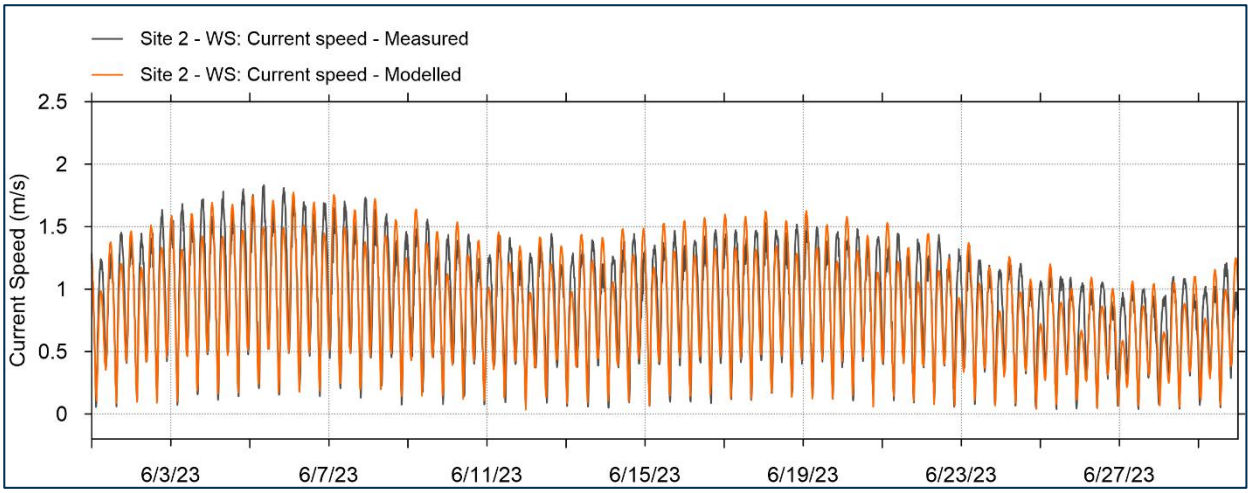

Figure 5-35: Time series comparison between simulated vs observed current speeds at Site 2 – WS in June 2023 (Local model)

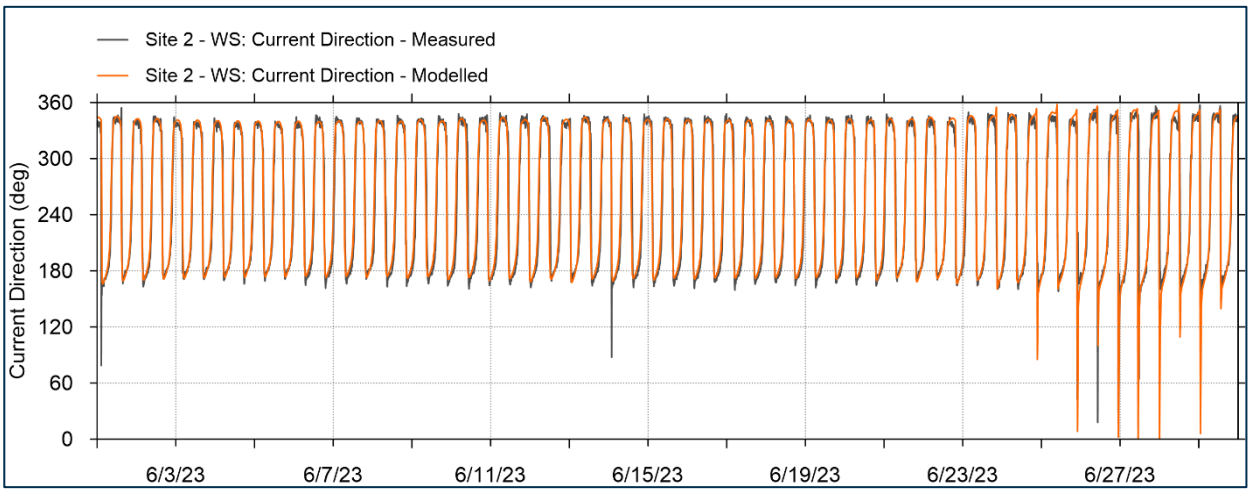

Figure 5-36: Time series comparison between simulated vs observed current directions at Site 2 – WS in June 2023 (Local model)

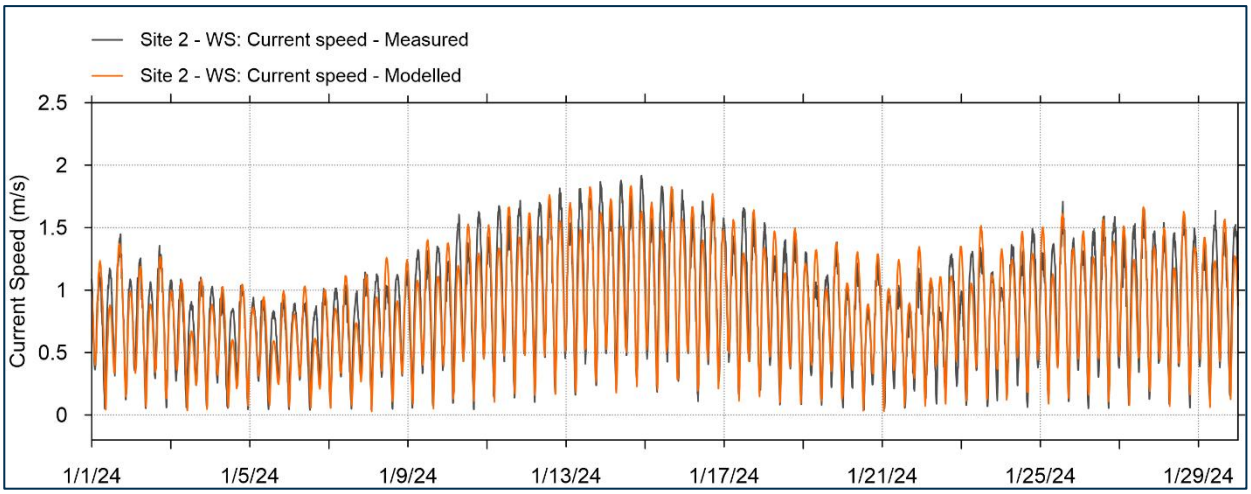

Figure 5-37: Time series comparison between simulated vs observed current speeds at Site 2 – WS in January 2024 (Local model)

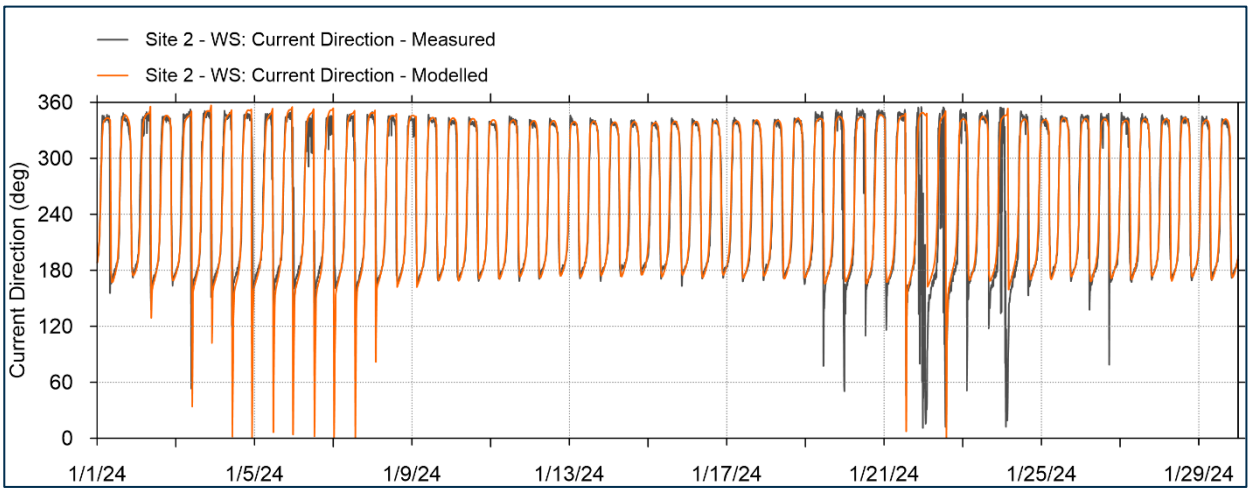

Figure 5-38: Time series comparison between simulated vs observed current directions at Site 2 – WS in January 2024 (Local model)

Table 5-8: Model errors in current speed at Site 2 – SIG current (local model)

Name of station	ME (m/s)	RMSE (m/s)	Std (m/s)	R
July 2023	0.04	0.15	0.14	0.88
January 2024	0.05	0.16	0.15	0.86
Spring tide (14 July – 24 July 2023)	0.05	0.14	0.13	0.88
Neap tide (25 July – 30 July 2023)	0.05	0.13	0.12	0.83

Note: *ME: Mean Error; RMSE: Root Mean Square Error; Std: Std. dev of Residuals; R: Coefficient of Determination*

Table 5-9: Model errors in current speed at Site 2 – WS current (local model)

Name of station	ME (m/s)	RMSE (m/s)	Std (m/s)	R
June 2023	0.04	0.17	0.17	0.82
January 2024	0.02	0.16	0.16	0.85
Spring tide (13 June – 23 June 2023)	0.02	0.16	0.16	0.82
Neap tide (1 January – 7 January 2024)	0.05	0.13	0.12	0.82

Note: *ME: Mean Error; RMSE: Root Mean Square Error; Std: Std. dev of Residuals; R: Coefficient of Determination*

Model Parameters

5.2.18 The settings applied to the Local model are summarized in **Table 5-10**.

Table 5-10: Settings for local MIKE21 model

Description	Setting
Minimum time step	0.01s
Maximum time step	60s
Critical Courant-Friedrichs-Lewy (CFL) number	0.8
Flood and dry	Included
Density type	Barotropic
Bed resistance	Manning number: 40[m1/3/s]
Eddy viscosity	0.28 (Smagorinsky formulation)

Description	Setting
Coriolis	Varying in domain
Wind forcing	Included

5.3 Model Results

Model Run Scenarios

5.3.1 The calibrated 2D hydrodynamic model has been run for a full spring-neap tidal cycle from 26th March to 11th April 2025. This time period was chosen as it has the highest tidal range in 2025, which produces the strongest tidal currents (**Figure 5-39**).

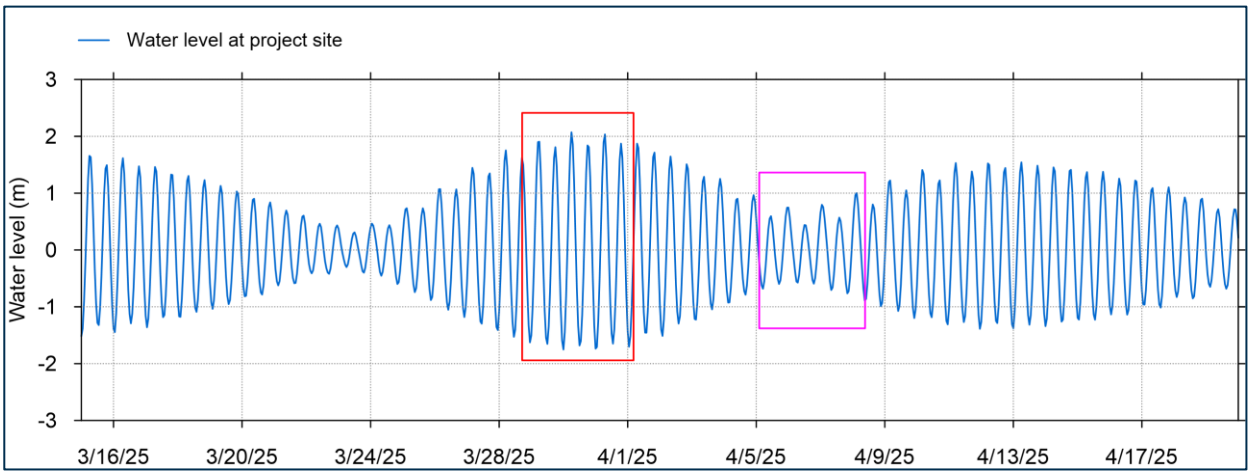

Figure 5-39: Modelled water levels at the WFD (red frame indicates spring tides and purple frame indicates neap tide)

5.3.2 The 2D HD model has been run for five layout scenarios: Baseline option and four turbine indicative layouts. The WDA turbine layouts which were modelled in the assessment are presented in **Table 5-11** and **Figure 5-40**. These include monopile WTG's for two WDA options of 15 MW and 24 MW, as well as 2 OSP's in the same proposed location for all layouts. Each of the 15 MW and 24 MW have a 'dense perimeter' and 'even spread' of WTGs. OSP's are modelled using a series of monopile structures.

5.3.3 In the MIKE21-HD model setup, the monopiles were input as a sub-grid feature using coordinates, structure type (circular pile) and diameter.

Table 5-11: WDA layout options

Type	Layout	Number	Structure	Diameter (m)
WTG	15 MW – Even Spread	144	Monopile	13.0
WTG	15 MW – Dense Perimeter	144	Monopile	13.0
WTG	24 MW – Even Spread	91	Monopile	15.0
WTG	24 MW – Dense Perimeter	91	Monopile	15.0
OSP	All	2	6 * Monopile (each OSP)	15.0

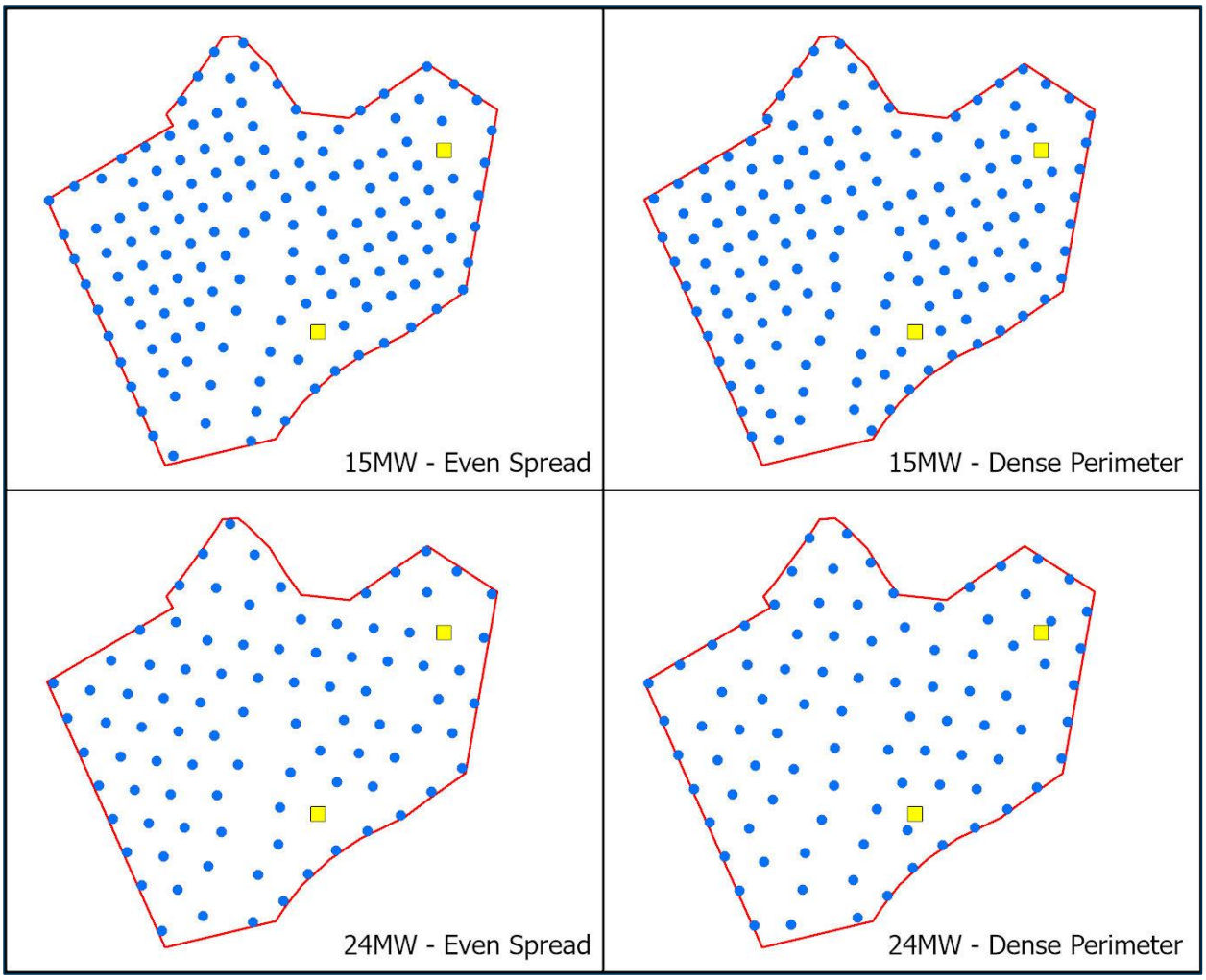

Figure 5-40: Indicative WTG(in blue) and OSP (in yellow) locations

Absolute Current Speed – Baseline

5.3.4 This section presents the absolute current speeds around the WDA for the baseline scenario. **Figure 5-41** and **Figure 5-42** present the predicted current speed and direction during spring tide for peak flood and peak ebb, respectively. **Figure 5-43** and **Figure 5-44** present the predicted current speed and direction during neap tide for peak flood and peak ebb, respectively. **Figure 5-45** presents the maximum current speed throughout the full spring-neap tidal cycle simulation.

5.3.5 The absolute current speed during the spring tide on peak flood is directed from south southwest to north northeast with a magnitude of up to 1.2 m/s in the south to 0.5 m/s in the north. During peak ebb, currents are directed from north to south with a magnitude of 0.4 m/s in the north to up to 1.0 m/s in the south.

5.3.6 The absolute current speed during neap tide on peak flood is directed from south to north with a magnitude of up to 0.5 m/s in the south to 0.1 m/s in the north. During peak ebb, currents are directed from north to south with a magnitude of 0.1 m/s in the north to up to 0.5 m/s in the south.

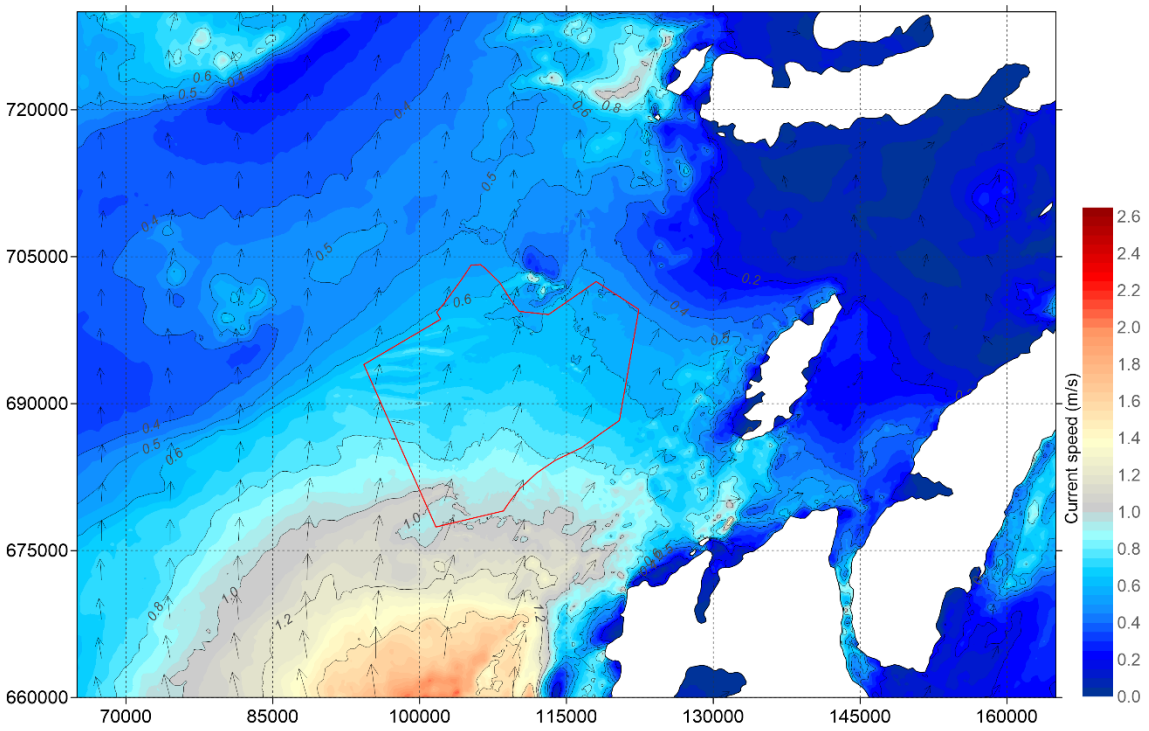

Figure 5-41: Baseline layout - Current speed during spring tide - peak flood (Local model)

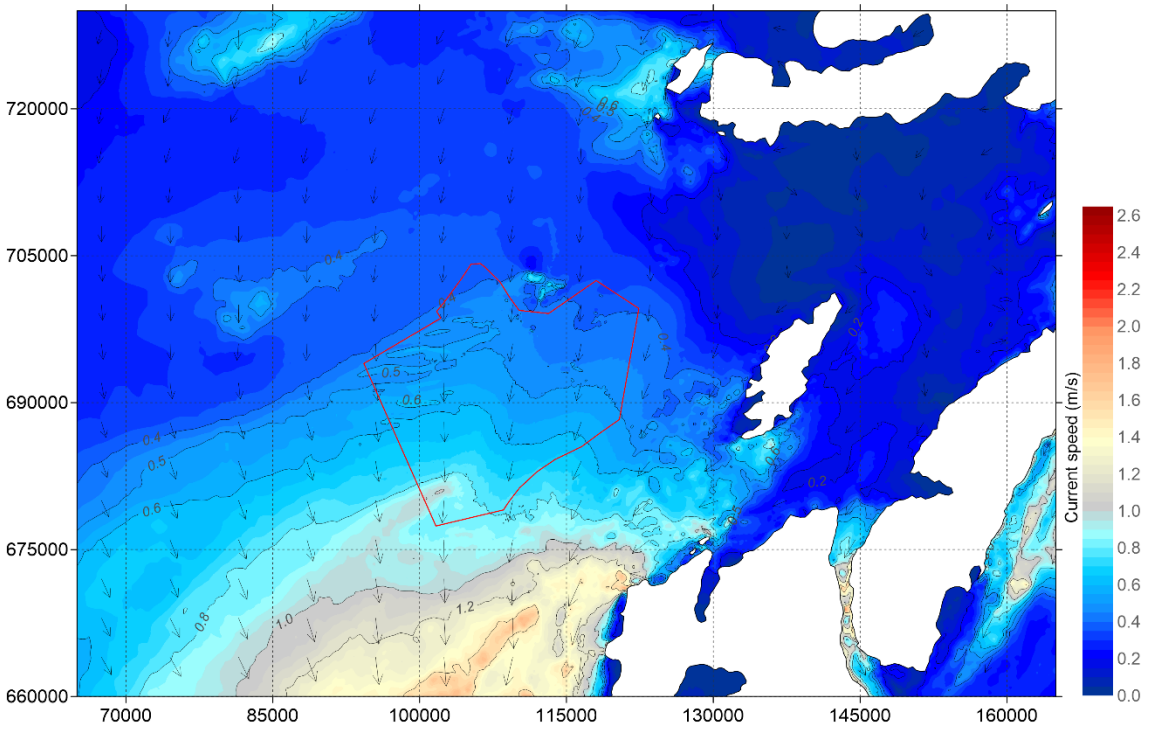

Figure 5-42: Baseline layout - Current speed during spring tide - peak ebb (Local model)

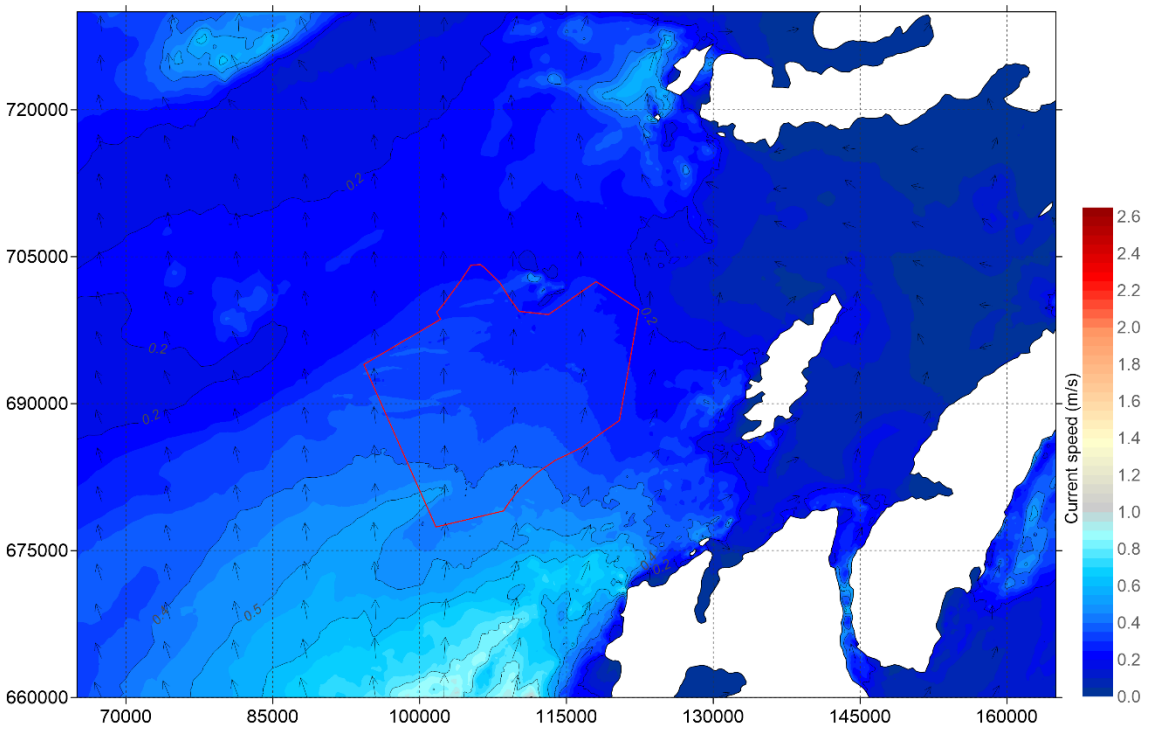

Figure 5-43: Baseline layout - Current speed during neap tide - peak flood (Local model)

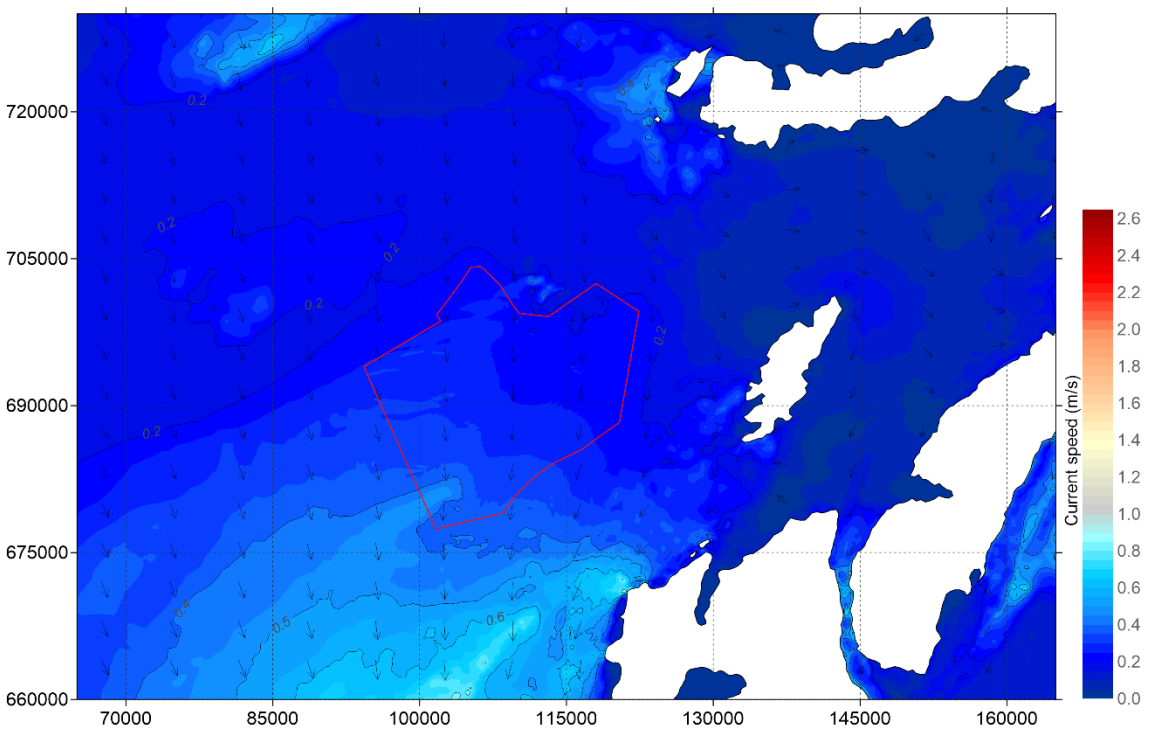

Figure 5-44: Baseline layout - Current speed during neap tide - peak ebb (Local model)

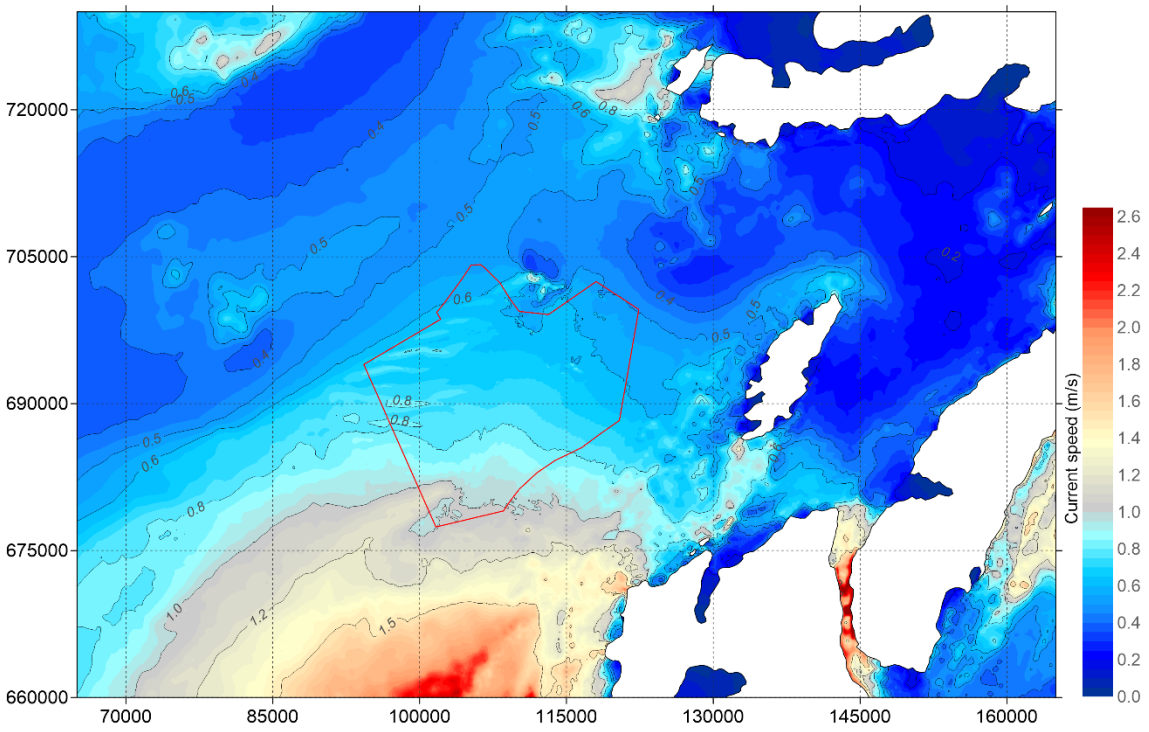

Figure 5-45: Baseline layout – Maximum current speed over 15 days (Local model)

Absolute Current Speed – 15 MW Dense Perimeter Layout

5.3.7 This section presents the absolute current speeds around the WDA for the 15 MW Dense Perimeter layout. **Figure 5-46** and **Figure 5-47** present the predicted current speed and direction during spring tide for peak flood and peak ebb, respectively. **Figure 5-48** and **Figure 5-49** present the predicted current speed and direction during neap tide for peak flood and peak ebb, respectively. **Figure 5-50** presents the maximum current speed throughout the full spring-neap tidal cycle simulation.

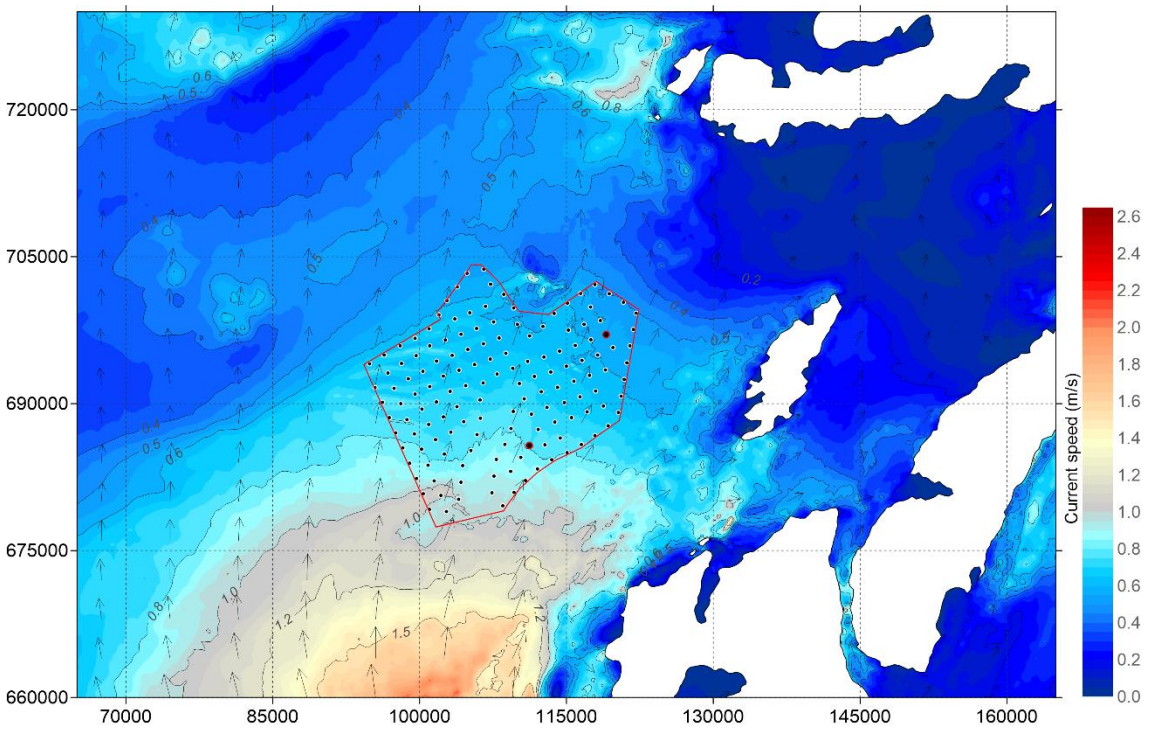

Figure 5-46: 15 MW - Dense Perimeter layout - Current speed during spring tide - peak flood (Local model)

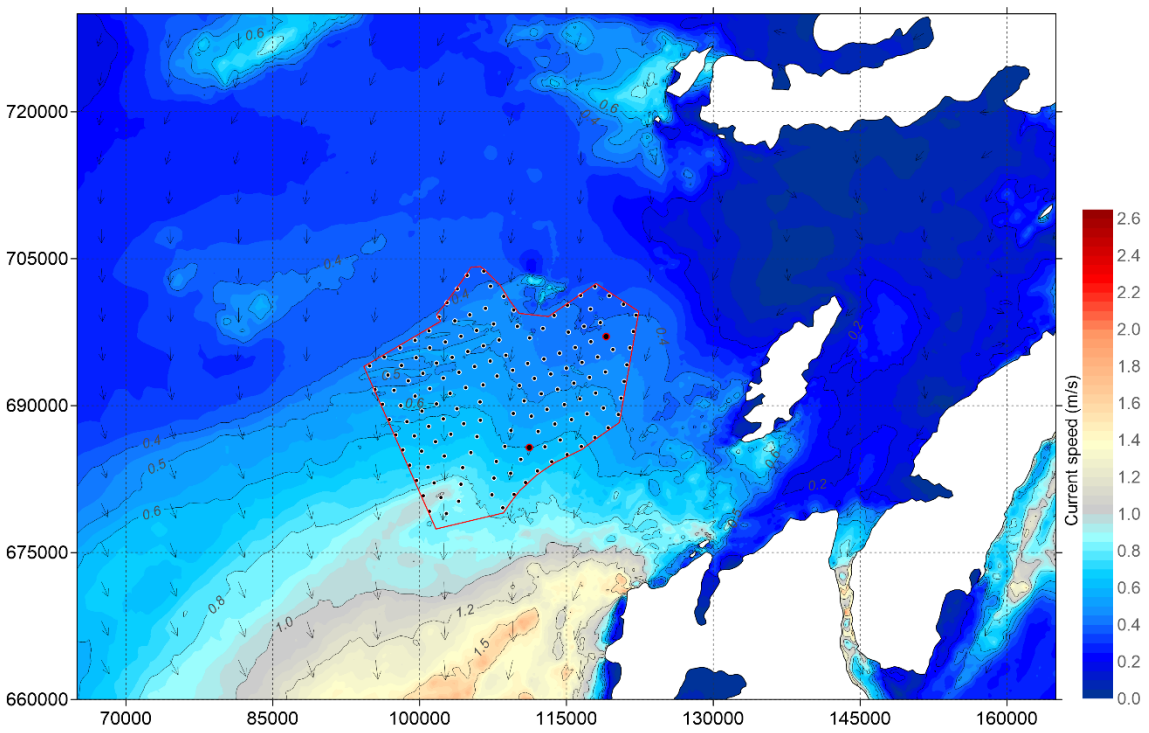

Figure 5-47: 15 MW - Dense Perimeter layout - Current speed during spring tide - peak ebb (Local model)

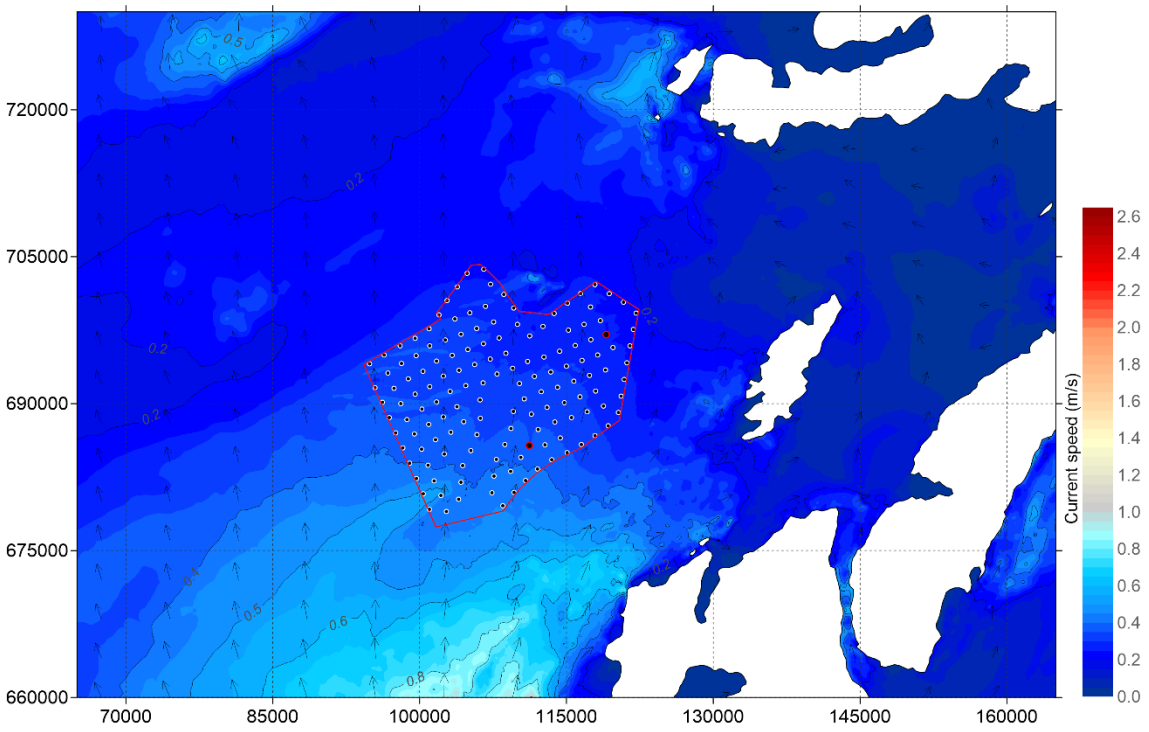

Figure 5-48: 15 MW - Dense Perimeter layout - Current speed during neap tide - peak flood (Local model)

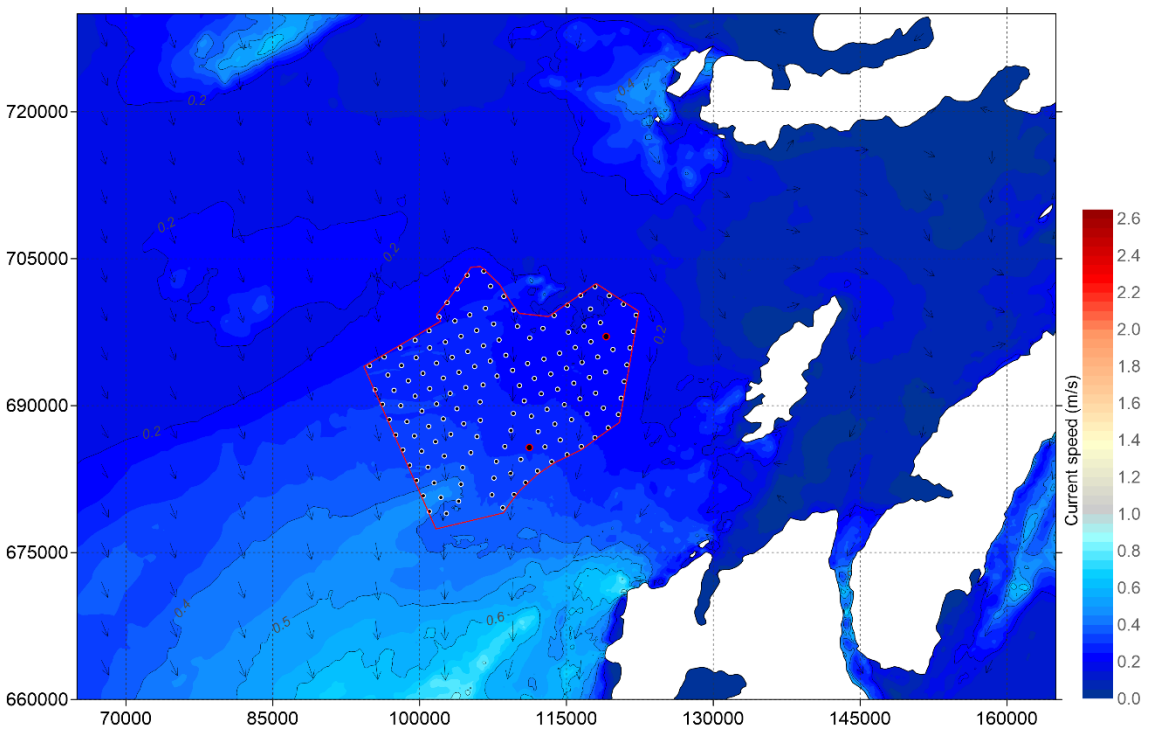

Figure 5-49: 15 MW - Dense Perimeter layout - Current speed during neap tide - peak ebb (Local model)

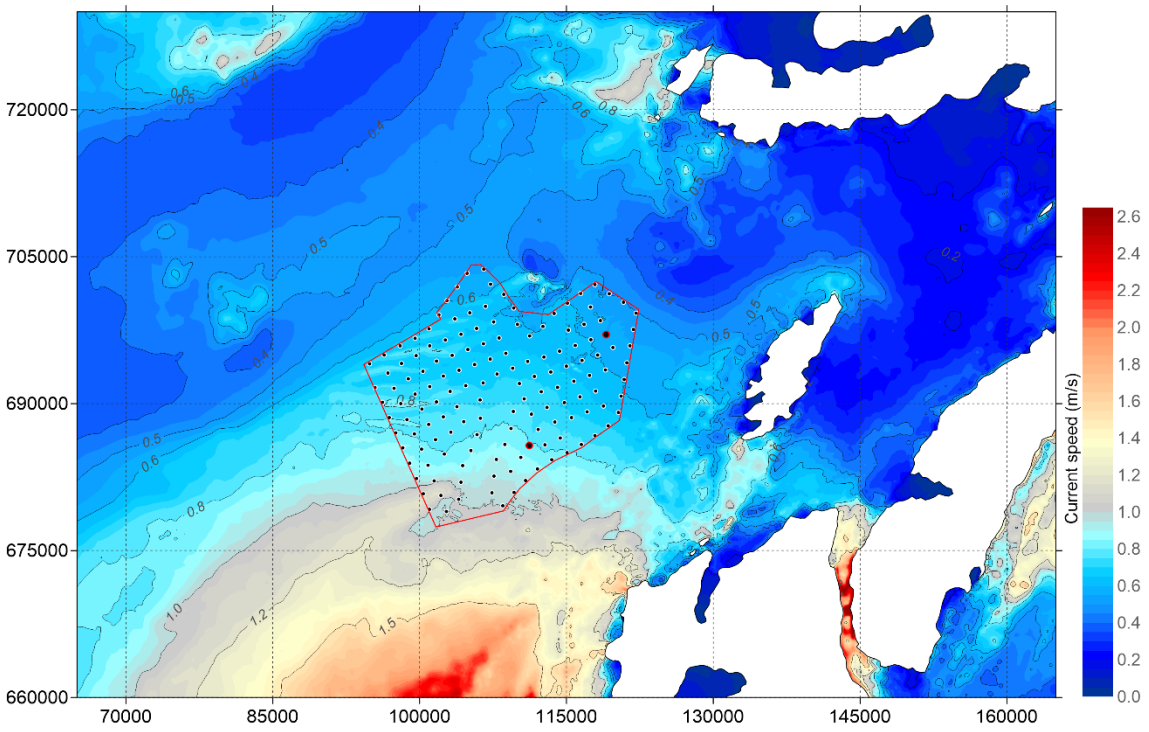

Figure 5-50: 15 MW - Dense Perimeter layout – Maximum current speed over 15 days (Local model)

Absolute Current Speed – 15 MW Even Spread Layout

5.3.8 This section presents the absolute current speeds around the WDA for the 15 MW Even Spread layout. **Figure 5-51** and **Figure 5-52** present the predicted current speed and direction during spring tide for peak flood and peak ebb, respectively. **Figure 5-53** and **Figure 5-54** present the predicted current speed and direction during neap tide for peak flood and peak ebb, respectively. **Figure 5-55** the maximum current speed throughout the full spring-neap tidal cycle simulation.

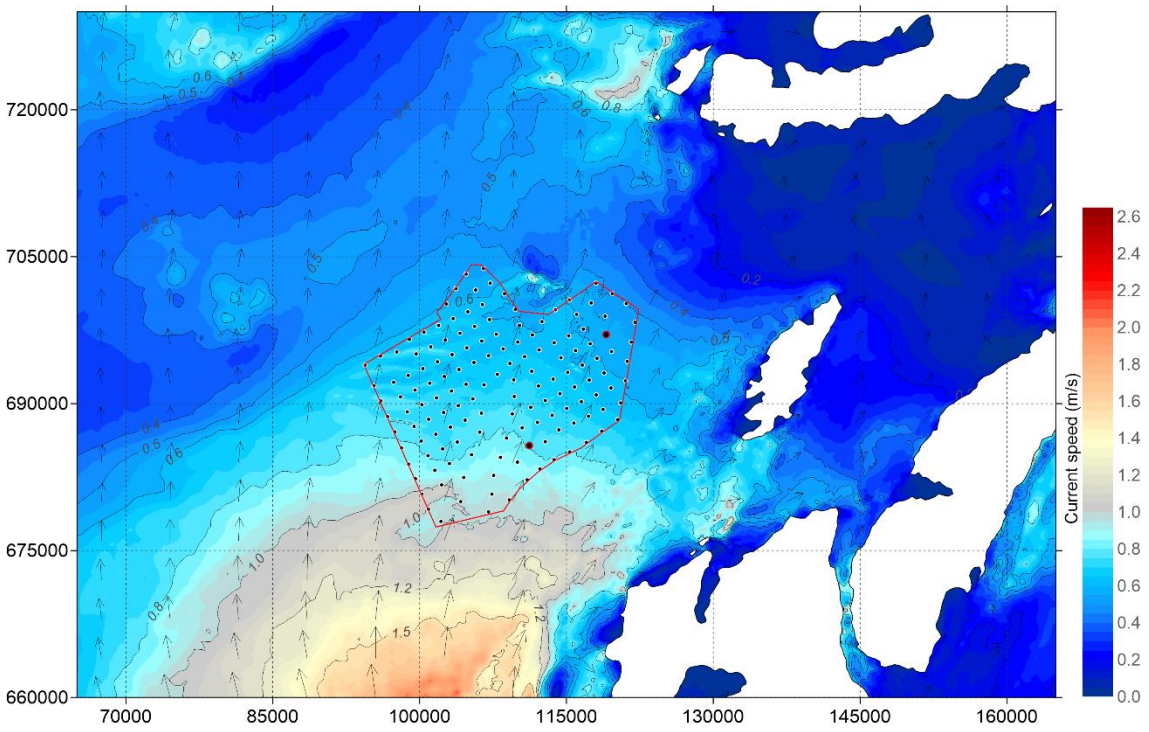

Figure 5-51: 15 MW - Even Spread layout - Current speed during spring tide - peak flood (Local model)

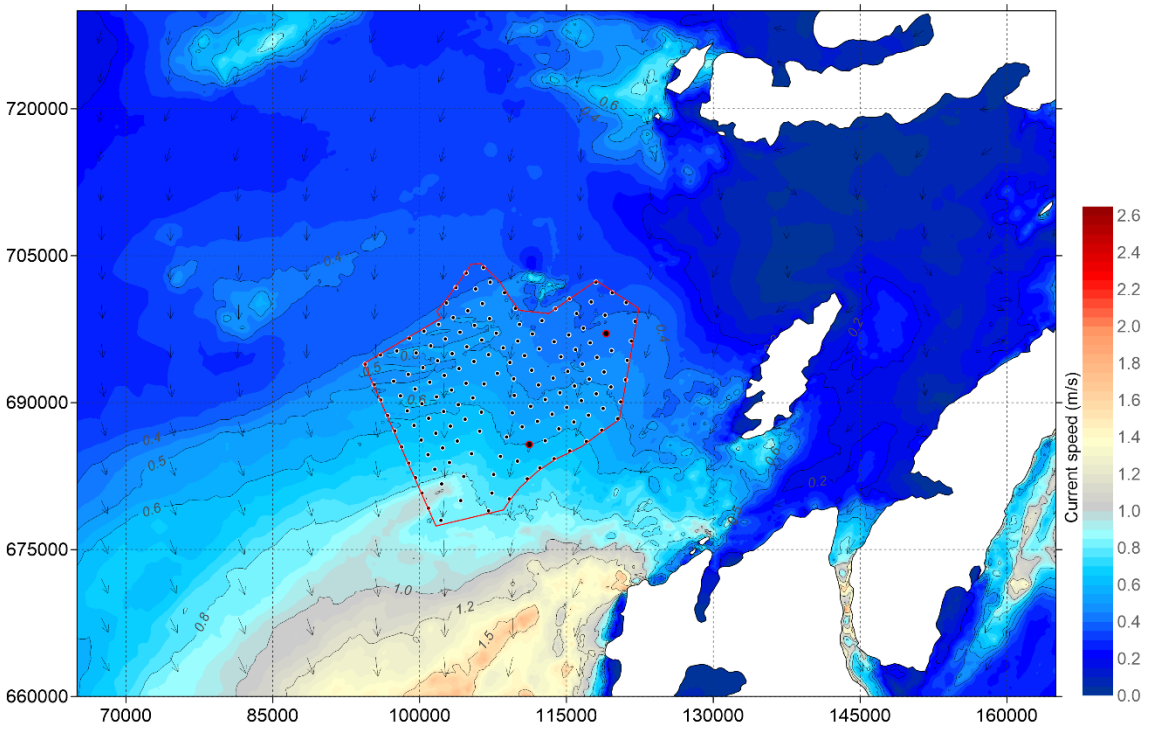

Figure 5-52: 15 MW - Even Spread layout - Current speed during spring tide - peak ebb (Local model)

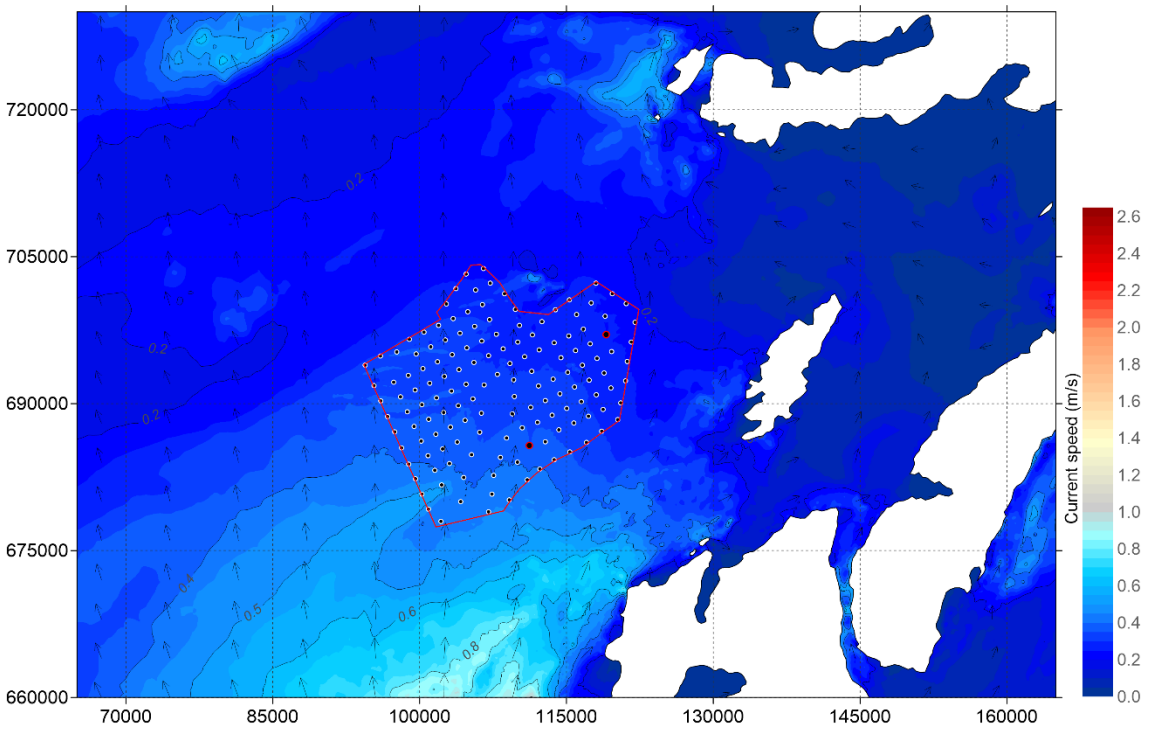

Figure 5-53: 15 MW - Even Spread layout - Current speed during neap tide - peak flood (Local model)

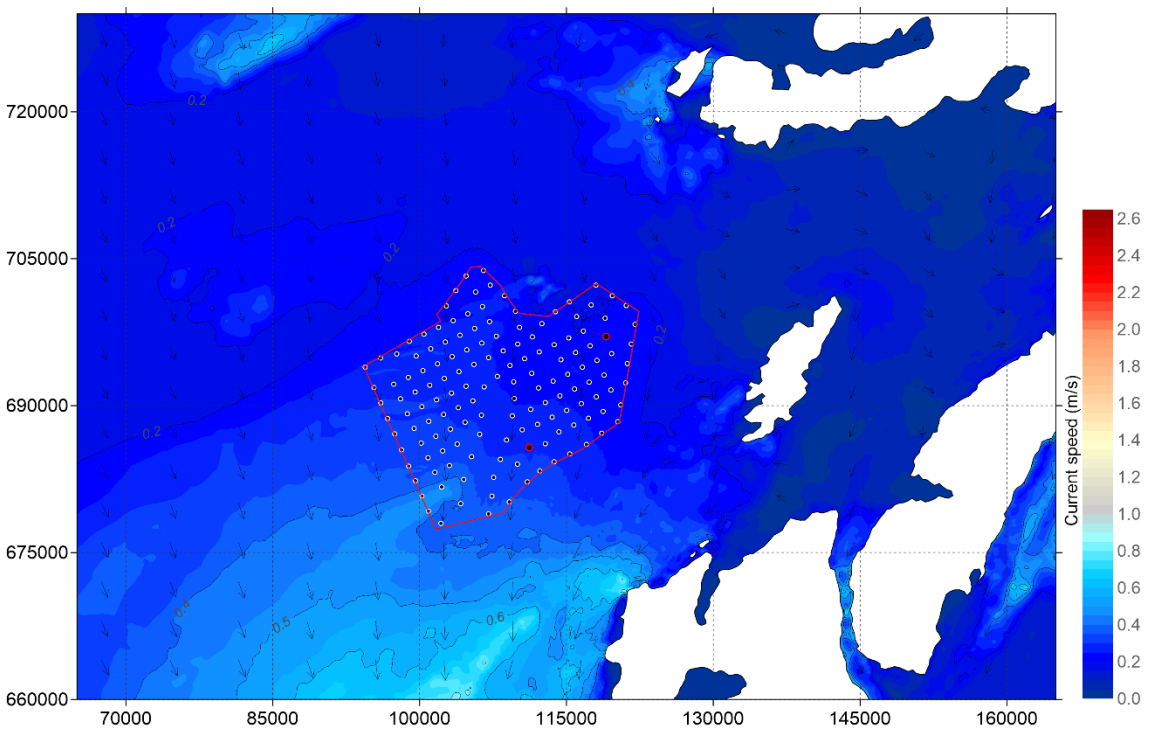

Figure 5-54: 15 MW - Even Spread layout - Current speed during neap tide - peak ebb (Local model)

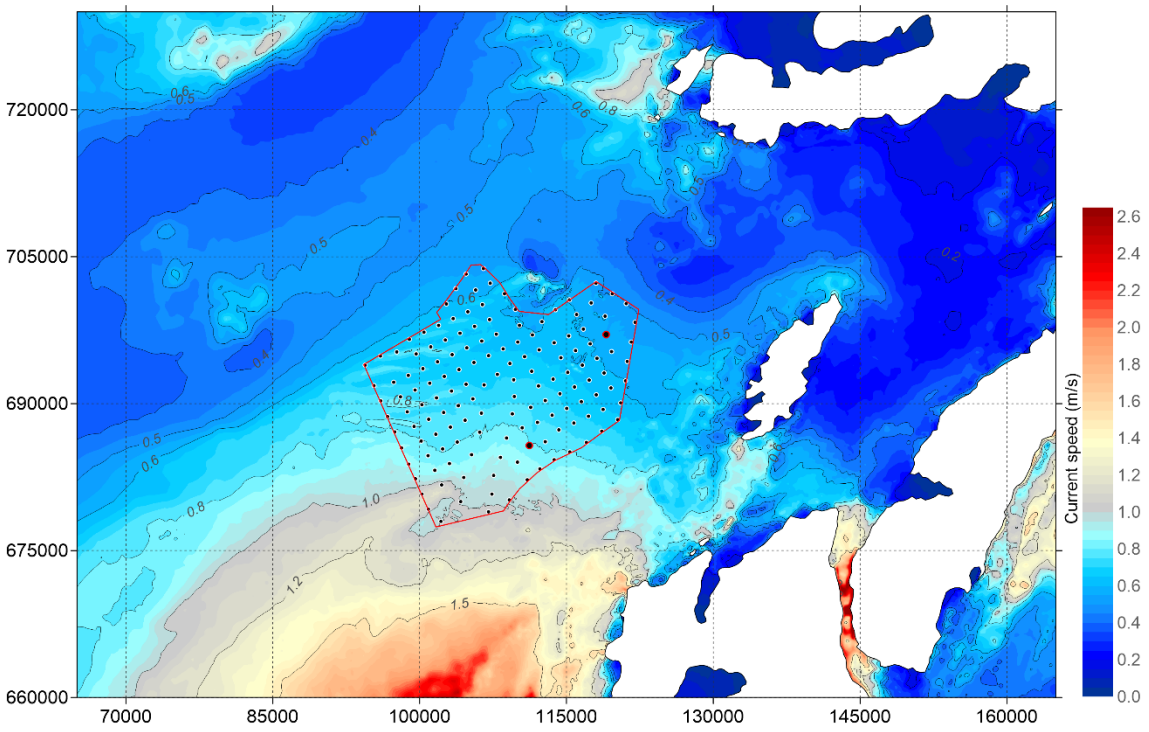

Figure 5-55: 15 MW - Even Spread layout – Maximum current speed over 15 days (Local model)

Absolute Current Speed – 24 MW Dense Perimeter Layout

5.3.9 This section presents the absolute current speeds around the WDA for the 24 MW Dense Perimeter layout. **Figure 5-56** and **Figure 5-57** present the predicted current speed and direction during spring tide for peak flood and peak ebb, respectively. **Figure 5-58** and **Figure 5-59** present the predicted current speed and direction during neap tide for peak flood and peak ebb, respectively. **Figure 5-60** the maximum current speed throughout the full spring-neap tidal cycle simulation.

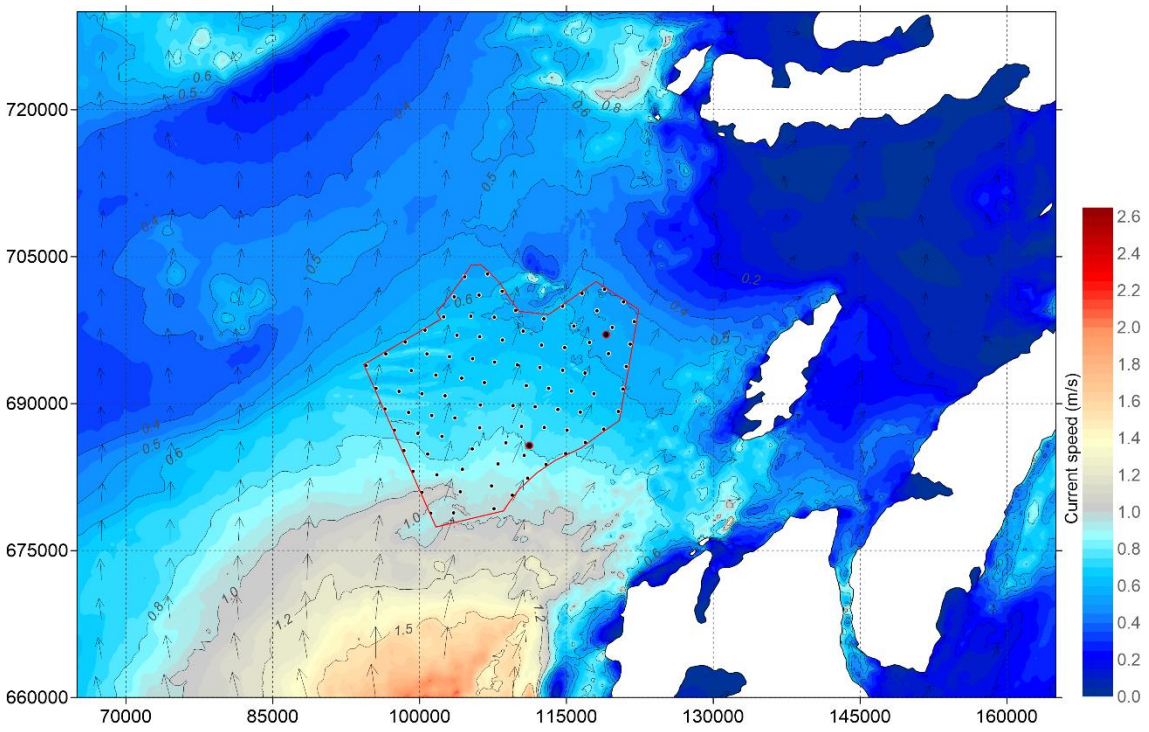

Figure 5-56: 24 MW - Dense Perimeter layout - Current speed during spring tide - peak flood (Local model)

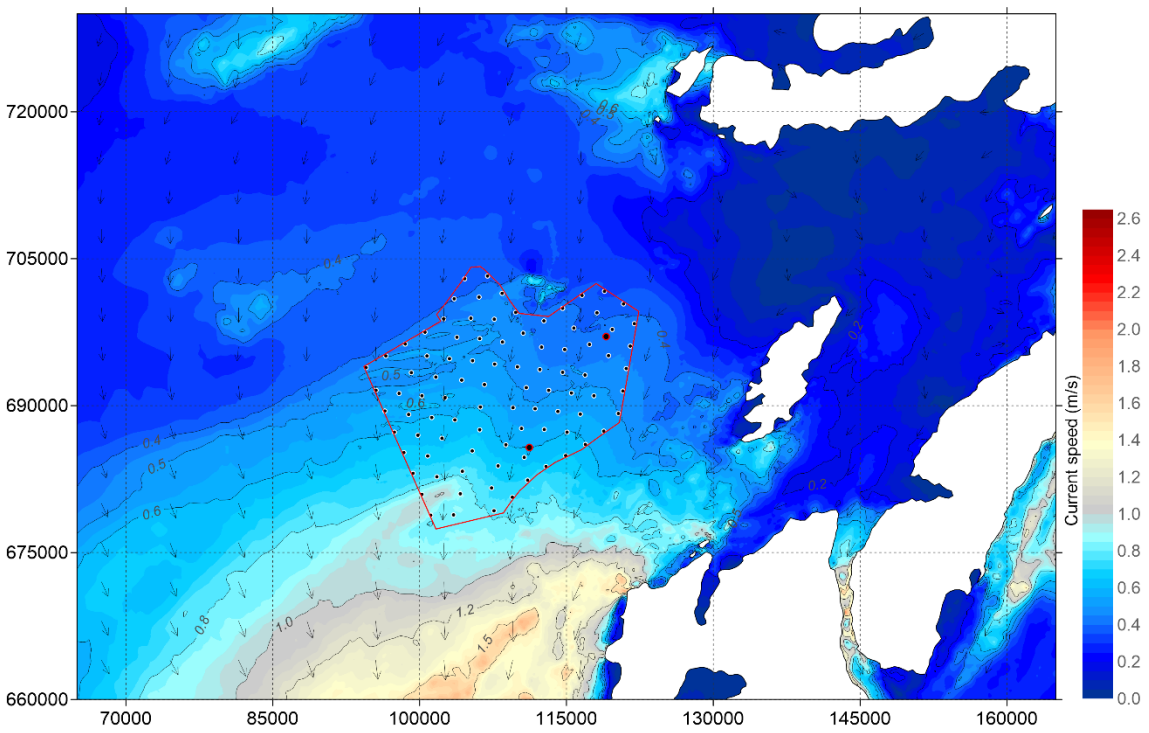

Figure 5-57: 24 MW - Dense Perimeter layout - Current speed during spring tide - peak ebb (Local model)

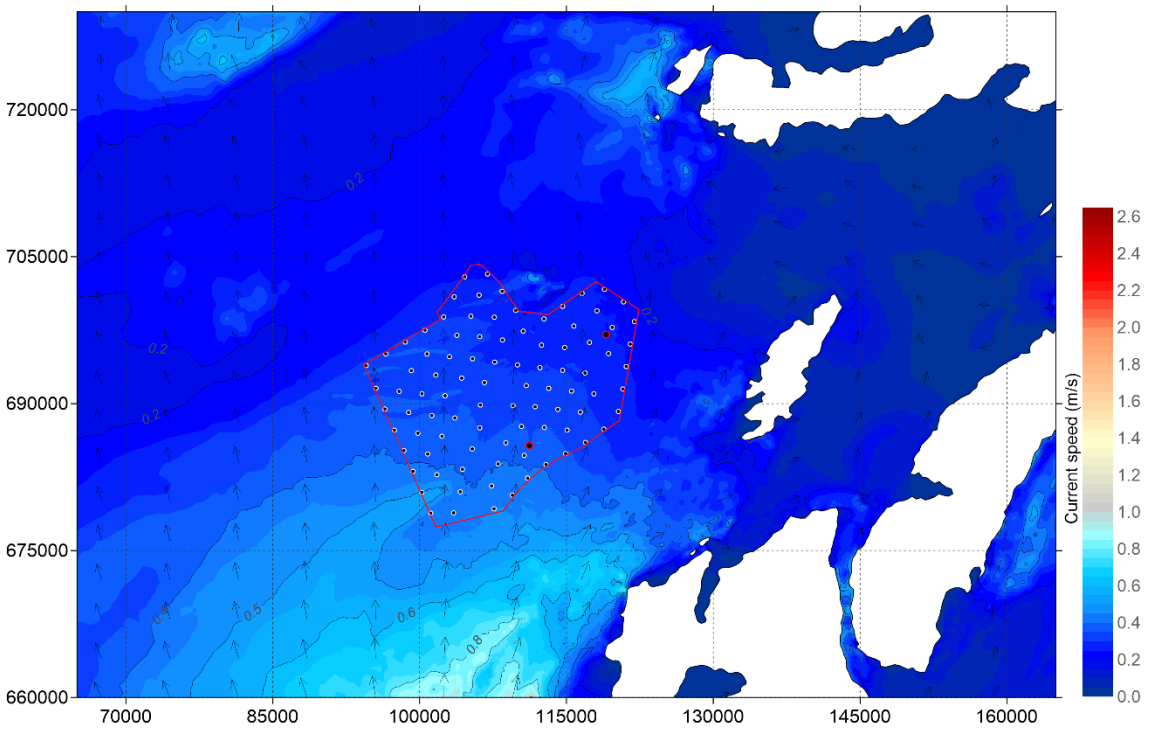

Figure 5-58: 24 MW - Dense Perimeter layout - Current speed during neap tide - peak flood (Local model)

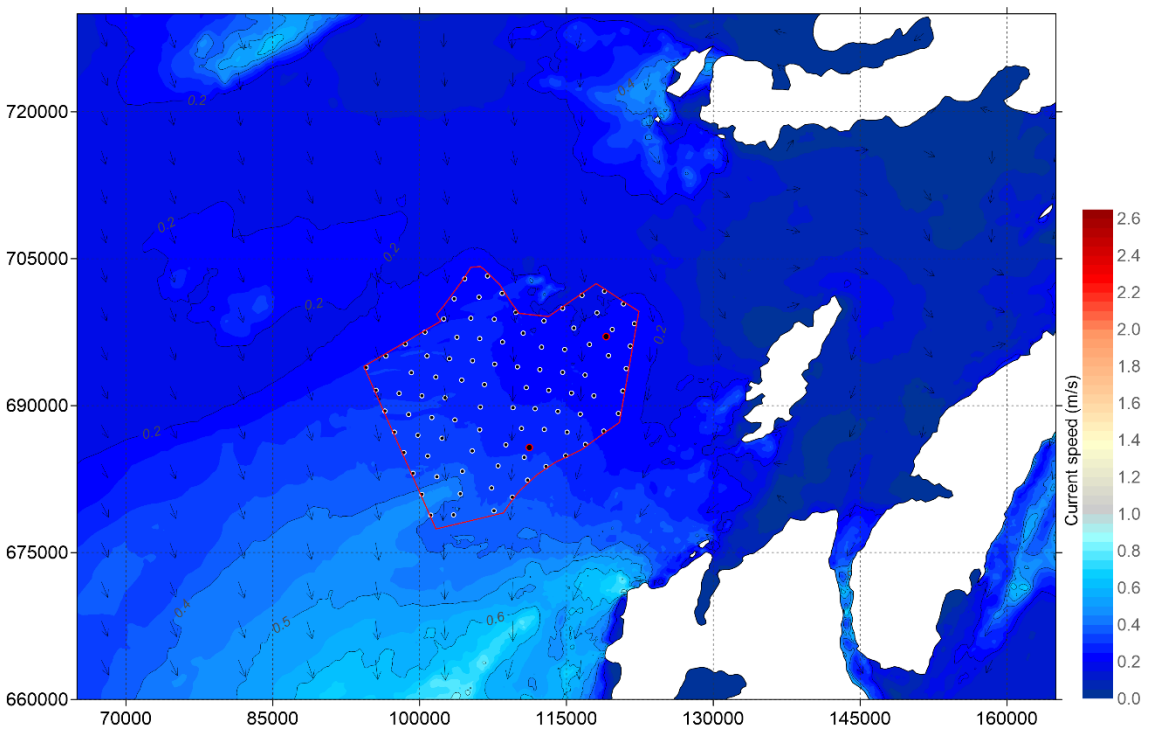

Figure 5-59: 24 MW - Dense Perimeter layout - Current speed during neap tide - peak ebb (Local model)

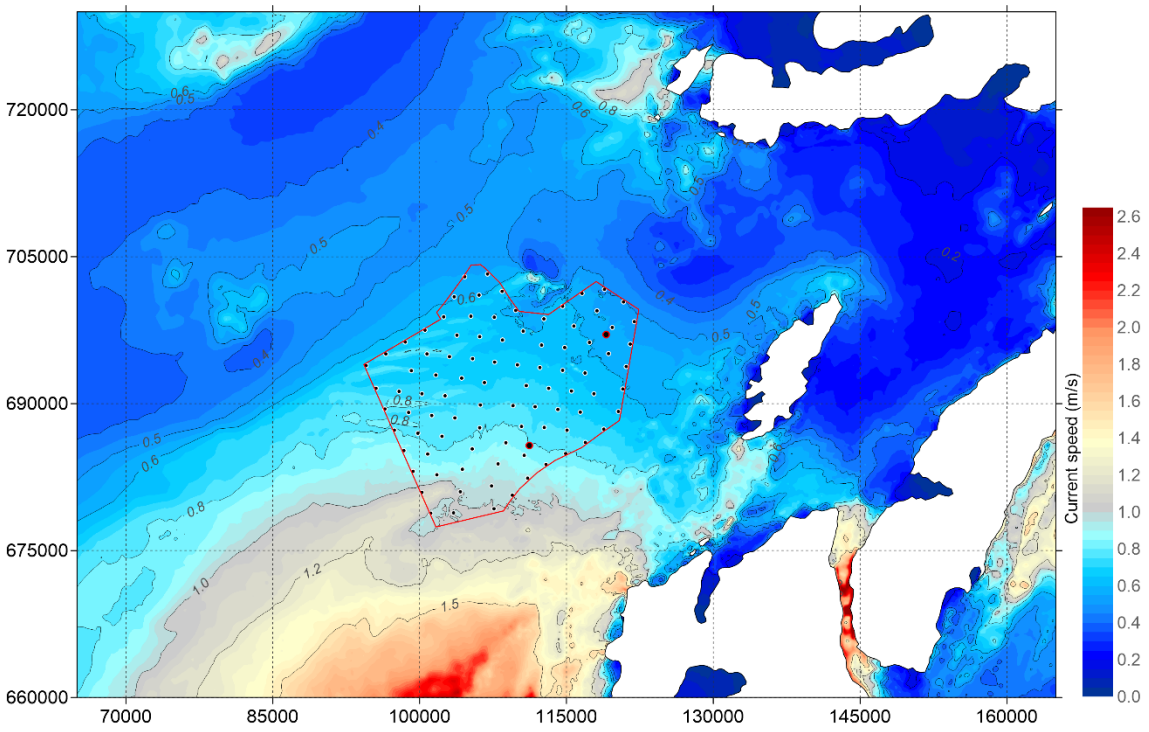

Figure 5-60: 24 MW - Dense Perimeter layout – Maximum current speed over 15 days (Local model)

Absolute Current Speed – 24 MW Even Spread Layout

5.3.10 This section presents the absolute current speeds around the WDA for the 24 MW Even Spread layout. **Figure 5-61** and **Figure 5-62** present the predicted current speed and direction during spring tide for peak flood and peak ebb, respectively. **Figure 5-63** and **Figure 5-64** present the predicted current speed and direction during neap tide for peak flood and peak ebb, respectively. **Figure 5-65** the maximum current speed throughout the full spring-neap tidal cycle simulation.

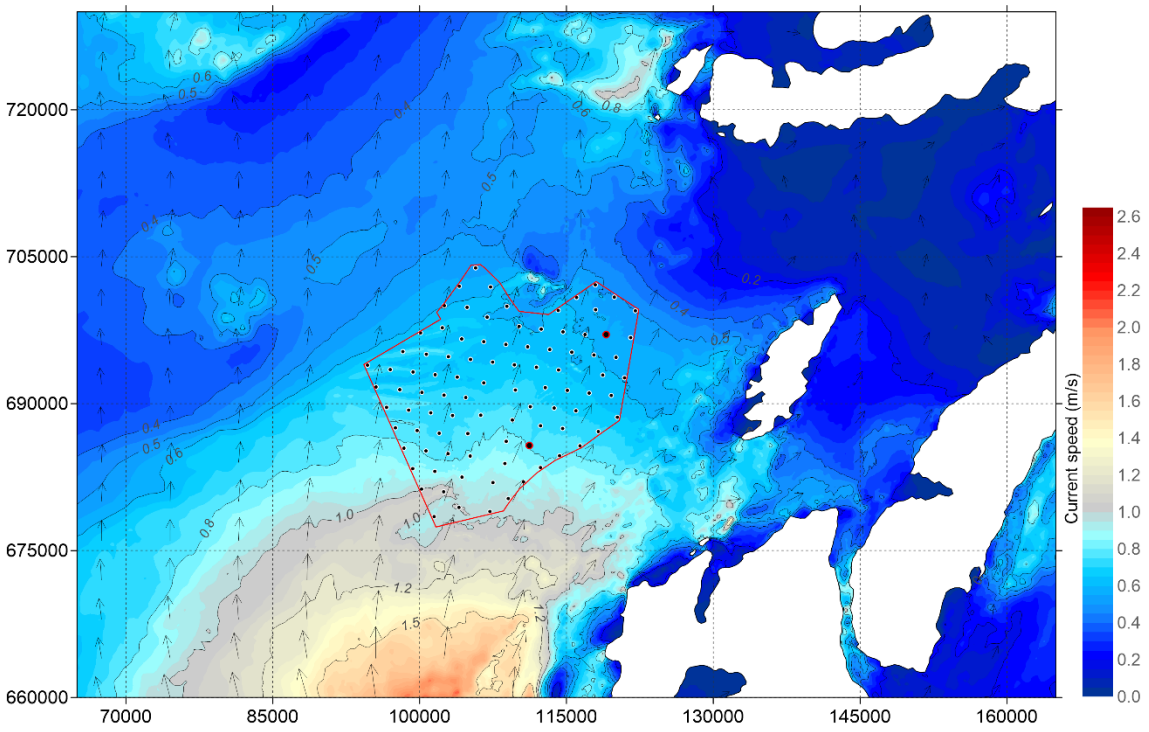

Figure 5-61: 24 MW - Even Spread layout - Current speed during spring tide - peak flood (Local model)

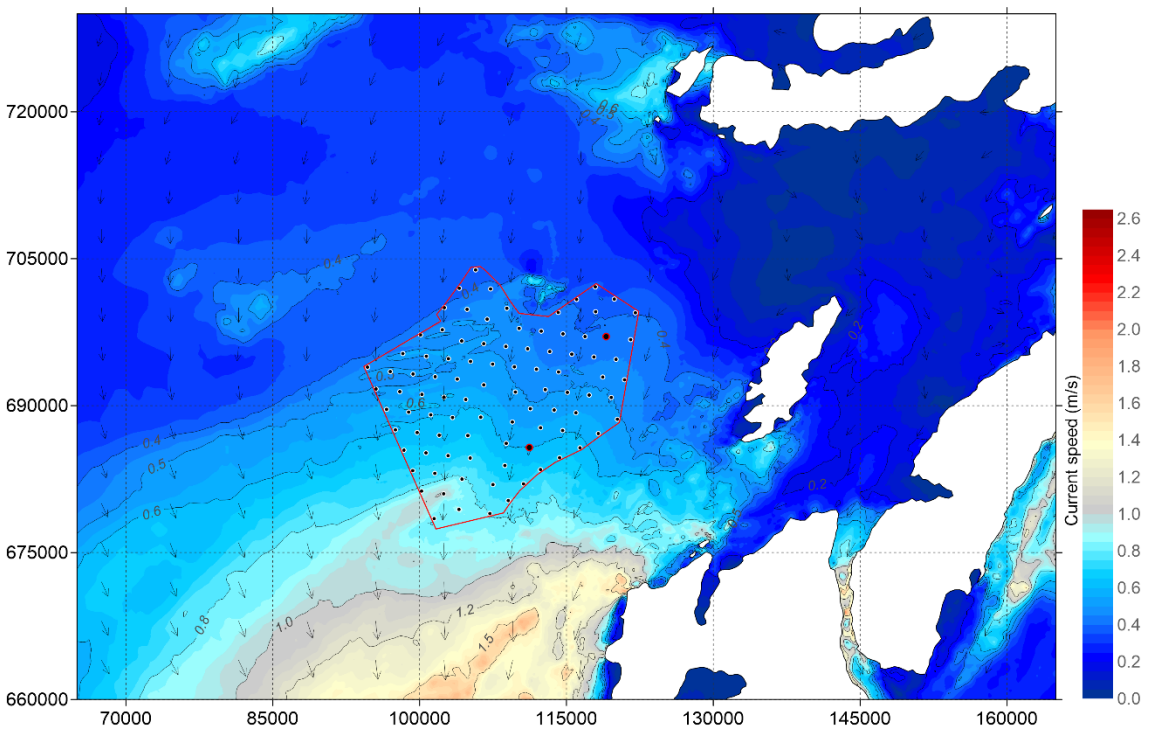

Figure 5-62: 24 MW - Even Spread layout - Current speed during spring tide - peak ebb (Local model)

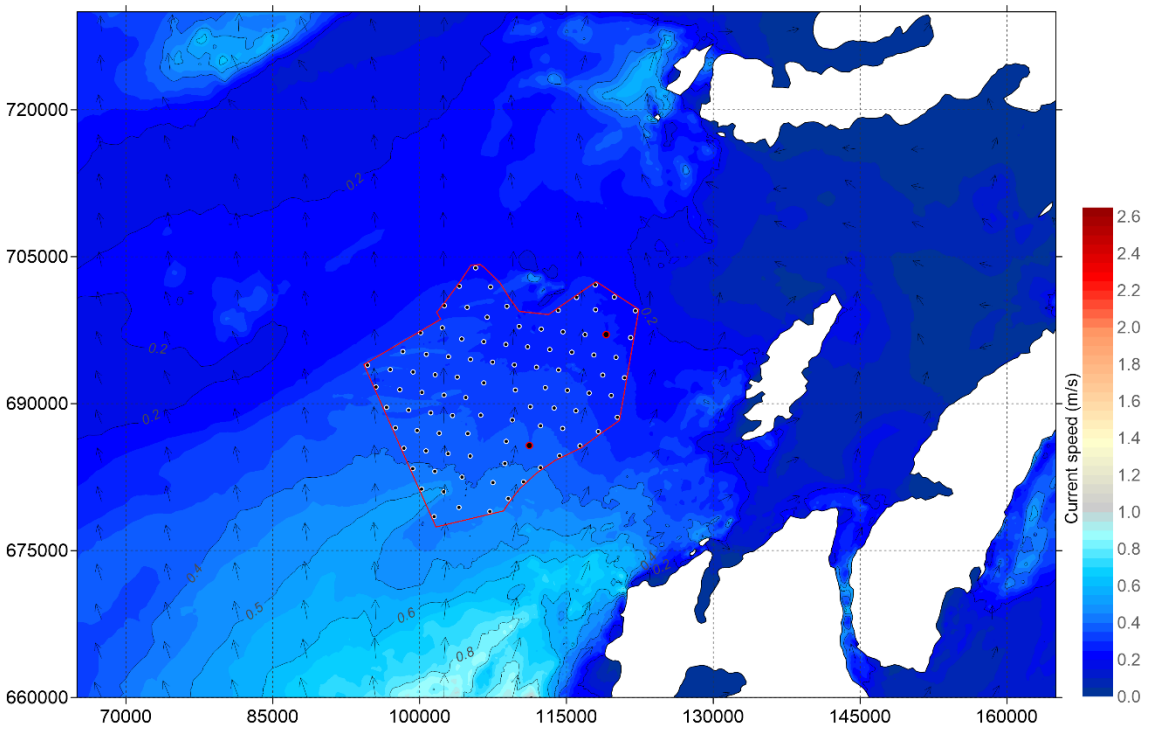

Figure 5-63: 24 MW - Even Spread layout - Current speed during neap tide - peak flood (Local model)

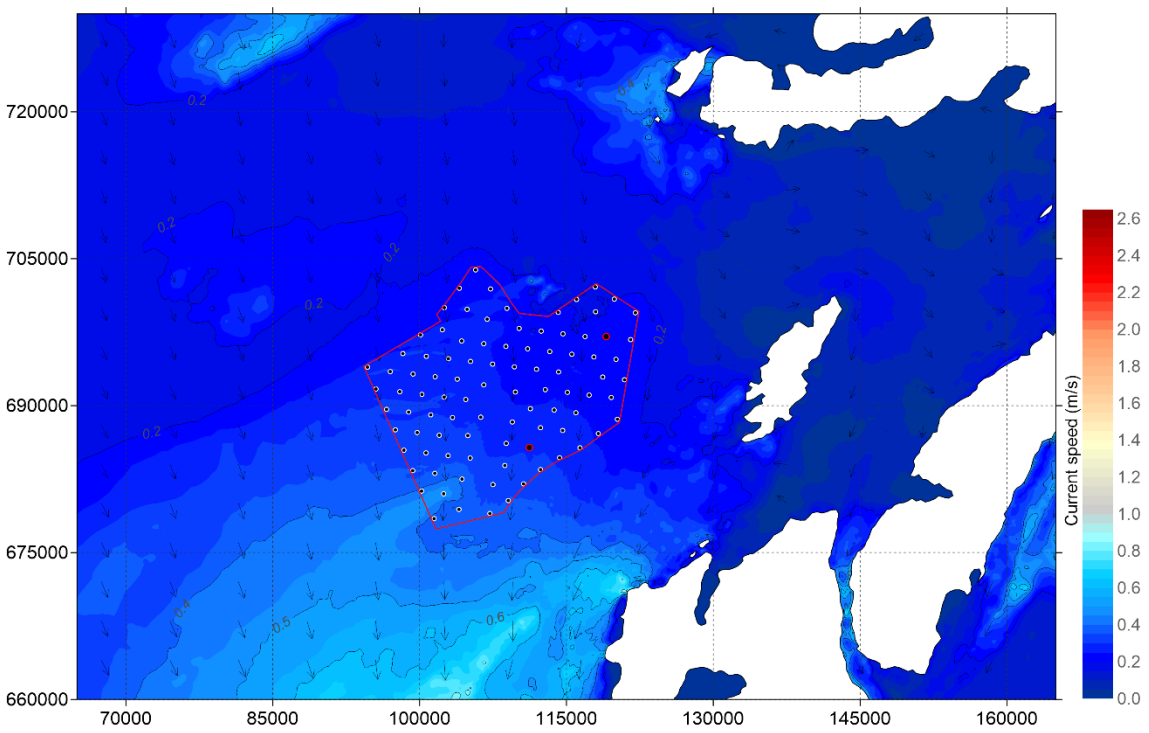

Figure 5-64: 24 MW - Even Spread layout - Current speed during neap tide - peak ebb (Local model)

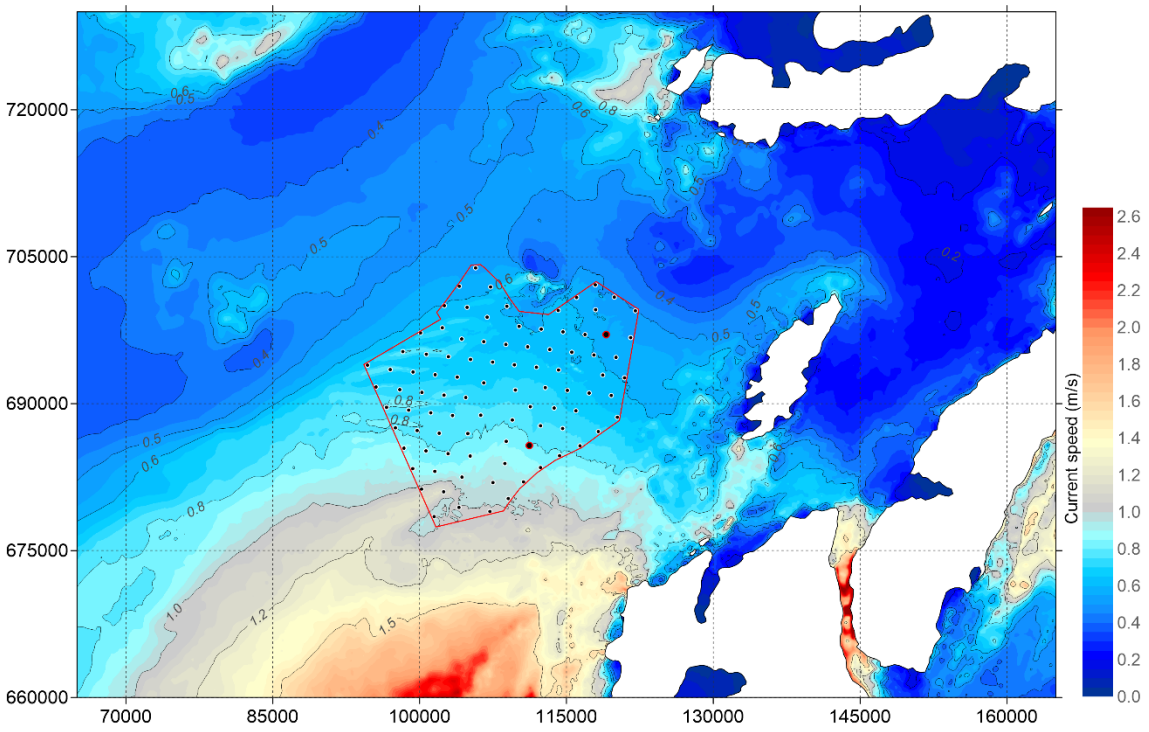

Figure 5-65: 24 MW - Even Spread layout – Maximum current speed over 15 days (Local model)

Impact on Current Speed – 15 MW Dense Perimeter Layout

5.3.11 This section presents the difference in absolute current speeds relative to the baseline around the WDA for the 15 MW Dense Perimeter layout. **Figure 5-66** and **Figure 5-67** present the predicted difference in current speed during spring tide for peak flood and peak ebb, respectively. **Figure 5-68** and **Figure 5-69** present the predicted difference in current speed during neap tide for peak flood and peak ebb, respectively. **Figure 5-70** presents the difference in maximum current speed throughout the full spring-neap tidal cycle simulation.

5.3.12 The results for difference in current speed between the 15 MW – Dense Perimeter layout and baseline scenario, indicate that all change <0.005 m/s is contained almost entirely within the WDA. At the Offshore Substation Platform (OSP) structures the change is greatest as expected, with a localized reduction of up to 0.06 m/s. The change is most pronounced on the peak flood stage of the spring tide.

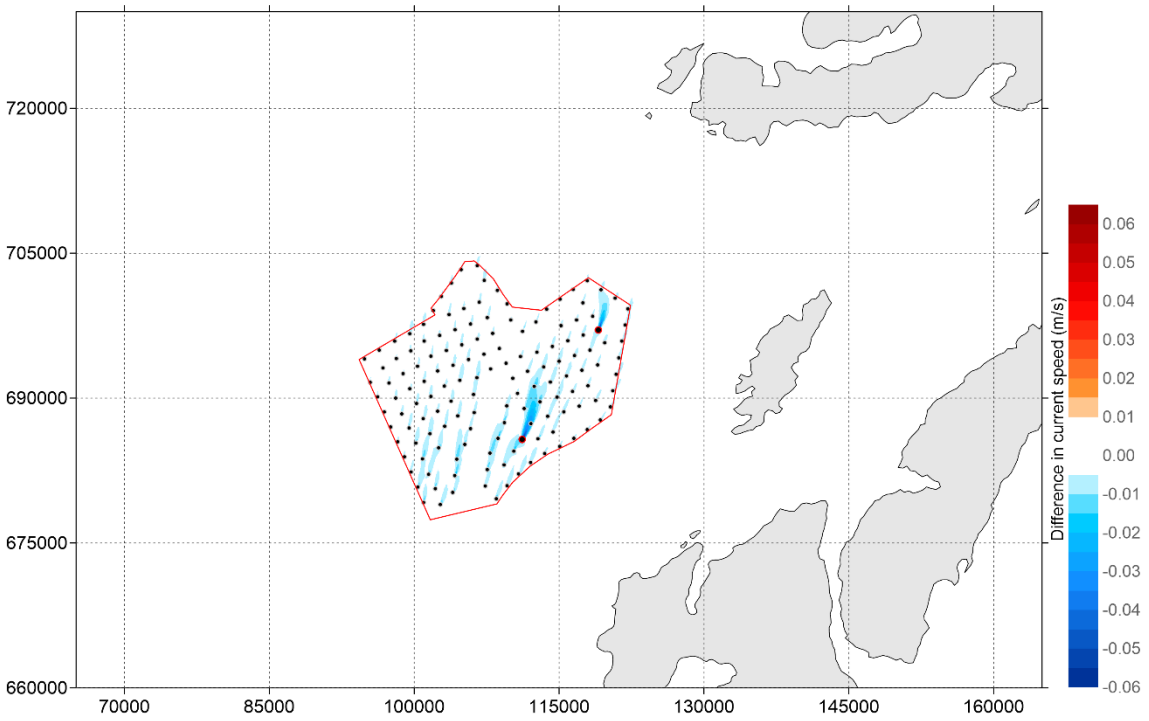

Figure 5-66 Difference in current speed (in meters) between 'Baseline' and '15 MW - Dense Perimeter layout' during spring tide (positive means increase of current speed by layout and vice versa) - peak flood

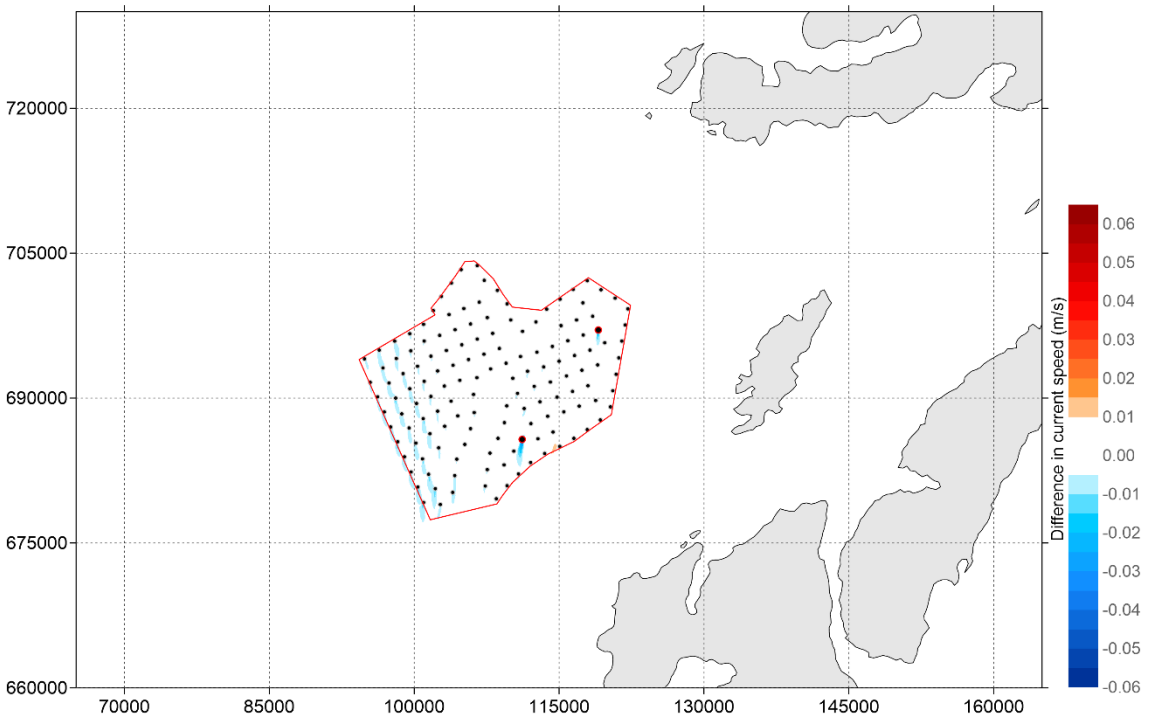

Figure 5-67 Difference in current speed (in meters) between 'Baseline' and '15 MW - Dense Perimeter layout' during spring tide (positive means increase of current speed by layout and vice versa) - peak ebb

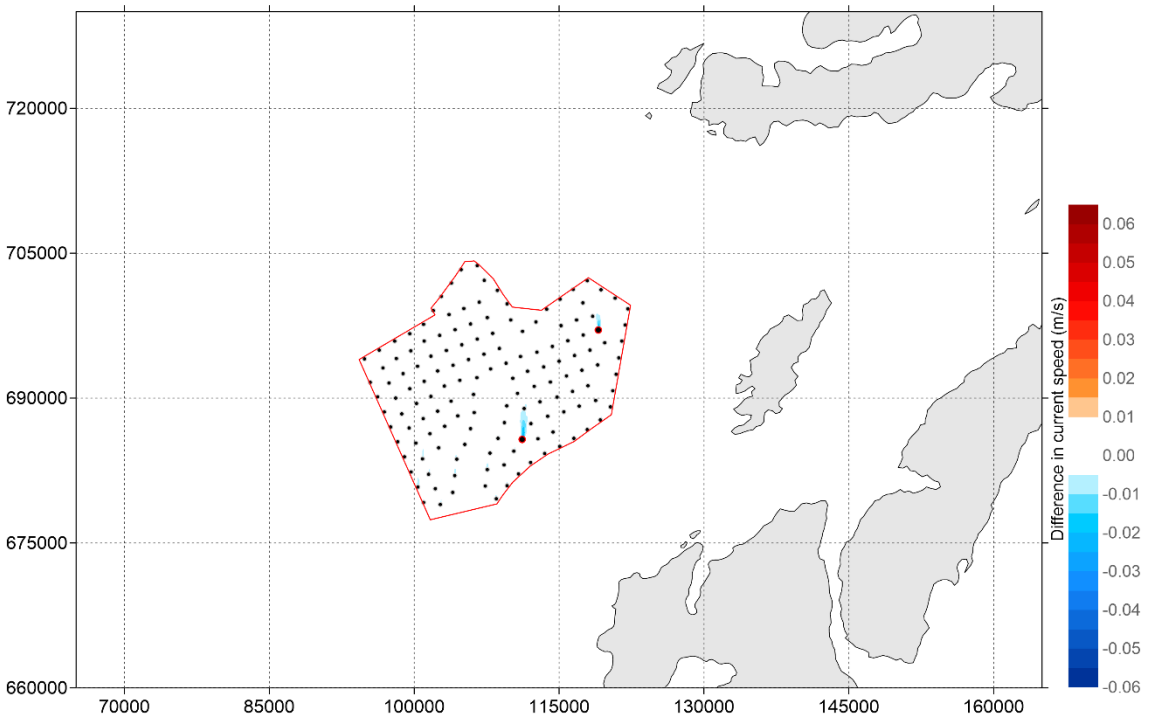

Figure 5-68 Difference in current speed (in meters) between 'Baseline' and '15 MW - Dense Perimeter layout' during neap tide (positive means increase of current speed by layout and vice versa) - peak flood

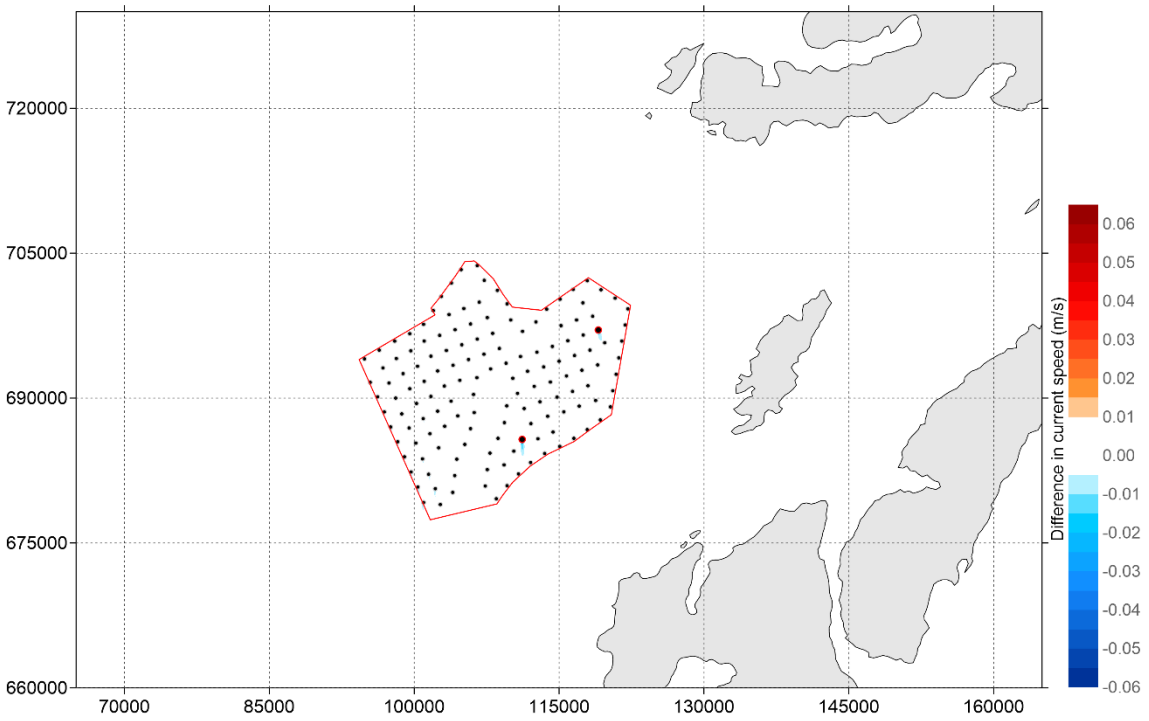

Figure 5-69 Difference in current speed (in meters) between 'Baseline' and '15 MW - Dense Perimeter layout' during neap tide (positive means increase of current speed by layout and vice versa) - peak ebb

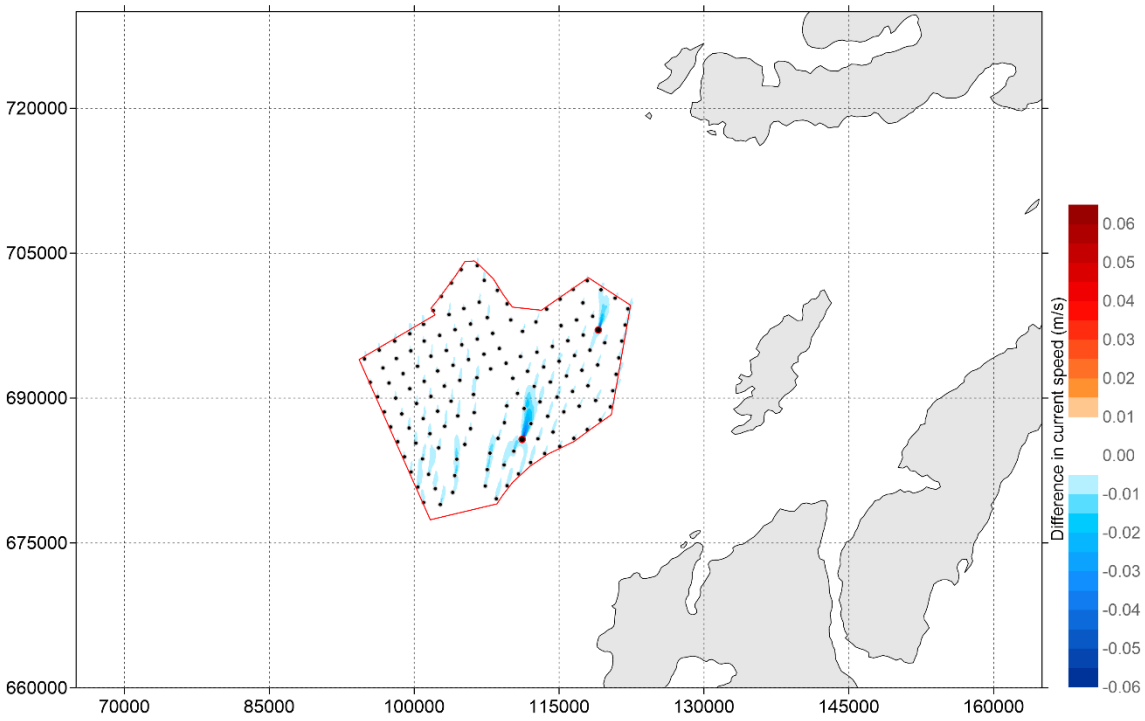

Figure 5-70 Difference in maximum current speed (in meters) between 'Baseline' and '15 MW - Dense Perimeter layout' over 15 days (positive means increase of current speed by layout and vice versa)

Impact on Current Speed – 15 MW Even Spread Layout

5.3.13 This section presents the difference in absolute current speeds relative to the baseline around the WDA for the 15 MW Even Spread layout. **Figure 5-71** and **Figure 5-72** present the predicted difference in current speed during spring tide for peak flood and peak ebb, respectively. **Figure 5-73** and **Figure 5-74** present the predicted difference in current speed during neap tide for peak flood and peak ebb, respectively. **Figure 5-75** presents the difference in maximum current speed throughout the full spring-neap tidal cycle simulation.

5.3.14 The results for difference in current speed between the 15 MW – Even Spread layout and baseline scenario, indicate that all change <0.005m/s is contained almost entirely within the WDA. The difference in current speed is very similar due to the 15 MW – Dense Perimeter layout.

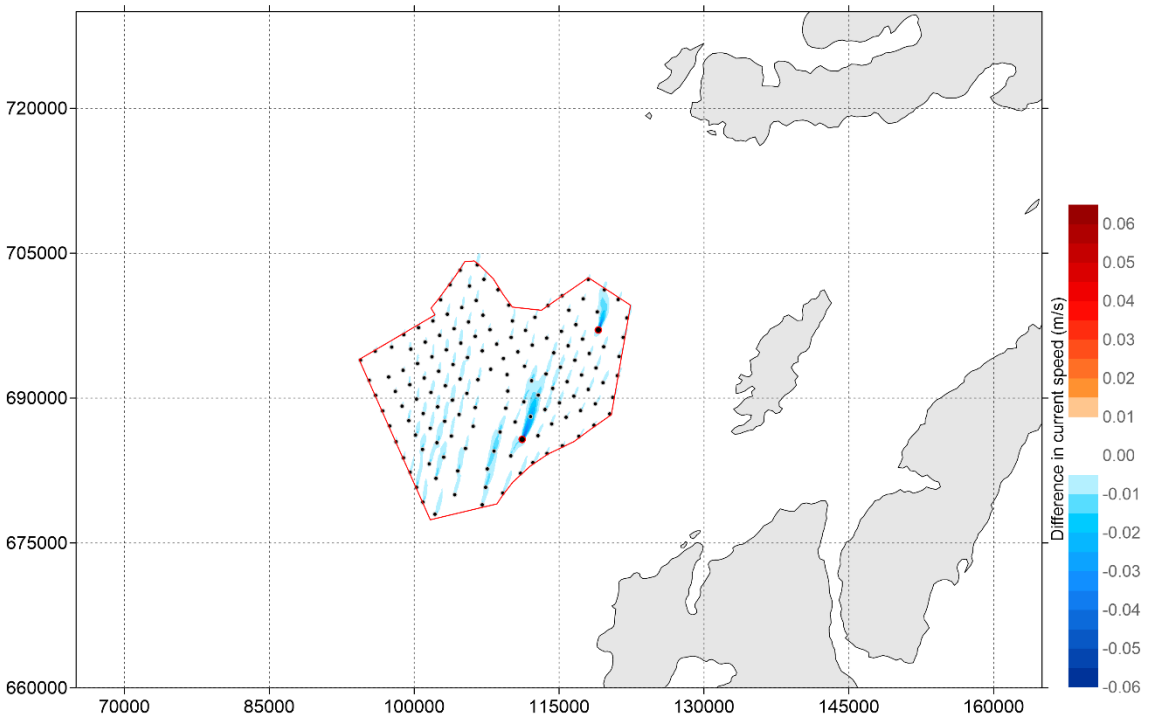

Figure 5-71 Difference in current speed (in meters) between 'Baseline' and '15 MW - Even Spread layout' during spring tide (positive means increase of current speed by layout and vice versa) - peak flood

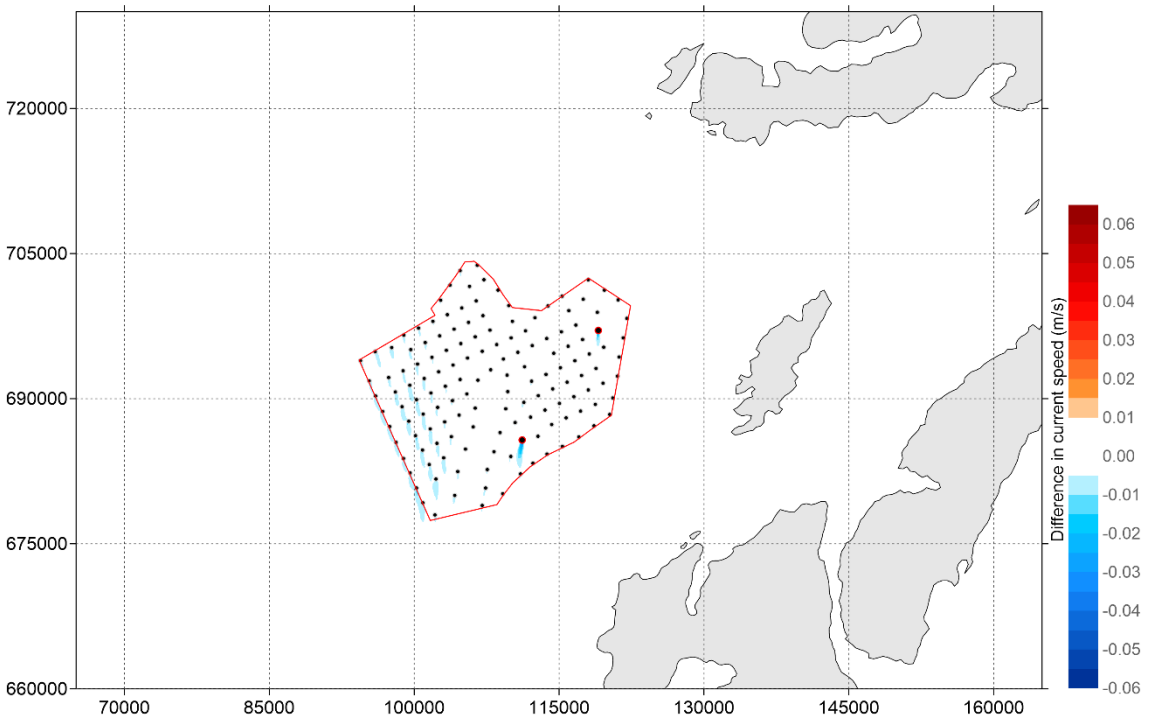

Figure 5-72 Difference in current speed (in meters) between 'Baseline' and '15 MW - Even Spread layout' during spring tide (positive means increase of current speed by layout and vice versa) - peak ebb

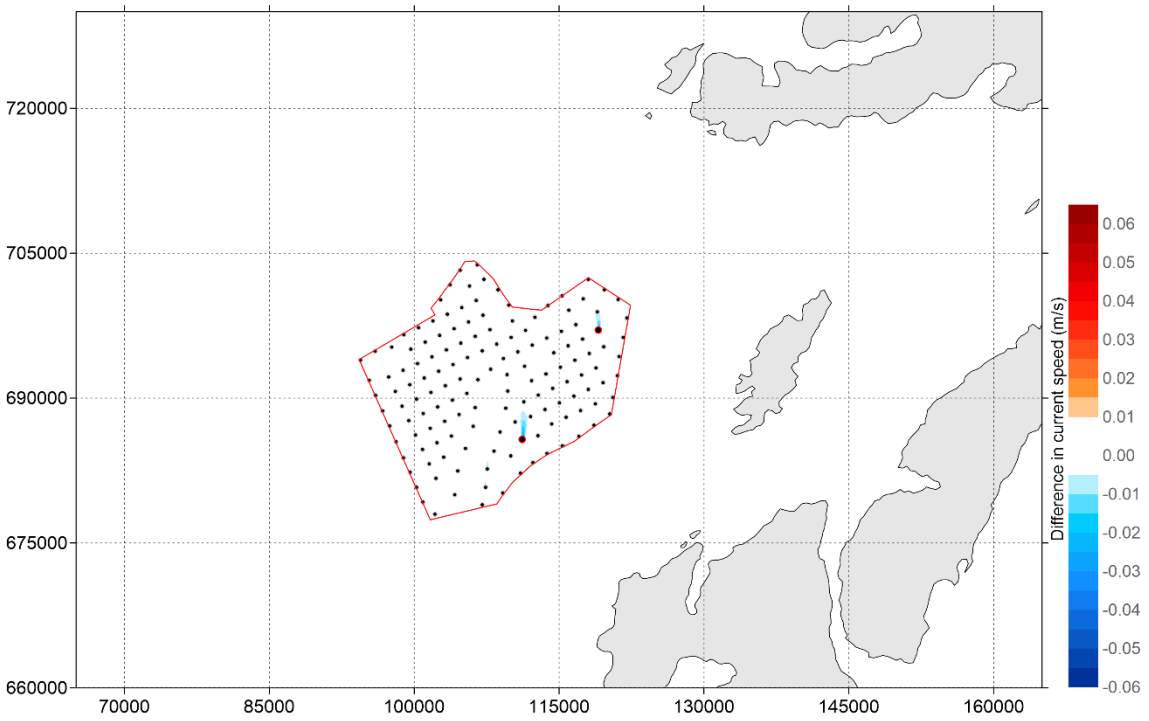

Figure 5-73 Difference in current speed (in meters) between 'Baseline' and '15 MW - Even Spread layout' during neap tide (positive means increase of current speed by layout and vice versa) - peak flood

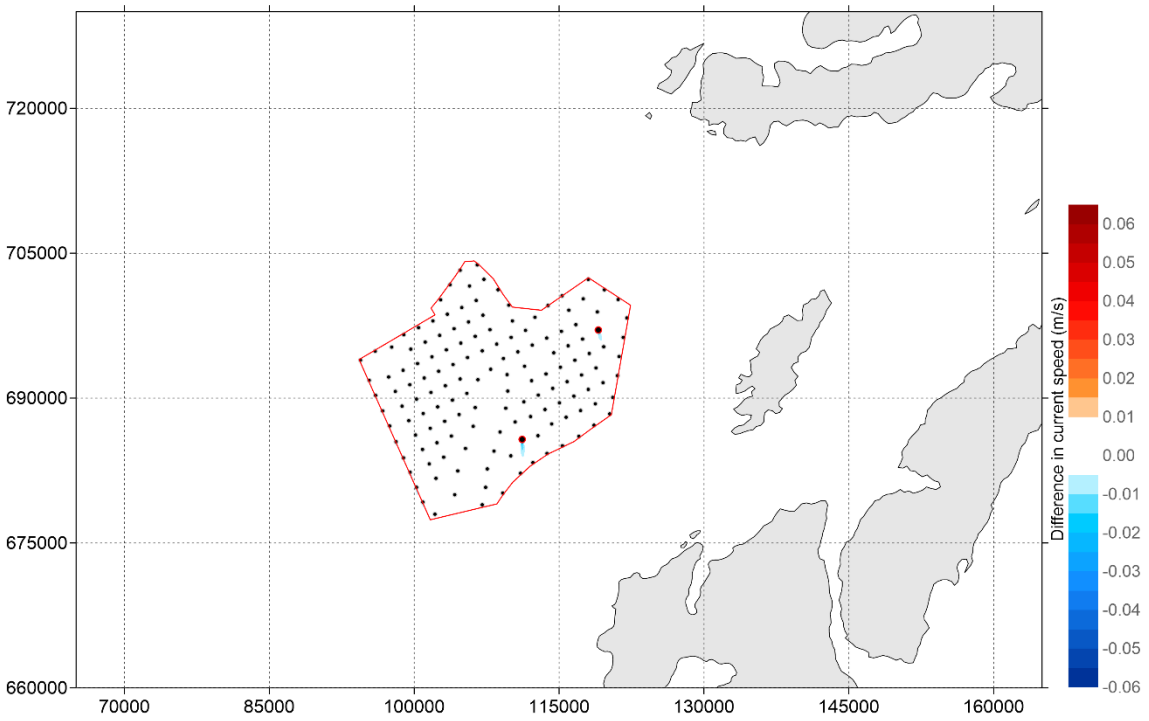

Figure 5-74 Difference in current speed (in meters) between 'Baseline' and '15 MW - Even Spread layout' during neap tide (positive means increase of current speed by layout and vice versa) - peak ebb

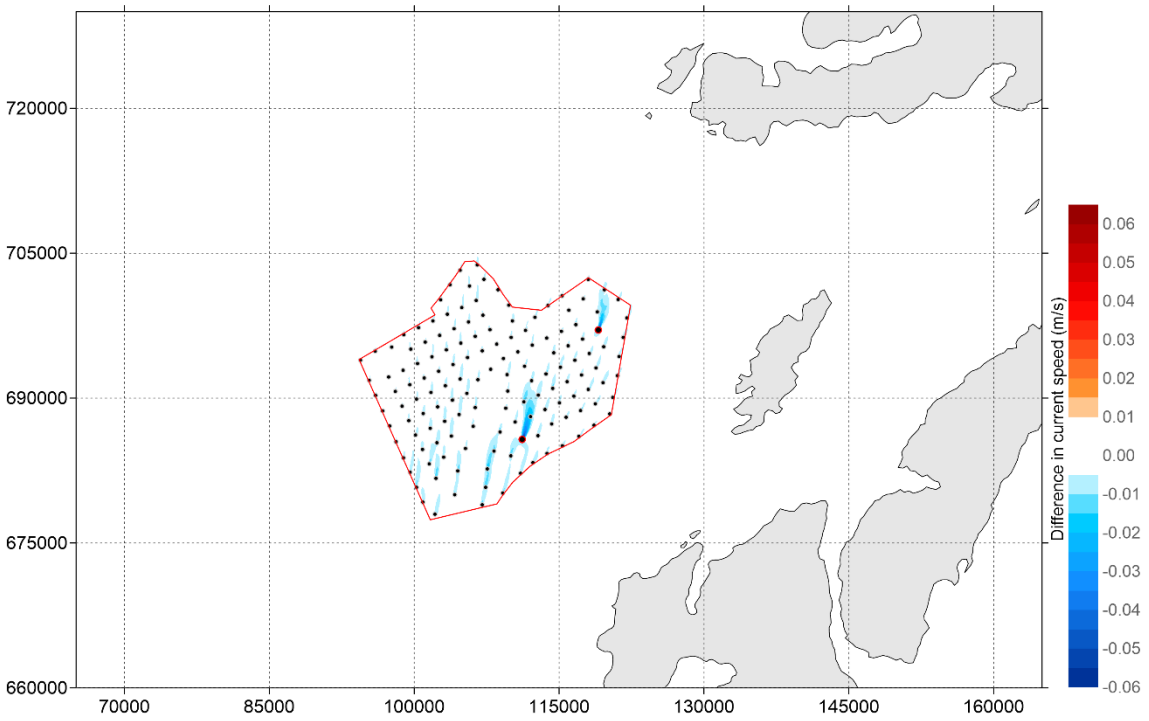

Figure 5-75 Difference in maximum current speed (in meters) between 'Baseline' and '15 MW - Even Spread layout' over 15 days (positive means increase of current speed by layout and vice versa)

Impact on Current Speed – 24 MW Dense Perimeter Layout

5.3.15 This section presents the difference in absolute current speeds relative to the baseline around the WDA for the 24 MW Dense Perimeter layout. **Figure 5-76** and **Figure 5-77** present the predicted difference in current speed during spring tide for peak flood and peak ebb, respectively. **Figure 5-78** and **Figure 5-79** present the predicted difference in current speed during neap tide for peak flood and peak ebb, respectively. **Figure 5-80** presents the difference in maximum current speed throughout the full spring-neap tidal cycle simulation.

5.3.16 The results for difference in current speed between the 24 MW – Dense Perimeter layout and baseline scenario, indicate that all change <0.005m/s is contained almost entirely within the WDA. The difference in current speed is very similar to both the 15 MW Dense Perimeter and 15 MW Even Spread layouts.

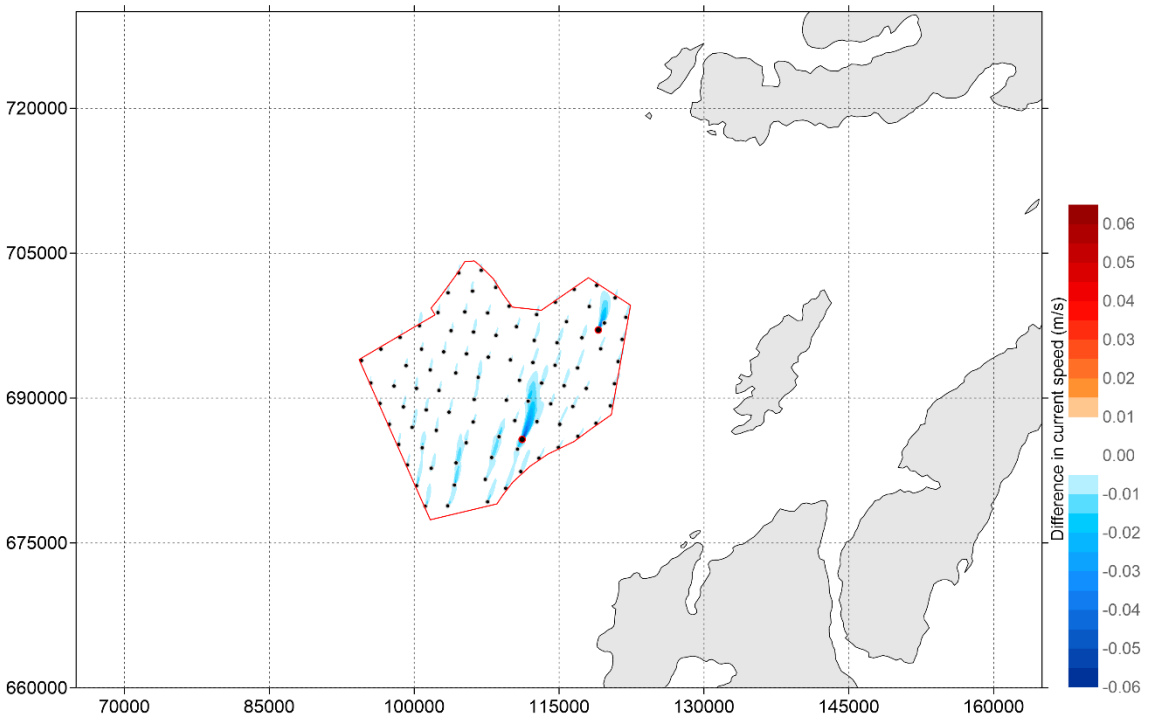

Figure 5-76 Difference in current speed (in meters) between 'Baseline' and '24 MW - Dense Perimeter layout' during spring tide (positive means increase of current speed by layout and vice versa) - peak flood

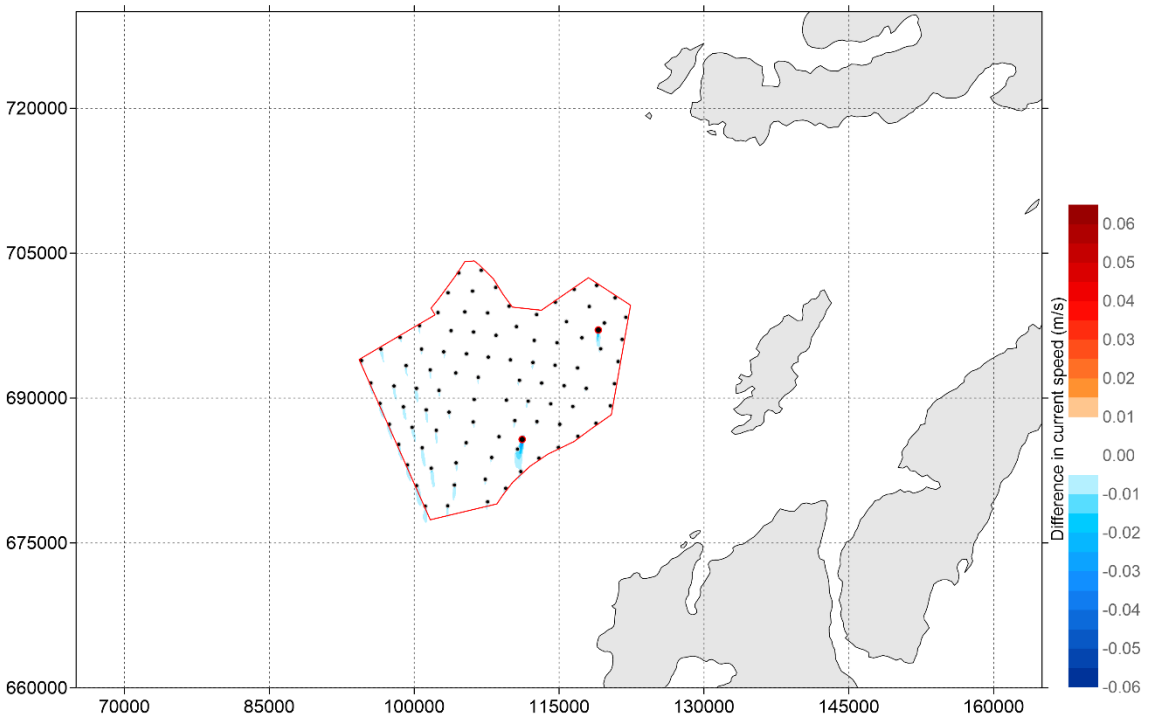

Figure 5-77 Difference in current speed (in meters) between 'Baseline' and '24 MW - Dense Perimeter layout' during spring tide (positive means increase of current speed by layout and vice versa) - peak ebb

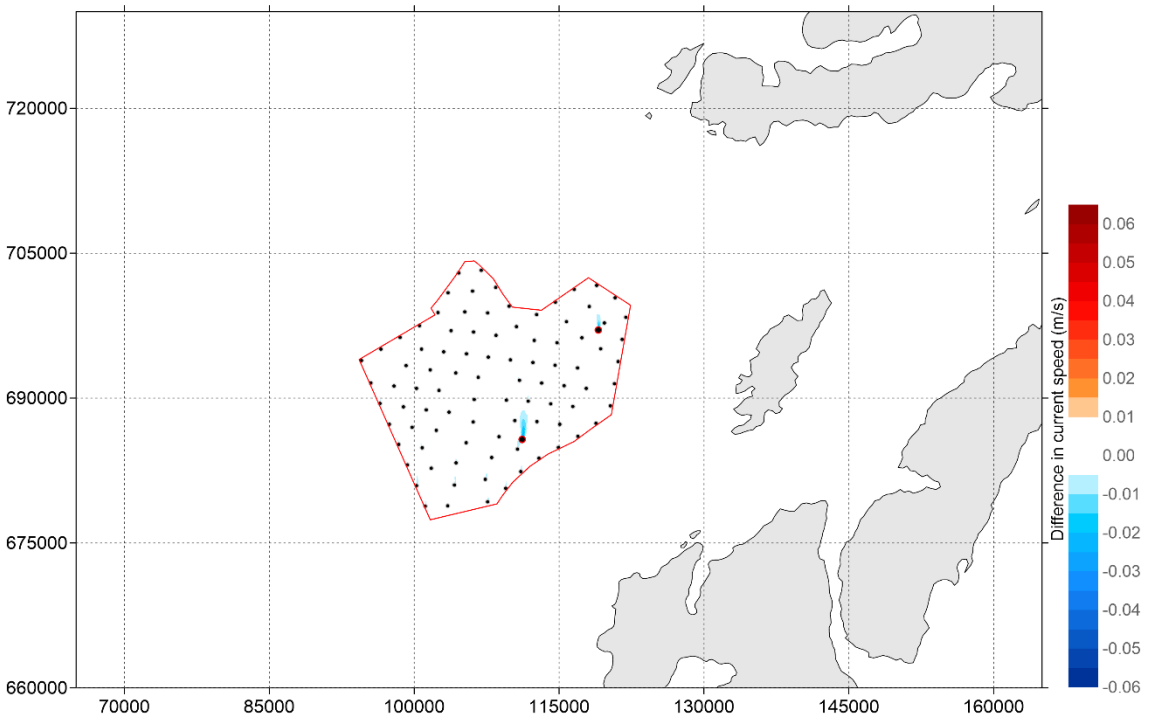

Figure 5-78 Difference in current speed (in meters) between 'Baseline' and '24 MW - Dense Perimeter layout' during neap tide (positive means increase of current speed by layout and vice versa) - peak flood

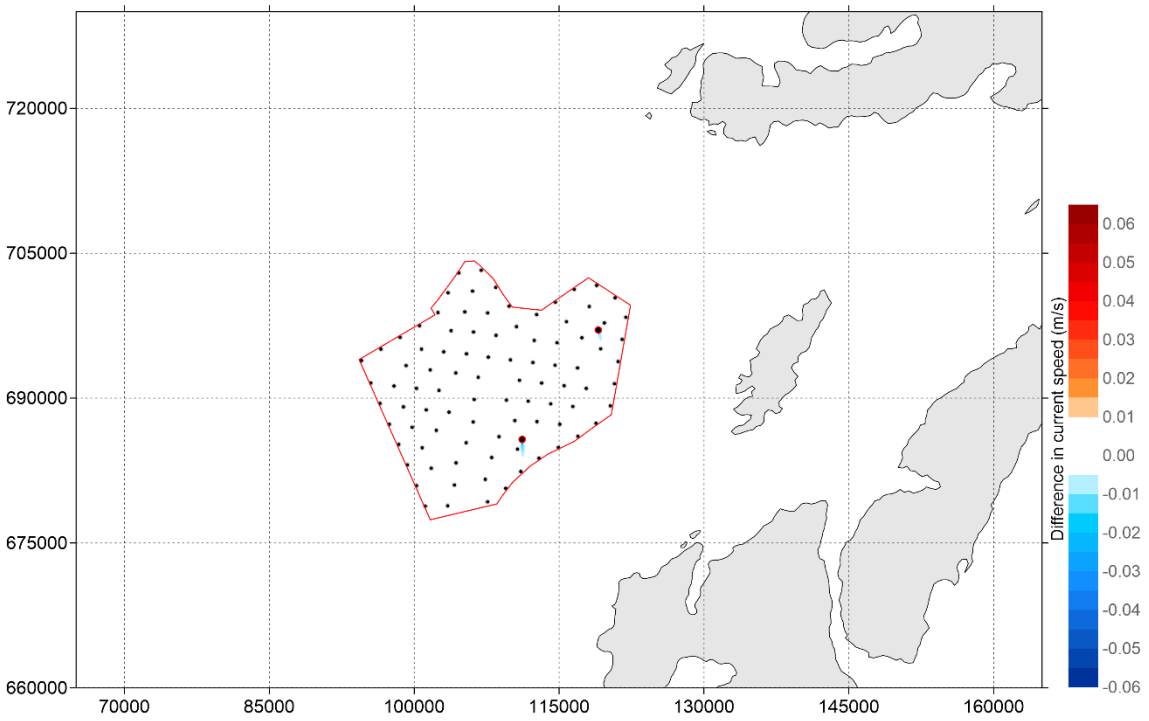

Figure 5-79 Difference in current speed (in meters) between 'Baseline' and '24 MW - Dense Perimeter layout' during neap tide (positive means increase of current speed by layout and vice versa) - peak ebb

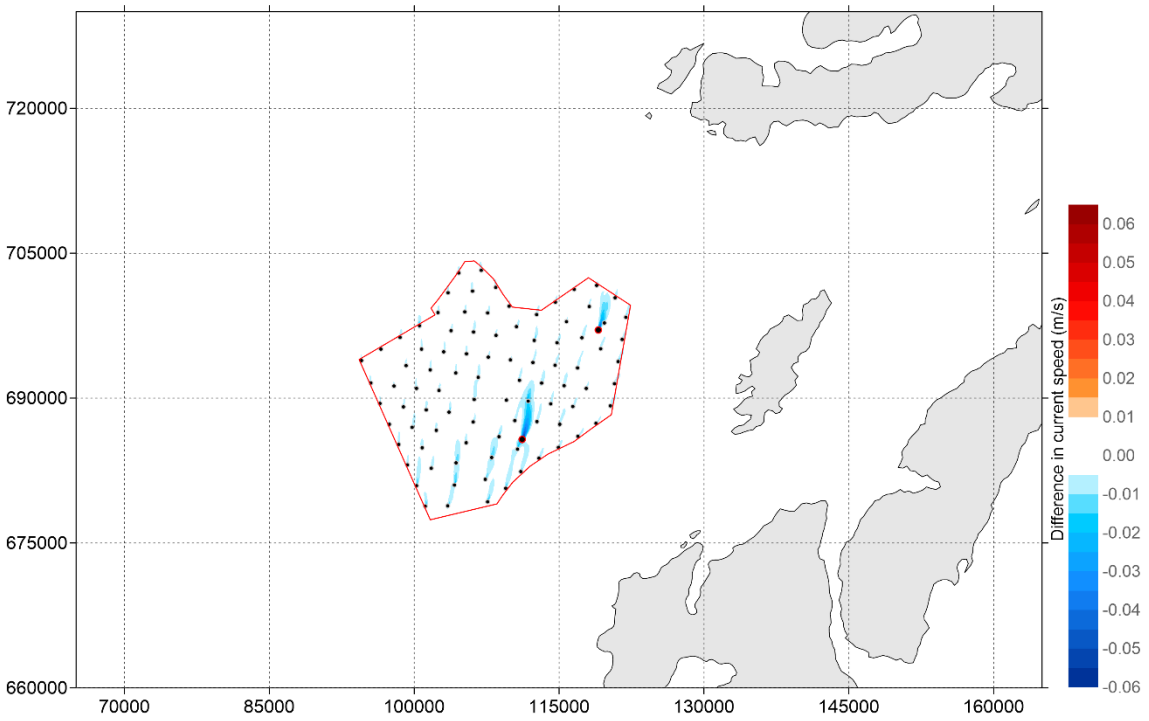

Figure 5-80 Difference in maximum current speed (in meters) between 'Baseline' and '24 MW - Dense Perimeter layout' over 15 days (positive means increase of current speed by layout and vice versa)

Impact on Current Speed – 24 MW Even Spread Layout

5.3.17 This section presents the difference in absolute current speeds relative to the baseline around the WDA for the 24 MW Even Spread layout. **Figure 5-81** and **Figure 5-82** present the predicted difference in current speed during spring tide for peak flood and peak ebb, respectively. **Figure 5-83** and **Figure 5-84** present the predicted difference in current speed during neap tide for peak flood and peak ebb, respectively. **Figure 5-85** presents the difference in maximum current speed throughout the full spring-neap tidal cycle simulation.

5.3.18 The results for difference in current speed between the 24 MW – Even Spread layout and baseline scenario, indicate that all change <0.005m/s is contained almost entirely within the WDA. The difference in current speed is very similar to all other layouts.

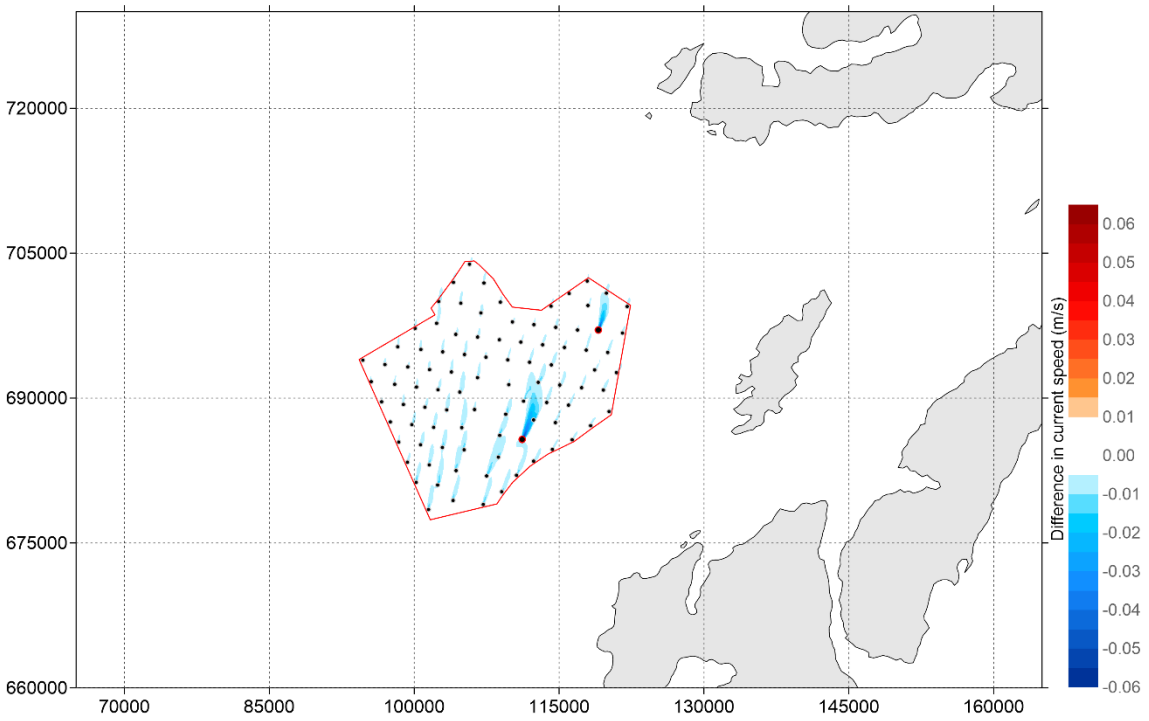

Figure 5-81 Difference in current speed (in meters) between 'Baseline' and '24 MW - Even Spread layout' during spring tide (positive means increase of current speed by layout and vice versa) - peak flood

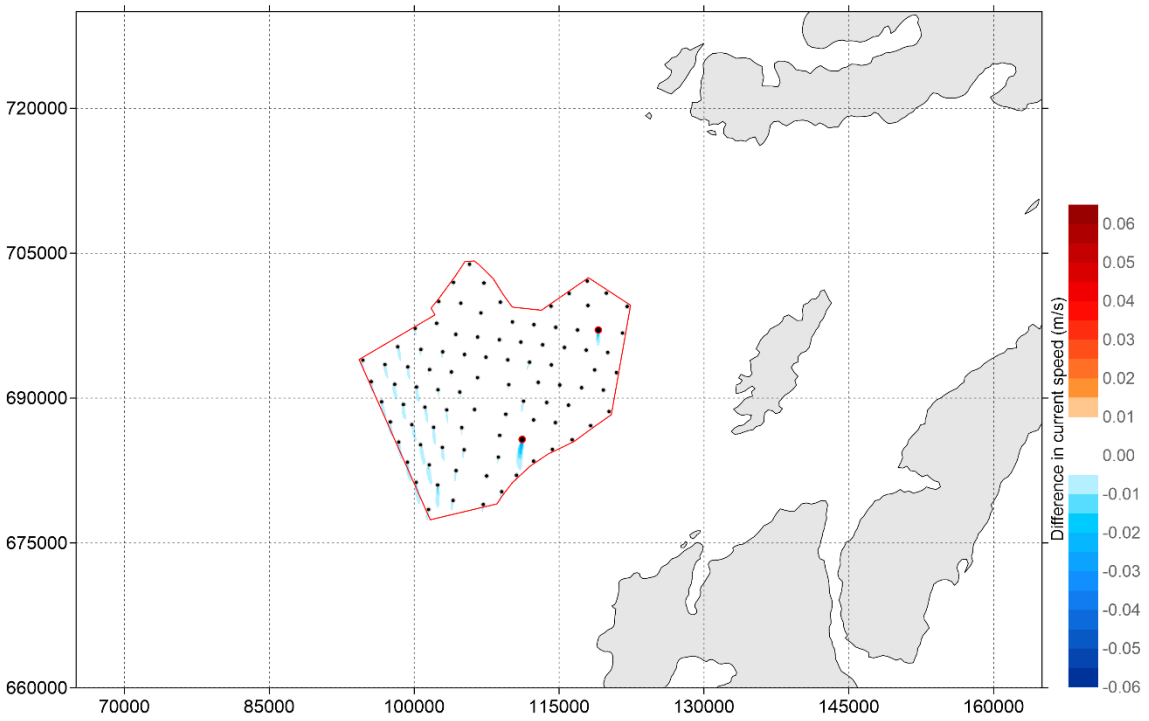

Figure 5-82 Difference in current speed (in meters) between 'Baseline' and '24 MW - Even Spread layout' during spring tide (positive means increase of current speed by layout and vice versa) - peak ebb

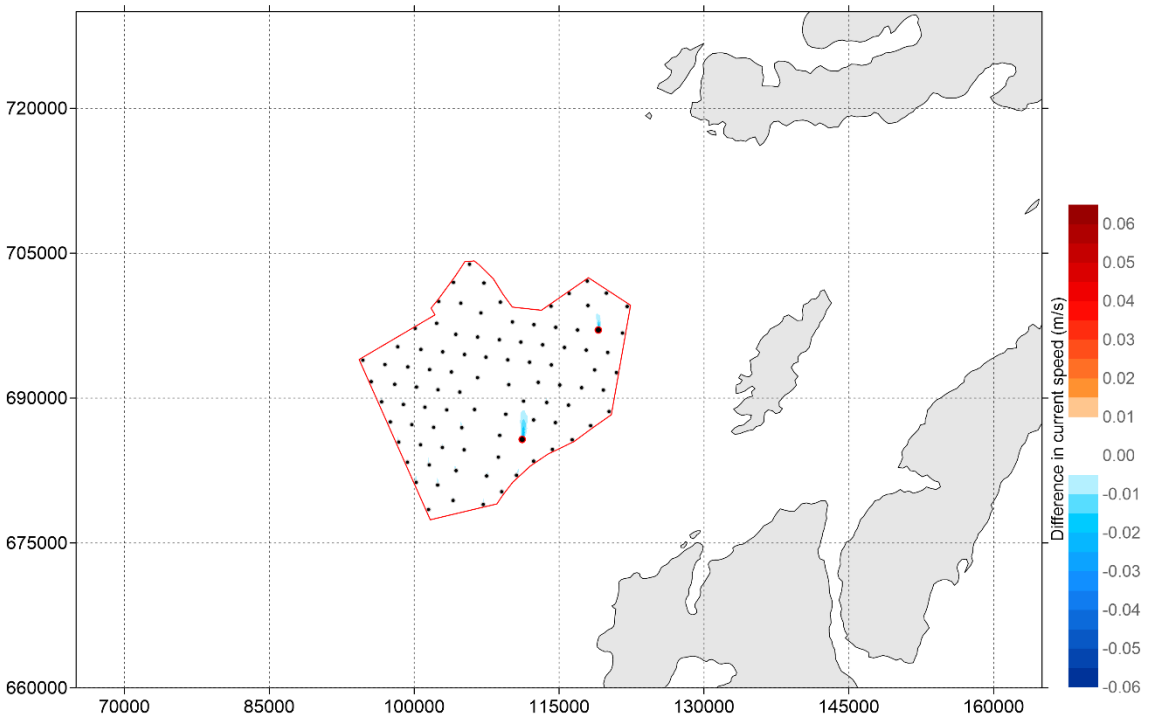

Figure 5-83 Difference in current speed (in meters) between 'Baseline' and '24 MW - Even Spread layout' during neap tide (positive means increase of current speed by layout and vice versa) - peak flood

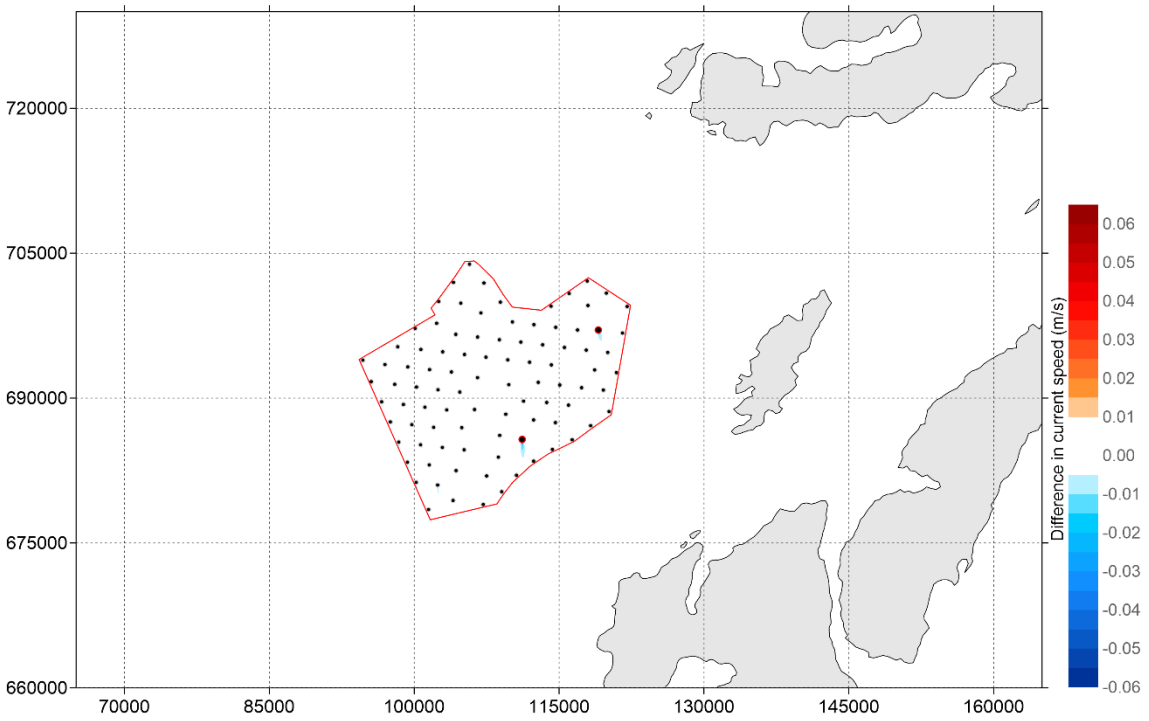

Figure 5-84 Difference in current speed (in meters) between 'Baseline' and '24 MW - Even Spread layout' during neap tide (positive means increase of current speed by layout and vice versa) - peak ebb

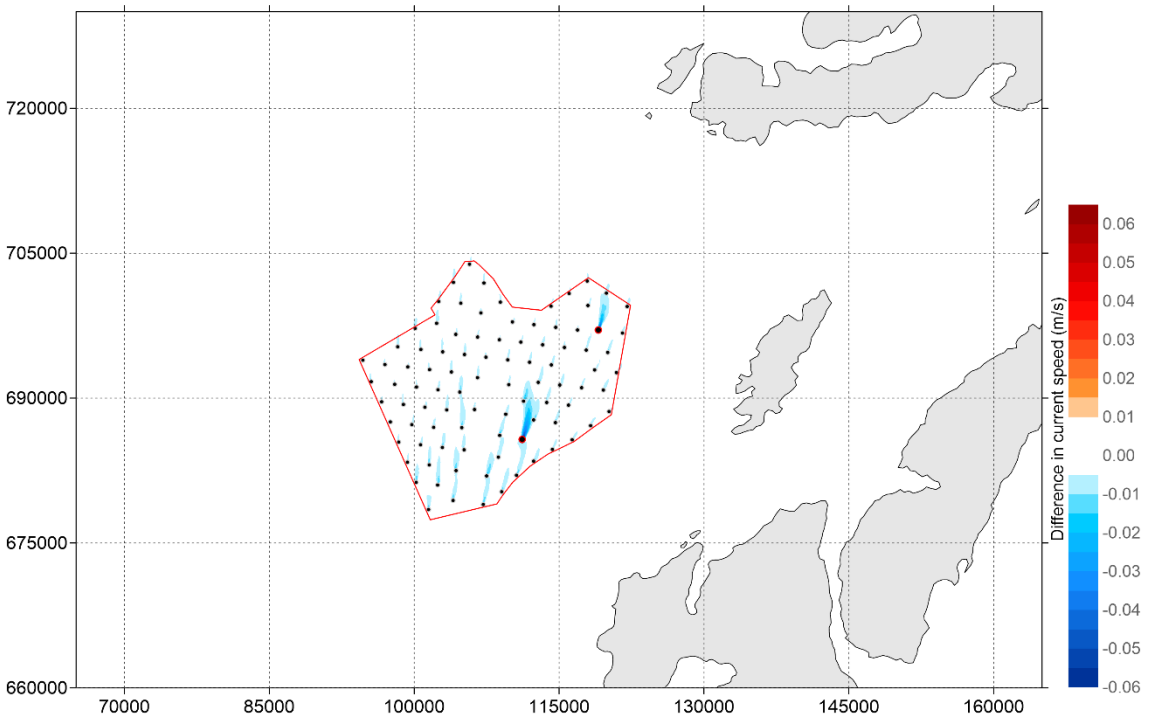

Figure 5-85 Difference in maximum current speed (in meters) between 'Baseline' and '24 MW - Even Spread layout' over 15 days (positive means increase of current speed by layout and vice versa)

Impact on Current Speed in Percentage – 15 MW Dense Perimeter Layout

5.3.19 This section presents the percentage difference in current speeds relative to the baseline around the WDA for the 15 MW Dense Perimeter layout. **Figure 5-86** and **Figure 5-87** present the predicted percentage difference in current speed during spring tide for peak flood and peak ebb, respectively. **Figure 5-88** and **Figure 5-89** present the predicted percentage difference in current speed during neap tide for peak flood and peak ebb, respectively. **Figure 5-90** presents the percentage difference in maximum current speed throughout the full spring-neap tidal cycle simulation.

5.3.20 The predicted percentage difference in current speed extending outside the WDA between the 15 MW – Dense Perimeter indicative layout and baseline scenario is more pronounced during the spring tide. At peak flood, the percentage difference is a reduction of up to 1.0% extending up to 2.5 km north of the WDA. At peak ebb, there is a reduction of up to 1.0% extending 8 km northwest of the WDA and an increase of up to 2.0% extending 7 km northeast of the WDA.

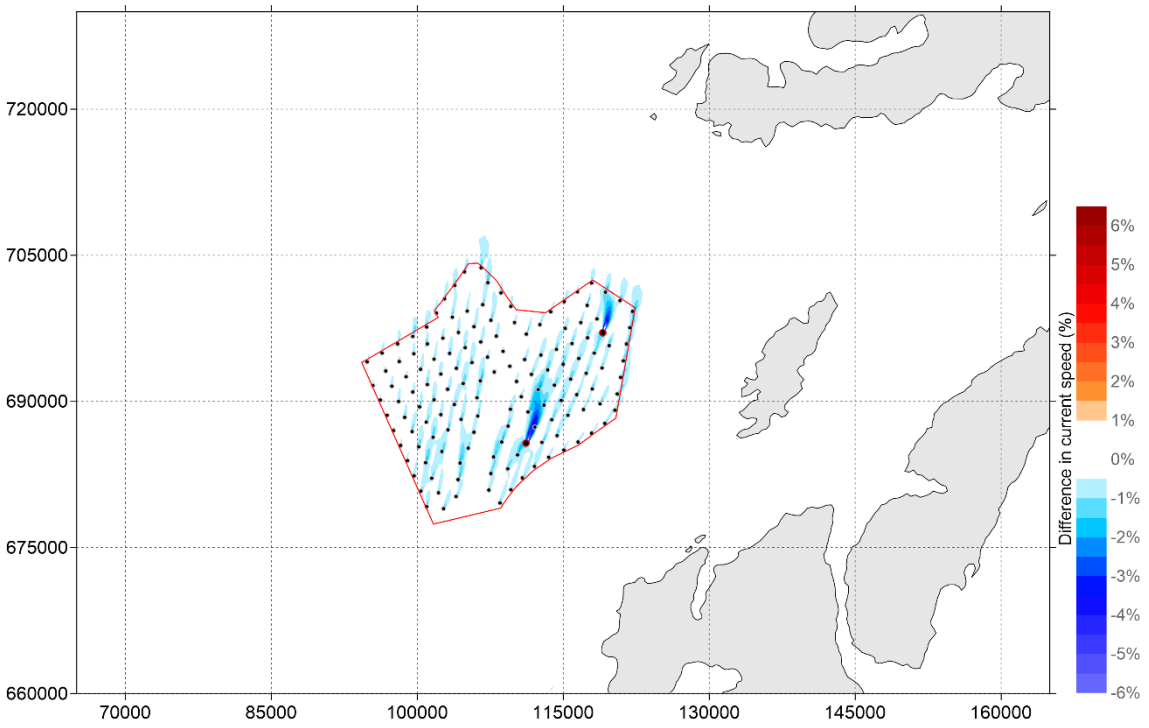

Figure 5-86 Percentage change of current speed between 'Baseline' and '15 MW - Dense Perimeter layout' during spring tide (positive means increase of current speed by layout and vice versa) - peak flood

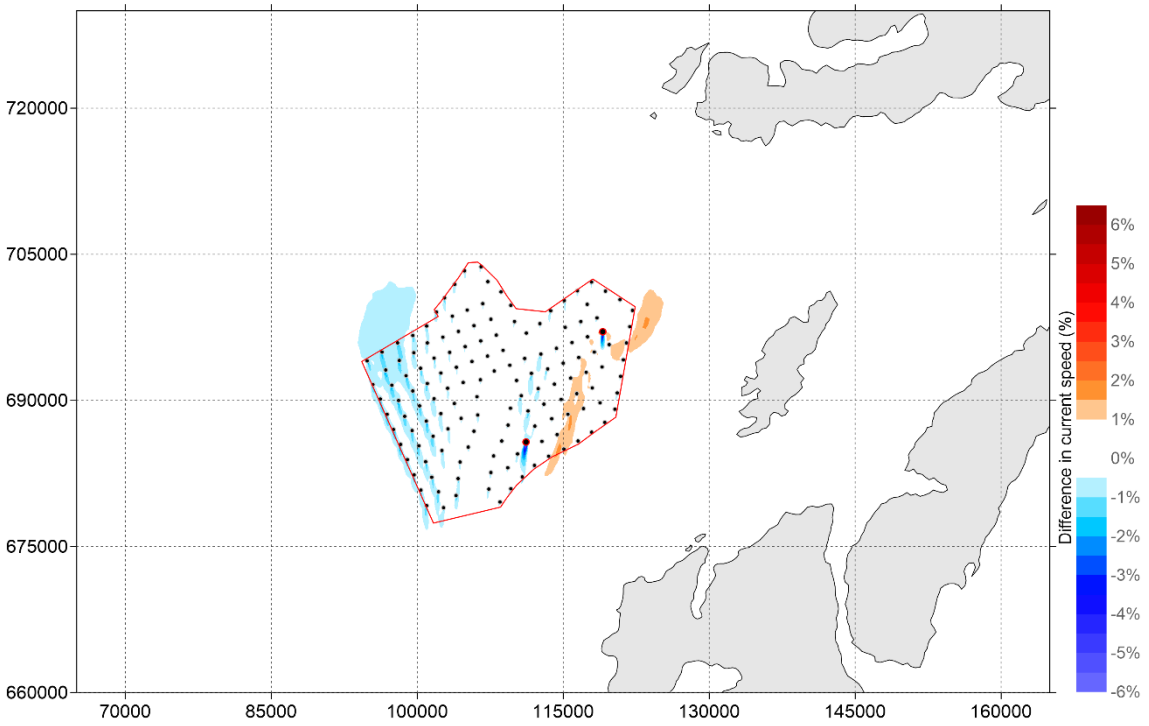

Figure 5-87 Percentage change of current speed between 'Baseline' and '15 MW - Dense Perimeter layout' during spring tide (positive means increase of current speed by layout and vice versa) - peak ebb

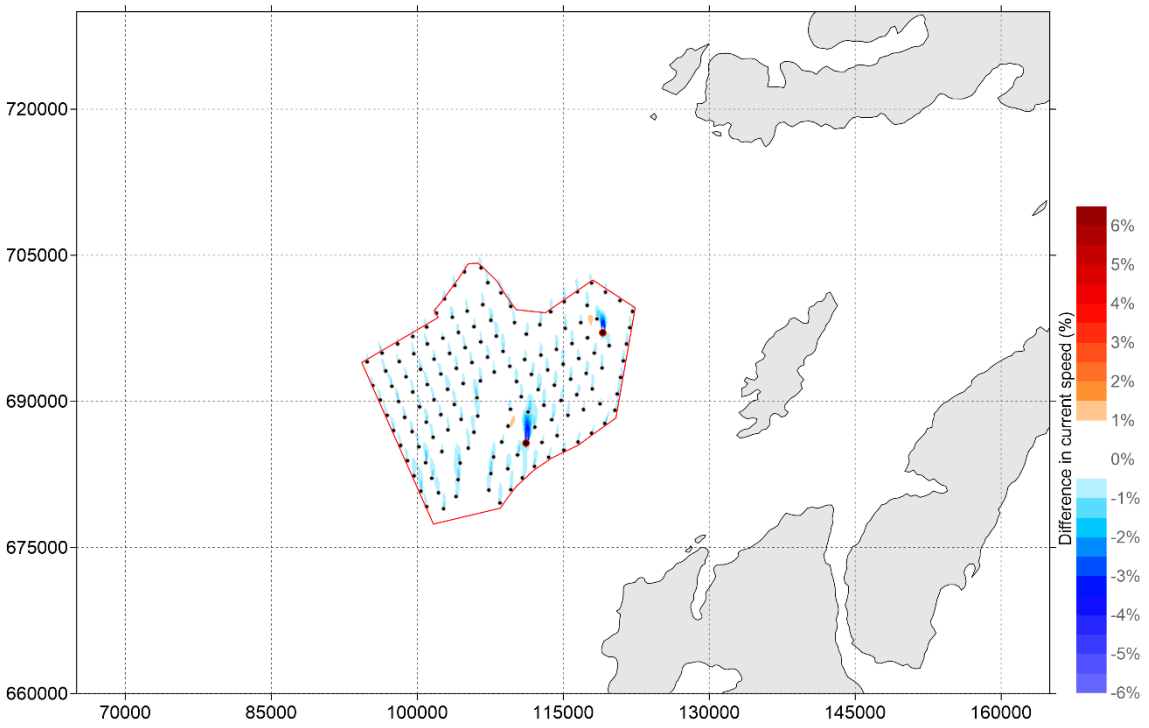

Figure 5-88 Percentage change of current speed between 'Baseline' and '15 MW - Dense Perimeter layout' during neap tide (positive means increase of current speed by layout and vice versa) - peak flood

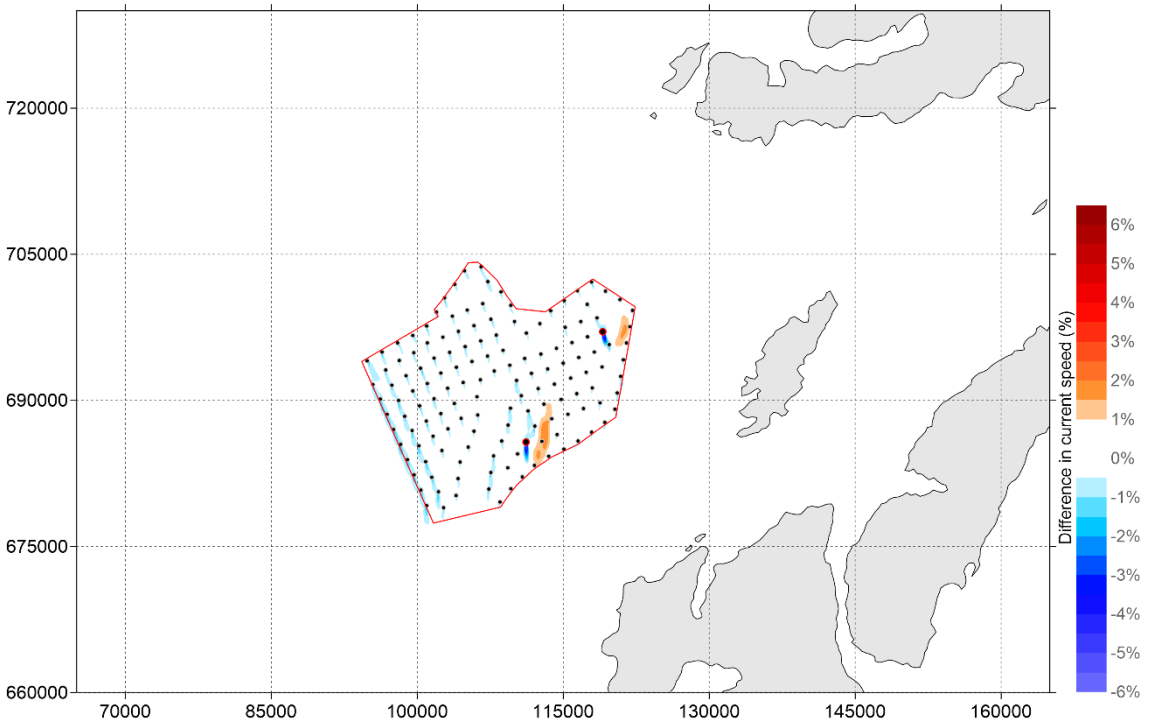

Figure 5-89 Percentage change of current speed between 'Baseline' and '15 MW - Dense Perimeter layout' during neap tide (positive means increase of current speed by layout and vice versa) - peak ebb

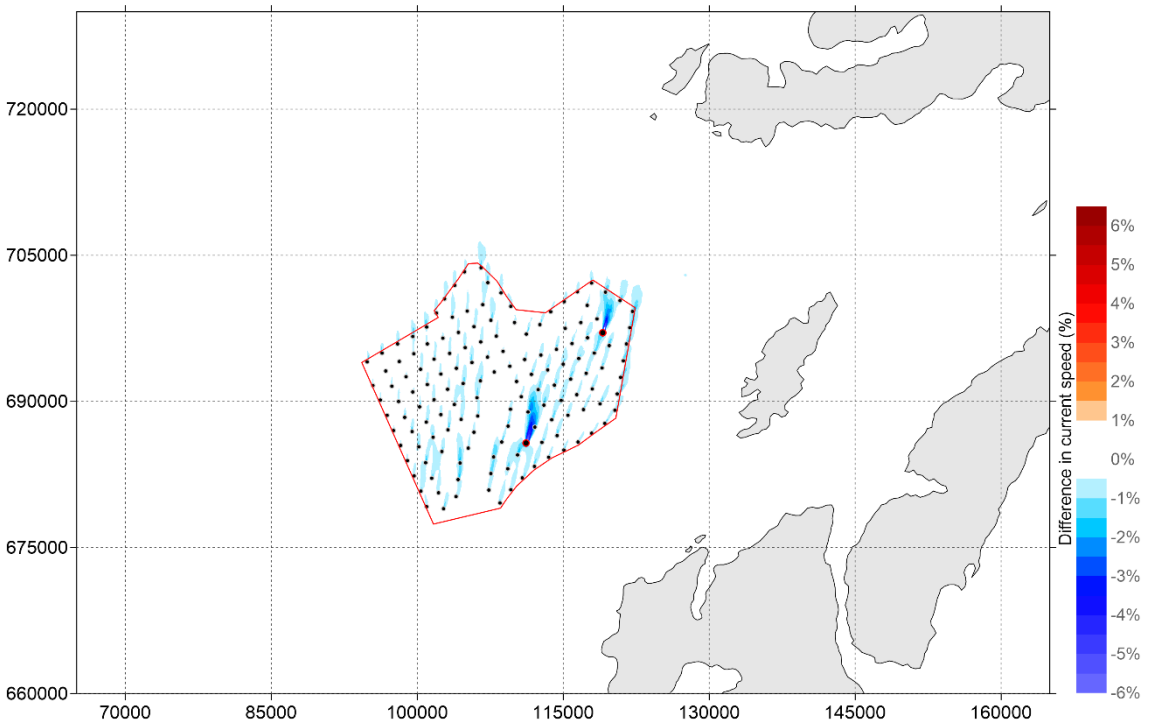

Figure 5-90 Percentage change of maximum current speed between 'Baseline' and '15 MW - Dense Perimeter layout' over 15 days (positive means increase of current speed by layout and vice versa)

Impact on Current Speed in Percentage – 15 MW Even Spread Layout

5.3.21 This section presents the percentage difference in current speeds relative to the baseline around the WDA for the 15 MW Even Spread layout. **Figure 5-91** and **Figure 5-92** present the predicted percentage difference in current speed during spring tide for peak flood and peak ebb, respectively. **Figure 5-93** and **Figure 5-94** present the predicted percentage difference in current speed during neap tide for peak flood and peak ebb, respectively. **Figure 5-95** presents the percentage difference in maximum current speed throughout the full spring-neap tidal cycle simulation.

5.3.22 The percentage change in current speed shows a very similar pattern for 15 MW Dense Perimeter, as presented above.

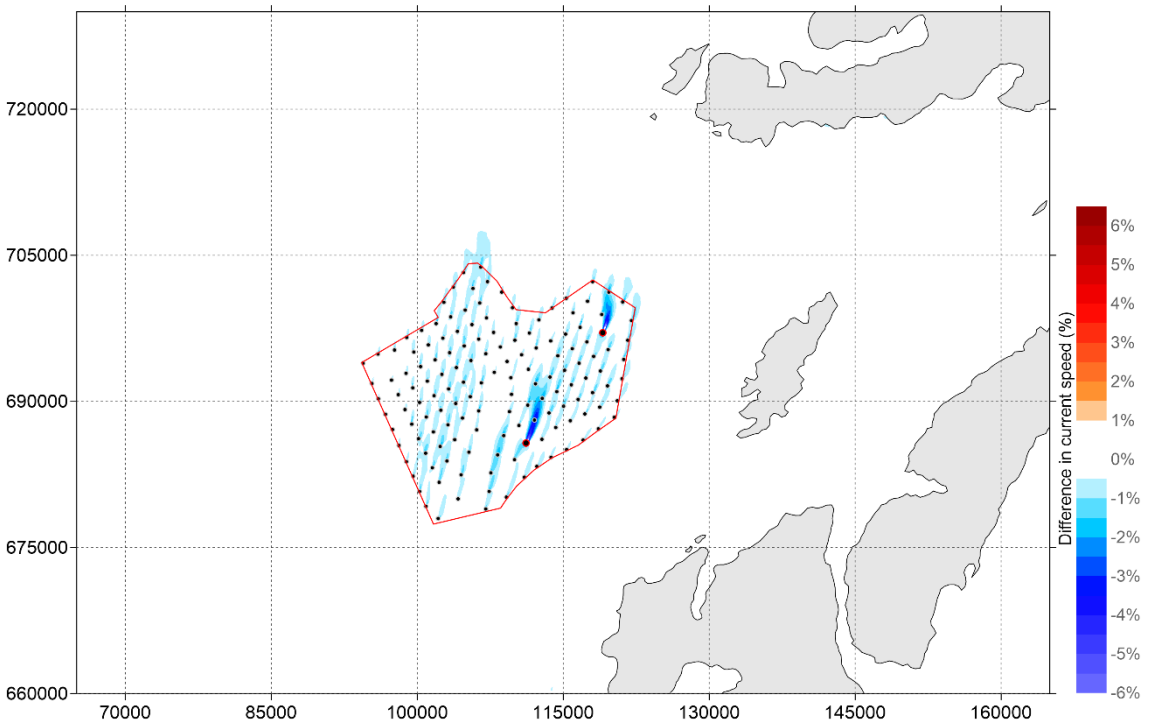

Figure 5-91 Percentage change of current speed between 'Baseline' and '15 MW - Even Spread layout' during spring tide (positive means increase of current speed by layout and vice versa) - peak flood

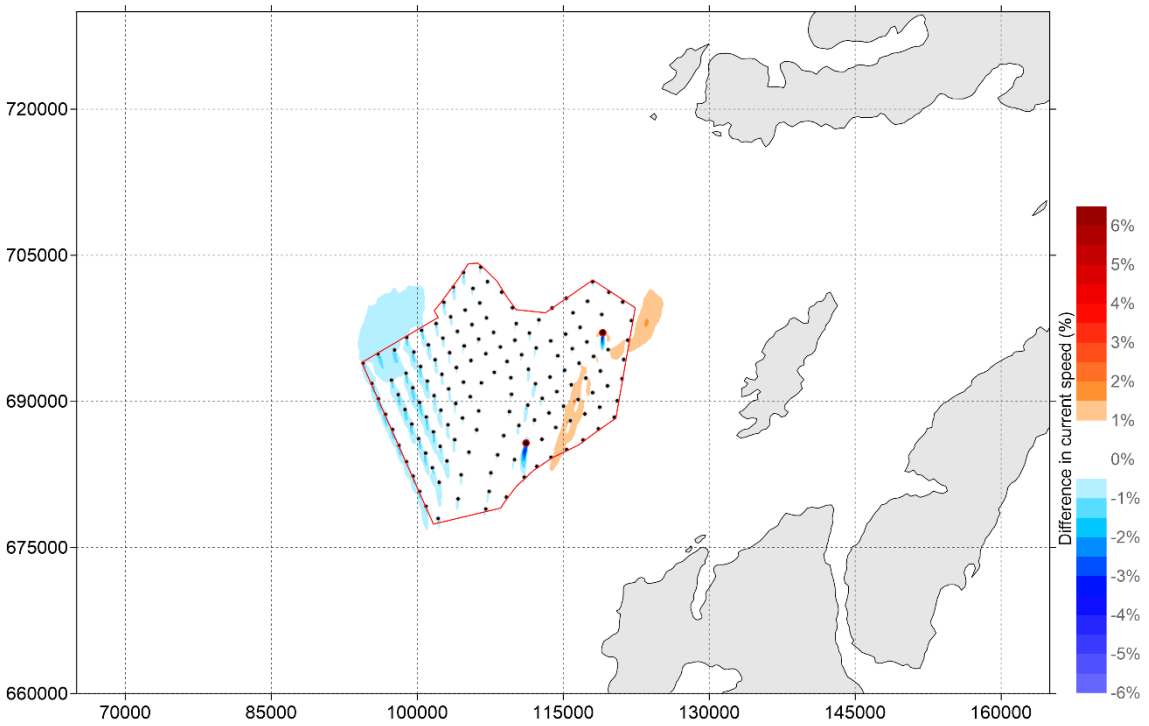

Figure 5-92 Percentage change of current speed between 'Baseline' and '15 MW - Even Spread layout' during spring tide (positive means increase of current speed by layout and vice versa) - peak ebb

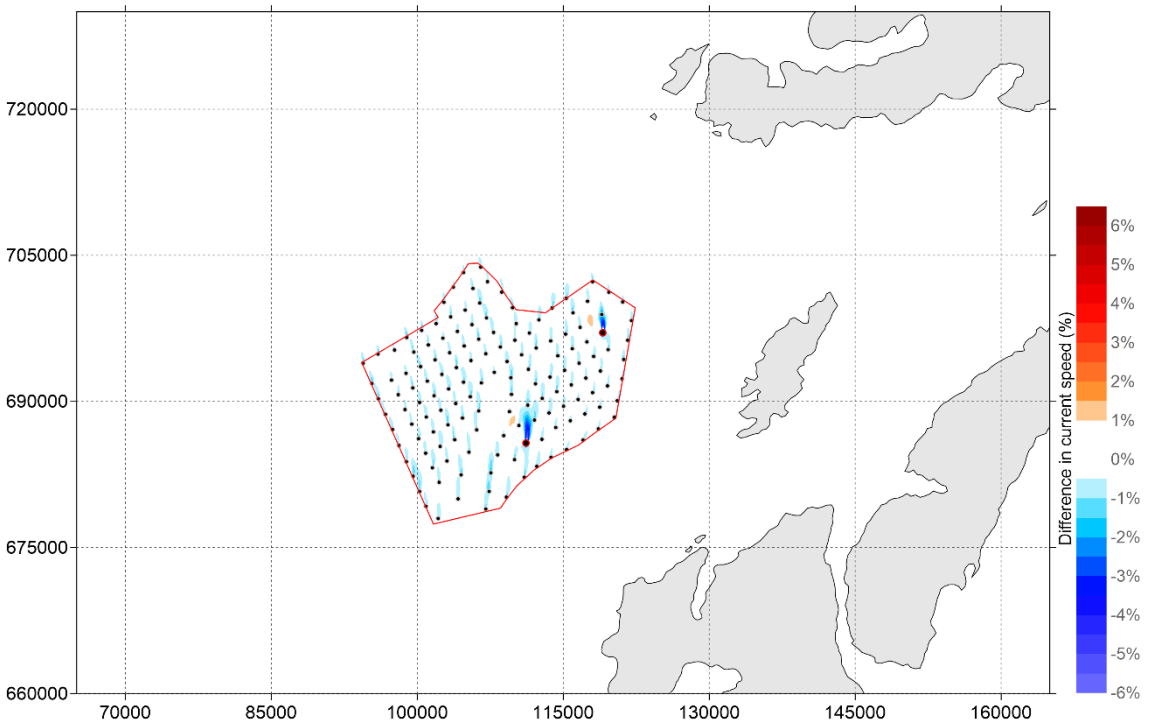

Figure 5-93 Percentage change of current speed between 'Baseline' and '15 MW - Even Spread layout' during neap tide (positive means increase of current speed by layout and vice versa) - peak flood

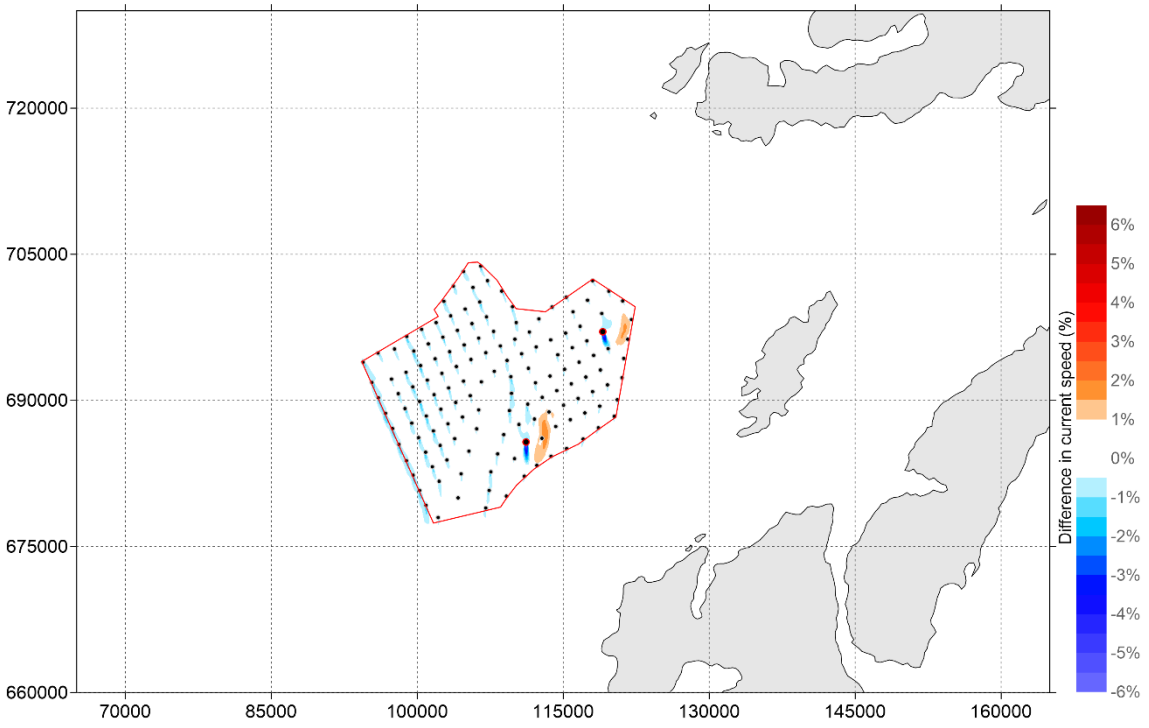

Figure 5-94 Percentage change of current speed between 'Baseline' and '15 MW - Even Spread layout' during neap tide (positive means increase of current speed by layout and vice versa) - peak ebb

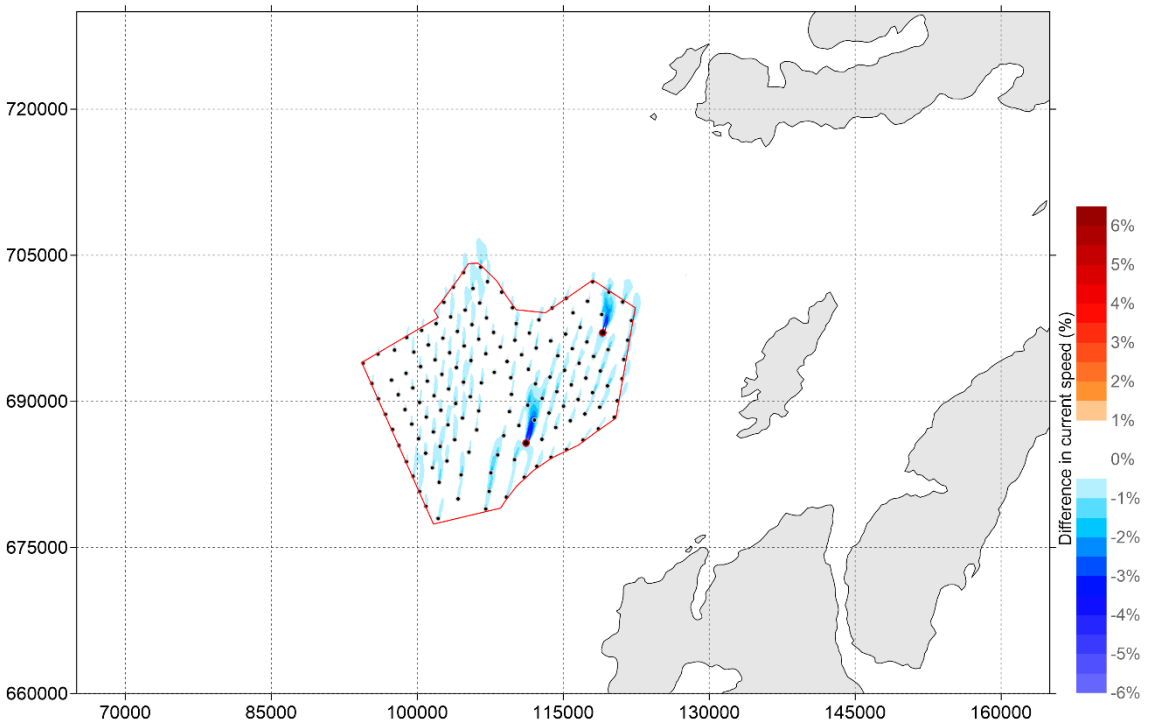

Figure 5-95 Percentage change of maximum current speed between 'Baseline' and '15 MW - Even Spread layout' over 15 days (positive means increase of current speed by layout and vice versa)

Impact on Current Speed in Percentage – 24 MW Dense Perimeter Layout

5.3.23 This section presents the percentage difference in current speeds relative to the baseline around the WDA for the 24 MW Dense Perimeter layout. **Figure 5-96** and **Figure 5-97** present the predicted percentage difference in current speed during spring tide for peak flood and peak ebb, respectively. **Figure 5-98** and **Figure 5-99** present the predicted percentage difference in current speed during neap tide for peak flood and peak ebb, respectively. **Figure 5-100** presents the percentage difference in maximum current speed throughout the full spring-neap tidal cycle simulation.

5.3.24 The predicted percentage difference in current speed extending outside the WDA between the 24 MW – Dense Perimeter layout and baseline scenario is more pronounced during the spring tide. At peak flood, the percentage difference is a reduction of up to 1.0% extending up to 1.5 km north of the WDA. At peak ebb, there is a reduction of up to 1.0% extending 3 km northwest of the WDA and an increase of up to 1.5% extending 4 km northeast of the WDA.

5.3.25 The percentage change in current speed outside the WDA is less than that predicted for the 15 MW layouts.

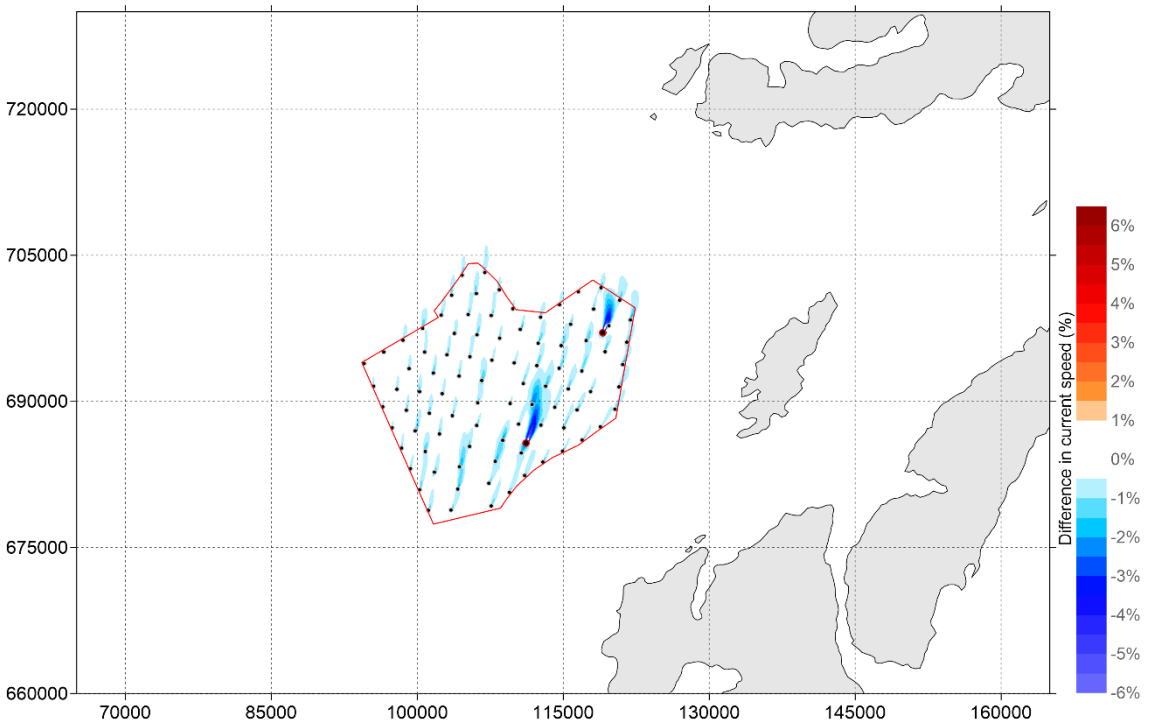

Figure 5-96 Percentage change of current speed between 'Baseline' and '24 MW - Dense Perimeter layout' during spring tide (positive means increase of current speed by layout and vice versa) - peak flood

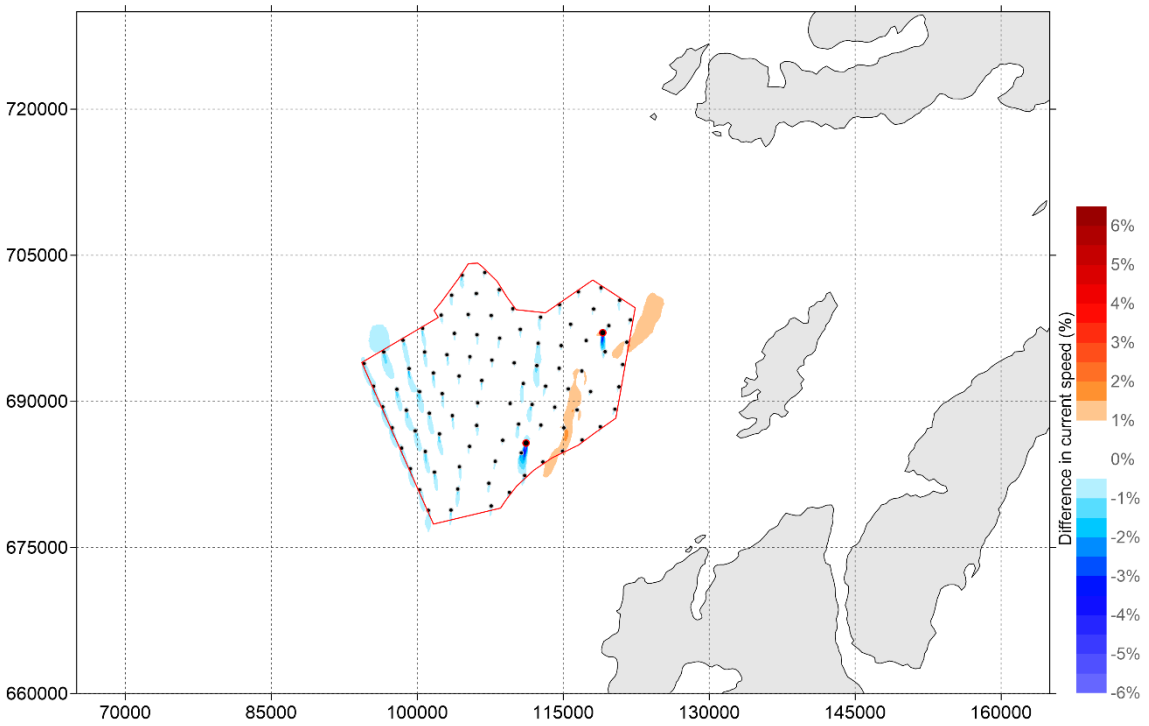

Figure 5-97 Percentage change of current speed between 'Baseline' and '24 MW - Dense Perimeter layout' during spring tide (positive means increase of current speed by layout and vice versa) - peak ebb

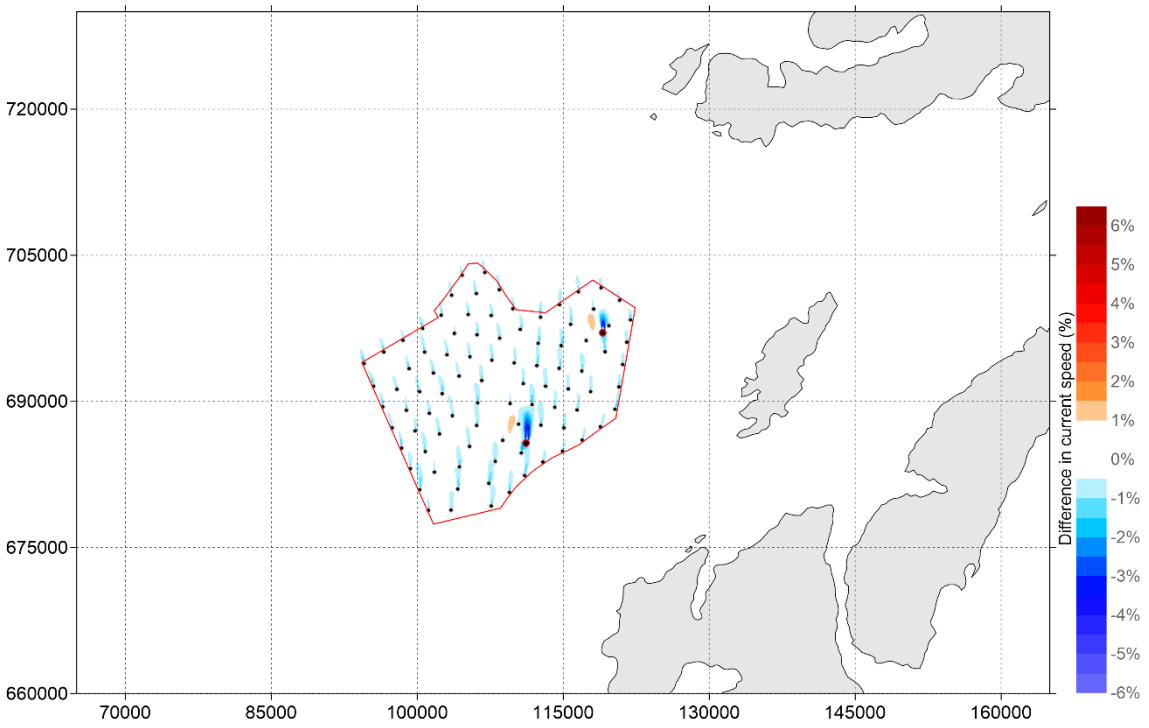

Figure 5-98 Percentage change of current speed between 'Baseline' and '24 MW - Dense Perimeter layout' during neap tide (positive means increase of current speed by layout and vice versa) - peak flood

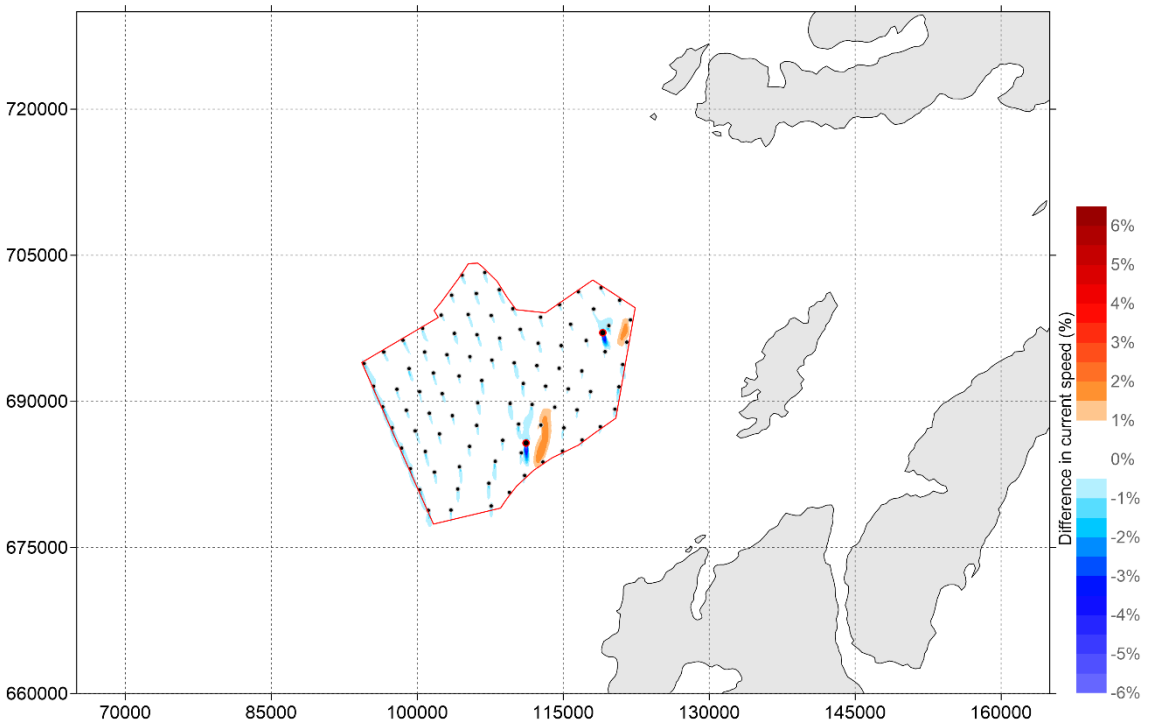

Figure 5-99 Percentage change of current speed between 'Baseline' and '24 MW - Dense Perimeter layout' during neap tide (positive means increase of current speed by layout and vice versa) - peak ebb

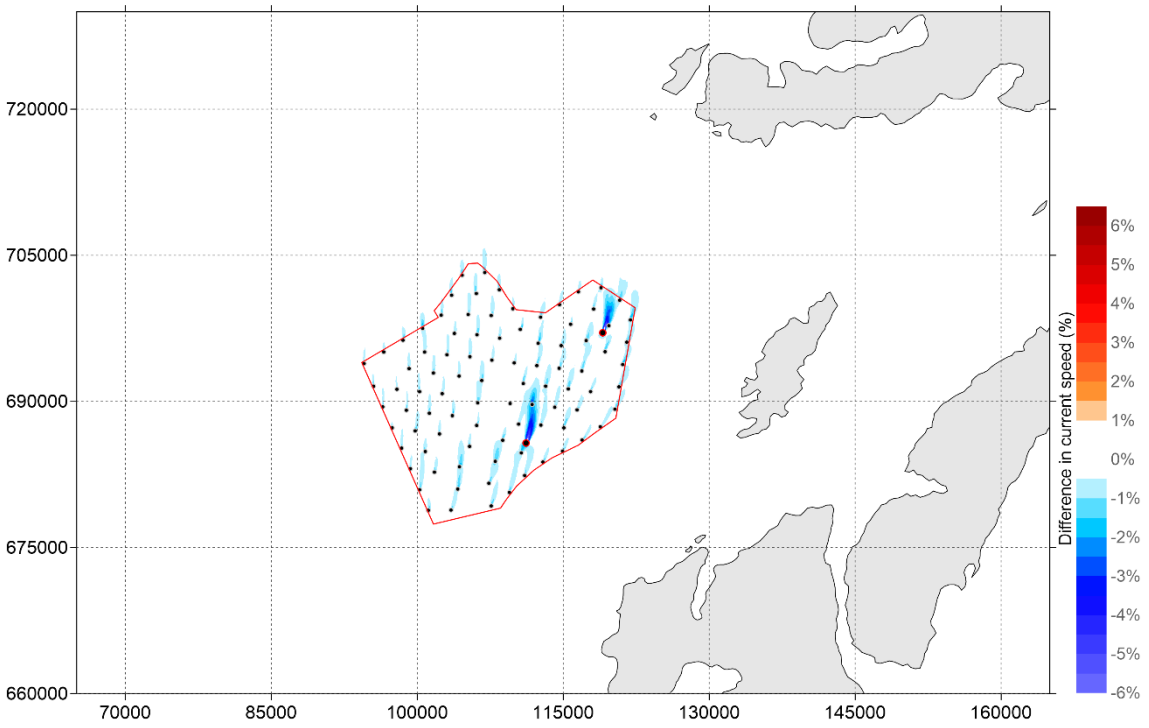

Figure 5-100 Percentage change of maximum current speed between 'Baseline' and '24 MW - Dense Perimeter layout' over 15 days (positive means increase of current speed by layout and vice versa)

Impact on Current Speed in Percentage – 24 MW Even Spread Layout

5.3.26 This section presents the percentage difference in current speeds relative to the baseline around the WDA for the 24 MW Even Spread layout. **Figure 5-101** and **Figure 5-102** present the predicted percentage difference in current speed during spring tide for peak flood and peak ebb, respectively. **Figure 5-103** and **Figure 5-104** present the predicted percentage difference in current speed during neap tide for peak flood and peak ebb, respectively. **Figure 5-105** presents the percentage difference in maximum current speed throughout the full spring-neap tidal cycle simulation.

5.3.27 The percentage change in current speed for the 24 MW – Even Spread layout is very similar to the results presented above for the 24 MW – Dense Perimeter layout.

5.3.28 The percentage change in current speed outside the WDA is less than that predicted for the 15 MW layouts.

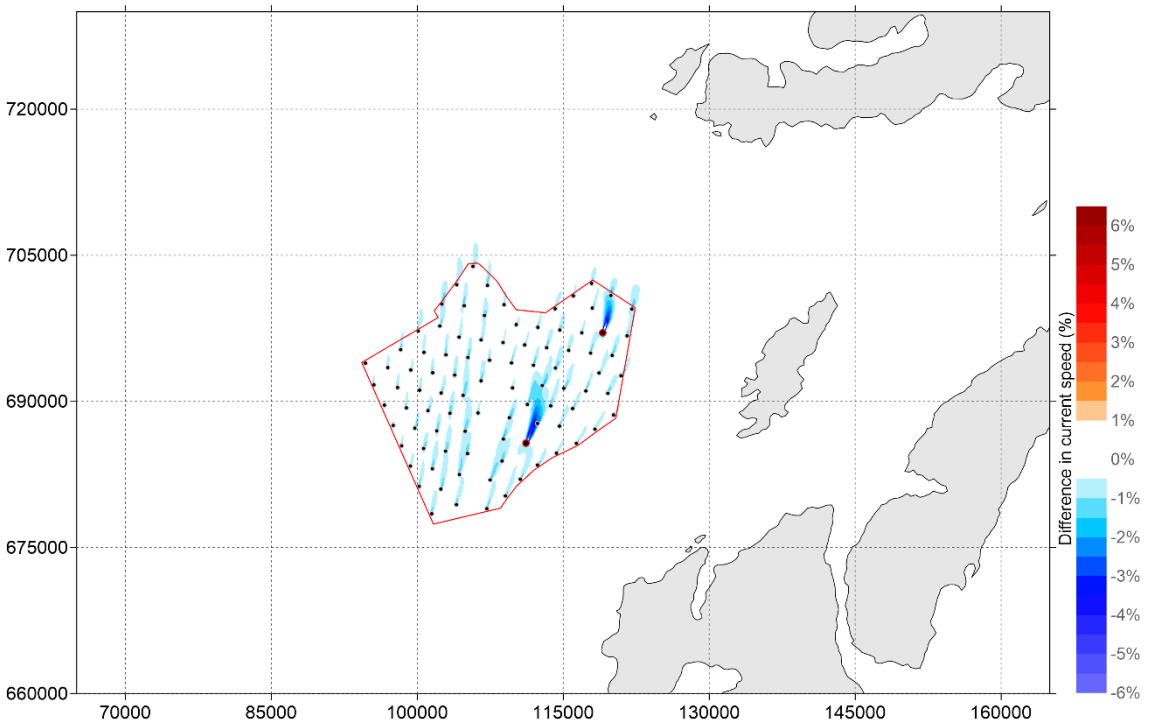

Figure 5-101 Percentage change of current speed between 'Baseline' and '24 MW - Even Spread layout' during spring tide (positive means increase of current speed by layout and vice versa) - peak flood

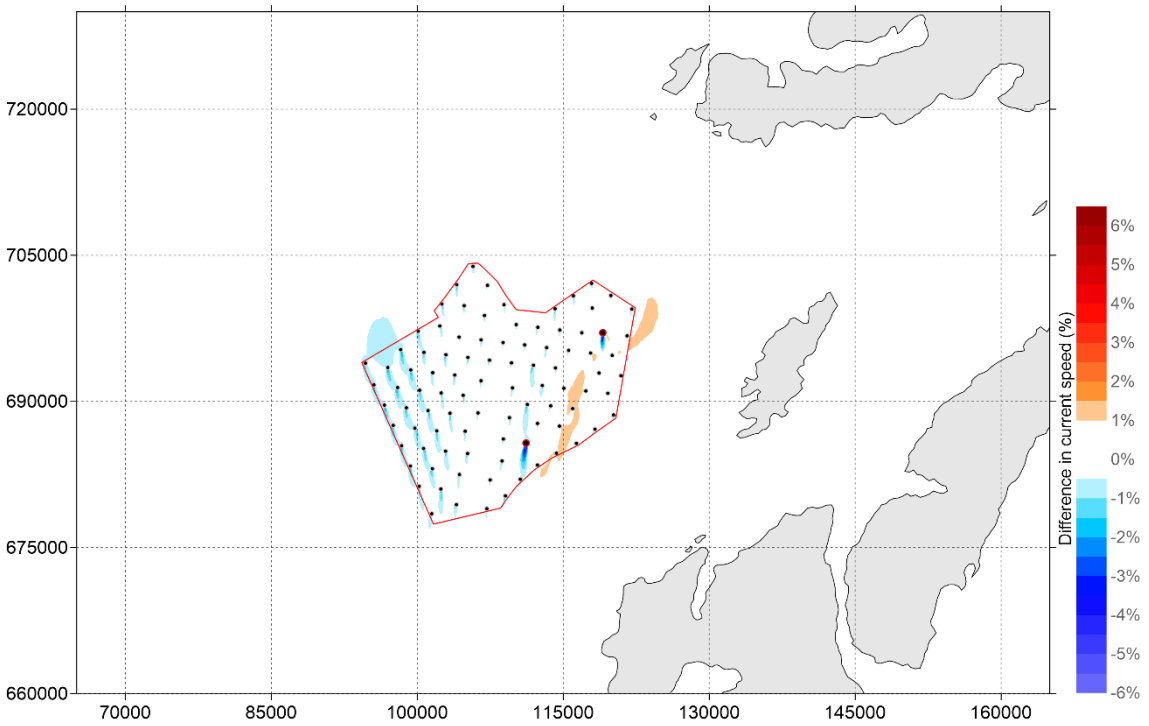

Figure 5-102 Percentage change of current speed between 'Baseline' and '24 MW - Even Spread layout' during spring tide (positive means increase of current speed by layout and vice versa) - peak ebb

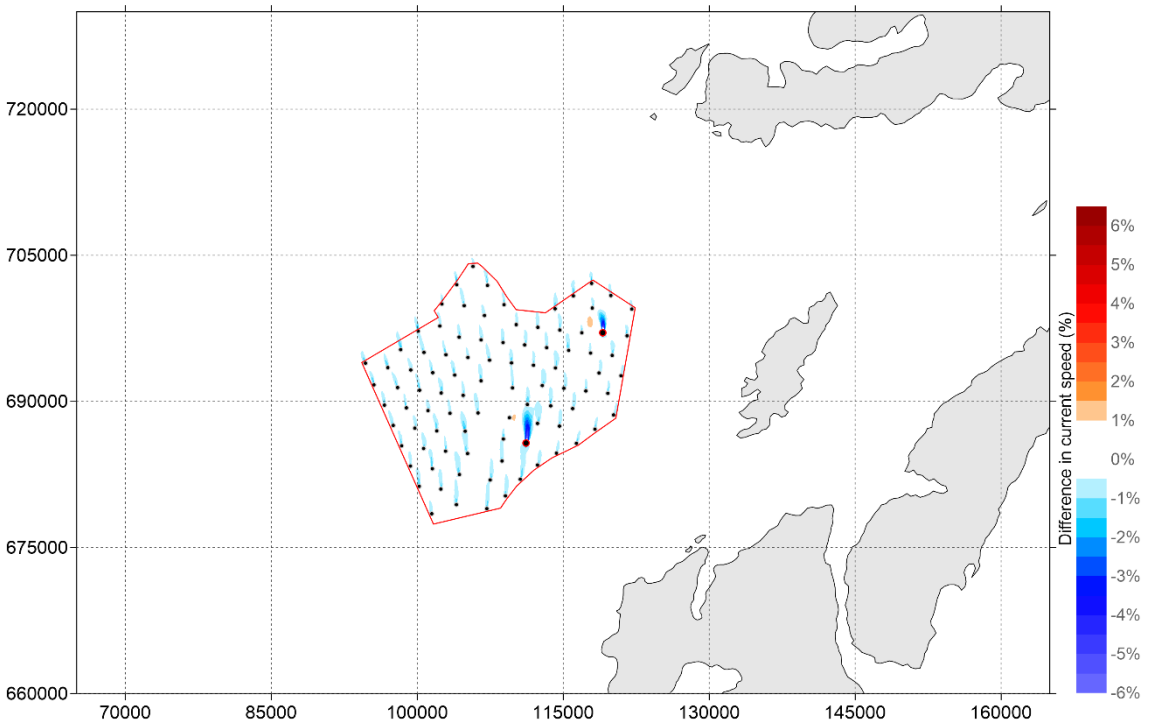

Figure 5-103 Percentage change of current speed between 'Baseline' and '24 MW - Even Spread layout' during neap tide (positive means increase of current speed by layout and vice versa) - peak flood

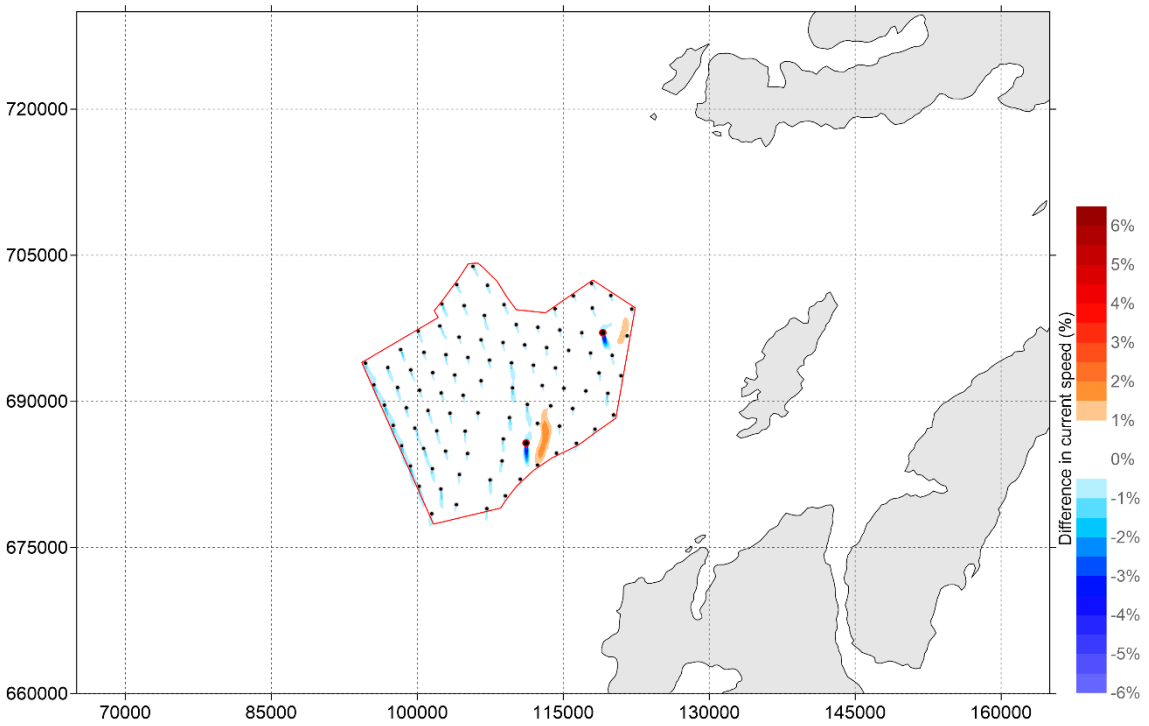

Figure 5-104 Percentage change of current speed between 'Baseline' and '24 MW - Even Spread layout' during neap tide (positive means increase of current speed by layout and vice versa) - peak ebb

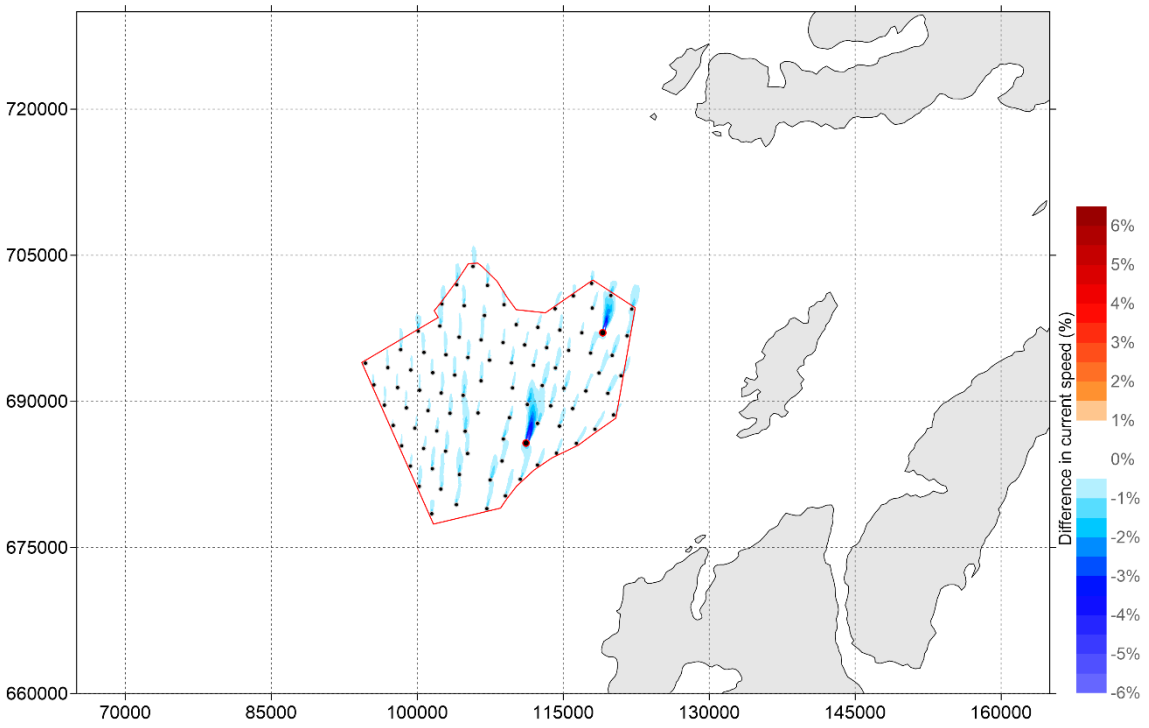

Figure 5-105 Percentage change of maximum current speed between 'Baseline' and '24 MW - Even Spread layout' over 15 days (positive means increase of current speed by layout and vice versa)

Comparison of Layouts (Current Speed)

5.3.29 From the results presented above, the model predicts that the effect on the current speeds is very similar between the two 15 MW layouts and between the two 24 MW layouts, with minimal difference between the 'Dense Perimeter' and 'Even Spread' indicative turbine layouts. In addition to this, the hydrodynamic model predicts that the increased number of monopiles (144) for the 15 MW WDA will have a greater effect on the current speed when compared with the 24 MW WDA, which has only 91 monopiles.

5.3.30 Most notably during spring tide, at peak flood, the 15 MW indicative turbine layouts predict a percentage reduction in current speed of 1.0% extending 2.5 km north of the WDA, compared with only 1.5 km for the 24 MW layouts. In addition to this, during peak ebb, percentage reductions of up to 1.0% extend 8 km northwest of the WDA for the 15 MW layouts and only 3 km for the 24 MW layouts. And percentage increase of up to 2.0% extending 7 km northeast of the WDA for the 15 MW layouts and up to 1.5% extending 4 km for the 24 MW layouts.

Absolute Bed Shear Stress – Baseline

5.3.31 This section presents the absolute bed shear stress around the WDA for the baseline scenario. **Figure 5-106** and **Figure 5-107** present the predicted bed shear stress during spring tide for peak flood and peak ebb, respectively. **Figure 5-108** and **Figure 5-109** present the predicted bed shear stress during neap tide for peak flood and peak ebb, respectively. **Figure 5-110** presents the maximum bed shear stress throughout the full spring-neap tidal cycle simulation.

5.3.32 The absolute bed shear stress during spring tide on peak flood is up to 2.4 N/m^2 in the south and 0.4 N/m^2 in the north. During peak ebb, bed shear stress is up to 0.4 N/m^2 in the north to up to 2.2 N/m^2 in the south.

5.3.33 The absolute bed shear stress during neap tide on peak flood is up to 0.6 N/m^2 in the south and 0.2 N/m^2 in the north. During peak ebb, bed shear stress is up to 0.2 N/m^2 in the north to up to 0.5 N/m^2 in the south.

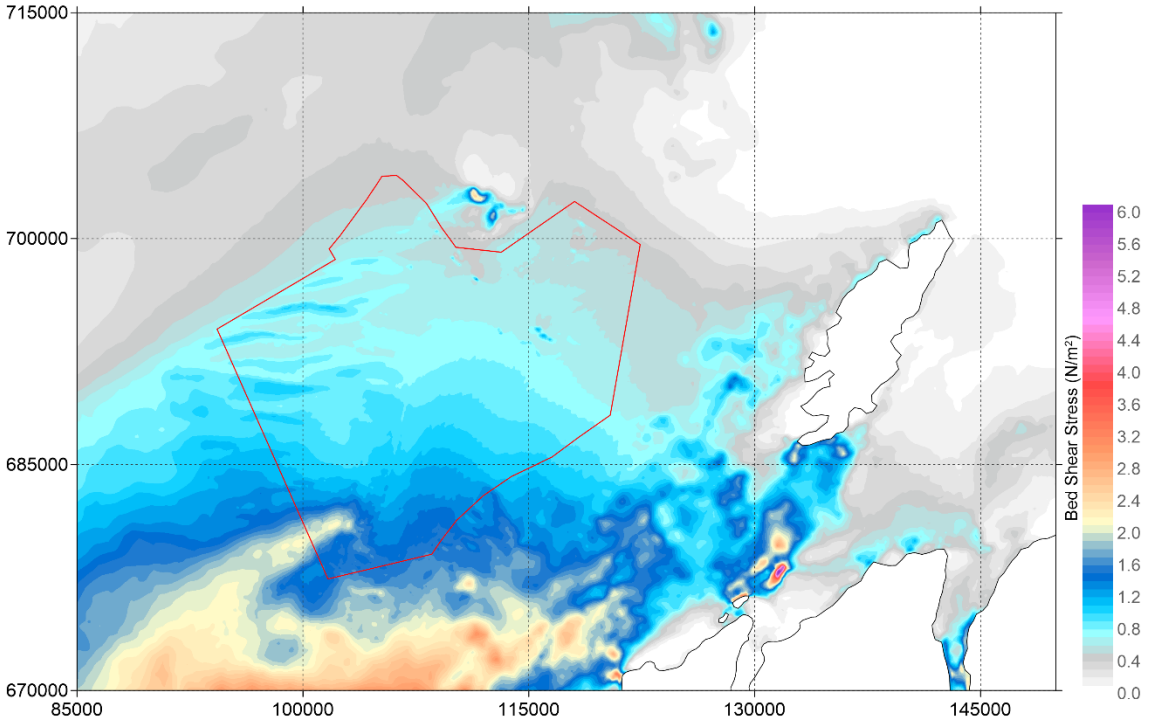

Figure 5-106: Baseline layout - Bed shear stress during spring tide - peak flood (Local model)

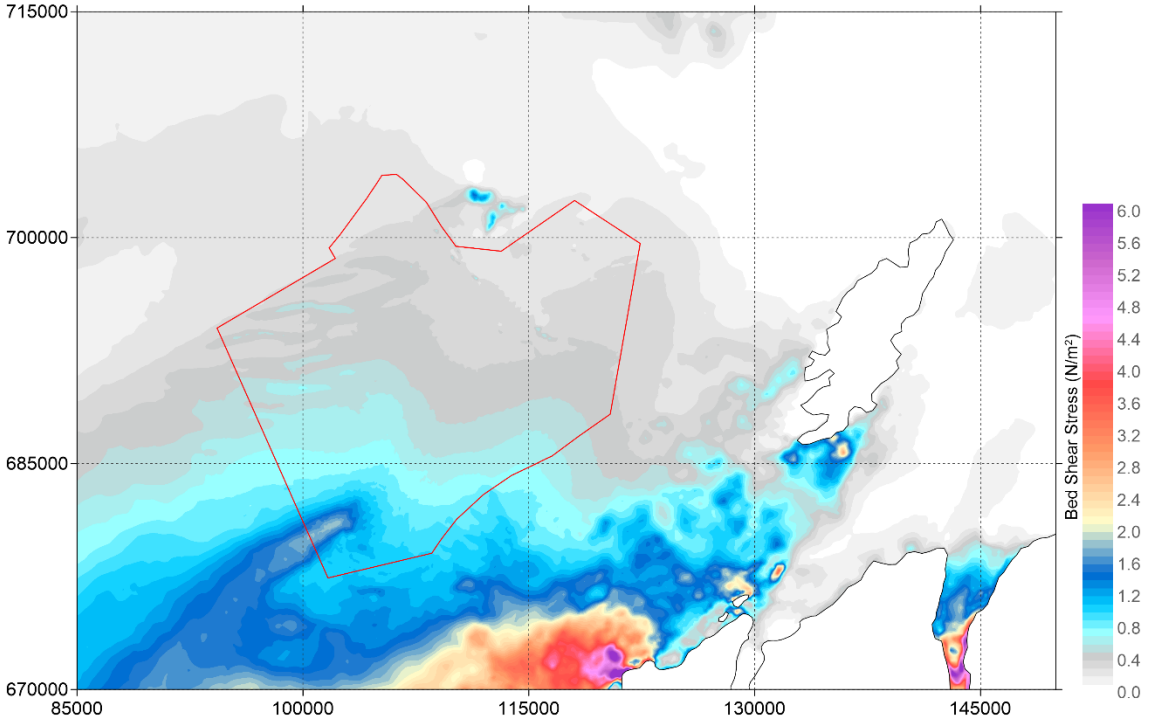

Figure 5-107: Baseline layout - Bed shear stress during spring tide - peak ebb (Local model)

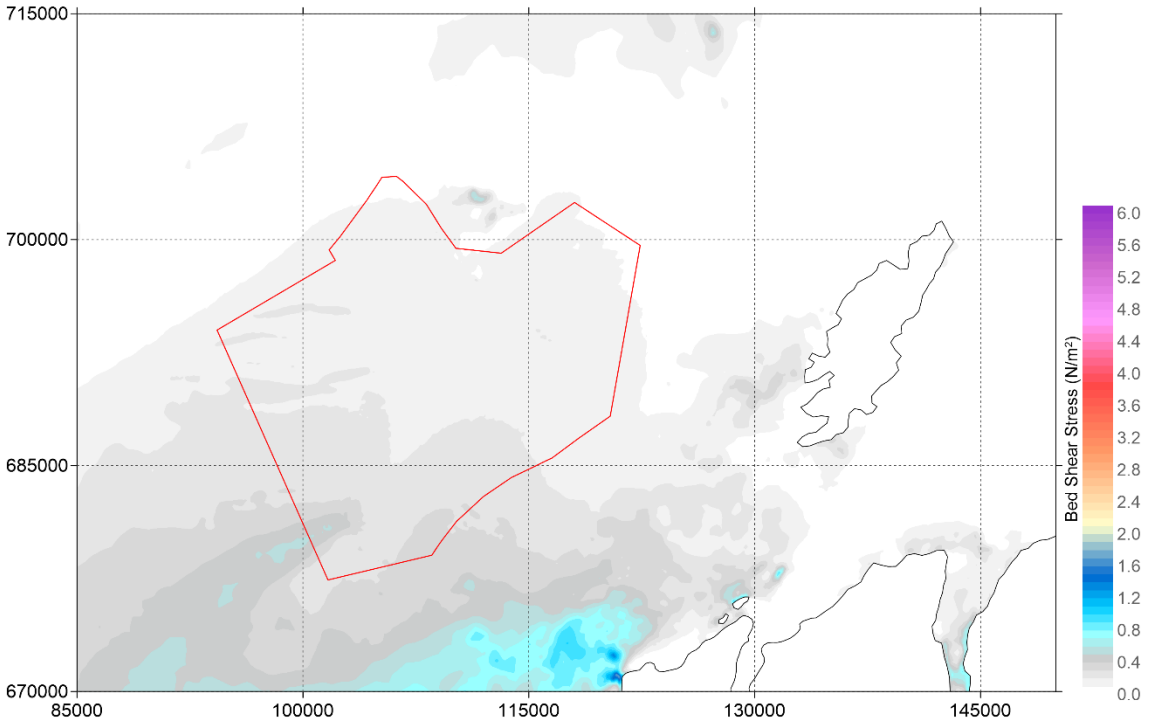

Figure 5-108: Baseline layout - Bed shear stress during neap tide - peak flood (Local model)

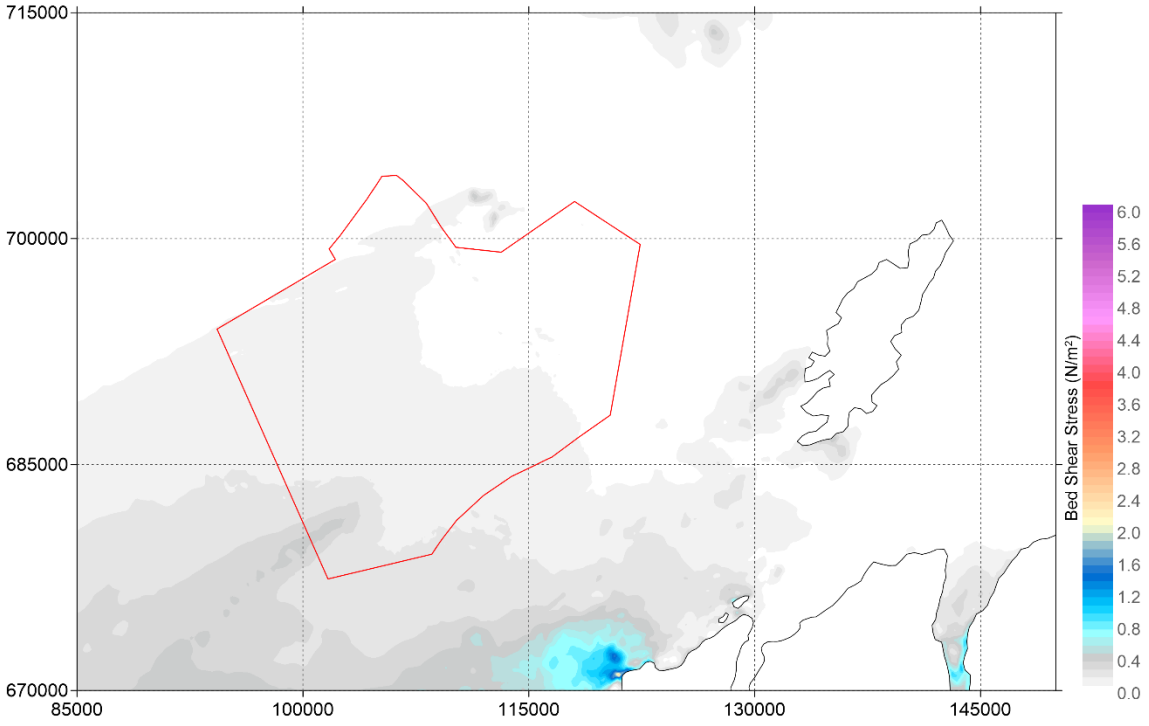

Figure 5-109: Baseline layout - Bed shear stress during neap tide - peak ebb (Local model)

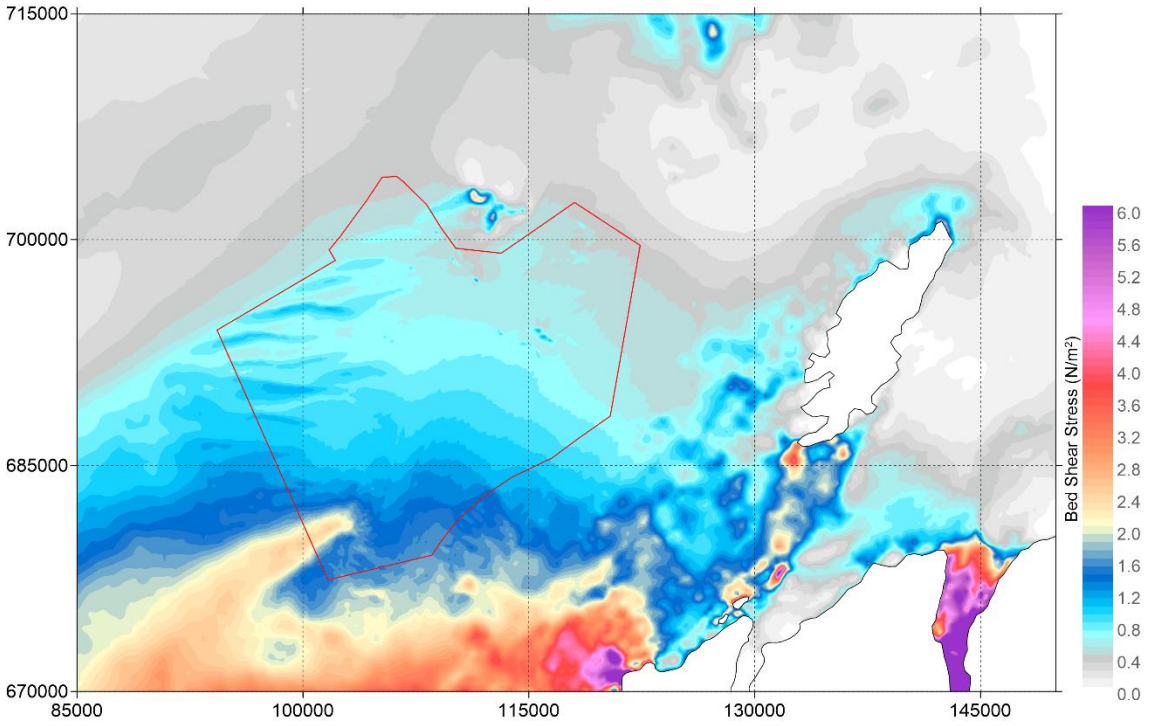

Figure 5-110: Baseline layout – Maximum Bed shear stress over 15 days (Local model)

Absolute Bed Shear Stress – 15 MW Dense Perimeter layout

5.3.34 This section presents the absolute bed shear stress around the WDA for the 15 MW Dense Perimeter layout. **Figure 5-111** and **Figure 5-112** present the predicted bed shear stress during spring tide for peak flood and peak ebb, respectively. **Figure 5-113** and **Figure 5-114** present the predicted bed shear stress during neap tide for peak flood and peak ebb, respectively. **Figure 5-115** presents the maximum bed shear stress throughout the full spring-neap tidal cycle simulation.

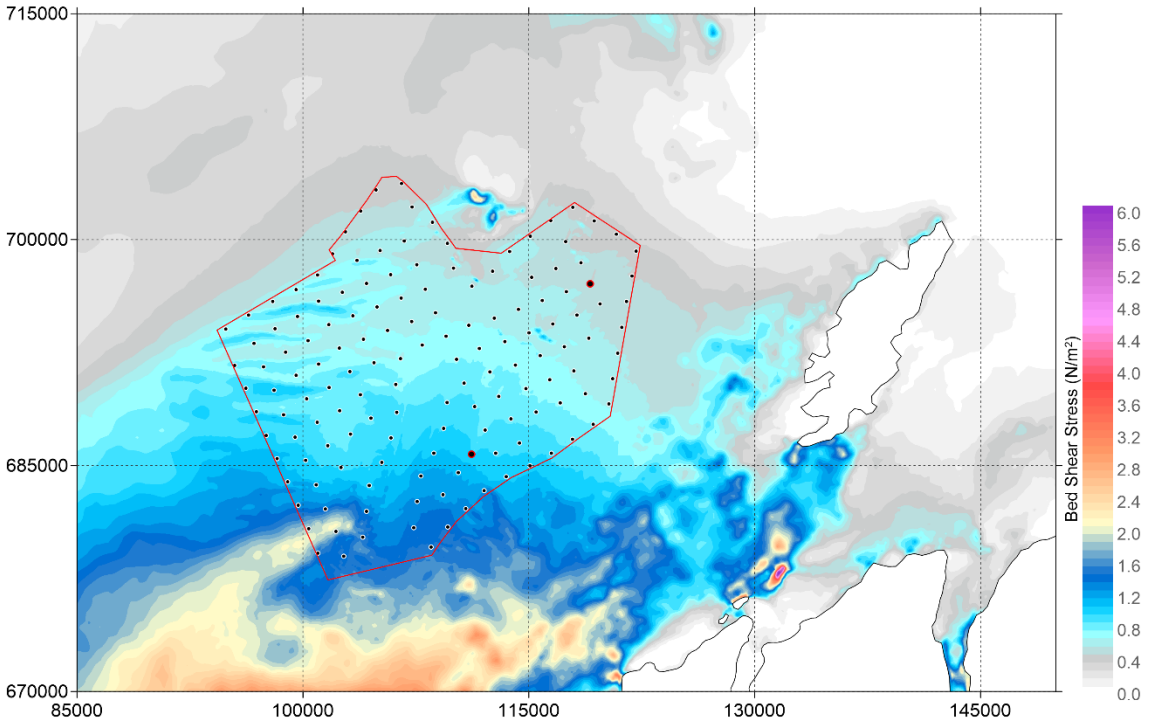

Figure 5-111: 15 MW - Dense Perimeter layout - Bed shear stress during spring tide - peak flood (Local model)

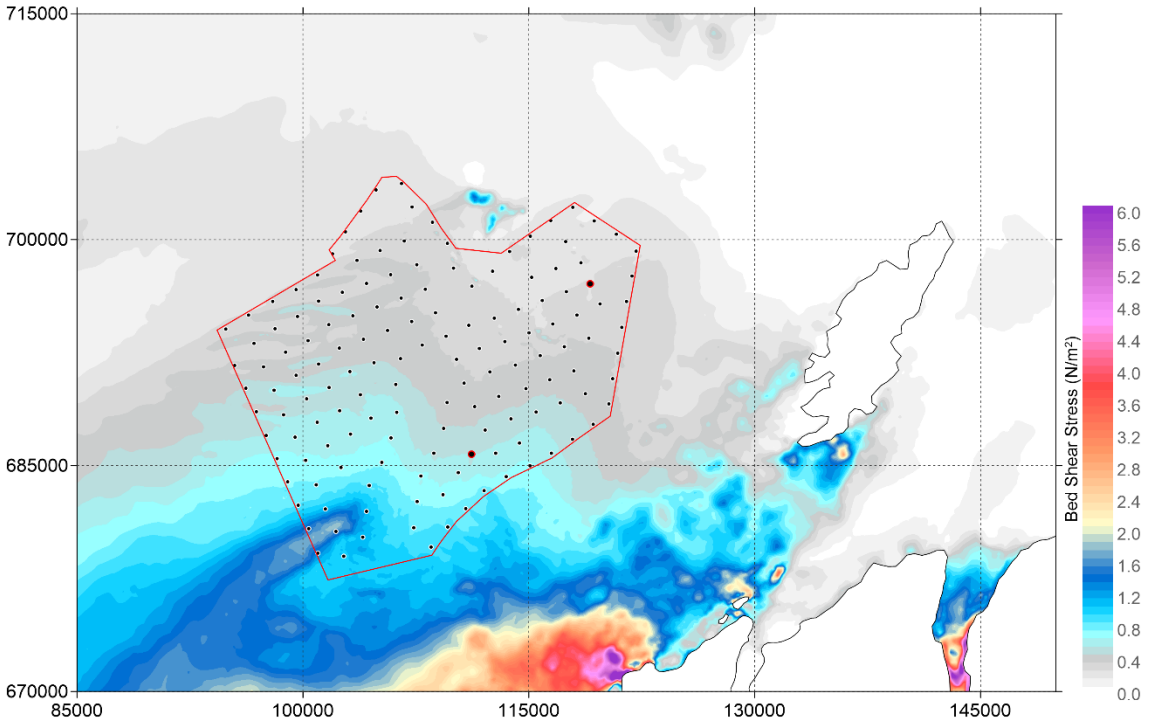

Figure 5-112: 15 MW - Dense Perimeter layout - Bed shear stress during spring tide - peak ebb (Local model)

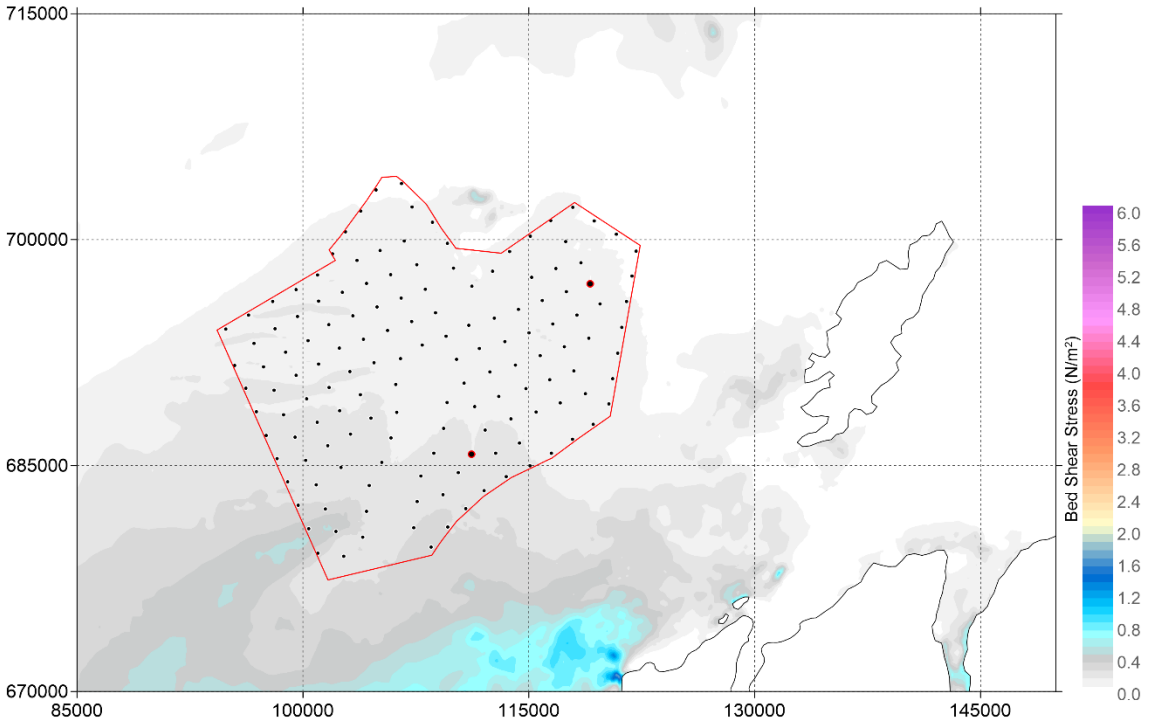

Figure 5-113: 15 MW - Dense Perimeter layout - Bed shear stress during neap tide - peak flood (Local model)

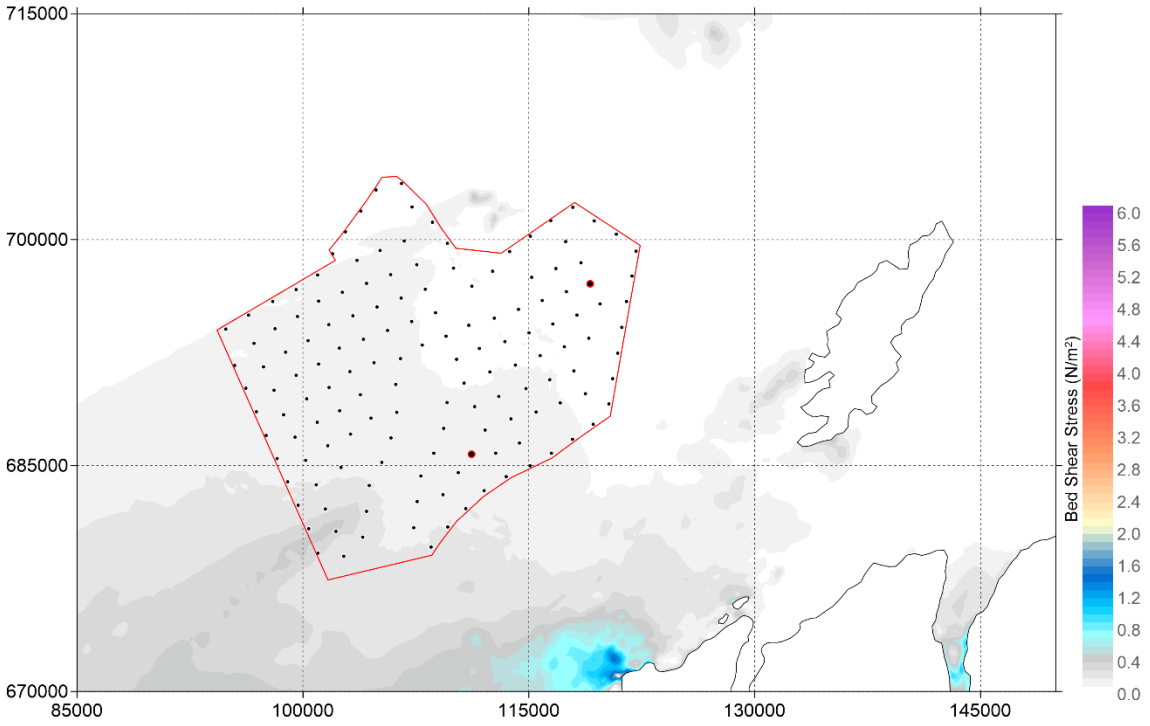

Figure 5-114: 15 MW - Dense Perimeter layout - Bed shear stress during neap tide - peak ebb (Local model)

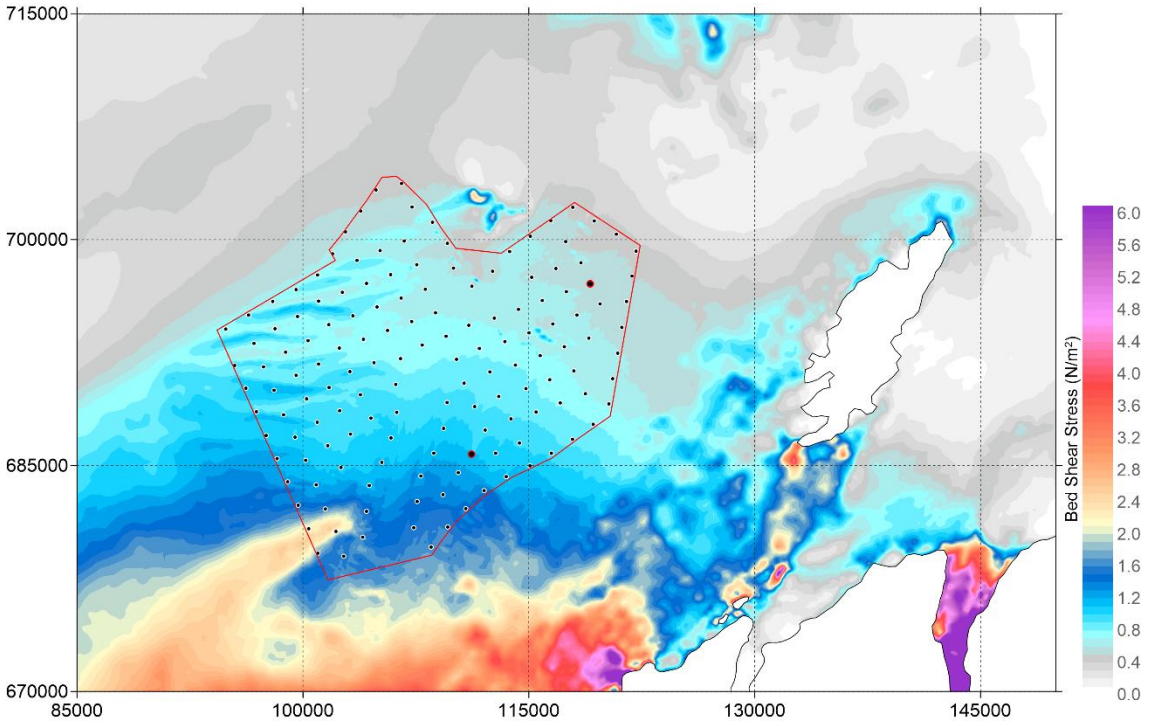

Figure 5-115: 15 MW - Dense Perimeter layout – Maximum Bed shear stress over 15 days (Local model)

Absolute Bed Shear Stress – 15 MW Even Spread layout

5.3.35 This section presents the absolute bed shear stress around the WDA for the 15 MW Even Spread layout. **Figure 5-116** and **Figure 5-117** present the predicted bed shear stress during spring tide for peak flood and peak ebb, respectively. **Figure 5-118** and **Figure 5-119** present the predicted bed shear stress during neap tide for peak flood and peak ebb, respectively. **Figure 5-120** presents the maximum bed shear stress throughout the full spring-neap tidal cycle simulation.

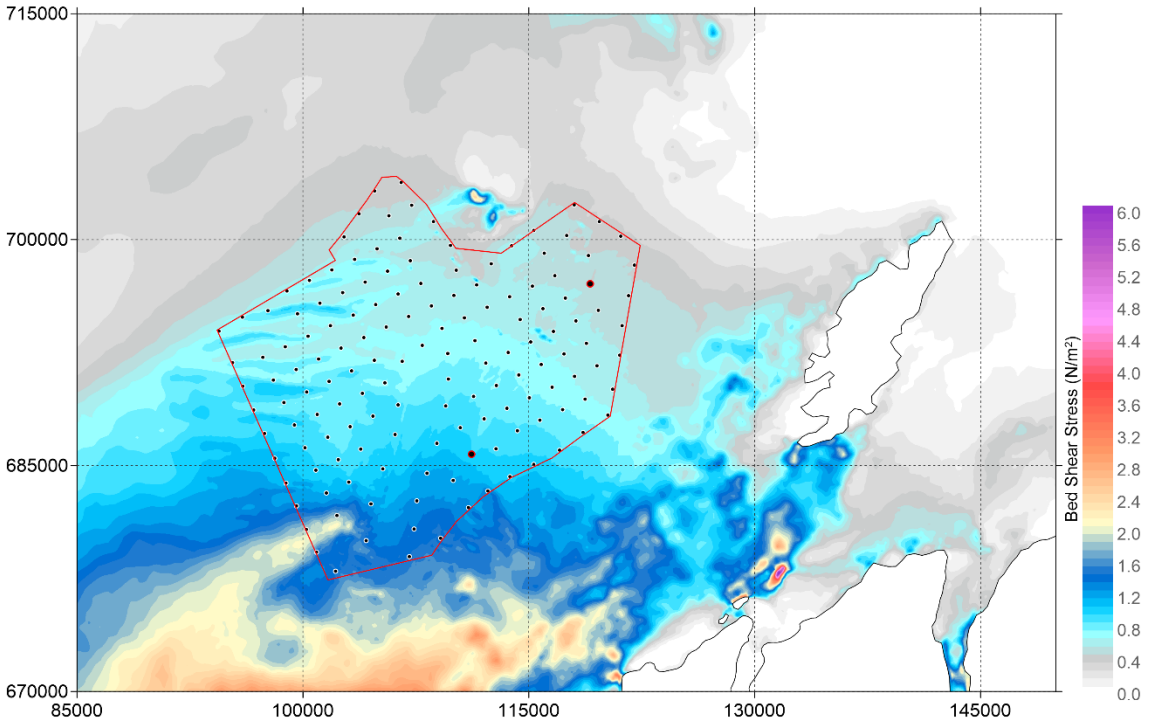

Figure 5-116: 15 MW - Even Spread layout - Bed shear stress during spring tide - peak flood (Local model)

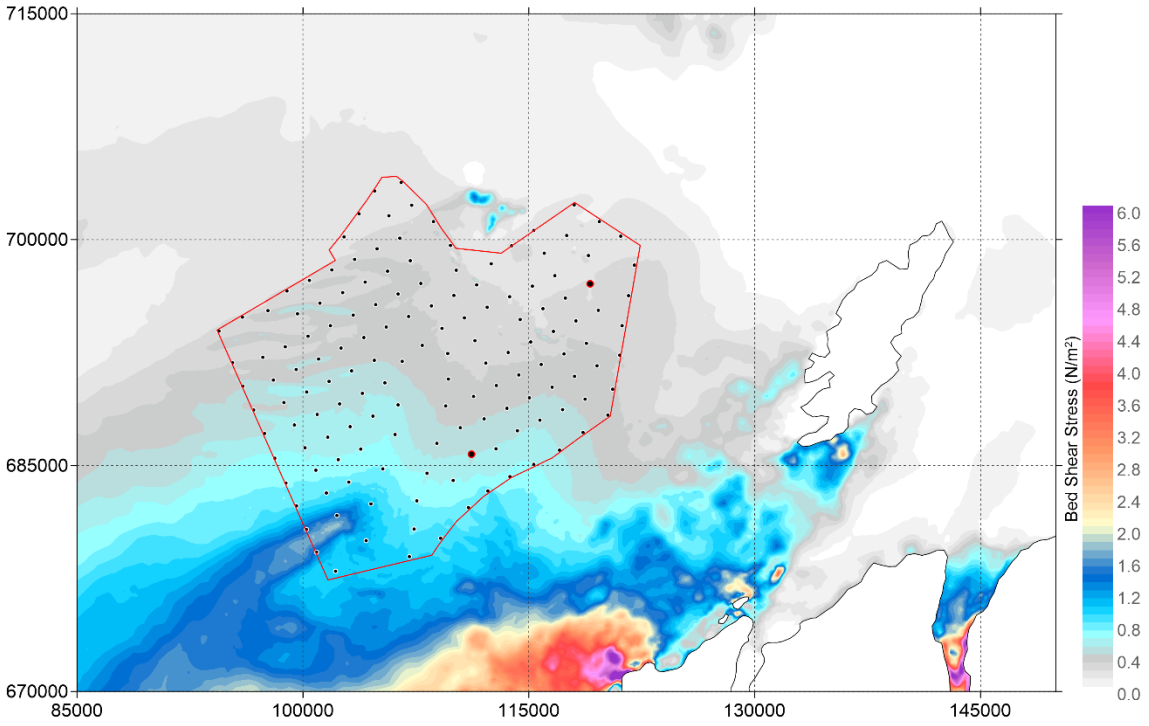

Figure 5-117: 15 MW - Even Spread layout - Bed shear stress during spring tide - peak ebb (Local model)

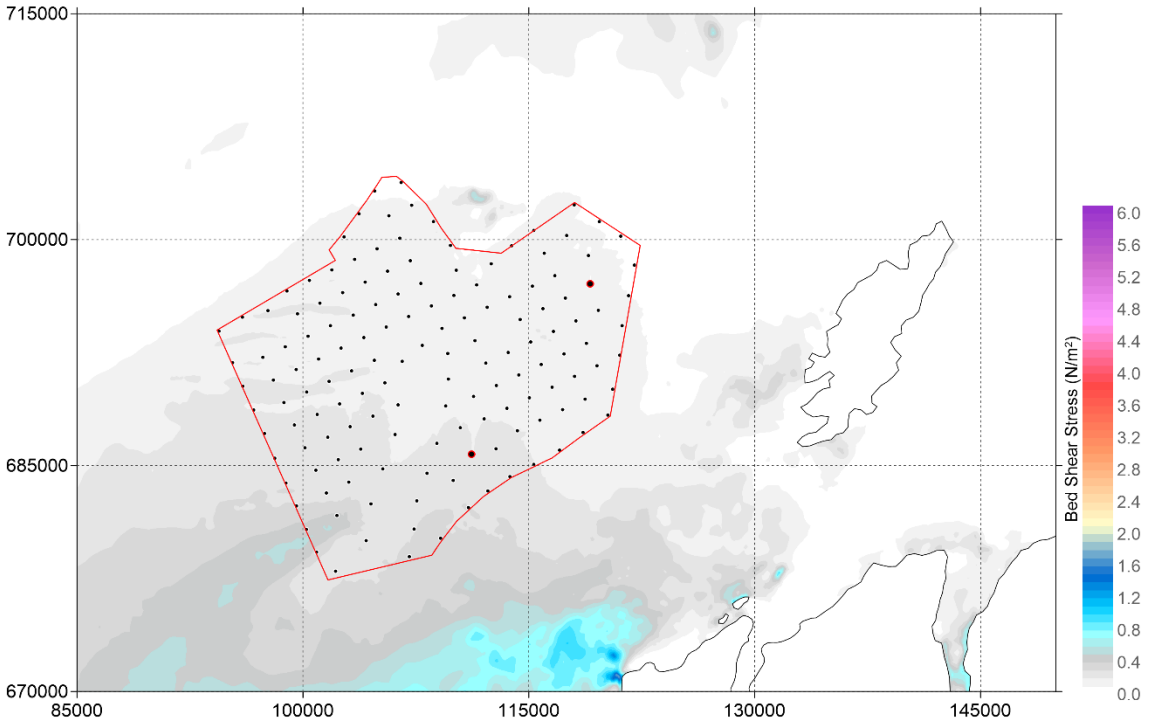

Figure 5-118: 15 MW - Even Spread layout - Bed shear stress during neap tide - peak flood (Local model)

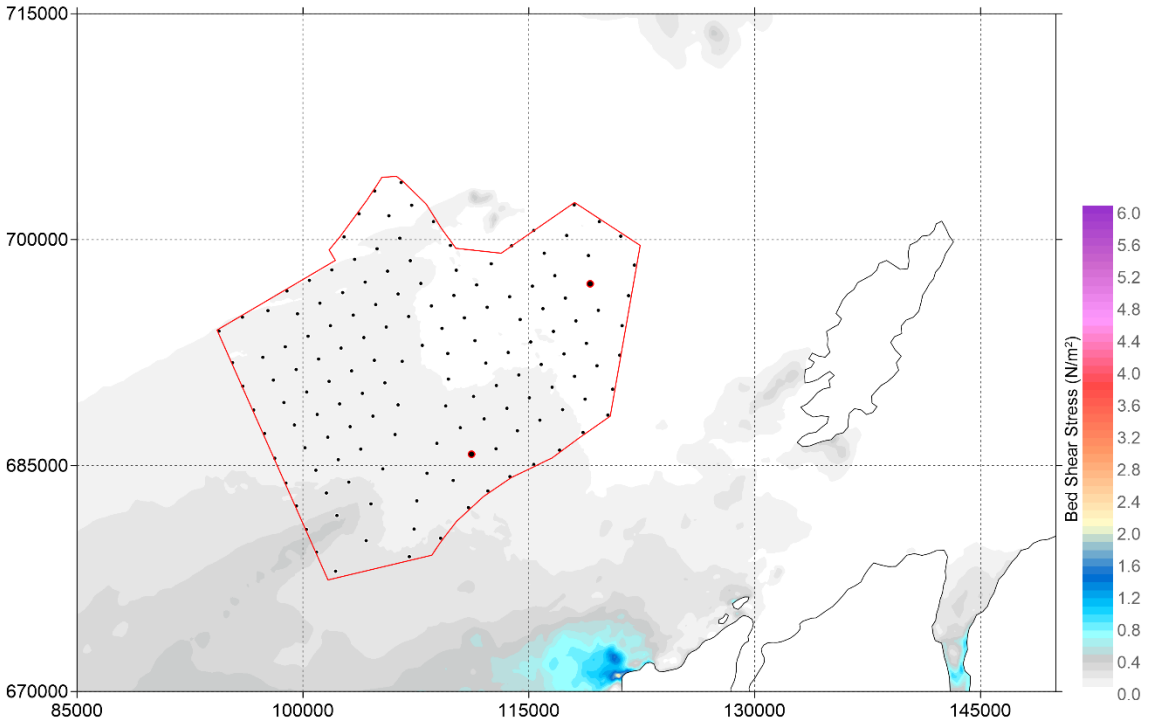

Figure 5-119: 15 MW - Even Spread layout - Bed shear stress during neap tide - peak ebb (Local model)

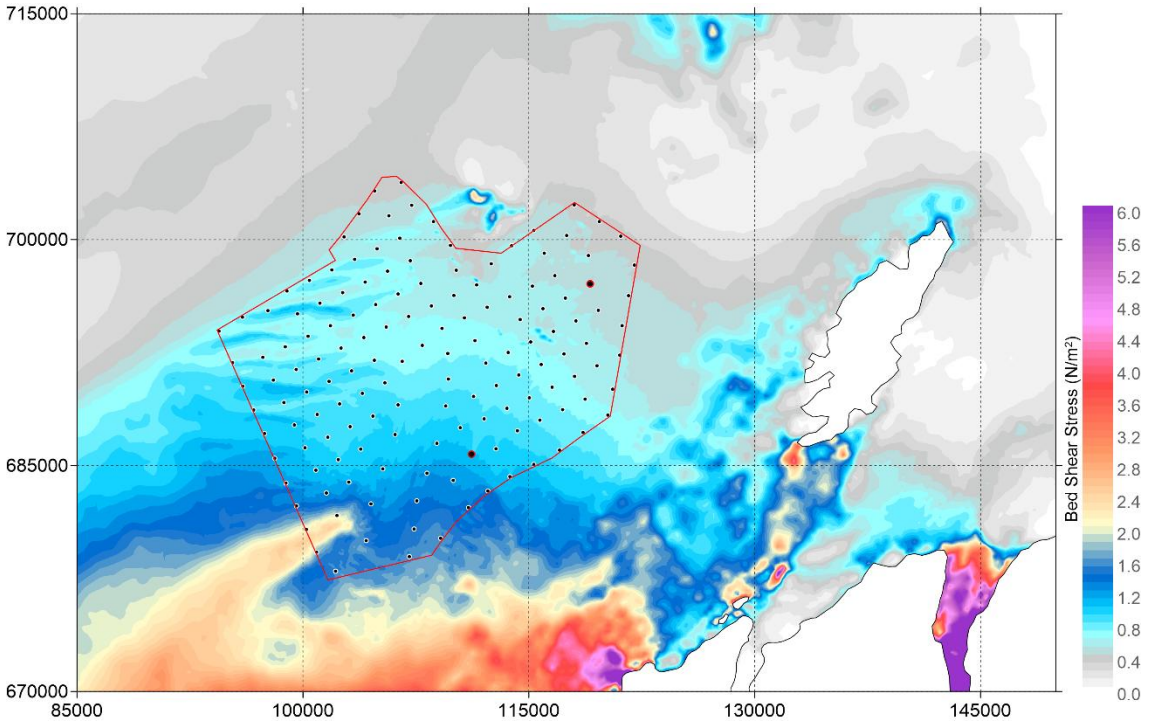

Figure 5-120: 15 MW - Even Spread layout – Maximum Bed shear stress over 15 days (Local model)

Absolute Bed Shear Stress – 24 MW Dense Perimeter layout

5.3.36 This section presents the absolute bed shear stress around the WDA for the 24 MW Dense Perimeter layout. **Figure 5-121** and **Figure 5-122** present the predicted bed shear stress during spring tide for peak flood and peak ebb, respectively. **Figure 5-123** and **Figure 5-124** present the predicted bed shear stress during neap tide for peak flood and peak ebb, respectively. **Figure 5-125** presents the maximum bed shear stress throughout the full spring-neap tidal cycle simulation.

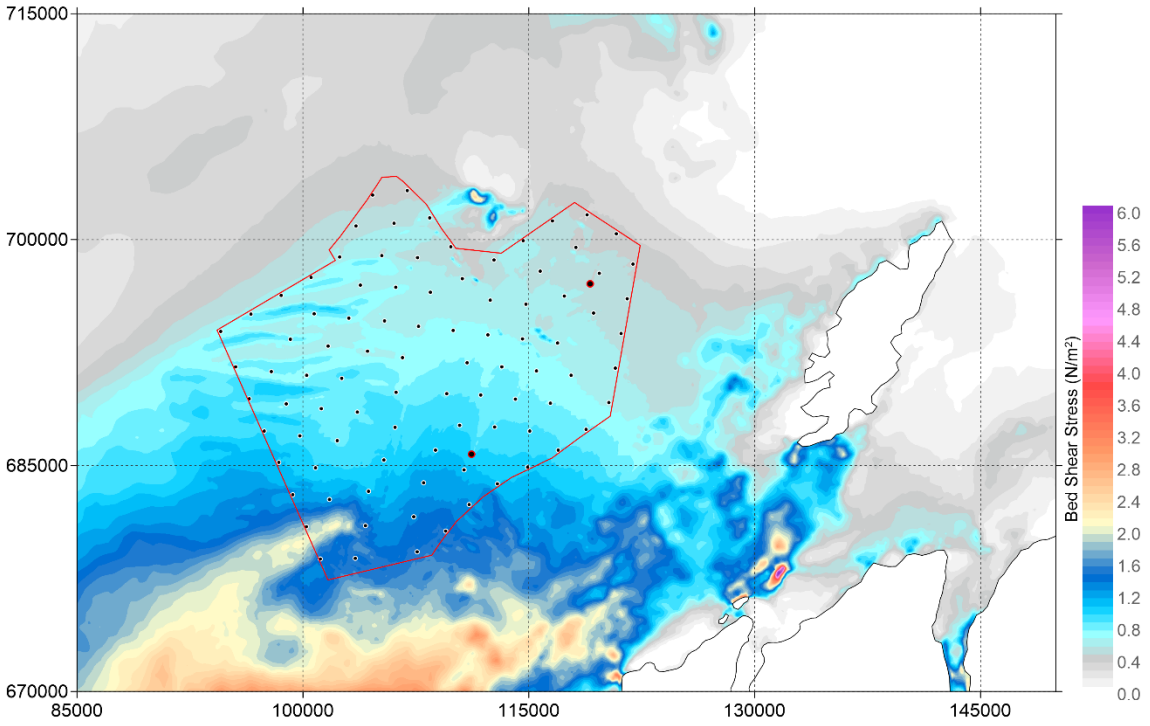

Figure 5-121: 24 MW - Dense Perimeter layout - Bed shear stress during spring tide - peak flood (Local model)

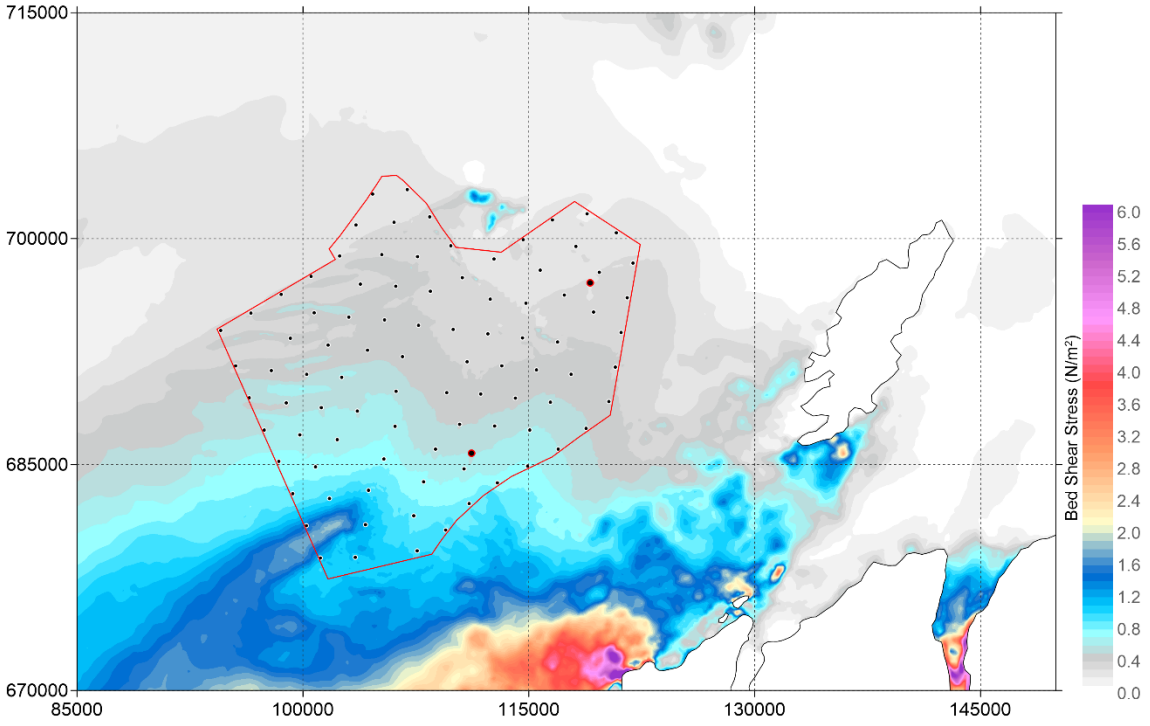

Figure 5-122: 24 MW - Dense Perimeter layout - Bed shear stress during spring tide - peak ebb (Local model)

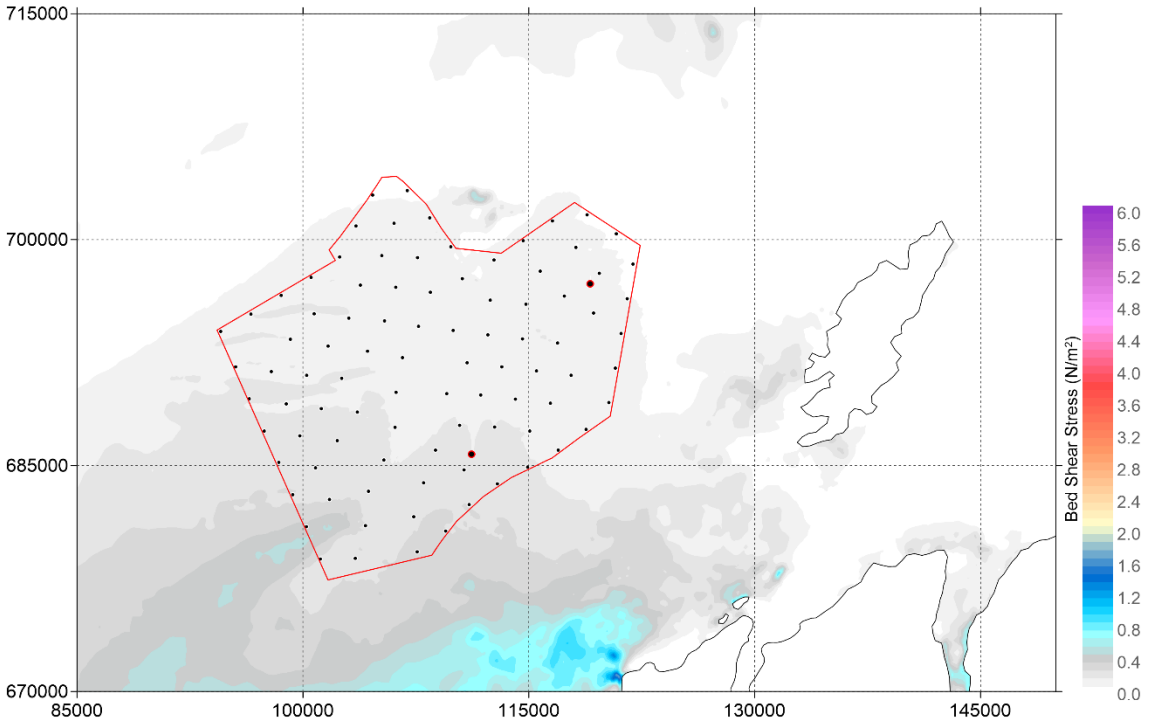

Figure 5-123: 24 MW - Dense Perimeter layout - Bed shear stress during neap tide - peak flood (Local model)

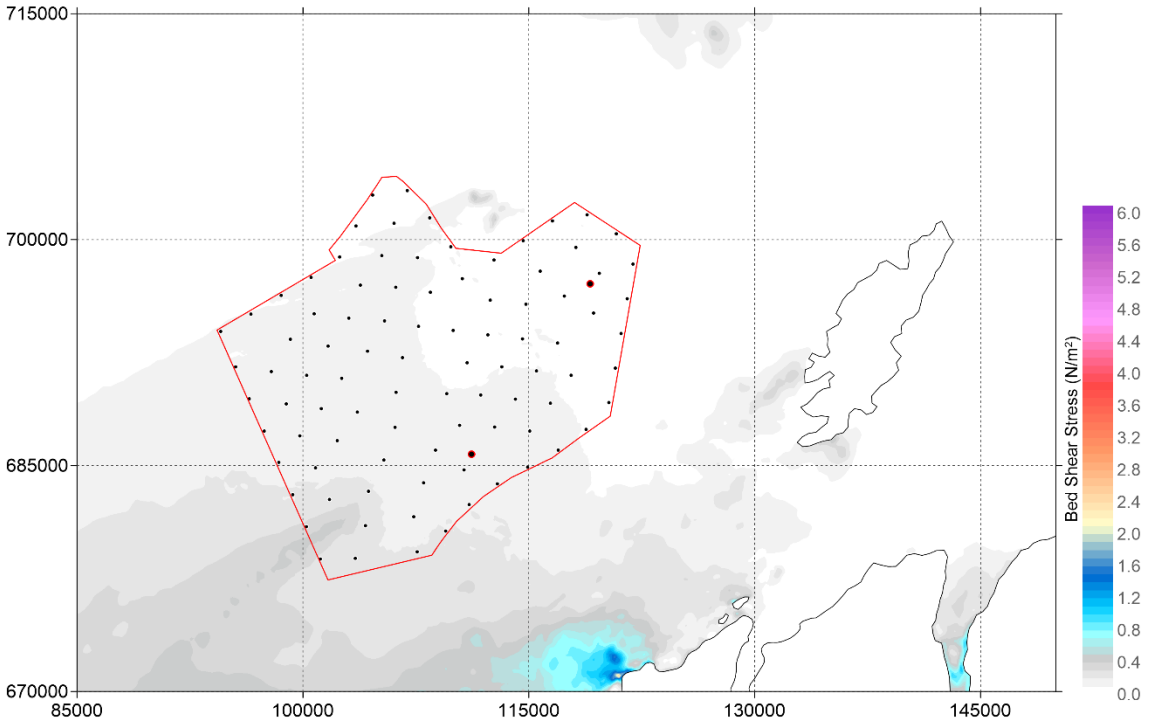

Figure 5-124: 24 MW - Dense Perimeter layout - Bed shear stress during neap tide - peak ebb (Local model)

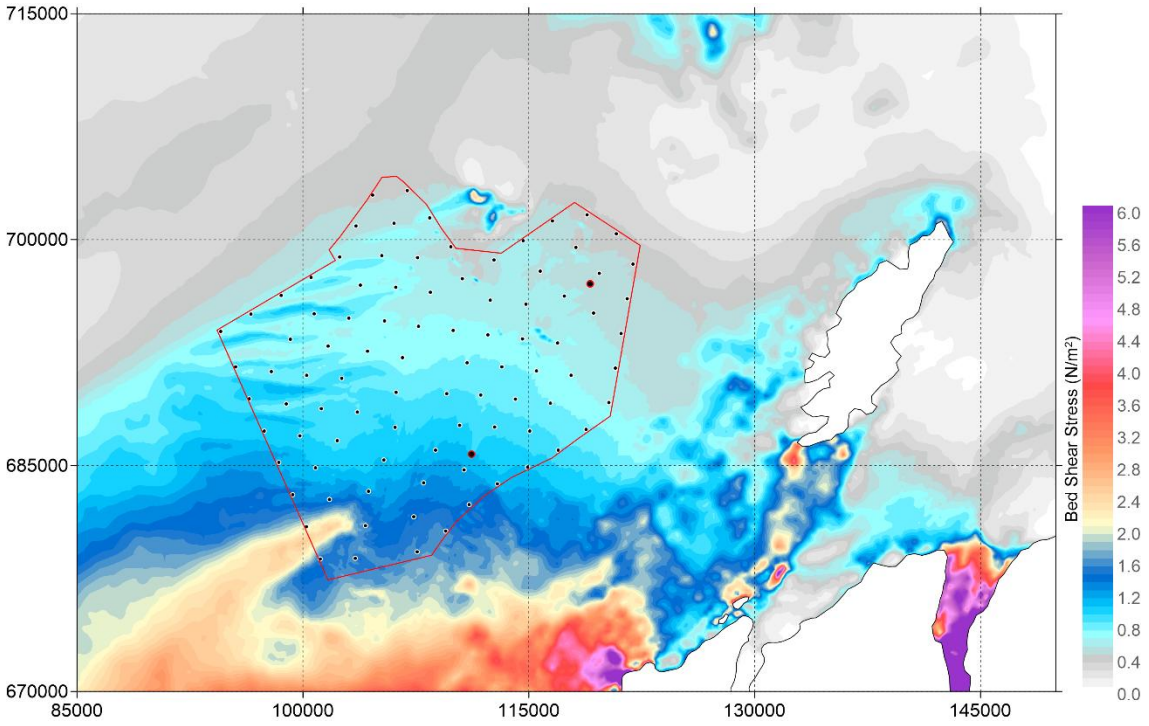

Figure 5-125: 24 MW - Dense Perimeter layout – Maximum Bed shear stress over 15 days (Local model)

Absolute Bed Shear Stress - 24 MW Even Spread layout

5.3.37 This section presents the absolute bed shear stress around the WDA for the 24 MW Even Spread layout. **Figure 5-126** and **Figure 5-127** present the predicted bed shear stress during spring tide for peak flood and peak ebb, respectively. **Figure 5-128** and **Figure 5-129** present the predicted bed shear stress during neap tide for peak flood and peak ebb, respectively. **Figure 5-130** presents the maximum bed shear stress throughout the full spring-neap tidal cycle simulation.

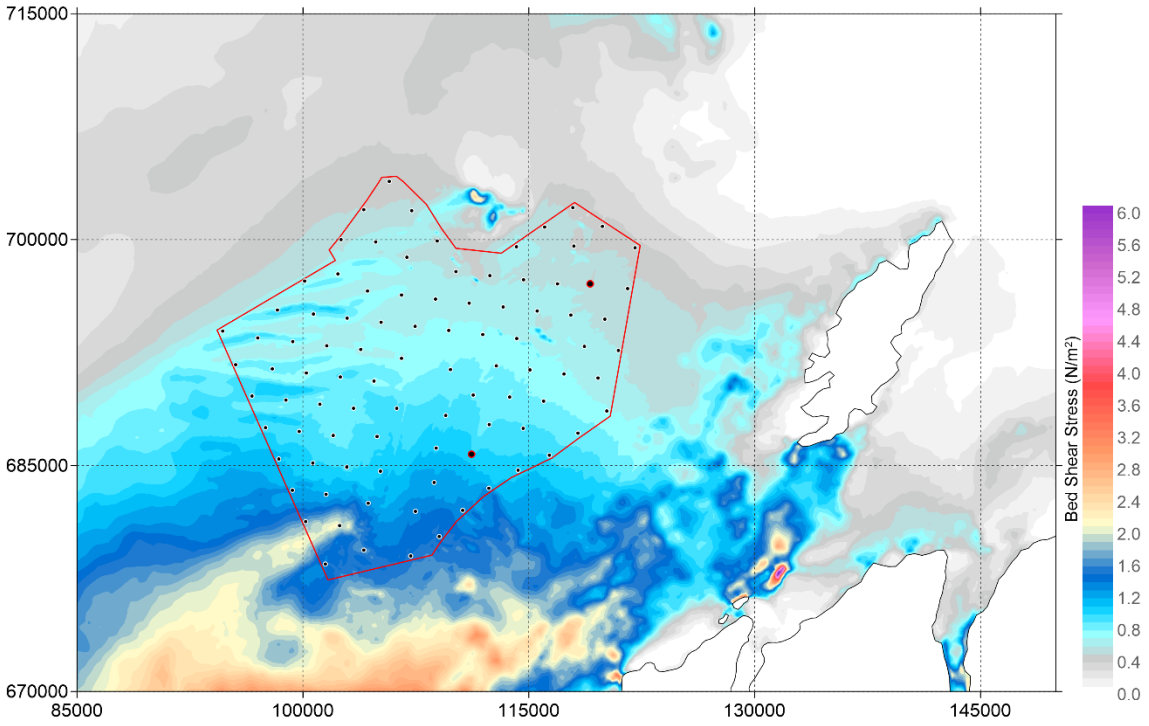

Figure 5-126: 24 MW - Even Spread layout - Bed shear stress during spring tide - peak flood (Local model)

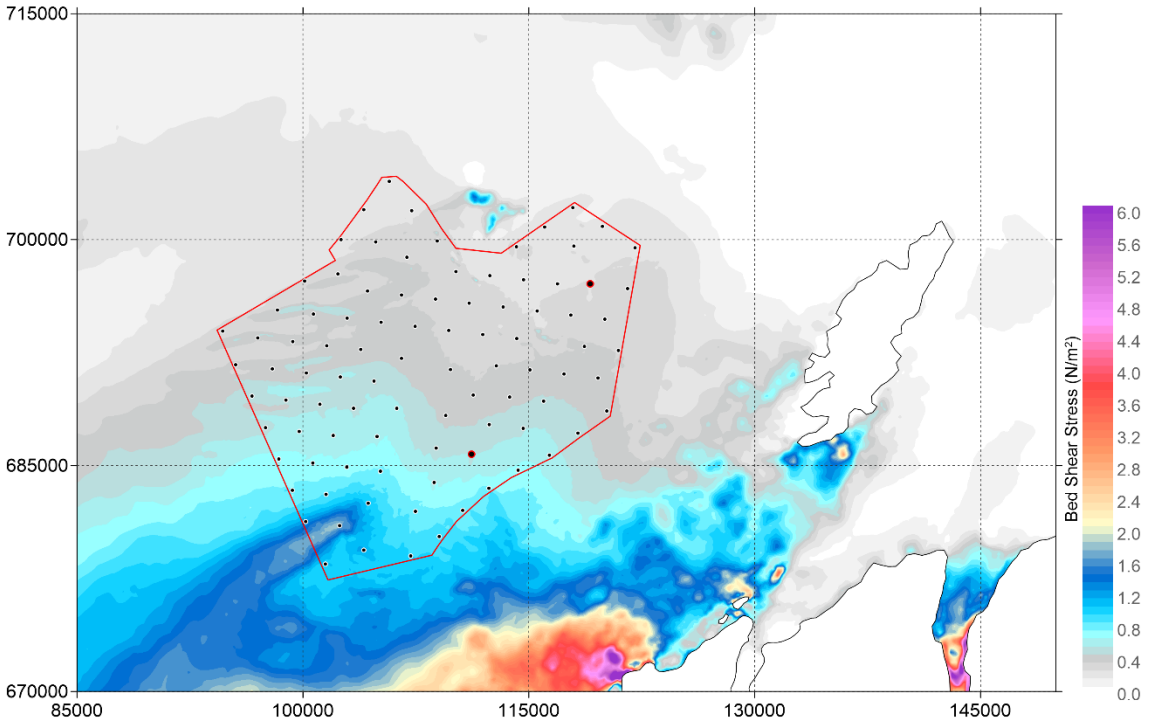

Figure 5-127: 24 MW - Even Spread layout - Bed shear stress during spring tide - peak ebb (Local model)

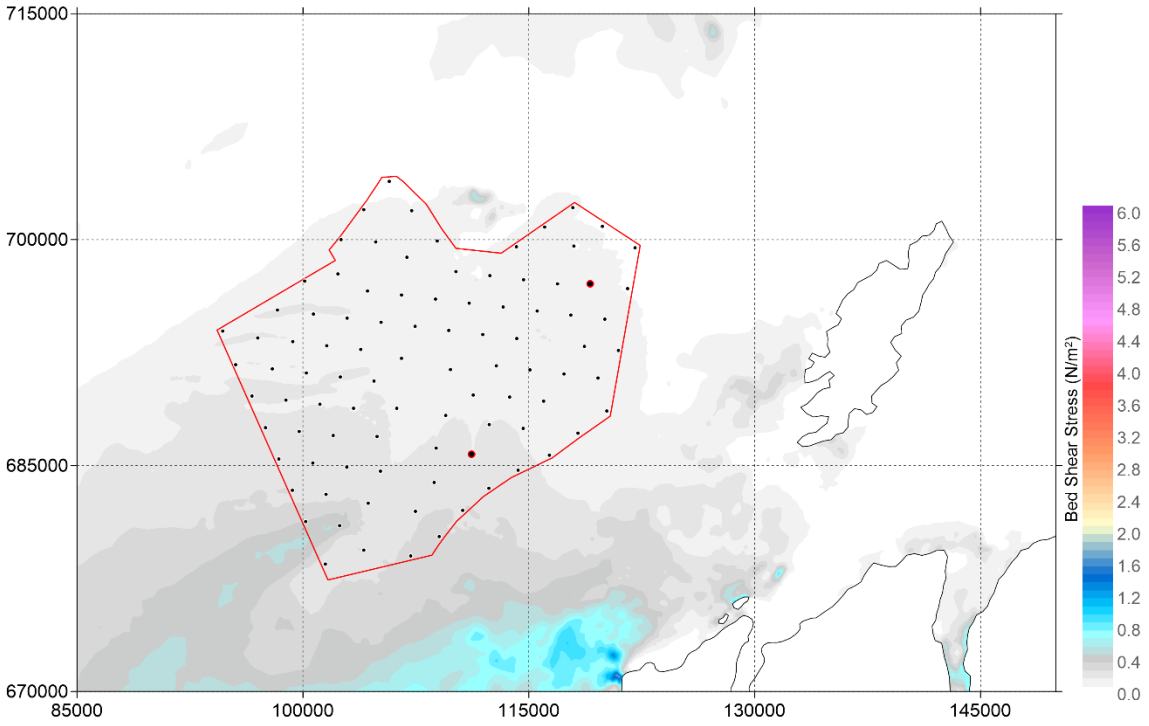

Figure 5-128: 24 MW - Even Spread layout - Bed shear stress during neap tide - peak flood (Local model)

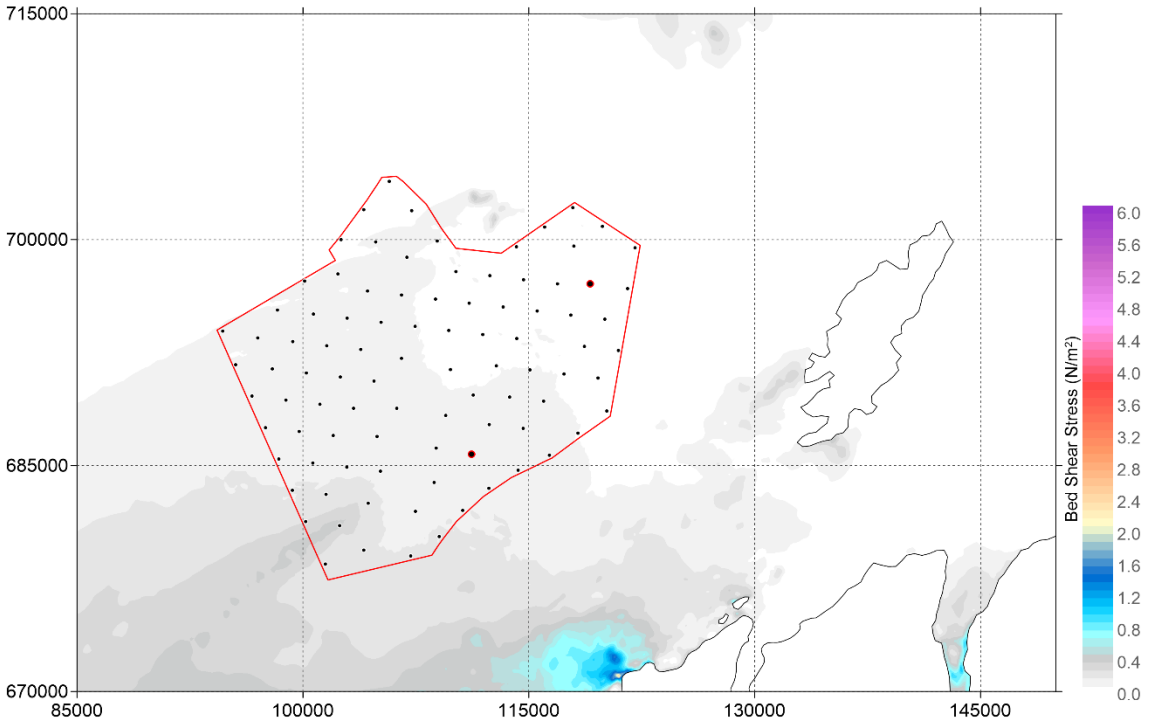

Figure 5-129: 24 MW - Even Spread layout - Bed shear stress during neap tide - peak ebb (Local model)

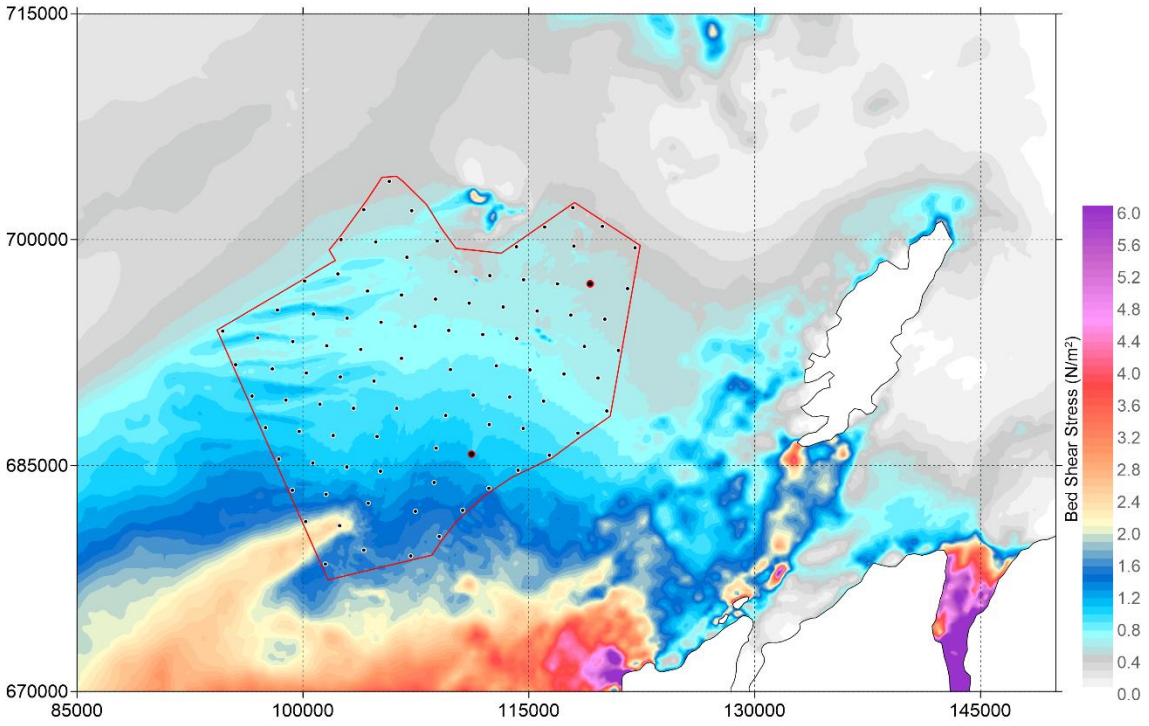

Figure 5-130: 24 MW - Even Spread layout – Maximum Bed shear stress over 15 days (Local model)

Impact on Bed Shear Stress – 15 MW Dense Perimeter Layout

5.3.38 This section presents the difference in absolute bed shear stress relative to the baseline around the WDA for the 15 MW Dense Perimeter layout. **Figure 5-131** and **Figure 5-132** present the predicted difference in bed shear stress during spring tide for peak flood and peak ebb, respectively. **Figure 5-133** and **Figure 5-134** present the predicted difference in bed shear stress during neap tide for peak flood and peak ebb, respectively. **Figure 5-135** presents the difference in maximum bed shear stress throughout the full spring-neap tidal cycle simulation.

5.3.39 The results for difference in bed shear stress between the 15 MW – Dense Perimeter layout and baseline scenario, indicate that during spring tide at peak flood the increase is <0.015 Nm^2 to the west of the site up to 2 km outside the WDA. To the north, east and south the reduction is <- 0.01 Nm^2, up to 4 km outside the WDA.

5.3.40 During spring tide at peak ebb, the increase is <0.02 Nm^2 to the east of the site up to 4 km outside the WDA. To the south and west, the reduction is <-0.025 Nm^2, up to 2 km outside the WDA and <-0.01 Nm^2 up to 4 km.

5.3.41 During neap tide the predicted change in bed shear stress is <0.01 Nm^2 outside the WDA.

5.3.42 At the OSP structures the change is greatest as expected, with a localized reduction of up to 0.13 Nm^2. The change is most pronounced on the peak flood stage of the spring tide.

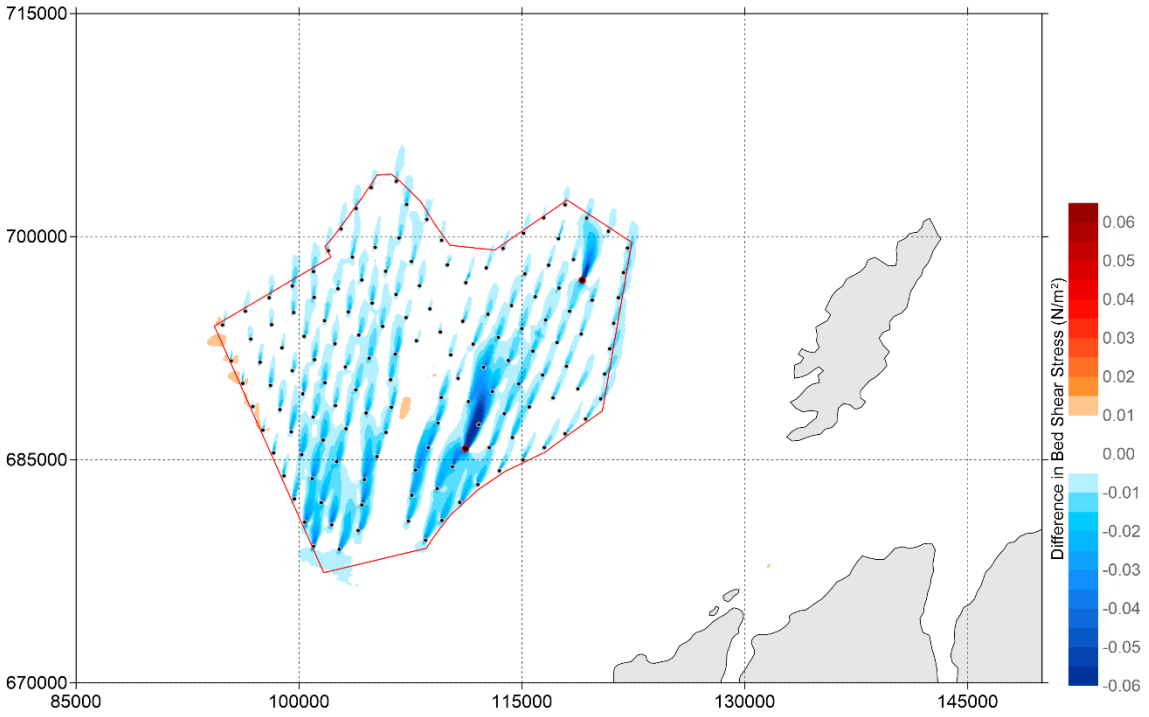

Figure 5-131: Difference in Bed shear stress (N/m2) between 'Baseline' and '15 MW - Dense Perimeter layout' during spring tide (positive means increase of bed shear stress by layout and vice versa) - peak flood

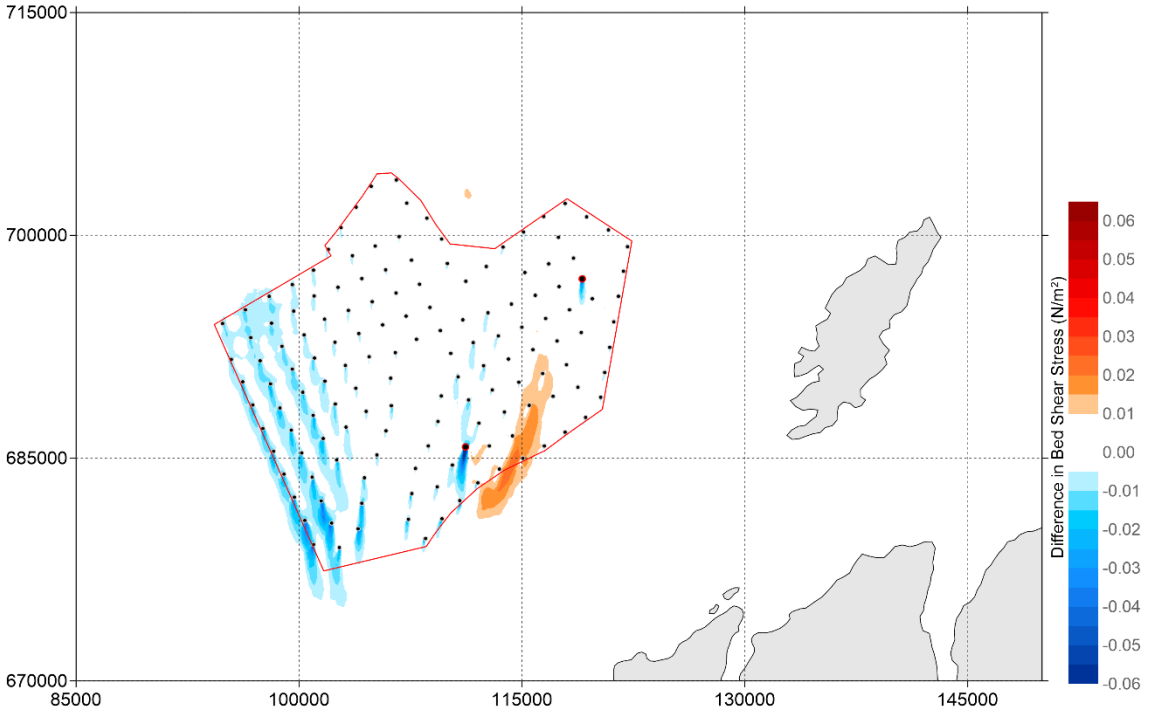

Figure 5-132: Difference in Bed shear stress (N/m^2) between 'Baseline' and '15 MW - Dense Perimeter layout' during spring tide (positive means increase of bed shear stress by layout and vice versa) - peak ebb

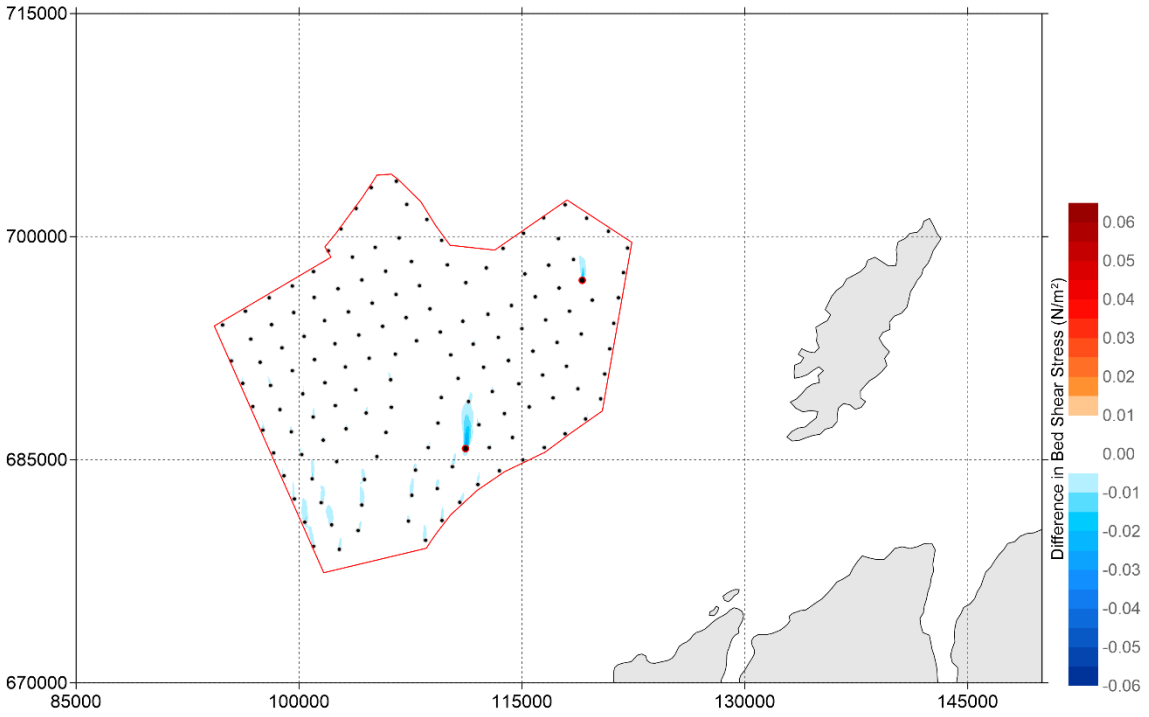

Figure 5-133: Difference in Bed shear stress (N/m^2) between 'Baseline' and '15 MW - Dense Perimeter layout' during neap tide (positive means increase of bed shear stress by layout and vice versa) - peak flood

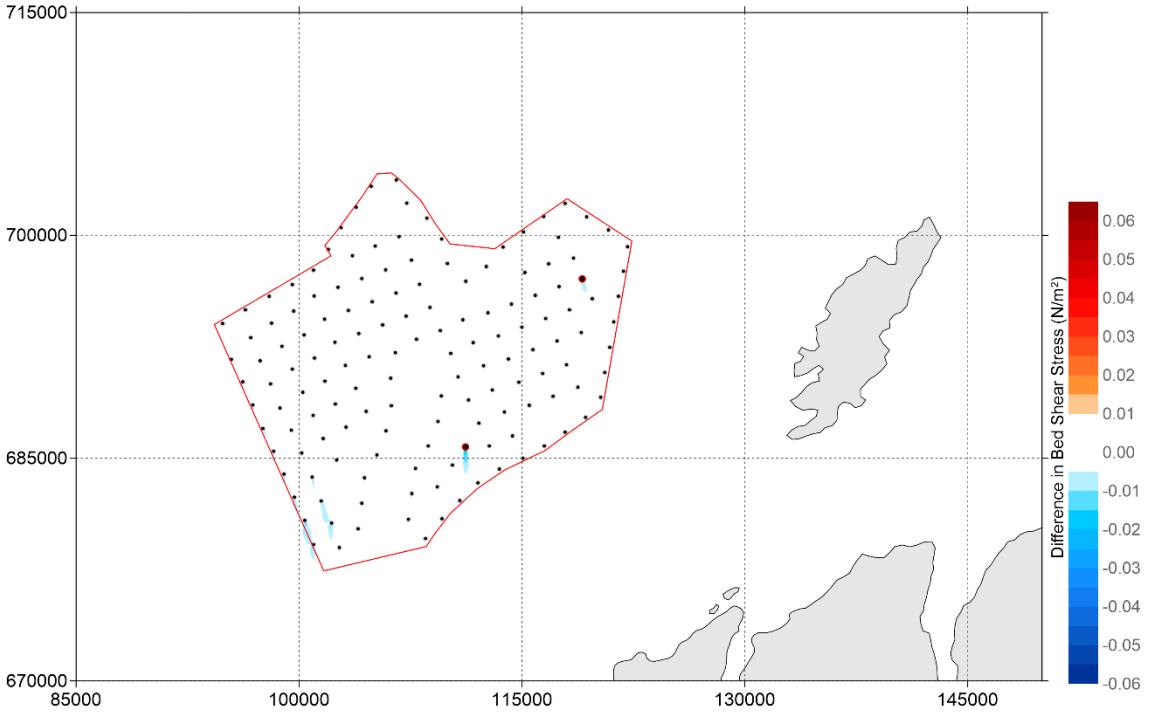

Figure 5-134: Difference in Bed shear stress (N/m^2) between 'Baseline' and '15 MW - Dense Perimeter layout' during neap tide (positive means increase of bed shear stress by layout and vice versa) - peak ebb

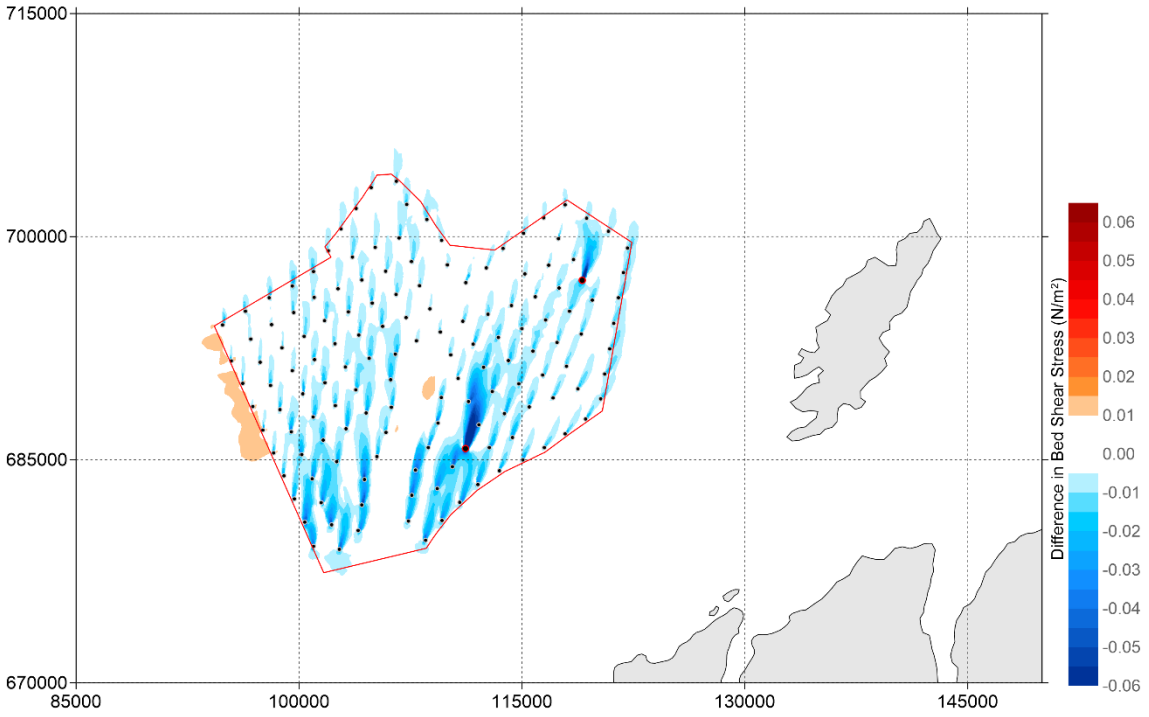

Figure 5-135: Difference in maximum Bed shear stress (N/m^2) between 'Baseline' and '15 MW - Dense Perimeter layout' over 15 days (positive means increase of bed shear stress by layout and vice versa)

Impact on Bed Shear Stress – 15 MW Even Spread Layout

5.3.43 This section presents the difference in absolute bed shear stress relative to the baseline around the WDA for the 15 MW Even Spread layout. **Figure 5-136** and **Figure 5-137** present the predicted difference in bed shear stress during spring tide for peak flood and peak ebb, respectively. **Figure 5-138** and **Figure 5-139** present the predicted difference in bed shear stress during neap tide for peak flood and peak ebb, respectively. **Figure 5-140** presents the difference in maximum bed shear stress throughout the full spring-neap tidal cycle simulation.

5.3.44 The difference in bed shear stress is very similar due to the 15 MW – Dense Perimeter layout.

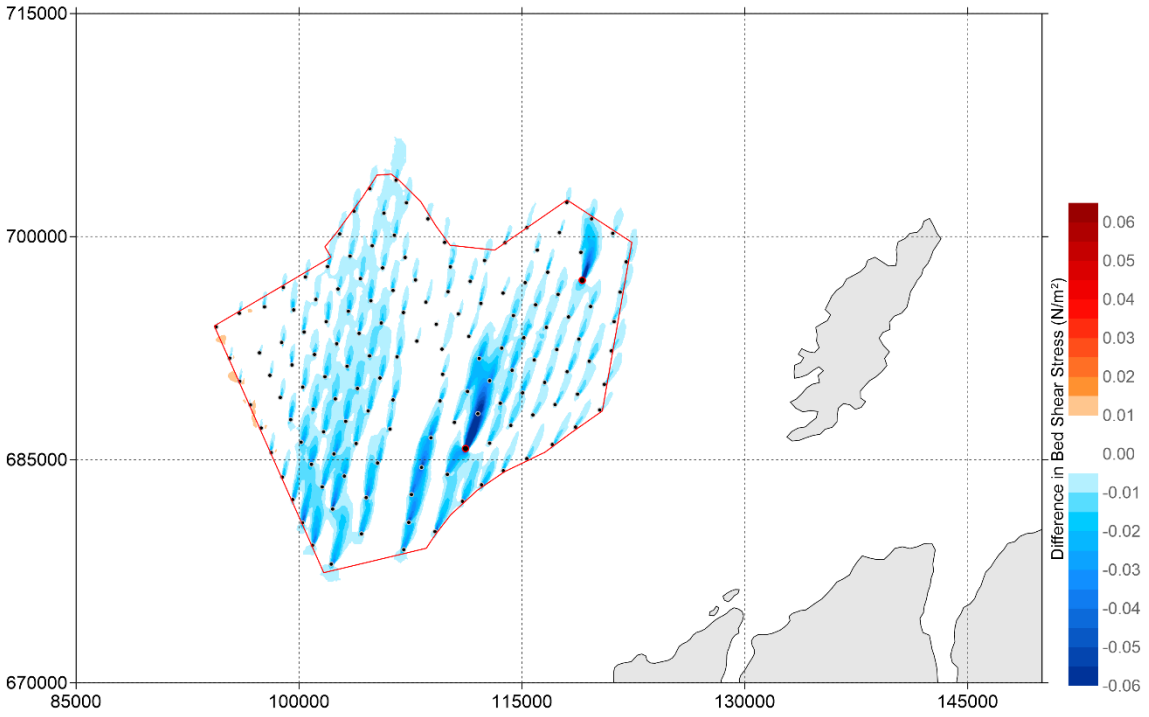

Figure 5-136: Difference in Bed shear stress (N/m^2) between 'Baseline' and '15 MW - Even Spread layout' during spring tide (positive means increase of bed shear stress by layout and vice versa) - peak flood

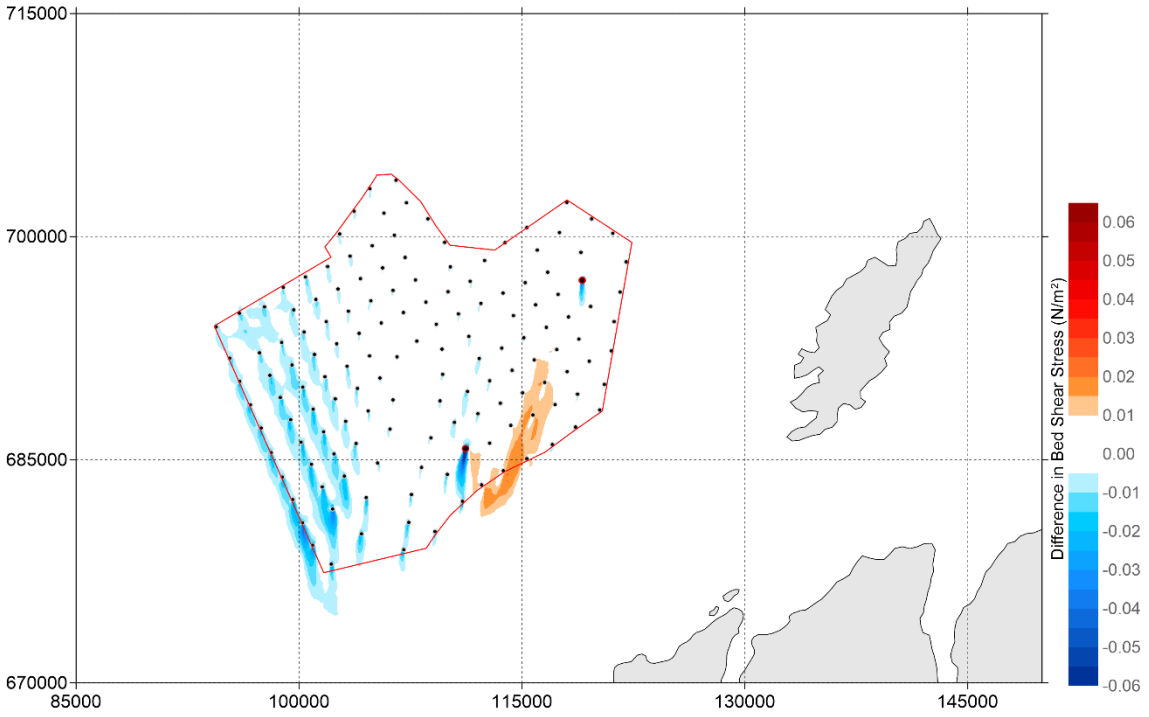

Figure 5-137: Difference in Bed shear stress (N/m^2) between 'Baseline' and '15 MW - Even Spread layout' during spring tide (positive means increase of bed shear stress by layout and vice versa) - peak ebb

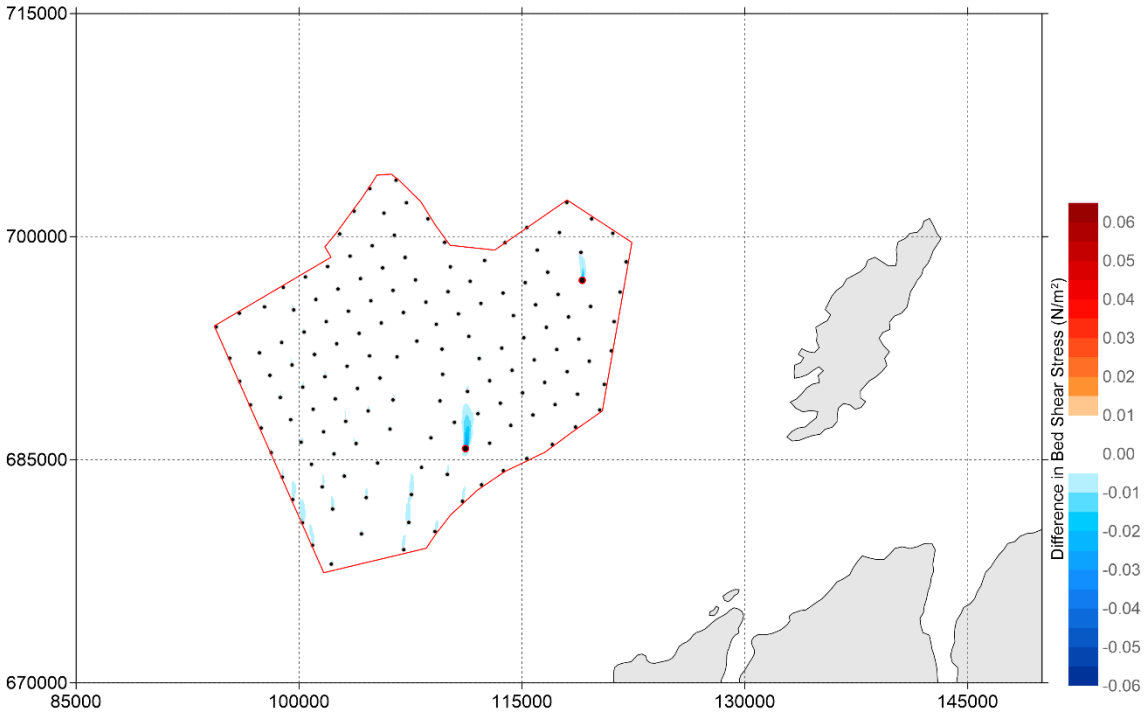

Figure 5-138: Difference in Bed shear stress (N/m^2) between 'Baseline' and '15 MW - Even Spread layout' during neap tide (positive means increase of bed shear stress by layout and vice versa) - peak flood

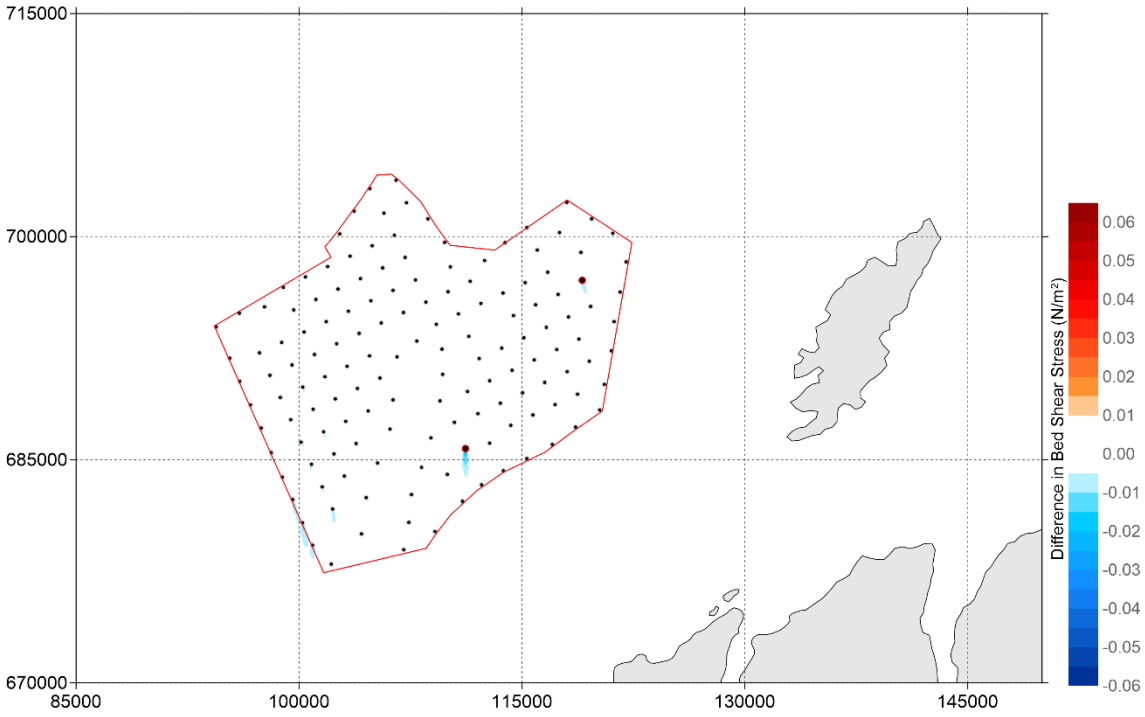

Figure 5-139: Difference in Bed shear stress (N/m^2) between 'Baseline' and '15 MW - Even Spread layout' during neap tide (positive means increase of bed shear stress by layout and vice versa) - peak ebb

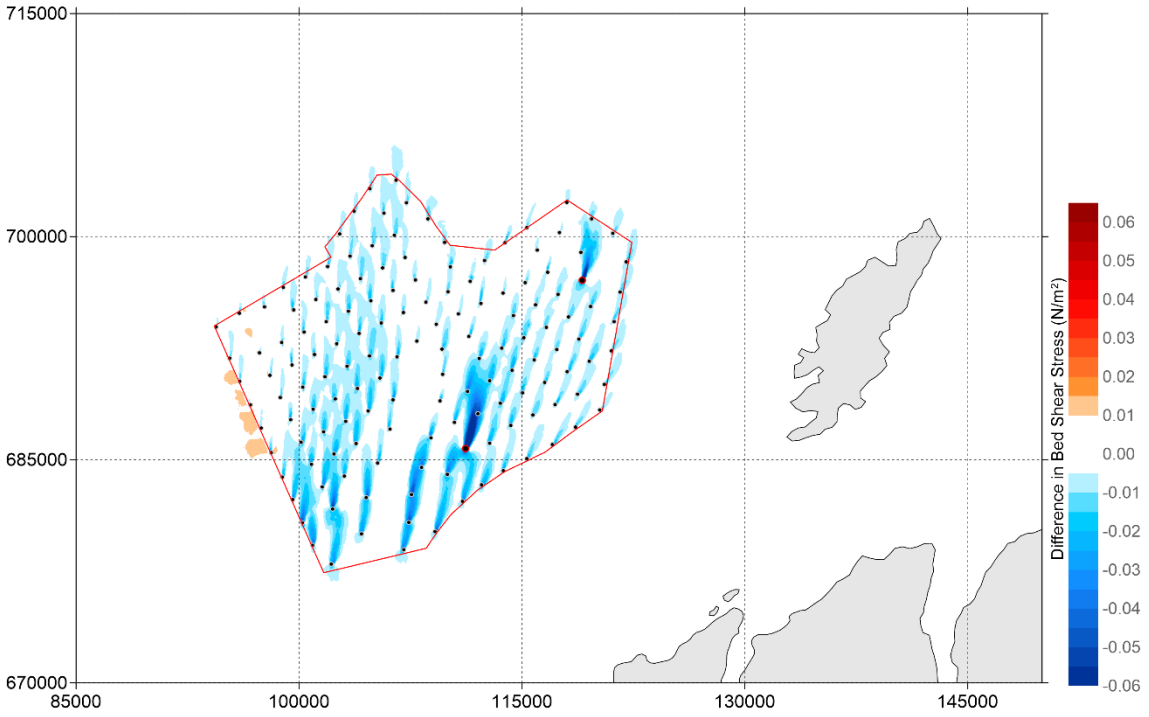

Figure 5-140: Difference in maximum Bed shear stress (N/m^2) between 'Baseline' and '15 MW - Even Spread layout' over 15 days (positive means increase of bed shear stress by layout and vice versa)

Impact on Bed Shear Stress – 24 MW Dense Perimeter Layout

5.3.45 This section presents the difference in absolute bed shear stress relative to the baseline around the WDA for the 24 MW Dense Perimeter layout. **Figure 5-141** and **Figure 5-142** present the predicted difference in bed shear stress during spring tide for peak flood and peak ebb, respectively. **Figure 5-143** and **Figure 5-144** present the predicted difference in bed shear stress during neap tide for peak flood and peak ebb, respectively. **Figure 5-145** presents the difference in maximum bed shear stress throughout the full spring-neap tidal cycle simulation.

5.3.46 The results for difference in bed shear stress between the 24 MW – Dense Perimeter layout and baseline scenario, indicate that during spring tide at peak flood the reduction is <-0.01 Nm^2, up to 2 km outside the WDA.

5.3.47 During spring tide at peak ebb, the increase is <0.02 Nm^2 to the east of the site up to 3 km outside the WDA. To the south and west, the reduction is <-0.025 Nm^2, up to 1.5 km outside the WDA and <-0.01 Nm^2 up to 3 km.

5.3.48 During neap tide the predicted change in bed shear stress is <0.01 Nm^2 outside the WDA.

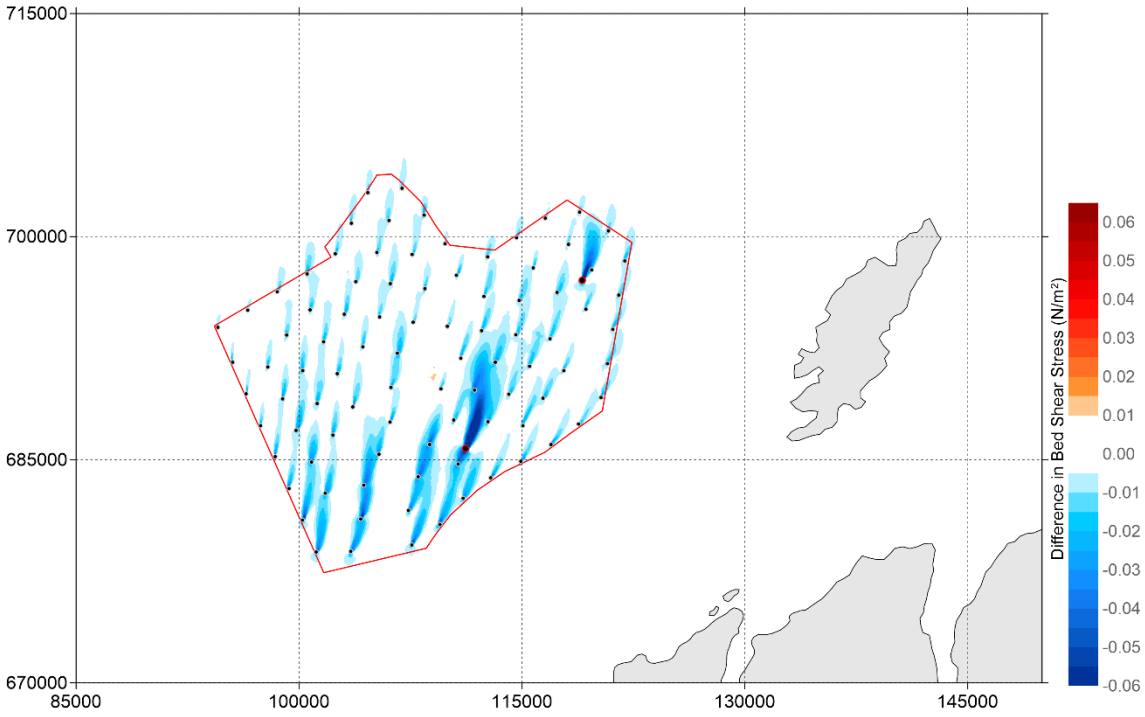

Figure 5-141: Difference in Bed shear stress (N/m^2) between 'Baseline' and '24 MW - Dense Perimeter layout' during spring tide (positive means increase of bed shear stress by layout and vice versa) - peak flood

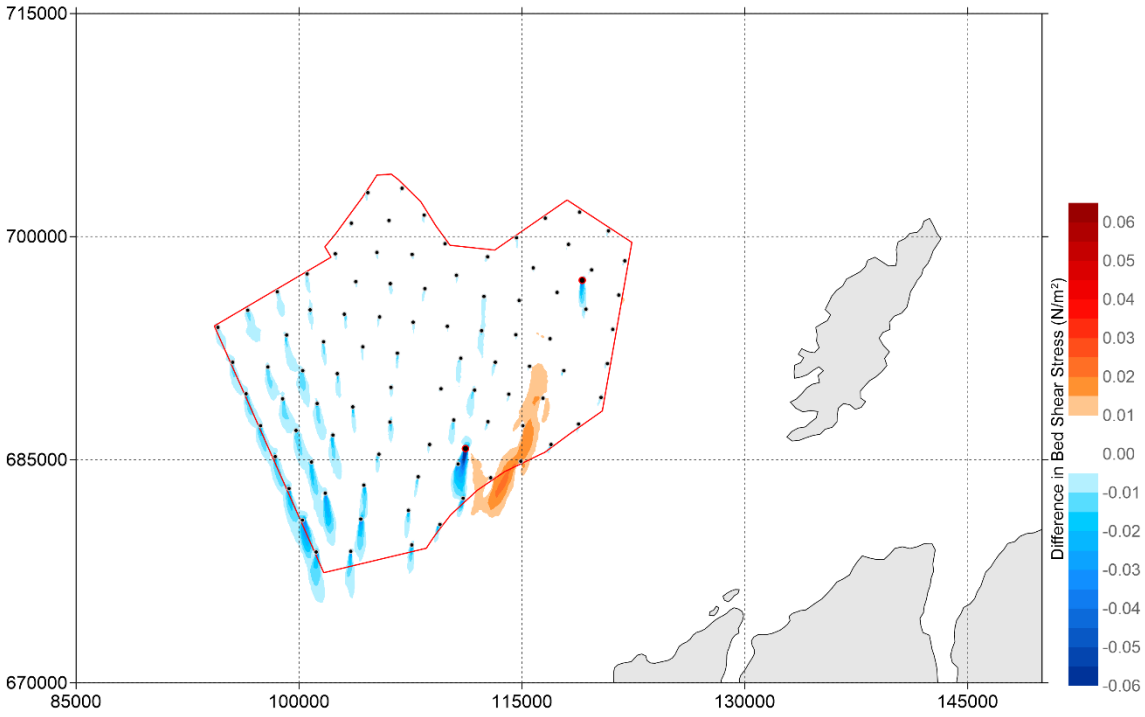

Figure 5-142: Difference in Bed shear stress (N/m^2) between 'Baseline' and '24 MW - Dense Perimeter layout' during spring tide (positive means increase of bed shear stress by layout and vice versa) - peak ebb

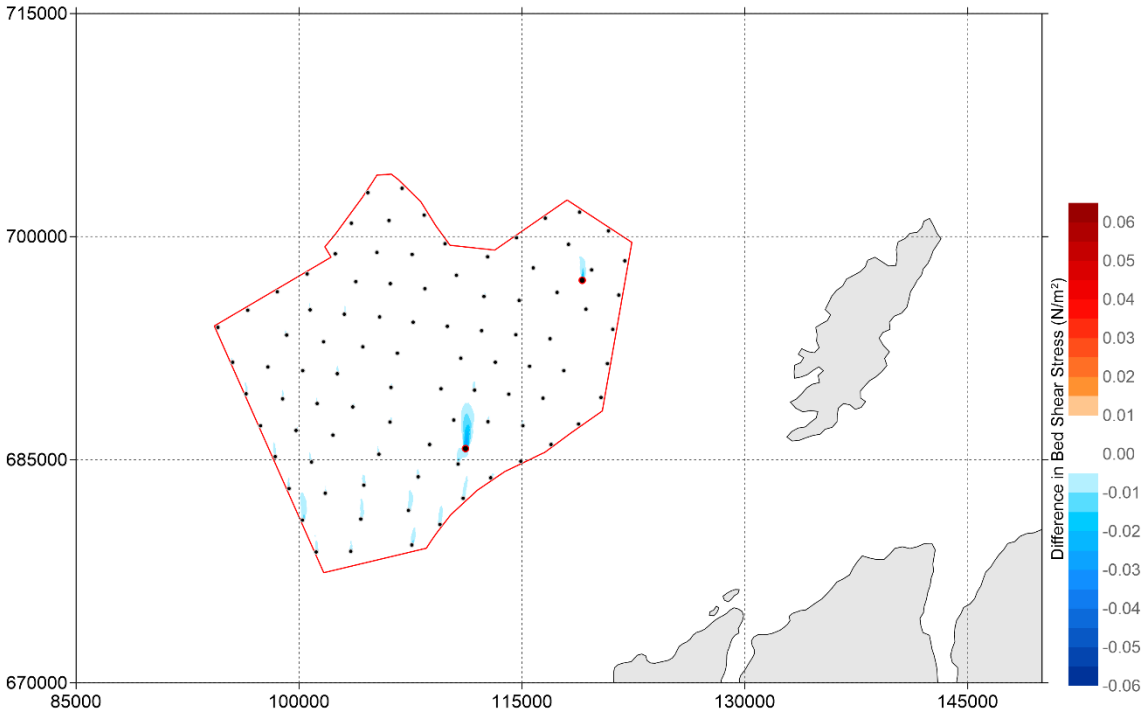

Figure 5-143: Difference in Bed shear stress (N/m^2) between 'Baseline' and '24 MW - Dense Perimeter layout' during neap tide (positive means increase of bed shear stress by layout and vice versa) - peak flood

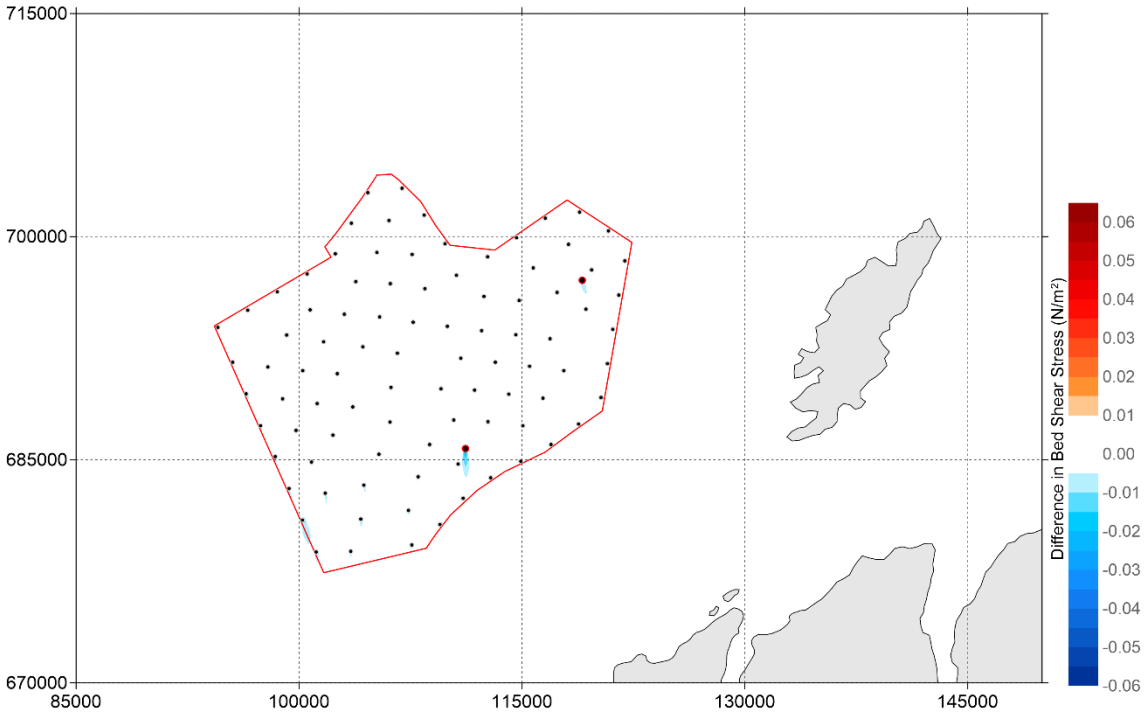

Figure 5-144: Difference in Bed shear stress (N/m^2) between 'Baseline' and '24 MW - Dense Perimeter layout' during neap tide (positive means increase of bed shear stress by layout and vice versa) - peak ebb

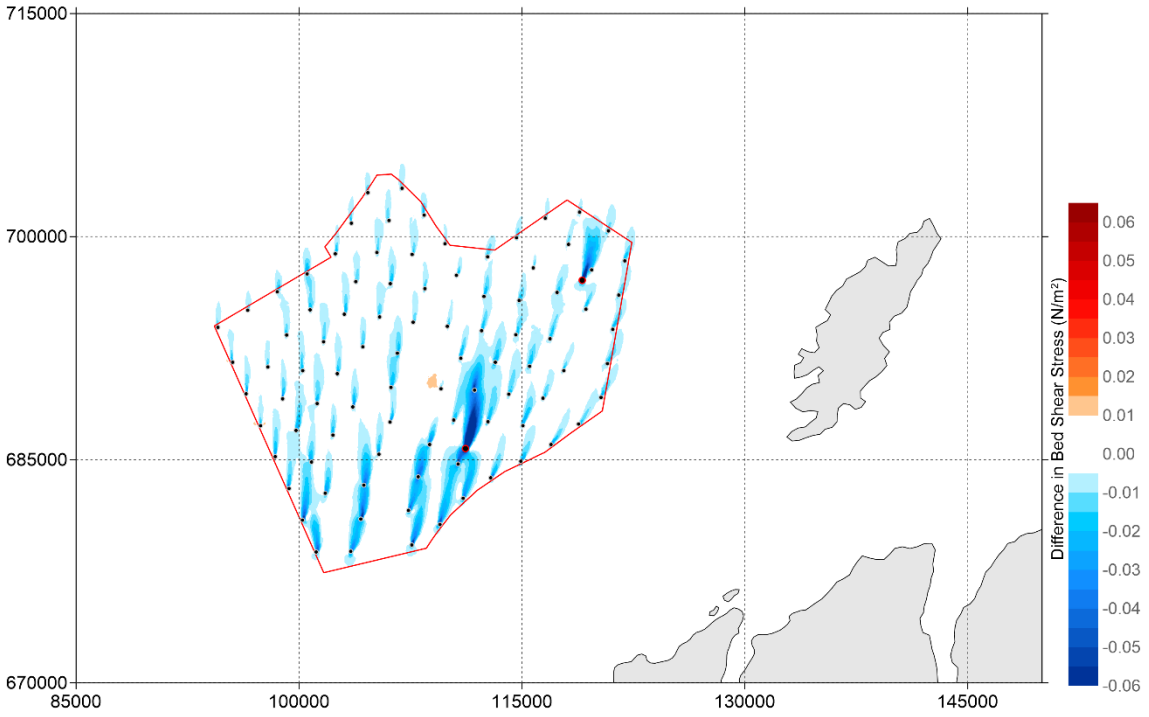

Figure 5-145: Difference in maximum Bed shear stress (N/m^2) between 'Baseline' and '24 MW - Dense Perimeter layout' over 15 days (positive means increase of bed shear stress by layout and vice versa)

Impact on Bed Shear Stress – 24 MW Even Spread layout

5.3.49 This section presents the difference in absolute bed shear stress relative to the baseline around the WDA for the 24 MW Even Spread layout. **Figure 5-146** and **Figure 5-147** present the predicted difference in bed shear stress during spring tide for peak flood and peak ebb, respectively. **Figure 5-148** and **Figure 5-149** present the predicted difference in bed shear stress during neap tide for peak flood and peak ebb, respectively. **Figure 5-150** presents the difference in maximum bed shear stress throughout the full spring-neap tidal cycle simulation.

5.3.50 The difference in bed shear stress is very similar to the one observed for the 24 MW – Dense Perimeter layout.

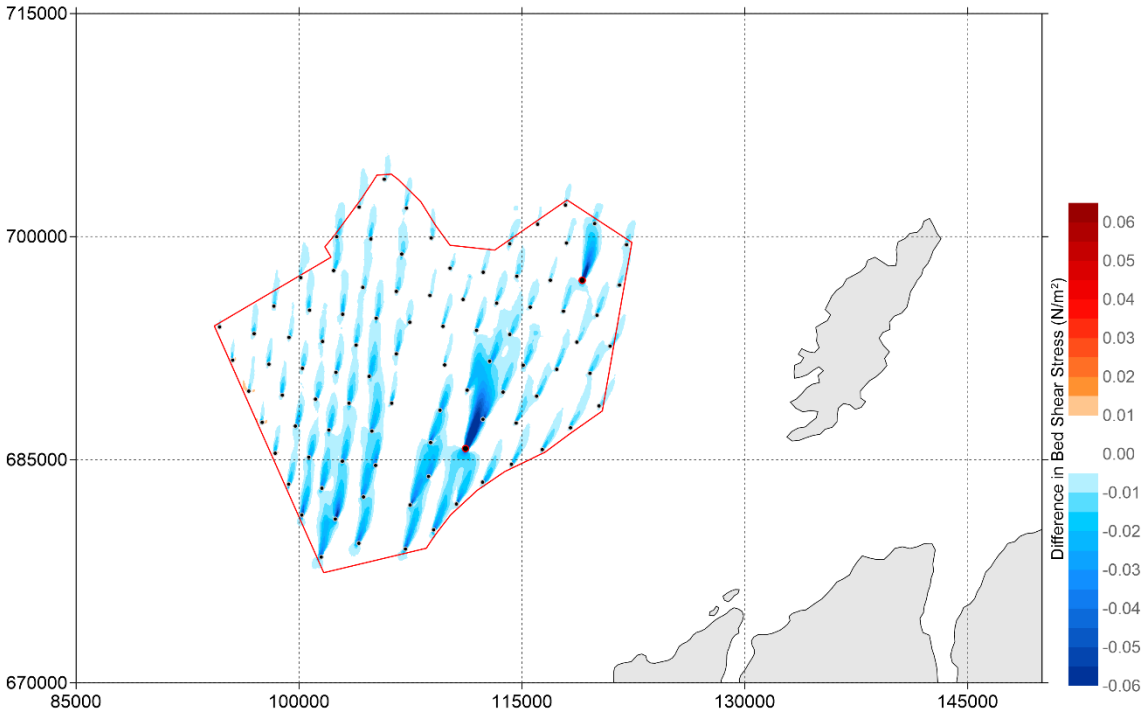

Figure 5-146: Difference in Bed shear stress (N/m^2) between 'Baseline' and '24 MW - Even Spread layout' during spring tide (positive means increase of bed shear stress by layout and vice versa) - peak flood

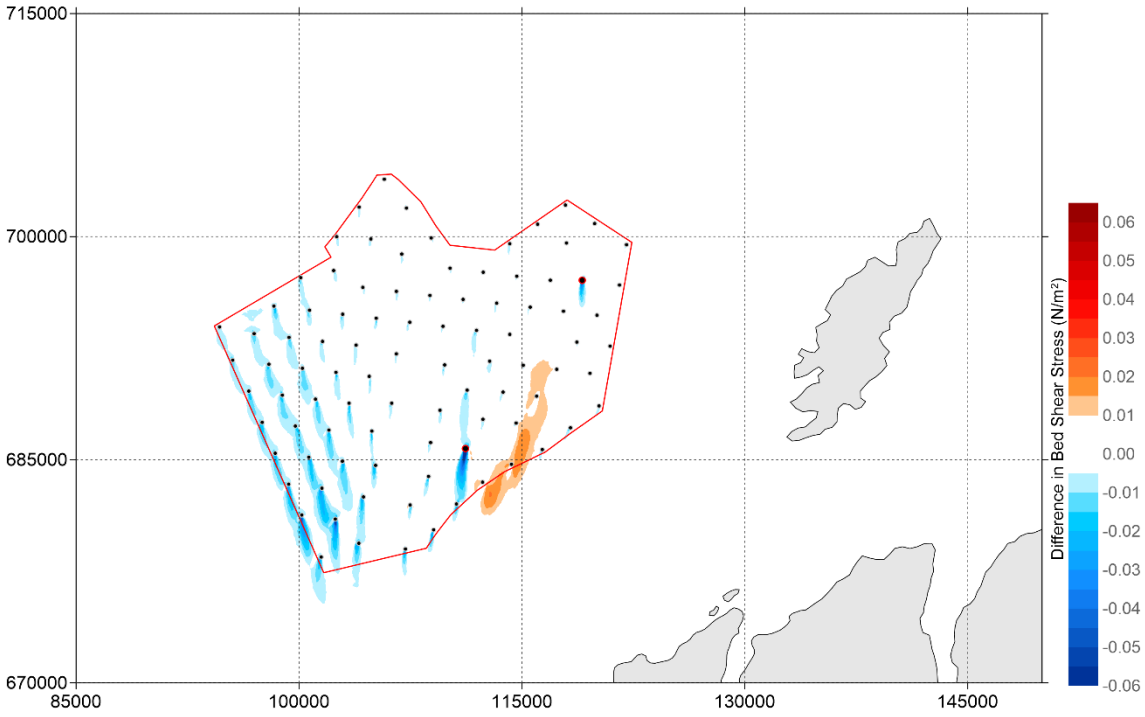

Figure 5-147: Difference in Bed shear stress (N/m^2) between 'Baseline' and '24 MW - Even Spread layout' during spring tide (positive means increase of bed shear stress by layout and vice versa) - peak ebb

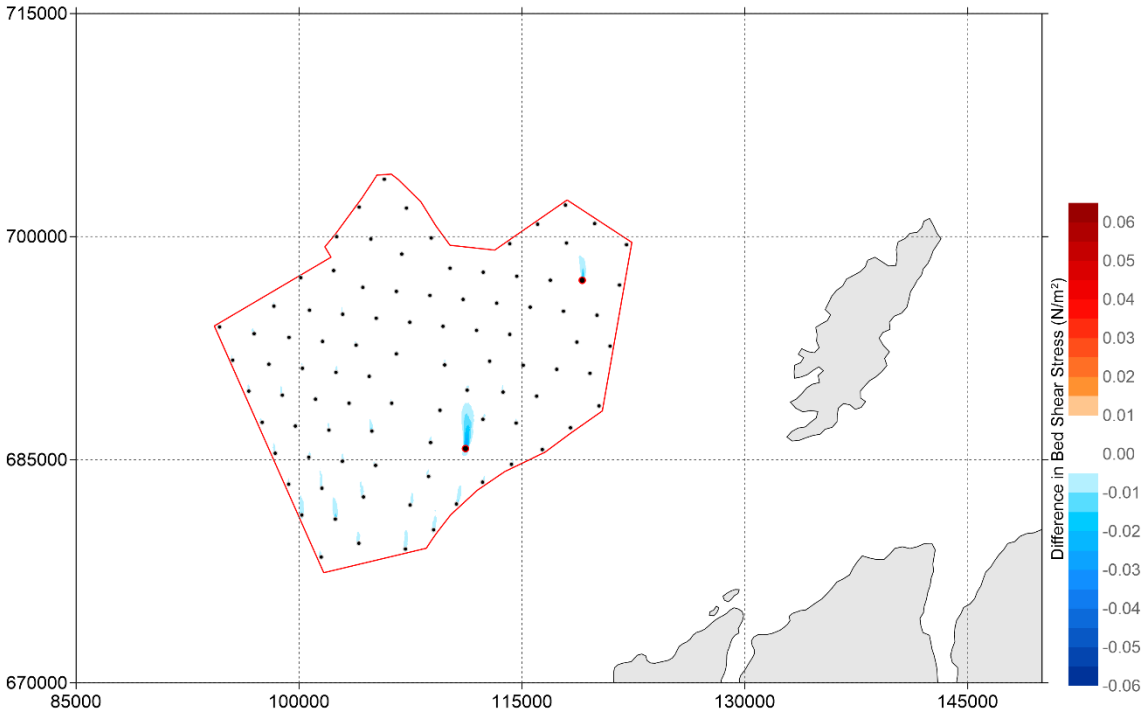

Figure 5-148: Difference in Bed shear stress (N/m^2) between 'Baseline' and '24 MW - Even Spread layout' during neap tide (positive means increase of bed shear stress by layout and vice versa) - peak flood

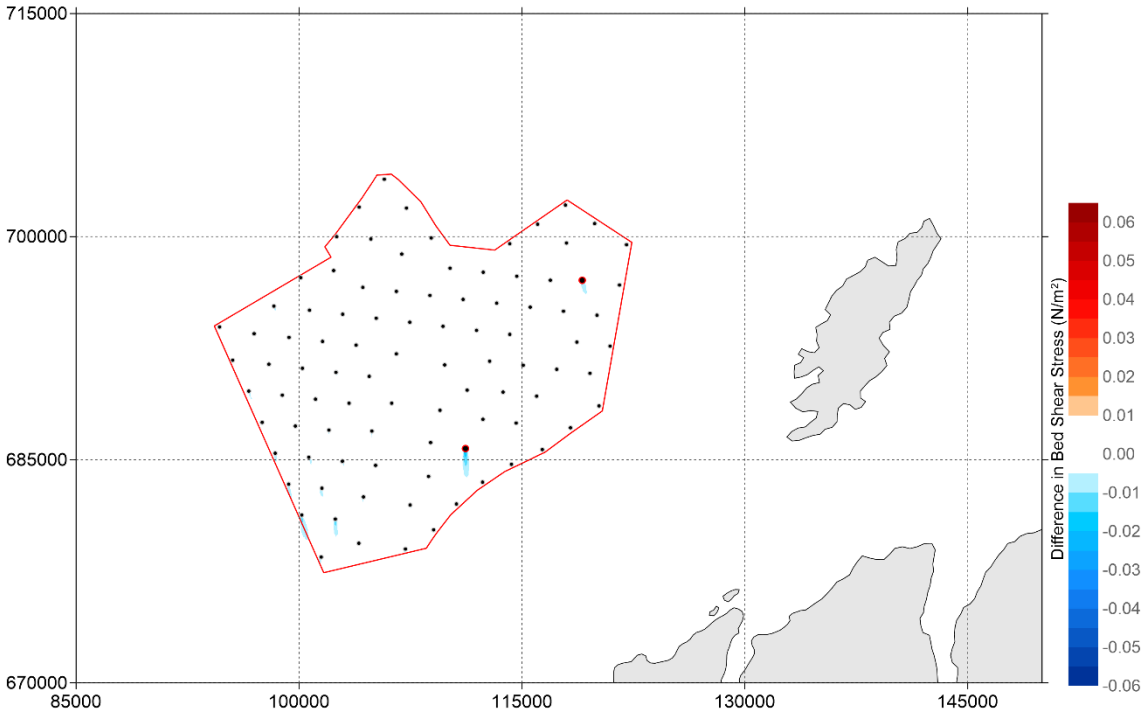

Figure 5-149: Difference in Bed shear stress (N/m^2) between 'Baseline' and '24 MW - Even Spread layout' during neap tide (positive means increase of bed shear stress by layout and vice versa) - peak ebb

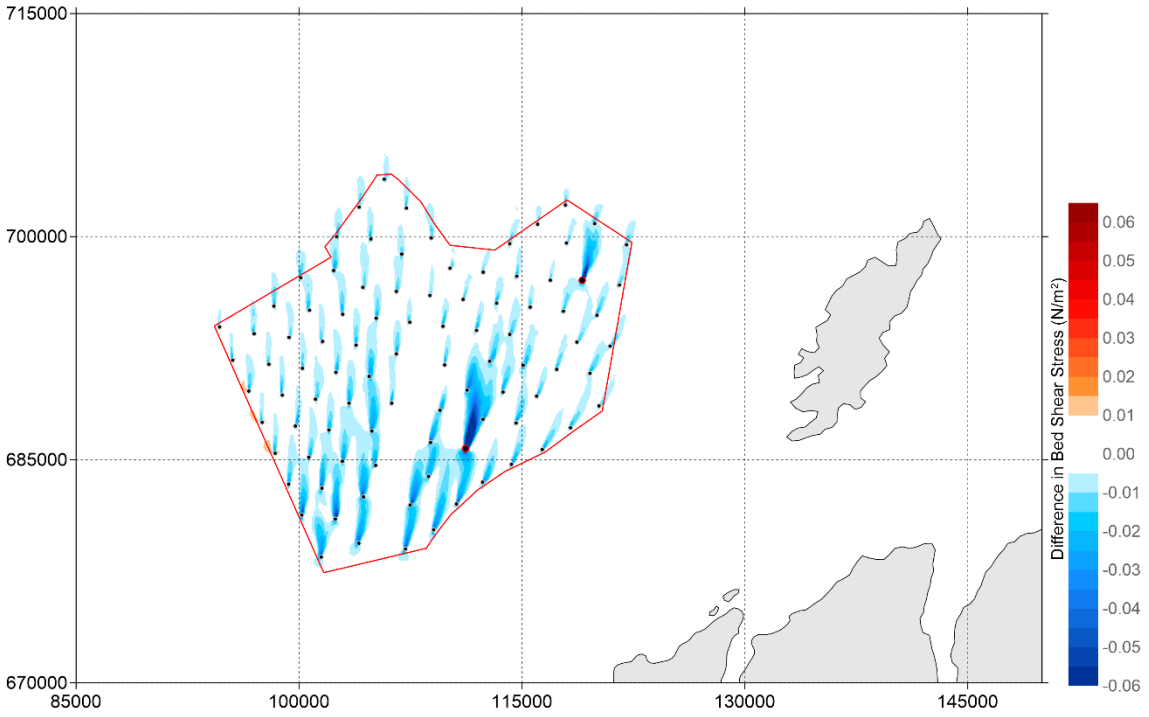

Figure 5-150: Difference in maximum Bed shear stress (N/m^2) between 'Baseline' and '24 MW - Even Spread layout' over 15 days (positive means increase of bed shear stress by layout and vice versa)

Impact on Bed Shear Stress in Percentage – 15 MW Dense Perimeter Layout

5.3.51 This section presents the percentage difference in bed shear stress relative to the baseline around the WDA for the 15 MW Dense Perimeter layout. **Figure 5-151** and **Figure 5-152** present the predicted percentage difference in bed shear stress during spring tide for peak flood and peak ebb, respectively. **Figure 5-153** and **Figure 5-154** present the predicted percentage difference in bed shear stress during neap tide for peak flood and peak ebb, respectively. **Figure 5-155** presents the percentage difference in maximum bed shear stress throughout the full spring-neap tidal cycle simulation.

5.3.52 The predicted percentage difference in bed shear stress extending outside the WDA between the 15 MW – Dense Perimeter layout and baseline scenario is more pronounced during the spring tide. At peak flood, the percentage difference is a reduction of up to 2.0% extending 2 km north of the WDA and up to 1.0% extending 5 km north of the WDA. In addition to this, there is a region of increased percentage difference in bed shear stress to the west of the WDA, up to 2.0% extending 3 km northwest of the WDA and up to 1.5% extending 8 km northwest of the WDA.

5.3.53 At peak ebb, there is a reduction of up to 2.0% extending 4 km northwest of the WDA and up to 1.0% 12 km northwest of the WDA. There is a region of increase of up to 3% extending 3 km northeast of the WDA and up to 1.5% extending 10 km northeast of the WDA.

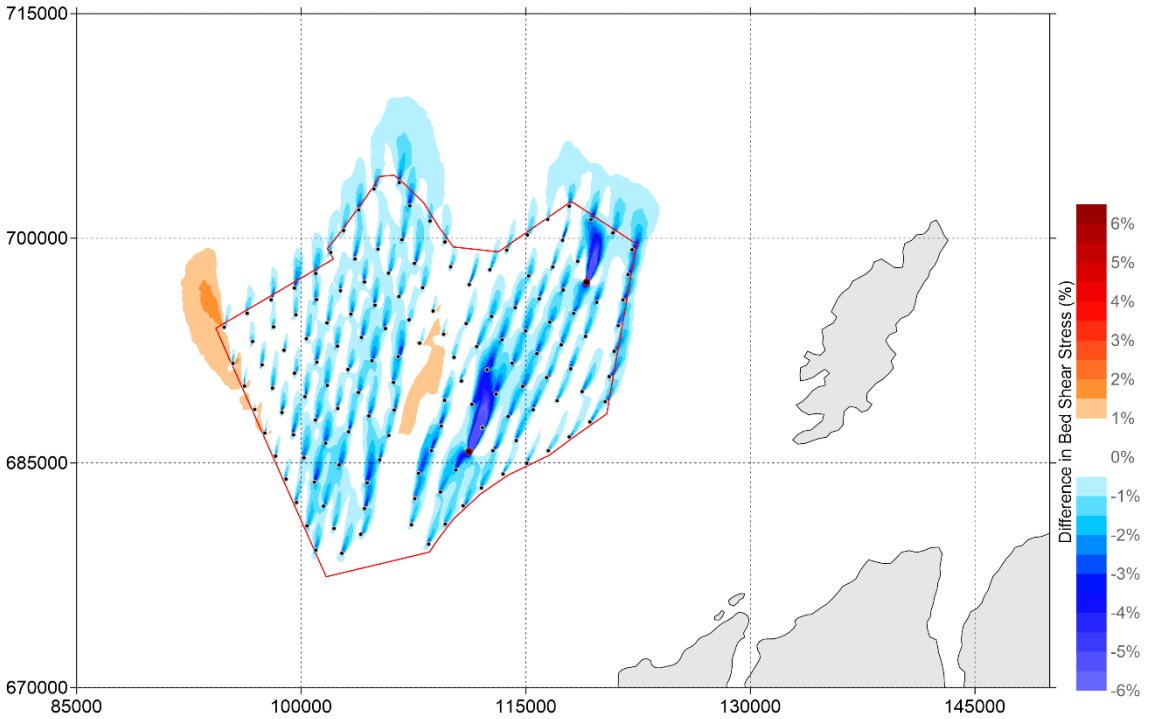

Figure 5-151: Percentage change of bed shear stress between 'Baseline' and '15 MW - Dense Perimeter layout' during spring tide (positive means increase of bed shear stress by layout and vice versa) - peak flood

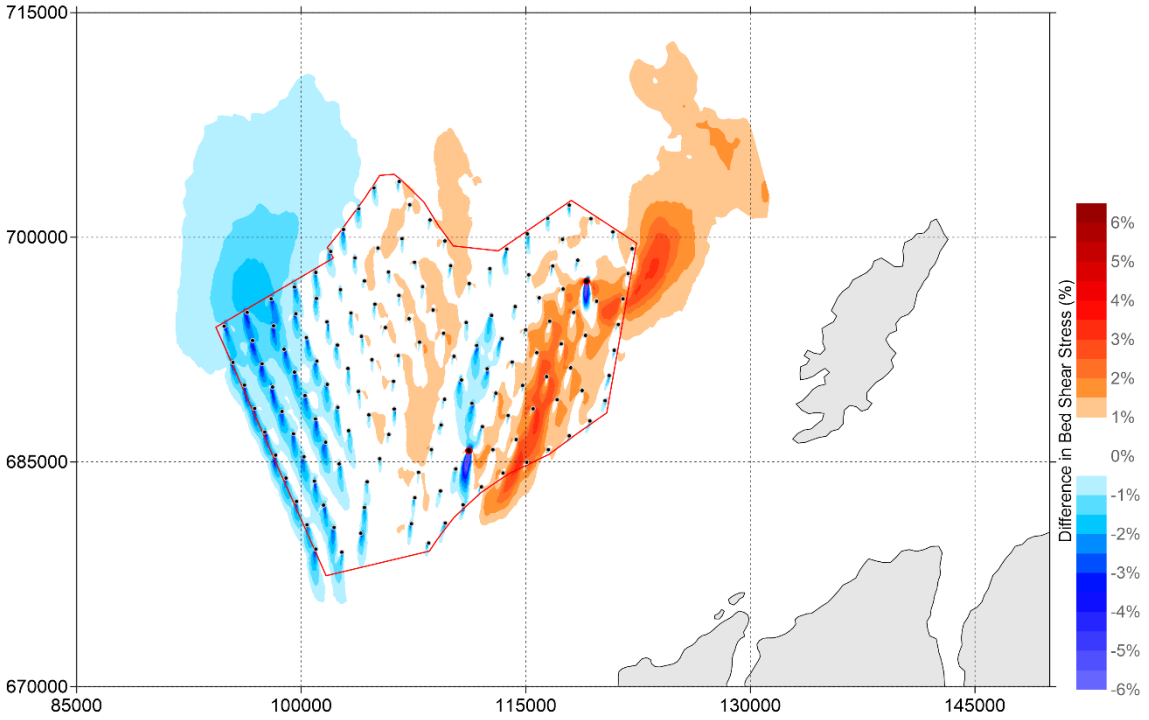

Figure 5-152: Percentage change of bed shear stress between 'Baseline' and '15 MW - Dense Perimeter layout' during spring tide (positive means increase of bed shear stress by layout and vice versa) - peak ebb

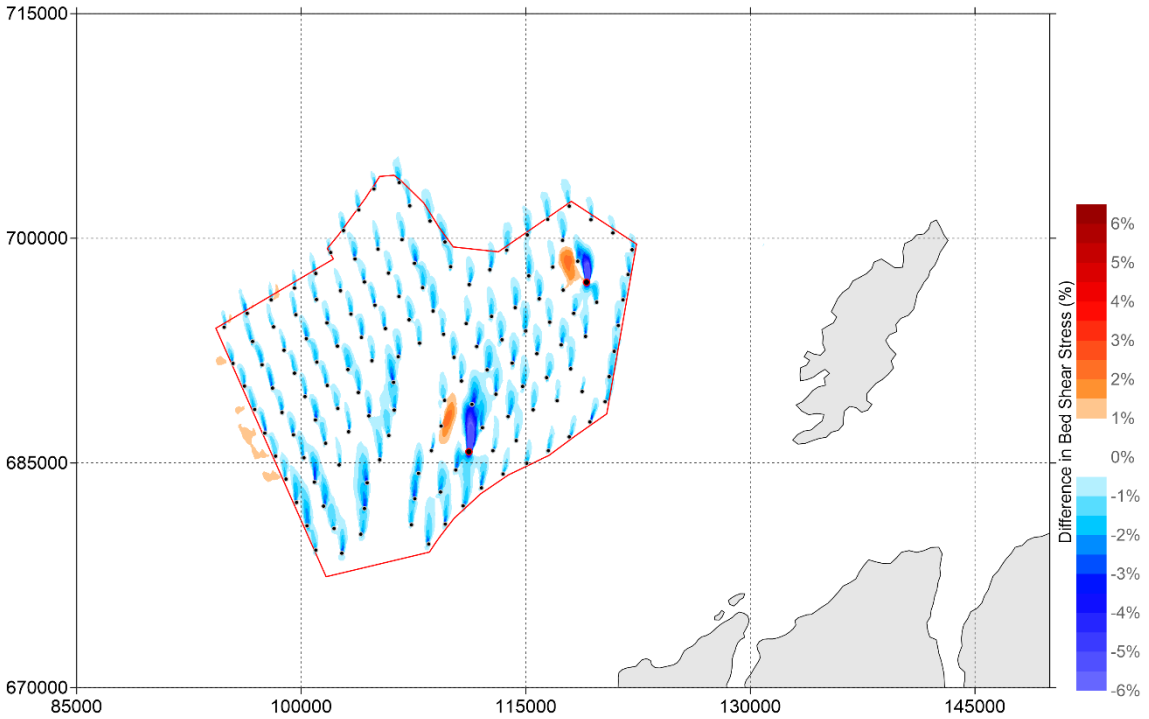

Figure 5-153: Percentage change of bed shear stress between 'Baseline' and '15 MW - Dense Perimeter layout' during neap tide (positive means increase of bed shear stress by layout and vice versa) - peak flood

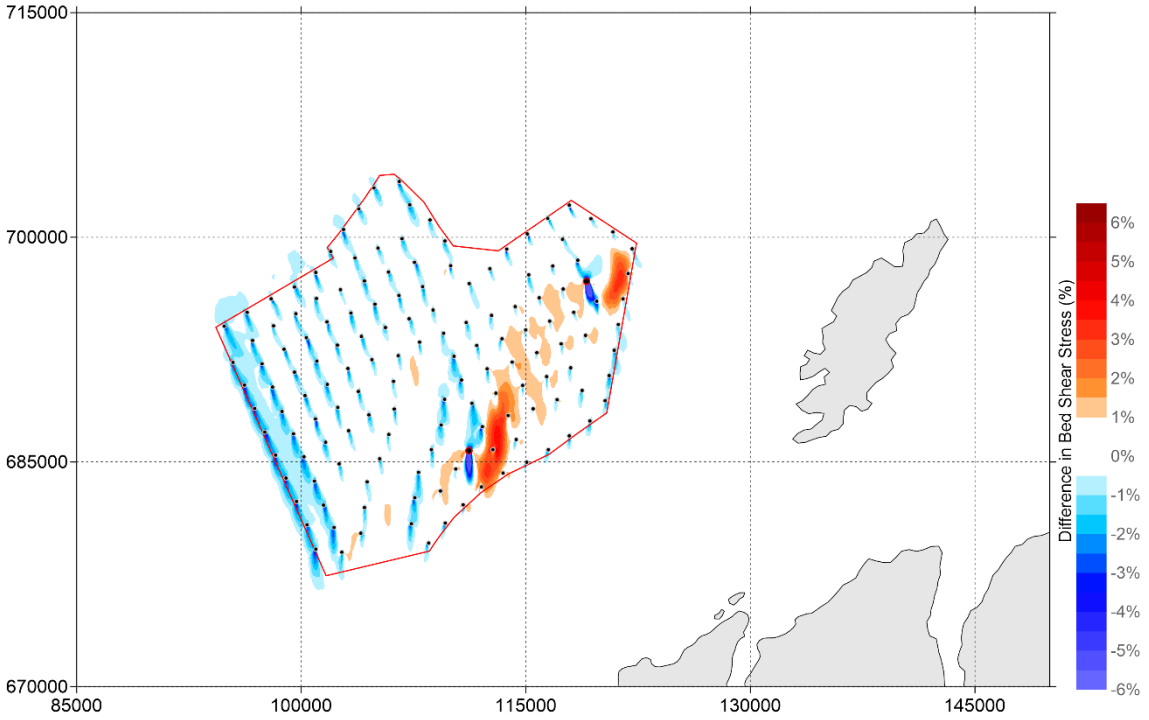

Figure 5-154: Percentage change of bed shear stress between 'Baseline' and '15 MW - Dense Perimeter layout' during neap tide (positive means increase of bed shear stress by layout and vice versa) - peak ebb

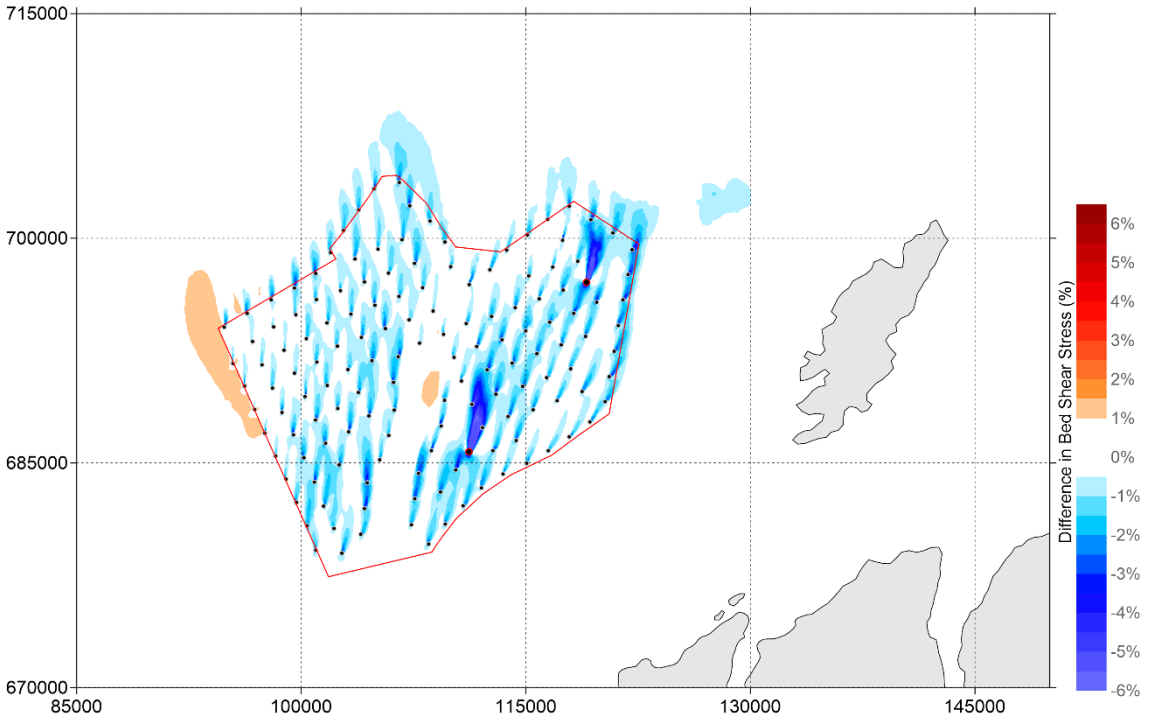

Figure 5-155: Percentage change of maximum current speed between 'Baseline' and '15 MW - Dense Perimeter layout' over 15 days (positive means increase of bed shear stress by layout and vice versa)

Impact on Bed Shear Stress in Percentage –15 MW Even Spread layout

5.3.54 This section presents the percentage difference in bed shear stress relative to the baseline around the WDA for the 15 MW Even Spread layout. **Figure 5-156** and **Figure 5-157** present the predicted percentage difference in bed shear stress during spring tide for peak flood and peak ebb, respectively. **Figure 5-158** and **Figure 5-159** present the predicted percentage difference in bed shear stress during neap tide for peak flood and peak ebb, respectively. **Figure 5-160** presents the percentage difference in maximum bed shear stress throughout the full spring-neap tidal cycle simulation.

5.3.55 The percentage change in bed shear stress shows a very similar pattern for 15 MW Dense Perimeter, as presented above.

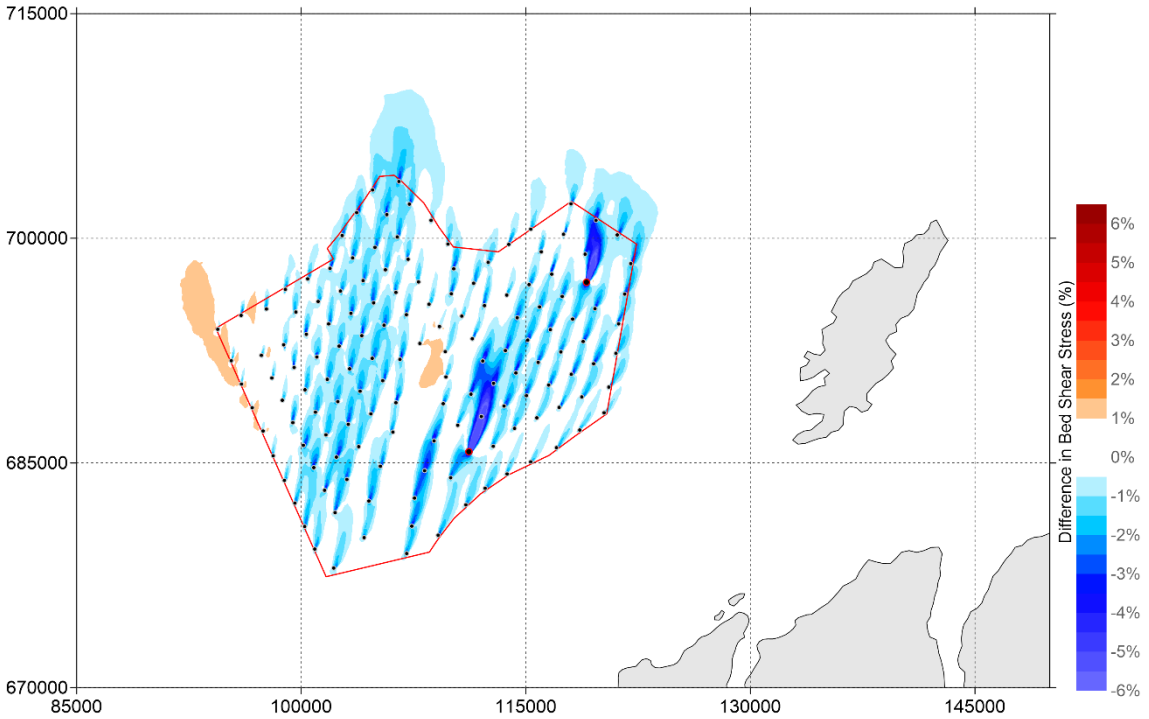

Figure 5-156: Percentage change of bed shear stress between 'Baseline' and '15 MW - Even Spread layout' during spring tide (positive means increase of bed shear stress by layout and vice versa) - peak flood

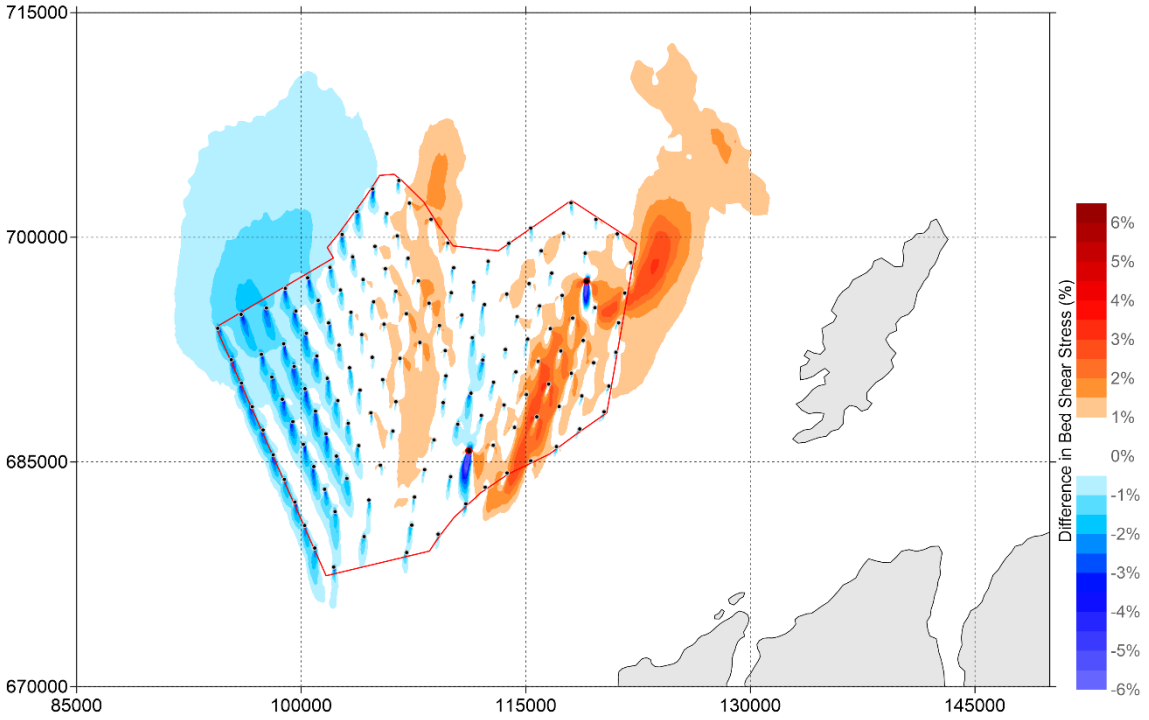

Figure 5-157: Percentage change of bed shear stress between 'Baseline' and '15 MW - Even Spread layout' during spring tide (positive means increase of bed shear stress by layout and vice versa) - peak ebb

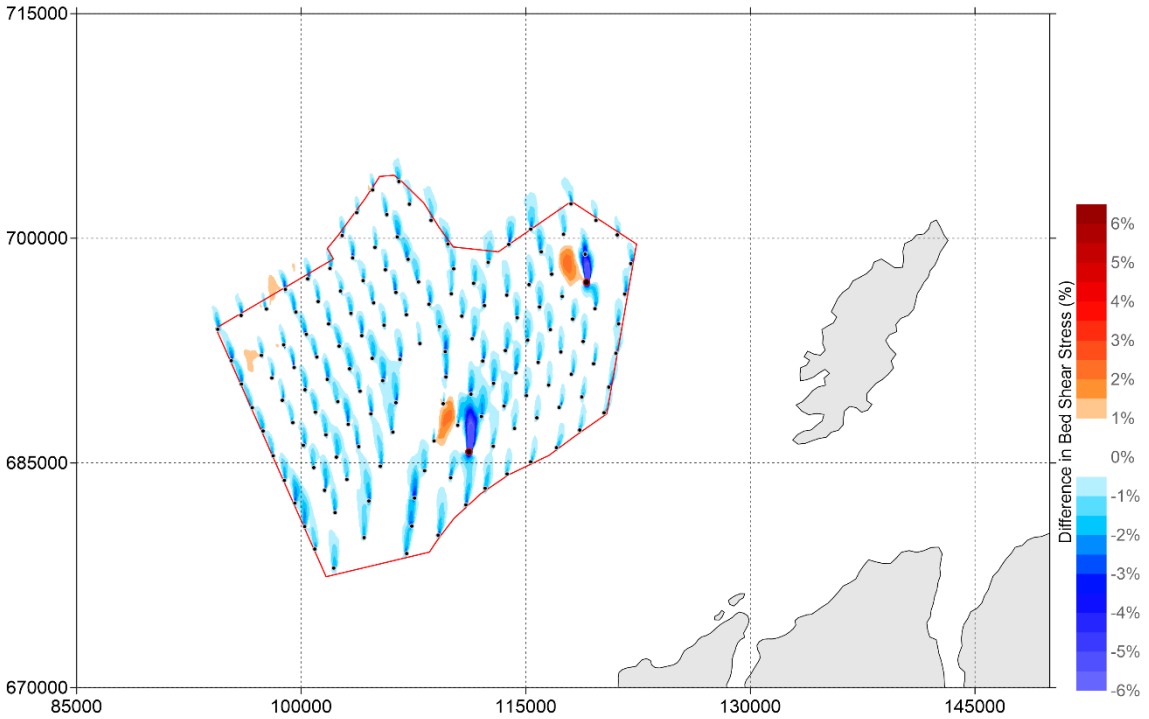

Figure 5-158: Percentage change of bed shear stress between 'Baseline' and '15 MW - Even Spread layout' during neap tide (positive means increase of bed shear stress by layout and vice versa) - peak flood

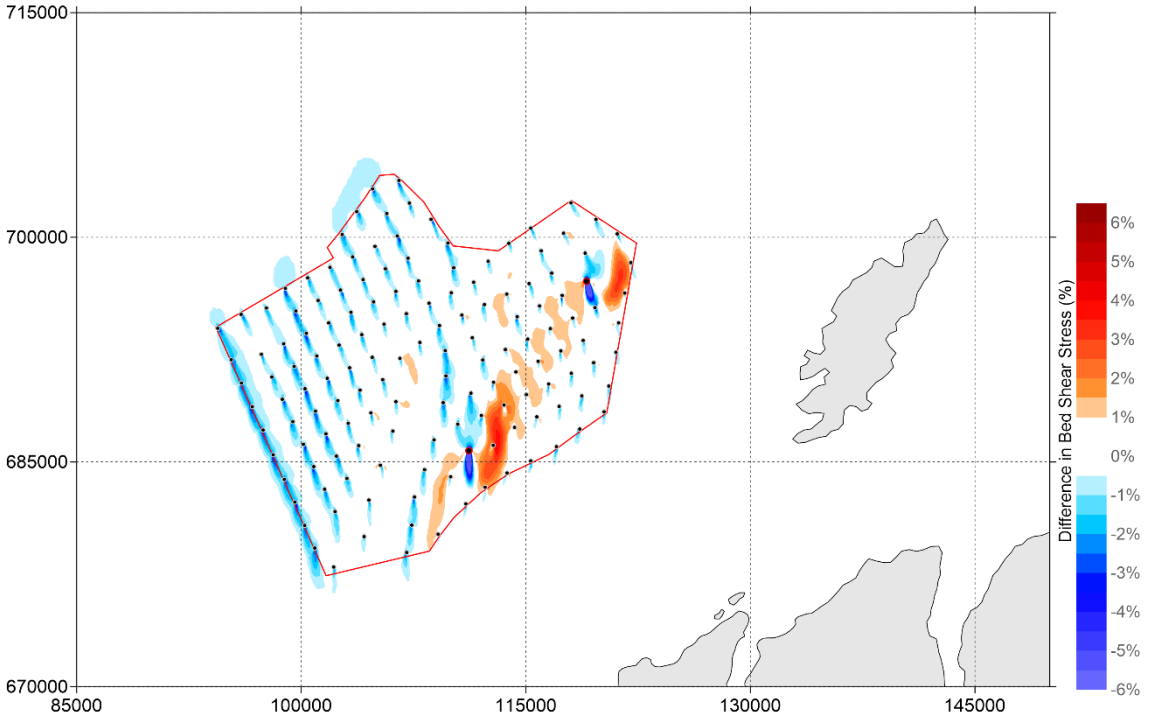

Figure 5-159: Percentage change of bed shear stress between 'Baseline' and '15 MW - Even Spread layout' during neap tide (positive means increase of bed shear stress by layout and vice versa) - peak ebb

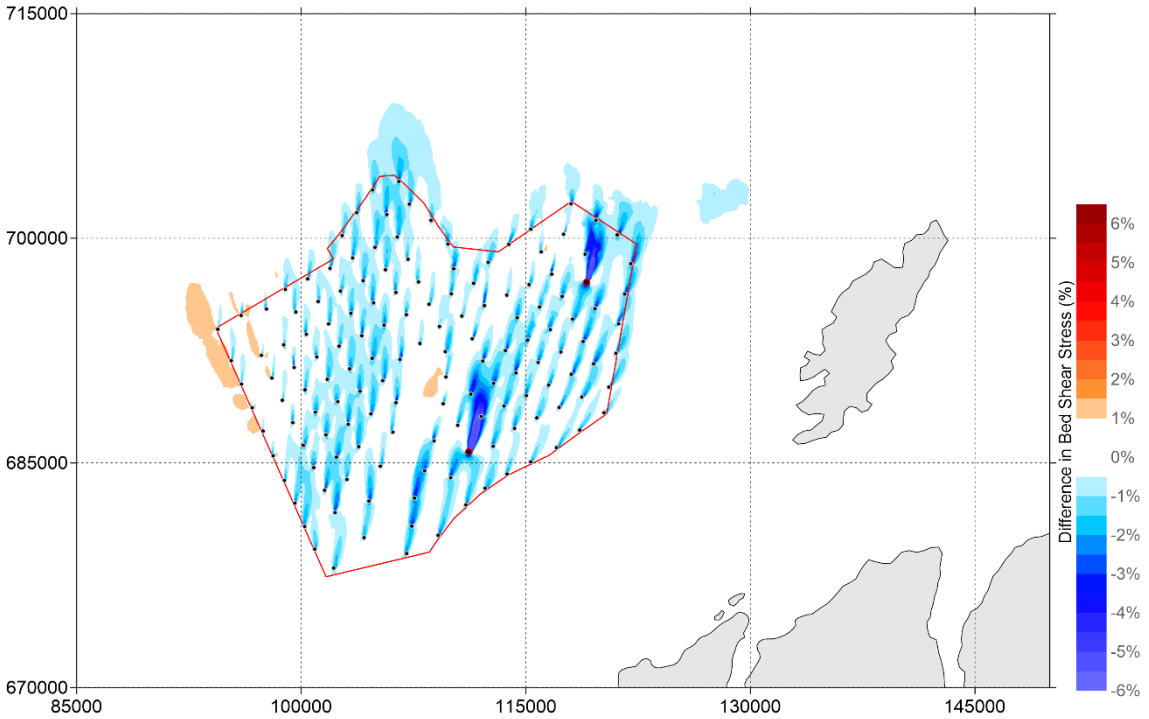

Figure 5-160: Percentage change of maximum current speed between 'Baseline' and '15 MW - Even Spread layout' over 15 days (positive means increase of bed shear stress by layout and vice versa)

Impact on Bed Shear Stress in Percentage – 24 MW Dense Perimeter Layout

5.3.56 This section presents the percentage difference in bed shear stress around the WDA for the 24 MW Dense Perimeter layout. **Figure 5-161** and **Figure 5-162** present the predicted percentage difference in bed shear stress during spring tide for peak flood and peak ebb, respectively. **Figure 5-163** and **Figure 5-164** present the predicted percentage difference in bed shear stress during neap tide for peak flood and peak ebb, respectively. **Figure 5-165** presents the percentage difference in maximum bed shear stress throughout the full spring-neap tidal cycle simulation.

5.3.57 The predicted percentage difference in bed shear stress extending outside the WDA between the 24 MW – Dense Perimeter layout and baseline scenario is more pronounced during the spring tide. At peak flood, the percentage difference is a reduction of up to 2% extending 1.5 km north of the WDA and up to 1% extending 4 km north of the WDA. In addition to this, there is a region of increased percentage difference in bed shear stress to the west of the WDA, up to 1.5% extending 2 km northwest of the WDA.

5.3.58 At peak ebb, there is a reduction of up to 2.0% extending 3 km northwest of the WDA and up to 1.0% 7 km northwest of the WDA. There is an increase of up to 3% extending 2.5 km northeast of the WDA and up to 1.5% extending 8 km northeast of the WDA.

5.3.59 The percentage change in bed shear stress outside the WDA is slightly less than predicted for the 15 MW layouts presented above.

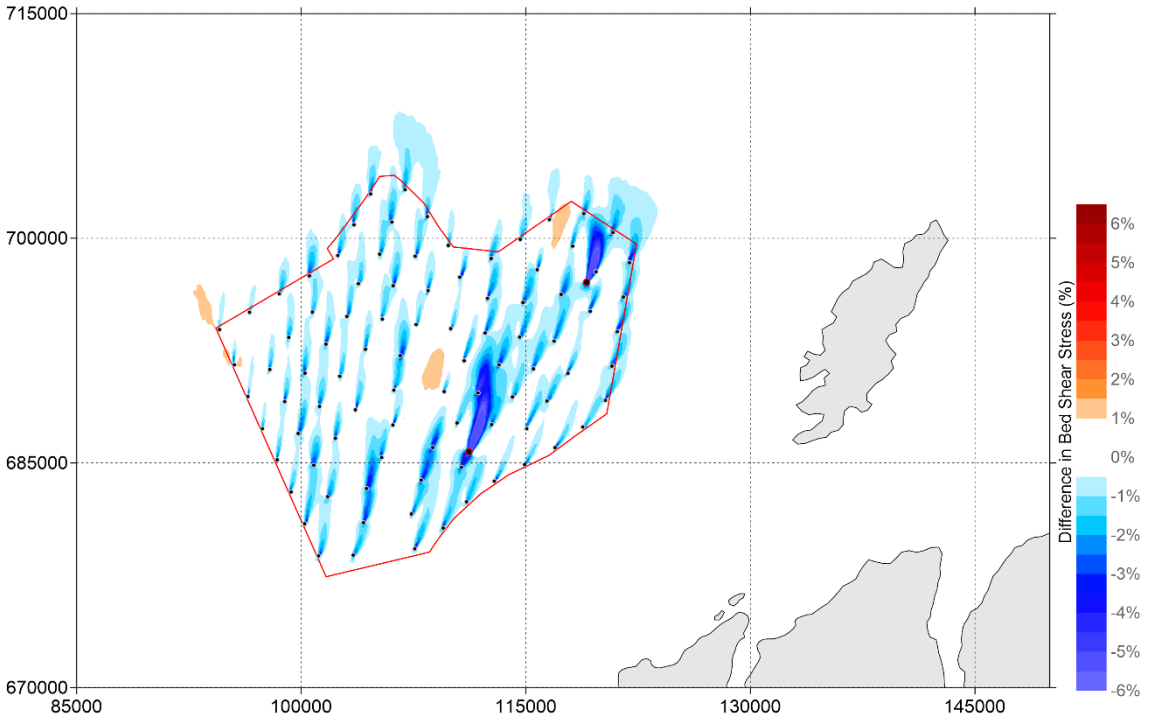

Figure 5-161: Percentage change of bed shear stress between 'Baseline' and '24 MW - Dense Perimeter layout' during spring tide (positive means increase of bed shear stress by layout and vice versa) - peak flood

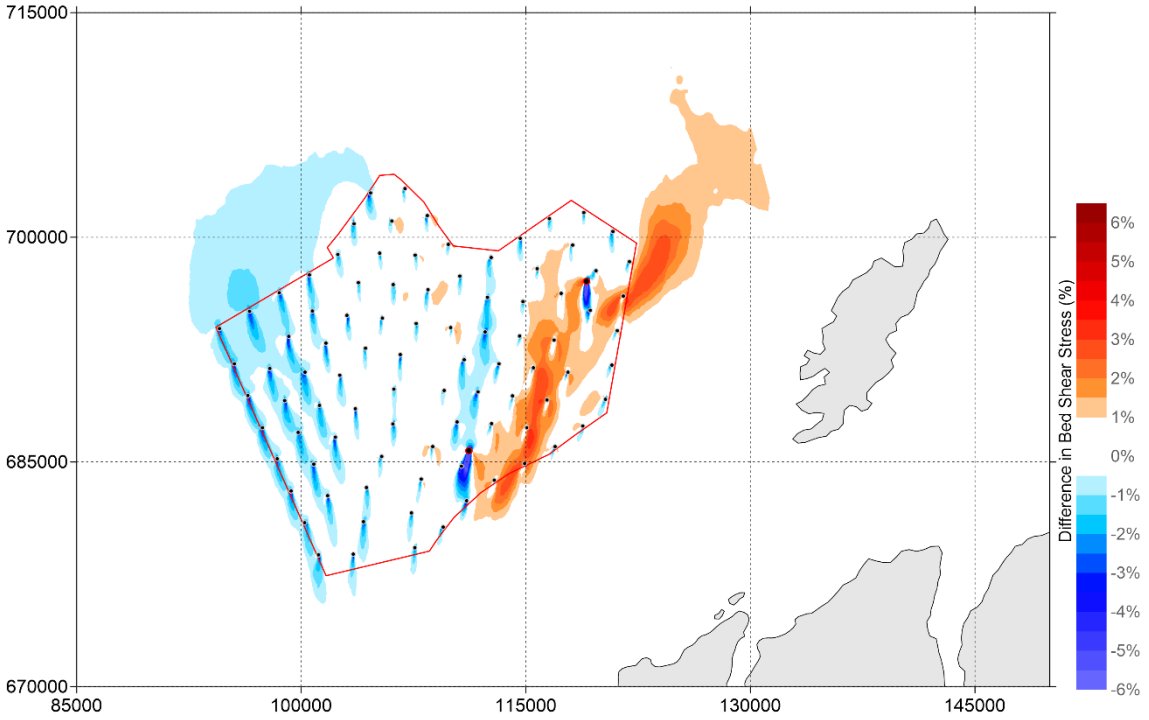

Figure 5-162: Percentage change of bed shear stress between 'Baseline' and '24 MW - Dense Perimeter layout' during spring tide (positive means increase of bed shear stress by layout and vice versa) - peak ebb

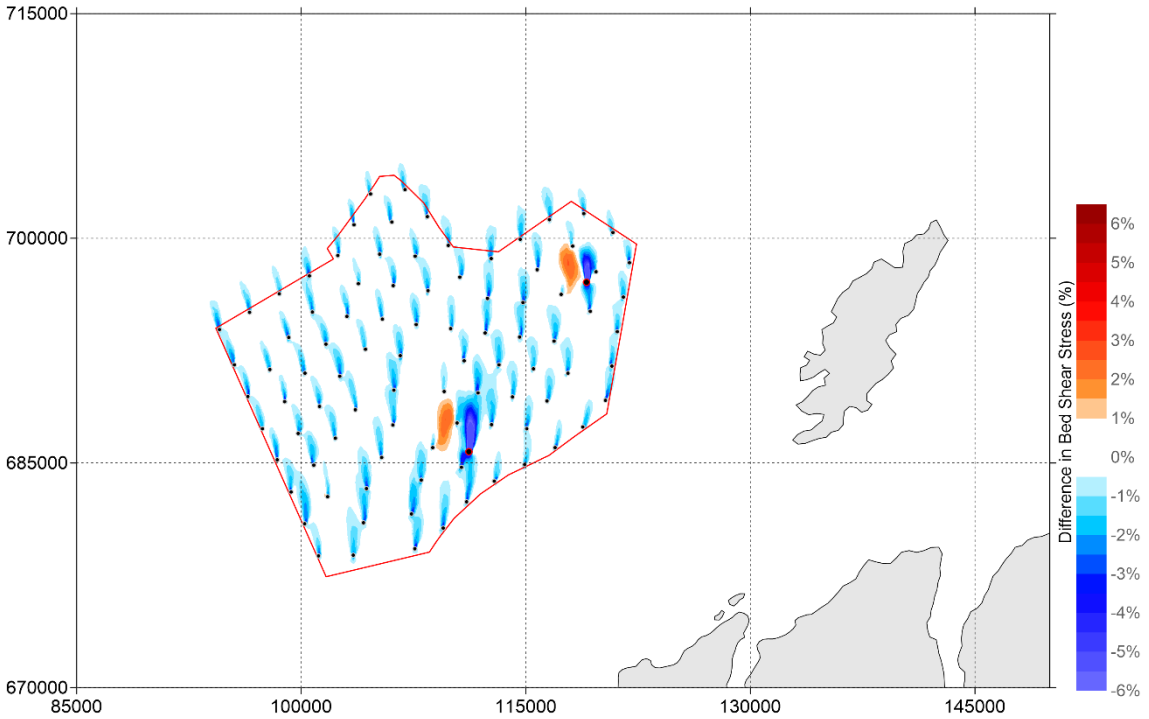

Figure 5-163: Percentage change of bed shear stress between 'Baseline' and '24 MW - Dense Perimeter layout' during neap tide (positive means increase of bed shear stress by layout and vice versa) - peak flood

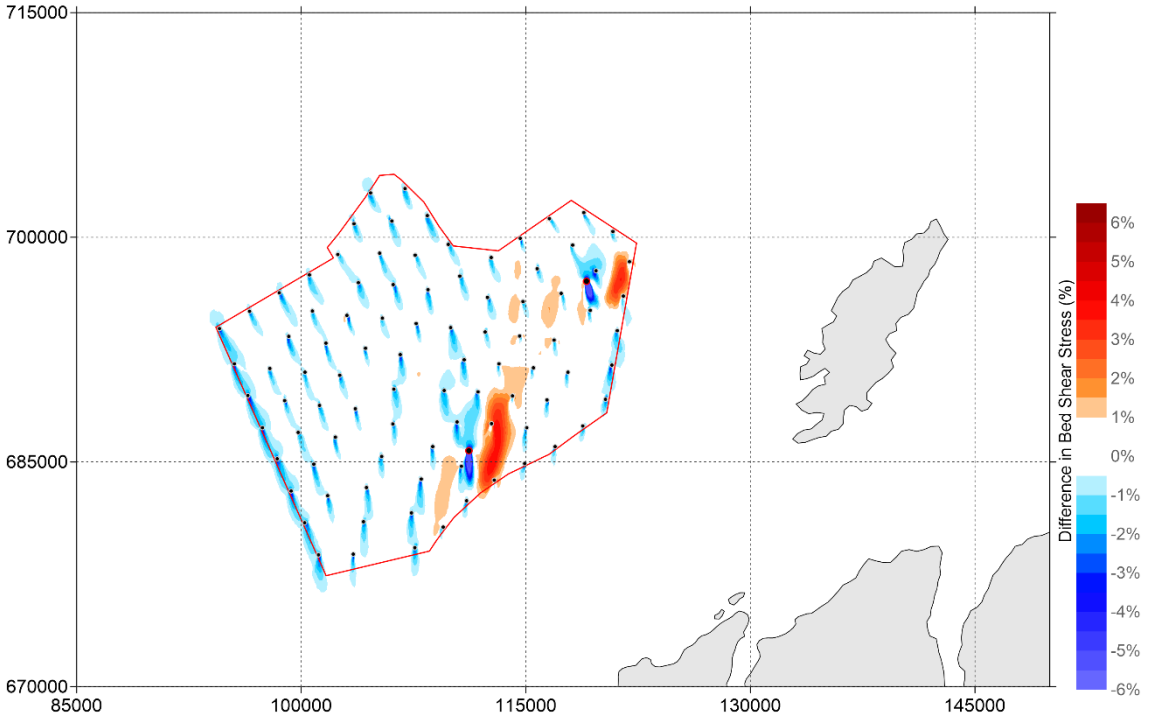

Figure 5-164: Percentage change of bed shear stress between 'Baseline' and '24 MW - Dense Perimeter layout' during neap tide (positive means increase of bed shear stress by layout and vice versa) - peak ebb

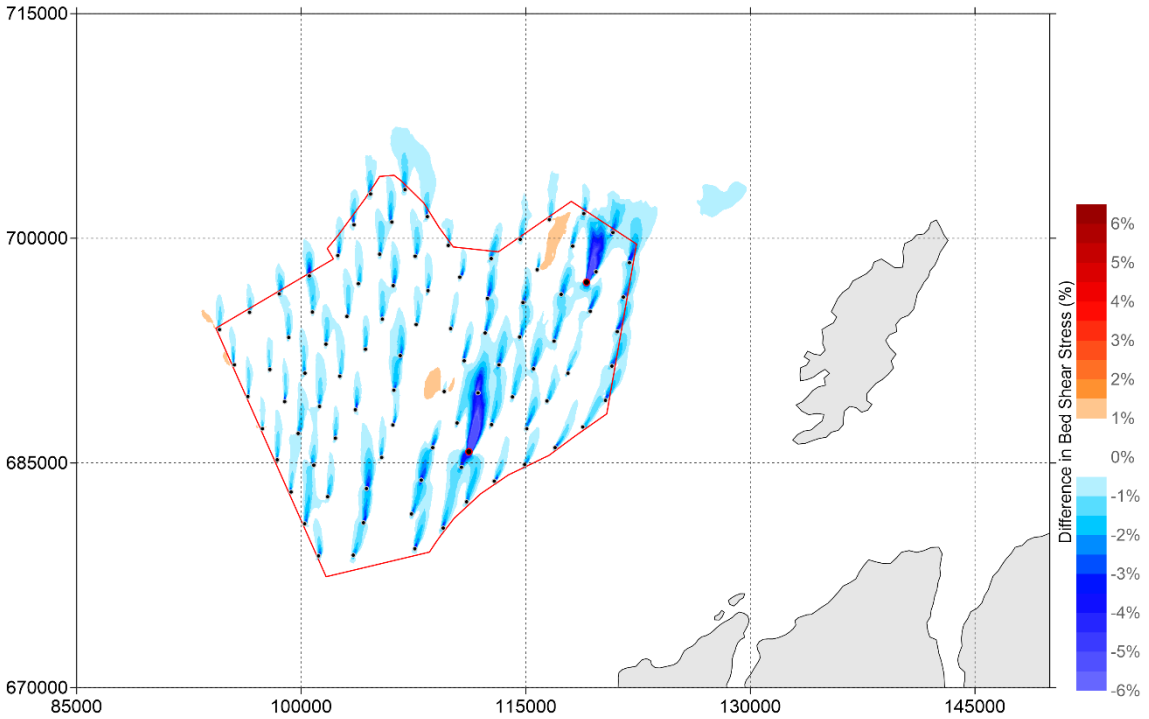

Figure 5-165: Percentage change of maximum current speed between 'Baseline' and '24 MW - Dense Perimeter layout' over 15 days (positive means increase of bed shear stress by layout and vice versa)

Impact on Bed Shear Stress in Percentage – 24 MW Even Spread layout

5.3.60 This section presents the percentage difference in bed shear stress relative to the baseline around the WDA for the 24 MW Even Spread layout. **Figure 5-166** and **Figure 5-167** present the predicted percentage difference in bed shear stress during spring tide for peak flood and peak ebb, respectively. **Figure 5-168** and **Figure 5-169** present the predicted percentage difference in bed shear stress during neap tide for peak flood and peak ebb, respectively. **Figure 5-170** presents the percentage difference in maximum bed shear stress throughout the full spring-neap tidal cycle simulation.

5.3.61 The percentage change in bed shear stress outside the WDA is less than predicted for the 15 MW layouts and very similar to the change predicted for the 24 MW – Dense Perimeter.

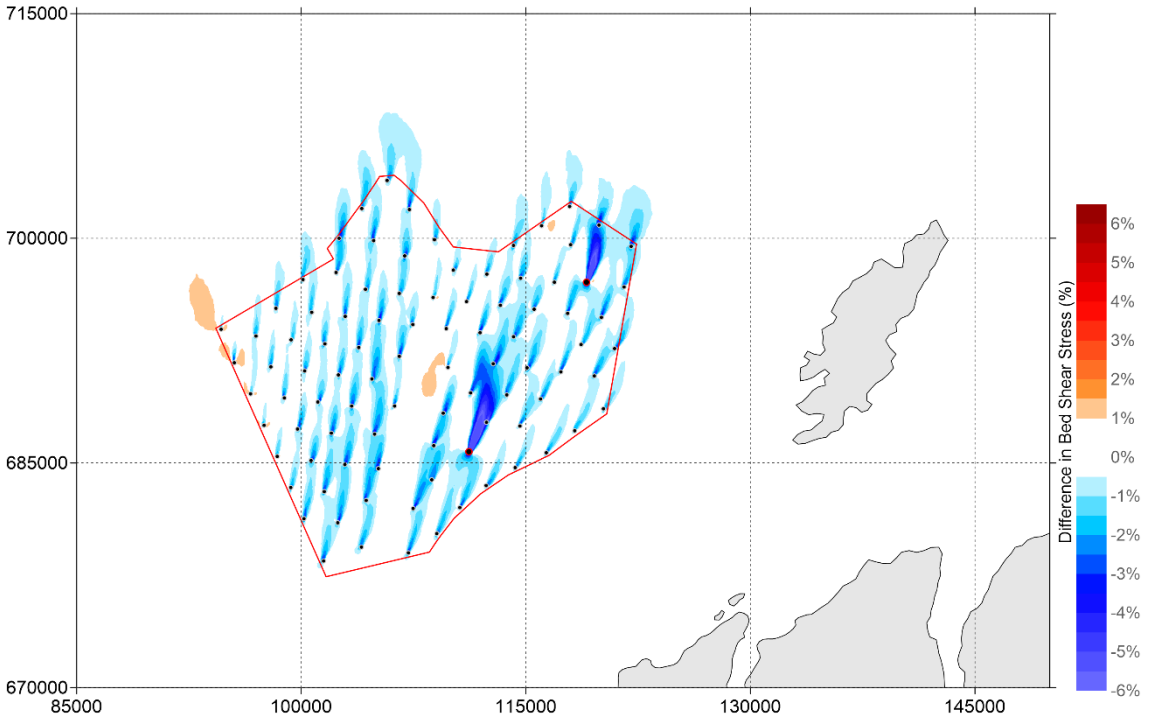

Figure 5-166: Percentage change of bed shear stress between 'Baseline' and '24 MW - Even Spread layout' during spring tide (positive means increase of bed shear stress by layout and vice versa) - peak flood

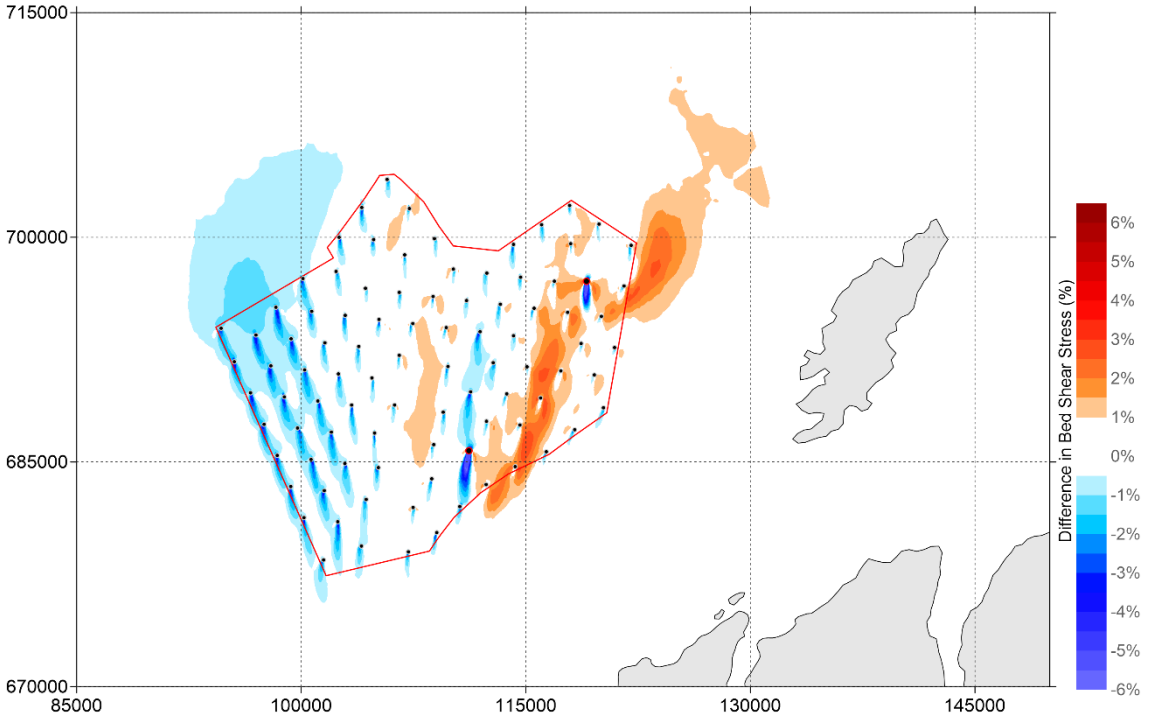

Figure 5-167: Percentage change of bed shear stress between 'Baseline' and '24 MW - Even Spread layout' during spring tide (positive means increase of bed shear stress by layout and vice versa) - peak ebb

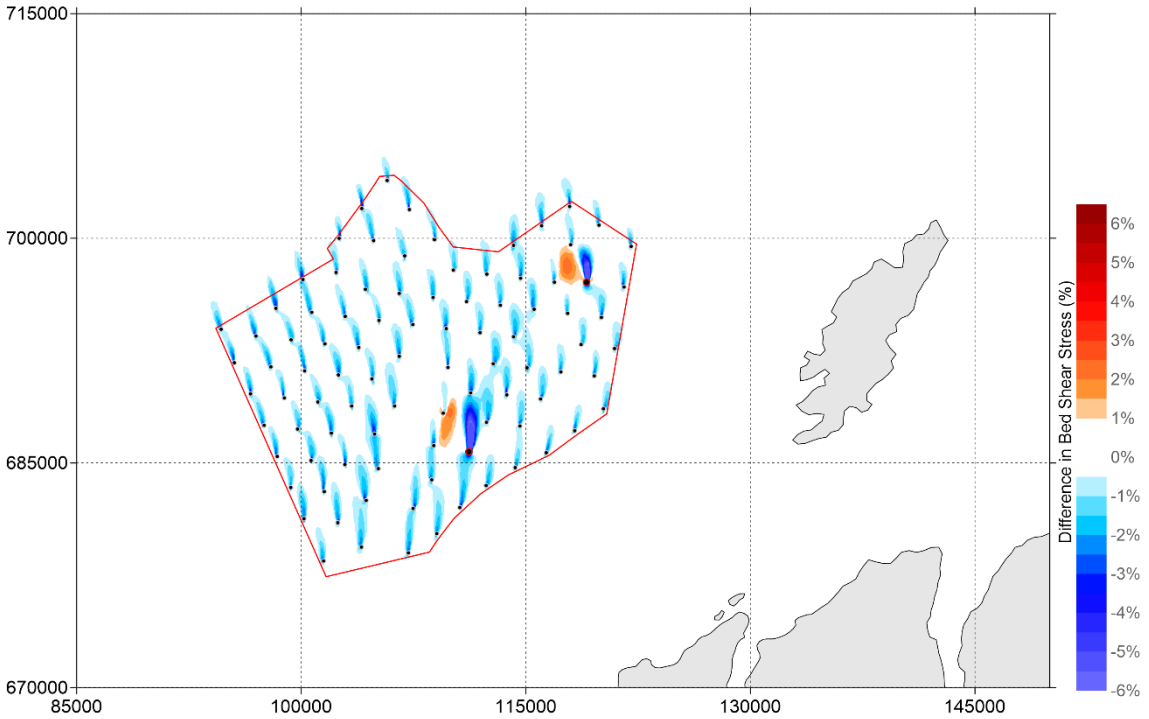

Figure 5-168: Percentage change of bed shear stress between 'Baseline' and '24 MW - Even Spread layout' during neap tide (positive means increase of bed shear stress by layout and vice versa) - peak flood

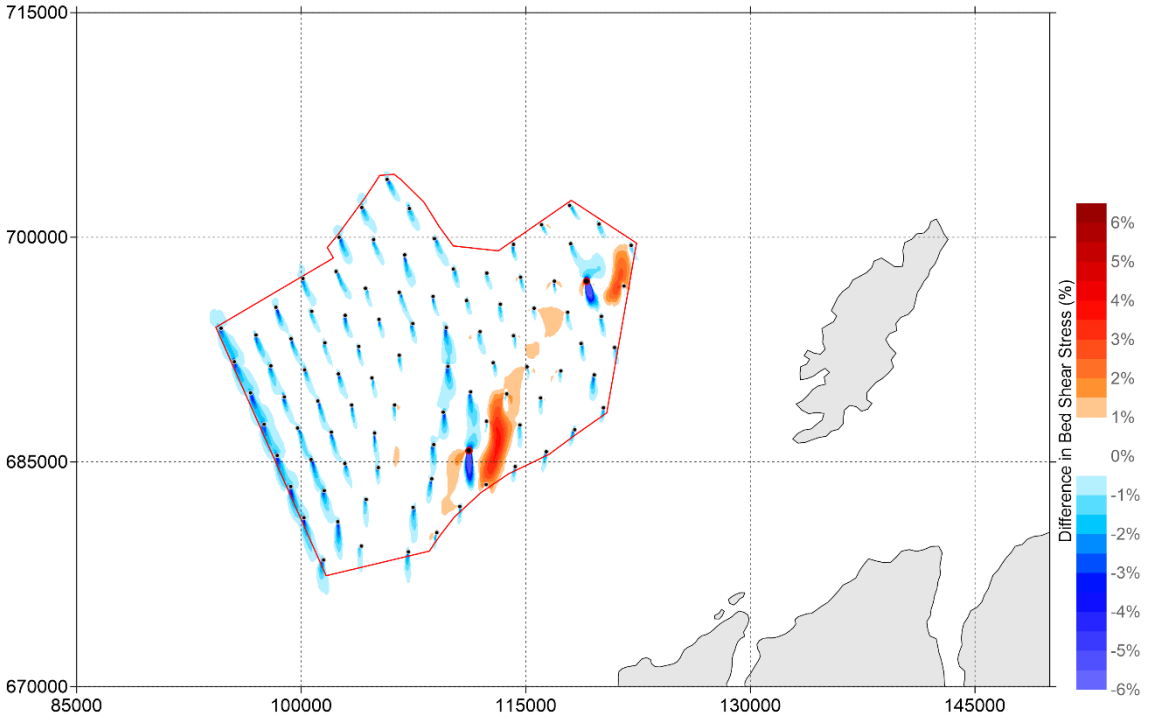

Figure 5-169: Percentage change of bed shear stress between 'Baseline' and '24 MW - Even Spread layout' during neap tide (positive means increase of bed shear stress by layout and vice versa) - peak ebb

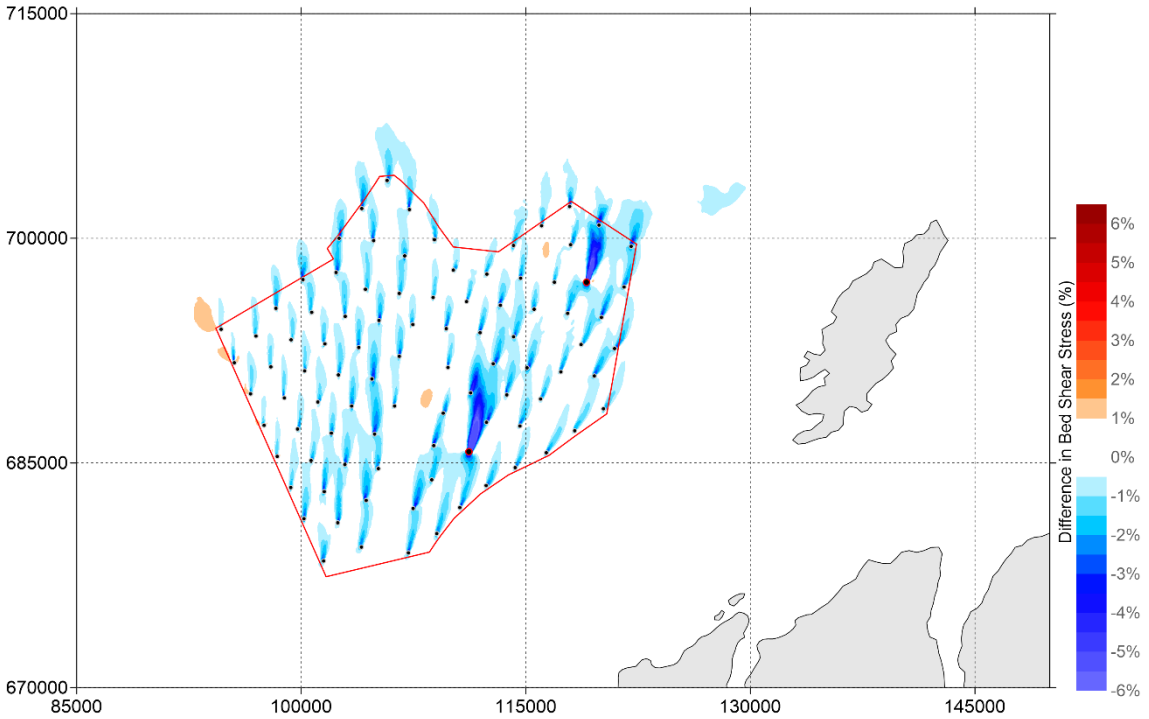

Figure 5-170: Percentage change of maximum current speed between 'Baseline' and '24 MW - Even Spread layout' over 15 days (positive means increase of bed shear stress by layout and vice versa)

Comparison of Layouts (Bed Shear Stress)

5.3.62 From the results presented above, the model predicts that the effect on the bed shear stress is very similar between the two 15 MW layouts and two 24 MW layouts, with minimal difference between the 'Dense Perimeter' and 'Even Spread' WDA's. In addition to this, the hydrodynamic model predicts that the increased number of monopiles (144) for the 15 MW WDA will have a greater effect on the bed shear stress when compared with the 24 MW WDA, which has only 91 monopiles.

5.3.63 Most notably during spring tide, where at peak flood the 15 MW layouts predict a percentage reduction in bed shear stress of 2.0% extending 2 km north of the WDA, compared with only 1.5 km for the 24 MW layouts. In addition to this, during peak ebb, percentage reductions of up to 2.0% extending 4 km northwest of the WDA for the 15 MW layouts and only 3 km for the 24 MW layouts. And percentage increase of up to 3.0% extending 3 km northeast of the WDA for the 15 MW layouts and up to 3.0% extending 2.5 km for the 24 MW layouts.

5.4 Summary and Conclusions on Hydrodynamic Modelling

5.4.1 A hydrodynamic modelling study has been undertaken using MIKE21 Hydrodynamic, to investigate the potential effect of the WDA on the surrounding hydrodynamic climate. The results will inform the assessment of significance in the relevant EIA chapters.

5.4.2 The study included the successful re-calibration of Haskoning's regional UK MIKE21 hydrodynamic model and development and calibration of a local MIKE21 hydrodynamic model, where comparisons were made to measured water level and current speed data at two survey locations (S1 and S2) and water levels at a class A tide gauge at Portrush. Model error statistics

comparing measured data with model results for regional and local MIKE21 models, were set against guidance published in EA (2022) and ABPmer (2013) studies on the calibration of hydrodynamic models for application in the coastal zone.

5.4.3 At Portrush the regional model demonstrated a very good agreement between modelled and measured water levels, with a RMSE of 0.09 m. This meets the requirement of RMSE < 0.1 m as suggested in the above guidance. At S1 and S2 the water levels again showed good agreement between measured and modelled data, with RMSE in all cases across both spring and neap tidal phases of < 0.2 m. For current speeds at both S1 and S2 the RMSE was < 0.2 m/s, satisfying the suggested guidance from the ABPmer (2013) study. Overall, from the results of the calibration, it was concluded that the performance of the model was suitable to be taken forward for the assessment simulations of the WDA layouts.

5.4.4 The local MIKE21 hydrodynamic model was simulated across a full spring-neap tidal cycle, for the baseline scenario and four indicative turbine layout options using monopile structures (15 MW Dense Perimeter, 15 MW Even Spread, 24 MW Dense Perimeter and 24 MW Even Spread). The results of the modelling were presented as absolute values, absolute difference and percentage difference in current speed and bed shear stress.

5.4.5 The model results suggest that current speeds are strongest at the southern end of the WDA, reaching up to 1.2 m/s on the northerly directed spring flood tide. Throughout the majority in the WDA the current speeds are between 0.4 m/s to 0.8 m/s on spring tide and 0.2 m/s to 0.4 m/s on neap tide.

5.4.6 Predicted simulations for the WDA options indicated that the more pronounced change in hydrodynamics occurs for the 15 MW WDA layouts, rather than the 24 MW WDA layouts. At peak flood, the percentage difference in current speed is a reduction of up to 1.0% extending up to 2.5 km north of the WDA. At peak ebb, there is a reduction in current speed of up to 1.0% extending 8 km northwest of the WDA and an increase of up to 2% extending 7 km northeast of the WDA.

5.4.7 For bed shear stress, at peak flood, the percentage difference is a reduction of up to 2% extending 2 km north of the WDA and up to 1% extending 5 km north of the WDA. In addition to this, there is a region of increased percentage difference in bed shear stress to the west of the WDA, up to 2% extending 3 km northwest of the WDA and up to 1.5% extending 8 km northwest of the WDA. At peak ebb, there is a reduction of up to 2.0% extending 4 km northwest of the WDA and up to 1.0% 12 km northwest of the WDA. There is a region of increase of up to 3% extending 3 km northeast of the WDA and up to 1.5% extending 10 km northeast of the WDA.

5.4.8 In summary, a change of up to 3% in both current speed and bed shear stress is predicted to be contained entirely within the boundary of the WDA.

6 Sediment Dispersion Modelling

6.1 Simulation Scenarios

6.1.1 This section of the report describes the sediment dispersion modelling exercise that was undertaken to investigate the suspended sediment dispersion and deposition arising from the drilling, seabed preparation, levelling and cable plough trenching activities inside the MachairWind WDA.

6.1.2 There are four proposed construction activities that are likely to cause sediment release into the water column. **Table 6-1** summarises the four dispersion model simulations that have been carried out.

Table 6-1: Sediment dispersion model simulations

ID	Name	Description
1	Structure drilling	Drilling for 48 (based on the worst-case scenario that up to 33% of turbine foundations could require drilling) randomly selected WTGs and 2 OSPs.
2	Structure bed preparation	Bed preparation for 144 WTGs and 2 OSPs.
3	Sandwave levelling	Levelling through sandwaves along three Inter-Array Cable (IAC) sections.
4	Cable plough trenching	Cable plough trenching of the IACs, export cable(s) and OSP link cables.

6.2 Dispersion Model Setup

6.2.1 For the purpose of the sediment dispersion model, the 2D hydrodynamic model described in **Section 5** has been developed into a 3D hydrodynamic model to simulate the suspended sediment transport throughout the water column.

6.2.2 The sediment dispersion model was then built in MIKE3-MT and is coupled with the 3D hydrodynamic model built in MIKE3-HD. The computational mesh of MIKE3-MT is identical to the MIKE3-HD mesh.

6.2.3 All sediment dispersion model simulations have been run for 30 days (24th March to 24th April 2025) to cover the full duration of the proposed construction activities and allow the plume to fully disperse after the activities have ended. This time period was chosen to coincide with reasonably large spring tides for a worst-case scenario.

6.2.4 The sediment dispersion model has been set up with 10 vertical layers to differentiate between SSCs throughout the water column, e.g. near the seabed and near the water surface.

6.2.5 In order to simulate the sediment dispersion close to natural conditions, wave disturbance effect using summer averaged wave conditions without storms has been included in the MIKE3-MT model.

6.2.6 In the model simulation, the dredger will release material along the centre line of the IAC and export cable routes in the WDA, or at a single point for WTG and OSP construction. This

adopted method for material release is conservative. The dredger will in reality move around the dredging area along multiple lines which means the sediment release will be more dispersed and thus the sediment concentration will be less.

6.3 Sediment Properties

6.3.1 The seabed sediment properties can be characterised by five sediment fractions, settling velocities and critical bed shear stresses which have been used in the suspended sediment dispersion modelling. The five fractions are shown in **Table 6-2**. The critical bed shear stress and fall velocities were calculated using the SandCalc software developed by HR Wallingford.

Table 6-2: Sediment settling velocity and critical bed shear stress

Sediment Type	Sediment Size (mm)	Settling Velocity (m/s)	Critical Shear Stress (N/m^2)
Silt/Clay	0.031	0.000554	0.0847
Fine sand	0.13	0.00935	0.1548
Medium Sand	0.3	0.0372	0.2025
Coarse Sand	1.3	0.135	0.657
Gravel	2	0.1734	1.166

6.3.2 The particle size distribution for each construction activity that has been applied to the model is uniform across the whole windfarm WDA and is detailed in **Table 6-3**.

Table 6-3: Particle size distribution

Sediment Type	Sediment Size (mm)	Percentage (%)
Silt/Clay	0.031	0.67
Fine sand	0.13	22.83
Medium Sand	0.3	51.68
Coarse Sand	1.3	20.4
Gravel	2	4.42

6.4 Sediment Release from Proposed Construction

6.4.1 **Table 6-4** summarises the construction volume, method, duration and sediment release rates for all four proposed construction activities. Trailing Suction Hopper Dredger (TSHD) and Cutter Suction Dredger (CSD) are the relevant acronyms in the table below.

Table 6-4: Summary of modelled construction activities inside windfarm WDA

Simulation	Activity	No. of structures or Length (km)	Volume (m^3)	Method	Production Rate (m^3/s)	Duration (days)	Sediment Release Rate (kg/s)
1	WTG Drilling	No. 48	501,744	CSD	1	0.12 per WTG	6
	OSP Drilling	No. 2	49,472	CSD	1	0.29 per OSP	6
2	WTG Bed preparation	No. 144	5,741,333	CSD	1	0.46 per WTG	6
	OSP Bed preparation	No. 2	219,740	CSD	1	1.27 per OSP	6
3	Sandwave Levelling	11.6 km	4,073,000	TSHD	1	47.14	15
4	IAC Plough Trenching	521.3 km	6,698,808	Cable plough	1.07	72.40	2,275.52
	Export Cable Plough Trenching	45.2 km	580,820	Cable plough	1.07	6.28	2,275.52
	OSP Link Cable Plough Trenching	15.9 km	204,315	Cable plough	1.07	2.21	2,275.52

6.5 Simulation 1 - Drilling for Structures (WTGs and OSPs)

6.5.1 As a worst-case scenario it has been assumed that up to a third of all WTGs (No. 48) could require drilling for installation. Those 48 WTGs have been chosen at random from a total of 144 WTGs in the WDA, and their locations are shown as red dots in **Figure 6-1**.

6.5.2 A total of 2 OSPs could also require drilling for installation and have been included in the simulation as shown in **Figure 6-1** (grey squares).

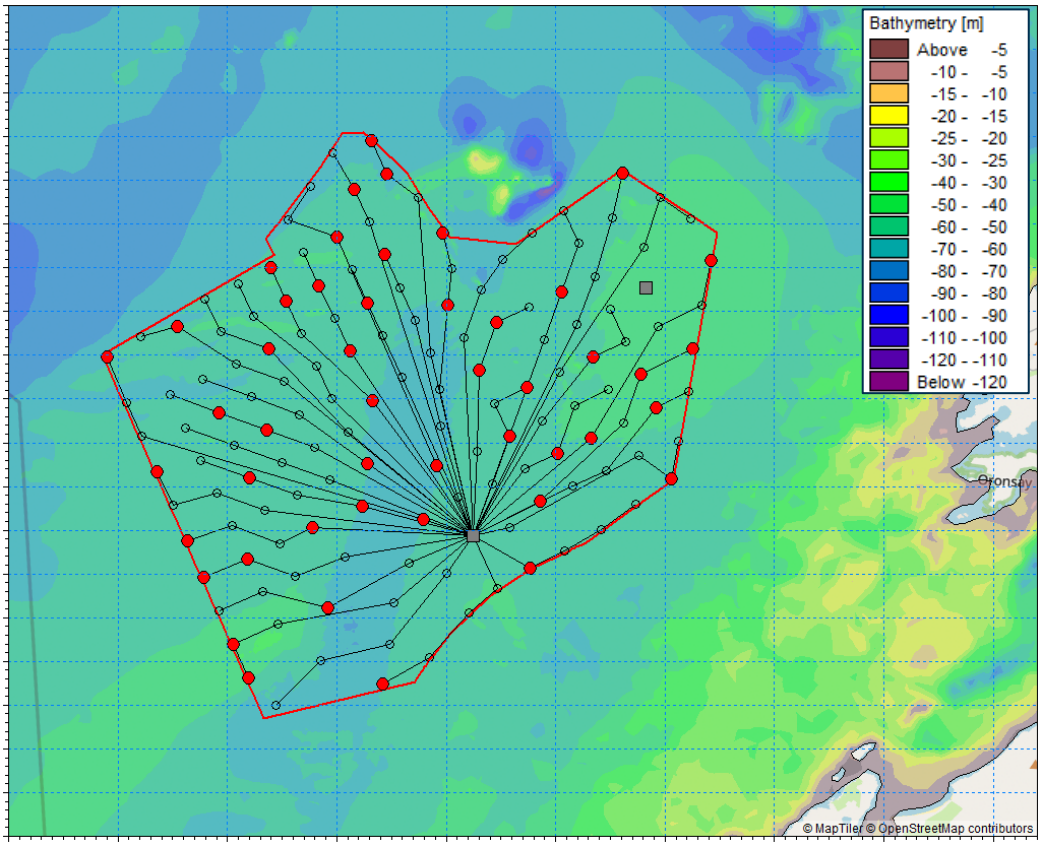

Figure 6-1: Location of drilling activities for WDA structures (red dot = 48 selected WTGs, grey square = 2 OSPs)

6.5.3 A total of 501,744 m^3 of seabed material would be released during the drilling activity for the 48 WTGs, and 49,472 m^3 for the 2 OSPs.

6.5.4 The total drilling period for each WTG is 0.12 days, and 0.29 days for each OSP using a CSD. For a worst-case scenario, the drilling activities for all structures have been simulated simultaneously.

6.5.5 The sediment release rate of the CSD is 6.0 kg/s and 50% of the material is released near the seabed and the other 50% near the water surface.

6.6 Simulation 2 – Bed Preparation for Structures (WTGs and OSPs)

6.6.1 As a worst-case scenario, it has been assumed that all 144 WTGs require bed preparation for installation and their locations are shown as red dots in **Figure 6-2**.

6.6.2 A total of 2 OSPs also require bed preparation for installation and have been included in the simulation as shown in **Figure 6-2** (grey square).

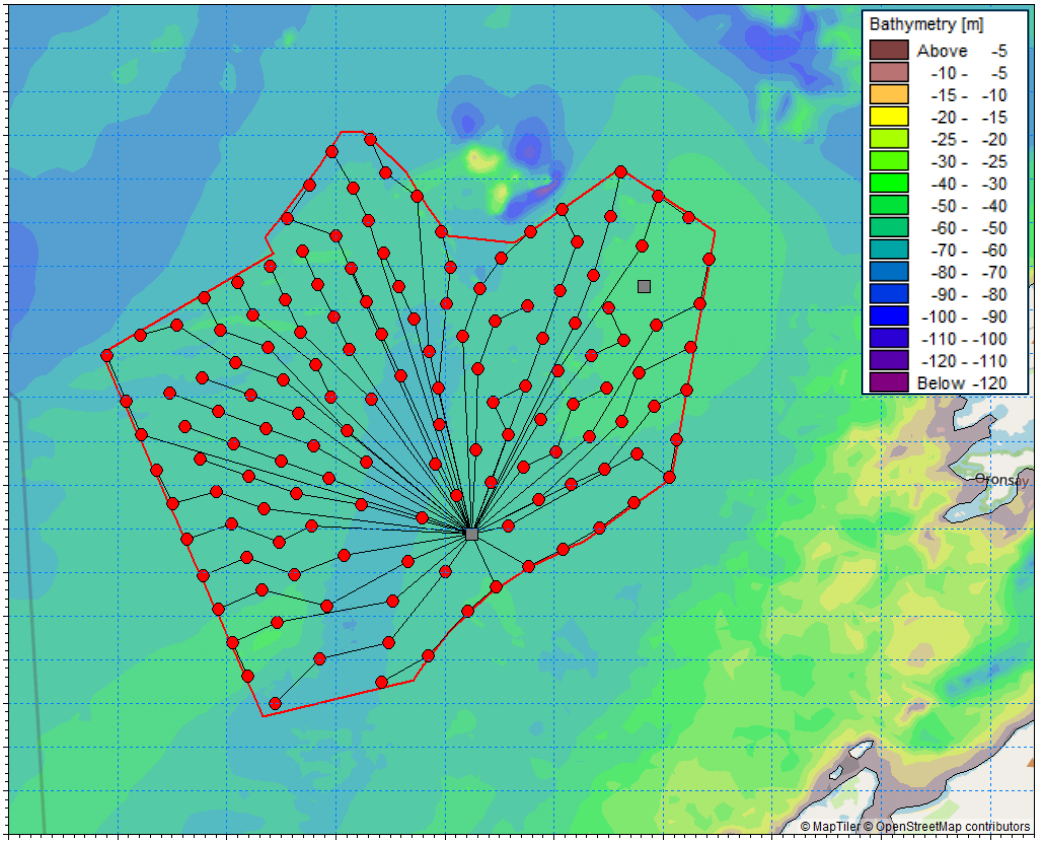

Figure 6-2: Location of bed preparation activities for WDA structures (red dot = 144 WTGs, grey square = 2 OSPs)

6.6.3 A total of 5,741,333 m^3 of seabed material will be released during the bed preparation activity for the 144 WTGs, and 219,740 m^3 for the 2 OSPs.

6.6.4 The total bed preparation period for each WTG is 0.46 days, and 1.27 days for each OSP using a CSD. For a worst-case scenario, the bed preparation activities for all structures have been simulated simultaneously.

6.6.5 The sediment release rate of the CSD is 6.0 kg/s and 50% of the material is released near the seabed and the other 50% near the water surface.

6.7 Simulation 3 – Array Cable Levelling

6.7.1 Levelling through sandwaves along the IACs is estimated to be required for a total length of 11.6 km. Three potential areas have been chosen, and the total length of levelling has been evenly divided between Area 1 and Areas 2/3 as shown in **Figure 6-3** (red thick line).

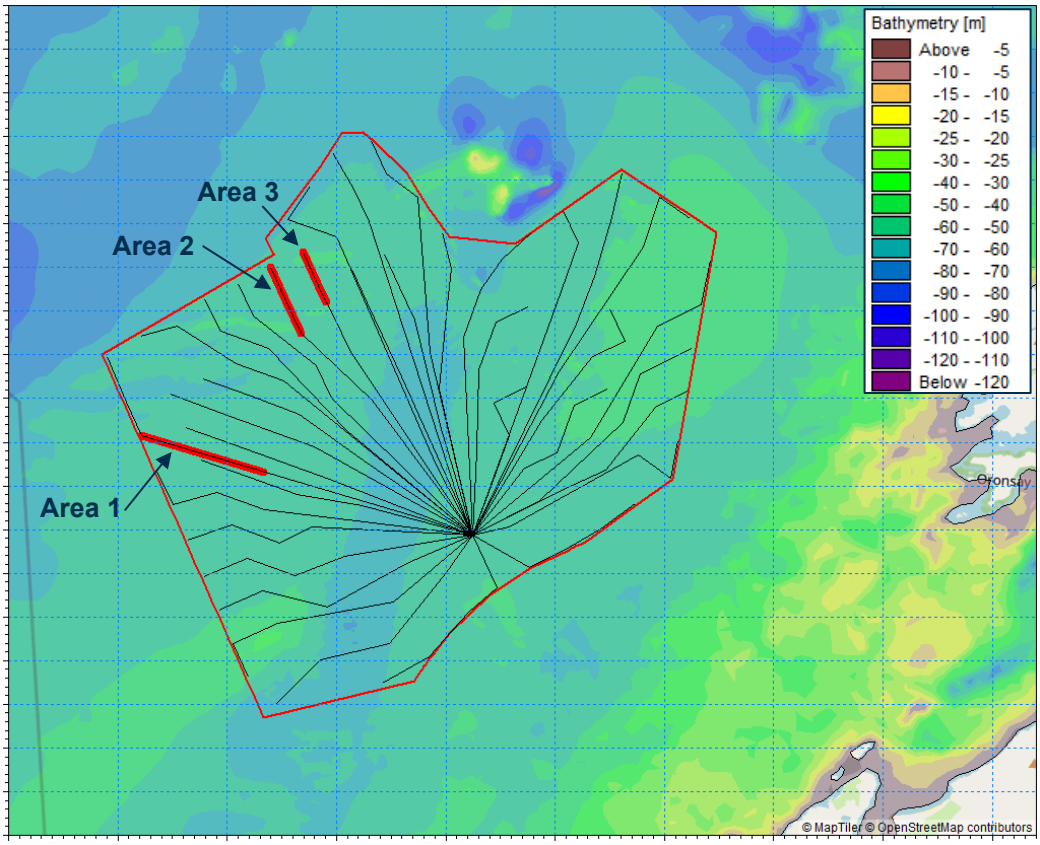

Figure 6-3: Location of array cable levelling activities (red line = indicative location of areas requiring levelling)

6.7.2 A total of 4,073,000 m^3 of seabed material will be released during the sandwave levelling activity, which is divided evenly between the three indicative levelling areas shown in **Figure 6-3**.

6.7.3 The total levelling period for the total length of 11.6 km is 47.14 days using a TSHD. In order to simulate the total levelling length within the 30-day MIKE3-MT model, Area 1 and Areas 2/3 each requiring levelling along a length of 5.8 km has been simulated separately covering a period of 23.57 days. The results of these two simulations have then been combined.

6.7.4 The sediment release rate of the TSHD is 15.0 kg/s and 50% of the material is released near the seabed and the other 50% near the water surface.

6.8 Simulation 4 – Cable Plough Trenching

6.8.1 The required total length of trenching inside the WDA is 582.4 km. The trenching length for each type of cable is detailed below and shown in **Figure 6-4** (colours as specified).

- Trenching length for IACs is 521.3 km (yellow/ turquoise /purple lines),
- Trenching length for for two export cable(s) is 45.2 km (pink and green lines),
- Trenching length for OSP Link Cable between OSP 1 and 2 is 15.9 km (orange line).

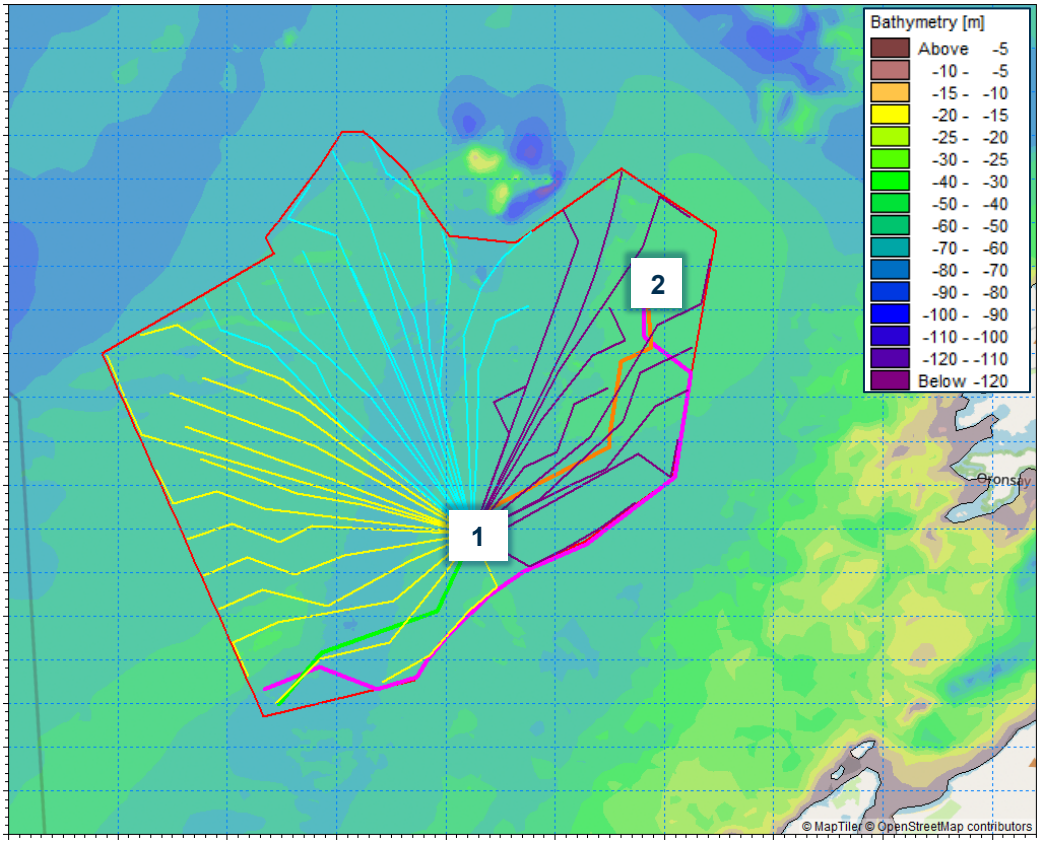

Figure 6-4: Location of array cable trenching activities (yellow / turquoise / black lines = IAC cables, pink and green lines = export cable(s), orange line = OSP Link cable, No. 1 and 2 = OSPs)

6.8.2 A total of 6,698,808 m^3 of seabed material will be released during the trenching activity for the IAC, and 580,820 m^3 for the export cable(s), and 204,315 m^3 for the OSP Link cable.

6.8.3 The total trenching period for the IACs is 72.4 days using a cable plough, and 6.28 days for the export cable(s), and 2.21 days for the OSP Link cable. In order to simulate the total trenching lengths within the 30-day MIKE3-MT model, the trenching activities (see **Figure 6-4**) have been split into the following four simulations. The results of these four simulations have then been combined:

- IAC cables 1 to 13 (yellow lines);
- IAC cables 14 to 25 (turquoise lines);
- IAC cables 26 to 36 (purple lines); and
- Two export cable(s) and OSP Link Cable (pink, green and orange lines).

6.8.4 The sediment release rate of the cable plough is 2,275.52 kg/s and the material is released near the seabed.

6.9 Presentation of Dispersion Model Results

6.9.1 **Section 6.10** to **Section 6.13** present the dispersion model results for the four proposed construction activities that have been simulated. For each simulation the model results are shown as:

- Maximum SSC contours showing the maximum at any one time during the entire model duration.
- Time series of SSC throughout the operational activities at points of interest P1 to P3 (see **Figure 6-5**), unless otherwise stated.
- Total sediment deposition thickness contours at the end of the simulation.

6.9.2 On the maximum SSC plots, the levels greater than 1 mg/l are shown. This value has been chosen because the WDA is characterized predominantly by an ambient level between 1 and 2 mg/l as defined in **Chapter 7 Marine Physical Environment**.

6.9.3 On the total sediment deposition thickness plots, levels greater than 5 cm are shown. This value has been chosen because it is the benchmark for a 'light' deposition event as defined by Marine Biological Association.

6.9.4 Each contour plot shows the dispersion model results and for geographical context the following (as relevant to each simulation):

- Machair Offshore Windfarm WDA as red outline;
- Machair Offshore Windfarm WTGs (circle) and OSPs (square);
- Machair Offshore Windfarm Inter-Array Cables (black lines);
- Machair Offshore Windfarm OSP Link cable; and
- Machair Offshore Windfarm export cable(s) inside the WDA.

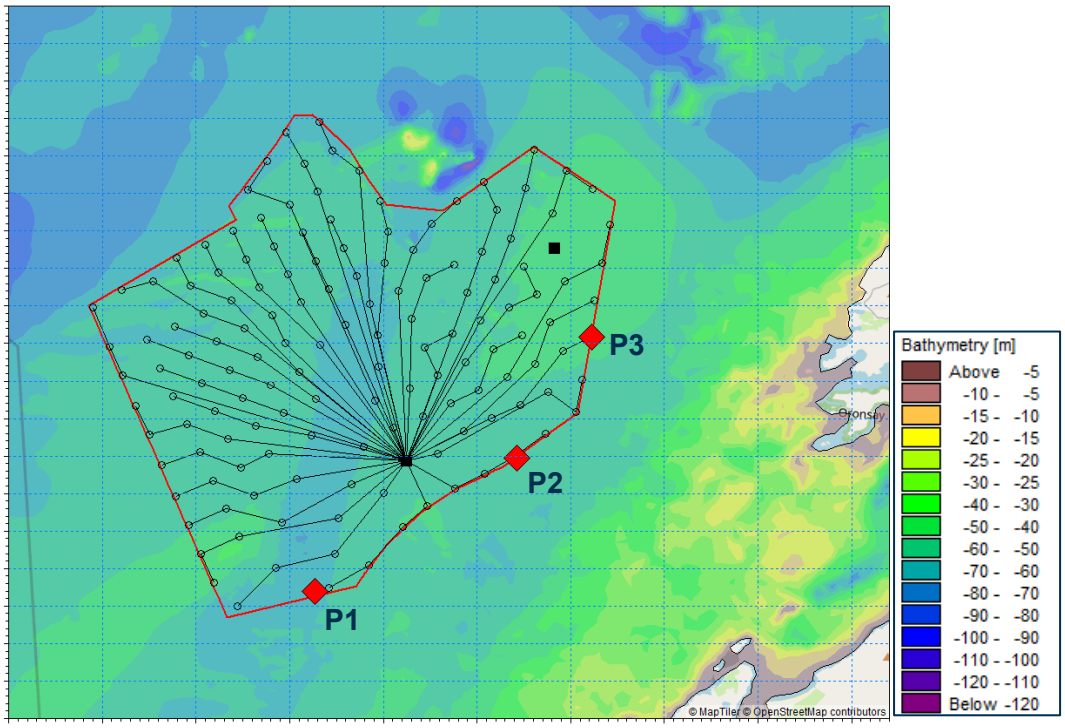

Figure 6-5: Model results extraction points P1 to P3

6.10 Simulation 1 Results - Drilling for Structures (WTGs and OSPs)

6.10.1 **Figure 6-6** to **Figure 6-8** show the maximum SSC which occurs during drilling activities for structures in the WDA near the seabed, in the middle of the water column and near the water surface respectively. The maximum suspended sediment is greatest near the seabed and occurs for the majority localised (up to 300 m diameter) around the WTGs and OSPs, with levels reaching 1 to 5 mg/l. Only in the south of the WDA do these maximum SSC levels extend beyond the WDA southwards in an elongated shape measuring up to 4 km in length and up to 1.5 km in width. The maximum SSC in the middle of the water column occurs localised around the WTGs and OSPs and is below 2 mg/l. The maximum SSC levels near the water surface also occur localised (up to 300 m diameter) around the WTGs and OSPs reaching 1 to 5 mg/l.

6.10.2 The time series plots show nugatory SSC at P1 to P3 during this activity and are therefore not presented here.

6.10.3 **Figure 6-9** shows that the total sediment deposition thickness which occurs during drilling activities for structures in the WDA is below 5 cm.

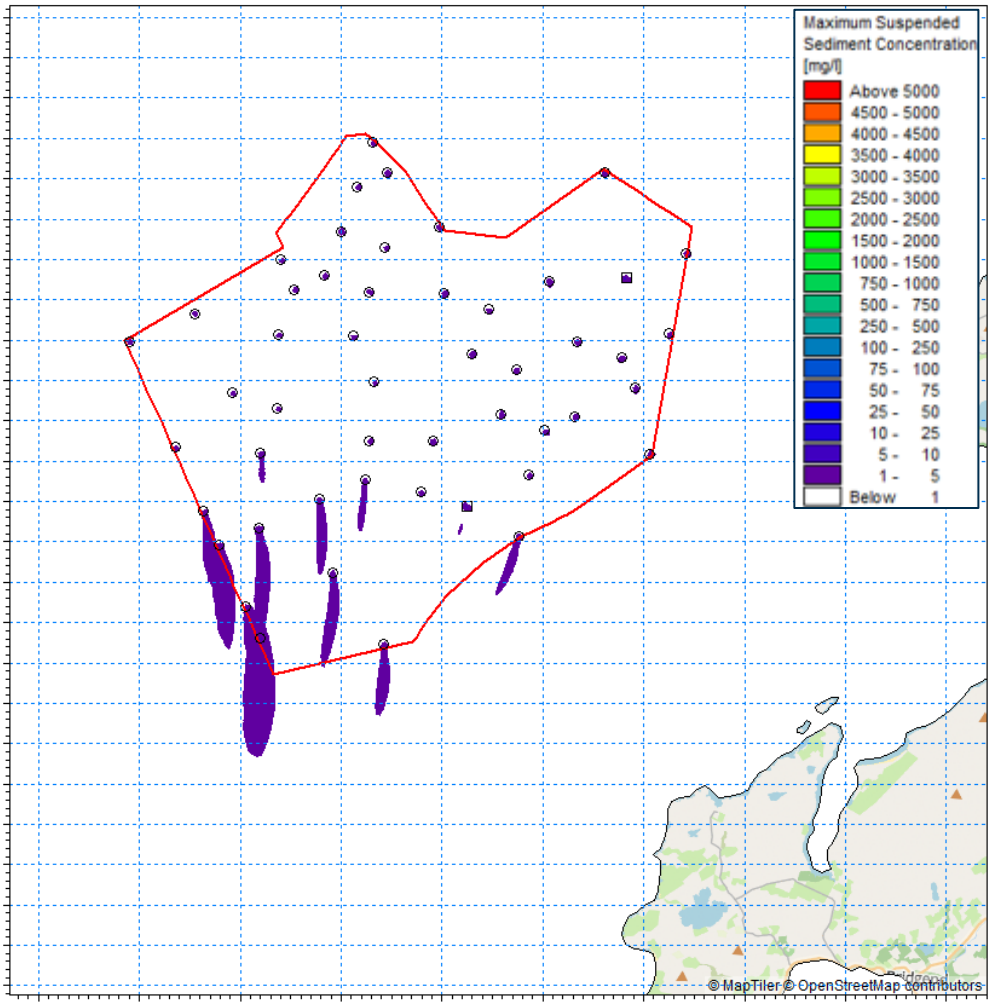

Figure 6-6: Maximum SSC during drilling activities for structures occurring near the seabed

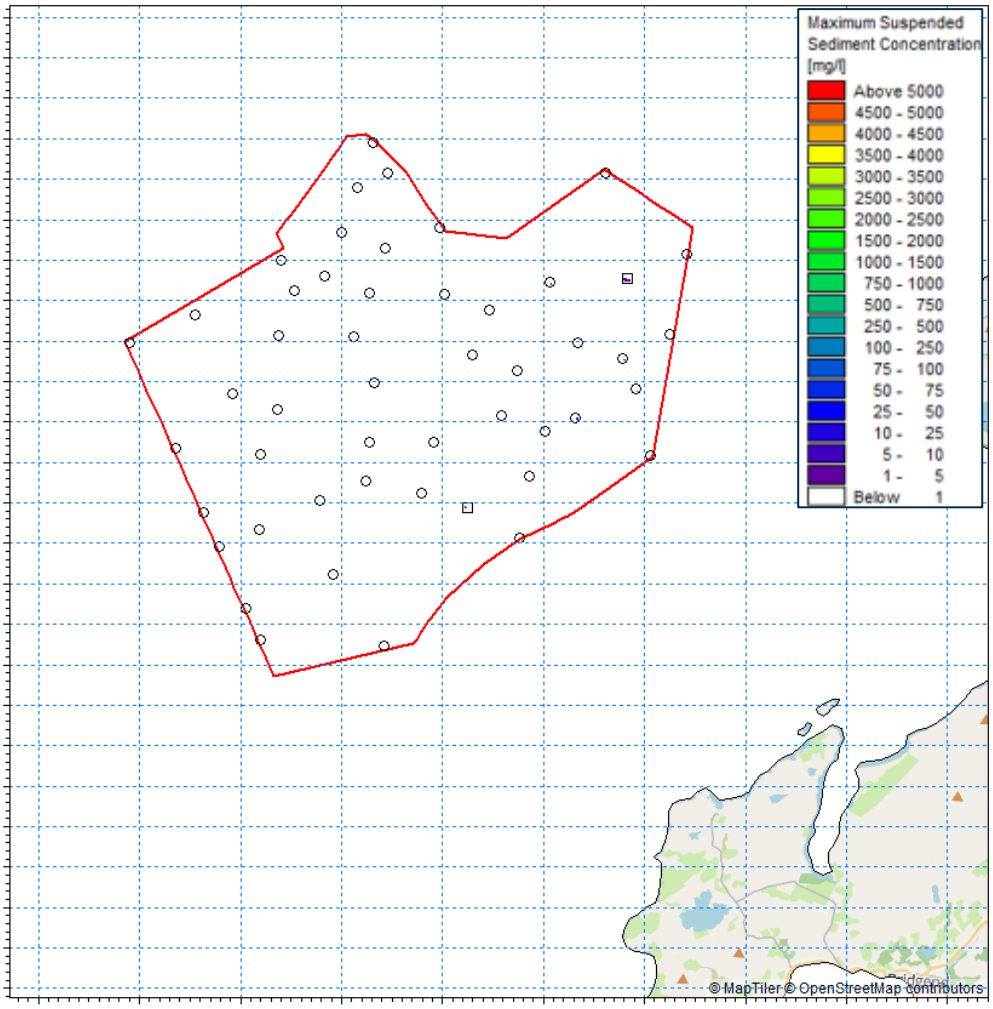

Figure 6-7: Maximum SSC during drilling activities for structures occurring in the middle of water column

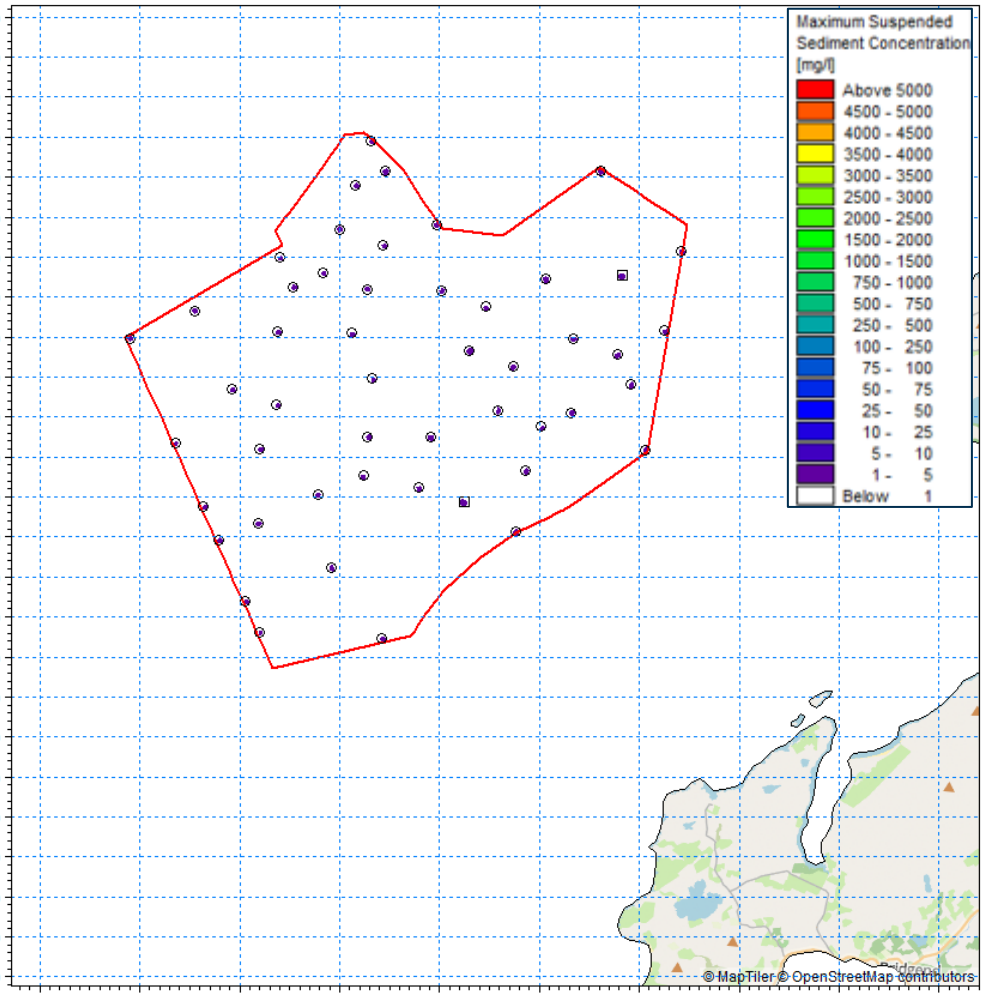

Figure 6-8: Maximum SSC during drilling activities for structures occurring near the water surface

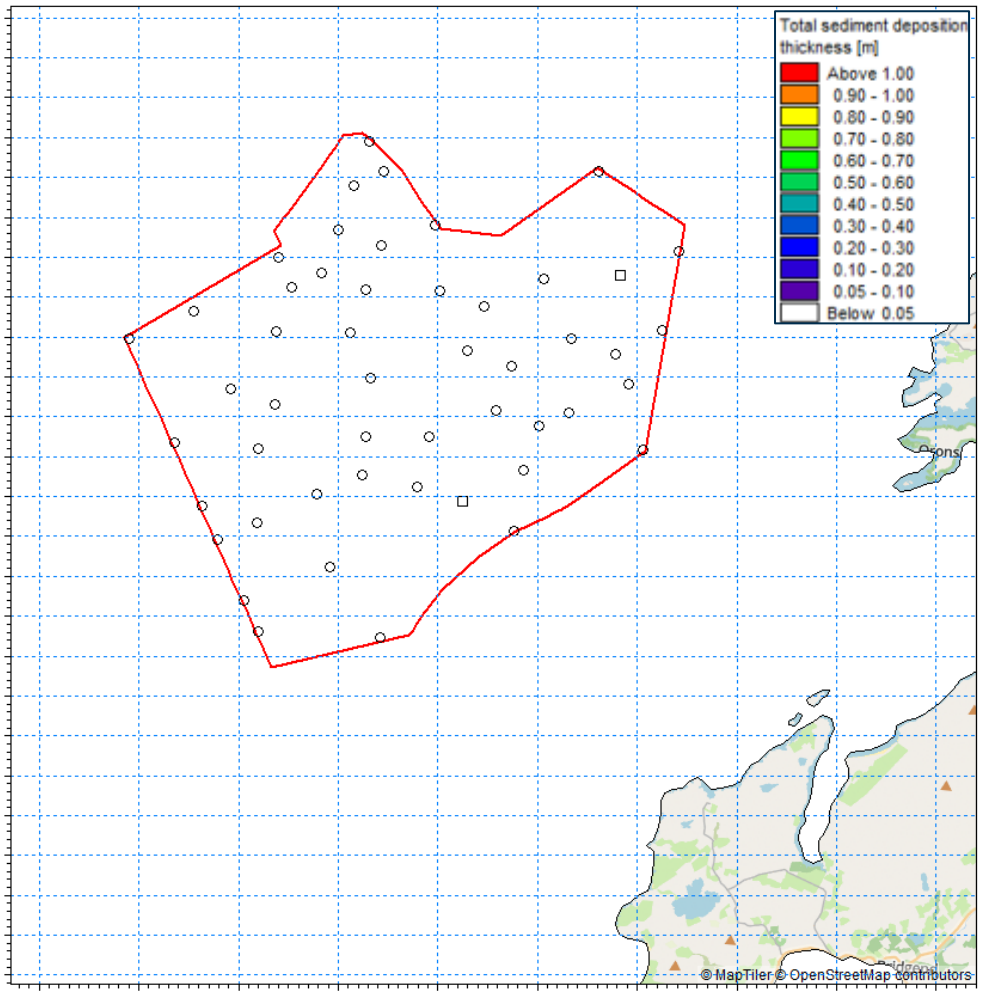

Figure 6-9: Total sediment deposition thickness during drilling activities for structures

6.11 Simulation 2 Results – Bed preparation for Structures (WTGs and OSPs)

6.11.1 **Figure 6-10** to **Figure 6-12** show the maximum SSC which occurs during bed preparation activities for structures in the WDA near the seabed, in the middle of the water column and near the water surface respectively. The maximum suspended sediment is greatest near the seabed and reach levels between 1 to 5 mg/l which cover almost the entire WDA. Only in the south of the WDA these maximum SSC levels extend beyond the WDA southwards in an elongated shape measuring up to 4 km in length and up to 2.5 km in width. The maximum SSC in the middle of the water column occurs localised around the WTGs and OSPs and is below 2 mg/l. The maximum SSC levels near the water surface also occur localised (up to 400 m diameter) around the WTGs and OSPs reaching 1 to 5 mg/l.

6.11.2 **Figure 6-13** to **Figure 6-15** show the time series data of SSC during bed preparation for structures in the WDA near the seabed, in the middle of the water column and near the water surface for three locations, namely P1, P2 and P3 respectively (shown as red points on **Figure 6-10** to **Figure 6-12**). The SSC levels at P1 are below 1 mg/l throughout the water

column. The SSC levels at P2 exceeding 1 mg/l last no longer than two hours with the peak of 2.4 mg/l occurring near the seabed. At P3 the SSC levels exceeding 1 mg/l last no longer than three hours with a maximum peak of 7.2 mg/l near the seabed and 5.2 mg/l near the water surface.

6.11.3 **Figure 6-16** shows that the total sediment deposition thickness which occurs during bed preparation activities for structures in the WDA is below 5 cm.

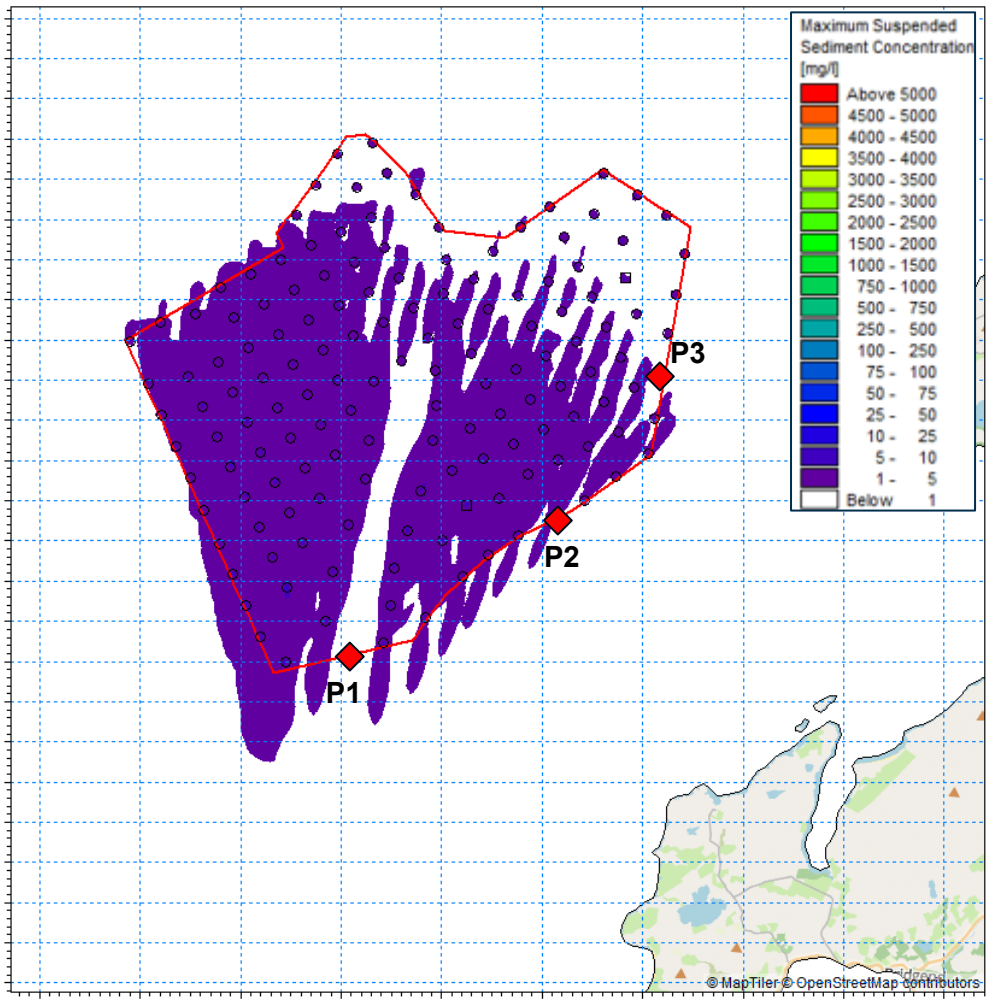

Figure 6-10: Maximum SSC during bed preparation activities for structures occurring near the seabed

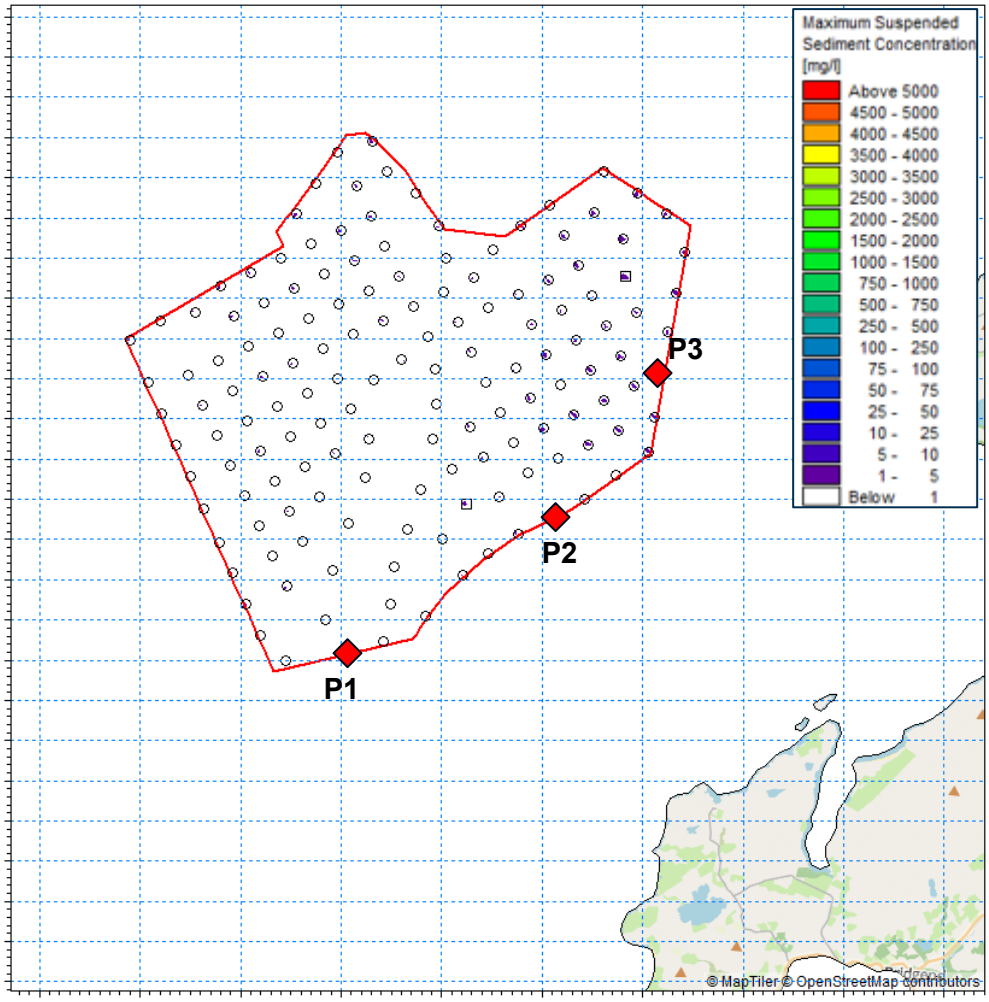

Figure 6-11: Maximum SSC during bed preparation activities for structures occurring in the middle of water column

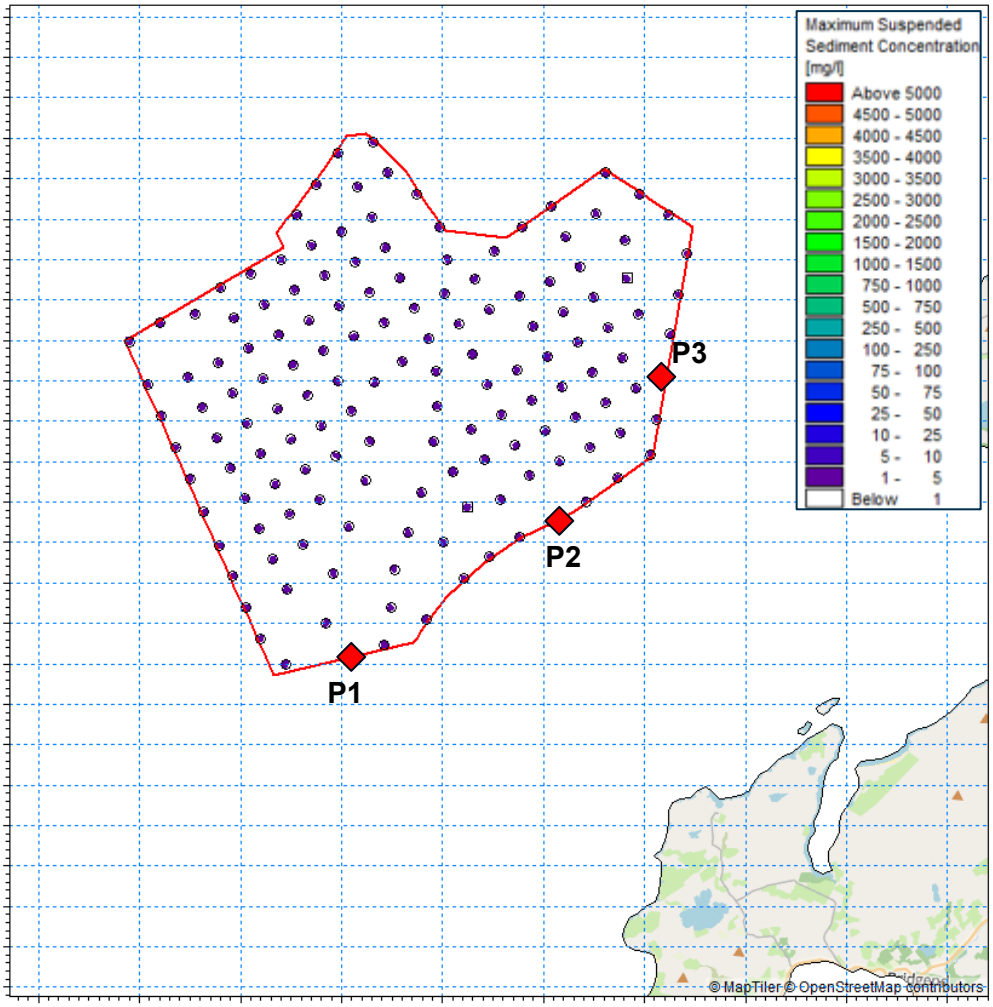

Figure 6-12: Maximum SSC during bed preparation activities for structures occurring near the water surface

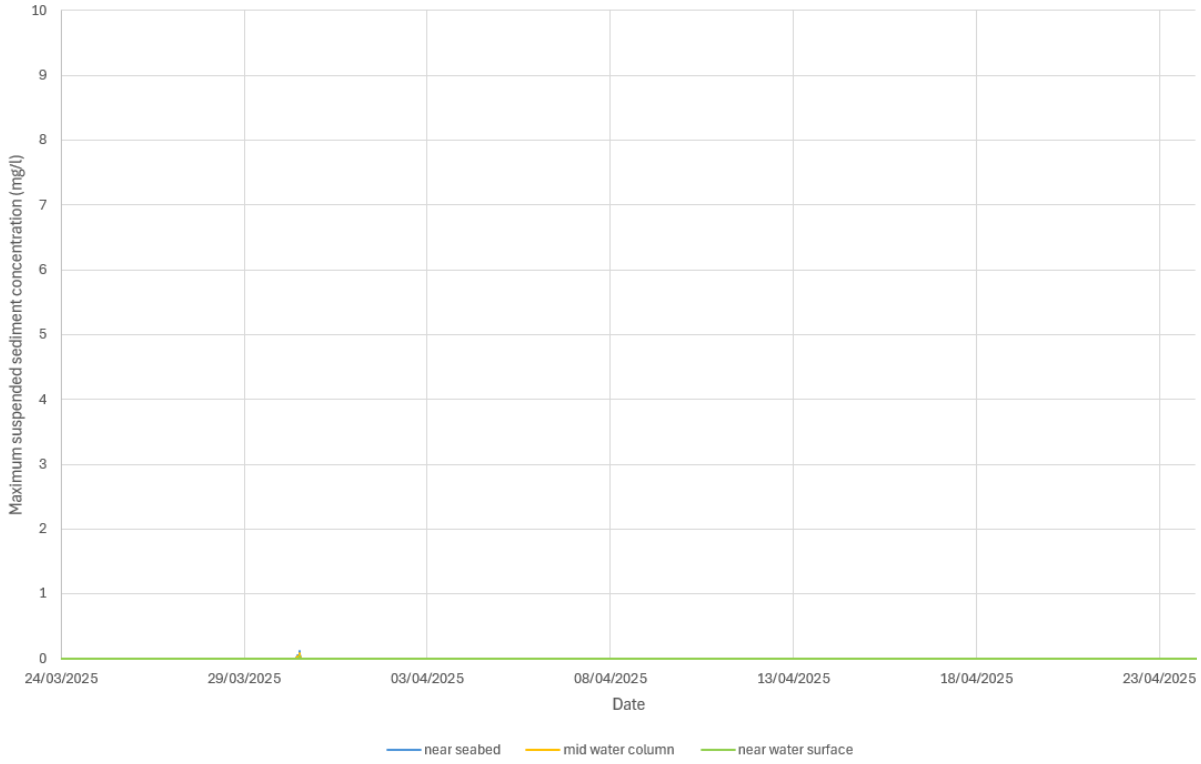

Figure 6-13: Time series of SSC at P1 during bed preparation activities for structures near seabed, middle of water column and near water surface

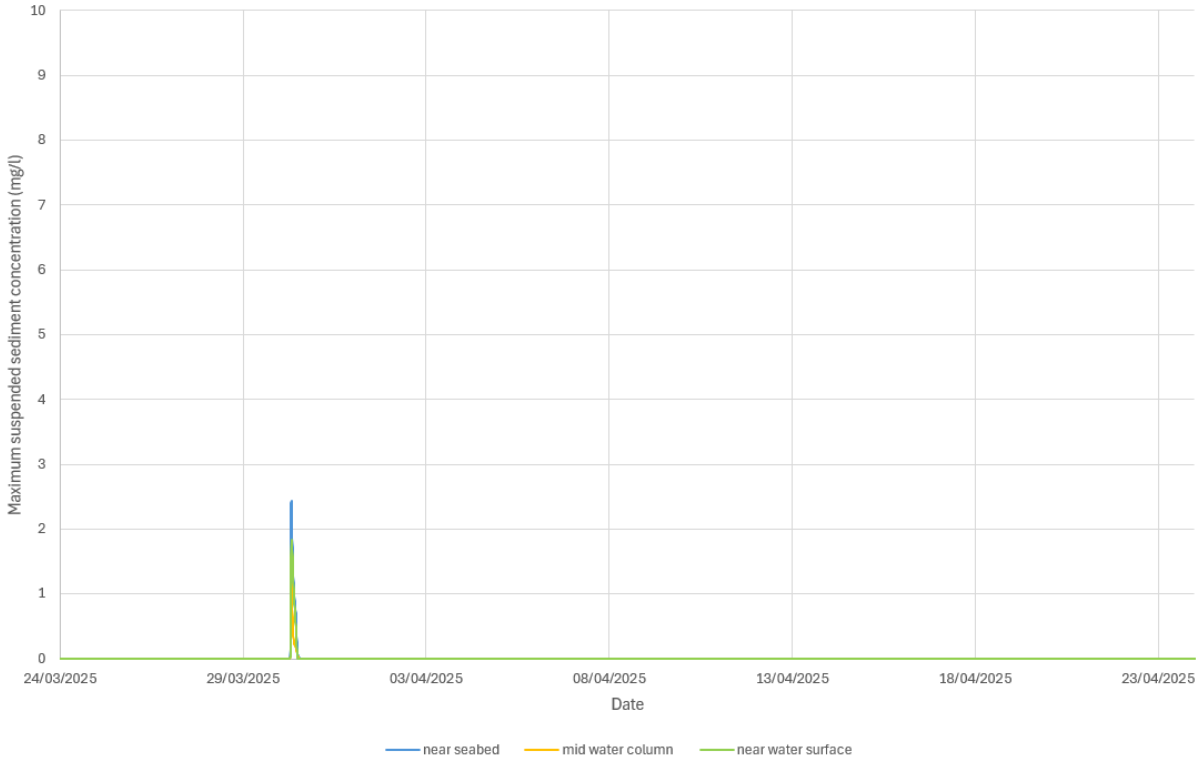

Figure 6-14: Time series of SSC at P2 during bed preparation activities for structures near seabed, middle of water column and near water surface

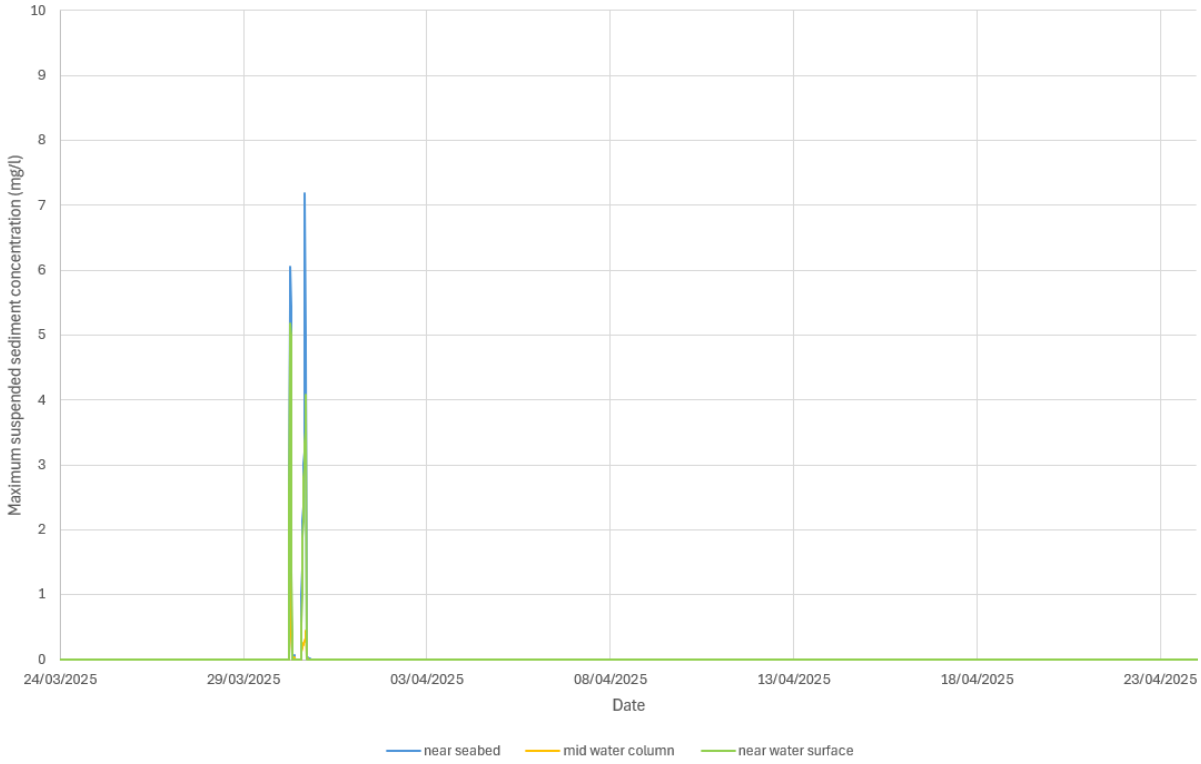

Figure 6-15: Time series of SSC at P3 during bed preparation activities for structures near seabed, middle of water column and near water surface

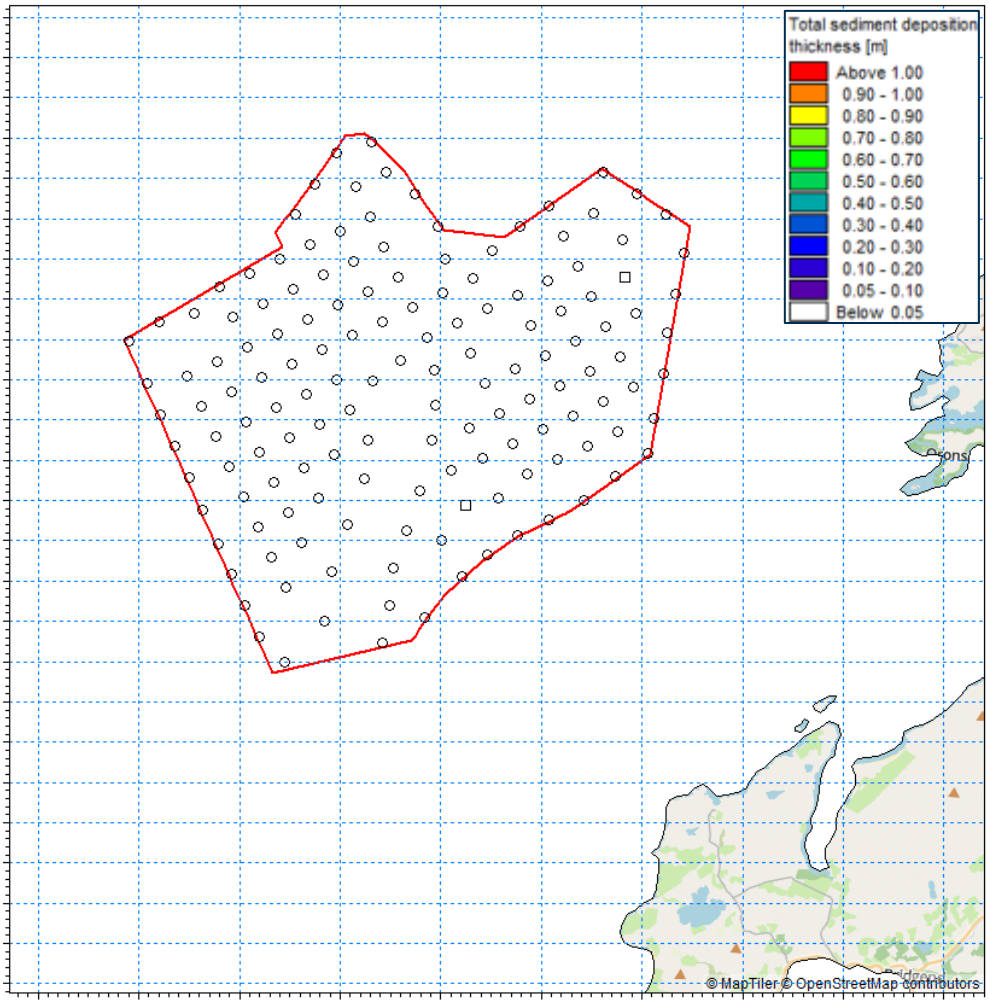

Figure 6-16: Total sediment deposition thickness during bed preparation activities for structures

6.12 Simulation 3 Results – Array Cable Levelling

6.12.1 **Figure 6-17** to **Figure 6-19** show the maximum SSC which occurs during sandwave levelling activities in the WDA near the seabed, in the middle of the water column and near the water surface respectively.[1] The maximum SSC is greatest near the seabed and occurs close to the IAC length that requires levelling. The maximum SSC levels near the seabed that reach between 25 and 40 mg/l only occur at small spots (up to diameter of 140 m) along the cable, maximum SSC levels between 5 and 25 mg/l mostly extend up to 250 m either side of the cable with only three areas extending by up to 1.3 km from the cable, whilst only maximum SSC levels between 1 and 5 mg/l extend between 0.5 and 5.0 km away from the cable. The maximum SSC in the middle of the water column occur localised around the cable with levels between 5 and 10 mg/l extending by up to 150 m either side and levels between 1 and 5 mg/l extending by up to 500 m either side. The maximum SSC levels near the water surface also occur localised around the cable reaching levels between 10 and 25 mg/l up to 120 m either side of the cable, whilst levels between 1 to 5 mg/l extend by up to 400 m either side.

[1] Note that the worst-case length of IACs is associated with connection into a single OSP and hence that is reflected in **Figure 6-17** to **Figure 6-19**.

6.12.2 The time series plots hardly show any SSC at P1 to P3 during this activity and are therefore not presented here.

6.12.3 **Figure 6-20** shows that the total sediment deposition thickness which occurs during sandwave levelling activities in the WDA is below 5 cm.

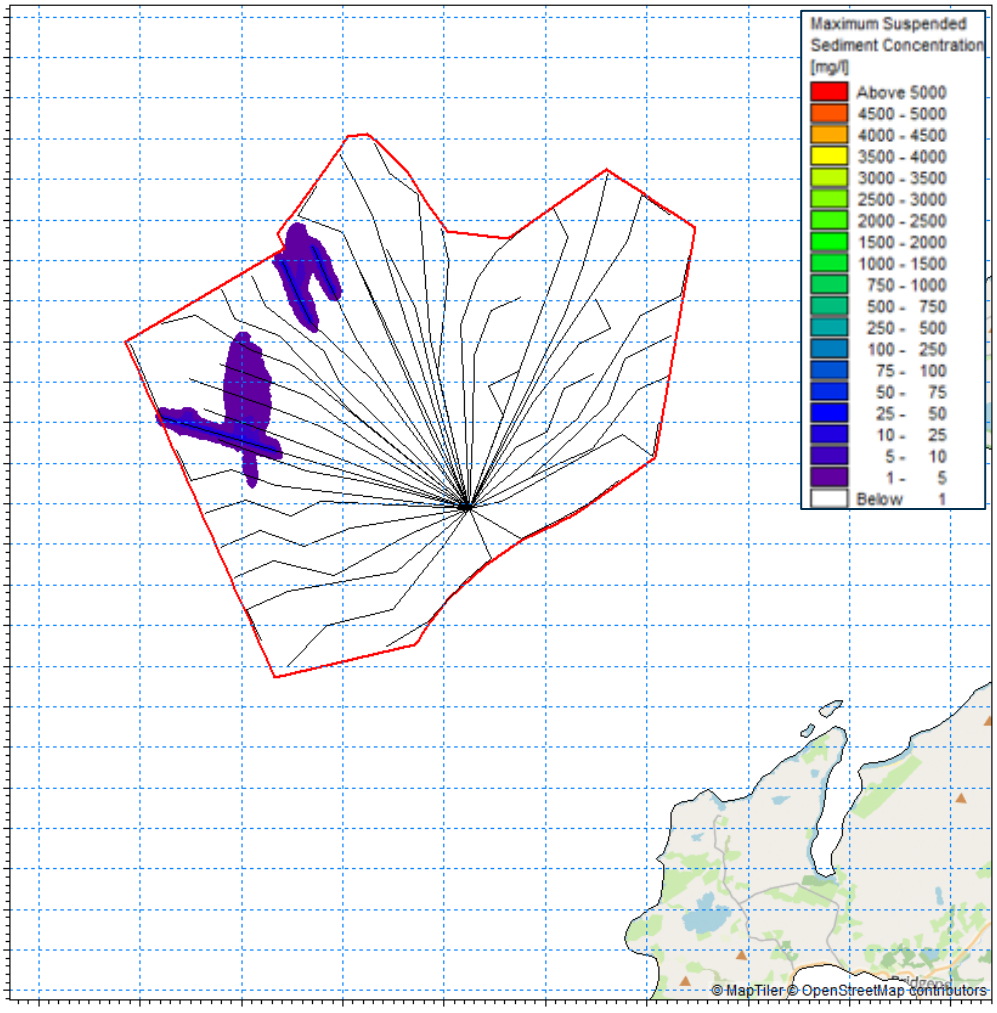

Figure 6-17: Maximum SSC during levelling activities for structures occurring near the seabed

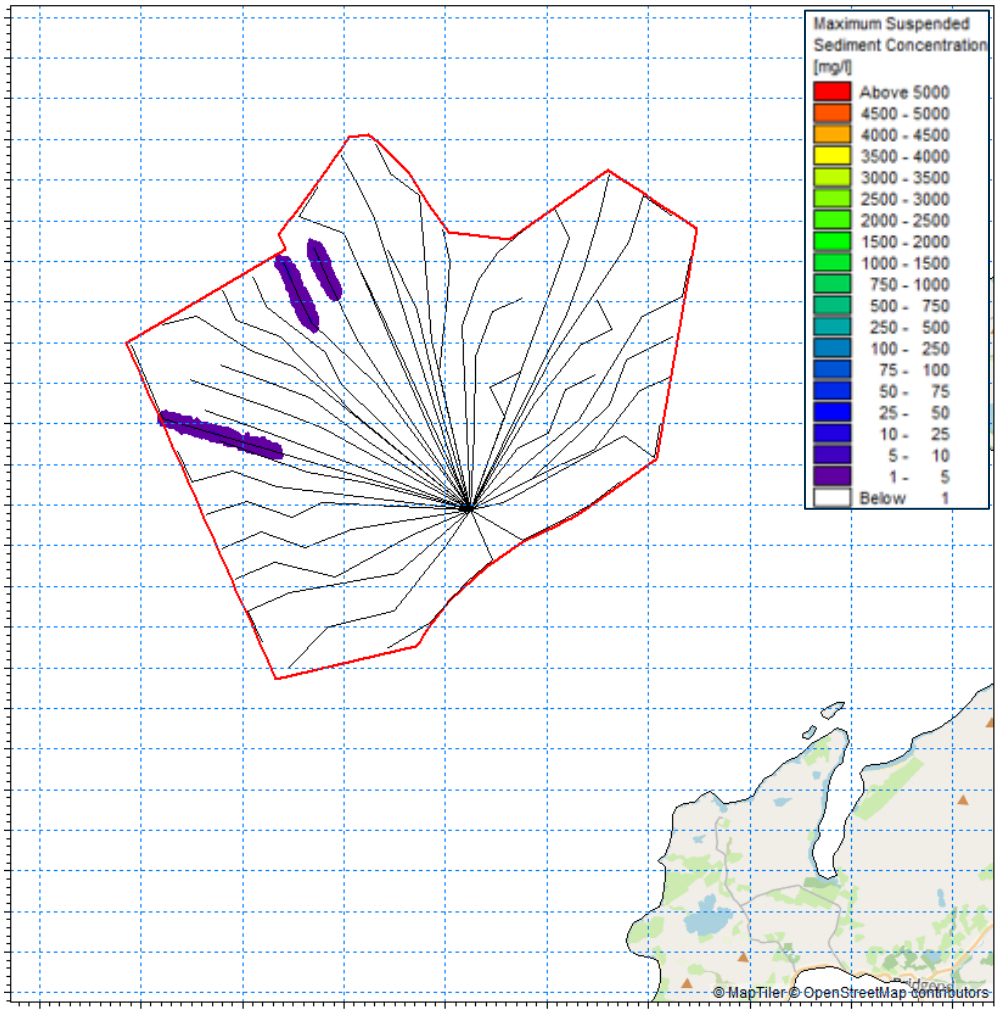

Figure 6-18: Maximum SSC during levelling activities for structures occurring in the middle of water column

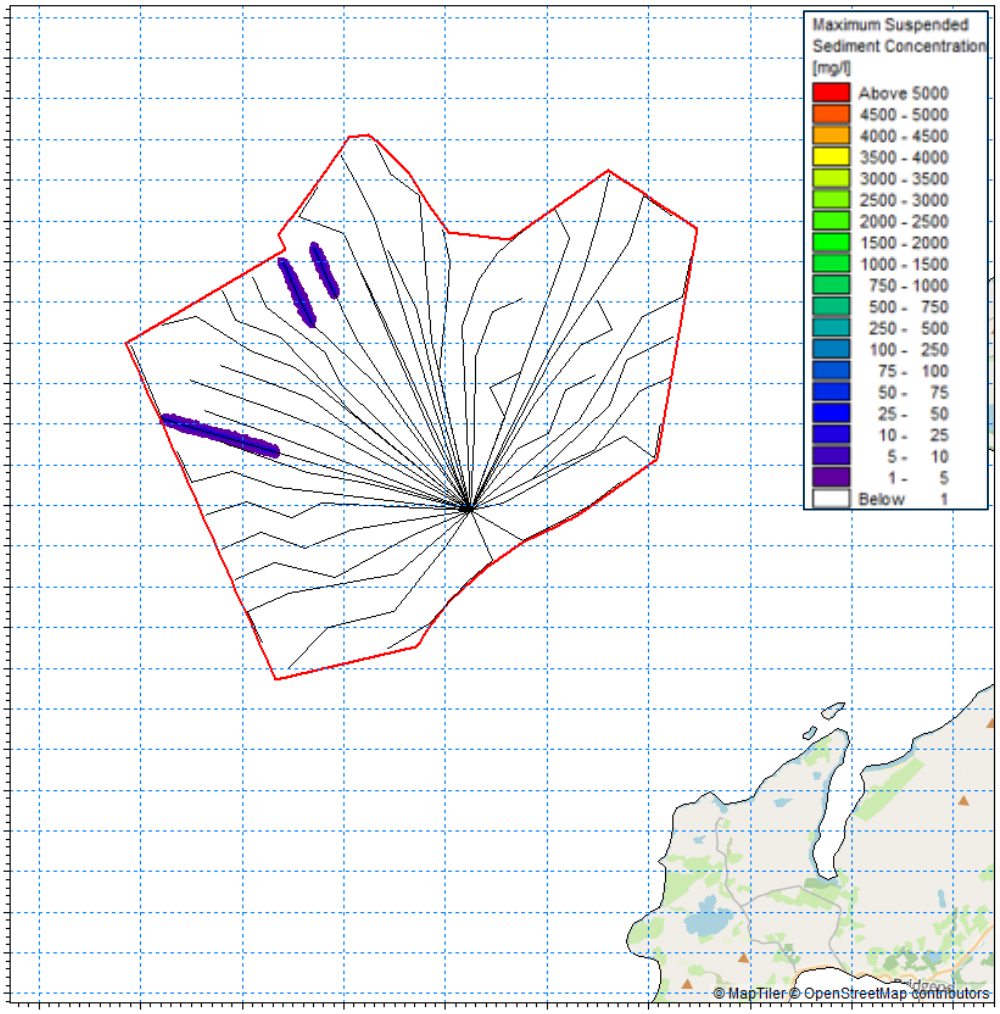

Figure 6-19: Maximum SSC during levelling activities for structures occurring near the water surface

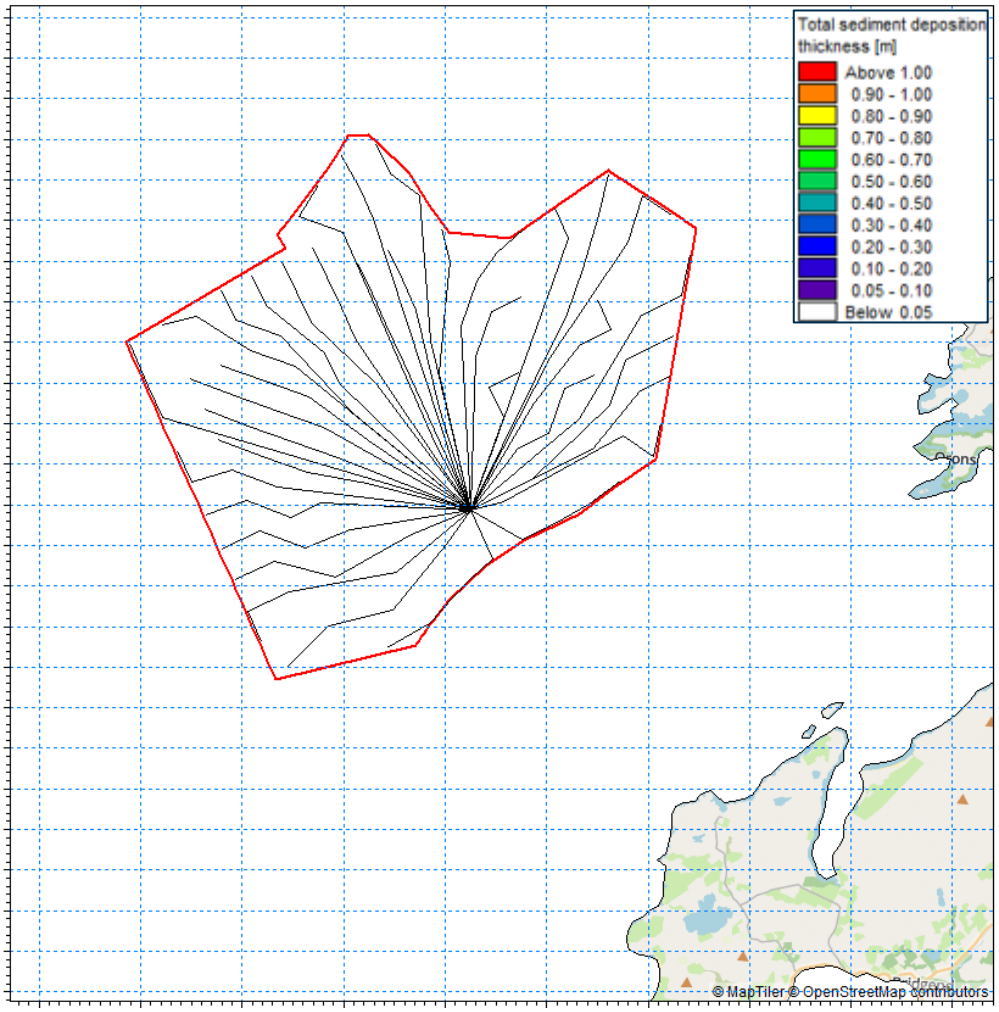

Figure 6-20: Total sediment deposition thickness during levelling activities for structures

6.13 Simulation 4 Results - Trenching

6.13.1 **Figure 6-21** to **Figure 6-23** show the maximum suspended sediment SSC which occurs during trenching activities along the cables in the WDA near the seabed, in the middle of the water column and near the water surface respectively. The maximum SSC is greatest near the seabed and gradually becomes less when reaching the water surface. The maximum SSC levels (equal or above 1 mg/l) near the seabed cover the whole of the WDA but only reach higher levels close to the cables. The maximum SSC levels close to the cables are on average between 1,500 and 2,500 mg/l extending by up to 150 m either side of the cable. Levels between 1 and 5 mg/l extend by approximately 8 km southwards beyond the WDA, and by approximately 3 km northwards. The maximum SSC levels (equal or above 1 mg/l) in the middle of the water column also cover the whole of the WDA but are below 50 mg/l, and levels between 1 and 5 mg/l extend by approximately 7.0 km southwards beyond the WDA, and by approximately 3.0 km northwards. The maximum SSC levels near the water surface reach between 1 and 5 mg/l and cover most of the WDA extending by up 5.0 km southwards and up to 2.5 km northwards beyond the WDA.

6.13.2 **Figure 6-24** to **Figure 6-26** show the time series data of SSC during trenching in the WDA near the seabed, in the middle of the water column and near the water surface for three locations, namely P1, P2 and P3 respectively (shown as red points on **Figure 6-21** to **Figure 6-23**). The SSC levels at P1 exceeding 1 mg/l only near the seabed and in the middle of the water column, and last less than 2 hours with a peak of 5,400 mg/l near the seabed and SSC levels of up to 5 mg/l in the middle of the water column. At P2 the SSC levels exceeding 1 mg/l near the seabed last approximately 8 hours with the peak at 2,200 mg/l. The SSC levels at P2 in the middle of the water column are considerably less, and levels exceeding 1 mg/l last less than 2 hours with a peak of 35 mg/l, whilst the SSC levels near the water surface are below 1 mg/l. The SSC levels at P3 exceeding 1 mg/l near the seabed last 1 to 2 hours with a peak of 9,700 mg/l, whilst the SSC levels in the middle of the water column are considerably less with a peak of 20 mg/l, and SSC levels near the water surface are all below 1 mg/l.

6.13.3 **Figure 6-27** shows the total sediment deposition thickness which occurs during trenching activities along the cables in the WDA. The deposition occurs along the cables and reaches levels of between 0.1 and 0.2 m on average which extends by up to 200 m either side of the cable. Deposition between 0.2 to 0.3 m occurs localised close to the cable but extends only by up to 100 m either side of the cable. There are some localised areas where the deposition is higher than 0.3 m. It occurs where several cables are close together. The deposition is highest near the OSP where all the cables 'meet', with levels reaching up to 4.0 m.

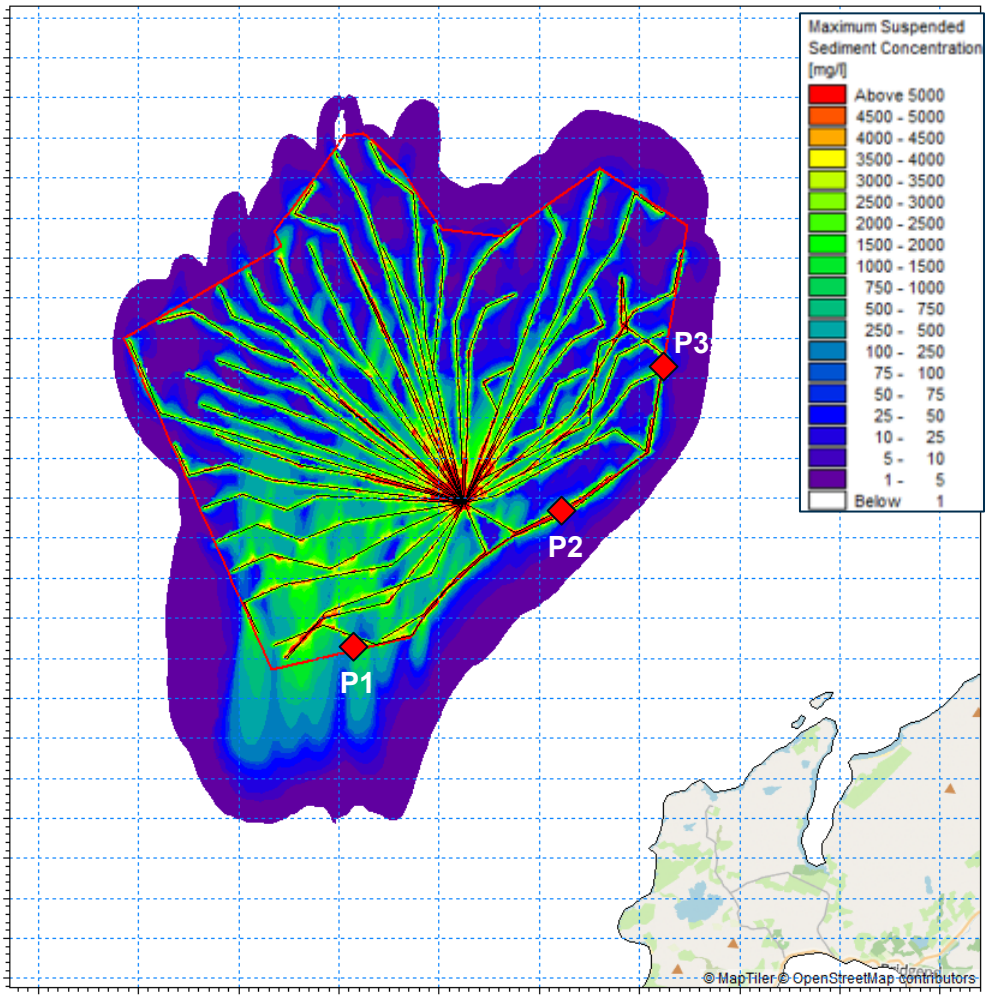

Figure 6-21: Maximum SSC during trenching activities for structures occurring near the seabed

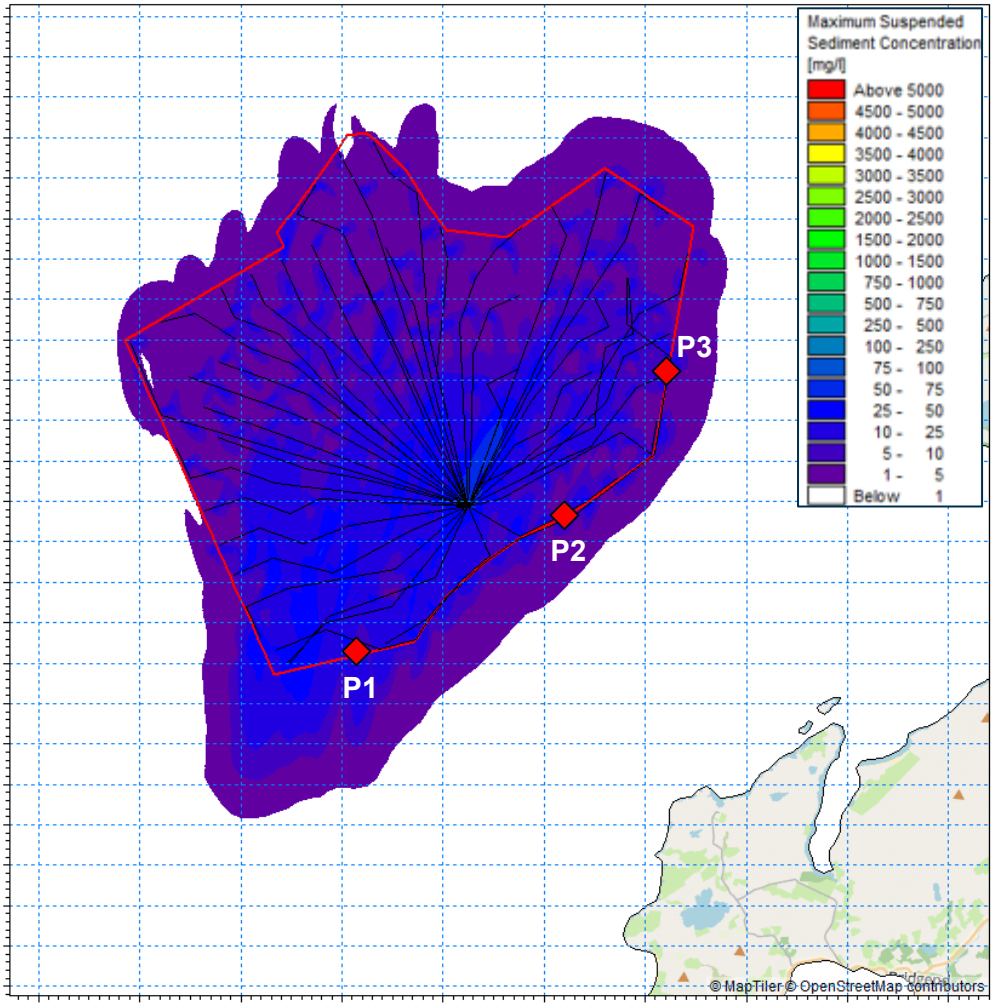

Figure 6-22: Maximum SSC during trenching activities for structures occurring in the middle of water column

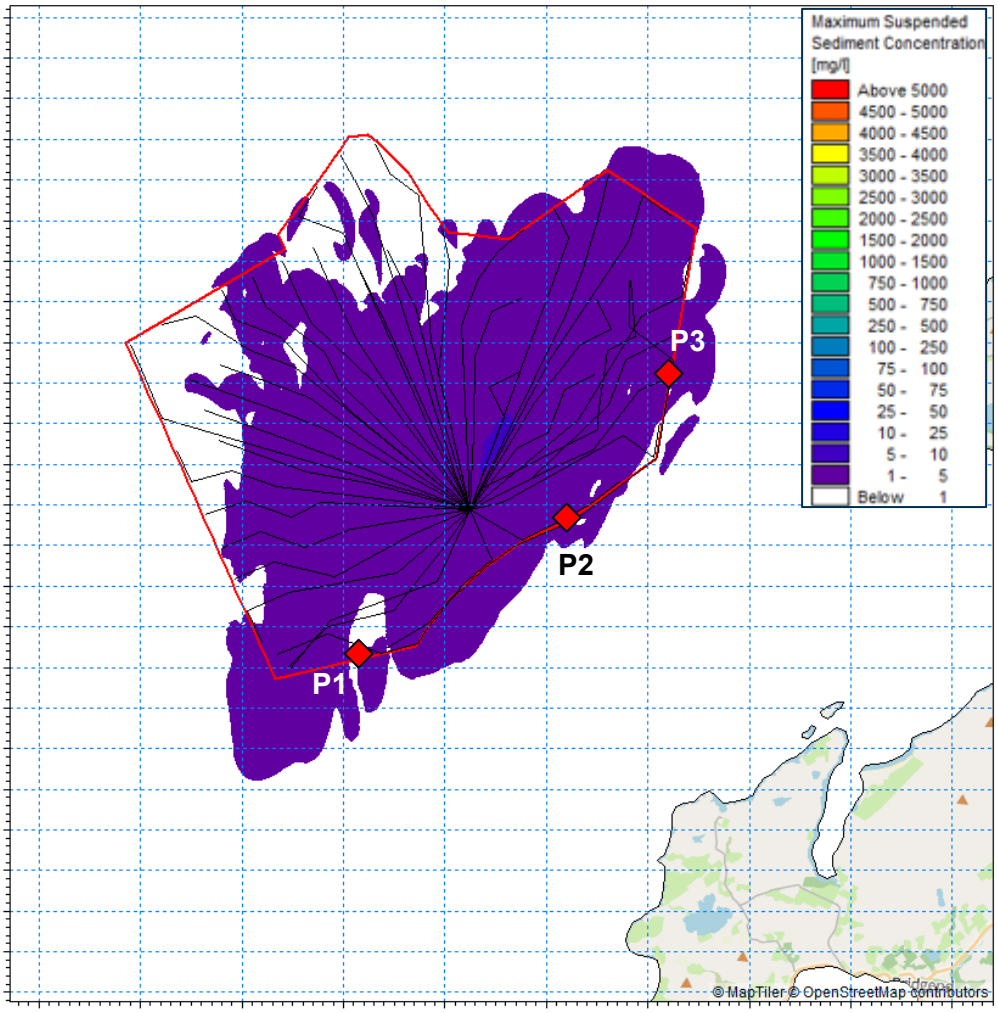

Figure 6-23: Maximum SSC during trenching activities for structures occurring near the water surface

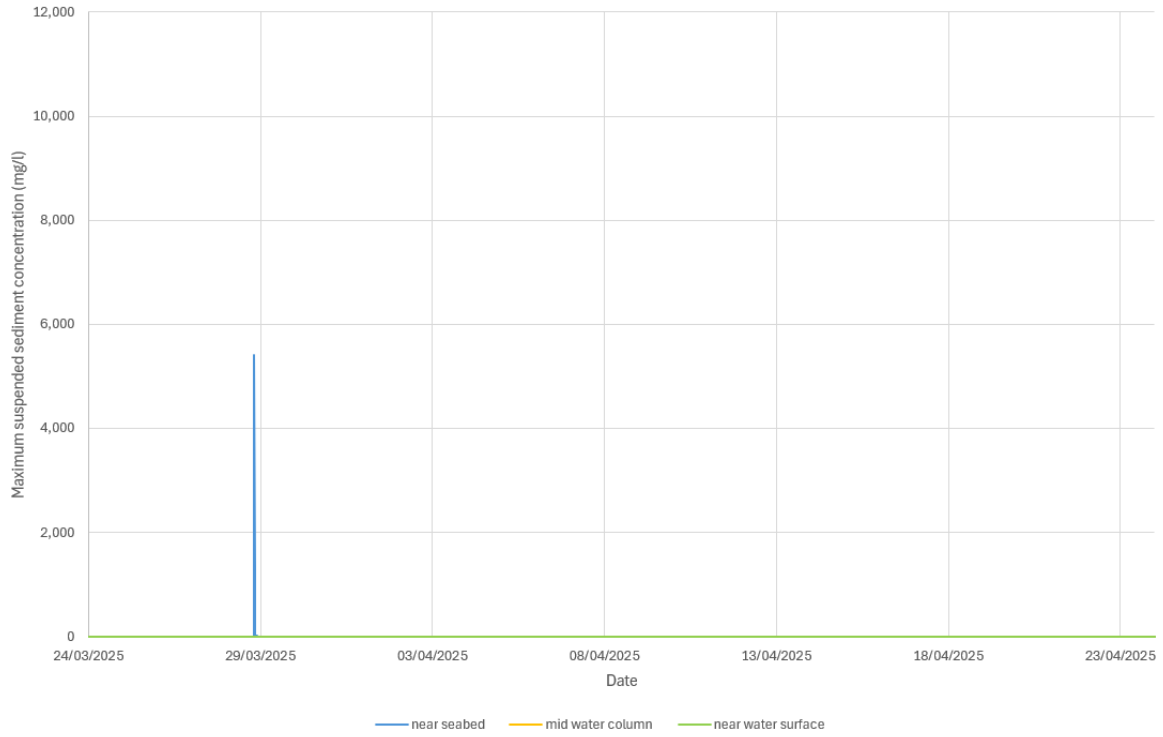

Figure 6-24: Time series of SSC at P1 during trenching activities for structures near seabed, middle of water column and near water surface

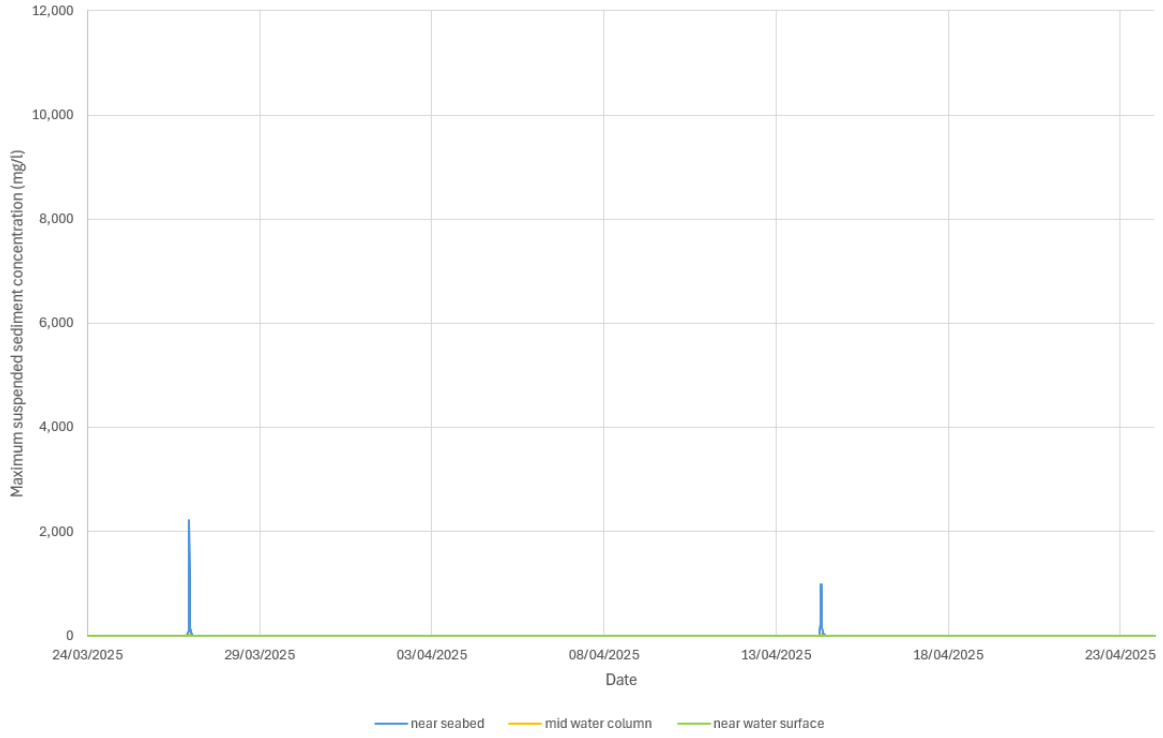

Figure 6-25: Time series of SSC at P2 during trenching activities for structures near seabed, middle of water column and near water surface

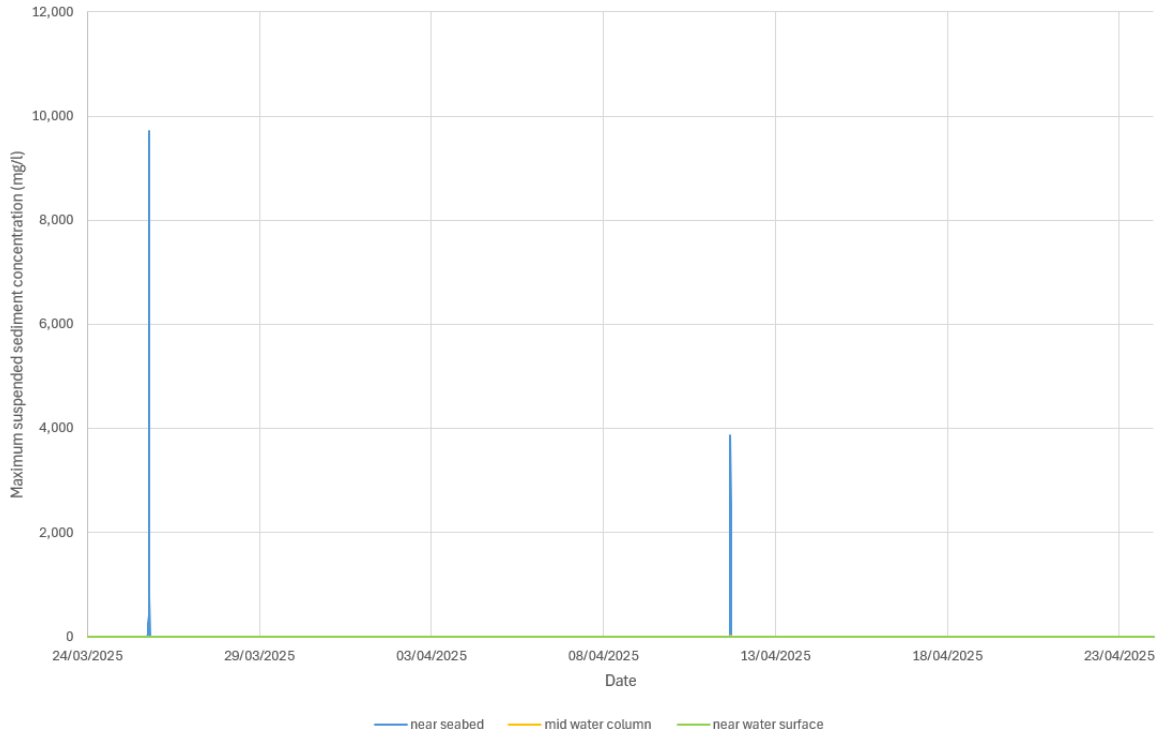

Figure 6-26: Time series of SSC at P3 during trenching activities for structures near seabed, middle of water column and near water surface

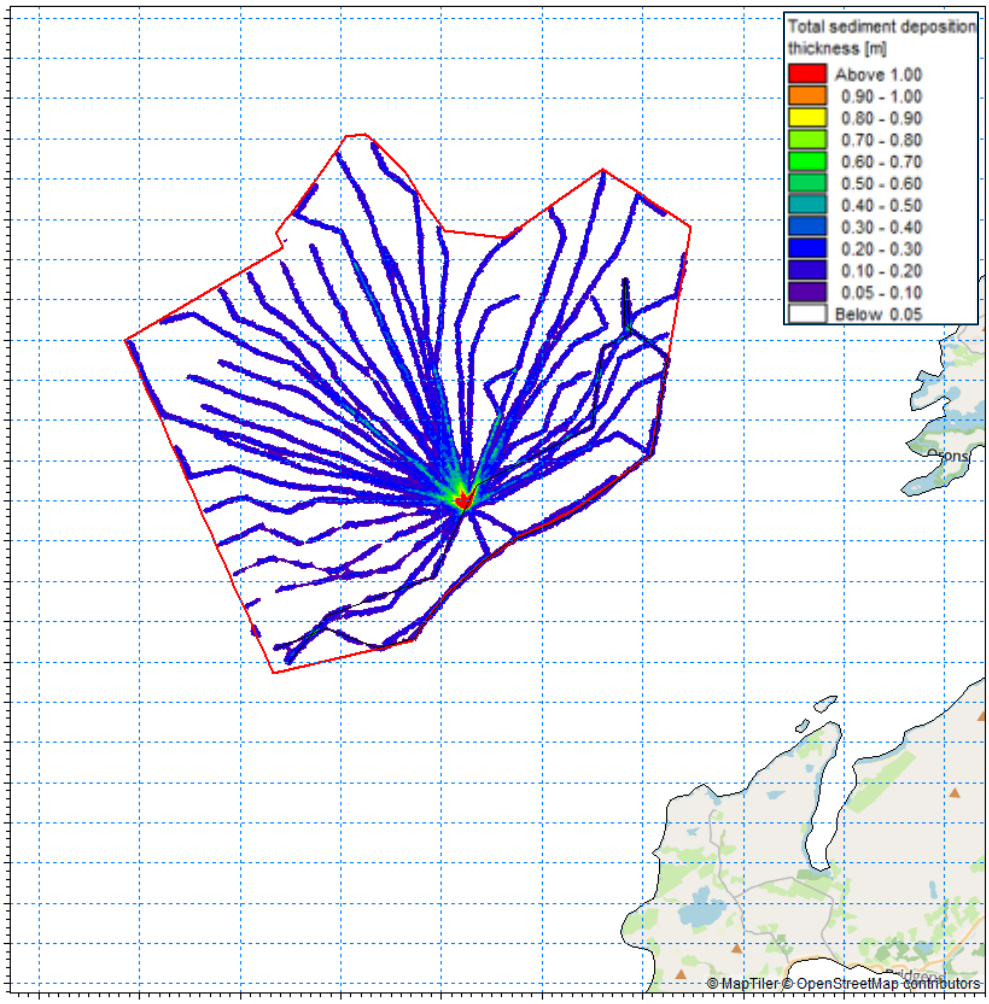

Figure 6-27: Total sediment deposition thickness during trenching activities for structures

6.14 Summary and Conclusion on Dispersion Modelling

6.14.1 The largest plume and highest SSCs are created by the cable trenching activities. The maximum SSC is greatest near the seabed and gradually becomes less when reaching the water surface. The maximum SSC levels occur close to the cables with an average between 1,500 and 2,500 mg/l. Maximum SSC levels between 1 and 5 mg/l extend by approximately 8 km southwards beyond the WDA, and by approximately 3 km northwards.

6.14.2 The drilling activities for foundations result in maximum SSCs of up to 5 mg/l, mainly localised around the WTGs and OSPs. Only in the south of the WDA and near the seabed the maximum SSC levels extend in elongated shapes southwards by up to 4 km beyond the WDA.

6.14.3 The bed preparation activities for structures result in maximum SSCs of up to 5 mg/l and they are localised around the WTGs and OSPs. SSC levels higher than 1 mg/l last less than 3 hours peaking at 7 mg/l.

6.14.4 The sandwave levelling activities show the greatest maximum SSCs near the seabed with SSC levels reaching 40 mg/l but only occurring in localised spots close to the cables. Maximum SSC levels between 1 and 5 mg/l extend by up to 5 km from the cable in three areas up to 2 km in width. However, all SSC levels above 1 mg/l occur within the WDA.

6.14.5 The total sediment deposition thickness which occurs during trenching activities along the cables in the WDA occurs close to the cables and reaches levels of between 0.1 and 0.2 m on average which extend by up to 200 m either side of the cable. There are some areas where the deposition is between 0.2 to 0.3 m extending by up to 100 m. The deposition is highest near the OSP where all the cables ‘meet’, with levels reaching up to 4 m.

6.14.6 The total sediment deposition thickness which occurs during drilling and bed preparation for structures and during sandwave levelling activities in the WDA is below 5 cm.

7 References

(1) *ABPmer, (2013). Numerical Model Calibration and Validation Guidance. ABP Marine Environmental Research Ltd, File Note R/1400/112. ABPmer, Southamton.*
(2) *BODC, (2024). British Oceanographic Data Centre. www.bodc.ac.uk*
(3) *CEFAS, (2025). Centre for Environment, Fisheries and Aquaculture Science.*
(4) *EMODnet, (2024). European Marine Observation Dataset*
(5) *Fugro, (2024). Wind Resource and Metocean Data Report. ScotWind MachairWind Resource and Metocean Campaign. Final Report. MCW-SCH-ENG-REP-FUG-00000.*
(6) *Fugro, (2024). WRM Measurement Campaign Operations Report. MCW-SCH-ENG-REP-FUG-000009.*
(7) *Jacobs and Environment Agency, (2022). Coastal Modelling Standards Update.*
(8) *Lund University, (2011). WAFO. A Matlab Toolbox for Analysis of Randon Waves and Loads.*
(9) *UKHO, (2025). Admiralty Seabed Bathymetry Portal. Seabed Mapping*